

University of Alberta

**Recombinant and Native Human Concentrative Nucleoside Transporters in
Intestine and Brain: Regulation and Importance in Adenosine
Signaling and Interactions with Drugs**

by



Thack(h) T. Lang

A thesis submitted to the Faculty of Graduate Studies and Research in partial
fulfillment of the requirements for the degree of Doctor of Philosophy

in

Medical Sciences - Oncology

Edmonton, Alberta

Spring, 2003.

National Library
of Canada

Acquisitions and
Bibliographic Services

395 Wellington Street
Ottawa ON K1A 0N4
Canada

Bibliothèque nationale
du Canada

Acquisitons et
services bibliographiques

395, rue Wellington
Ottawa ON K1A 0N4
Canada

Your file *Votre référence*

ISBN: 0-612-82129-3

Our file *Notre référence*

ISBN: 0-612-82129-3

The author has granted a non-exclusive licence allowing the National Library of Canada to reproduce, loan, distribute or sell copies of this thesis in microform, paper or electronic formats.

The author retains ownership of the copyright in this thesis. Neither the thesis nor substantial extracts from it may be printed or otherwise reproduced without the author's permission.

L'auteur a accordé une licence non exclusive permettant à la Bibliothèque nationale du Canada de reproduire, prêter, distribuer ou vendre des copies de cette thèse sous la forme de microfiche/film, de reproduction sur papier ou sur format électronique.

L'auteur conserve la propriété du droit d'auteur qui protège cette thèse. Ni la thèse ni des extraits substantiels de celle-ci ne doivent être imprimés ou autrement reproduits sans son autorisation.

Canada

University of Alberta

Library Release Form

Name of Author: Thack(h) T. Lang

Title of Thesis: Recombinant and Native Human Concentrative Nucleoside Transporters in Intestine and Brain: Regulation and Importance in Adenosine Signaling and Interactions with Drugs.

Degree: Doctor of Philosophy

Year this Degree Granted: 2003

Permission is hereby granted to the University of Alberta Library to reproduce single copies of this thesis and to lend or sell such copies for private, scholarly or scientific research purposes only.

The author reserves all other publication and other rights in association with the copyright in the thesis, and except as herein before provided, neither the thesis nor any substantial portion thereof may be printed or otherwise reproduced in any material form whatever without the author's prior written permission.



13105-41A Street
Edmonton, Alberta
T5A 2T8

Date: Feb. 3, 2003.

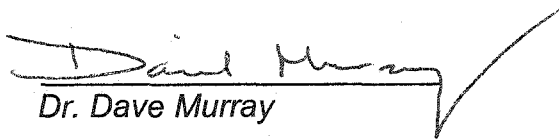
University of Alberta

Faculty of Graduate Studies and Research

The undersigned certify that they have read, and recommend to the Faculty of Graduate Studies and Research for acceptance, a thesis entitled "*Recombinant and Native Human Concentrative Nucleoside Transporters in Intestine and Brain: Regulation and Importance in Adenosine Signaling and Interactions with Drugs*" submitted by *Thack(h) Trung Lang* in partial fulfillment of the requirements for the degree of *Doctor of Philosophy in Medical Sciences-Oncology*.



Dr. Carol E. Cass



Dr. Dave Murray



Dr. Andy Shaw



Dr. James Young



Dr. Chris Cheeseman
(External examiner)



Dr. Fiona Parkinson
(External examiner)

Thesis approval date: Feb 3, 2003

This thesis is dedicated to my loving family, my father, Khanh, my mother, Lily,
my three sisters, Anh, Donna and Mai.

Abstract

Human cells possess multiple nucleoside transporters with overlapping substrate selectivities that belong to either the equilibrative (ENT) or concentrative (CNT) nucleoside transporter family. CNT-mediated activities have been observed in intestine and brain where they are hypothesized to function in nucleoside and nucleoside drug absorption and adenosine signaling, respectively.

Analysis of various normal and neoplastic human cell lines failed to identify any lines that exhibited a single human (h) CNT in isolation. A nucleoside transport-deficient mutant line, derived from a human lymphoblastoid cell line, was used to generate stable transfectants that possessed a single type of human nucleoside transporter. These transfectants were used to study the role of hCNT family members in drug interaction and drug sensitivity.

Structure-activity studies of hCNT1 and hCNT2 revealed important features for permeant recognition. These transporters exhibited differences in their affinities for caffeine, nicotine and adenosine receptor ligands.

While hCNT2 transported purine nucleosides and deoxynucleosides with high activity, it also accepted halogenated uridine analogs. hCNT1 interacted with several adenosine analogs. The degree of sensitivity of hCNT2 stable transfectants to uridine and adenosine analog drugs (5-fluorouridine, floxidine and cladribine, fludarabine, respectively) was reflected in their affinities and patterns of transport activity by hCNT2.

Generation of antibodies against hCNT2 enabled localization of recombinant hCNT2 to plasma membranes of stably transfected cells. Localization studies with anti-hCNT3 antibodies in polarized Caco-2 intestinal epithelial cells showed trafficking of native hCNT3 from intracellular sites to plasma membranes during Caco-2 differentiation. Increased hCNT3 at plasma membranes was associated with increased hCNT3 activity at apical membranes. Higher levels of hCNT3 were also observed in regions of small intestine than large intestine.

The distribution of hCNT2, hCNT3 and adenosine receptors in human brain was assessed by quantitative immunoblot analysis using the Typhoon Imager. Levels of adenosine A₁ receptors were positively correlated with the levels of hCNT2. This suggested a possible relationship between hCNT2 and sites of adenosine action.

While these studies show that CNTs are involved in drug interaction and adenosine-mediated signaling, they also raise greater awareness of the potential for regulation of hCNT3 in differentiated intestinal cells.

Acknowledgements

This thesis was completed with the support of numerous people and they have my thanks and gratitude. I would like to thank my supervisor, Dr. Carol Cass, for taking me on and allowing me to undertake a variety of projects during the course of my studies. She is a role model and a great teacher. I am grateful for all her support, encouragement and help in scientific writing. I could not have asked for a better supervisor.

The staff and students in Carol's laboratory are a wonderful group of people and they are like a second family to me. I would like to thank each and every one of them from the bottom of my heart for making my scientific experience a great one. I would particularly like to thank: Ms. Geraldine Baron, Dr. Miguel Cabrita, Ms. Pat Carpenter, Dr. Marilyn Clarke, Dr. Imogen Coe, Dr. Vijaya Damaraju, Dr. Allan Doucette, Mr. Adam Elwi, Dr. Kathryn Graham, Dr. Lori Jennings, Dr. Karen King, Ms. Jackie Leithoff, Dr. Rajam Mani, Dr. Jihan Marjan, Ms. Delores Mowles, Mr. Pete Panayides, Ms. Cheryl Santos, Ms. Milada Selner, Dr. Elizabeth Silver, Ms. Michelle Seth-Smith, Mr. Frank Visser, Dr. Clarence Wong, Ms. Jing Zhang and Ms. Lily Zombar.

I would like to thank our collaborators: Drs. Steve Baldwin, Charlie Hao, John Mackey, Michael Sawyer and Jim Young for their expert advice and provisions of clinical samples; the vivarium staff (Dan and Gail) for the maintenance of animals; Dr. Xie-Jun Sun for his assistance with confocal microscopy.

I would like to thank the staff and students in the Department of Oncology for their friendship and sharing of many laughs. I would particularly like to thank the staff in Dr. Carol Cass's office (Cheryl, Cynthia, Jennifer and Lori) and the medical librarian, Linda, for all their assistance over the years. I would also like to thank: Drs. Roseline Godbout, Michael Hendzel, Judith Hugh, Linda Pilarski, Charlette Spencer, Joan Turner and Michael Weinfeld for all the scientific discussions. It was a pleasure interacting with them.

My gratitude to members of my supervisory committee (Drs. Dave Murray, Andy Shaw, Jim Young) and members of my examining committee (Drs. Chris Cheeseman and Fiona Parkinson) for taking the time to read my thesis so thoroughly and providing useful suggestions and discussions.

I appreciate the interactions with members of the CIHR (formerly MRC) Molecular Biology of Membrane Group and I thank them for providing wonderful opportunities to develop skills in giving scientific presentations. The Oncology 660 seminar series (Thursday noon) also provided a great atmosphere for scientific interactions, and I have presented at these forums on several occasions and I appreciate everyone's keen interests and suggestions.

My final thanks extend to my immediate family and friends for their love and support. They have seen me through good and bad times, and have shown me tremendous patience. My parents, Khanh and Lily (Thuan), my sisters (Anh, Donna and Mai) have always been there for me and provided me with the opportunity to pursue my dreams. I am grateful to my friends: Andy, Eric, Fabio,

Mike, Nam, Jason, Kevin, Sharon, Sheri and Tanya for all their kindness and understanding over the years.

Table of Contents

Chapters	Page
I. Introduction	1
I.1. Nucleoside transporters: a brief overview of their significance	2
I.2. Importance of physiological nucleosides	3
I.2.1. Purine nucleosides	4
I.2.2. Pyrimidine nucleosides	6
I.3. Nucleoside analogs	7
I.3.1. Anticancer nucleosides	9
I.3.2. Antiviral nucleosides	10
I.4. Intracellular metabolism of nucleosides and nucleoside analogs	12
I.5. Multiplicity of nucleoside transport processes in cells	13
I.5.1. Equilibrative nucleoside transport processes	14
I.5.2. Concentrative nucleoside transport processes	15
I.6. The superfamily of nucleoside transport proteins	16
I.6.1. Equilibrative nucleoside transporter (ENT) family	18
I.6.1.1. Distribution of ENTs in cells and tissues	21
I.6.2. Concentrative nucleoside transporter (CNT) family	23
I.6.2.1. hCNT1	24
I.6.2.2. hCNT2	25
I.6.2.3. hCNT3	26
I.6.2.4. Distribution of CNT mRNAs in mammalian cells and tissues	28

I.6.2.5.	Location of sodium-dependent nucleoside transport processes in cells and tissues	29
I.6.2.6.	Location of CNT proteins in cells and tissues.....	30
I.7.	Regulation of nucleoside transporters	31
I.8.	Goals of the present work.....	32
I.9.	Rationale.....	33
I.10.	Nucleoside-transport deficient human cells	34
I.11.	Approach	35
II.	Materials and Methods	52
II.1.	Materials	53
II.2.	General molecular biology procedures	54
II.2.1.	DNA primers and DNA sequencing	55
II.3.	Plasmid construction.....	55
II.3.1.	pcDNA3/LacZ	55
II.3.2.	pcDNA3/hCNT1	55
II.3.3.	pcDNA3/hCNT2	56
II.3.4.	pGFP-C1/hCNT3	57
II.3.5.	pcDNA3/hCNT3.....	57
II.4.	Southern blot analysis	58
II.5.	RNA preparation and northern blot analysis	58
II.6.	Reverse transcription-polymerase chain reaction (RT-PCR) analysis ..	59
II.7.	Taqman real-time quantitative RT-PCR.....	60
II.8.	SDS-polyacrylamide gel electrophoresis and immunoblotting	62

II.9.	Protein quantitation.....	63
II.10.	Growth and maintenance of cell lines	64
II.10.1.	Suspension cell lines	65
II.10.2.	Adherent cell lines.....	66
II.10.3.	Trypan blue dye exclusion	67
II.10.4.	Cloning cells by limiting dilution	68
II.11.	Transient transfections.....	68
II.11.1.	DEAE-dextran transfection.....	68
II.12.	Stable transfection and selection of transfectants in Chapter III	69
II.12.1.	Electroporation and selection in geneticin.....	69
II.12.2.	Cloning of Stable Transfectants in Semi-Solid Medium.....	70
II.13.	Assessment of transfection efficiencies	71
II.13.1.	In situ β -galactosidase staining	71
II.13.2.	Semi-quantitative β -galactosidase activity assay	71
II.14.	Transepithelial electrical resistance measurements.....	72
II.15.	Nucleoside transport assays with suspension cells.....	73
II.16.	Nucleoside uptake assays with adherent cells	74
II.17.	Preparation of membranes from cells	75
II.17.1.	Membranes from yeast	75
II.17.2.	Membranes from tissue culture cells.....	76
II.17.3.	Membranes from tissues of the human brain.....	77
II.17.4.	Membranes from tissues of the gastrointestinal tract.....	78
II.17.5.	Membranes from human red blood cells.....	80

II.18.	Generation of anti-peptide antibodies	81
II.19.	Testing of antibody production by enzyme-linked immunadsorbant assay (ELISA).....	82
II.20.	Immunization protocols	82
II.20.1.	Production of polyclonal antibodies in rabbits	83
II.20.2.	Production of monoclonal antibodies in mice.....	84
II.21.	Immunoaffinity purification of polyclonal and monoclonal antibodies	85
II.21.1.	Enrichment of polyclonal antibodies.....	86
II.21.2.	Enrichment of immunoglobulins by protein G affinity chromatography.....	86
II.22.	Indirect immunofluorescence confocal microscopy.....	87
 III. Characterization of Endogenous Nucleoside Transporters Present in Human Cell Lines and Generation of Transient and Stable Transfectants..94		
III.1.	Introduction.....	95
III.2.	Results.....	99
III.2.1.	Molecular characterization of cultured human cells derived from different tissue origins	99
III.2.1.1.	Analysis of hENT1 and hENT2 mRNAs in various human cell lines	99
III.2.1.2.	Analysis of hCNT1 and hCNT2 mRNAs in various human cell lines	100
III.2.1.3.	RT-PCR and Taqman RT-PCR analyses of nucleoside transporter mRNAs in Caco-2 and HeLa cells.....	101

III.2.2.	Functional characterization of nucleoside transporters present in HeLa cells	104
III.2.3.	Production and characterization of transient transfectants in HeLa cells	106
III.2.3.1.	Analysis of DEAE-dextran toxicity to HeLa cells.....	107
III.2.3.2.	Optimization of DEAE-dextran transfection conditions and assessment of transfection efficiency by in situ cytochemical staining of transfected HeLa cells.....	107
III.2.3.3.	HeLa cells transiently transfected with hCNT1 cDNA: characterization of hCNT1-mediated uridine transport activity.....	109
III.2.3.4.	Stability of nucleoside transport activity of HeLa cells transiently transfected with hCNT1 cDNA over time	110
III.2.3.5.	HeLa cells transiently transfected with hCNT2 cDNA: characterization of hCNT2 protein production and functional activity.....	111
III.2.4.	Characterization of CEM and CEM-ARAC cells: demonstration of hENT1 in CEM cells and its absence in CEM-ARAC cells.....	112
III.2.5.	Presence of hENT1 mRNA in CEM, but not in CEM-ARAC cells	113
III.2.6.	Analysis of nucleoside transport activities in CEM and CEM-ARAC cells	113
III.2.7.	Demonstration of endogenous hENT1 in CEM, but not in CEM-ARAC, cells by immunoblot analysis.....	114
III.2.8.	Production and isolation of stable transfectants of CEM-ARAC cells	116

III.2.8.1.	Optimization of transfection conditions for electroporation...	116
III.2.8.2.	Determination of appropriate exposure concentration of geneticin for selection of CEM-ARAC stable transfectants	120
III.2.8.3.	Production of hCNT2 stable transfectants of CEM-ARAC cells	121
III.2.8.4.	Integration of hCNT2 cDNA into the genome of ARAC/D2 cells	122
III.2.8.5.	Detection of hCNT2 mRNA in ARAC/D2 cells but not in CEM or CEM-ARAC cells.....	123
III.2.8.6.	Stability of the nucleoside-transport phenotype in ARAC/D2 cells	124
III.2.8.7.	Transport characteristics of ARAC/D2 cells: Na ⁺ -dependency and cif-type activity.....	124
III.2.8.8.	Production of hCNT1 stable transfectants of CEM-ARAC cells	125
III.2.8.9.	Production of hENT2 stable transfectants of CEM-ARAC cells..	127
III.2.9.	Comparison of the nucleoside transport activity by T- lymphoblastoid cell lines producing hCNT2, hCNT1, hENT2, and hENT1 in isolation	129
III.3.	Discussion	130
IV.	Structure-Activity and Structure-Cytotoxicity Studies of hCNT1 and hCNT2 in TLCT1 and ARAC/D2 Stable Transfectants	176

IV.1.	Introduction	177
IV.2.	Results	180
IV.2.1.	Analysis of the nucleoside structural determinants for interaction with hCNT2 in ARAC/D2 cells.....	180
IV.2.2.	Structure-activity relationships of hCNT2: inhibition of uridine uptake by purine and pyrimidine nucleosides and by nucleobases	180
IV.2.3.	Kinetics of uridine uptake and interactions of halogenated-uridine analogs with hCNT2.....	183
IV.2.4.	Transport characteristics of ARAC/D2 cells: hCNT2-mediated transport of physiological and modified nucleosides.....	185
IV.2.5.	Transport of 5-fluorouridine by hCNT2	186
IV.2.6.	Analysis of the chemosensitivity of cytotoxic nucleoside drugs in ARAC/D2, CEM and CEM-ARAC cells	187
IV.2.7.	Enhanced sensitivity to purine and pyrimidine nucleoside drugs in hCNT2-producing ARAC/D2 cells	188
IV.2.8.	Comparative studies of hCNT1 and hCNT2 in TLCT1 and ARAC/D2 stable transfectants: transporter interactions with analogs of uridine and adenosine	190
IV.2.8.1.	Kinetics of uridine transport by hCNT1 in TLCT1 cells.....	190
IV.2.8.2.	Comparison of the inhibitory activities of uridine analogs on uridine uptake by hCNT1 and hCNT2 in stable transfectants	191
IV.2.8.3.	Inhibition of ³ H-uridine transport into TLCT1 and ARAC/D2 cells by L-adenosine, but not by L-uridine	192

IV.2.8.4. Comparison of the inhibitory activities of adenosine analogs on uridine uptake by hCNT1 and hCNT2 in stable transfectants	193
IV.2.8.5. Concentration-effect relationships of adenosine analogs and nicotine for inhibition of ³ H-uridine transport into TLCT1 and ARAC/D2 cells	195
IV.2.8.6. Comparison of the inhibitory constants of adenosine analogs and nicotine in TLCT1 and ARAC/D2 cells	196
IV.2.8.7. Assessment of transportability of natural and therapeutic nucleosides by hCNT1 and hCNT2 in TLCT1 and ARAC/D2 cells	197
IV.3. Discussion.....	200
IV.3.1. Analysis of the molecular determinants for interaction with hCNT2 and correlation of drug transport with in vitro sensitivity.....	200
IV.3.2. Comparative studies of hCNT1 and hCNT2 in TLCT1 and ARAC/D2 stable transfectants: transporter interactions with analogs of uridine, adenosine and adenine and with nicotine	204
IV.3.3. Conclusion.....	208
Chapter V.....	231
V. Production and Characterization of Antibodies Against hCNT2 and hCNT3	231
V.1. Introduction.....	232
V.2. Results.....	235
V.2.1. Generation of anti-hCNT2 antibodies.....	235

V.2.1.1.	Choosing appropriate peptide sequences of hCNT2 for raising anti-peptide antibodies	235
V.2.1.2.	Characterization of anti-hCNT2 antibodies.....	236
V.2.1.3.	Assessment of anti-hCNT2 peptide antibody production by ELISA	237
V.2.1.4.	Demonstration of specificity of anti-hCNT2 peptide antibodies by immunoblot analysis	237
V.2.1.5.	Demonstration of anti-hCNT2 antibody reactivity with hCNT2 in ARAC/D2 cells by immunofluorescence.....	239
V.2.2.	Generation of anti-hCNT3 antibodies	240
V.2.2.1.	Choosing appropriate peptide sequence of hCNT3 for raising anti-peptide antibodies	240
V.2.2.2.	Characterization of anti-hCNT3 antibodies.....	241
V.2.2.3.	Demonstration of specificity of anti-hCNT3 antibodies by immunoblot analysis.....	242
V.2.2.4.	Production of hCNT3 and hCNT3 tagged with green fluorescent protein (GFP) in HeLa cells	243
V.2.2.5.	Detection of recombinant hCNT3 in HeLa cells transiently transfected with hCNT3 cDNA	245
V.2.2.6.	Detection of hCNT3 in transiently transfected HeLa cells by immunofluorescence with anti-hCNT3 antibodies	245
V.2.2.7.	Detection of hCNT3-GFP staining in HeLa cells transiently transfected with pGFP-C1/hCNT3 by immunofluorescence analysis.....	246

V.3. Discussion	248
VI. Localization of Recombinant hCNT2 in Stably Transfected Cells and Alterations in Distribution of Native hCNT3 in Caco-2 Cells	275
VI.1. Introduction	276
VI.2. Results	281
VI.2.1. Localization of recombinant hCNT2 in stably transfected human T- lymphoblastoid cells	281
VI.2.2. Localization of hCNT3 during Caco-2 cellular differentiation	283
VI.2.2.1. Functional characterization of nucleoside transporters present in Caco-2 cells	283
VI.2.2.1.1 Demonstration of hENT1-, hENT2- and hCNT3-mediated uptake into Caco-2 cells.	284
VI.2.2.2. Growth properties and differentiation of Caco-2 cells	285
VI.2.2.2.1 Growth characteristics of Caco-2 cells	286
VI.2.2.2.2 Transepithelial electrical resistance (TEER): assessment of differentiation status in Caco-2 cells	286
VI.2.2.3. Localization of endogenous hCNT3 at different times during Caco-2 differentiation	287
VI.2.2.4. Abundance of hCNT3 in plasma membranes at different times during Caco-2 differentiation	290
VI.2.2.5. Stimulation of hCNT3-mediated uridine transport activities detected at the apical membrane of Caco-2 cells over time in culture ...	291

VI.2.3. Relative abundance of hCNT3 protein in the gastrointestinal tract....	292
VI.3. Discussion.....	293
VII. Distribution and Localization of CNT Proteins in Human Brain and Vascular Endothelial Cells: Relationship Between Their Location and Site of Adenosine Action	316
VII.1. Introduction	317
VII.2. RESULTS.....	321
VII.2.1. Distribution of hCNT2, hCNT3 and adenosine A1 receptors within the major divisions of the human brain	321
VII.2.2. Correlation of hCNT2 and hCNT3 protein abundance with adenosine A ₁ receptor	322
VII.2.3. Demonstration of hCNT2 and hCNT3 in human endothelial cells by immunoblot analysis.....	324
VII.2.4. Localization of hCNT2 and hCNT3 to plasma membranes of HUVEC by immunofluorescence confocal microscopy	325
VII.3. Discussion.....	328
VIII. General Conclusions and Discussion	347
VIII.1. Characterization of endogenous nucleoside transporters present in cultured human cell lines	348
VIII.2. Generation of transfectants for assessing nucleoside analog interactions with hCNTs.....	350

VIII.3.	Correlation of nucleoside drug transport capabilities with <i>in vitro</i> drug sensitivities	353
VIII.4.	Production of antibodies against CNT proteins	355
VIII.5.	Subcellular location of recombinant hCNT2 and regulation of hCNT3 distribution and abundance during intestinal cell differentiation	356
VIII.6.	Relationships between the distribution and location of CNTs and sites of adenosine action	358
IX.	Bibliography.....	361

List of Tables

Table I-1. Mediated transport of clinically relevant nucleoside drugs by mammalian concentrative and equilibrative transport processes and proteins	37
Table I-2. Nucleoside transport processes and their corresponding proteins in human cells.....	38
Table I-3. Tissue and cellular distribution of concentrative and equilibrative nucleoside transporters in mammals	39
Table II-1. TaqMan primers and probes used in Chapter III	90
Table II-2. Description of cell lines and their properties used in this thesis.....	91
Table III-1. Comparison of the relative expression levels of nucleoside transporter mRNAs in HeLa cells by quantitative Taqman RT-PCR.....	137
Table III-2. Summary of northern and RT-PCR analyses of mRNA expression in various human cell lines.....	138
Table III-3. Transfection efficiencies assessed by <i>in situ</i> β -galactosidase staining of HeLa cells transfected with different concentrations of plasmid and DEAE-dextran	139
Table III-4. Uptake of ^3H -uridine by representative geneticin-resistant clones of CEM-ARAC cells.....	140
Table IV-1. Inhibition of uridine uptake by hCNT2 in ARAC/D2 cells by ribonucleosides, arabinonucleosides and nucleobases: identification of candidate permeants and inhibitors of hCNT2.....	210

Table IV-2. Inhibitor constants (K_i values) for inhibition of uridine transport by hCNT2 in ARAC/D2 cells	212
Table IV-3. Comparison of Michaelis-Menten constants for the transport of uridine and 5-fluorouridine by hCNT2 in ARAC/D2 and hENT1 in CEM cells	213
Table IV-4. Effects of continuous exposures to cytotoxic nucleoside drugs and doxorubicin on proliferation rates of CEM, CEM-ARAC and ARAC/D2 cells	214
Table IV-5. K_i values for inhibition of uridine transport by hCNT1 in TLCT1 and hCNT2 in ARAC/D2 cells by analogs of uridine	215
Table IV-6. Inhibitory activities of adenine and adenosine analogs and nicotine on uridine transport by hCNT1 in TLCT1 and hCNT2 in ARAC/D2 cells ...	216
Table IV-7. K_i values for inhibition of uridine transport by hCNT1 in TLCT1 and hCNT2 in ARAC/D2 cells by analogs of adenine and adenosine	217
Table IV-8. Comparison of the levels of nucleoside and drug transport by hCNT1 and hCNT2 in TLCT1 and ARAC/D2 cells.....	218

List of Figures

Figure I-1. Main structural modifications to transform a natural nucleoside into a nucleoside analog	40
Figure I-2. Chemical structures of uridine and several fluorinated-uridine analogs (5-fluorouridine, 5-fluoro-2'-deoxyuridine and 5-fluoro-5'-deoxyuridine) used in gastrointestinal cancers	41
Figure I-3. Chemical structures of the natural nucleoside adenosine and its analogs cladribine and fludarabine employed in treatment of different types of human leukemia	42
Figure I-4. Chemical structures of guanosine and arabinonucleosides used in the treatment of leukemias and viral diseases.....	43
Figure I-5. Chemical structures of thymidine and its analogs used in treatment of human immunodeficiency virus (HIV)	44
Figure I-6. Chemical structures of 2-deoxycytidine and its analogs used in treatment of human immunodeficiency virus (HIV).....	45
Figure I-7. Chemical structures of inosine and its analog 2',3'-dideoxyinosine used in treatment of human immunodeficiency virus (HIV)	46
Figure I-8. Nucleoside permeation into human cells via different routes.....	47
Figure I-9. Structural characteristics of CNTs and ENTs	48
Figure I-10. Relationships among functionally characterized members of the vertebrate concentrative nucleoside transporter family.....	49
Figure I-11. Predicted topological model of hCNT2	50

Figure I-12. Proposed topological model of hCNT3 indicating the major landmarks	51
Figure II-1. Information on the mammalian expression plasmid pcDNA3 utilized in this thesis	92
Figure II-2. Information on the plasmid used to generate GFP fusion proteins..	93
Figure III-1. Analysis of hENT1 mRNA expression in human cell lines by northern blot analysis.....	141
Figure III-2. Analysis of hENT2 mRNA expression in human cell lines by northern blot analysis.....	142
Figure III-3. Analysis of hCNT1 mRNA expression in human cell lines by northern blot analysis.....	143
Figure III-4. Analysis of hCNT2 mRNA expression in human cell lines by northern blot analysis.....	144
Figure III-5. RT-PCR analysis of nucleoside transporter mRNAs in Caco-2 cells	145
Figure III-6. Cycle time plot for real time Taqman RT-PCR analysis in HeLa cells	146
Figure III-7. Inhibitory effects of NBMPR or dilazep on uridine uptake by HeLa cells.....	147
Figure III-8. Analysis of DEAE-dextran toxicity to HeLa cells	148
Figure III-9. A representative bright field image of <i>in situ</i> staining for β -galactosidase activity in HeLa cells.....	149

Figure III-10. Long time courses of uridine uptake by HeLa cells transiently transfected with hCNT1 cDNA	150
Figure III-11. Short-time courses of uridine uptake by HeLa cells transiently transfected with hCNT1 cDNA	151
Figure III-12. Analysis of nucleoside transport activities in HeLa cells transiently transfected with hCNT1 cDNA at various times after transfection	152
Figure III-13. Time course of uridine uptake by HeLa cells transiently transfected with hCNT2 cDNA	153
Figure III-14. RT-PCR analysis for the presence of hENT1 mRNA in CEM and CEM-ARAC cells.....	154
Figure III-15. Comparison of uridine uptake by CEM and CEM-ARAC cells over short and long time periods.....	155
Figure III-16. Immunoblot analysis demonstrating hENT1 in CEM cells, but not in CEM-ARAC cells.....	156
Figure III-17. Amino acid sequence alignment of hENT1 and mENT1	157
Figure III-18. Determination of viability of CEM-ARAC cells for electroporation using constant capacitance of 25 μ F and graded changes in voltage strength	158
Figure III-19. The effects of DNA concentration on the transfection efficiency of CEM-ARAC cells electroporated at 25 μ F and 1000 V	159
Figure III-20. Determination of viability of CEM-ARAC cells for electroporation using constant capacitance of 3 μ F and graded changes to voltage strength	160

Figure III-21. The effect of DNA concentration on transfection efficiency of CEM-ARAC cells electroporated at 3 μ F and 1400 V	161
Figure III-22. Determination of viability of CEM-ARAC cells for electroporation using constant capacitance of 960 μ F and graded changes to voltage strength.....	162
Figure III-23. The effect of DNA concentration on transfection efficiency of CEM-ARAC cells electroporated using optimized electroporation conditions of 960 μ F and 190 V	163
Figure III-24. The growth-inhibitory effects of geneticin on CEM-ARAC cells ..	164
Figure III-25. Genomic integration of hCNT2 cDNA into ARAC/D2 cells	165
Figure III-26. Expression of hCNT2 mRNA in ARAC/D2 cells, but not in CEM or CEM-ARAC cells.....	166
Figure III-27. Nested RT-PCR demonstrating hCNT2 mRNA in ARAC/D2 cells, but not in CEM or CEM-ARAC cells.....	167
Figure III-28. Stability of hCNT2-mediated uridine transport activity in ARAC/D2 cells over 25 generations	168
Figure III-29. Demonstration of sodium-dependent, hCNT2-mediated uptake by ARAC/D2 stable transfectants	169
Figure III-30. Effects of natural nucleosides and dilazep on uridine influx into ARAC/D2 stable transfectants	170
Figure III-31. Sodium-dependent, carrier-mediated uptake by TLCT1 stable transfectants	171

Figure III-32. Demonstration of <i>cit</i> -type activity by TLCT1 stable transfectants	172
Figure III-33. Time course of uridine uptake by TLET2 stable transfectants....	173
Figure III-34. Demonstration of <i>ei</i> -type activity by TLET2 stable transfectants	174
Figure III-35. Comparison of uridine transport activity in T-lymphoblastoid cell lines producing either hCNT2, hCNT1, hENT2 or hENT1.....	175
Figure IV-1. Effects of nucleoside analogs on uridine uptake by hCNT2 in ARAC/D2 cells	219
Figure IV-2. Kinetic analysis of uridine transport mediated by hCNT2 in ARAC/D2 cells	220
Figure IV-3. The concentration dependence of hCNT2-mediated uridine transport into ARAC/D2 cells by fluorinated uridine analogs	221
Figure IV-4. Transport of purine and pyrimidine nucleosides by hCNT2 in ARAC/D2 cells	222
Figure IV-5. Chemical structures of capecitabine and 5-fluoro-5'-deoxyuridine	223
Figure IV-6. Antiproliferative activities of 5-fluorouridine, 5-fluoro-2'-deoxyuridine and 5-fluoro-5'-deoxyuridine on ARAC/D2 cells.....	224
Figure IV-7. Kinetic analysis of uridine transport mediated by hCNT1 in TLCT1 cells.....	225
Figure IV-8. Concentration dependent inhibition of uridine transport by 5-fluoro- 5'-deoxyuridine in hCNT1- and hCNT2-producing stable transfectants.....	226

Figure IV-9. Effects of L-uridine and L-adenosine on uridine influx into hCNT1-containing TLCT1 and hCNT2-containing ARAC/D2 cells	227
Figure IV-10. Inhibition of uridine transport by N ⁶ -(p-aminobenzyl)adenosine and 5'-deoxyadenosine in hCNT1-containing TLCT1 and hCNT2-containing ARAC/D2 cells	228
Figure IV-11. Structural similarities between caffeine and adenosine.....	229
Figure IV-12. Inhibition of uridine transport by caffeine and nicotine in hCNT1-containing TLCT1 and hCNT2-containing ARAC/D2 cells	230
Figure V-1. Hydrophilicity plot of hCNT2 protein sequence identifying hydrophilic regions	252
Figure V-2. Hydropathy plot of the chosen polypeptide TL3273 of hCNT2.....	253
Figure V-3. Topological prediction of hCNT2	254
Figure V-4. Amino acid sequence alignment of polypeptides TL3273, CNT2, CNT1 and CNT3	255
Figure V-5. Monitoring anti-hCNT2 peptide antibody production in rabbits by ELISA.....	256
Figure V-6. Monitoring anti-hCNT2 peptide antibody production in mice by ELISA.....	257
Figure V-7. Immunoreactivity of anti-hCNT2 antibodies against recombinant hCNT2 produced in yeast and ARAC/D2 stable transfectant	258
Figure V-8. Detection of recombinant hCNT2 in HeLa cells transiently transfected with hCNT2 cDNA by immunoblot analysis.....	260

Figure V-9. Anti-hCNT2 antibodies primarily stain plasma membranes of hCNT2 stably transfected ARAC/D2 cells but not of transporter-deficient CEM-ARAC cells.....	261
Figure V-10. Plasma membrane labeling of hCNT2 stably transfected ARAC/D2 cells in the presence, but not in the absence, of anti-hCNT2 antibodies ...	262
Figure V-11. Hydropathy plot of the chosen polypeptide TL3360 of hCNT3....	263
Figure V-12. Topological prediction of hCNT3 orientation in the membrane ...	264
Figure V-13. Amino acid sequence alignment of polypeptides TL3360, hCNT3, hCNT2 and hCNT1	265
Figure V-14. Hydropathy plot of the chosen polypeptide TL3361 of hCNT3....	266
Figure V-15. Amino acid sequence alignment of polypeptides TL3361, hCNT3, hCNT2 and hCNT1	267
Figure V-16. Immunoreactivity of anti-hCNT3 antibodies against recombinant hCNT3 produced in yeast	268
Figure V-17. Uridine transport activities in HeLa cells transiently transfected with untagged or GFP-tagged hCNT3 cDNA.....	270
Figure V-18. Detection of recombinant hCNT3 in HeLa cells transiently transfected with hCNT3 cDNA by immunoblot analysis.....	271
Figure V-19. Detection of hCNT3 in pcDNA3/hCNT3 transiently transfected HeLa cells by immunofluorescence analysis with anti-hCNT3 antibodies .	272
Figure V-20. Immunofluorescence analysis of pcDNA3 transiently transfected HeLa cells with anti-hCNT3 antibodies	273

Figure V-21. Detection of hCNT3 in pGFP-C1/hCNT3 transiently transfected HeLa cells by immunofluorescence analysis	274
Figure VI-1. Anti-hCNT2 antibodies with reactivity of plasma membranes of hCNT2-producing ARAC/D2 cells but not transporter-deficient CEM-ARAC cells.....	299
Figure VI-2. Localization of hCNT2 to the cell surface above the actin cytoskeleton in hCNT2-producing ARAC/D2 cells	300
Figure VI-3. Colocalization of hCNT2 staining with the T-cell specific CD3 cell surface marker.....	301
Figure VI-4. The absence of immunostaining of hCNT2 in transporter-deficient CEM-ARAC cells.....	302
Figure VI-5. Time course of uridine uptake by Caco-2 cells in the presence and absence of sodium.....	303
Figure VI-6. Inhibitory effects of dilazep and NBMPR on uridine uptake by Caco-2 cells.....	304
Figure VI-7. Growth curve of Caco-2 cells	305
Figure VI-8. Transepithelial electrical resistance (TEER) values of Caco-2 cell monolayers cultured on collagen-coated polycarbonate inserts	306
Figure VI-9. Absence of immunofluorescent signal in Caco-2 cells stained with secondary antibodies alone	307
Figure VI-10. Localization of hCNT3 to the endoplasmic reticulum in day 4 Caco-2 cell cultures	308

Figure VI-11. Reduced colocalization of hCNT3 with endoplasmic reticulum marker in day 11 Caco-2 cell cultures.....	309
Figure VI-12. Cell surface localization of hCNT3 in day 15 Caco-2 cell cultures	311
Figure VI-13. Predominant cell surface localization of hCNT3 in day 18 Caco-2 cell cultures.....	312
Figure VI-14. Immunoblot analysis of hCNT3 production in membrane preparations from Caco-2 cells after 4, 11, and 18 days in culture.....	313
Figure VI-15. Sodium-dependent uridine transport activities in Caco-2 cultures after 4, 11, and 18 days.....	314
Figure VI-16. Immunoblot analysis of well-differentiated Caco-2 cells and biopsies of human tissues from different regions of gastrointestinal tract .	315
Figure VII-1. Differential distribution and abundance of hCNT2 and hCNT3 within the major divisions of the human brain	335
Figure VII-2. Immunodetection of adenosine A1 receptors within the major divisions of the human brain	336
Figure VII-3. Quantitation of the relative abundance of hCNT2 in the major divisions of the human brain	337
Figure VII-4. Quantitation of the relative abundance of hCNT3 in the major divisions of the human brain	338
Figure VII-5. Quantitation of the relative abundance of adenosine A1 receptors in the major divisions of the human brain	339

Figure VII-6. Comparison of the abundance of hCNT2 and adenosine A1 receptors in human brain	340
Figure VII-7. Comparison of the abundance of hCNT3 and adenosine A1 receptors in human brain	341
Figure VII-8. Demonstration of hCNT2 and hCNT3 in human umbilical vein endothelial cells (HUVEC)	342
Figure VII-9. Localization of hCNT2 to cell surfaces of human umbilical vein endothelial cells (HUVEC)	343
Figure VII-10. Profile of colocalized immunofluorescent signals from anti-hCNT2 polyclonal and monoclonal antibody staining of HUVEC	344
Figure VII-11. Localization of hCNT3 to cell surfaces of human umbilical vein endothelial cells (HUVEC)	345
Figure VII-12. Profile of colocalized immunofluorescent signals from anti-hCNT3 polyclonal and monoclonal antibody staining of HUVEC	346

List of Abbreviations, Symbols and Nomenclature

A ₆₀₀	absorbance at 600 nm
AIDS	acquired immunodeficiency syndrome
araA	9-β-D-arabinofuranosyladenine
araC	1-β-D-arabinofuranosylcytosine
araG	9-β-D-arabinofuranosylguanine
BCA	bicinchoninic acid
BeWo	human choriocarcinoma cell line
BSA	bovine serum albumin
bp	base pair (s)
CNT	concentrative nucleoside transporter
CSF	cerebralspinal fluid
AZT	3'-deoxy-3'-azidothymidine
3TC	(-)-2',3'-dideoxy-3'-thiacytidine
ddC	2',3'-dideoxycytidine
dCK	deoxycytidine kinase
dGK	deoxyguanosine kinase
d4T	2',3'-didehydro-3'-deoxythymidine
ddl	2',3'-dideoxyinosine
DNA	deoxyribonucleic acid
cDNA	complementary DNA
Ct	cycle threshold

<i>cib</i>	concentrative, insensitive to NBMPR, broadly selective
<i>cif</i>	concentrative, insensitive to NBMPR, formycin B is permeant
<i>cit</i>	concentrative, insensitive to NBMPR, thymidine is permeant
cs	concentrative, sensitive to NBMPR
csg	concentrative, sensitive to NBMPR, guanosine is permeant
CdA	2-chloro-2'-deoxyadenosine
CCRF-CEM	human T-lymphoblastic leukemia cell line
CD	cluster differentiation
CNS	central nervous system
CNT	concentrative nucleoside transporter
CPM	counts per minute
Cy5	indodicarbocyanine
DAPI	4',6-diamidino-2-phenylindole
DMEM	Dulbecco's modified Eagle's medium
DMSO	dimethyl sulfoxide
DTT	dithiothreitol
dNTP	deoxyribonucleotide triphosphate
ECL	enhanced chemiluminescence
ENT	equilibrative nucleoside transporter

EDTA	ethylenediaminetetraacetic acid
<i>ei</i>	equilibrative, insensitive to NBMPR
<i>es</i>	equilibrative, sensitive to NBMPR
ELISA	enzyme-linked immunosorbent assay
F-araA	9- β -D-arabinofuranosyl-2-fluoroadenine
FBS	fetal bovine serum
FITC	fluoroisothiocyanin
GAPDH	glyceraldehyde phosphate dehydrogenase
HAT	hypoxanthine aminopterin thymidine selection medium
HEK	human embryonic kidney
HUVEC	human umbilical vein endothelial cells
HEPES	N-2-hydroxyethylpiperzine-N'-2-ethane sulfonic acid
HI	heat-inactivated
HS	horse serum
HEK	human embryonic kidney
HeLa	human cervical cancer cell line
hSPNT1	human sodium-dependent purine nucleoside selective transporter 1, also known as hCNT1
HRP	horseradish peroxidase
hr	hour (s)
h	human

IC ₅₀	concentration that reduced uptake by 50%
KLH	keyhole limpet hemocyanin
kb	kilobase (s)
kDa	kilodalton (s)
mRNA	messenger RNA
MNNG	N-methyl-N-nitroso-N'-nitroguanidine
M	molar
mol	mole
NMDG	N-methyl-D-glucammonium
μF	microfaraday
μg	microgram
μM	micromolar
μl	microlitre
mA	milliampere (s)
mg	milligram
ml	millilitre
mM	millimolar
min	minutes (s)
ng	nanogram
NBMPR	nitrobenzylmercaptapurine ribonucleoside (6- [(4-nitrobenzyl)thiol]-9-β-D-riboouranosyl purine)
OD	optical density
PMA	phorbol 12-myristate 13-acetate

PMSF	phenylmethanesulfonyl fluoride
PBS	phosphate-buffered saline
PBST	PBS containing Tween 20
PAGE	polyacrylamide gel electrophoresis
PCR	polymerase chain reaction
PVDF	polyvinylidene fluoride
pmol	picomole
r	rat
RBC	red blood cell
RNA	ribonucleic acid
RPMI	Roswell Park Memorial Institute
sec	second (s)
Na ⁺	sodium
SDS	sodium dodecyl sulfate
SD	standard deviation
TEER	transepithelial electrical resistance
Tris	tris(hydroxymethyl)aminomethane
TPBS	Tween-20, phosphate-buffered saline
TTBS	Tween-20, Tris-buffered saline
V	volt

Chapter I

I. Introduction

I.1. Nucleoside transporters: a brief overview of their significance

Flux of nucleosides across cellular plasma membranes can occur by passive diffusion or by one or more mediated processes, that involve specific membrane proteins termed nucleoside transporters, which are capable of translocating substances at a relatively faster rate than passive diffusion. Carriers for the transport of nucleosides are either of the equilibrative facilitated diffusion type or of the concentrative sodium/cotransporter type, belonging respectively to the ENT or CNT family of nucleoside transport proteins.

Although most cells can synthesize nucleotides via *de novo* biosynthetic pathways, nucleoside transporters provide an energetically more favorable route to acquire nucleotide precursors in the form of nucleosides. Nucleoside transporters, therefore, likely play an important role in nucleoside salvage in highly active cells such as intestinal and brain cells, and their actions to attain nucleosides from dietary sources and body fluids may be a potential route for nucleoside drug entry into diseased cells.

Nucleoside uptake into cells varies throughout the cell cycle [1], and as a result of cellular differentiation and other growth-related stimuli [2-6]. Although there is substantial information on the regulation of other transporters [7, 8], evidence for the regulation of nucleoside transporters is beginning to emerge [9].

A large body of work on adenosine transport by nucleoside transporters of mainly the equilibrative-type implicates these transporters in regulating the local intracellular and extracellular adenosine concentrations [10]. Extracellular adenosine acts as a signaling molecule through binding to adenosine receptors

located at the cell surface, ultimately leading to a variety of physiological effects on many organs that are targets of adenosine receptor control, such as the central nervous system [11]. Extracellular adenosine pools utilized in the stimulation or inactivation of adenosine receptors are believed to be due, in part, to fluxes mediated via nucleoside transporters.

The role of nucleoside transporters, therefore, appears to be quite diverse, including modulation of adenosine interaction with its receptor to mediate various physiological functions, as well as providing a route of entry for metabolically important natural nucleosides and therapeutic nucleoside drugs. While these functions are better understood for the ENTs, the significance of CNTs is poorly understood. This study aims at providing further insights into the regulation and importance of the CNTs in nucleoside drug therapeutics and adenosine signaling.

1.2. Importance of physiological nucleosides

Nucleosides and their associated metabolic products are involved in many biological processes and play a major role in structural, metabolic, energetic and regulatory functions of the cell. Pyrimidine and purine nucleotides are precursors for DNA and RNA synthesis. Some specialized mammalian cells such as bone marrow, erythrocytes, leukocytes, intestinal enterocytes and certain brain cells are deficient in *de novo* nucleotide synthetic pathways [12-14], and therefore rely primarily on the salvage of exogenous nucleosides and nucleobases to maintain nucleotide pools to meet metabolic demands.

1.2.1. Purine nucleosides

Adenosine is a low-affinity permeant of certain nucleoside transport process, and a high-affinity, high-capacity permeant of other transport processes [15]. Adenosine exhibits a multitude of effects in mammalian tissues, particularly in excitable tissues such as the heart and brain, where it has been proposed to be a mediator in local vasoregulation, cardiac mechanical and electrical function, synaptic transmission in the central nervous system and modulator of platelet function and cell adhesion [16-18]. These actions by adenosine are mostly mediated by its interactions with adenosine receptors (A_1 , A_{2A} , A_{2B} and A_3) located at the plasma membranes of target cells [19, 20]. Adenosine can reduce the activity of excitable tissues (e.g., by slowing the heart rate) or increase the delivery of metabolic substrates (e.g., by inducing vasodilation) [16, 21], and therefore help to couple the rate of energy expenditure to the energy supply. Relative to the heart, adenosine has been shown to act as a cardioprotector during periods of hypoxia and ischemia [22-25].

While exhibiting protective effects on certain cell types, extracellular adenosine also regulates cellular growth by inhibition of cell proliferation [26, 27] and apoptosis [28-31] in both neoplastic and normal cell types. In experiments performed on human astrocytoma, murine myoblastic and human blood vessel endothelial cells, the antiproliferative effects of adenosine or possibly adenosine triphosphate were shown to be dependent, not upon interaction with adenosine receptors, but rather upon uptake into cells [32-34]. In some cases, the effects of adenosine triphosphate on cells were indirect through metabolism to

adenosine [34], suggesting that mediated adenosine uptake into cells was required for adenosine-induced apoptosis.

In the CNS (central nervous system), adenosine appears to also display this dual role of promoting either cell protection or toxicity [35, 36]. For example, this opposing effect of adenosine has been demonstrated *in vitro* utilizing glial cells, whereby adenosine can mediate protection or apoptosis depending on the pathway of adenosine signaling [37]. Generally, adenosine is viewed as a neuroprotector in the brain through interaction with adenosine A₁ receptors by preventing the release of different neurotransmitters [35].

Since the four types of adenosine receptors may be activated by different ranges of adenosine concentrations [38], the levels of adenosine available to interact and activate these receptors help determine the different physiological responses to adenosine. Therefore, the control of adenosine concentrations in the extracellular milieu under different physiological conditions can influence the degree of receptor stimulation and the consequent actions of adenosine. The existence of high affinity (apparent K_m of 0.8 μM) and low affinity (apparent K_m of 259 μM) adenosine transport processes have been detected in adult rat and chick embryo brains [39, 40]. However, neuronal cells appear to possess a larger component of high-affinity nucleoside transport systems for adenosine than glial cells [41, 42]. Interactions between nucleoside transporters and adenosine receptors has been suggested, since the adenosine A₂/A₁ receptor agonist, 5'-N-ethylcarboxamidoadenosine, was capable of stimulating adenosine transport [22].

The purine nucleoside, guanosine, is toxic to some forms of cancer, and though its cytotoxicity is pronounced in cancers with upregulated guanine nucleotide synthesis [43], its mechanism of action is poorly understood. There is a body of evidence in the cancer literature that points to guanine bases and nucleosides as potential antineoplastic agents [44, 45]. Several chemically modified guanine bases and nucleosides have been shown to be effective against various types of cancer cells [46]. More interestingly, guanosine has been shown to be toxic to some neoplastic cells [47-49]. While uptake of extracellular guanosine appears to result in growth inhibition of cancer cells, it has also been shown that guanosine itself reduces apoptosis and protects renal cells from ischemic injury [50].

1.2.2. Pyrimidine nucleosides

An important difference between purine and pyrimidine metabolism in mammals is that pyrimidines are recycled from nucleosides, particularly uridine, whereas purines are recycled partly from their bases [51]. There is little evidence that pyrimidine bases, such as uracil, can be salvaged and reincorporated into nucleotides by mammals. For example, patients with genetically blocked pyrimidine synthesis respond to oral uridine but not to uracil [52], although both substances are known to be transported across the gut [12]. Uridine is a permeant of all mammalian nucleoside transporters identified to date [15, 53]. The physiological significance of the apparent universal transportability of this compound is uncertain, although its importance in cells cannot be dismissed. The availability of uridine is particularly crucial for the synthesis of

DNA, RNA and biomembranes via the formation of pyrimidine nucleotide-lipid conjugates [54], and thus is essential for cellular function and growth.

Uridine possesses similar properties to adenosine in that it appears to act as a signaling molecule as well as a therapeutic agent [55-57]. For example uridine is often employed in combination with fluoropyrimidine chemotherapy to protect against side effects like myelosuppression [56]. Like adenine nucleotides, uridine nucleotides interact with pyrimidinoceptors located at the cell surface [58] and modulate numerous cellular events such as depolarization and hormone release [55].

The basal concentrations of uridine in the bone marrow, plasma, cerebral spinal fluid (CSF) and other body fluids range from 3 to 8 μM , and it is actively salvaged by cells, resulting in the intracellular uridine concentration typically being comparatively higher than the extracellular concentration [51]. It has been shown recently that uridine can induce differentiation of human neuroblastoma cells through protein kinase C mediated signaling pathways [57]. Although nucleoside transporters were not mentioned in this study, uptake across the plasma membrane was likely required for differentiation. The pyrimidine nucleoside, thymidine, has also been employed to modulate the therapeutic activity of numerous anti-metabolites, most notably 5-fluorouracil, araC and methotrexate [59].

1.3. Nucleoside analogs

Due to the varied metabolic fates of natural nucleosides and their key role in nucleic acid metabolism, many nucleoside analogs have been synthesized

with the aim of developing clinically useful drugs. To date, twelve nucleoside analogs have been identified that possess clinical applications in the treatment of neoplastic and viral diseases [60-62], and more will likely be identified in the future. A representative structure of a natural nucleoside and the main structural modifications to yield some of the more common nucleoside analogs are depicted in Figure I-1. Similar to natural nucleosides, most nucleoside drugs execute their biological activity at intracellular sites, but due to their hydrophilicity, do not permeate the lipid bilayer of plasma membranes readily in the absence of functional nucleoside transport proteins. A few pyrimidine-based nucleosides such as zidovudine (3'-deoxy-3'-azidothymidine, AZT) [63-65], lamivudine (3TC) [66], stavudine (d4T) [67] and troxacitabine [68] are sufficiently hydrophobic that some permeation into target cells evidently occurs via passive diffusion at rates sufficient to achieve pharmacologic activity.

The presence or absence of nucleoside transporters at the plasma membrane appears to have a profound impact on the *in vitro* and often *in vivo* pharmacological actions of many nucleoside drugs [62, 69, 70]. For instance, cells that are made incapable of transporting nucleosides by genetic mutations [71-74] or treatment with nucleoside transport inhibitors [75-79] exhibit low levels of nucleoside drug uptake and are resistant to a variety of nucleoside analogs with anticancer activity. While *in vitro* experiments have documented that nucleoside-transport deficient cells are resistant to cytotoxic nucleosides, the importance of nucleoside-transport deficiency in clinical resistance has not been as well established, presumably due to the difficulty in conducting transport

assays on malignant cells, and the associated heterogeneity of clinical tumor specimens. Still, there is some evidence that high abundance of nucleoside transporters is associated with increased nucleoside drug uptake and positive clinical outcome in patients with leukemia [80-84].

1.3.1. Anticancer nucleosides

Nucleoside drugs are important clinically in the treatment of hematological malignancies and solid tumors [62]. Pyrimidine nucleoside analogs such as gemcitabine (2',2'-difluoro-2'-deoxycytidine) and capecitabine (N4-pentyloxycarbonyl-5'-deoxy-5-fluorocytidine) possess a broad range of clinical applications against solid tumors. Some of their therapeutic activities include breast, ovarian, bladder, head and neck and pancreatic cancers [62, 85]. The basis for the clinical activity of these two compounds against solid tumors is unknown, although it may be due to differences between their cellular pharmacologies and those of other nucleoside drugs. The major active metabolite of capecitabine is 5-fluoro-5'-deoxyuridine, which has been shown recently to be transported by a member of the CNT family [86]. Among pyrimidine-based derivatives, fluorinated pyrimidines and their nucleosides (5-fluorouridine, 5-fluoro-2'-deoxyuridine, 5-fluoro-5'-deoxyuridine) constitute an important class of anticancer agents that exhibit activity against disseminated human cancers, especially of the gastrointestinal tract, breast and ovary [60, 87, 88]. The chemical structure of these uridine-based analogs together with the natural nucleoside uridine is presented in Figure 1-2. 5-Fluorouridine is used for the treatment of superficial bladder cancers that represent about 80% of bladder

cancers [89, 90]. Another important pyrimidine nucleoside analog, araC (1- β -D-arabinofuranosylcytosine, cytarabine), which has been extensively studied with respect to its mechanism of action and transportability into cells [91, 92], is primarily employed in the management of myelogenous leukemia [85, 93].

The purine-nucleoside analogs such as cladribine (2-chloro-2'-deoxyadenosine) and fludarabine (9- β -D-arabinosyl-2-fluoroadenine) exhibit clinical activity for different hematological malignancies [18, 94-98]. Cladribine and fludarabine share in their ability to induce apoptosis of human lymphoid cells [99], although cladribine appears to exhibit a higher degree of efficacy against chronic lymphoid malignancies such as chronic lymphocytic leukemia, hairy cell leukemia and cutaneous T-cell lymphoma [94, 96]. Both compounds share structural resemblance to adenosine, but otherwise are resistant to deamination by adenosine deaminase. Their chemical structures and that of adenosine are presented in Figure I-3. AraC's guanine congener, 9- β -D-arabinofuranosylguanine (araG), is selectively toxic to T-lymphoblasts, whereas araC exhibits equal toxicity to both T- and B- cells [100, 101]. A prodrug of araG is in clinical trials and shows promise in treatment of lymphoid malignancies specifically of the T-cell origin [102, 103]. The similarities and differences between the chemical structures of the two pyrimidine and purine arabinonucleosides can be seen in Figure I-4.

1.3.2. Antiviral nucleosides

Several nucleoside analogs are employed in the treatment of viral diseases [61, 104, 105], and many nucleoside analogs are currently being

evaluated for their activity as antiviral agents. The modified derivatives of natural nucleosides currently approved for treating human immunodeficiency virus (HIV) and herpes virus infections are presented in Figures 1-4, 1-5, 1-6 and 1-7. Antiviral nucleoside analogs must be activated intracellularly to their triphosphate forms to enable their incorporation into newly synthesized viral DNA, ultimately leading to inhibition of viral reverse transcription and prevention of viral replication [106]. Several studies reveal the contribution of nucleoside transport systems in the translocation of antiviral nucleoside drugs into cells [61], implicating their role in the multi-step process of antiviral activation.

The thymidine analog, zidovudine (3'-azido-2',3'-dideoxythymidine, AZT) is the prototypical antiretroviral drug widely employed for the treatment of HIV infection [107]. Although it is transported to a large extent by a member of the CNT family [108, 109], organic ion transporters also appear to possess the capacity for mediating zidovudine uptake into cells [110]. Other nucleoside drugs such as didanosine (2',3'-dideoxyinosine, ddi), zalcitabine (2',3'-dideoxycytidine, ddC) and lamivudine ((-)-2',3'-dideoxy-3'-thiacytidine, 3TC) have been used in combination with viral protease inhibitors for HIV infection [111]. One of the newest antiviral thymidine derivatives stavudine (2',3'-didehydro-3'-deoxythymidine, d4T) is currently in clinical trials for the treatment of HIV, and in contrast to other nucleoside analog drugs, it appears not to be mediated by nucleoside transport systems of the equilibrative type [67]. Transport of this compound by sodium-dependent nucleoside transporters has not been characterized. The purine nucleoside analogs, including vidarabine (araA, 9- β -

D-arabinofuranosyladenine), acyclovir (9-(2-hydroxyethoxymethyl)guanine) and ganciclovir (9-(1,3-dihydroxy-2-propoxymethyl)guanine) are used against herpes simplex virus [60].

While the current state of knowledge of the transport of clinically important nucleoside drugs by the human concentrative nucleoside transporters is limited, it was anticipated that the efforts of the present study will further add to the body of information in this area. The present state of knowledge of the transportability of the clinically useful anticancer and antiviral nucleoside analog drugs by mammalian nucleoside transporters is summarized in Table I-1. Included are those nucleoside drugs for which transport has been demonstrated directly, by measuring fluxes, or indirectly by showing either inhibition of mediate-uptake by drug or inhibition of drug action by simultaneous exposure to NBMPR (for the equilibrative NBMPR-sensitive process).

I.4. Intracellular metabolism of nucleosides and nucleoside analogs

Nucleoside and nucleoside analog permeation across the plasma membrane is usually followed by subsequent intracellular metabolism. For most nucleoside drugs, the triphosphate derivative is the major determinant of cytotoxic action through its incorporation into DNA and/or RNA. The stepwise phosphorylation process not only activates the nucleoside drug, but also serves to prevent efflux since phosphorylated nucleosides (i.e., nucleotides) do not readily permeate plasma membranes. Once inside cells, the conversion into different phosphorylated derivatives is catalyzed by several phosphorylating

enzymes, including deoxycytidine kinase (dCK) and deoxyguanosine kinase (dGK).

The location of dCK is in the cytoplasm [112] and its substrate preference appears to be nonspecific in that it is known to phosphorylate both pyrimidine and purine deoxynucleoside derivatives such as cytarabine, cladribine, fludarabine and araG, among others [113]. In contrast dGK, which also phosphorylates araG, is present in mitochondria [114] and may be a potential contributor to the side-effects or efficacy of nucleoside drug treatment due to mitochondrial toxicity.

1.5. Multiplicity of nucleoside transport processes in cells

Up until the cloning of cDNAs encoding for nucleoside transporters responsible for nucleoside fluxes observed in cells, early studies relied on cultured cell lines as well as isolated cells and tissues to characterize transport processes. Many of these studies were complicated by the coexistence of two or more functionally distinct transport processes [115], which makes the analysis of fluxes complex. It is now recognized that there are multiple transporters for nucleosides that are either of the equilibrative facilitated diffusion type or of the concentrative sodium/cotransporter type. The equilibrative transport processes act to translocate nucleosides down their transmembrane concentration gradient and are bi-directional facilitators, whereas concentrative processes are inwardly directed symporters, which can translocate nucleosides against their concentration gradients though coupled movement of sodium down its electrochemical gradient. The classification of nucleoside transport processes is

based on permeant specificities, sensitivity to inhibition by diagnostic agents and type of transport [13]. The functional difference between concentrative and equilibrative transport processes is depicted diagrammatically in Figure I-8.

1.5.1. Equilibrative nucleoside transport processes

In mammalian cells, there are two facilitated processes of broad permeant selectivity for purine and pyrimidine nucleosides that can be distinguished by the difference in their sensitivities to inhibition by the synthetic nucleoside analog, NBMPR. These equilibrative transport processes have been divided into two subtypes (*es* and *ei*) on the basis of their sensitivity (*es*) or insensitivity (*ei*) to inhibition by NBMPR. The *es* process is inhibited at low concentrations (<1 nM) of NBMPR as a result of interaction of NBMPR with high-affinity binding sites (K_d of 0.1-1 nM), while the *ei* process is not affected by NBMPR up to micromolar concentrations [115, 116]. A number of other structurally unrelated substances, including dilazep, dipyridamole and draflazine, are inhibitors of both *es* and *ei* processes. These agents are coronary vasodilators by acting to prevent the uptake of adenosine into metabolizing cells through inhibition of equilibrative transport processes, this ultimately leads to a local increase in adenosine pools available to prolong the effects on adenosine receptors. This prolongation is responsible for the vasodilatory effects of these transport inhibitors and many studies have explored these transport inhibitors in the development of cardioprotective therapies [25, 117, 118].

1.5.2. Concentrative nucleoside transport processes

Detailed studies of the substrate specificity, and hence the possible number of different sodium-nucleoside cotransporters, has mainly involved the examination of the inhibitory effects of nucleosides on the influx of radioactive permeants. Two systems of nomenclature have been employed, one based on trivial names (*cif*, *cit*, *cib*, *csg* and *cs*) utilizing the classification scheme described by Cass *et al.* [13], and the other employed numerical designations for concentrative processes (N1-N5) to signify order of discovery. The latter system is no longer used and subsequent descriptions of nucleoside transport processes will employ the trivial names, *cif*, *cit*, *cib*, *csg* and *cs*.

There is evidence for six sodium-dependent (concentrative) nucleoside transport processes as revealed by identification of differential inhibition characteristics and permeant selectivities of nucleoside uptake by whole cells and by brush border membrane vesicles isolated from various organs [53]. These concentrative processes consist of a heterogeneous group, with a mixed pattern of overlapping permeant selectivities that can result in an elaborate phenotype whereby one nucleoside may be simultaneously transported by more than one process within a cell or tissue. Thus, it is pertinent to have an experimental system that can discriminate between the various concentrative nucleoside transporter types.

The *cif*, *cit* and *cib* processes share in their insensitivity to NBMPR inhibition, although they differ in their permeant selectivities. The *cif*, *cit* and *cib* processes exhibit selectivity for purine nucleosides, pyrimidine nucleosides or

both, respectively, but also can accept adenosine and uridine as permeants. A *cit*-like system has been found in human kidneys, which also accepts the purine nucleoside guanosine as a permeant [119]. The *cs* and *csg* processes, which have been identified, respectively, in freshly isolated leukemia cells [120] and human acute promyelocytic leukemia NB4 cells [121], are sensitive to NBMPR inhibition, hence their designation as *cs* (concentrative-sensitive). The *cs* process appears to accept adenosine analogs as permeants while the *csg* process prefers guanosine. The identity of the proteins associated with the observed *cs* and *csg* processes remains to be determined.

In general, the permeant affinities of the sodium-dependent transport processes are higher than equilibrative processes. Increasing the concentration of sodium appears to increase the affinity of the transporter for the nucleosides without much effect on the maximum velocity for nucleoside uptake [122, 123]. The sodium/nucleoside coupling ratios estimated from sodium activation curves at fixed nucleoside concentrations are 1:1 for *cif* and *cit*, and 2:1 for *cib* when conducted with either native or recombinant CNT proteins [2, 123-129].

1.6. The superfamily of nucleoside transport proteins

Since 1994, the proteins responsible for the majority of nucleoside transport processes observed in mammalian cells have been identified through molecular cloning of their cDNAs and functional characterization in expression systems in either *Xenopus* oocytes or cultured cells [2, 130-139]. This has substantially advanced knowledge of the functional and structural relationships among mammalian nucleoside transporters. The correspondence between

nucleoside transport processes and human transport proteins identified and characterized to date is shown in Table I-2. These nucleoside transport proteins comprise two functionally distinct protein families that have been designated ENT and CNT, depending on whether they mediate, respectively equilibrative (E) or concentrative (C) nucleoside transport processes [140]. The two functionally characterized members of the ENT family, hENT1 and hENT2, which mediate respectively *es* and *ei* transport activity, share in their ability to transport a broad range of purine and pyrimidine nucleosides as well as several nucleobases, but otherwise are different in their sensitivity to NBMPR.

In contrast, several of the CNT family members that have been functionally characterized, including hCNT1 and hCNT2, exhibit a more defined permeant selectivity. The hCNT1 protein, which exhibits *cit* transport activity, prefers pyrimidine nucleosides, although it also possesses the capacity to transport adenosine with low activity. The hCNT2 protein exhibits *cif*-type activity and is purine-nucleoside selective, although it also transports uridine. hCNT3 exhibits *cib* transport activity and is unique among hCNTs in its ability to accept both purine and pyrimidine nucleosides as permeants.

The difference in functional properties between ENTs and CNTs also extends to their distinct structural arrangements. Figure I-9 shows the different architectural designs between ENTs and CNTs, as predicted from algorithms and biochemical studies using antibodies against various regions of the proteins [140-143].

1.6.1. Equilibrative nucleoside transporter (ENT) family

The human ENTs, hENT1 and hENT2, have primary sequences of 456 amino acids and are 49% identical and 69% similar at the amino acid level with highly conserved transmembrane segments. Almost all mammalian ENT proteins identified to date possess either 456 or 457 amino acid residues and have predicted membrane topologies typically comprised of 11 transmembrane segments that are connected mostly by short hydrophilic loops, except for the two distinctly large loops, one of which is extracellular and the other intracellular (see Figure I-9). Portions of the large intracellular loop, which connects transmembrane domains 6 and 7, have previously been employed as immunogenic epitopes in the production of antibodies against hENT1 [144], and there is experimental evidence of its cytosolic location through the use of glycosylation scanning mutagenesis in combination with antibodies [142]. The extracellular loop, which is between transmembrane domains 1 and 2, contains a consensus site for N-linked glycosylation that has been confirmed experimentally to be glycosylated at asparagine 48 of hENT1 [142]. This result is consistent with early studies that utilized site-specific photolabeling of plasma membranes of red blood cells with ³H-NBMPR and demonstrated that the es-type transporter migrated as a glycoprotein on SDS-polyacrylamide gel electrophoresis [143, 145, 146].

Both hENT1 and hENT2 are inhibited by coronary vasodilators such as dilazep and draflazine as well as dipyridamole. However, there are species differences in the sensitivities of the ENTs to these transport inhibitors, with the

most well known example being the difference between human cells in comparison to rat and mouse cells [115, 147]. Differences in nucleoside transport capacity have been noted for *es* processes in red blood cell preparations of human compared to mouse, rat and guinea-pig [148]. Also, the rat homolog of ENT1 is less sensitive to inhibition by dipyridamole, dilazep and draflazine than its human counterpart [149-151]. Therefore, the experimental design must be carefully defined and studies performed with non-human systems cannot be assumed applicable to the human nucleoside transporters because of species difference in their functional characteristics.

However, a large body of information can be found for hENT1, due mainly to the availability of cell types such as human red blood cells, which possess exclusively the *es*-type transport process [152]. On the contrary, much less is known about hENT2, which is typically present in cells and tissues together with other nucleoside transporters. In cells where it is present, its activity is often very low in comparison to hENT1-mediated activity, which is typically responsible for the majority of the observed flux [153, 154]. The generation of a stable cell line that possesses recombinant hENT2 as its only nucleoside transporter would provide a useful model system in which to study the characteristics of this transporter.

The cDNA encoding hENT1 was isolated from a placental cDNA library by screening using oligonucleotide probes based on sequence information acquired from the amino terminus of highly purified *es* transporter from human red blood cells [135]. The hENT1 gene has been mapped to chromosome 6p21.1-p21.2

[155]. Although the hENT1 protein shares several molecular properties with the human red cell glucose transporter (GLUT1) [156, 157], hENT1 has no amino acid homology to GLUT1 [135]. The es transporter from human red blood cells is heterogeneously glycosylated and migrates as a broad band on SDS polyacrylamide gel electrophoresis with an apparent molecular mass between 45 and 65 kDa [158]. The hENT1 cDNA encodes a protein of 456 amino acids with a predicted molecular mass of 50 kDa. When hENT1 cDNA is expressed in oocytes, ³H-uridine transport by hENT1 is inhibited by both purine and pyrimidine nucleosides and by low concentrations of NBMPR, dilazep, and dipyridamole, which is typical of an es-type transporter [135].

The human cDNA encoding for hENT2 protein was isolated from human placenta by RT-PCR using degenerate oligonucleotide primers based on similarities between the hENT1 and hENT2 sequences [136]. The hENT2 cDNA was also independently cloned by functional complementation in the nucleoside-transport deficient CEM-ARAC human leukemia cell line using a HeLa cell cDNA library [137, 138]. Expression of full-length hENT2 cDNA in either *Xenopus* oocytes or cultured CEM-ARAC cells demonstrated functional transport activity characteristic of an ei-type transporter with broad substrate selectivities as revealed by inhibition and direct transport studies [136, 137].

Recombinant hENT2 is insensitive to NBMPR inhibition up to 10 μ M [137] and exhibits the capacity to transport nucleobases, including adenine, hypoxanthine, uracil and thymine, with apparent K_m values ranging between 740 μ M and 2600 μ M [139, 159]. This is consistent with earlier studies that

demonstrated that the nucleobase hypoxanthine is a permeant of the *ei* transporter in human endothelial cells [160]. Furthermore, hENT2 appears to be unique among the functionally characterized human ENTs in its ability to accept antiviral nucleoside analogs of the 3'-deoxyribosyl type [161]. While rCNT1 accepts AZT as a permeant [109], there is sufficient evidence to indicate that hENT2 exhibits a capacity to transport this antiviral drug as well [109].

1.6.1.1. Distribution of ENTs in cells and tissues

Homologs of ENTs have been identified in a wide range of eukaryotes, including plants, fungi, insects, nematodes, and protozoan parasites [53, 140]. The hENT1 protein is considered to be ubiquitous [15], based on evidence of its activity in almost all cell types and tissues examined. However, hENT2 mRNA expression and nucleoside transport activity is not as widespread as that of hENT1 (see Table I-3). rENT2 mRNA has been detected in different regions of rat brain, including hippocampus, cortex, striatum and cerebellum [162] in conjunction with rENT1 mRNA, which appears to exhibit widespread distribution in neurons of the hippocampus, dentate gyrus and cerebellum [163]. The presence of ENT-mediated nucleoside transport activities in the central nervous system has been demonstrated via isotopic flux analysis with ³H-adenosine in mammalian brain preparations [164, 165]. In addition, the distribution of the *es*-type transporter (ENT1) has been examined by ligand-binding studies with ³H-NBMPR in post mortem human brain and rat brain [166, 167]. More recently, a comparison of the regional location of hENT1 and hENT2 using antibodies against the human ENTs established that the two proteins exhibited different

distributions within post mortem human brain [144]. These studies and others [10, 21] have provided a functional link between regulation of endogenous adenosine by nucleoside transporters, specifically members of the ENT family, and adenosine-mediated neuromodulation of adenosine receptor stimulation.

Hybridization analysis of RNA from a variety of human tissues has revealed that hENT2 mRNA is expressed at variable levels in a variety of tissues, including intestine, kidney, heart, lung, colon, prostate, pancreas, salivary gland, thyroid gland, thymus and heart, with the highest mRNA abundance in skeletal muscle [136, 137, 168, 169]. Studies of hENT2-mediated nucleoside fluxes in cultured human cell lines have suggested a moderate to broad tissue distribution, although it is often present in lower abundance and generally in association with hENT1 and occasionally with members of the CNT family. Most cultured human cell lines that have been characterized possess both hENT2- and hENT1-mediated nucleoside transport activities, including cervical cancer HeLa cells, erythroleukemia K562 cells and choriocarcinoma BeWo cells [138, 153, 154, 160, 170, 171]. Several tissues, including intestine, epididymis and brain, have also been demonstrated to contain hENT2 activity [144, 172, 173]. Most studies of ENT2 have been conducted with transporters other than hENT2, and a more refined summary of the distribution of mammalian ENT2 by analysis of mRNA expression or the presence of ENT protein or activity is presented in Table I-3.

1.6.2. Concentrative nucleoside transporter (CNT) family

The mammalian CNTs are encoded by a gene family that is unrelated to other known transporter gene families. Almost nothing was known about CNT proteins until the molecular cloning from rat jejunum by functional expression selection in *Xenopus* oocytes of a cDNA encoding for the first-to-be-discovered member of the CNT family, designated rCNT1 [63]. Since the cloning of rCNT1, more than 40 CNT family members have been identified in both eukaryotes and prokaryotes. In comparison to the eukaryotic transporters, the prokaryotic transporters such as NupC from *E. coli* are smaller proteins and appear to mediate nucleoside symport using the transmembrane gradient of protons rather than sodium ions [174, 175]. The *E. coli* NupC has many homologs in other bacteria, including several that cause human diseases (e.g., *Haemophilus influenza*, *Bacillus subtilis* and *Helicobacter pylori*) [176].

Analyses of the amino acid sequences of the transporters by predictive algorithms in combination with biochemical studies utilizing glycosylation scanning mutagenesis and other approaches have provided evidence that mammalian CNTs possess 13 transmembrane segments [141], whereas the prokaryotic CNTs lack the first three transmembrane segments and tend to possess relatively shorter carboxyl termini. The mammalian CNTs have very different predicted topologies than the ENTs (as depicted in Figure I-9), as would be expected given that these proteins possess unrelated primary sequences, and thus must have different ancestries.

Despite the structural similarities between mammalian CNT family members, the difference in their permeant selectivities has enabled the design of experiments based on the generation of chimeric proteins of recombinant CNTs [177, 178]. These chimeric studies in conjunction with site-directed mutagenesis of CNT1 and CNT2 proteins have identified important amino acid residues within transmembrane domains 7 and 8 of CNTs that are involved in permeant binding [177, 178].

1.6.2.1. *hCNT1*

The cDNAs encoding for the pyrimidine-nucleoside selective hCNT1 were cloned by hybridization screening and RT-PCR of a human intestinal cDNA library based on rCNT1 sequences [133]. Two hCNT1 cDNA isolates were cloned yielding proteins with 648 and 650 amino acid residues, and a predicted molecular mass of 71 kDa. The hCNT1 gene is located on chromosome 15q25-26 and the deduced amino acid sequences of hCNT1 shares 83% identity with rCNT1 sequences (see Figure I-10). Expression of hCNT1 cDNA in *Xenopus* oocytes yielded functional nucleoside transport activity and inhibition characteristics typical of the *cit*-type process, with the ability to mediate preferentially the uptake of pyrimidine nucleosides and to some extent adenosine as well [133]. Recombinant hCNT1, when produced in *Xenopus* oocytes, mediates uridine transport with high affinity (apparent K_m value of 42 μ M) and also possesses the ability to transport the antiviral 3'-deoxynucleoside analog, zidovudine (see Figure I-5 for chemical structure). It has also been shown that recombinant hCNT1 mediates the uptake of gemcitabine with

relatively high affinity with apparent K_m values of 32 μM and 24 μM respectively in hCNT1 cDNA transfected HeLa cells [66, 69] and cRNA microinjected oocytes of *Xenopus laevis* [179].

1.6.2.2. hCNT2

The cDNAs encoding hCNT2 and hSPNT1 were cloned respectively from human intestine and kidney by RT-PCR amplification strategies and functional expression of their cDNAs in *Xenopus* oocytes [131, 132]. The two independently isolated cDNAs encoding hCNT2 and hSPNT1 shared similar functional characteristics when expressed in *Xenopus* oocytes of producing functional nucleoside transport activities typical of *cif*-type processes [131, 132]. The predicted hCNT2 and hSPNT1 proteins both possess 658 amino acids, and their amino acid sequences differed only at residue 75, having an arginine in hCNT2 [132] and a serine in hSPNT1 [131].

The cDNA encoding hCNT2 isolated by Ritzel *et al* [132] was used in the studies presented in this thesis. The predicted molecular mass of hCNT2 protein is 72 kDa and there are five consensus sites for N-linked glycosylation, two of which are located in the interior region of the protein, and three within the carboxyl-terminal tail. Experimental evidence to ascertain if hCNT2 is a glycoprotein is not available. The hCNT2 protein also possesses several consensus sites for protein kinase A and C phosphorylation, indicating that it may be regulated by a protein-kinase dependent mechanism. The functional significance of the phosphorylation sites remains to be explored.

The hCNT2 protein shares 83% and 72% amino acid identity with rCNT2 and hCNT1, respectively. A comparison of the molecular properties of mammalian CNTs is shown in Figure I-10. Most of the divergence within CNT family members is located at regions close to the amino terminus and carboxyl terminus of the protein. These key differences between CNTs were kept in mind in developing synthetic peptide epitopes for raising specific antibodies against hCNT2. The proposed architectural model of hCNT2, based on predictive algorithms for polytopic membrane proteins and experimental evidence using glycosylation scanning mutagenesis analysis of rCNT1 [141] is presented in Figure I-11. The topological model shown in Figure I-11 reveals the location of the synthetic peptide utilized in the generation of anti-hCNT2 polyclonal and monoclonal antibodies (see Chapter V).

1.6.2.3. *hCNT3*

The identification of novel CNT sequences from mammary gland and colon adenocarcinoma in the GenBank database, which were speculated to represent sequences corresponding to the unidentified *cib*-type transporter, provided the basis for the isolation of a partial open reading frame of hCNT3 by RT-PCR of RNA preparations of cells known to possess *cib* activity [2]. The partial sequence that was obtained was extended by 5'-RACE amplification of mRNA from differentiated HL-60 cells, which exhibit *cib* activity, to generate the entire open reading frame of hCNT3 [2]. In contrast to the similar chromosomal locations of hCNT1 and hCNT2, both of which have been mapped to chromosome 15 [132, 133], the hCNT3 gene is located on chromosome 9q22.2

[2]. Upstream sequences of the hCNT3 gene consists of a phorbol myristate acetate response element, which is thought to be associated with the transcriptional regulation of hCNT3 mRNA expression in HL-60 cells [2]. The hCNT3 cDNA encodes a predicted protein of 691 amino acid residues with a predicted molecular mass of 76 kDa.

The hCNT3 protein shares 78% amino acid identity with mCNT3 and 57% identity with a CNT protein designated hfCNT from an evolutionarily ancient marine vertebrate, the Pacific hagfish [177]. Cells from hagfish have been shown to possess *cib* activity [177]. Phylogenetic analysis places the CNT3 protein, from human and mouse closest to the hagfish CNT, in a different CNT subfamily from the human and mouse CNT1 and CNT2 proteins, as depicted in Figure I-10. Similar to other CNT family members, hCNT3 also possesses multiple consensus sites at the carboxyl terminus for N-linked glycosylation grouped in close proximity at asparagine⁶³⁶ and asparagine⁶⁶⁴. The proposed topological model of hCNT3, which is presented in Figure I-12, is based on predictive algorithmic analysis; there is biochemical evidence for the 13-transmembrane domain model from studies of rCNT1, which has been shown to possess an intracellular amino terminus and an extracellular carboxyl terminus [141].

Recombinant hCNT3 produced in *Xenopus* oocytes exhibited sodium-dependent uptake of both purine and pyrimidine nucleosides [2] that was typical of the *cib*-type process, as observed in earlier transport studies conducted with brain choroid plexus and microglia and jejunum of the small intestine [128, 129,

180]. The hCNT3 protein transports several physiological purine and pyrimidine nucleosides (e.g., adenosine, guanosine, inosine, cytidine, thymidine and uridine) with high affinity [2]. The apparent K_m values for these nucleosides were in the range between 15 μM and 53 μM [2], which is comparable to the general high-affinity interaction of nucleosides with hCNT1 and hCNT2. The sodium/nucleoside coupling estimated from sodium activation curves of recombinant hCNT3-mediated nucleoside uptake in *Xenopus* oocytes suggested a stoichiometry of 2:1 [2]. This stoichiometry is consistent with the stoichiometries observed in experiments with the naturally occurring *cib*-type transporters from brain [128, 129].

1.6.2.4. Distribution of CNT mRNAs in mammalian cells and tissues

Among CNTs, CNT1 and CNT2 proteins are not as widely distributed in mammalian cells and tissues as the ENTs. While the tissue distribution of hCNT1 has not been determined, there is evidence of rCNT1 mRNA expression in kidney as well as in different regions of the small intestine including jejunum, ileum and duodenum at varying levels [63, 181], but not in colon [181]. Also, RT-PCR analysis using rCNT1-specific primers to PCR amplify preparations of RNA from rat brain tissue has shown that rCNT1 mRNA is present in numerous regions of the brain, including cerebral cortex, cerebellum, hippocampus, striatum, brain stem, superior colliculus, hypothalamus and choroid plexus [182]. Molecular techniques employing northern blot analysis and RT-PCR have identified CNT2 transcripts in a variety of mammalian tissues including intestine, liver, kidney, brain, placenta, lung, skeletal muscle, pancreas, heart and

stomach, although the levels of transcript appeared to vary between tissues [131, 132, 168, 182].

While CNT mRNAs appear to be expressed mainly in specialized cell types, the distribution of CNT3 mRNA appears to be much more widespread than that of CNT1 and CNT2 mRNAs. The highest level of hCNT3 mRNA expression was observed in mammary gland, bone marrow, trachea and pancreas, with varying levels in different regions of the intestine, and comparatively much lower levels in kidney [2]. A moderate level of hCNT3 mRNA was expressed in liver, lung, placenta, prostate, testis, and numerous other tissues, most notably the heart and different areas of the brain [2]. It is uncertain whether these findings reflect the presence of physiologically significant amounts of CNT proteins. No immunoblot analyses of human tissues have yet been performed due to the lack of available antibodies against the human CNTs.

1.6.2.5. Location of sodium-dependent nucleoside transport processes in cells and tissues

Indirect evidence for the presence of concentrative nucleoside transport processes has come from numerous experimental preparations, including mammalian tissues, isolated intact cells and membrane vesicles. A summary of the cellular and tissue location of the various CNT-mediated activities is presented in Table I-3. Sodium-dependent nucleoside transport has been suggested to be present in rat brain [165, 183], rat and mouse macrophages [127, 184, 185], mouse splenocytes [186, 187], thymocytes [188] and bone

marrow granulocyte-macrophage progenitor cells [189], rabbit and rat jejunum [190-192], liver [193], and hepatocytes [194], rat, rabbit, bovine and human renal epithelium [119, 123, 195]. Human intestinal brush border membranes appear to possess sodium-dependent nucleoside transport activity suggestive of the *cit*- and *cif*-type processes [196, 197]. Despite the numerous reports of sodium-dependent nucleoside transport processes, there is relatively little detailed information on the kinetic properties and drug selectivities of *cit*, *cif* or *cib* processes in human cells. Most studies have been restricted to membrane vesicles [125, 195, 196], and there are only a few investigations that have been conducted with recombinant concentrative transporters in human cells [66, 74, 198].

Currently, the promyelocytic leukemia HL-60 cell line is the only example of a cultured human line that has been clearly shown to exhibit sodium-dependent nucleoside transport activity of the *cib* type [2, 199]. In many cases, the level of sodium-dependent transport activity in cultured cells is so low that it is only revealed following the inhibition of either the *es* and/or *ei* transport process [127, 200, 201]. No cultured human cell line has yet been identified that naturally exhibits either the *cif* or *cit* process.

1.6.2.6. Location of CNT proteins in cells and tissues

Mammalian CNT family members are present mainly in highly differentiated tissues. Immunolocalization studies of CNT1 in rat tissues have shown that it is located at the brush-border membranes of polarized intestinal epithelial cells and renal cortical tubular cells as well as the bile canalicular

membranes of hepatic parenchymal cells [141]. Nucleoside transport studies have provided evidence for both *cif*- and *cit*-type activities in rat renal brush-border membrane preparations and human intestinal brush-border membrane preparations [196, 202], observations that are consistent with the current view of the role of the CNTs in luminal absorption of nucleosides. Recombinant fusion proteins of rCNT1 and rCNT2 that were tagged with green fluorescent protein and produced in renal epithelial Madin-Darby canine kidney (MDCK) cells were located primarily in apical membranes [203]. Further evidence of CNT trafficking to apical membranes comes from studies of recombinant hCNT1 and hENT1 produced simultaneously as fluorescently-labeled fusion proteins in MDCK cells, which revealed that hCNT1 localizes to apical membranes, while hENT1 localizes to basolateral membranes [204]. These results suggest that the CNTs may possess targeting elements that guide them to apical membranes of polarized epithelial cells.

1.7. Regulation of nucleoside transporters

Although there is considerable information pertaining to the mechanisms that underlie regulation of other mammalian transporters [7, 8], relatively little is known about the regulation of nucleoside transporters. Nucleoside uptake varies throughout the cell cycle [1], as a result of cellular differentiation and other growth-related stimuli [2-6]. In epithelial cells such as hepatocytes, rCNT2 mRNA expression and nucleoside transport activity are highly regulated during cell-cycle progression and differentiation [9]. In murine bone marrow macrophages, the inhibition of cell proliferation by interferon-gamma results in

selective down-regulation of ENT1 mRNA and a concurrent stimulation of CNT1 and CNT2 mRNA expression [205].

Differentiation of human promyelocytic leukemic HL-60 cells to monocyte/macrophage-like cells by exposure to phorbol esters [206, 207] is accompanied by an increase in sodium-dependent transport of both purine and pyrimidine nucleosides that is associated with a decline in nucleoside transport of the equilibrative type [3, 199]. Quantitative Taqman RT-PCR analysis combined with nucleoside transport assays comparing parental and differentiated HL-60 cells showed that cell differentiation leads to a stimulation of hCNT3 mRNA levels that is paralleled by augmentation of *cib*-type nucleoside transport activity [2]. In the few examples available, cellular differentiation appears to ultimately lead to an increase in CNT-mediated nucleoside transport activity and a reduction in ENT-mediated transport, although there are obviously cell- and tissue-specific differences [208]. As a consequence, there is little consensus in the literature as to the nature of the regulation of nucleoside transporters in various cell types and tissues.

1.8. Goals of the present work

The overall goal of the research presented in this thesis was to examine the role of the CNTs in nucleoside drug sensitivity and adenosine signaling, and to gain a better understanding of their subcellular distribution and regulation of their trafficking. It was hypothesized that generation of a panel of stable cell lines that exhibit a single type of nucleoside transporter in isolation and specific

antibodies against the transporters would provide the necessary tools to achieve these goals. The objectives were to:

- 1) functionally express cDNAs encoding various nucleoside transporters by stable transfection in a transport-deficient T-lymphoblast cell line,
- 2) undertake structure-activity and structure-cytotoxicity relationship studies of hCNTs and compare the transport properties of hCNTs,
- 3) generate and characterize polyclonal and monoclonal antibodies against hCNTs,
- 4) determine the location of recombinant hCNT2 in stably transfected cells and examine changes in distribution of native hCNT3 in polarized intestinal epithelial cells,
- 5) examine and compare the distribution and location of hCNT2 and hCNT3 in human brain and endothelial cells with that of adenosine A1 receptors.

I.9. Rationale

A key to understanding the physiological role of a specific nucleoside transport process is the functional production of the protein responsible for the distinct transport process. Molecular cloning of cDNAs encoding the major nucleoside transporters of human cells [2, 131-133, 135-137] has provided the tools to produce recombinant nucleoside transport proteins for detailed studies. It is critical to choose an expression system that is capable of both functional expression as well as adequate production of recombinant protein. Bacterial expression systems, such as *Escherichia coli*, are often not suitable for the production of eukaryotic membrane proteins due to the possible formation of

inclusion bodies because of improper folding; this typically leads to the loss of activity of the protein [209]. Also *E. coli* possesses two nucleoside transport systems, *nupC* and *nupG*, that mediate the transport of a broad range of nucleosides [174, 210]. Similarly, the yeast (*Saccharomyces cerevisiae*) expression system is complicated by interferences of a purine-cytosine permease, encoded by *FCY2* [211, 212], as well as evidence of uridine and cytidine mediated uptake by the *FUI1* protein and another unidentified transporter [176, 213]. These endogenous transporters in the host cells may pose complications in the interpretation of kinetics and permeant selectivities.

Ideally, it is desirable to express human cDNAs encoding for a specific nucleoside transporter type in human cells that lack endogenous transport activity. The distinct advantage is that the transporter DNA sequences, which are derived from human sources, are more likely to be properly expressed because the host cell is also of human origin, and therefore should possess a full complement of functional post-transcriptional and post-translational activities. As such, expression of nucleoside transporter cDNAs in human cells for investigation will likely be more physiologically applicable than expression in bacteria or yeast.

I.10. Nucleoside-transport deficient human cells

Multiple nucleoside transporters with overlapping permeant selectivities are naturally present in most human cells [153, 200, 201]. Presently, the only human cell line that has been shown to be nucleoside-transport deficient is the CEM-ARAC line, a drug resistant mutant that was derived from the human T-

lymphoblastoid CEM cell line [214], which was originally isolated from patients with acute lymphocytic leukemia [71]. The nucleoside transport process present in the CEM cell line has been well characterized and is exclusively of the *es*-type [138, 215]. The CEM-ARAC transport-defective mutants were isolated from wildtype CEM cells that were mutagenized with MNNG (N-methyl-N-nitroso-N'-nitroguanidine) [214, 216]. The mutagenized cells were subsequently selected by their resistance to araC (1- β -D-arabinofuranosylcytosine), a drug that was selectively cytotoxic to wildtype CEM at low concentrations, but not to CEM-ARAC cells.

The isolated CEM-ARAC mutants failed to transport cytidine and 2'-deoxycytidine and lost high-affinity NBMPR binding sites [214], suggesting an absence of *es*-type transporter. Although the exact molecular mechanism of this genetic defect in nucleoside transport deficiency was not determined, the transport deficiency of CEM-ARAC cells was well documented [138, 214, 216]. The CEM-ARAC cell line was utilized in the cloning of the human equilibrative, NBMPR-insensitive nucleoside transporter by functional complementation of the nucleoside transport deficiency [137].

I.11. Approach

In the present work, the transport-deficiency of CEM-ARAC cells was used to advantage in the production of stable transfectants that exhibit a single type of nucleoside transporter. These stable cell lines provided new *in vitro* models in the same genetic background for study and comparison of the different nucleoside transporters. Emphasis was focused on studies of hCNT1

and hCNT2, and their interactions with drugs and nucleoside analogs. The successful generation of antibodies specifically against hCNT2 and hCNT3 yielded reagents that were employed in studies aimed at determining their subcellular location and tissue distribution, and their roles in nucleoside utilization and pharmacology in intestine and brain.

Table I-1. Mediated transport of clinically relevant nucleoside drugs by mammalian concentrative and equilibrative transport processes and proteins

Drug	Transported by:		Primary use	Reference
	Concentrative transporters	Equilibrative transporters ¹¹		
Pyrimidine nucleoside analogs				
FUrd	hCNT2, hCNT3	es	Bladder cancer	[2, 74]
FdUrd ²	hCNT2, hCNT3	es, ei	Colorectal cancer	[2, 74, 217, 218]
dFUrd ³	hCNT1	es		[86, 219]
Idoxuridine	hCNT2	es	Herpes virus	[74, 218]
Cytarabine	hCNT1	es, ei	Leukemia	[66, 82, 93, 220, 221]
Gemcitabine	hCNT1, hCNT3	hENT1, hENT2	Solid tumor	[2, 66, 69, 179]
Zalcitabine ⁴	hCNT3	es	HIV	[2, 222, 223]
Zidovudine ⁵	rCNT1, hCNT1, hCNT3	es	HIV	[2, 63, 66, 109, 224]
Purine nucleoside analogs				
Cladribine ⁶	hCNT2, hCNT3	hENT1, hENT2	Hairy-cell leukemia	[2, 74, 225]
Fludarabine ⁷	hCNT2, hCNT3	hENT1, hENT2	Leukemia, lymphoma	[2, 74, 225]
Pentostatin ⁸	ND ¹	es		
Vidarabine ⁹	hCNT2	es, ei	Herpes virus	[74, 226, 227]
Ganciclovir	ND ¹	es		[228, 229]
Didanosine ¹⁰	rCNT2	es	HIV	[198, 223]

¹Not determined; ²also called floxidine; ³5-fluoro-5'-deoxyuridine; ⁴also called ddC; ⁵also called AZT; ⁶also called CdA; ⁷also called F-araA; ⁸also called 2'-deoxycoformycin; ⁹also called araA; ¹⁰also called ddl

¹¹Included are nucleoside drugs for which transport has been established either directly by measuring fluxes of the process (i.e., es and ei process) or indirectly by showing inhibition of drug action by simultaneous exposure to NBMPR. Drugs tested for transportability by recombinant proteins are shown with transporter names (i.e., hENT1, hENT2)

Table I-2. Nucleoside transport processes and their corresponding proteins in human cells

Transport process	Permeant selectivity	Na ⁺ / nucleoside stoichiometry	Transport protein	Reference	
<i>Trivial</i>	<i>Numerical</i>				
Concentrative transporters			CNT family		
<i>cif</i> ⁴	N1	Purine nucleosides & uridine	1:1	hCNT2 ¹	[131, 132]
<i>cit</i> ⁵	N2	Pyrimidine nucleosides & adenosine	1:1	hCNT1	[133]
<i>cit</i> ⁵	N4	Pyrimidine nucleosides & adenosine & guanosine	ND ²	ND ²	[119, 230]
<i>cib</i> ⁶	N3	Purine & pyrimidine nucleosides	2:1	hCNT3	[2, 134, 231]
<i>cs</i> ⁷	N5	Formycin B, cladribine, fludarabine	ND ²	ND ²	[120]
<i>csg</i> ⁸	N6	Guanosine	ND ²	ND ²	[121]
Equilibrative transporters			ENT family		
<i>es</i> ⁹	NA ³	Purine & pyrimidine nucleosides	NA ³	hENT1	[135]
<i>ei</i> ¹⁰	NA ³	Purine & pyrimidine nucleosides & nucleobases	NA ³	hENT2	[136-139]

¹Also named hSPNT

²Not determined

³Not applicable

⁴letters designate concentrative, insensitive to NBMPR, formycin B selectivity

⁵letters designate concentrative, insensitive to NBMPR, thymidine selectivity

⁶letters designate concentrative, insensitive to NBMPR, broad selectivity

⁷letters designate concentrative, sensitive to NBMPR

⁸letters designate concentrative, sensitive to NBMPR, guanosine selectivity

⁹letters designate equilibrative, sensitive to NBMPR

¹⁰letters designate equilibrative, insensitive to NBMPR

Table I-3. Tissue and cellular distribution of concentrative and equilibrative nucleoside transporters in mammals

Transporter	Transport process	mRNA expression	Reference	Functional activity	Reference
CNT2	<i>cif</i>	intestine, liver kidney, brain, placenta, lung, skeletal muscle, pancreas, heart, stomach,	[131, 132, 168, 182]	liver, intestine, kidney, macrophage, monocytes, L1210 leukemic cells, spleen	[119, 123, 124, 126, 127, 196, 232-235]
CNT1	<i>cit</i>	liver, placenta, brain, kidney, intestine	[63, 132, 168, 182]	intestine, kidney	[119, 123, 196, 233-235]
CNT3	<i>cib</i>	intestine, kidney, liver, heart, lung, pancreas, prostate, testis, trachea, mammary gland, placenta, bone marrow, brain, HL-60 cells	[2, 180]	choroid plexus, microglia	[128, 129, 236]
NA ¹ ENT1	<i>cit/N4</i> <i>es</i>	ND ² expressed in most tissues & cells	ND ² [135, 168]	kidney produced in most tissues and cells	[119, 125] [15, 53]
ENT2	<i>ei</i>	intestine, kidney, heart, lung, colon, prostate, pancreas, salivary gland, thyroid gland, thymus, heart, skeletal muscle, brain	[136, 137, 162, 168, 169]	brain, epididymis, intestine, Walker 256 rat carcinosarcoma cells, S49 mouse lymphoma cells, HeLa cervical cancer cells, umbilical vein endothelial cells, K562 erythroleukemia cells, BeWo choriocarcinoma cells	[144, 153, 154, 160, 170-173, 237]

¹Not applicable

²Not determined

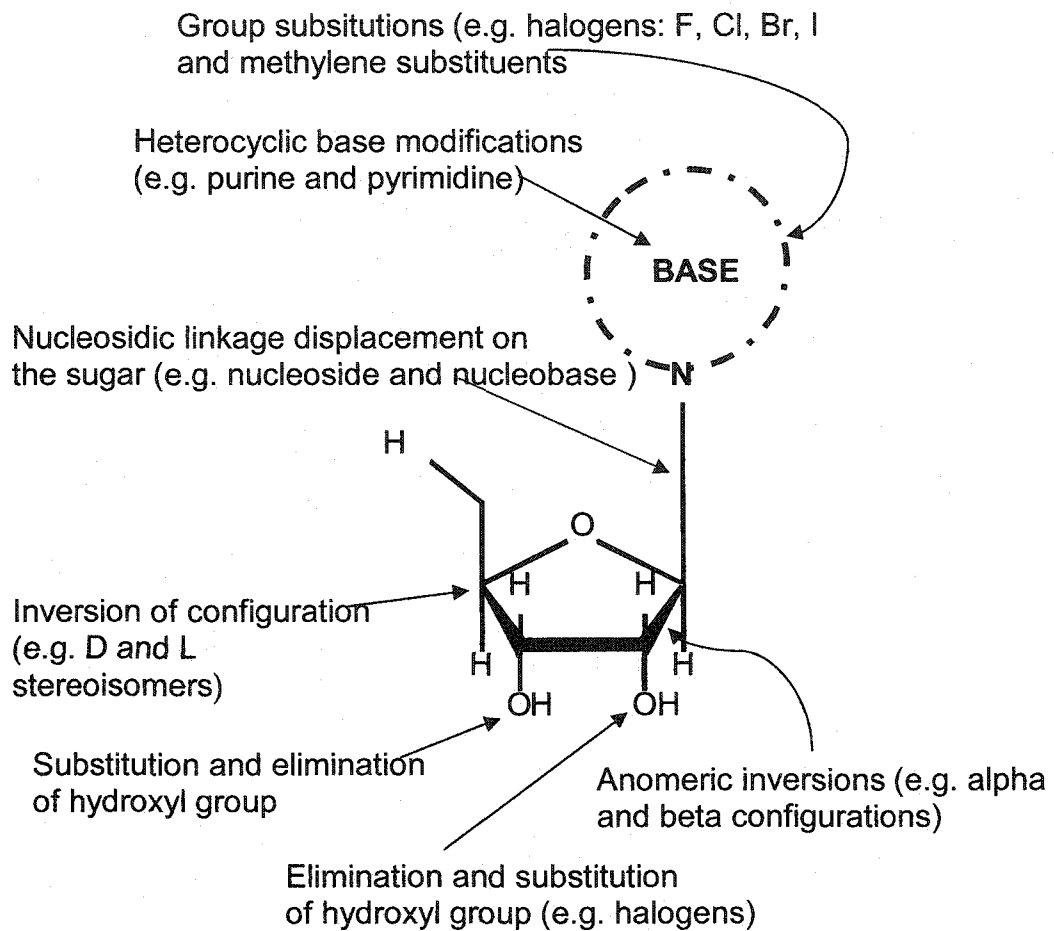


Figure I-1. Main structural modifications to transform a natural nucleoside into a nucleoside analog

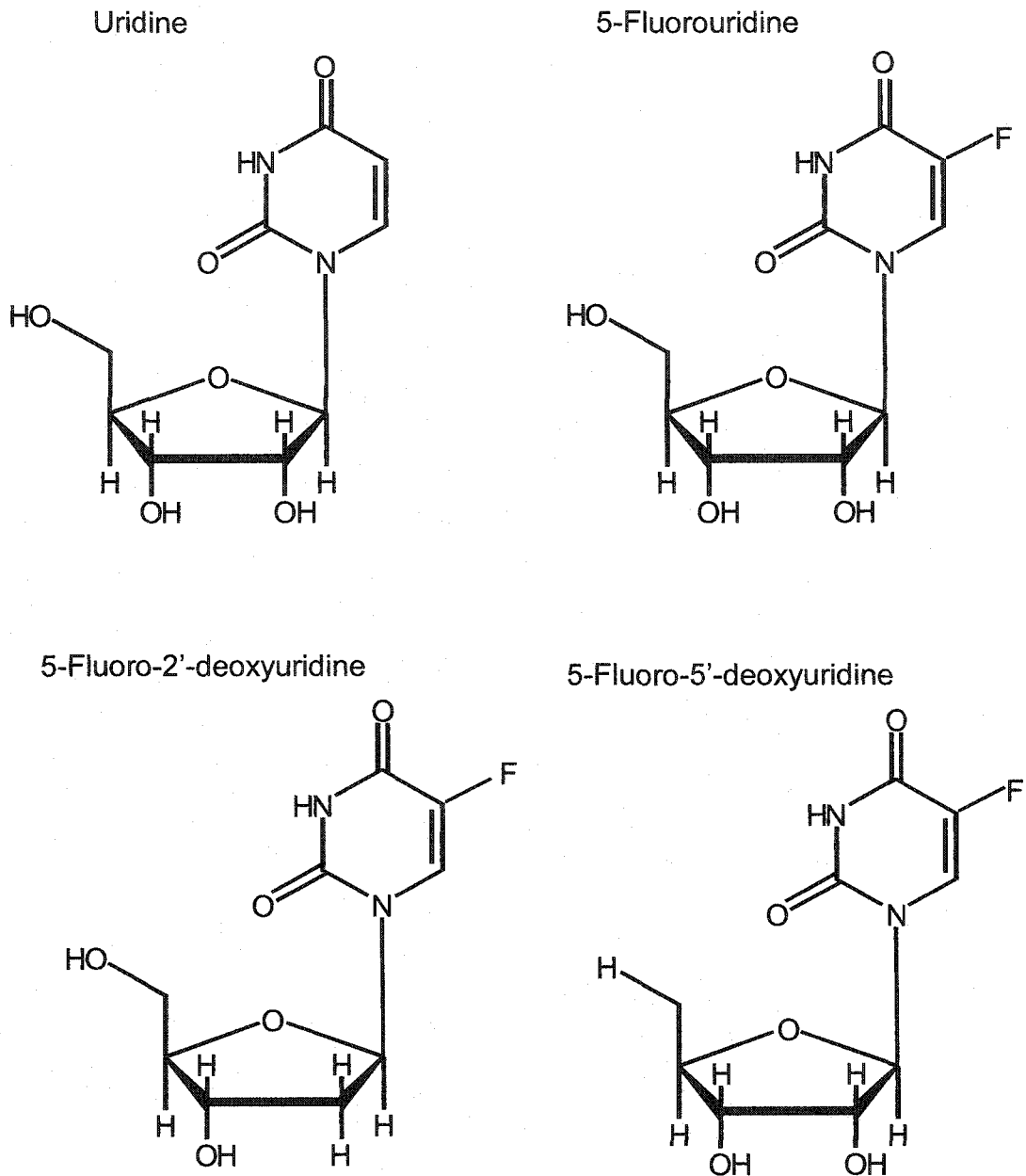


Figure I-2. Chemical structures of uridine and several fluorinated-uridine analogs (5-fluorouridine, 5-fluoro-2'-deoxyuridine and 5-fluoro-5'-deoxyuridine) used in gastrointestinal cancers

Depicted are the chemical structures of uridine and three treatment derivatives (5-fluorouridine (FUrd), 5-fluoro-2'-deoxyuridine (FdUrd, floxidine) and 5-fluoro-5'-deoxyuridine (dFUrd))

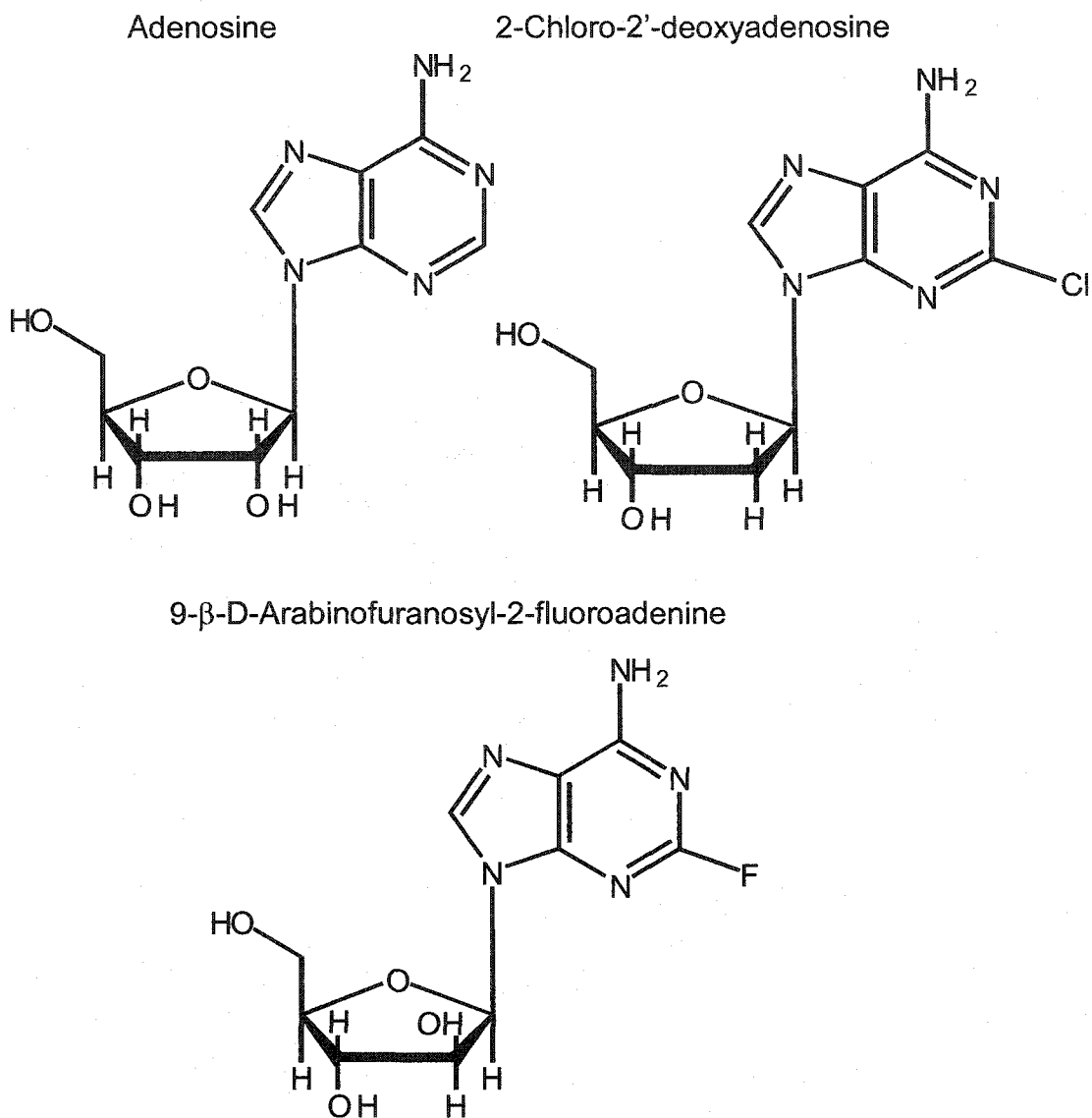


Figure I-3. Chemical structures of the natural nucleoside adenosine and its analogs cladribine and fludarabine employed in treatment of different types of human leukemia

Depicted are the chemical structures of adenosine and two purine-based derivatives 2-chloro-2'-deoxyadenosine (cladribine, CdA) and 9-β-D-arabinofuranosyl-2-fluoroadenine (fludarabine, F-araA).

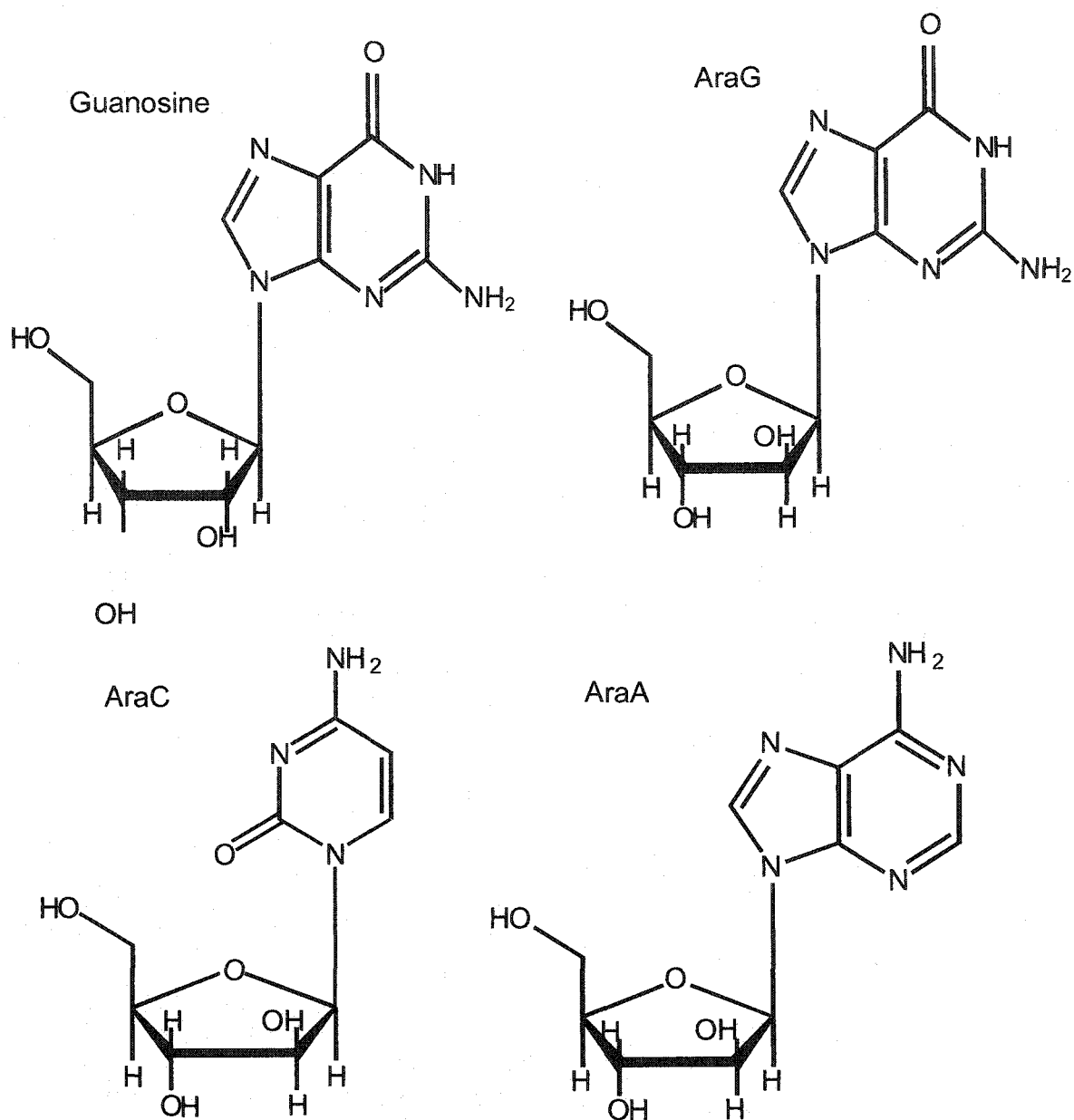


Figure I-4. Chemical structures of guanosine and arabinonucleosides used in the treatment of leukemias and viral diseases

Depicted are the chemical structures of guanosine and two purine-based arabinonucleosides araG (9- β -D-arabinofuranosylguanine), araA (9- β -D-arabinofuranosyladenine, vidarabine) and the pyrimidine-based arabinonucleoside araC (1- β -D-arabinofuranosylcytosine, cytarabine).

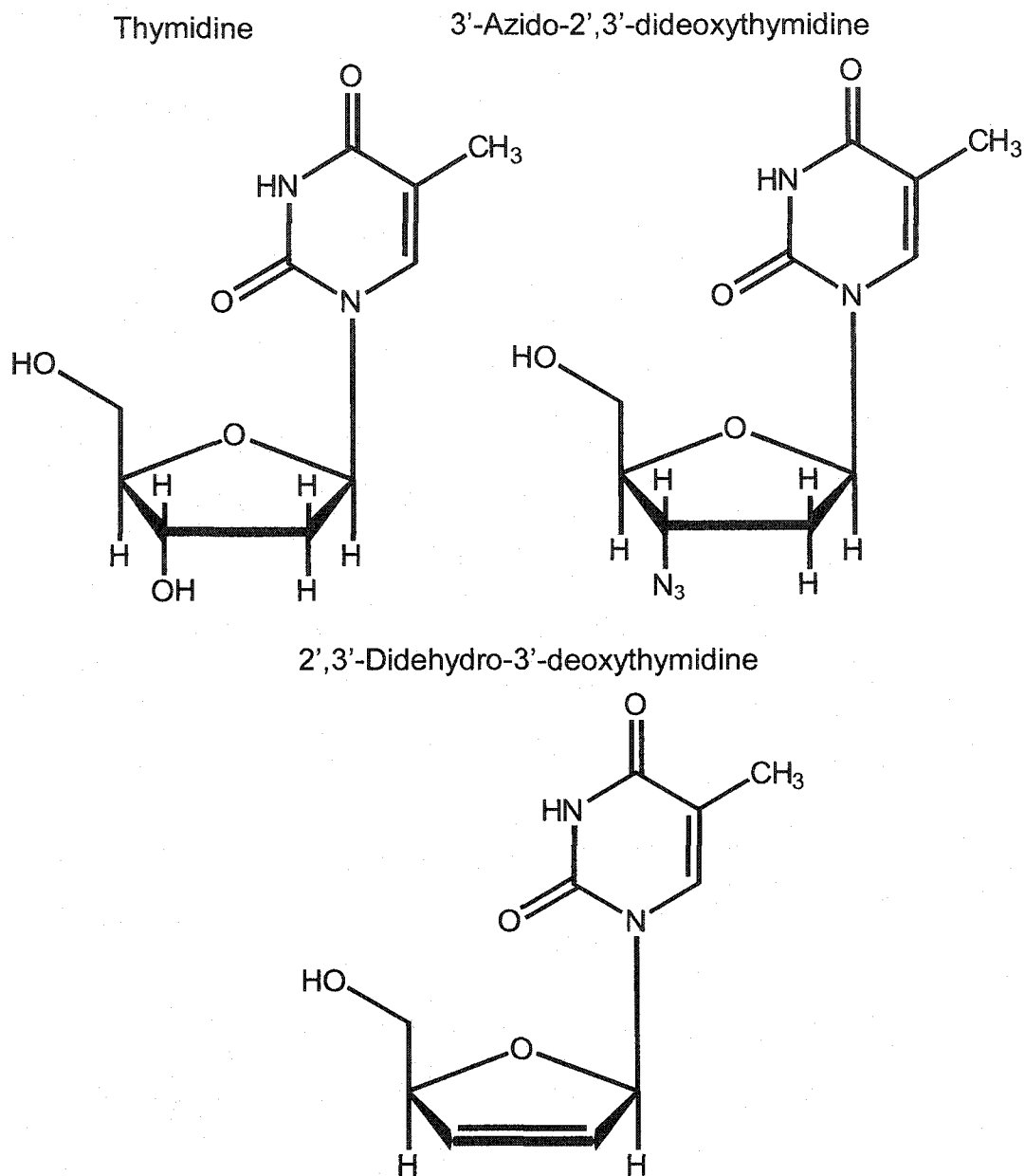
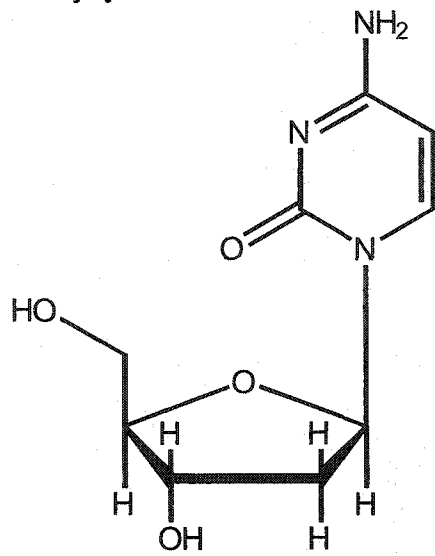


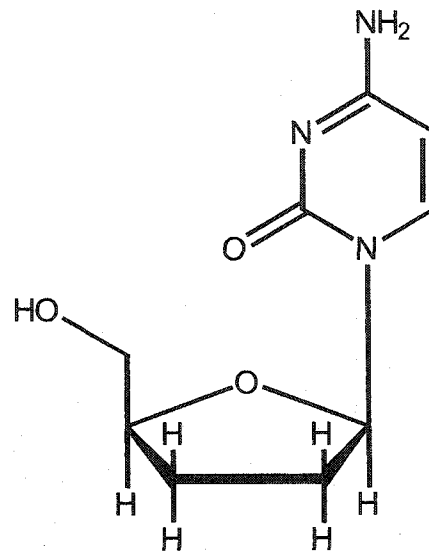
Figure I-5. Chemical structures of thymidine and its analogs used in treatment of human immunodeficiency virus (HIV)

Depicted are the chemical structures of thymidine, 3'-azido-2',3'-dideoxythymidine (zidovudine, AZT) and 2',3'-dideohydro-3'-deoxythymidine (stavudine, d4T).

2'-Deoxycytidine



2',3'-Dideoxycytidine



(-)-2',3'-Dideoxy-3'-thiacytidine

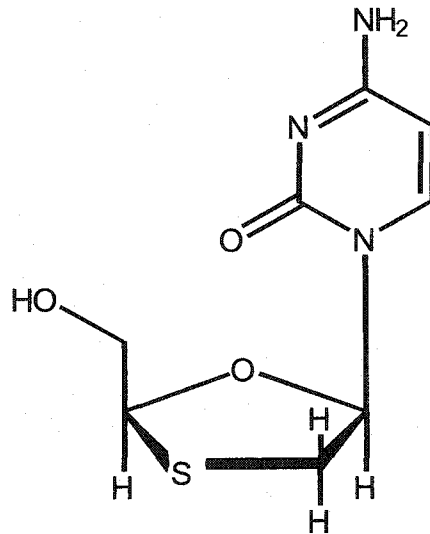


Figure I-6. Chemical structures of 2-deoxycytidine and its analogs used in treatment of human immunodeficiency virus (HIV)

Depicted are the chemical structures of cytidine, (-)-2',3'-dideoxy-3'-thiacytidine (lamivudine, 3TC) and 2',3'-dideoxycytidine (zalcitabine, ddC).

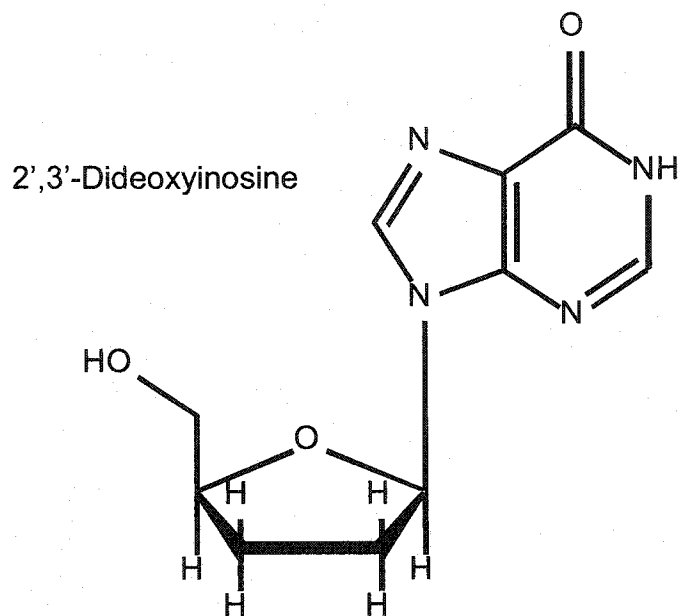
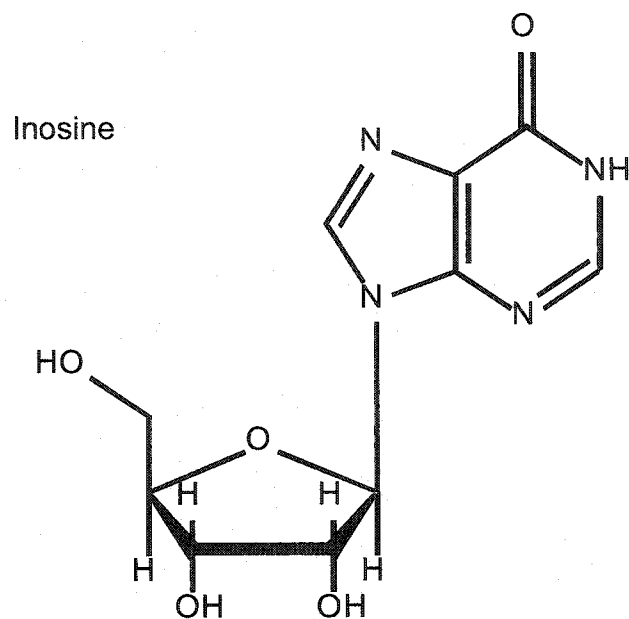


Figure I-7. Chemical structures of inosine and its analog 2',3'-dideoxyinosine used in treatment of human immunodeficiency virus (HIV)

Depicted are the chemical structures of inosine and 2',3'-dideoxyinosine (didanosine, ddl).

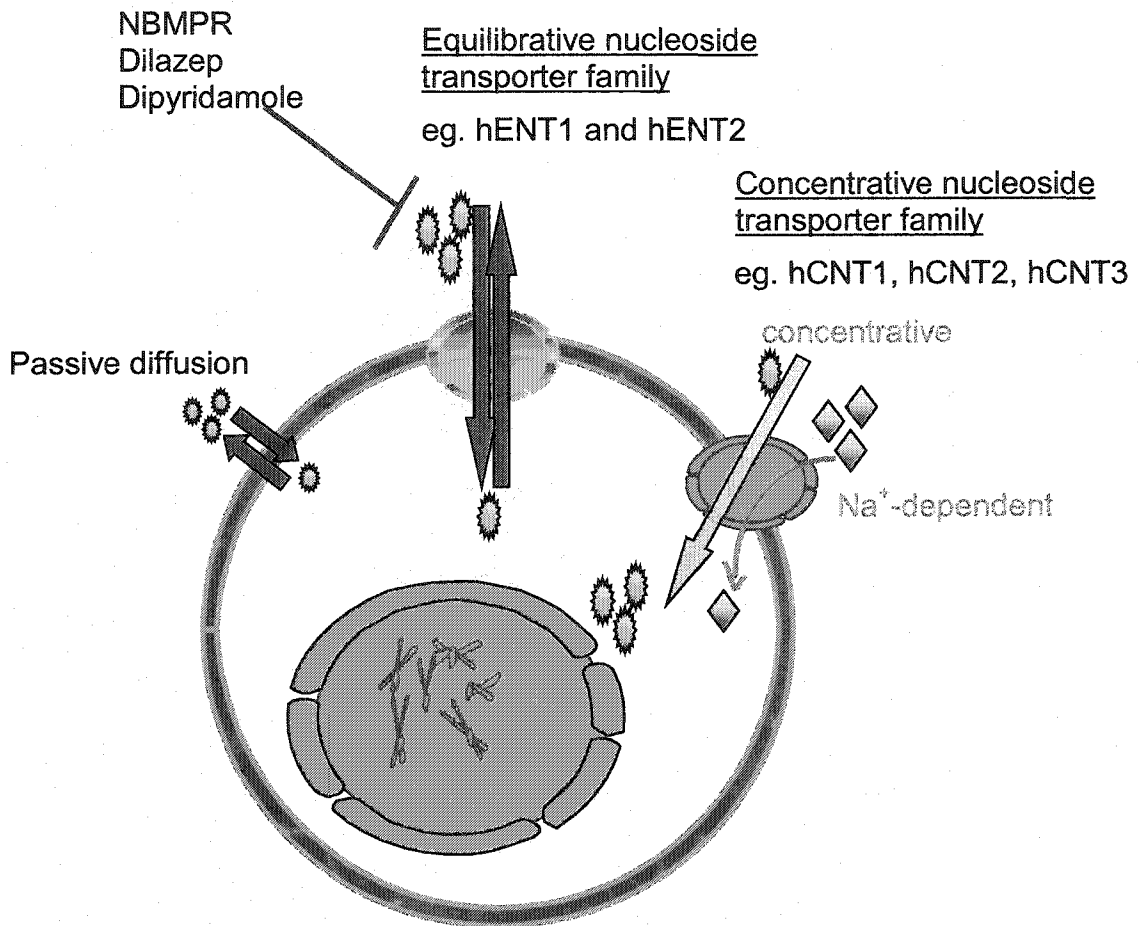


Figure I-8. Nucleoside permeation into human cells via different routes

Shown are the various routes of entry into mammalian cells for a variety of nucleosides and nucleoside drugs.

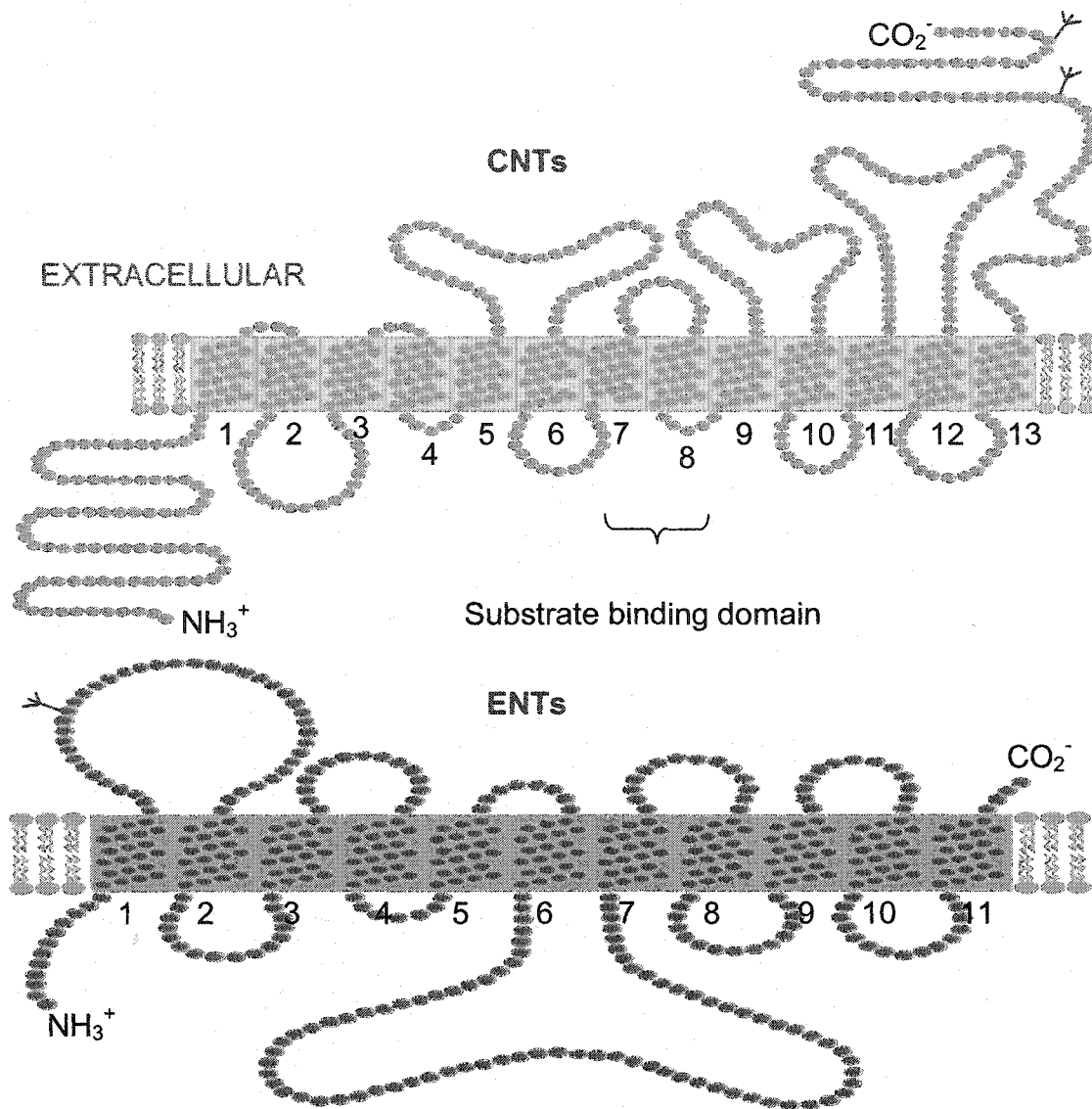



Figure I-9. Structural characteristics of CNTs and ENTs

Shown are the typical architectural designs of hCNTs (e.g. hCNT1, hCNT2) and hENTs (e.g. hENT1, hENT2). Predicted glycosylation of asparagine residue as shown in the hCNT topology model () is based on experimental evidence of the rat homolog rCNT1, indicating that the carboxyl terminus is extracellular [141]. Transmembrane domains 7 and 8 of CNTs implicated in substrate binding are indicated [177]. Glycosylation of asparagine⁴⁸ of hENTs as indicated is based on glycosylation scanning mutagenesis studies of hENT1 [142]. Adapted from Baldwin *et al.* [140].

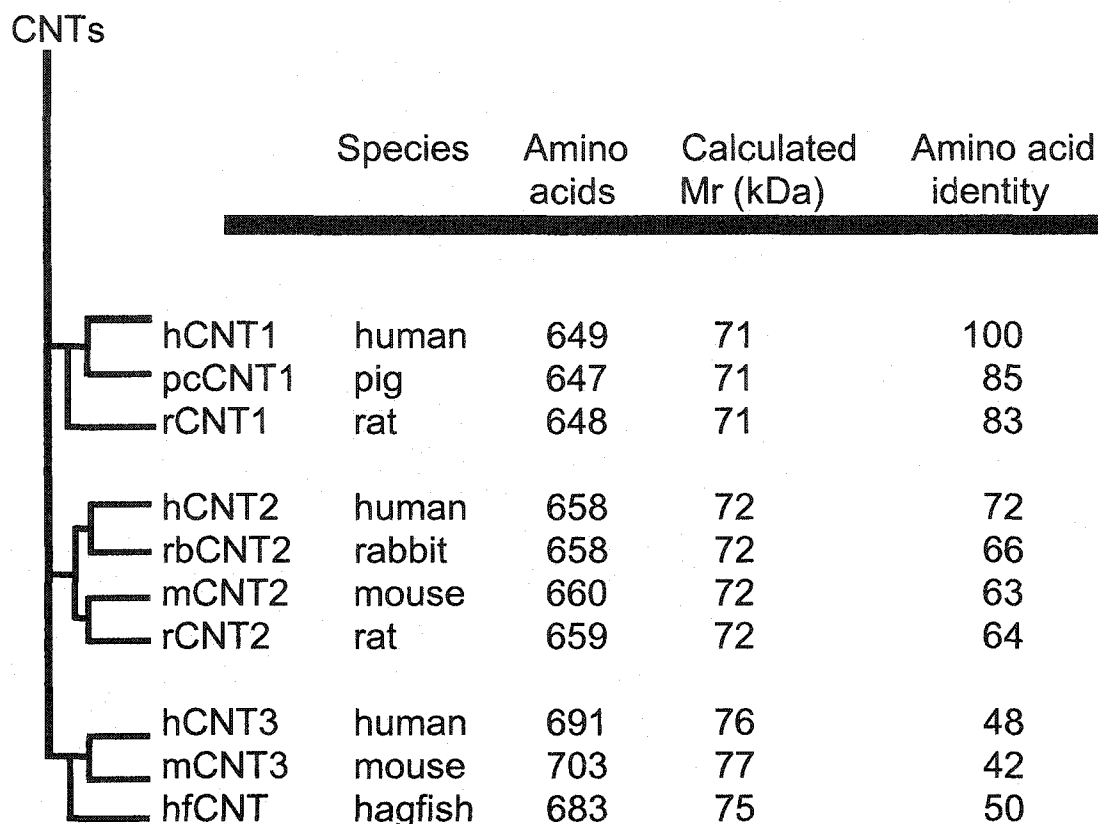


Figure I-10. Relationships among functionally characterized members of the vertebrate concentrative nucleoside transporter family

The amino acid sequences of functionally characterized members of the CNT family were deduced from the nucleotide sequences obtained from GenBank data bases. The sequences of CNT proteins were aligned using the BESTFIT program of the University of Wisconsin Genetics Computer Group (GCG, Madison, WI, USA) for the UNIX operating system. The properties of CNT proteins were determined using PepTool software and shown are the calculated Mr (molecular mass, kDa) and percent amino acid identities. Phylogenetic tree of functionally characterized CNT family members was constructed employing ClustalW software and grouped into evolutionary tree using GCG Pileup and Growtree software.

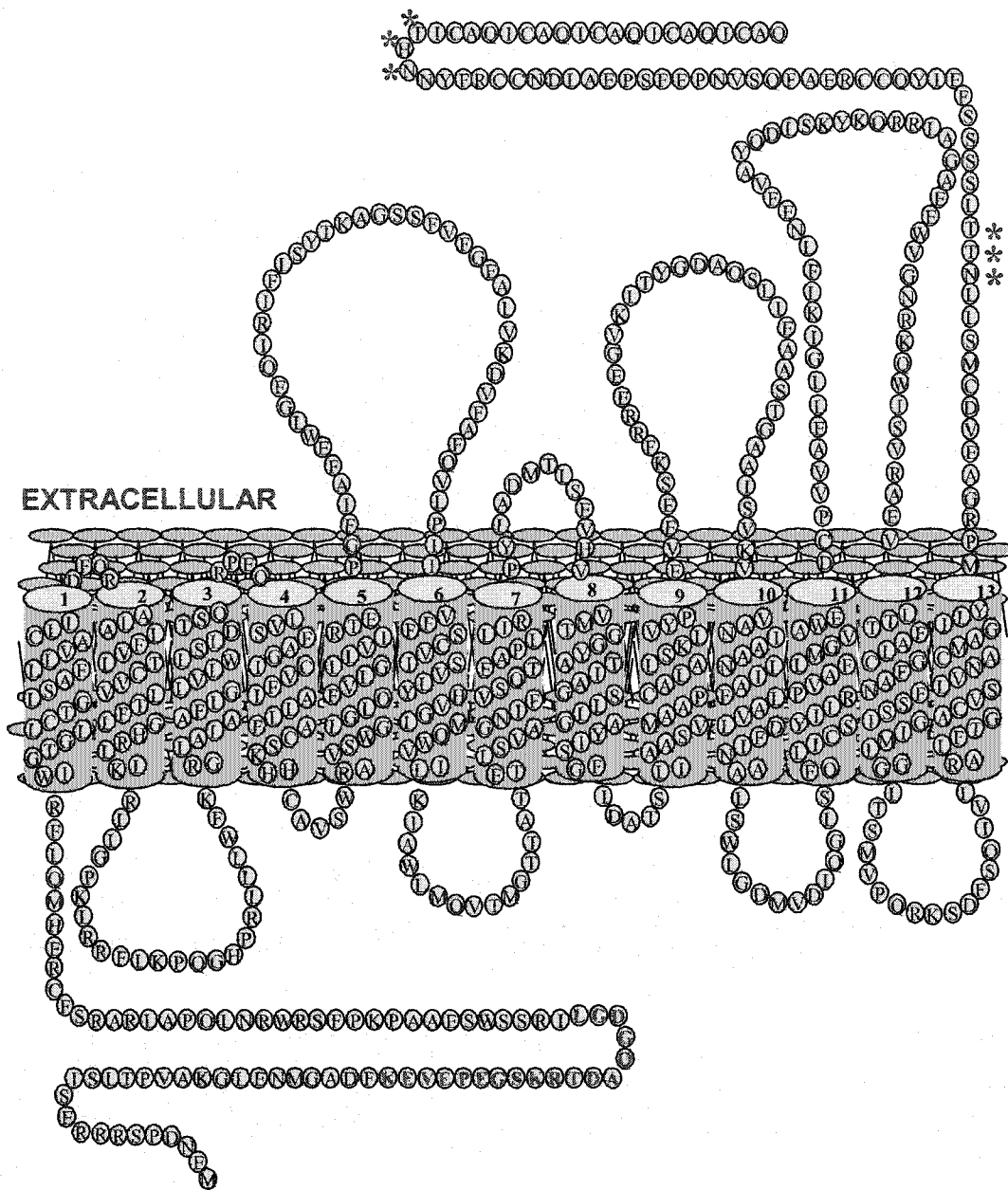


Figure I-11. Predicted topological model of hCNT2

Depicted is the predicted topology model of hCNT2 generated using TopPredII protein structure analysis software and TopPredII calculations for polytopic membrane proteins. hCNT2 is predicted to possess 13 transmembrane domains and the potential N-linked glycosylation consensus sites are indicated (***) . Letters represent amino acid residues. Shown is the synthetic peptide epitope (in red, bold characters) employed in generating anti-hCNT2 polyclonal and monoclonal antibodies (described in Chapter V). Adapted from Hamilton *et al.* [141].

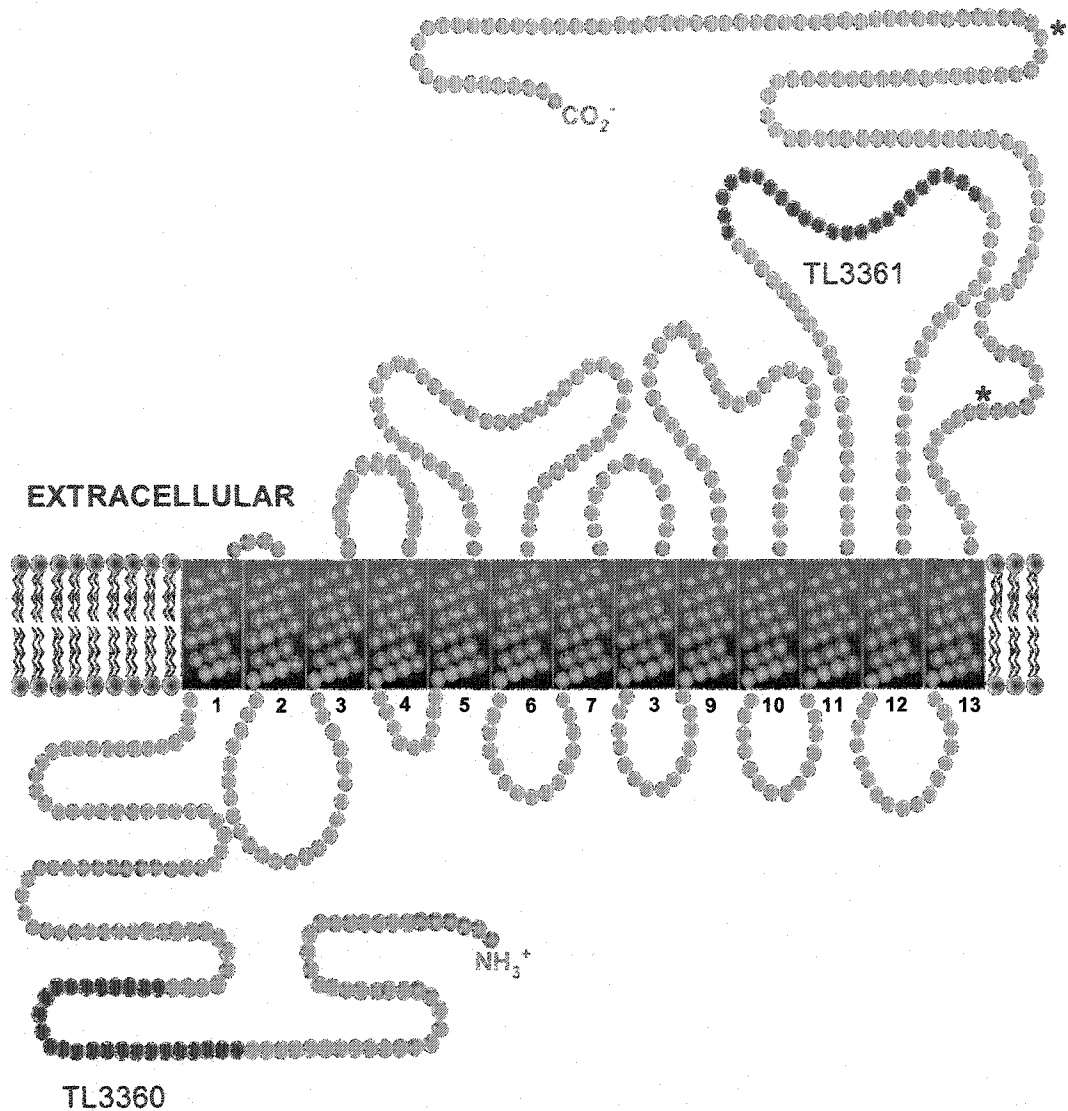


Figure I-12. Proposed topological model of hCNT3 indicating the major landmarks

Depicted is the predicted topology model of hCNT3 produced using the TopPredII protein structure analysis software and TopPredII calculations for polytopic membrane proteins (as described in Chapter V). hCNT3 is predicted to possess 13 transmembrane domains and the potential N-linked glycosylation consensus sites are indicated (*) at asparagine⁶³⁶ and asparagine⁶⁶⁴. Shown (in red, bold characters) are the synthetic peptide epitopes (TL3360, TL3361) employed to generate anti-hCNT3 polyclonal and monoclonal antibodies (described in Chapter V).

Chapter II

II. Materials and Methods

II.1. Materials

Radioisotopes were purchased from Moravsek Biochemicals Inc. (Brea, CA) and ^3H -nucleosides were purified by high-performance liquid chromatography using water-methanol gradients on a C18 reverse-phase column. All chemicals were of analytical grade and obtained from either Sigma-Aldrich (Oakville, ON), Fisher Scientific (Nepean, ON) or the Cross Cancer Institute Pharmacy (Edmonton, AB), unless otherwise stated. Dilazep employed in earlier experiments was a gift from F. Hoffman La Roche and Co. (Basel, Switzerland) and in later experiments was purchased from Sigma-Aldrich. Cell culture supplies were from Gibco BRL. The adenosine A1 receptor rabbit polyclonal antibodies (A-268) were purchased from Sigma (St. Louis, MI). All peroxidase-conjugated secondary antibodies and Cy5-conjugated goat anti-rabbit secondary antibodies were purchased from Jackson Laboratories Inc. (West Grove, PA). All Alexa Fluor secondary antibodies, Alexa Fluor 488 phalloidin, DIOC5 (3',3'-dipentylloxacarbocyanine iodide) endoplasmic reticulum dye and DNA-intercalating agent 4',6-diamidino-2-phenylindole (DAPI) used for immunofluorescence were purchased from Molecular Probes (Eugene, OR). Anti-CD3 (fluoroisothiocyanin) FITC conjugated monoclonal antibodies were a gift from Dr. Linda Pilarski (Oncology, University of Alberta). The enhanced chemiluminescence (ECL) and ECL PLUS detection kits were purchased from Amersham Pharmacia Biotech Inc. (Dorval, PQ). Polyvinylidene fluoride (PVDF) membranes were purchased from Millipore (Bedford, MA). COMPLETE

protease inhibitor tablets and DOSPER liposomal transformation reagent were purchased from Boehringer Mannheim (Lavel, PQ).

II.2. General molecular biology procedures

General molecular biology procedures were adapted from general procedures described by Ausubel *et al.* [238]. Transformation of Top10F' and JM109 strain *Escherichia coli* (Invitrogen, San Diego, CA) was, respectively, by the heat-shock method [238] or electroporation using a CELL-PORATOR (Gibco BRL, Rockville, MD) according to the manufacturer's instructions. Transformed *E. coli* were grown in Luria broth (1% (w/v) bacto-tryptone, 0.5% (w/v) bacto-yeast extract, 1% (w/v) NaCl, pH 7.0) with ampicillin (50 µg/ml) or kanamycin (100 µg/ml) at 37°C in a shaker at 200 RPM. *E. coli* stock cultures were stored (1:1) in freezing solution (65% glycerol, 0.1 M MgSO₄, 0.025 M Tris-Cl, pH 8.0) at -80°C.

Preparation of plasmid DNA was performed using Mini, Midi or Maxi Plasmid Purification Kits from Qiagen according to the manufacturer's instructions (Qiagen, Mississauga, ON). Microbiological media were purchased from Difco/BD Diagnostic Systems (Sparks, MD). Taq polymerase was purchased from Gibco/BRL Life Technologies (Burlington, ON) and Pwo polymerase was purchased from Boehringer Mannheim/Roche Molecular Biochemicals (Lavel, PQ). Restriction enzymes and T4 ligase were purchased from Gibco/BRL Life Technologies unless otherwise stated. DNA samples were resolved by electrophoresis on a 1% (w/v) agarose gel (Gibco/BRL Life Technologies) in Tris/acetate/EDTA electrophoresis buffer (Tris-acetate, 2 mM

Na₂EDTA·2H₂O, pH 8.5) alongside 1-kb DNA molecular weight markers (Gibco/BRL Life Technologies)

II.2.1. DNA primers and DNA sequencing

DNA primers were synthesized using Perkin Elmer/Applied Biosystems DNA Synthesizers (Foster City, CA). DNA for use as template in DNA sequencing was prepared using the Qiagen Plasmid Purification kit (Qiagen Corp., Mississauga, ON) according to the manufacturer's instructions. DNA sequences were determined by *Taq* DyeDeoxy terminator cycle sequencing with an automated Model 310 DNA sequencer (Applied Biosystems, Foster City, CA). DNA sequencing results were analyzed using EditView/AutoAssembler software (Applied Biosystems). Sequence alignments were generated using MacVector™ DNA analysis software (Oxford Molecular, Madison, WI).

II.3. Plasmid construction

II.3.1. pcDNA3/LacZ

The LacZ open reading frame was excised from pcDNA1-AMP/LacZ (Invitrogen, Carlsbad, CA) using HindIII and XhoI restriction enzymes and subcloned into pcDNA3 (Invitrogen).

II.3.2. pcDNA3/hCNT1

The open reading frame of hCNT1 was PCR-amplified using hCNT1 cDNA in the original cloning vector, pGem (Clontech, Palo, Alto, CA) as template and the following 5'EcoRI- and 3'XbaI-containing primers (restriction sites

underlined): 5'-GGGAATTCATGGAGGAACCTGCAGCCAGCCCTG-3' and 5'-CCTCTAGATCACTGTGCGCAGATCGTGTG-3'. The EcoRI-hCNT1-XbaI fragment was subcloned into the polylinker region downstream of the enhancer/promoter sequences of the immediate early gene of human cytomegalovirus of the mammalian expression vector pcDNA3 (Invitrogen). The vector map of pcDNA3 is shown in Figure II-1. The structure of pcDNA3/hCNT1 was verified by restriction endonuclease mapping and DNA sequencing. pcDNA3/hCNT1 was transformed into Top10F' *E. coli* by the heat-shock method and plasmid DNA for use in transfections was prepared using the Qiagen Maxi Plasmid Purification Kit (Qiagen) according to the manufacturer's instructions.

II.3.3. pcDNA3/hCNT2

The open reading frame of hCNT2 [132] was excised from the original cloning vector, pBluescript II KS(+) (Stratagene, La Jolla, CA), using EcoRI and XbaI restriction enzymes and subcloned into the polylinker region downstream of the enhancer/promoter sequences of the immediate early gene of human cytomegalovirus of the mammalian expression vector pcDNA3 (Invitrogen). The structure of pcDNA3/hCNT2 was verified by restriction endonuclease mapping and DNA sequencing. pcDNA3/hCNT2 was transformed into electrocompetent JM109 *E. coli* (Invitrogen) and plasmid DNA for use in transfections was prepared using the Qiagen Maxi Plasmid Purification Kit (Qiagen) according to the manufacturer's instructions.

II.3.4. pGFP-C1/hCNT3

The open reading frame of hCNT3 was PCR-amplified using hCNT3 cDNA in the original cloning vector pBluescript II KS(+) (Stratagene) as template and the following 5'BglIII and 3'XhoI containing primers (restriction sites underlined): 5'- CCAGATCTATGGAGCTGAGGAGTACAGCAGCCC-3' and 5'- GGCTCGAGTCAAAATGTATTAGAGATCCCATTGCAGT-3'. The BglIII-hCNT3-XhoI fragment was subcloned into the polylinker in frame with the upstream GFP open reading frame and the cytomegalovirus promoter of pGFP-C1 (Clontech). The GFP stop codon was replaced by the polylinker and therefore hCNT3 was produced as a fusion protein with hCNT3 at the C-terminus of GFP. The vector map of pGFP-C1 is shown in Figure II-2. The structure of pGFP-C1/hCNT3 was verified by restriction endonuclease mapping and DNA sequencing. pGFP-C1/hCNT3 was transformed into electrocompetent JM109 *E. coli* (Invitrogen) and plasmid DNA for use in transfections was prepared using the Qiagen Maxi Plasmid Purification Kit (Qiagen) according to the manufacturer's instructions

II.3.5. pcDNA3/hCNT3

The open reading frame of hCNT3 was excised from pGFP-C1/hCNT3 using BglIII and XhoI restriction enzymes and subcloned into pcDNA3 (Invitrogen) using compatible restriction sites BamHI and XhoI. The structure of pcDNA3/hCNT3 was verified by restriction endonuclease mapping and DNA sequencing. pcDNA3/hCNT3 was transformed into Top10F' *E. coli* by the heat-shock method and plasmid DNA for use in transfections was prepared using the

Qiagen Maxi Plasmid Purification Kit (Qiagen) according to the manufacturer's instructions.

II.4. Southern blot analysis

Genomic DNA was prepared from cells by the proteinase K-RNase method [249], cleaved with EcoRI (Gibco BRL), subjected to electrophoresis on a 0.8% agarose gel with size markers (1-kb DNA ladder, Gibco BRL) and transferred to Hybond-N⁺ membranes (Amersham, Piscataway, NJ). The hybridization probes were prepared by (i) PCR amplification of the full length hCNT2 cDNA from pcDNA3/hCNT2, (ii) separation on agarose gels, (iii) purification on a G10 sepharose column, (iv) ³²P radiolabeling using a Pharmacia random primer oligolabeling kit (5 x 10⁸-10⁹ dpm/μg of DNA), and (v) purification by gel filtration chromatography on a Nick Column (Pharmacia). Hybridization was conducted under high stringency (65°C, 1 h) using Express Hybridization solution (Pharmacia) according to the manufacturer's instructions. Autoradiography was carried out by exposure to Kodak X-OMAT XAR film at -80°C.

II.5. RNA preparation and northern blot analysis

Total RNA was prepared from 10⁷ actively proliferating tissue culture cells using either TRIzol reagent (Gibco/BRL Life Technologies) or Qiagen Rneasy total RNA isolation columns according to the manufacturers' instructions. RNA samples (15-20 μg) were heated at 60°C for 10 min and combined with loading buffer (0.25% bromophenol blue (w/v), 0.25% xylene cyanol (w/v), 50% glycerol (v/v), 1 mM EDTA). RNA was resolved by electrophoresis on a denaturing 1%

(w/v) agarose/formaldehyde gel and transferred to Hybond-N membranes (Amersham, Oakville, ON) by upward capillary transfer [249]. RNA was UV-crosslinked to the Hybond-N membranes by StrataLinker (Stratagene Corp.). Hybridization ^{32}P -probes were prepared by random primer labeling of cDNA fragments using a T7 Quick Prime Kit according to the manufacturer's instructions (Pharmacia, Dorval, PQ). Hybond-N membranes were incubated with ^{32}P -probes in ExpressHyb solution according to the manufacturer's instructions (Clontech, Palo Alto, CA). The membranes were washed 3 times at 37°C in 2X SSC (standard sodium citrate, 0.3M sodium chloride, 0.03M sodium citrate)/0.1% SDS and in 0.1X SSC/0.1% SDS. The hybridization complexes were detected by exposure to Kodak X-OMAT XAR film (Kodak) at -80°C.

II.6. Reverse transcription-polymerase chain reaction (RT-PCR) analysis

Poly(A)⁺ RNA was isolated from actively proliferating cells using the FastTrack 2.0 Isolation Kit (Invitrogen, Carlsbad, CA) according to the manufacturer's instructions. mRNA concentrations were determined spectrophotometrically. For cDNA synthesis reactions, Superscript RT kits (Gibco BRL) were used following the manufacturer's instructions. Oligonucleotide primers specific for hENT1 were ES2 and ES4, which corresponded, respectively, to hENT1 cDNA residues 4-21 (sense, 5'-CACCATGACAACCAGTCACCAGCCT-3', start codon underlined) and ⁺414-⁺437 (antisense, 5'-GACCTGATATACTCCATTCTCC-3') derived from the 3'-

untranslated regions. Oligonucleotide primers specific for hCNT2 were NT2D and JM23, which corresponded, respectively, to residues 1528-1549 (sense, 5'-GGAATGGAGGAGTGGATGAGG-3') and 1949-1971 (antisense, 5'-GCTGTGGATTCTACAACAATACC-3'). Nested-PCR was performed on "first-round" hCNT2 products using NT2KG25 and NT2KG26 internal primer sets, which corresponded, respectively, to residues 1562-1584 (sense, 5'-GGATTTCTGTGAGAGCTGAAATC-3') and 1920-1939 (antisense, 5'-GAATTTCAATGCTATGGCCC-3'). Amplifications were performed on a Robocycler Temperature Cycler (Stratagene) as follows: 5 min at 94°C, 25 cycles (94°C for 1 min, 57°C for 2 min, 72°C for 2 min) and 20 min at 72°C. PCR products were subjected to electrophoresis on a 1% agarose gel with size markers (1-kb DNA ladder, Gibco BRL) and bands that migrated with the expected mobilities of hENT1 and hCNT2 were excised, gel-purified and sequenced in one direction for confirmation of identity.

II.7. Taqman real-time quantitative RT-PCR

Taqman PCR was performed in which cDNAs were used as templates to quantify the relative levels of transporter transcripts present by detection of PCR products in real-time using the Taqman 7700 sequence detection system (Applied Biosystems). Total RNA was isolated from 10^7 actively proliferating cells using RNeasy Columns (Qiagen, Mississauga, ON) according to the manufacturer's instructions. The cDNA was synthesized by reverse transcription using the Applied Biosystems Reverse Transcription Kit (Applied Biosystems, Foster City, CA) following the manufacturer's instructions. The Taqman

Universal Master Mix Kit (Applied Biosystems) was used to prepare reactions with triplicate samples for real-time PCR, in which cDNA (2 μ l) was mixed with 2X Universal PCR Master Mix (25 μ l), primers (300 μ M) and probes (100 μ M) in a total volume of 50 μ l. Cycling conditions were as recommended by the manufacturer (1 cycle each of 2 min at 50°C and 10 min at 95°C, followed by 40 cycles of 15 sec at 95°C and finally 1 min at 60°C).

The DNA probes for Taqman reactions were purchased from Applied Biosystems and Biosource International (Camarillo, CA). The probe and primer-combinations for glyceraldehyde-3-phosphate dehydrogenase (GAPDH), which was used in control reactions, were purchased from Applied Biosystems as a Taqman RNA Control Reagent Kit (Applied Biosystems). The DNA primers specific for human CNTs and ENTs were designed with Primer Express software (Applied Biosystems). The sequence of primers and probes employed to detect hENT1, hENT2, hCNT1, hCNT2 and hCNT3 are shown in Table II-1.

The data are expressed in cycle threshold values (Ct). The Ct value is the PCR cycle number at which the accumulated fluorescent signal in a particular reaction crossed a threshold level of fluorescence above background; the threshold was set within the linear phase of the exponential PCR reaction. Validation assays (Applied Biosystems, User Bulletin 2) with nucleoside transporter and GAPDH cDNAs demonstrated that they were amplified with equal efficiencies (K. Graham, S. Perdue, D. Mowles, C. Santos, J. Mackey, C. Cass, Unpublished results). The relative quantitation of transcripts was determined using GAPDH as an internal control to correct for differences in RNA

concentrations by subtracting the Ct values for GAPDH (Applied Biosystems, User Bulletin 2). The results were normalized to the expression level of an arbitrary reference (i.e., $\Delta Ct - \Delta Ct_{\text{reference}} = \Delta\Delta Ct$) and presented as the value obtained from the equation $2^{-\Delta\Delta Ct}$.

II.8. SDS-polyacrylamide gel electrophoresis and immunoblotting

Membrane preparations or cell extracts were solubilized in an equal volume of sample loading buffer (4% SDS (w/v), 20% glycerol (v/v), 2% β -mercaptoethanol (v/v), 0.01% bromophenol blue (w/v), 20 mM Tris-HCl pH 6.8), heated at 70°C for 5 min and subjected to SDS-polyacrylamide gel electrophoresis (SDS-PAGE) following the method of Laemmli as described in Ausubel *et al.* [238, 239]. Samples were electrophoretically resolved using 10% SDS-polyacrylamide gels along with prestained protein markers (Biorad). Electrophoretically separated proteins were transferred to PVDF membranes by electroblotting at 200-400 mA constant current for 2-3 hr using a semi-dry electroblotter (Owl Scientific Inc., Portsmouth, NH) in 10 mM Tris, 100 mM glycine and 10% methanol (v/v). Transfer efficiency was verified by staining the PVDF membrane with non-permanent dye solution (diluted 1:10 with distilled water) of 2% Ponceau S (3-hydroxy-4-[2-sulfo-4-(sulfophenylazo)phenylazo]-2,7-naphthalene disulfonic acid) in 30% trichloroacetic acid and 30% sulfonosalicic acid.

Detection of proteins by immunoblotting [240, 241] was accomplished by subjecting PVDF membranes to the following order of steps: i) incubation overnight at 4°C with 5% skim milk powder (w/v) in TTBS (0.2% Tween 20, 20

mM Tris-HCl, pH 7.6 and 137 mM NaCl), ii) incubation for 2-3 hr at room temperature with primary antibodies diluted with 2% skim milk powder (w/v) in TTBS, iii) washing with TTBS over a period of 1-2 hr, iv) incubation for 1 hr with horseradish peroxidase conjugated secondary antibodies diluted with 2% skim milk powder (w/v) in TTBS, v) washing with TTBS over a period of 1-2 hr and vi) detection by enhanced chemiluminescence (ECL) or ECL Plus according to the manufacturer's instructions (Amersham-Pharmacia Biotech). Visualization was by exposure to Fuji RX film (Fuji Medical Systems, Stamford, CT).

Quantitation was by detection of chemifluorescence at 450 nm using a Typhoon 9400 Variable Mode Imager (Amersham-Pharmacia Biotech, Sunnyvale, CA) and importing electronic images into ImageQuant version 5.2 software (Amersham-Pharmacia Biotech) for data analysis. Individual bands were corrected for background signals and the signal intensities of bands were quantitatively determined by "Volume Analysis" (Typhoon User Guide, Amersham-Pharmacia Biotech). The "volume", which is the integrated intensity of all pixels in a particular band, was calculated and expressed in arbitrary units corresponding to the Typhoon signal detected. The resulting data were exported to Excel (Microsoft Corp.) and Prism (GraphPad Software Inc.) for further analysis and plotting.

II.9. Protein quantitation

Quantitation of protein content was by the bicinchoninic acid (BCA) assay method [242] using 96-well plates. Ten μ l portions of solution containing either i) unknown protein sample, ii) graded concentrations of bovine serum albumin

(Sigma) or iii) no protein was mixed with 200- μ l portions of BCA reagent (Sigma) and incubated at 37°C for 30 min according to the manufacturer's instructions. Absorbance of samples was determined at 600 nm using a 96-well plate reader and SOFTmax program (Molecular Devices). The protein content of unknown samples was determined from a standard curve constructed from the results obtained with bovine serum albumin.

II.10. Growth and maintenance of cell lines

Media, sera, antibiotics and collagen were obtained from either Gibco/BRL Life Technologies (Burlington, ON) or Sigma-Aldrich. Tissue culture flasks and plates were obtained from either Falcon (Becton Dickinson Labware, Franklin Lakes, NJ), Corning (Corning, NY) or Nunc (Roskilde, Denmark). Tissue culture bottles for suspension cultures were obtained from Gibco/BRL Life Technologies. Cells were grown as suspension or adherent cultures. A list of cell lines and their properties is shown in Table II-2.

Suspension cultures were subcultured at regular intervals (3-5 days) by dilution to 50,000 cells/ml in T-25 flasks or 50-ml tissue culture bottles. Adherent cultures were subcultured at regular intervals (3-7 days) by trypsinization and seeding at 1×10^5 cells/T-25 flask, unless otherwise stated. Cells were incubated at 37°C in a humidified (95%) atmosphere of 5% CO₂ in air, and cell numbers were determined using a Coulter Z2 electronic particle counter equipped with a size analyzer (Coulter Electronics, Burlington, ON). The cell lines used in this study were periodically demonstrated to be free of *Mycoplasma* by direct culture in agar/cell-free medium (Provincial Health Laboratory,

Edmonton, AB). Cell cultures ≥ 30 subculture generations were discarded (unless otherwise stated) and new cultures were started from mycoplasma-free, stock cultures stored in 10% dimethyl sulfoxide in growth medium in liquid nitrogen.

II.10.1. Suspension cell lines

K562 and NB4 cells were maintained in Roswell Park Memorial Institute (RPMI) 1640 (Gibco BRL) medium supplemented with 10% fetal bovine serum (FBS) (v/v). S49 and L-1210/B23.1 murine cells, which exhibit only *es* activity [243-245], were maintained in RPMI 1640 medium supplemented with 10% horse serum (HS) (v/v). AE1 cells, which were derived from S49 cells and are nucleoside transport-defective [237, 243, 245, 246], were maintained in Dulbecco's modified Eagle's medium (DMEM) (Gibco BRL) supplemented with 10% heat-inactivated horse serum (HIHS) (v/v). The CCRF-CEM (American Type Culture Collection CCL-119) cell line (hereafter referred to as CEM), which is a human T-lymphoblast line that was originally derived from a patient with acute lymphocytic leukemia, exhibits *es* nucleoside transport activity [75]. CEM-ARAC-8C (hereafter referred to as CEM-ARAC) is a nucleoside-transport defective subline that was selected for resistance to cytarabine by Dr. B. Ullman (Oregon Health Sciences University, Portland, OR) [214]. CEM and its derivatives were maintained in RPMI 1640 medium supplemented with 10% FBS (v/v) and, for CEM-ARAC cells, with 0.25 μM tubercidin and 0.5 μM cytarabine or, for stable transfectants (ARAC/D2, TLCT1 and TLET2), with 0.2 $\mu\text{g}/\mu\text{l}$ geneticin.

II.10.2. Adherent cell lines

HeLa S3 (hereafter referred to as HeLa) cells were maintained in RPMI 1640 medium supplemented with 10% calf serum (CS) (v/v). MCF7, MDA-MB-435S (hereafter referred to as 435S) and 180/1 cells were maintained in DMEM supplemented with 10% FBS (v/v). HEK 293 cells were maintained in DMEM supplemented with 5% FBS (v/v) and 5% CS (v/v). BeWo cells were maintained in RPMI 1640 medium supplemented with 10% FBS (v/v). Caco-2 cells (generations 25-40) were grown in DMEM supplemented with 20% FBS (v/v) on collagen-coated matrix using conditions adapted from Hidalgo *et al* [247]. Growth media were changed daily and cell were subcultured at weekly intervals on collagen-coated tissue culture Transwell polycarbonate membrane inserts (Nunc) or plates by dilution such that the initial population density was 30,000 cells/cm².

Primary cultures of human umbilical vein endothelial cells (HUVEC) were isolated from human umbilical cords using established procedures in the laboratory of Dr. Judith Hugh (Laboratory Medicine, Cross Cancer Institute, Edmonton). HUVEC were grown on 1% gelatin-coated tissue culture plates or flasks in growth medium composed of medium 199 (Gibco/BRL Life Technologies) supplemented with 20% fetal bovine serum (v/v), 100 mg endothelial cell growth supplement (Sigma), 4 mM L-glutamine and 10,000 units/ml penicillin/streptomycin solution (Gibco/BRL Life Technologies). Cords were rinsed twice with PBS and then incubated for 20 min with 0.2% collagenase in PBS. The cell suspension was collected, centrifuged and the cell pellet was

resuspended in medium 199 enriched with endothelial cell growth supplement, 100 µg/ml streptomycin, 100 units/ml penicillin, 0.25 µg/ml amphotericin and 20% FCS and plated on 1% gelatin-coated tissue culture plates. The cells were grown at 37°C in a humidified (95%) atmosphere of 5% CO₂ in air for 24 hr. Medium was changed to remove red blood cells and incubated in growth medium for 4-6 days to form confluent monolayers. HUVEC were further subcultured with media changes and cells were used for experiments in the third to fourth passage. Endothelial cells were verified by their cobblestone morphology and immunofluorescence staining with antibody against von-Willebrandfactor antigen (Dako, Dakopatts, Denmark).

II.10.3. Trypan blue dye exclusion

The number of viable cells was determined using trypan blue staining and a hemocytometer (Scientific Instrument, Buffalo, NY) [248]. A 0.5-ml solution of 0.4% trypan blue (Sigma-Aldrich) in HBSS was mixed with 0.1 ml cell suspension in a small tube. The mixture was inverted three times and left to stand at room temperature for 5 min. One drop of the mixture was dispensed onto the counting chamber of a hemocytometer using a steril Pasteur pipet. The mixture was allowed to settle for 2 min and then counted using a light microscope set at 100x magnification. A hand-held counter (ENM Supplies, England) was used to count the total number of cells and total number of viable (unstained) cells. The percentage of viable cells was determined as follows:

$$\text{Percent viable cells} = (\text{number of unstained cells} / \text{total number of cells}) \times 100$$

II.10.4. Cloning cells by limiting dilution

A suspension of cells in growth medium was prepared such that it contained 10 cells/ml, and 0.1 ml of this suspension was dispensed into 96-well plates using a multichannel pipet (Nunc) [248, 249]. Thus, some wells may have received near 10 cells/well, some between 1-10 cells/well, some 1 cell/well, and some may have received no cells at all. Plates were agitated frequently to keep the diluted cells uniformly suspended in the medium and incubated at 37°C in a humidified (95%) atmosphere of 5% CO₂ in air.

II.11. Transient transfections

II.11.1. DEAE-dextran transfection

Transfection using the DEAE-dextran method was adapted from general procedures described for transfection of mammalian cell lines [108, 250, 251]. Actively proliferating HeLa cells were plated in growth medium and grown to approximately 60-70% confluency in 100-mm plates. Growth medium was removed from plates and cells were washed with PBS (pH 7.4) after which 5 ml of DMEM supplemented with 10% NuSerum (Gibco/BRL) and 100 µM chloroquine was added. Cells were then transfected with 3 µg of either pcDNA3, pcDNA3/LacZ, pcDNA3/hCNT1, pcDNA3/hCNT2, pcDNA3/hCNT3 or pGFP-C1/hCNT3 (prepared as described in section II.2.) and 10 mg/ml DEAE-dextran mixture in PBS (pH 7.4), which was added dropwise to cells. Cells were incubated for 4 hr at 37°C, after which 3 ml of PBS containing 10% DMSO (v/v) was added for 2 min at room temperature. Cells were washed with PBS three

times and incubated in DMEM supplemented with 10% NuSerum for 24 hr at 37°C. Cells were then trypsinized, pooled and plated in growth medium on appropriate tissue culture plates for 48 hr at 37°C prior to transport assays. Transfection efficiencies were monitored by *in situ* β -galactosidase staining of cells that had been transfected in parallel with pcDNA3/LacZ [252].

II.12. Stable transfection and selection of transfectants in Chapter III

For transfections, pcDNA3, pcDNA3/LacZ, pcDNA3/hCNT1, pcDNA3/hCNT2 or pcDNA3/hENT2 were (i) purified on a Qiagen Midi column (as described in section II.2.) from JM109 or Top10F' *E. coli* cultures that had been grown in the presence of 50 μ g/ml ampicillin, (ii) linearized with BglII restriction enzyme, and (iii) diluted to 0.25 μ g/ μ l with RPMI 1640 medium that contained no glutamine (hereafter referred to as Gln-free RPMI).

II.12.1. Electroporation and selection in geneticin

Transfection by electroporation was adapted from general procedures described for electroporation of mammalian cell lines [253-258]. For electroporation, recipient cells were prepared from actively proliferating CEM-ARAC cultures by (i) centrifugation (800 x g, 10 min), (ii) resuspension at 5×10^4 cells/ml in RPMI 1640 medium with 10% HHS, and (iii) incubation at 37°C in a humidified (95%) atmosphere of 5% CO₂ in air for 72 hr to a concentration of about 4×10^5 cells/ml, after which they were (iv) collected by centrifugation (800 x g, 10 min), (v) washed twice with Gln-free RPMI and (vi) concentrated in Gln-free RPMI to 3×10^8 cells/ml.

Electroporation was performed using a gene pulser [253, 257] equipped with a capacitance extender (Biorad, ON) and a 4-mm gap cuvette (Biorad) in which was placed 170 μ l of cell suspension and 30 μ l of the linearized plasmid mixture. After electroporation (190 V, 960 μ F, 65-75 ms), cells were (i) resuspended in RPMI 1640 supplemented with 15% HIHS, 100 units/ml penicillin and 100 μ g/ml streptomycin (Gibco BRL) and (ii) incubated for 24 h at 37°C in a humidified (95%) atmosphere of 5% CO₂ and air, after which they were (iii) triturated, (iv) diluted to 2 x 10⁵ cells/ml with RPMI 1640 supplemented with 10% HIHS, (v) incubated at 37°C for an additional 24 h, (vi) collected by centrifugation (800 x g, 10 min), (vii) resuspended at 1 x 10⁵ cells/ml in RPMI 1640 supplemented with 10% HIHS and 0.2 μ g/ μ l geneticin (G418, Life Technologies Inc., Gaithersberg, MD), and (viii) incubated at 37°C in a humidified (95%) atmosphere of 5% CO₂ with medium changes at 3-4 day intervals for approximately one month.

II.12.2. Cloning of Stable Transfectants in Semi-Solid Medium.

Geneticin-resistant cells were identified by cloning of cells in soft-agarose by a modification of the method of Sato *et al.* [259]. Geneticin-resistant cells were grown in soft-agarose cloning medium that consisted of equal volumes of fresh RPMI 1640 supplemented with 0.2 μ g/ μ l G418, 20% HIHS, 1 mM α -ketoglutarate (Sigma, Oakville, ON) and 6 mM glutamine and the same medium that had been "conditioned" by exposure to actively proliferating CEM-ARAC cells for 24 h. Geneticin-selection cultures were suspended in cloning medium with 1% Seaplaque agarose (Mandel, Guelph, ON) to yield 5 x 10³-1 x 10⁴

cells/100-mm plate (Fisher Scientific, Ottawa, ON) and incubated for three weeks at 37°C in a humidified (95%) atmosphere of 5% CO₂ in air. Surviving colonies were picked, expanded and screened for nucleoside transport activity in transport assays as described in section II.15.

II.13. Assessment of transfection efficiencies

II.13.1. *In situ* β -galactosidase staining

To determine transfection efficiencies with DEAE-dextran transfections (section II.11.1), parallel cultures were transfected with pcDNA3 or pcDNA3 containing the *E. coli* LacZ gene (pcDNA3/LacZ) and *in situ* β -galactosidase staining was assessed [260, 261]. Cultures were grown for 72 h after which they were harvested, fixed (0.5% glutaraldehyde in PBS) for 15 min at room temperature and washed twice (PBS adjusted to pH 7.4) by centrifugation (800 x g, 5 min). The resulting cell pellets were incubated in 1-ml portions of staining solution that consisted of 1 mg/ml 5-bromo-4-chloro-3-indoyl- β -D-galactopyranoside, 20 mM potassium ferricyanide/ferrocyanide and 2 mM MgCl₂ in PBS for 24 h at 37°C. Transfection efficiencies were estimated by determination of the proportion of green-stained cells using a hemacytometer.

II.13.2. *Semi-quantitative* β -galactosidase activity assay

To determine transfection efficiencies with the electroporation method of transfection (section II.12.1), parallel cultures were transfected with pcDNA3 or pcDNA3/LacZ and β -galactosidase activity was assessed [262, 263]. Cultures

were grown for 72 h after which they were harvested and assayed following the manufacturer's instructions (Gene Therapy Systems Inc., San Diego, CA). Cells were separated from transfection medium by centrifugation, washed three times with PBS (pH 7.4) and incubated in 2500 μ l lysis buffer (Gene Therapy Systems Inc.) for 10-15 min at room temperature with constant swirling to ensure complete cell lysis. Cells were observed under light microscopy to confirm complete lysis. Cell lysates (100 μ l) were transferred to individual tubes and centrifuged (2500 x g, 10 min) to pellet insoluble material. The supernatant was collected and 300 μ l o-nitrophenyl- β -D-galactopyranoside (Gene Therapy Systems Inc.) was added, after which the mixture was incubated at room temperature for 1 hr. Absorbance readings of samples at 400 nm were determined using a spectrophotometer.

II.14. Transepithelial electrical resistance measurements

Transepithelial electrical resistance (TEER) readings of cell monolayers were determined using the Millicell-(ERS) Epithelial Resistance System (Millipore, Bedford, MA) following the manufacturer's suggestions. Electrical resistance values were calculated by multiplying the voltage changes by the surface area of the polycarbonate membrane and then applying Ohm's law. TEER values obtained in the absence of cells (caused by the electrical system and the collagen-coated, polycarbonate membrane) were considered background. For each experiment, electrical resistance values were corrected for background, which ranged from 33-48 ohm-cm².

II.15. Nucleoside transport assays with suspension cells

Initial rates of nucleoside uptake were measured at room temperature using the oil-stop method [264, 265] with actively proliferating cells. Cells were harvested by centrifugation (800 x g, 10 min), washed twice in either sodium-containing transport buffer (5 mM D-glucose, 20 mM Tris-HCl, 3 mM K₂HPO₄, 1 mM MgCl₂·6H₂O, 2 mM CaCl₂ and 130 mM NaCl, pH 7.4) or sodium-free transport buffer (NaCl was substituted with N-methyl-D-glucammonium chloride) and then resuspended in sodium-containing or sodium-free transport buffer. Transport assays involving adenosine and deaminase-sensitive adenosine analogs were conducted in the presence of 2 μM 2'-deoxycoformycin to prevent deamination [266-268]. Time courses of uptake of ³H-nucleosides were determined using rapid sampling procedures in which the transport process was initiated by addition of cells to the ³H-nucleoside solution (1:1) and terminated by rapid addition of excess cold nucleoside solution followed by immediate centrifugation (16,000 x g, 30 s) through transport oil [mixture of paraffin oil (Fisher Scientific, Ottawa, ON) and silicone 550 oil (Dow Corning, Mississauga, ON) with final specific gravity of 1.03 g/ml] to separate the cells from the permeant solution. Replicate assay mixtures were exposed to either ¹⁴C-polyethyleneglycol or ³H₂O to determine trapped extracellular and intracellular water volumes, respectively. The cell pellets were solubilized in 0.5 ml of 5% Triton-X 100 and cell-associated radioactivity was determined by liquid scintillation counting. Transport rates were derived from regression analysis of

the linear component of uptake and kinetic parameters (apparent K_m and V_{max} values) were calculated using Prism (GraphPad Software Inc., San Diego, CA).

II.16. Nucleoside uptake assays with adherent cells

Nucleoside uptake assays were performed using adapted procedures described for uptake assays with HeLa and Caco-2 cells [170, 247, 269]. Cells were attached to tissue culture 35-mm plates (Falcon) or collagen-coated Transwell membrane inserts (Nunc) (2-3 samples/condition) at room temperature in sodium-containing or sodium-free transport buffer (as described in section II.10.2.). For assay conditions in the presence of sodium, cells were washed twice with sodium-containing transport buffer. For assays in the absence of sodium, cells were washed twice with sodium-free transport buffer. For assays that required inhibition of ENT-mediated processes, cells were incubated with 200 μ M dilazep or 0.1 μ M NBMPR for 15 min at room temperature prior to uptake measurements and uptake assays were conducted in the presence of 200 μ M dilazep or 0.1 μ M NBMPR. Uptake assays involving adenosine and deaminase-sensitive adenosine analogs were conducted in the presence of 2 μ M 2'-deoxycoformycin to prevent deamination [266-268].

For transport experiments with tissue culture plates, uptake was initiated by adding 1.5 ml of transport buffer containing 3 H-labeled permeant solution. For transport experiments with Transwell membrane inserts, uptake was initiated by adding 1 ml of transport buffer containing 3 H-labeled permeant solution to the apical (upper) compartment of the Transwell insert (the basal (lower) compartment was continuously exposed to sodium-containing transport buffer).

Uptake was stopped by quickly aspirating permeant solution and immersing the cells in 1.5 litres of ice-cold sodium-free transport buffer. Membrane inserts were removed from the plastic supports with the Membrane Removal Tool (Nunc) and placed in scintillation vials. Cells were solubilized in 1.25 ml of 5% Triton X-100 (v/v) and 5 ml of EcoLite scintillation fluid was added for measurement of radioactivity by liquid scintillation counting.

II.17. Preparation of membranes from cells

All procedures for preparation of membranes were conducted on ice using buffer solutions that were chilled from 0 to 4°C and centrifugations were performed at 4°C. Buffer solutions (prepared just before using) employed for membrane preparations contained protease inhibitor tablets (Complete Protease Inhibitors, Boehringer Mannheim), 0.3 mM phenylmethylsulfonyl fluoride (PMSF) and 0.5 mM dithiothreitol (DTT). The protein content of membrane preparations was determined by the bicinchoninic acid (BCA) assay method [242] as described in section II.9. Membrane preparations were quick frozen in liquid nitrogen and stored in PBS that contained protease inhibitor cocktail (one Complete Protease Inhibitor tablet, 0.3 mM PMSF and 0.5 mM DTT) at -80°C until use.

II.17.1. Membranes from yeast

Yeast membranes were used in characterization of antibodies against hCNTs and were prepared using previously established procedures [213, 270]. Yeast constructs (pYES2, pYES2/hCNT2myc, pYGE15 and

pYGE15/hCNT3myc) were generously provided by F. Visser or J. Zhang (Department of Oncology, University of Alberta). Yeast transformed with the different plasmids were grown to an OD₆₀₀ of approximately 1.0 ± 0.3 . Yeast were i) harvested by centrifugation at 500 x g for 5 min, ii) resuspended in yeast breaking buffer (0.2 mM EDTA, 0.5 mM DTT and 10 mM Tris-HCl, pH 7.5), iii) lysed by vortexing in the presence of glass beads (425-600 μ M, Sigma) for 15 min and iv) centrifuged at 500 x g for 5 min to remove unbroken cells and glass beads. The resulting yeast cell lysates (i.e., the supernatant) were centrifuged at 100,000 x g for 1 hr and the protein content of the resulting membrane preparations was determined (as described in section II.9) prior to storage at -80°C .

II.17.2. Membranes from tissue culture cells

Actively proliferating tissue culture cells (1×10^8 - 3×10^8 cells) were harvested and washed by centrifugation three times in PBS (pH 7.4) and the resulting cell pellets were resuspended in 10 volumes of swelling buffer (10 mM Tris-HCl, pH 7.4, 1 mM ZnCl₂, 0.5 mM DTT and 0.3 mM PMSF). Cells were lysed with a Polytron homogenizer (Brinkmann Instruments, Westbury, NY) and unbroken cells and nuclei were removed by centrifugation at 900 x g for 20 min. The supernatant was collected and membranes were isolated by centrifugation at 13000 x g for 30 min. Membrane pellets were resuspended in homogenization buffer (5 mM K₂HPO₄, 0.5 mM ZnCl₂, pH 5.0) with 9.25% sucrose (w/v), Dounce homogenized several times and centrifuged at 13000 x g for 30 min. The unfractionated membranes were either resuspended in PBS that

contained protease inhibitors cocktail (Complete Protease Inhibitors, 0.3 mM PMSF and 0.5 mM DTT) and stored frozen at -80°C or used immediately for isolation of plasma membranes.

Enriched plasma membranes were isolated using established procedures [271]. Unfractionated membranes were layered onto a discontinuous (45%, 30%, 25%, 20% and 15%) sucrose gradient and centrifuged at 3500 x g for 45 min. Plasma membranes were collected between the 20% and 30% sucrose layers and 0.66 mM EDTA was added. The mixture was centrifuged at 11000 x g for 1 hr, and the resulting pellets were resuspended in 15% DMSO (v/v) and centrifuged 27000 x g for 25 min. The protein content of the resulting enriched plasma membrane preparations was determined (as described in section II.9) prior to storage at -80°C.

II.17.3. Membranes from tissues of the human brain

Membranes from human brain tissues were prepared as described by Jennings *et al* [144]. Human brain was obtained by Dr. Chunhai Hao (Laboratory Medicine and Pathology, University Hospital and University of Alberta) at autopsy less than 4 hr postmortem from a 42-year-old male who had no history of neurological or psychiatric disease and passed away as a result of pulmonary failure. Dissection of the brain into its major divisions (cerebral cortex (divided into frontal, parietal, temporal and occipital lobes), hippocampus, thalamus, basal ganglia (divided into caudate nucleus, putamen and globus pallidus), brainstem (divided into the medulla, midbrain and pons) and cerebellum) was performed in the laboratory of Dr. Chunhai Hao. Dissected brain tissues were

collected and stored at -80°C by Dr. L. Jennings (Department of Oncology, University of Alberta, now at University of California, San Diego, Department of Pharmacology).

Enriched membrane preparations of frontal, parietal, temporal and occipital lobes of cerebral cortex, cerebellum and thalamus were prepared by Dr. L. Jennings, and medulla, midbrain, pons, hippocampus, caudate nucleus, putamen and globus pallidus were prepared by T. Lang. Brain tissues were minced with a razor blade, homogenized with a Polytron (Brinkmann Instruments) in 10 volumes of 1 mM EDTA, 300 mM sucrose, 0.02% NaN_3 and 100 mM Tris-HCl, pH 7.2 and centrifuged at $1000 \times g$ for 15 min. Supernatants were then filtered through six layers of cheesecloth and filtrates were centrifuged at $150000 \times g$ for 45 min. Supernatants were discarded, pellets were homogenized with the Polytron in 10 volumes of 1 mM EDTA, 0.02% NaN_3 and 100 mM Tris-HCl (pH 7.2) and centrifuged at $150000 \times g$ for 45 min. The homogenization step was repeated two more times. The pellets were resuspended in two volumes of 1 mM EDTA, 0.02% NaN_3 and 20 mM Tris-citrate (pH 7.5) and protein content of the resulting enriched membrane preparations was determined by the BCA assay method prior to storage at -80°C .

II.17.4. Membranes from tissues of the gastrointestinal tract

Biopsies of tissues from different regions of the gastrointestinal (GI) tract, from six different patients who had no prior history of GI disease were obtained by Dr. Clarence Wong (Department of Oncology, Cross Cancer Institute and Department of Medicine, Gastroenterology, University of Alberta) under an

approved protocol. All study patients volunteered for the study after informed consent was given and endoscopies were performed at the Cross Cancer Institute and University of Alberta Hospital, Edmonton, Alberta. Upper gastrointestinal endoscopies were performed with diagnostic Fujinon and Olympus endoscopes. Multiple tissue biopsies, each measuring 4-10 mm diameter, were taken from the lumen of the esophagus, stomach and duodenum with standard biopsy forceps. Patients undergoing colonoscopy were given 4 litres of polyethylene glycol bowel preparation the day before the examination. Fujinon and Olympus colonoscopes were used to obtain multiple biopsies from colon, ileum and jejunum. Suspected malignant tissue was biopsied when observed, with duplicate samples sent for histological confirmation.

Biopsied samples were either fixed in formalin for histological analysis, or immediately snap frozen to be used for preparation of membranes as described elsewhere [238]. GI biopsies used in this study were from normal GI tissue as determined from histological analysis. Thawed GI tissues were minced with a razor blade and homogenized with a Polytron (Brinkmann Instruments) in 5 volumes of 300 mM sucrose, 25 mM imidazole, 1 mM EDTA (pH 7.2), 1 mM leupeptin, and 0.5 mM phenylmethylsulfonyl fluoride. The homogenates were centrifuged in an Eppendorf centrifuge at 4,000 x g for 15 min. Supernatants were then filtered through six layers of cheesecloth and filtrates were centrifuged at 150000 x g for 45 min. Supernatants were discarded, pellets were homogenized with the Polytron in 10 volumes of 1 mM EDTA, 0.02% NaN₃ and 100 mM Tris-HCl (pH 7.2) and centrifuged at 150,000 x g for 45 min. The

homogenization step was repeated two more times. The pellets were resuspended in two volumes of 1 mM EDTA, 0.02% NaN₃ and 20 mM Tris-citrate (pH 7.5) and the protein content of the resulting membrane preparations was determined by the BCA method (section II.9) prior to storage at -80°C. Immunoblot analyses (section II.8) utilized pooled membrane preparations from six patients.

II.17.5. Membranes from human red blood cells

Human blood was collected by the medical laboratory staff at the Cross Cancer Institute from volunteers under an approved protocol (J. Mackey, Medical Oncology, Cross Cancer Institute). The blood, which was obtained in heparinized tubes, was centrifuged at 1000 x g for 45 min and the buffy coats and plasma were aspirated off, leaving behind red blood cells. Membranes of red blood cells were prepared as described elsewhere [272, 273]. The red blood cells were washed three times by resuspension in isotonic 172 mM Tris buffer (pH 7.6) and centrifugation at 1000 x g for 45 min. The resulting pellets were resuspended in hypotonic 11.1 mM Tris buffer (pH 7.6) and centrifuged at 20000 x g for 45 min. The supernatants were removed, and the washing and centrifugation steps were repeated several times until the membrane pellets were colorless. The red blood cell membranes were then resuspended in seven volumes of 0.1 mM EDTA and 50 mM Tris buffer (pH 11.1), incubated for 15 min and then centrifuged at 22000 x g for 25 min. The supernatants were removed and the membrane pellets were subjected to three washing and centrifugation (22000 x g for 25 min) steps with 50 mM Tris-HCl (pH 8.0). The protein content

of the resulting membrane preparations was determined (as described in section II.9) prior to storage at -80°C.

II.18. Generation of anti-peptide antibodies

Synthetic peptides corresponding to amino acid sequences of hCNT2 and hCNT3 were synthesized and conjugated to either keyhole limpet hemocyanin (KLH) or bovine serum albumin (BSA) by the Alberta Peptide Institute (University of Alberta, Edmonton, AB, Canada). Peptide-KLH and peptide-BSA conjugates were purified by the Alberta Peptide Institute to greater than 95% homogeneity.

The peptide conjugates, which were received from the Alberta Peptide Institute as lyophilized material, were difficult to redissolve directly into PBS since the aqueous solubility of the peptide-conjugates was low. The peptide-conjugates (1-2 mg) were initially dissolved in 100-200 μ l of 8 M urea in a 1.5-ml Eppendorf microfuge tube and incubated at 37°C for 4 hr with occasional 30-sec vortexing. The samples were then centrifuged for 5 min at 1000 x g in a table top centrifuge (Eppendorf, Hamburg, Germany), the supernatants were transferred into a 6000-8000 molecular weight cut-off dialysis bag (VWR International, Mississauga, ON) and dialyzed i) first against 0.1 M ammonium bicarbonate for 24 hr at 4°C and ii) then against PBS (pH, 7.4). Peptide-conjugates were stored in PBS (pH, 7.4) at -20°C until use.

II.19. Testing of antibody production by enzyme-linked immunoadsorbant assay (ELISA)

Antisera from rabbits, mice or supernatants from hybridoma cultures were screened for immunoreactivity by ELISA using a 96-well plate reader (Molecular Devices) and a 96-well plate washer (Brinkmann Instruments, Mississauga, ON) [238, 274]. The 96-well plates (Falcon) were coated with peptide conjugated to bovine serum albumin (200 ng/well) and stored overnight at 4°C. Plates were washed twice with PBS and incubated overnight at 4°C with 300 µl of 5% skim milk powder (w/v) in PBST (PBS (pH 7.4) and 0.2% Tween 20 (v/v)) to reduce non-specific binding to the plates. Graded dilutions of antisera were added to individual wells (50 µl/well) and incubated at room temperature for 2 hr. The plates were washed three times with PBST after which 50 µl of horseradish peroxidase conjugated secondary antibodies were added to each well and the plates were then incubated at room temperature for 2 hr. The plates were washed three times with PBST and 50 µl PBS (pH, 8.0) containing one tablet of tetramethylbenzidine dihydrochloride was added to each well according to the manufacturer's suggestions (Sigma). Absorbance at 650 nm was determined using a 96-well plate reader and SOFTmax program (Molecular Devices).

II.20. Immunization protocols

Female New Zealand White rabbits, which were virus-free and barrier-maintained, were purchased from Charles River Laboratories (St. Constant, PQ). BALB/c barrier-maintained female mice were purchased from Health Sciences

Laboratory Animal Services (Faculty of Medicine and Dentistry, University of Alberta, Edmonton, AB). Rabbits and mice were maintained in quarantine for a minimum of one week prior to immunization. Blood for preimmune sera was collected in the Cross Cancer Institute Vivarium from rabbits (5-7 ml) and mice (100-200 μ l) 5-7 days before immunization. Immunization of rabbits and mice was performed at the Cross Cancer Institute Vivarium by Gail Hipperson, Vivarium Manager, in association with vivarium personnel according to standard animal handling procedures approved by the Cross Cancer Institute Animal Care Committee.

II.20.1. Production of polyclonal antibodies in rabbits

Immunization of rabbits was performed according to Cross Cancer Institute Vivarium standard operating procedures and methods of Harlow and Lane [275]. Rabbits were immunized by intramuscular injection of approximately 100 μ g of peptide-KLH conjugate in PBS (pH 7.4) mixed 1:1 with Freund's complete adjuvant (Gibco/BRL Life Technologies) in a 350- to 400- μ l volume. Booster intramuscular injections (2-4, depending on immune response to antigen as determined by ELISA) of 100 μ g of peptide-KLH conjugate in PBS (pH 7.4) mixed 1:1 with Freund's incomplete adjuvant (Gibco/BRL Life Technologies) were performed 21-23 days after first injection and 21-25 days apart from each other. Test bleeds (approximately 5 ml) were collected 10-11 days after every injection. Sera were collected from blood samples by incubating blood at 37°C for 30 min, followed by overnight incubation at 4°C, and then centrifugation at

1000 x g for 30 min at 4°C. The resulting supernatants (sera) were stored at -20°C.

II.20.2. Production of monoclonal antibodies in mice

Immunization of mice was performed according to Cross Cancer Institute Vivarium standard operating procedures and methods of Harlow and Lane [275]. Mice were immunized by intraperitoneal injection of approximately 50 µg of peptide-KLH conjugate in PBS (pH 7.4) mixed 1:1 with Freund's complete adjuvant in a 100-µl volume. Two booster intraperitoneal injections of 50 µg of peptide-KLH conjugate in PBS (pH 7.4) mixed 1:1 with Freund's incomplete adjuvant in a 100-µl volume were performed 14 and 35 days after first injection. Test bleeds were collected 10-11 days after each injection. Sera were collected from test bleeds by incubating the blood at 37°C for 30 min, followed by overnight incubation at 4°C, and then removal of cells by centrifugation at 1000 x g for 30 min at 4°C. The resulting supernatants (sera) were collected and stored at -20°C.

For a responding mouse that produced the desired antisera as determined by ELISA and immunoblot analysis (described in section II.8), an intravenous injection of 50 µg of peptide-KLH conjugate in PBS (pH 7.4) in a 100-µl volume was administered 21-31 days after the final booster injection. After 3-4 days, the mouse was sacrificed, its spleen was removed and splenic lymphocytes were harvested for hybridoma production.

Hybridomas were generated with assistance from either Ms. Milada Selner or Ms. Pat Carpenter using similar procedures to those described in Harlow and Lane [275]. Hybridomas were produced by fusion of spleen cells of immunized mice with murine myeloma non-secreting PC/NSI/1-AG4-1 cells, using polyethylene glycol (Sigma) as the fusing agent [276]. Hybridomas were selected by prolonged culture (30-60 days) in HAT selection medium (100 μ M hypoxanthine, 16 μ M aminopterin and 0.4 μ M thymidine supplemented with 20% heat-inactivated FBS, 2 mM L-glutamine, 0.5 mM oxaloacetic acid and 1 mM sodium pyruvate) in the presence of 50 μ g/ml gentamycin antibiotic. The supernatants from hybridoma cultures were subjected to primary screenings by ELISA with peptide-BSA conjugates (section II.19). Hybridoma-culture supernatants exhibiting strong positive results on ELISA were also subjected to immunoblot analysis (section II.8). The positive hybridoma cultures identified were subjected to limiting dilution to obtain clonal populations. Hybridoma clones were stored in 10% DMSO in growth media in liquid nitrogen. For serum-free monoclonal antibody preparations, hybridomas were grown in serum-free growth medium (Gibco/BRL Life Technologies). Monoclonal antibodies obtained from hybridoma supernatants were stored at -20°C.

II.21. Immunoaffinity purification of polyclonal and monoclonal antibodies

Antibody purification procedures were performed in the cold room at 4°C and buffer solutions were chilled to 0 to 4°C. Protein content of purified antibody

preparations was determined by the bicinchoninic acid (BCA) assay method [242] as described in section II.9.

II.21.1. Enrichment of polyclonal antibodies

Enrichment of antibodies was adapted from general procedures described in Harlow and Lane [274]. Nitrocellulose paper was coated with a 0.2 mg/ml solution of peptide-BSA conjugate in PBS (pH 7.4) and non-specific binding was blocked by incubation of the coated nitrocellulose paper in TPBS containing 5% skim milk powder (w/v) overnight. The nitrocellulose paper was washed with TPBS three times and antisera from the rabbit that was injected with the peptide conjugate (peptide-KLH, section II.20.1.) was applied to the nitrocellulose paper and incubated overnight with gentle shaking to allow immunoglobulin binding to peptide. The bound immunoglobulins were eluted by addition of 2 ml of 0.1 M glycine (pH 2.5), followed by neutralization with 0.3 ml of 1 M Tris-HCl (pH 9.0). The eluted immunoglobulin fractions were concentrated into small volumes in PBS (pH 7.4) using Centriprep 50 centrifugal protein filter units (Millipore) by centrifugation at 1500 x g for 40 min at 4°C. Polyclonal antibodies were further enriched by protein G column as described below.

II.21.2. Enrichment of immunoglobulins by protein G affinity chromatography

Polyclonal and monoclonal antibodies were purified on protein G columns (Amersham-Pharmacia Biotech) following the methods of Harlow and Lane [274, 275]. Protein G columns were equilibrated with PBS according to the

manufacturer's instructions (Amersham-Pharmacia Biotech). Polyclonal antibody preparations from the Centriprep 50 centrifugal protein filter unit (as described in section II.22.1.) or supernatants from serum-free hybridoma cultures were passed through protein G columns that were subsequently washed with a minimum of 10 column volumes of PBS (pH 7.4) until no protein was detected by monitoring the absorbance of the eluate at 280 nm. Bound immunoglobulins were eluted from protein G columns using 50 mM glycine (pH 3.0), which was added stepwise at approximately half column volume per step. The eluate from each step was collected in tubes containing 1/10 column volume of 1 M Tris (pH 8.0) and mixed gently to bring pH back to neutral. The immunoglobulin-containing fractions were identified by absorbance readings at 280 nm. The protein content of the enriched antibody preparations was determined by the BCA assay method (section II.9).

II.22. Indirect immunofluorescence confocal microscopy

Cell staining used modified procedures described elsewhere [274, 275, 277]. Grade #1 glass coverslips (VWR) were coated with either poly-L-lysine, gelatin or Type I calf skin collagen (all from Sigma), following the manufacturer's recommendations. Cells were attached by i) growing on collagen-, gelatin- or poly-L-lysine-coated coverslips positioned in the wells of 6-well tissue culture plates (Falcon) for 4-24 hr, ii) growing on transwell collagen-coated polycarbonate inserts (Nunc) or iii) cytocentrifugation onto coverslips at 1200 x g for 10 min using Cytospin (VWR). Cells were fixed and permeabilized with either i) freshly made 4% paraformaldehyde (w/v) in PBS (pH 7.4) for 5 min, followed

by PBS containing 0.5% Triton X-100 for 5 min (all at room temperature) or ii) 100% methanol for 5 min at -20°C.

The coverslips were washed three times with PBS (pH 7.4), and then incubated in 4% goat serum (Sigma) in PBS (pH 7.4) overnight at 4°C to reduce non-specific binding. Coverslips were incubated with 50 µl portions of primary antibodies diluted between 1:10 to 1:1000 in PBS containing 2% goat serum for 2 hr at room temperature in a humidified chamber. Coverslips were rinsed with PBS containing 0.1% Triton X-100 and washed three times with PBS prior to a 1-hr incubation with 50 µl portions of appropriate Alexa Fluor secondary antibodies (e.g., Alexa-fluor 488, Alexa-fluor 546 and Alexa-fluor 594) diluted between 1:500 to 1:1000 in PBS containing 1% goat serum. Coverslips were rinsed with PBS containing 0.1% Triton X-100 and washed three times with PBS. Coverslips were mounted onto #1 glass slides (VWR) with approximately 10 µl of a 90% glycerol-PBS-based medium sometimes containing 1 mg/ml paraphenylenediamine and 0.5 µg/ml DAPI.

Slides were visualized with an LSM-510 laser-scanning confocal microscope (Carl Zeiss, Toronto, ON) with multitrack setting, which collects the images of channels arising from laser lines of various wavelengths using appropriate filters. Individual channels were separated (e.g., DAPI (365 nm) GFP/Alexa-fluor (488 nm), Alexa-fluor (546 nm), Alexa-fluor (594 nm) and CY5 (620 nm)) from collected images using the LSM-510 software, and were exported as single channel 12-bit TIFF images into Metamorph 4.6 (Universal Imaging Corp., Downingtown, PA), where background noise was subtracted from

all images. Images were assembled and printed on a NP-1600 sublimation printer (Codonics, Middleburg Heights, OH).

Table II-1. TaqMan primers and probes used in Chapter III

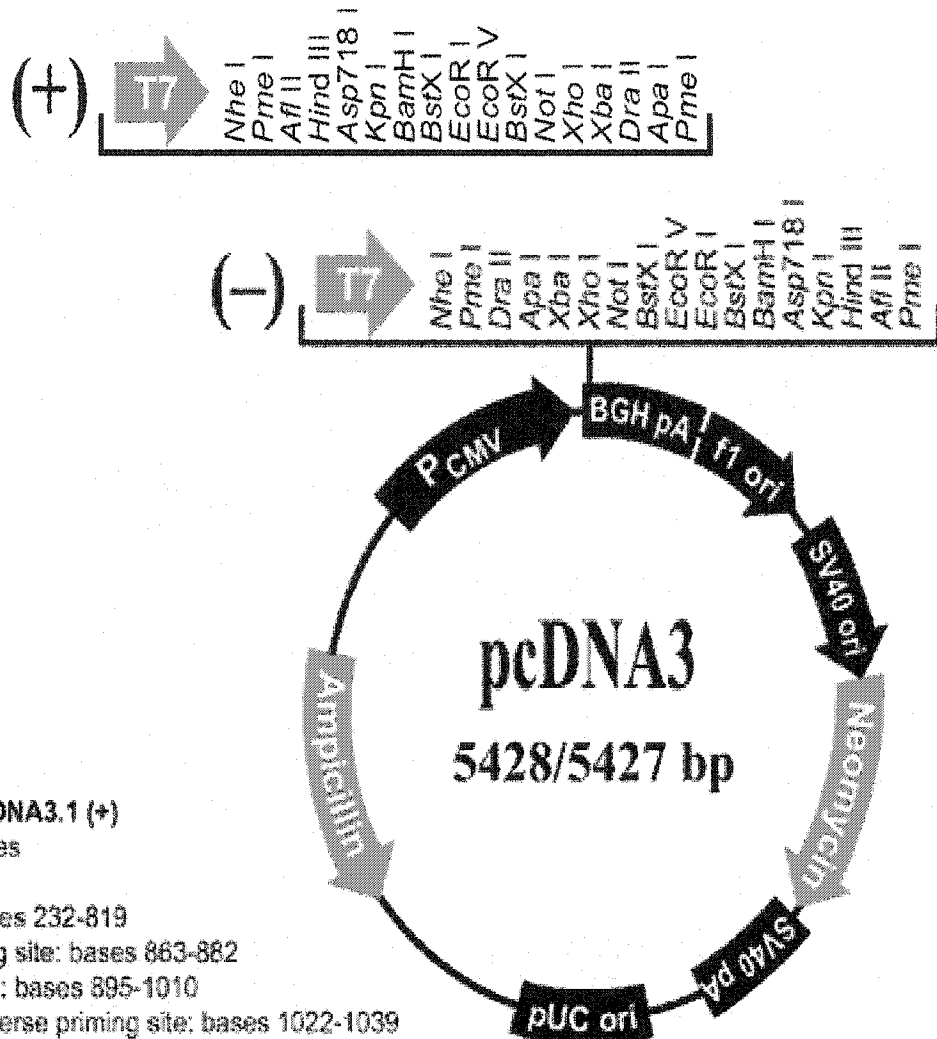
hENT1:	
Sense primer	5'-CACCAGCCTCAGGACAGATACAA
Antisense primer	5'-GTGAAATACTGAGTGGCCGTCAT
Probe	5'-FAM-CCACGGGAGCAGCGTTCCCA
hENT2:	
Sense primer	5'-ATGAGAACGGGATTCCCAGTAG
Antisense primer	5'-GCTCTGATTCCGGCTCCTT
Probe	5'-TET-CAGAAAGTAGCTCTGACCCTGGATCTTGACCT
hCNT1:	
Sense primer	5'-TCTGTGGATTTGCCAATTTTCAG
Antisense primer	5'-CGGAGCACTATCTGGGAGAAGT
Probe	5'-TET-TGGGAGGCTTGACCTCCATGGTCC
hCNT2:	
Sense primer	5'-CAAACACCACAGCGCAGTGT
Antisense primer	5'-TGACCAAGATCCCAAAGACAAA
Probe	5'-TET-CCTAGGCCCGAAAACACTGTCCTCCA
hCNT3:	
Sense primer	5'-GGGTCCCTAGGAATCGTGATC
Antisense primer	5'-CGAGGCGATATCACGCTTTC
Probe	5'-FAM-CGGACTIONCACATCCATGGCTCCTTC

TET: tetrochloro-6-carboxy-fluorescein

FAM: 6-carboxy-fluorescein

Table II-2. Description of cell lines and their properties used in this thesis

Cell Lines	Tissue origin	Growth Properties	Reference
Human:			
CEM	acute lymphoblastic leukemia; peripheral blood; T-lymphoblast	suspension	ATCC
CEM-ARAC			Drs. B Ullman , J Belt [214]
ARAC/D2			[74] This study
TLCT1	adenocarcinoma; cervix	adherent and suspension	This study
TLET2			This study
HeLa			ATCC
K562			ATCC
NB4			ATCC
MCF7	adenocarcinoma; mammary gland; breast	adherent	ATCC
MDA-MB-435S (435S)	ductal carcinoma; mammary gland; breast	adherent	ATCC
180/1	squamous cell cervical cancer	adherent	Dr. R Britten (Cross Cancer Institute, Edmonton, AB)
BeWo	choriocarcinoma; placenta kidney; transformed with adenovirus 5 DNA	adherent	ATCC
HEK 293		adherent	Dr. J. Casey from ATCC
Caco-2	colorectal adenocarcinoma; colon	adherent	ATCC
Mouse:			
S49	lymphoma; B-lymphocyte	suspension	[237]
AE1			[243]
L-1210/b23.1	lymphocytic leukemia myeloma	suspension	[244]
PC/NSI/1-			ATCC
AG4-1			[278]



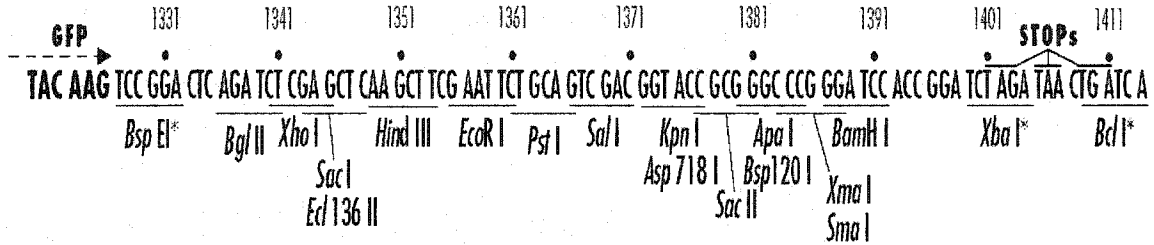
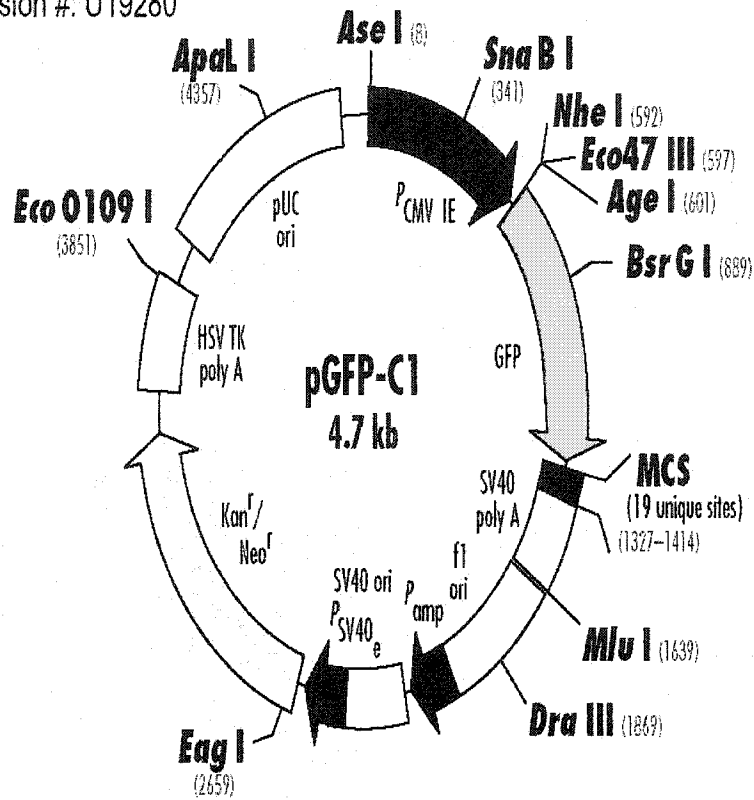
Comments for pcDNA3.1 (+)
5428 nucleotides

- CMV promoter: bases 232-819
- T7 promoter/priming site: bases 863-882
- Multiple cloning site: bases 895-1010
- pcDNA3.1/BGH reverse priming site: bases 1022-1039
- BGH polyadenylation sequence: bases 1028-1252
- f1 origin: bases 1298-1726
- SV40 early promoter and origin: bases 1731-2074
- Neomycin resistance gene (ORF): bases 2136-2930
- SV40 early polyadenylation signal: bases 3104-3234
- pUC origin: bases 3617-4287 (complementary strand)
- Ampicillin resistance gene (*bla*): bases 4432-5428 (complementary strand)
- ORF: bases 4432-5292 (complementary strand)
- Ribosome binding site: bases 5300-5304 (complementary strand)
- bla* promoter (P3): bases 5327-5333 (complementary strand)

Figure II-1. Information on the mammalian expression plasmid pcDNA3 utilized in this thesis

Image obtained from manufacturer's brochure (Invitrogen)

GenBank Accession #: U19280



Restriction Map and Multiple Cloning Site (MCS) of pGFP-C1. Unique restriction sites are in bold.

Figure II-2. Information on the plasmid used to generate GFP fusion proteins

Image obtained from manufacturer's brochure (Invitrogen)

Chapter III

III. Characterization of Endogenous Nucleoside Transporters Present in Human Cell Lines and Generation of Transient and Stable Transfectants*

* Portions of this chapter have been published previously [279].

III.1. Introduction

The heterogeneity in expression and functional activity of nucleoside transporters that naturally occurs in mammalian cells (see e.g., [115, 153, 200, 201]) makes the study of a particular transporter of interest often difficult. One of the aims of the work in this chapter was to examine the expression profiles of nucleoside transporter mRNAs in various human cell lines and subsequently characterize the associated nucleoside transport activities. Several human cell lines of different tissue origins were analyzed, including neoplastic and/or normal cell types of lung, kidney, intestine, cervix and breast, as well as various blood cells derived from patients with acute myelogenous leukemia or chronic lymphocytic leukemia. The molecular and functional characterization of the cell lines was undertaken to i) increase knowledge of the nucleoside transporter profiles of cell lines that are used to study nucleoside chemotherapy drugs and ii) provide information needed for the development of new *in vitro* model systems to study the interactions of nucleosides and nucleoside analogs with particular transporters of interest.

Knowledge of the expression profiles and functional activities of nucleoside transporters present in the different cell lines aided in the selection of two cell lines (HeLa and CEM-ARAC) to be used as recipients for gene transfer studies in which exogenous nucleoside transporter cDNAs were introduced transiently or stably into recipient cells. There were no cell lines known when this study was initiated that naturally possessed hCNT1, hCNT2 and hENT2 in isolation, which was consistent with the absence of a suitable model system in

which to study these transporters. HeLa cells, which lacked functional evidence of CNTs, were chosen as recipients to introduce coding sequences corresponding to hCNT1 and hCNT2 by transient transfection. This work provided transient transfectants in HeLa cells for study of recombinant CNTs.

There are only a few examples of human cell types, such as red blood cells and the CCRF-CEM (hereafter referred to as CEM) human leukemia cell line, that naturally exhibit a single nucleoside-transport process (the prototypic equilibrative NBMPR-sensitive (*es*) process) [75, 145, 215, 226, 280]. These cell types have been used extensively to study the *es*-transport process in the absence of other processes, and much is known about its functionality [53].

A transport-deficient subline of CEM, designated CEM-ARAC, was isolated from mutagenized CEM cells that were exposed to MNNG (N-methyl-N-nitroso-N'-nitroguanidine) by selection for resistance to araC (1- β -D-arabinofuranosylcytosine) [214, 216]. The isolated CEM-ARAC mutants failed to transport cytidine and 2'-deoxycytidine, and also lost high-affinity NBMPR binding sites [214], suggesting an absence of the *es*-type transporter that was present in CEM cells. Although the exact molecular mechanism for the nucleoside transport defect was not determined, the transport deficiency of CEM-ARAC cells was well documented [138, 214, 216]. The CEM-ARAC cell line was utilized in the cloning of the human equilibrative, NBMPR-insensitive nucleoside transporter (i.e., hENT2) by functional complementation of the nucleoside transport deficiency [137].

In the work described in this chapter, the CEM-ARAC cell line was shown to exhibit a complete deficiency in nucleoside transport capability and this was due to the lack of hENT1 mRNA expression since none was detected by RT-PCR. In contrast, the CEM line, which expressed hENT1 mRNA, was capable of NBMPR-sensitive nucleoside transport and possessed membrane proteins that were recognized by antibodies specific for hENT1.

When this work was initiated, there were no human model systems that exhibit a single type of transporter (i.e., hCNT1, hCNT2 or hENT2) that could be utilized to study specifically hCNT1, hCNT2 or hENT2 in the absence of other types of transporters. These nucleoside transporters are generally present in low abundance and often in association with the ubiquitously expressed, high-activity hENT1 [140]. The unique characteristic of nucleoside-transport deficiency of the CEM-ARAC line was used to advantage to create new experimental models by introducing the different nucleoside transporters (hCNT2, hCNT1 and hENT2) by transfer of their cDNAs into CEM-ARAC cells.

Electroporation was utilized in the stable transfection of CEM-ARAC cells [253, 257, 258]. The same expression constructs that were used to successfully produce functional nucleoside transporters in HeLa cells by transient transfection were employed for stable transfection of CEM-ARAC cells. Transfectants that had acquired and were expressing the introduced cDNAs were identified by screening geneticin-resistant cultures for acquisition of sodium-dependent uptake of ³H-labeled uridine by comparing uptake in the transfectants with that in transport-deficient CEM-ARAC cells.

Procedures developed for gene-transfer in the production of the CNT-containing transfectants in CEM-ARAC cells [279] were subsequently employed for generation of hCNT1 and hENT2 transfectants in the same host cells. Characterization of stable transfectants was based on the analysis of i) mRNA expression, ii) protein production, iii) sodium-dependent and sodium-independent transport of ³H-uridine and iv) their sensitivity to inhibition by diagnostic permeants of human *cif*-, *cit*- and *ei*- type transporters [13, 131-133, 136, 137]. The generation of a series of stable and transient transfectants in CEM-ARAC and HeLa cells, respectively, provided model systems for the studies described in subsequent chapters of the different nucleoside transporters.

III.2. Results

III.2.1. Molecular characterization of cultured human cells derived from different tissue origins

Human cells often possess multiple nucleoside transporters and the underlying contributions of the different transport systems to the overall fluxes observed is difficult to interpret [121, 153, 200, 201]. The following studies examined different human cell lines derived from a variety of tissue origins i) to identify transcripts corresponding to the known nucleoside transporters that have been cloned [2, 132, 133, 135, 136] and, in some instances, ii) to determine whether the nucleoside transport activities observed in cells corresponded with the identity of the expressed mRNAs. The nucleoside transporter profiles of the human cell lines tested served as the basis for the subsequent choice of recipient cell lines for introduction of cDNAs encoding recombinant nucleoside transporters by transient or stable transfections.

III.2.1.1. Analysis of hENT1 and hENT2 mRNAs in various human cell lines

Northern blot analyses were utilized to identify mRNAs encoding the different nucleoside transporters in human cell lines. The presence of transcripts for glyceraldehyde-3-phosphate dehydrogenase (GAPDH) was employed as a positive control for all northern blot experiments because of its constitutive expression in many cell types [238]. The experiments of Figure III-1 examined different human cell lines (CEM, NB4, K562, Caco-2, BeWo, HeLa, MCF7, 435S, 180/1 and HEK 293) for expression of hENT1 mRNA. The results showed

relatively high levels of hENT1 mRNA in nine of the cell lines examined and moderate levels in MCF7 lines compared to the levels observed for the GAPDH controls. These results, which indicated that hENT1 mRNA was expressed in all of the cell lines analyzed, were consistent with the general understanding that hENT1 is present in a wide range of cell types [15, 140].

The experiments of Figure III-2 were undertaken to determine if hENT2 mRNA was present in Caco-2, CEM, CEM-ARAC, HeLa, K562, MCF7 and NB4 cells. Expression of hENT2 mRNA was clearly evident in HeLa and NB4 cells, but not in CEM or CEM-ARAC cells. Although the northern blot of Figure III-2 did not convincingly demonstrate the presence of hENT2 mRNA in MCF7, K562 and Caco-2 cells, the original blot (prior to electronic conversion) showed faint bands corresponding to hENT2 mRNA for each of the three cell lines.

III.2.1.2. Analysis of hCNT1 and hCNT2 mRNAs in various human cell lines

The experiments of Figure III-3 analyzed different cell lines (Caco-2, 435S, CEM, HeLa, K562, MCF7, BeWo, HEK 293 and NB4) for the presence of hCNT1 mRNA. The results revealed that hCNT1 mRNA was present in HeLa, 435S and HEK 293 cells. The finding of hCNT1 mRNA expression in cervical cancer HeLa cells was unexpected since there had been no previous reports of hCNT1 activity in this cell line. However, the demonstration of hCNT1 mRNA in HEK 293 cells, which were derived from human kidney, was consistent with the previous report of hCNT1 mRNA in human kidney as revealed by northern blot analysis [133].

The experiments of Figure III-4 examined ten human cell lines for expression of hCNT2 mRNA. Although control GAPDH mRNA was detected in all of the cell lines, hCNT2 mRNA was not detected in any of the cell lines. The absence of hCNT2 mRNA was in contrast to the expression profile of hENT1 mRNA in these cell lines.

III.2.1.3. RT-PCR and Taqman RT-PCR analyses of nucleoside transporter mRNAs in Caco-2 and HeLa cells

At the time the northern analyses of Figures III-1 to III-4 were undertaken, hCNT3 cDNA had not yet been cloned. Subsequent to the successful cloning of hCNT3 cDNA [2], experiments were undertaken with Caco-2 and HeLa cells in which transcripts of the five transporters were assessed in the same preparations, since both cell lines were being used to study different members of the concentrative nucleoside transporter family by transient expression technique.

Expression of hENT1 mRNA in Caco-2 cells was determined by RT-PCR analysis in the experiment of Figure III-5 (Panel A). Poly(A)⁺ RNA, which was isolated from Caco-2 cells, was reverse-transcribed and subjected to amplification by PCR. The plasmid pcDNA3/hENT1, which was employed as a positive control for RT-PCR, yielded PCR-amplification of hENT1 DNA and is shown in lane 3. Identical PCR-conditions with RNA from Caco-2 cells (lane 2) produced PCR products of similar mobilities to those that were produced with pcDNA3/hENT1, demonstrating the presence of hENT1 mRNA in Caco-2 cells. PCR reactions in which DNA template from Caco-2 cells was substituted with

water resulted in no bands (lane 1) whereas reactions that employed human β -actin specific primers produced the expected bands (Panel F). RT-PCR analysis of RNA preparations from Caco-2 cells also revealed the presence of hENT2 mRNA (Panel B). The presence of hENT1 and hENT2 mRNAs in Caco-2 cells was also reported by Ward *et al*, [269].

In the northern analyses presented in Figures III-1 to III-4, hCNT1 and hCNT2 mRNAs were not detected in Caco-2 cells. The results of the experiments of Figure III-5 confirmed the absence of hCNT1 and hCNT2 mRNAs in Caco-2 cells (Panels C and D). The experiments of Figure III-5 also determined whether hCNT3 mRNA was present in Caco-2 cells (Panel E). The plasmid pcDNA3/hCNT3, which was employed as a positive control for RT-PCR, is shown in lane 3. Identical PCR conditions with RNA from Caco-2 cells (lane 2) produced a band of similar mobility to the one that was produced with pcDNA3/hCNT3 and no band was present in PCR reactions with water substituted DNA template control (lane 1). These results demonstrated for the first time the presence of hCNT3 mRNA in an adherent cultured cell line. Studies of native hCNT3 in the Caco-2 cell model of intestinal epithelium are described in Chapter VI.

It was planned to use HeLa cells as recipients for introduction of concentrative nucleoside transporter cDNAs because of their high transfection efficiency using the DEAE-dextran method of gene transfer [238, 250, 251]. However, the unexpected presence of hCNT1 mRNA in HeLa cells raised the possibility that endogenous hCNT1-mediated transport activity would interfere

with the analysis of nucleoside fluxes arising from recombinant concentrative nucleoside transporters introduced by transient transfection. Although previous studies with ENT inhibitors and nucleoside transport measurements in HeLa cells have demonstrated equilibrative-type processes, they failed to show sodium-dependent processes [153, 198].

The experiments of Figure III-6 were undertaken to compare the relative expression levels of ENT and CNT mRNAs in HeLa cells by quantitative Taqman RT-PCR. This technique overcomes the non-quantitative limitation of conventional RT-PCR by allowing the measurement of an accumulating PCR product in real time using a Taqman automated detector [281, 282]. Taqman oligonucleotide probes for PCR reactions contain a fluorescent reporter, which increases in direct proportion to the amount of PCR product in a reaction (Applied Biosystems, User Bulletin 2).

Figure III-6 is a visual representation of the fluorescence emitted by the formation of PCR products specific for GAPDH, hCNT1, hCNT2 and hCNT3. The results demonstrated that GAPDH mRNA was expressed at much higher levels than hCNT1 mRNA, whereas hCNT2 and hCNT3 mRNAs were not expressed above the threshold determined for the experiment. The relative quantitation of nucleoside transporter mRNA expression in HeLa cells is presented in Table III-1. Quantitation of relative levels of nucleoside transporter mRNA used the "Comparative Ct (cycle threshold) Method" (Applied Biosystems, User Bulletin 2) in which GAPDH was employed as the internal control to correct for differences in RNA concentrations between different preparations as

previously described [2]. The calculated results, in which the relative levels of ENT mRNA were normalized to the hCNT1 mRNA level, showed a 598-fold difference, with more hENT1 mRNA than hCNT1 mRNA. Although hENT2 mRNA was expressed at lower levels than hENT1 mRNA, there was still 156-fold more hENT2 mRNA than hCNT1 mRNA. The values for the other CNT transcripts were well below the threshold set for the experiment.

A summary of the results of the molecular analyses of human cell lines is presented in Table III-2. Collectively these results suggested that the expression of CNT transcripts was less frequent than that of ENT transcripts, and this finding was consistent with the current notion of the more limited tissue distribution of the CNTs [15]. Based on the nucleoside transporter expression profiles of the human cell lines, it was decided that HeLa cells were appropriate candidates for use as recipient cells for the transient introduction of cDNAs encoding for the various CNTs. HeLa cells were shown to express very low levels of hCNT1 mRNA, and were not expected to exhibit significant functional activity, although functional assessment of the nucleoside transporters present in HeLa cells was undertaken to confirm this conclusion.

III.2.2. Functional characterization of nucleoside transporters present in HeLa cells

To determine the endogenous nucleoside transport activities present in HeLa cells, radioisotopic flux analysis was undertaken with ³H-uridine. Uridine was employed since it is considered to be a universal permeant of all nucleoside

transporters [13, 231] and it also exhibits important characteristics such as high solubility and stability in solution.

HeLa cells are known to possess both ENT activities (*es* and *ei*), but they have not previously been shown to possess CNT activities [153, 198]. To ascertain whether HeLa cells also possessed functional CNT activities, the uptake of 10 μM uridine was measured in sodium-containing or sodium-free transport buffer in the experiment of Figure III-7 to assess the inhibitory effects of dilazep or NBMPR on uridine uptake. Uridine uptake into HeLa cells in sodium-containing transport buffer in the presence of dilazep was negligible in the time period of 30 sec. Extension of uridine uptake into HeLa cells in the presence of dilazep to 240 sec, revealed little, if any, detectable uridine uptake, indicating that ENT processes were exclusively contributing to the mediated uridine fluxes observed in HeLa cells. When uridine uptake measurements were conducted in sodium-free transport buffer, rapid uptake of uridine was observed, and this uptake was similar to that observed in sodium-containing transport buffer, suggesting the absence of any detectable sodium-dependent (i.e., concentrative) processes.

To distinguish between *es* and *ei* transport activities in HeLa cells, uridine uptake was performed in the presence of 0.1 μM NBMPR, which did not completely inhibit uridine uptake, and in the presence of 200 μM dilazep, which completely inhibited uridine uptake (Figure III-7). This result suggested that the residual uridine flux observed in the presence of NBMPR was due to mediated uptake by the *ei* transport mechanism. Comparison of the transport rates, which

were calculated from the initial rates of uptake of the NBMPR-sensitive and NBMPR-insensitive components, revealed that the *es* process was the major contributor to the observed uridine uptake (1.65 ± 0.057 pmol/ 10^6 cells/sec), and the *ei* process was a minor component (0.33 ± 0.044 pmol/ 10^6 cells/sec).

III.2.3. Production and characterization of transient transfectants in HeLa cells

When this work was undertaken, functional characteristics of human *cif* and *cit* processes were known primarily from studies of recombinant transporters (hCNT2, hCNT1) in oocytes of *Xenopus laevis* [132, 133]. With the availability of nucleoside transporter cDNAs, it became possible to study recombinant nucleoside transport proteins by expression of their cDNAs in a variety of expression systems. The nucleoside transport characteristics of recombinant transporters produced in human cells may be different from those observed using non-human expression systems.

The studies outlined below attempted to further characterize nucleoside transporter properties of human CNTs in cultured human cervical cancer HeLa cells. The molecular and functional studies described in sections III.2.1 and III.2.2 established that HeLa cells were good host cells for introduction of cDNAs encoding for CNTs. The DEAE (diethyl-aminoethyl)-dextran transfection technique had previously been successfully used to produce functional rCNT1 in cultured monkey kidney COS-1 cells [108]. Modifications of the DEAE-dextran procedure for transfection of COS-1 cells were thus applied to HeLa cells.

III.2.3.1. Analysis of DEAE-dextran toxicity to HeLa cells

Because DEAE-dextran is known to be toxic to cells [295], the concentrations that decreased viability of HeLa cells were determined. HeLa cells were exposed to graded concentrations of DEAE-dextran and cell viability was assessed at 2, 4, and 24 hr after exposure by assessing the ability of HeLa cells to exclude trypan blue. Short exposure times of 2 and 4 hr were chosen since a maximum of 4 hr is required for efficient transfection using DEAE-dextran [238, 251, 283]. The results of Figure III-8 showed that the concentration of DEAE-dextran that decreased the number of viable cells after 24-hr exposures was approximately 350 $\mu\text{g/ml}$; shorter exposures of 2 and 4 hr of the same concentrations did not decrease cell viability. However, a decrease in viability was evident at short exposure times at 400 $\mu\text{g/ml}$ DEAE-dextran and greater decreases in viability were observed at higher concentrations. Since a 2- to 4-hr exposure to DEAE-dextran was needed for efficient transfection [238, 251, 283], DEAE-dextran concentrations of 100 to 350 $\mu\text{g/ml}$, which were well below those that exhibited toxicity against HeLa cells during short exposures, were used in subsequent experiments to optimize transfection efficiency.

III.2.3.2. Optimization of DEAE-dextran transfection conditions and assessment of transfection efficiency by in situ cytochemical staining of transfected HeLa cells

The LacZ gene introduced into pcDNA3 to yield pcDNA3/LacZ was used as a reporter in transfection experiments that were undertaken to optimize transfection conditions. The activity of the gene product, β -galactosidase, which

catalyzes the hydrolysis of β -galactosides, was assayed to give an indication of transfection efficiency [260, 261]. Cells transfected with pcDNA3/LacZ appeared green following fixation and incubation with β -galactosides under the appropriate conditions. A representative bright field image of HeLa cells stained for β -galactosidase activity is shown in Figure III-9. Cellular staining of an aqua-green color was indicative of positive β -galactosidase activity, whereas HeLa cells that were colorless were assumed to have not been transfected with pcDNA3/LacZ.

Transfection conditions for HeLa cells were optimized by varying two important parameters, notably the concentrations of DEAE-dextran and DNA utilized for transfection. The results summarized in Table III-3 revealed that 200 $\mu\text{g/ml}$ of DEAE-dextran together with 1.5 μg of DNA generated the highest transfection efficiency (i.e., 42%). At the highest (3 μg) and lowest (0.5 μg) DNA concentrations, substantial decreases in transfection efficiencies were apparent at all DEAE-dextran concentrations tested. The lowest (100 $\mu\text{g/ml}$) DEAE-dextran concentration that was used yielded the lowest transfection efficiencies, regardless of the amount of pcDNA3/LacZ DNA used. Thus, subsequent transfection experiments with HeLa cells were proportionally scaled up using 200 $\mu\text{g/ml}$ of DEAE-dextran and 1-1.5 μg of the appropriate preparation of plasmid DNA.

III.2.3.3. *HeLa cells transiently transfected with hCNT1 cDNA: characterization of hCNT1-mediated uridine transport activity*

The transfection efficiency for production of hCNT1 transient transfectants was expected to be 30-37%, based on results from parallel transfection experiments with pcDNA3/LacZ and analysis of *in situ* β -galactosidase activity as described in Figure III-9. Following transfection of pcDNA3/hCNT1 into HeLa cells, uridine influx analysis was conducted to determine conditions needed to obtain initial rates of uptake for kinetic studies. Dilazep was employed as the inhibitor because of its intrinsic high solubility in aqueous solution and capacity to completely inhibit *es* and *ei* processes (i.e., ENT-mediated) [147, 246].

A time course of 10 μ M uridine uptake into HeLa cells transiently transfected with hCNT1 cDNA is presented in Figure III-10. The results showed that HeLa cells transfected with pcDNA3/hCNT1 exhibited uridine uptake that was linear over the time period of 60 sec when sodium was present in the transport buffer, whereas no detectable uptake was observed in sodium-free transport buffer. HeLa cells transfected with pcDNA3, without the hCNT1 coding region, showed no detectable uridine uptake, regardless of the presence or absence of sodium in the transport buffer. These results suggested that pcDNA3/hCNT1, when introduced in HeLa cells, was expressed, resulting in production of functional hCNT1.

Subsequent transport experiments were conducted using shorter time intervals of 10 sec to establish initial rates of uptake while still maintaining maximum differentiation between sodium-dependent and sodium-independent

uptake processes. The experiment of Figure III-11 was performed over a 10-sec time period in sodium-containing or sodium-free transport buffer with HeLa cells transfected with either pcDNA/hCNT1 or pcDNA3. The results showed that hCNT1-transfected HeLa cells exhibited linear uptake of uridine over the 10-sec time period, with an initial rate that was approximately 39-fold greater than that observed for pcDNA3-transfected HeLa cells (i.e., 0.78 ± 0.03 versus 0.02 ± 0.01 pmol/ 10^6 cells/sec, respectively). These results demonstrated that it was possible to measure initial rates of uptake mediated by recombinant hCNT1 in transiently transfected HeLa cells.

III.2.3.4. Stability of nucleoside transport activity of HeLa cells transiently transfected with hCNT1 cDNA over time

In transiently transfected cells, the introduced DNA is not incorporated into the host cell genome, and the expression levels of the introduced DNA decreases over time [258, 283]. To investigate the changes in the level of nucleoside transport activity as a function of time after transfection of pcDNA3/hCNT1 into HeLa cells, initial rates of uptake were obtained from 10-sec time courses of 10 μ M uridine uptake at 24, 48, 72 and 96 hr after transfection. The results are presented as transport rates (pmol/ 10^6 cells/sec) and are presented in Figure III-12. The results showed that uridine transport activity in sodium-containing transport buffer was evident 24 hr after transfection and the transport rates were significantly higher than those observed in sodium-free transport buffer (0.28 ± 0.01 and 0.035 ± 0.05 pmol/ 10^6 cells/sec respectively). The highest transport rates were obtained at 72 hr post-transfection and

decreased transport rates were apparent at 96 hr post-transfection. No detectable uridine uptake was observed in HeLa cells transfected with pcDNA3 when transport assays were performed in either the presence or absence of sodium. In subsequent experiments in which HeLa cells were transfected by the DEAE-dextran technique, transport assays were conducted between 48 and 72 hr post-transfection.

III.2.3.5. HeLa cells transiently transfected with hCNT2 cDNA: characterization of hCNT2 protein production and functional activity

Earlier studies described *cif*-type processes in membrane vesicle preparations from different organs such as intestine and kidney [190, 196]. The molecular cloning of the cDNA encoding for hCNT2 [131, 132], which demonstrated that hCNT2 was the protein responsible for the *cif*-type activities observed in human cells, enabled a more specific approach for studying hCNT2 by expression of its cDNA in HeLa cells. One of the objectives of generating transient transfectants of hCNT2 in HeLa cells was to ascertain whether the pcDNA3/hCNT2 construct, when expressed in human cells, would yield functional hCNT2 at the plasma membrane. Demonstration of hCNT2 functional activity and *cif*-type characteristics in transient transfectants would indicate that the pcDNA3/hCNT2 construct should produce a similar outcome when introduced into cells by stable transfection. Transient transfection of HeLa cells with pcDNA3/hCNT2 was accomplished using analogous transfection conditions that were used for generation of the hCNT1 transient transfectants. Transfection efficiencies for the production of hCNT2 transient transfectants were expected to

be approximately 30% as determined from parallel transfection experiments with pcDNA3/LacZ.

The functionality of recombinant hCNT2 produced in HeLa cells was examined by conducting uridine transport assays as presented in Figure III-13. The results showed that pcDNA3/hCNT2-transfected HeLa cells exhibited rapid uptake of uridine that was linear over 10 sec when performed in the presence of sodium, yielding a transport rate of 0.677 ± 0.029 pmol/ 10^6 cells/sec. In the absence of sodium, residual uridine uptake (0.072 ± 0.007 pmol/ 10^6 cells/sec) was observed. In a second experiment (not shown) in which cells were subjected to three additional washes with sodium-free transport buffer before transport assays, the uridine uptake in cells transfected with pcDNA3/hCNT2 (0.043 ± 0.002 pmol/ 10^6 cells/sec) was similar to that in cells transfected with pcDNA3 (0.041 ± 0.003 pmol/ 10^6 cells/sec). The low level of uridine uptake in the absence of sodium was not observed in another experiment, which was performed using identical conditions to the experiment in Figure III-13; this experiment yielded initial rates of uridine uptake in pcDNA3/hCNT2 and pcDNA3, respectively, of 0.049 ± 0.009 and 0.045 ± 0.011 pmol/ 10^6 cells/sec.

III.2.4. Characterization of CEM and CEM-ARAC cells: demonstration of hENT1 in CEM cells and its absence in CEM-ARAC cells

The human T-lymphoblastoid CEM line has been shown previously to exhibit equilibrative NBMPR-sensitive nucleoside transport activity [315] and the CEM-ARAC subline lacks the capacity for transporting cytidine and binding NBMPR [214]. The results presented in section III.2.1.1 had established that

CEM cells possessed transcripts for hENT1, but not for other nucleoside transporters. The nature of the nucleoside transport competency and deficiency, respectively, of CEM and CEM-ARAC cells was explored further in the work presented in this section. The aim was to determine the molecular basis of the transport defect of CEM-ARAC cells, and specifically to establish if they were appropriate recipient cells for stable transfection of nucleoside transporter cDNAs.

III.2.5. Presence of hENT1 mRNA in CEM, but not in CEM-ARAC cells

To ascertain if hENT1 was expressed in CEM-ARAC cells, high-sensitivity RT-PCR with primers designed to detect full-length hENT1 transcripts was undertaken with RNA isolated from CEM and CEM-ARAC cells. The results of Figure III-14 showed a PCR product of the expected size in reactions conducted with RNA from CEM cells, but not in reactions with RNA from CEM-ARAC cells. Reactions with human β -actin specific primers produced the expected bands in both CEM and CEM-ARAC cells. The control PCR reactions in which water was substituted for DNA template resulted in no bands. The unique CEM-derived PCR product was sequenced and demonstrated correspondence to the hENT1 coding sequence that was previously cloned from human placenta [135].

III.2.6. Analysis of nucleoside transport activities in CEM and CEM-ARAC cells

NBMPR binds to CEM cells with high affinity, long considered to be a hallmark of the presence of the NBMPR-sensitive process [170, 215, 284].

Ullman *et al* described the absence of high-affinity binding of NBMPR in CEM-ARAC cells [214], and concluded that the *es* process was absent from CEM-ARAC cells.

A comparison of initial rates of uptake of 10 μM ^3H -uridine by CEM and CEM-ARAC cells (Figure III-15) revealed rapid uptake of uridine in CEM cells, whereas uptake was not detected in CEM-ARAC cells. The extent to which uridine entered CEM-ARAC cells via passive diffusion was assessed by extending the time course of uridine uptake into CEM-ARAC cells over longer time periods. Minimal uridine uptake was detected into CEM-ARAC cells over the 5-min time period, and the amount of uridine uptake over longer incubations of up to 10 min was low, at best.

III.2.7. Demonstration of endogenous hENT1 in CEM, but not in CEM-ARAC, cells by immunoblot analysis

To ascertain whether the absence of uridine transport activity in CEM-ARAC cells was due to the absence of hENT1 protein as expected from the absence of hENT1 mRNA (section III.2.5), immunoblot analysis was conducted on enriched plasma membranes prepared from CEM-ARAC and CEM cells. Monoclonal antibodies raised against a synthetic peptide [144] were employed to detect hENT1 in the immunoblot of Figure III-16. As a control to assess the immunoreactivity of the anti-hENT1 monoclonal antibodies, human red blood cell (RBC) membranes was also included in the analysis. RBCs have been used for studies of the prototypic *es* process for many years [285, 286]. The immunoblot results showed that the immunoreactive protein of RBCs migrated as a broad

band with an apparent molecular mass of 51 kDa, demonstrating the presence of hENT1 in human RBC. The predicted molecular mass of hENT1 is approximately 50 kDa and the native protein of human RBC is known to be heterogeneously glycosylated [158]. A broad immunoreactive band of similar mobility to that observed in RBC membrane preparations was also observed in CEM, but not in CEM-ARAC, preparations. This result showed for the first time that the hENT1 protein was present in CEM cells, and was absent in CEM-ARAC cells.

The immunoreactivity of the anti-hENT1 monoclonal antibodies against murine ENT1, which had not been previously established, was examined using cellular lysates from three murine (L1210/B23.1, S49 and AE1) cancer cell lines. Amino acid sequence alignment of hENT1 and mENT1 (mouse ENT1) in the region (amino acid residues 254-271 of hENT1) used for production of monoclonal antibodies against hENT1 showed only 17% amino acid identity (Figure III-17). Although cross-reactivity was not expected, the experiment of Figure III-16 revealed faintly immunoreactive species that migrated as sharp bands in preparations from L1210/B23.1 and S49 cells, but not from AE1 cells, which have been shown to lack the capacity for es-mediated nucleoside transport [237, 243, 245, 246]. The apparent cross-reactivity of the anti-hENT1 monoclonal antibodies with a band of approximately 52 kDa in the S49 preparations that was absent in the AE1, suggested that the 10D7G2 monoclonal antibodies also recognized mENT1. The detection of similar

immunoreactive material in L1210/B23.1 murine leukemia cells was consistent with the es-type process known to be present in this cell line [244].

III.2.8. Production and isolation of stable transfectants of CEM-ARAC cells

The studies described in sections III.2.4-III.2.7 indicated that CEM-ARAC cells lacked endogenous nucleoside transporters, and thus were ideally suited to serve as the recipient cells for creation of stable transfectants that produced a single type of nucleoside transporter in isolation. In addition, the relative simplicity of culturing suspension cells for transport studies was useful. Electroporation was employed as a method of choice for gene transfer since higher frequencies of stable integration of the introduced DNA is usually achieved relative to other transfection methodologies [257, 258]. Also, once electrical parameters for electroporation were established for transfection of a particular transporter cDNA, similar parameter settings could be applied to transfections with other nucleoside transporter cDNAs.

III.2.8.1. Optimization of transfection conditions for electroporation

Although high levels of cell death are common after electroporation, a range of 40-60% viability has been found to yield reasonable transfection efficiencies [255, 256]. In these studies, the electroporation parameters (i.e., voltage and capacitance settings) were varied to determine conditions that achieved approximately 50% viability of CEM-ARAC cells after electroporation. Prior to electroporation, CEM-ARAC cells and pcDNA3/LacZ in PBS were

combined, placed in 4-mm gap cuvettes and incubated on ice for 10 min. Control cultures of CEM-ARAC cells without pcDNA3/LacZ were treated identically. Electroporation parameters that used a low constant capacitance setting while varying the voltage in the range of 1000-2000 V were initially tested with CEM-ARAC cells because these parameters have been used to obtain stable transfectants in many cell types [253]. The experiment of Figure III-18, in which the capacitance was maintained at 25 μ F while the voltage of the electrical pulse was increased in stepwise fashion, revealed that most of the CEM-ARAC cells were killed at the lowest voltage setting of 1000 V for the experiment. Increases in voltage resulted in corresponding decreases in the number of viable CEM-ARAC cells. Voltage settings of 1800-2000 V produced almost complete CEM-ARAC cell kill after electroporation. Similar results were obtained with CEM-ARAC cells devoid of pcDNA3/LacZ DNA in electroporation medium (not shown). CEM-ARAC cells that were subjected to the electroporation conditions of 1000 V and 25 μ F, which yielded the highest number of viable cells in the experiment of Figure III-18, were chosen for determination of transfection efficiency by analysis of β -galactosidase activity.

To assess the effects of different amounts of DNA on the transfection efficiency of CEM-ARAC cells electroporated at 25 μ F and 1000 V, the experiment of Figure III-19 was undertaken. Analysis of β -galactosidase activity in CEM-ARAC cells was performed 72 hr after electroporation of pcDNA3/LacZ by measuring the appearance of a bright yellow end product from β -galactosidase hydrolysis of its substrate o-nitrophenyl- β -D-galactopyranoside

[262]. The results presented in Figure III-19 shows the level of β -galactosidase activity in CEM-ARAC cells electroporated with pcDNA3/LacZ. For most of the pcDNA3/LacZ DNA concentrations tested, the electroporation conditions of 1000 V and 25 μ F yielded only small differences between CEM-ARAC cells electroporated in the presence and absence of pcDNA3/LacZ. Lowering the voltage below 1000 V while maintaining capacitance at 25 μ F has been previously shown to increase viability, but to also decrease the transfection frequency [253].

In the experiment of Figure III-20, the capacitance was lowered from 25 μ F to 3 μ F, and voltage settings ranging from 1000-2000 V were tested. The results showed a dramatic increase in CEM-ARAC cell viability relative to the results shown in Figure III-18, particularly at the lower voltage settings of 1000-1400 V. Further increases in voltage from 1400-2000 resulted in decreases in CEM-ARAC cell viability below 50%. The electrical pulse setting of 1400 V at 3 μ F yielded approximately 50% viable CEM-ARAC cells after electroporation. CEM-ARAC cells that were subjected to this electroporation condition were chosen for analysis of β -galactosidase activity.

The experiment of Figure III-21 shows the β -galactosidase activity of CEM-ARAC cells electroporated with varying pcDNA3/LacZ DNA concentrations using the new electrical pulse setting of 1400 V and 3 μ F. The results revealed low β -galactosidase activities for the majority of the pcDNA3/LacZ plasmid concentrations examined. Plasmid concentrations of 9-11 μ g of pcDNA3/LacZ gave the highest levels of β -galactosidase activity.

It has been shown that some cells of the hematopoietic lineage are electroporated more effectively in tissue culture medium without serum and at low voltage/high capacitance settings, which yield 10-fold longer electrical pulses than the more commonly used setting [255]. These settings would, in theory, extend the membrane pore opening time and facilitate an increase in the number of DNA molecules to enter cells [287]. These electroporation conditions were assessed in the experiments in which PBS was replaced by glutamine-free RPMI 1640 and CEM-ARAC cells were electroporated with pcDNA3/LacZ using a Gene Pulser that was equipped with a capacitance extender set at 960 μ F. The experiment of Figure III-22, which tested voltage settings ranging from 100 to 300 V, yielded high viability of CEM-ARAC cells at the lower voltage settings and a gradual decrease in viability as a function of increasing voltage. Since voltage settings of 180 and 200 V resulted in approximately 58% and 45% viable CEM-ARAC cells, respectively, after electroporation, a voltage setting of 190 V was used to obtain approximately 50% viability.

To determine the best concentration of DNA to use with the revised electroporation conditions of 190 V and 960 μ F, the experiment of Figure III-23 was undertaken. Presented is the β -galactosidase activity of CEM-ARAC cells electroporated with pcDNA3/LacZ DNA. The results showed a modest increase in the level of β -galactosidase activity for most of the pcDNA3/LacZ DNA concentrations tested compared to those observed in Figures III-19 and III-21, particularly at pcDNA3/LacZ DNA concentrations from 8-11 μ g. Although the β -galactosidase activities fluctuated at the lower (2-7 μ g) pcDNA3/LacZ DNA

concentrations, they were fairly constant at the higher pcDNA3/LacZ concentrations (8-11 µg). Subsequent electroporation of CEM-ARAC cells with pcDNA3 containing the coding sequences for the different nucleoside transporters utilized 9 µg of DNA and electrical pulse parameters of 190 V and 960 µF.

III.2.8.2. Determination of appropriate exposure concentration of geneticin for selection of CEM-ARAC stable transfectants

The neomycin analog, geneticin, was used as a selective agent for transfected cells harbouring the neomycin resistance gene [288]. The pcDNA3 vector possesses a neomycin resistance gene downstream of the polylinker (see Figure II-1), and therefore confers geneticin resistance on cells that have been stably transfected, enabling them to grow in media containing geneticin.

It has been shown that the amount of geneticin required in culture media to inhibit the growth of cells not transfected with the neomycin resistance marker varied with different cell types [238, 288]. Therefore, the experiment of Figure III-24 was undertaken to determine the minimum concentration of geneticin required to kill all non-transfected CEM-ARAC cells. CEM-ARAC cells in early exponential growth were exposed to growth media that contained graded concentrations of geneticin and the growth inhibitory effects of increasing geneticin concentrations were expressed as the percentage of growth rates of untreated (control) CEM-ARAC cells. The results of Figure III-24 showed that 48-hr exposures to geneticin produced relatively low growth inhibitions, even at high concentrations, compared to that observed during 72-hr and 120-hr

exposures. Geneticin exposure times of 72 or 120 hr resulted in maximal growth inhibition of CEM-ARAC cells, which was apparent at geneticin concentrations of $\geq 150 \mu\text{g/ml}$. This result suggested that there was a lag period before the growth inhibitory effect of geneticin became apparent, and therefore prolonged exposures to geneticin would be necessary to select transfected cells that have incorporated the neomycin resistance gene. Therefore, the procedure for the selection of geneticin-resistant CEM-ARAC cells was accomplished using prolonged exposures to a geneticin concentration of $200 \mu\text{g/ml}$.

III.2.8.3. Production of hCNT2 stable transfectants of CEM-ARAC cells

The established electroporation conditions for gene-transfer (described in section III.2.8.1-III.2.8.2) were employed to stably introduce the hCNT2 coding sequence into transport-deficient CEM-ARAC cells. The construct, pcDNA3/hCNT2, was shown in section III.2.3.5 to be expressed properly in transient transfection experiments with human cervical cancer HeLa cells since sodium-dependent transport activity was observed after transfection, indicating the presence of functional hCNT2 at the cell surface. Electroporation of CEM-ARAC cells with pcDNA3/hCNT2 was accomplished using the optimized electrical pulse parameters of 190 V and $960 \mu\text{F}$. Isolation of hCNT2 stable transfectants with the introduced pcDNA3/hCNT2 was based on selection for geneticin resistance by growth in $200 \mu\text{g/ml}$ geneticin as described in section III.2.8.2.

Surviving geneticin-resistant clones were isolated and individually expanded, and their nucleoside-transport activities were compared with those of

CEM-ARAC cells by quantitating cellular uptake of radioactivity during 5-min exposures to 10 μ M 3 H-uridine. More than 4000 clones were produced and of the several hundred that were tested for their capacity to accumulated 3 H-uridine, only a few exhibited nucleoside transport activity. Representative results are shown in Table III-4. The D2 clone exhibited the highest uridine uptake activity and was therefore selected and recloned by limiting dilution. Subsequent uridine uptake measurements with the CEM-ARAC/hCNT2-D2 reclone, hereafter referred to as ARAC/D2, yielded no further enrichment in uridine transport activity (values \pm S.D. ranged from 1987 ± 247 cpm/ 10^6 cells to 2208 ± 92 cpm/ 10^6 cells), indicating that the transport-competent phenotype was stable.

III.2.8.4. Integration of hCNT2 cDNA into the genome of ARAC/D2 cells

Genomic DNA from ARAC/D2 cells was examined to determine if pcDNA3/hCNT2 was integrated into the host cell genome in the experiment of Figure III-25. High-stringency hybridization with full length hCNT2 cDNA of EcoR1-digested genomic DNA revealed a single unique band of 3.4 kb in ARAC/D2, but not in CEM-ARAC preparations and two faint bands of 2.1 kb and 1.7 kb in both preparations. The unique 3.4-kb band in ARAC/D2 preparations suggested integration of hCNT2 cDNA into host genomic DNA, whereas the 2.1- and 1.7-kb bands were evidently derived from the endogenous hCNT2 gene, since they were both observed in the transfected and untransfected cell preparations. The stronger signal observed for CEM-ARAC preparations, relative to that for ARAC/D2 preparations, was because a greater quantity of

genomic DNA (15 versus 10 µg, respectively) was analyzed to increase the likelihood of detecting endogenous hCNT2 DNA.

III.2.8.5. Detection of hCNT2 mRNA in ARAC/D2 cells but not in CEM or CEM-ARAC cells

Poly(A)⁺ RNA from actively proliferating cultures of ARAC/D2, CEM and CEM-ARAC cells was analyzed by RT-PCR, followed by nested-PCR in the experiments of Figures III-26 and III-27. When pcDNA3/hCNT2 was used as the template, fragments with gel mobilities expected for the 458-bp (Figure III-26) and 425-bp (Figure III-27) products of the external- and nested-hCNT2 primers were produced. Although PCR products that migrated with the same mobilities as those obtained with the hCNT2-plasmid preparations were detected in both rounds of PCR with the ARAC/D2 preparations, PCR products were not detected after either round (of 25 cycles each) conducted with the CEM and CEM/ARAC preparations. Sequencing of the nested-PCR product from the ARAC/D2 preparations demonstrated exact correspondence with the cloned hCNT2 DNA sequence from human intestine [132]. These results established that (i) CEM and CEM/ARAC cells lacked hCNT2 mRNA, indicating that their lack of endogenous hCNT2 activity was due to low (or no) expression of the hCNT2 gene, and (ii) ARAC/D2 cells contained hCNT2 mRNA, evidently produced by expression of the introduced hCNT2 cDNA.

III.2.8.6. Stability of the nucleoside-transport phenotype in ARAC/D2 cells

The stability of the acquired nucleoside transport activity of the hCNT2 stable transfectant was assessed by determining uridine transport rates in parallel cultures of ARAC/D2 cells that were maintained in either the presence or absence of geneticin over many passages. Geneticin-containing and geneticin-free cultures were analyzed at passage 10, 20 and 25 for cellular uptake of ^3H -uridine in the presence or absence of sodium as shown in the experiment of Figure III-28. Uridine transport rates were relatively constant in the cultures that were maintained in geneticin over 25 passages (about 100 days in culture) and there was no substantial decline in uridine transport rates observed in the cultures maintained in the absence of geneticin over the same number of passages. These results demonstrated the long-term stability of the acquired nucleoside transport activity even in the absence of geneticin-selection pressure. Therefore, stable transfectants were routinely propagated in the absence of geneticin for experimental purposes, although stock cultures were maintained in geneticin to exclude the possibility of developing revertants.

III.2.8.7. Transport characteristics of ARAC/D2 cells: Na^+ -dependency and cif-type activity

The nature of the acquired nucleoside-transport capability of ARAC/D2 cells was assessed by comparing time courses of uptake of $10\ \mu\text{M}$ ^3H -uridine in the presence or absence of sodium by ARAC/D2 cells with those of CEM-ARAC or CEM cells as shown in the experiment of Figure III-29. In the presence of sodium, ARAC/D2 cells exhibited initial uptake rates (i.e., transport) that were

25-fold greater than those of CEM-ARAC cells, whereas in the absence of sodium, uptake rates were negligible. This indicated that the observed stimulation of uridine transport activity required the presence of an inwardly directed sodium gradient. Uridine uptake by CEM cells, which possessed only hENT1 activity, reached equilibrium at around 60 sec and was not dependent on the sodium gradient. No measurable uridine uptake was observed in CEM-ARAC cells in either the presence or absence of sodium, which was consistent with the nucleoside-transport deficiency previously established for this cell line [71, 214].

Natural nucleosides that are diagnostic for the *cif*-type transport process were assessed for their ability to inhibit sodium-dependent uridine transport in ARAC/D2 cells. The experiment of Figure III-30 revealed that sodium-stimulated uridine transport was completely inhibited by either 1 mM inosine or guanosine. Thymidine and dilazep did not significantly reduce uridine transport when tested at 1 mM. Collectively, the observed inhibition characteristics of ARAC/D2 cells were consistent with those described for naturally occurring *cif*-type transporters of human intestine and kidney epithelia [119, 196].

III.2.8.8. Production of hCNT1 stable transfectants of CEM-ARAC cells

A similar gene-transfer methodology based on the electroporation conditions used to obtain the ARAC/D2 stable transfectants was employed to introduce hCNT1 cDNA into CEM-ARAC cells. Approximately 3400 geneticin-resistant clones were isolated and expanded for isotopic flux analyses with 10 μ M 3 H-labeled uridine, which were performed in the presence or absence of sodium

over a 4-min time period. Of the approximately 223 clones that were examined initially for uridine uptake activity, six clones exhibited consistently high uridine uptake values during repeated uridine uptake measurements. These six transport-positive clones were recloned by limiting dilution in geneticin as described in section II.12.2. The clone TLC2-A33DT1 (hereafter referred to as TLCT1) was kept for further analysis because it exhibited similar uridine uptake values before and after recloning.

The acquired nucleoside transport activity of the TLCT1 transfectants was characterized in the experiment of Figure III-31, in which uptake of $10\ \mu\text{M}$ ^3H -uridine was measured over 240-sec intervals in the presence or absence of sodium. The results revealed a stimulation of uridine uptake in the presence of sodium that was linear over the time period analyzed and yielded a rate of 0.278 ± 0.008 pmol/ μl cell water/sec. In contrast, uridine uptake in the absence of sodium was negligible and was similar to the uptake observed in the presence of excess nonradiolabeled uridine to block mediated flux of ^3H -uridine.

To ascertain the functional characteristics of the acquired nucleoside transport activity, various diagnostic nucleosides and nucleoside analogs were tested for their ability to inhibit uridine uptake into TLCT1 cells. Figure III-32 shows the inhibitory activity of various test compounds (thymidine, guanosine, cytidine and NBMPR) on uridine transport by TLCT1 cells. The results demonstrated that uridine transport in the absence of additives was stimulated by the presence of sodium whereas in the absence of sodium, negligible uridine uptake was observed. The addition of pyrimidine nucleosides (cytidine and

thymidine) in the presence of sodium completely inhibited uridine transport into TLCT1 cells. NBMPR was employed to assess the presence, if any, of NBMPR-sensitive process in TLCT1 cells. Uridine uptake into TLCT1 cells was not inhibited by either 2 mM guanosine or 10 μ M NBMPR, which was employed to assess the presence, if any, of NBMPR-sensitive process in TLCT1 cells. This inhibition profile was typical of the pyrimidine-nucleoside selective hCNT1, which has previously been described in studies of recombinant hCNT1 produced in *Xenopus* oocytes by Ritzel *et al.* [133].

III.2.8.9. *Production of hENT2 stable transfectants of CEM-ARAC cells*

The hENT2 coding sequence was PCR-amplified from the original cloning vector pBluescript KS with the appropriate restriction sites for subcloning into the pcDNA3 vector. Similar electroporation conditions that were employed in the production of ARAC/D2 and TLCT1 transfectants were applied to introduce hENT2 cDNAs into CEM-ARAC cells. Of the more than 1000 geneticin resistant-clones isolated and expanded, the clone TLC63-G109BT2 (hereafter referred to as TLET2) exhibited the highest uridine uptake activity. The TLET2 transfectants were recloned by limiting dilution in geneticin and the measured nucleoside transport activity (0.102 ± 0.01 pmol/ μ l cell water/sec) was similar to the transport activity observed prior to recloning (0.098 ± 0.02 pmol/ μ l cell water/sec). This result demonstrated the consistency of nucleoside transport activities and the apparent stability of the acquired nucleoside transport phenotype of the TLET2 transfectants.

Time courses of uridine uptake into the TLET2 transfectants were determined, an example of which is shown in Figure III-33, demonstrating linear uptake of uridine over a time period of 240 sec. The addition of 200 μ M dilazep reduced uridine influx to negligible levels that were similar to those observed in the presence of 3 mM nonradiolabeled uridine. The sensitivity to inhibition by dilazep indicated that the TLET2 transfectants exhibited an ENT-like nucleoside transport process.

To demonstrate that the uptake of uridine by TLET2 cells was mediated by recombinant hENT2, the effects of several test compounds on uridine uptake were examined in the experiments of Figure III-34. These experiments were performed in sodium-containing transport buffer in the presence of i) 3 mM diagnostic nucleoside or nucleobase, ii) 0.1 μ M NBMPR or iii) 200 μ M dilazep. There was no change in uridine transport rates when uptake was performed in either sodium-containing or sodium-free transport buffer in the absence of additives. This result was indicative of an equilibrative transport mechanism since the removal of sodium had no effect on uridine uptake. The addition of purine (guanosine) or pyrimidine (thymidine, cytidine) nucleosides or the nucleobase hypoxanthine reduced uridine influx to levels similar to that observed in the presence of dilazep. The inhibition of uridine uptake by hypoxanthine in TLET2 transfectant, which may be indicative of transportability of this compound, was consistent with the unique ability of hENT2, among nucleoside transporters, to transport hypoxanthine [289, 290]. NBMPR did not inhibit uridine uptake at 0.1 μ M, which was expected since hENT2 is insensitive to NBMPR [136, 137,

289]. Collectively, these results suggested that the TLET2 stable transfectants produced recombinant hENT2 since the inhibitory activities of the various test compounds were typical of an *ei*-type transporter [15, 136, 137, 289, 290].

III.2.9. Comparison of the nucleoside transport activity by T-lymphoblastoid cell lines producing hCNT2, hCNT1, hENT2, and hENT1 in isolation

The experiments of Figure III-35 were undertaken to compare the relative abilities of the different nucleoside transporters to mediate the uptake of the universal permeant uridine. The uptake of 10 μM ^3H -uridine was measured in the presence of sodium and uridine transport rates were obtained from the slopes of linear portions of time courses. The results revealed that the hCNT1 transfectants exhibited a uridine transport rate of 0.288 ± 0.004 pmol/ μl cell water/sec, which was approximately three-fold higher than those of the hCNT2 and hENT2 transfectants. The uridine transport rates for the hCNT2 and hENT2 stable transfectants (0.110 ± 0.001 pmol/ μl cell water/sec and 0.098 ± 0.003 pmol/ μl cell water/sec respectively) were similar. However, of the four transporters test, native hENT1 in CEM cells exhibited the highest uridine transport rate (0.802 ± 0.091 pmol/ μl cell water/sec).

III.3. Discussion

For many cell types, the occurrence of heterogeneous nucleoside transport processes with complex overlapping substrate selectivities poses difficulty in the interpretation of flux measurements and characterization of nucleoside transportability. Mutagenesis and phenotypic selection methods have been used to develop mutants or derivatives of the murine L1210 leukemia, which exhibits multiple nucleoside transport processes [201], that each possess a single process (*es*, *cif*) for analysis of individual nucleoside transporter types [201, 244]. In addition, a stable transfectant with the rat pyrimidine-nucleoside selective transporter (rCNT1) has been produced in a nucleoside-transport deficient L1210 cell line [159]. However, species differences in nucleoside transporter interaction with substrates have been reported for both ENT and CNT family members [147, 148, 291, 292].

While earlier studies of human nucleoside transporters with cultured human cell lines yielded much profitable information (for examples, see [115]), they also revealed the heterogeneity of nucleoside transporters present in human cells. Accordingly, the aim of the work in this chapter was to develop human cell models with the same genetic background for study of a single nucleoside transport activity. Various human cell lines of different tissue origin were analyzed for expression of nucleoside transporter mRNAs and two (HeLa and CEM-ARAC cells) demonstrated suitability for transfection purposes.

The expression profiles for hCNTs and hENTs in the human cell lines examined correlated well with their nucleoside transport activities shown in this

study and elsewhere. In comparison to the limited distribution of the CNT mRNAs, the ENT mRNAs were expressed in a broader range of cell lines, with hENT1 mRNA being expressed in all the cell lines examined. The presence of hENT1 mRNA in BeWo, CEM, NB4, K562, Caco-2, HeLa, MCF7 and 435S cells was consistent with the *es* processes reported for these cell types [121, 153, 154, 170, 171, 200, 215, 269, 293, 294].

Although hENT2 mRNA had not previously been shown in NB4, MCF7 and K562 cells, it was consistent with the observed *ei*-type transport activities reported in these cell lines [121, 200]. The demonstration of hENT2 mRNA in HeLa cells was also established for the first time in this work. In the past, HeLa cells have been used to study the endogenous *ei*-mediated process [153, 170, 265].

None of the cell lines analyzed expressed hCNT2 mRNA, which is consistent with the current status of the lack of a model cell line for studying hCNT2 [140]. The demonstration of hCNT1 mRNA in HEK 293 cells, which were derived from human kidney, was consistent with a previous report of hCNT1 mRNA in human kidney by northern blot analysis [133]. Also, transport activity of the *cit* process, which is indicative of the presence of hCNT1, has been described in preparations from human, pig, cow and rat kidney [123, 195, 230].

The expression of hCNT1 mRNA in HeLa cells was unexpected since transport assays did not reveal any sodium-dependent (i.e., concentrative) transport activities, although equilibrative processes were readily detectable. Measurements of the relative levels of nucleoside transporter mRNA expression

in HeLa cells by real-time quantitative RT-PCR failed to detect hCNT2 and hCNT3 mRNAs. Although hCNT1 mRNA was detected in these experiments, the levels of hENT1 and hENT2, respectively, were 598-fold and 156-fold greater than hCNT1 mRNA levels, indicating that hCNT1 mRNA was present in very small amounts in HeLa cells. This result corresponded well with the uridine transport activities observed in HeLa cells, in which hENT1 was the major contributor to influx of 10 μ M uridine (1.65 ± 0.057 pmol/ 10^6 cells/sec), followed by hENT2 (0.33 ± 0.044 pmol/ 10^6 cells/sec), with no evidence of CNT-mediated activities.

HeLa cells were chosen as recipients for transient transfections of CNTs (hCNT1 and hCNT2) because they lacked functional CNT-mediated activities. The ENT-mediated activities in HeLa cells could be inhibited by dilazep [75]. Generation of transient transfectants in HeLa cells provided confirmation that pcDNA3 containing the different nucleoside transporter cDNAs, when introduced into cultured human cells, resulted in functional nucleoside transporters. The same constructs were employed for production of stable transfectants in CEM-ARAC cells.

Interestingly, in a single experiment that examined sodium-dependency of uridine uptake into HeLa cells transiently transfected with hCNT2 cDNA, a low level of uridine uptake was observed in the absence of sodium and the presence of dilazep. This may have been due to trace amounts of sodium left behind from the incomplete removal of cell culture growth media after standard washing with sodium-free transport buffer. In subsequent experiments, additional washes of

HeLa cell monolayers with sodium-free transport buffer prior to uptake measurements in the absence of sodium and in the presence of dilazep effectively decreased uptake values to the levels observed with pcDNA3 transfected cells. A small amount of uncoupled transport (slippage) has been observed in transport experiments conducted in the absence of sodium with recombinant CNT proteins produced in the *Xenopus*-oocyte expression system [63, 180].

At the time this study was undertaken, the molecular identity of the protein linked to the deficiency in nucleoside transport capability of CEM-ARAC cell line had not yet been determined, although it was predicted, based on the *es*-like functionality of the parental CEM line, to be hENT1. The present work established by RT-PCR and DNA sequencing of the resulting products that CEM cells possessed, whereas CEM-ARAC cells lacked, mRNA that corresponded to the identified coding sequence of placental hENT1 [135]. The absence of hENT1 mRNA and hENT1 protein, combined with the inability to transport uridine and other nucleosides in isotopic flux analysis, indicated that hENT1 was exclusively responsible for mediating nucleoside uptake in CEM cells. This conclusion is consistent with the detection of the *es* process in CEM cells by radioisotopic flux analysis and NBMPR photoaffinity labeling [75, 137, 215].

The transport deficiency of the CEM-ARAC cell line was exploited in the production of stable transfectants with a single nucleoside transporter type. Gene transfer by electroporation was employed to introduce nucleoside transporter coding sequences into the genome of CEM-ARAC cells, thereby

generating a series of isogenic cell lines, each producing a specific nucleoside transporter of interest. Although electroporation generally requires more optimization of transfection conditions than the DEAE-dextran method, electroporation produces a greater frequency of exogenous DNA integration into the host cell genomic DNA [258, 295]. Also, once electroporation conditions are optimized, similar conditions can be applied for production of other stable transfectants. In the current work, the optimal conditions for electroporation were established during the production of hCNT2 transfectants.

Isolation of stable transfectants that had acquired the introduced nucleoside transporter cDNA was based on selection for a surrogate marker by growth in geneticin. Geneticin is an aminoglycoside that inhibits protein synthesis in mammalian cells by interfering with ribosomal function [296]. Expression of the bacterial APH gene, which encodes for aminoglycoside 3'-phosphotransferase, in mammalian cells therefore results in detoxification of geneticin [297, 298].

Many of the hCNT2 stable transfectants, despite their resistance to geneticin, did not exhibit nucleoside transport activity when assayed directly by measuring ³H-uridine accumulation into cells. This failure may have been due to (i) loss of the nucleoside transporter insert, although the geneticin-resistance marker was retained, or (ii) unsuitable integration of nucleoside transporter sequences (e.g., in intervening (i.e. non-expressed) regions of the host cell genome) for functional expression. However, a number of geneticin-resistant transfectants exhibited low uridine transport activity, suggesting integration of hCNT2 cDNA into

genomic regions that resulted in low level production of transporter protein at the cell surface.

The hCNT2 stable transfectant named ARAC/D2 is the first stable transfectant to have been produced in human cells that lacked endogenous nucleoside transporters. Southern blots of EcoR1-digested genomic DNA from ARAC/D2 cells indicated incorporation of hCNT2 DNA into host-cell genomic DNA. Recloning of the hCNT2-producing ARAC/D2 line under geneticin selection did not significantly increase nucleoside transport activity of cultures, suggesting that the line was clonal in origin. The acquisition of functional hCNT2 protein at the cell surface was demonstrated by the presence of sodium-dependent transport of guanosine, adenosine, inosine and uridine, but not thymidine, a permeant selectivity that is typical of native *cif*-type transporters [119, 196].

The generation of the hCNT2 stable transfectant of CEM-ARAC cells served as a guide for production of other (e.g., hCNT1 and hENT2) stable transfectants in the same host cell line. Comparison of the uridine transport activity of stable transfectants producing different recombinant nucleoside transporters revealed that the hCNT1 transfectants exhibited approximately 3-fold higher transport activity compared to hCNT2 and hENT2 transfectants when tested at 10 μ M uridine. However, native hENT1 in CEM cells exhibited a much higher uridine transport rate relative to the recombinant nucleoside transporters produced in CEM-ARAC cells. This may have been due to differences in

expression of native versus recombinant nucleoside transporters, or to real differences in their capacities to transport uridine.

The goal of the work in this chapter was to develop new cellular model systems for study of nucleoside transporters in isolation from other nucleoside transporter types. Characterization of various human cell lines established that HeLa and CEM cells were suitable for transfection purposes. Transient transfection of HeLa cells enabled the production of transient transfectants that produced either hCNT1 or hCNT2. Stable transfection technique generated stable cell lines that produced hCNT1, hCNT2 or hENT2 in isolation. The availability of these stable transfectants opens the possibility for transporter type-specific designs of permeants and inhibitors. In addition, they provide appropriate model systems for studies, such as those described in subsequent chapters, that compared the properties of different nucleoside transporters.

Table III-1. Comparison of the relative expression levels of nucleoside transporter mRNAs in HeLa cells by quantitative Taqman RT-PCR

Total RNA was isolated from actively proliferating HeLa cells and cDNAs were synthesized by reverse transcription and subjected to Taqman PCR as described in Materials and Methods (section II.7). The data are expressed as the cycle threshold values (Ct), which are the PCR cycle number at which the accumulated fluorescent signal in each reaction crossed a threshold (a level of fluorescence) above background, which was set within the linear phase of the exponential PCR reaction. The relative levels of mRNA were calculated by the Comparative Ct Method (section II.7).

	Ct	Average Ct	ΔCt^1	$\Delta\Delta Ct^2$	Relative to hCNT1 ³
hCNT1	34.32 34.57 34.57	34.48±0.08	14.21±0.12	0.00±0.12	1
hENT1	25.18 25.20 25.41	25.26±0.07	4.98±0.11	(-)9.22±0.11	598
hENT2	27.55 26.46 27.58	27.20±0.37	6.92±0.38	(-)7.29±0.38	156
hCNT2	38.87 36.44 38.03	37.78±0.71	Below threshold	Below threshold	N/A
hCNT3	40.00 40.00 39.48	39.83±0.17	Below threshold	Below threshold	N/A
GAPDH	20.37 20.11 20.36	20.28±0.08	N/A	N/A	N/A

¹The ΔCt value was determined by subtracting the average of the control GAPDH Ct values from the average Ct value obtained for each nucleoside transporter (hENT1, hENT2, hCNT1, hCNT2 or hCNT3). The standard deviation of the difference was calculated from the standard deviations of the control GAPDH and nucleoside transporter values using the following formula:

$$s = \sqrt{s_1^2 + s_2^2} \quad \text{where: } s = \text{standard deviation}$$

²The results are normalized to the level of the hCNT1 ΔCt value

³The levels of hENT1 and hENT2 mRNA relative to hCNT1 mRNA were determined by the formula: $2^{-\Delta\Delta Ct}$

Table III-2. Summary of northern and RT-PCR analyses of mRNA expression in various human cell lines

For northern blot analyses, total RNA was isolated from human colon carcinoma Caco-2, kidney HEK 293, breast adenocarcinoma MCF7, breast ductal carcinoma 435S, squamous cell cervical cancer 180/1, cervical adenocarcinoma HeLa, chronic myelogenous leukemia K562, acute promyelocytic leukemia NB4, acute lymphoblastic leukemia CEM, choriocarcinoma BeWo cells as described in Figures III-1-III-4. For RT-PCR, mRNA was isolated from human acute lymphoblastic leukemia CEM and CEM-ARAC cells, followed by cDNA synthesis and PCR-amplification as described in section II.6. For Taqman RT-PCR, total RNA was isolated from HeLa cells, cDNA was synthesized and subjected to real-time PCR using the Taqman 7700 sequence detection system as described in Figure III-6. Results are scored as + (presence of specific transcripts) or - (absence of specific transcripts). Individual entries are based on results of at least two separate experiments that yielded similar results. Unless otherwise noted, positive (+) and negative (-) entries are based on results of northern analysis.

Cell line	hCNT3	hCNT2	hCNT1	hENT2	hENT1	GAPDH/actin
Caco-2	+ ⁵	- ⁵	- ⁵	+ ⁵	+ ⁵	+ ⁵
HEK293	ND ¹	-	+	ND ¹	+	+
MCF7	ND ¹	-	-	+	+	+
435S	ND ¹	-	+	ND ¹	+	+
180/1	ND ¹	-	ND ¹	ND ¹	+	+
HeLa	- ²	- ²	+ ²	+ ²	+ ²	+ ²
K562	ND ¹	-	-	+	+	+
NB4	ND ¹	-	-	+	+	+
CEM	ND ¹	- ³	-	-	+ ⁴	+ ^{3,4}
CEM-ARAC	ND ¹	- ³	ND ¹	-	- ⁴	+ ^{3,4}
BeWo	ND ¹	-	-	ND ¹	+	+

¹Not determined

²Also demonstrated by Taqman RT-PCR as described in Figure III-6

³Also demonstrated by RT-PCR as described in Figures III-26 and III-27

⁴Also demonstrated by RT-PCR as described in Figure III-14

⁵Also demonstrated by RT-PCR as described in Figure III-5

Table III-3. Transfection efficiencies assessed by *in situ* β -galactosidase staining of HeLa cells transfected with different concentrations of plasmid and DEAE-dextran

HeLa cells were transfected on 60-mm plates as described in Materials and Methods (section II.11.1) with different pcDNA3/LacZ and DEAE-dextran concentrations as indicated below. After 72 hr, cells were fixed and stained for β -galactosidase activity as described in Materials and Methods (section II.13.1) and as shown in Figure III-9. Cells were counted using a hemocytometer at 100x magnification by bright-field microscopy as described in section II.10.3. The results are calculated as the percent of green staining in the total population and are expressed as the mean of duplicate sample determinations.

Amount of DEAE-dextran ($\mu\text{g/ml}$)	Amount of pcDNA3/LacZ (μg)	Percentage of positive cells
100	0.5	3
100	1	1
100	1.5	<1
100	2	<1
100	2.5	<1
100	3	<1
150	0.5	10
150	1	32
150	1.5	24
150	2	18
150	2.5	1
150	3	<1
200	0.5	<1
200	1	32
200	1.5	42
200	2	28
200	2.5	5
200	3	1
250	0.5	5
250	1	10
250	1.5	20
250	2	24
250	2.5	28
250	3	11
300	0.5	<1
300	1	2
300	1.5	10
300	2	15
300	2.5	20
300	3	<1
350	0.5	<1
350	1	<1
350	1.5	5
350	2	12
350	2.5	10
350	3	<1

Table III-4. Uptake of ³H-uridine by representative geneticin-resistant clones of CEM-ARAC cells

Cultures were expanded from individual surviving clones as described in section II.10. Cells were incubated at room temperature for 5 min in the presence of 10 μ M ³H-uridine in sodium-containing transport buffer (1 x 10⁶ cells/ml), and cell-associated radioactivity was determined as described in section II.15. Net uptake was determined by taking the difference of the total uptake for each clone and the CEM-ARAC uptake. Shown are values (mean \pm SD of triplicate determinations, n = 2) from assays with 40 of > 4000 cloned populations of transfected cells.

Clone	Uridine uptake ¹ (cpm/10 ⁶ cells)	Clone	Uridine uptake ¹ (cpm ¹ /10 ⁶ cells)
CEM-ARAC	87 \pm 4		
D1	157 \pm 17	D21	247 \pm 17
D2	1987 \pm 247	D22	157 \pm 25
D3	187 \pm 10	D23	89 \pm 7
D4	122 \pm 15	D24	92 \pm 4
D5	137 \pm 17	D25	167 \pm 14
D6	547 \pm 74	D26	354 \pm 21
D7	218 \pm 101	D27	234 \pm 13
D8	981 \pm 237	D28	222 \pm 17
D9	567 \pm 127	D29	187 \pm 22
D10	167 \pm 16	D30	487 \pm 57
D11	883 \pm 456	D31	125 \pm 11
D12	987 \pm 128	D32	857 \pm 16
D13	906 \pm 89	D33	167 \pm 13
D14	501 \pm 24	D34	191 \pm 9
D15	123 \pm 11	D35	174 \pm 28
D16	127 \pm 14	D36	421 \pm 24
D17	324 \pm 156	D37	137 \pm 8
D18	257 \pm 134	D38	147 \pm 12
D19	348 \pm 125	D39	142 \pm 23
D20	246 \pm 111	D40	197 \pm 47

¹cpm, counts per min

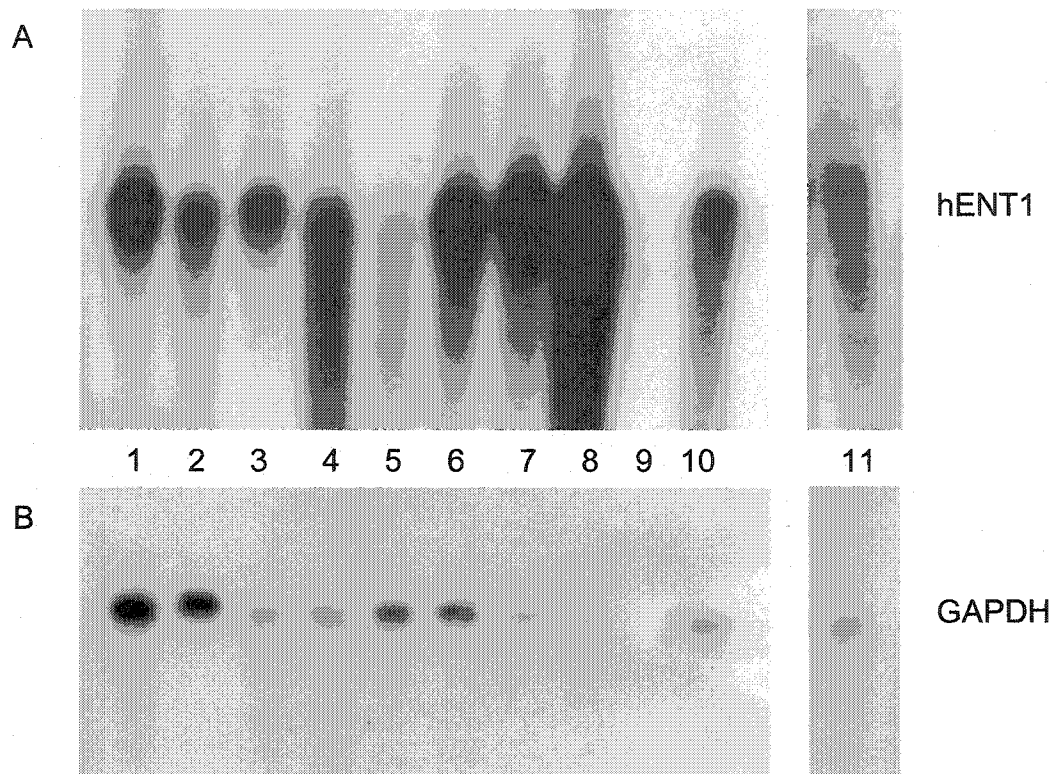


Figure III-1. Analysis of hENT1 mRNA expression in human cell lines by northern blot analysis

Total RNA (15-20 μ g) was isolated from human cell lines and electrophoretically resolved on denaturing agarose/formaldehyde gels (Materials and Methods, section II.5), and transferred to Hybond-N membranes (section II.5). The 1371-bp fragment of hENT1 cDNA and 970-bp fragment of GAPDH (glyceraldehyde-3-phosphate dehydrogenase) cDNA were labeled with 32 P and hybridized to the RNA blots as described in section II.5. Detection was by exposure to autoradiographic film at -80°C . The lanes are: CEM (lane 1), Caco-2 (lane 2), HeLa (lane 3), K562 (lane 4), MCF7 (lane 5), NB4 (lane 6), HEK 293 (lane 7), 180/1 (lane 8), negative control (lane 9, loading buffer), BeWo (lane 10) and 435S (lane 11).

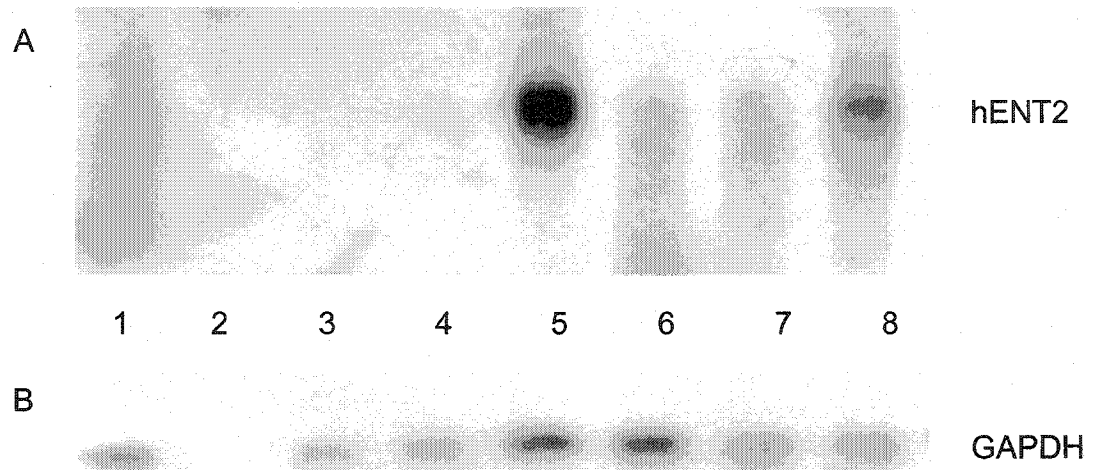


Figure III-2. Analysis of hENT2 mRNA expression in human cell lines by northern blot analysis

Northern blot analysis was conducted as described in the legend to Figure III-1, except that a ^{32}P -labeled 1320-bp fragment of hENT2 cDNA was used to detect hENT2 transcripts. The lanes are: Caco-2 (lane 1), negative control (lane 2, loading buffer), CEM (lane 3), CEM-ARAC (lane 4), HeLa (lane 5), K562 (lane 6), MCF7 (lane 7), and NB4 (lane 8).

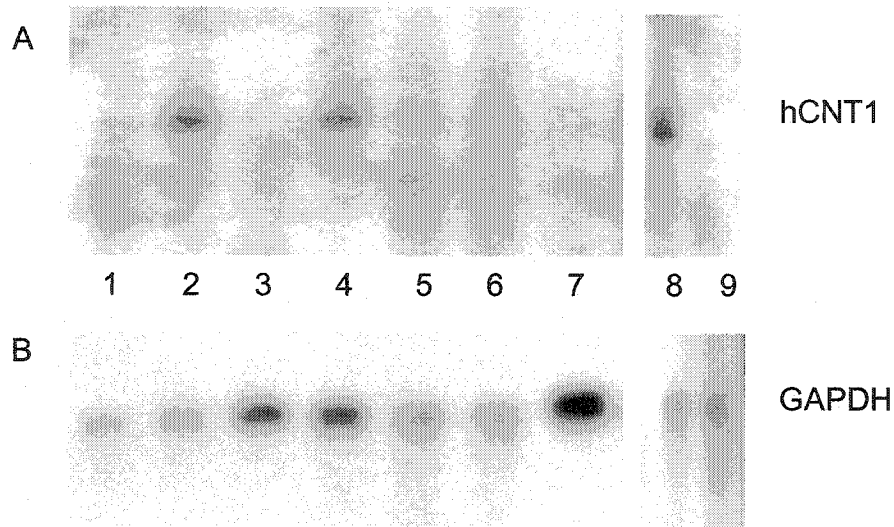


Figure III-3. Analysis of hCNT1 mRNA expression in human cell lines by northern blot analysis

Northern blot analysis was conducted as described in the legend to Figure III-1, except that a ^{32}P -labeled 1939-bp fragment of hCNT1 cDNA was used to detect hCNT1 transcripts. The lanes are: Caco-2 (lane 1), 435S (lane 2), CEM (lane 3), HeLa (lane 4), K562 (lane 5), MCF7 (lane 6), BeWo (lane 7), HEK 293 (lane 8) and NB4 (lane 9).

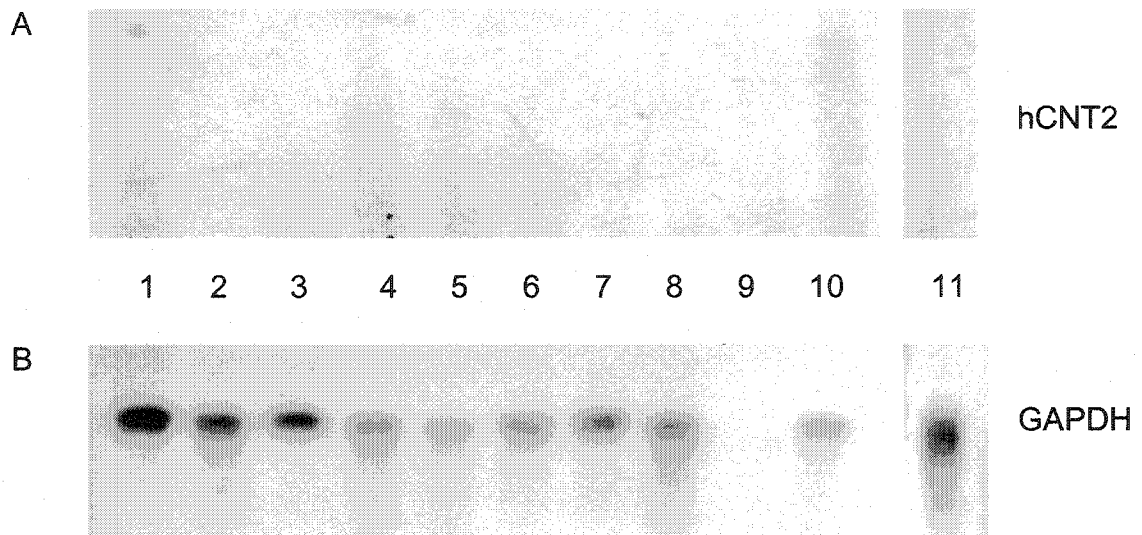


Figure III-4. Analysis of hCNT2 mRNA expression in human cell lines by northern blot analysis

Northern blot analysis was conducted as described in the legend to Figure III-1, except that a ^{32}P -labeled 1950-bp fragment of hCNT2 cDNA was used to detect hCNT2 transcripts. The lanes are: CEM (lane 1), Caco-2 (lane 2), HeLa (lane 3), K562 (lane 4), MCF7 (lane 5), NB4 (lane 6), HEK 293 (lane 7), 180/1 (lane 8), negative control (lane 9, loading buffer), BeWo (lane 10) and 435S (lane 11).

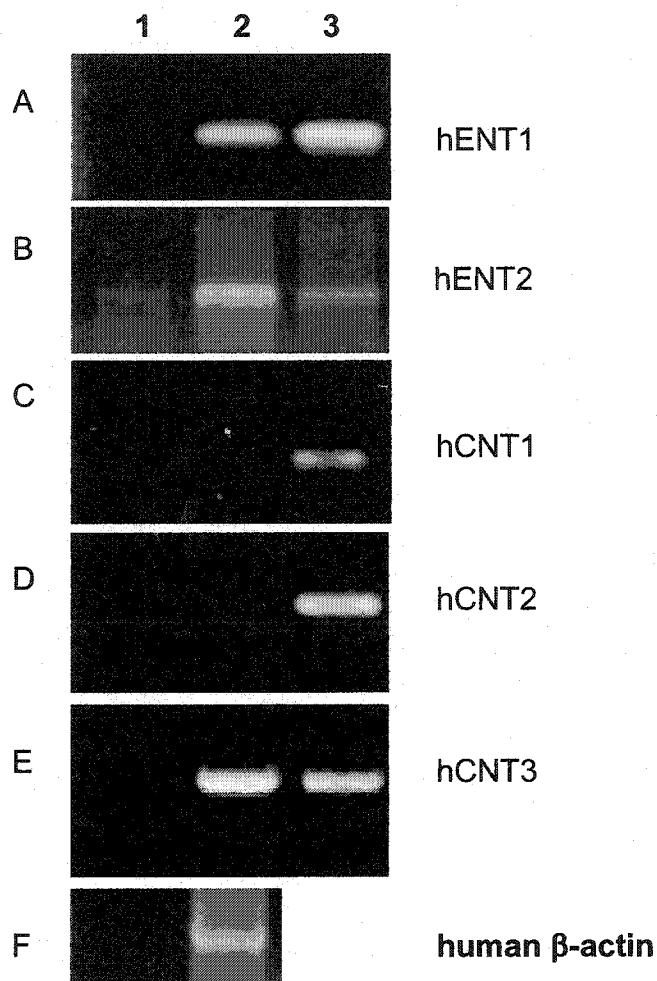


Figure III-5. RT-PCR analysis of nucleoside transporter mRNAs in Caco-2 cells

Poly(A)⁺ RNA was isolated from Caco-2 cells (passage 25-40) that had been grown for 19 days in culture and first-strand cDNA was synthesized by reverse transcription (Materials and Methods, section II.6). The cDNAs were PCR-amplified with primers specifically designed to detect the full-length open reading frame of hENT1, hENT2, hCNT1, hCNT2 and hCNT3. PCR reactions with water substituted (lane 1), Caco-2 cDNA (lane 2) and plasmid (pcDNA3/hENT1, pcDNA3/hENT2, pcDNA3/hCNT1, pcDNA3/hCNT2 or pcDNA3/hCNT3; lane 3) as DNA template were performed as described in Materials and Methods (section II.6). The products of PCR reactions were separated on a 1% agarose gel and the bands that migrated with the expected mobility of hENT1, hENT2, hCNT1, hCNT2, hCNT3 and human β -actin are indicated.

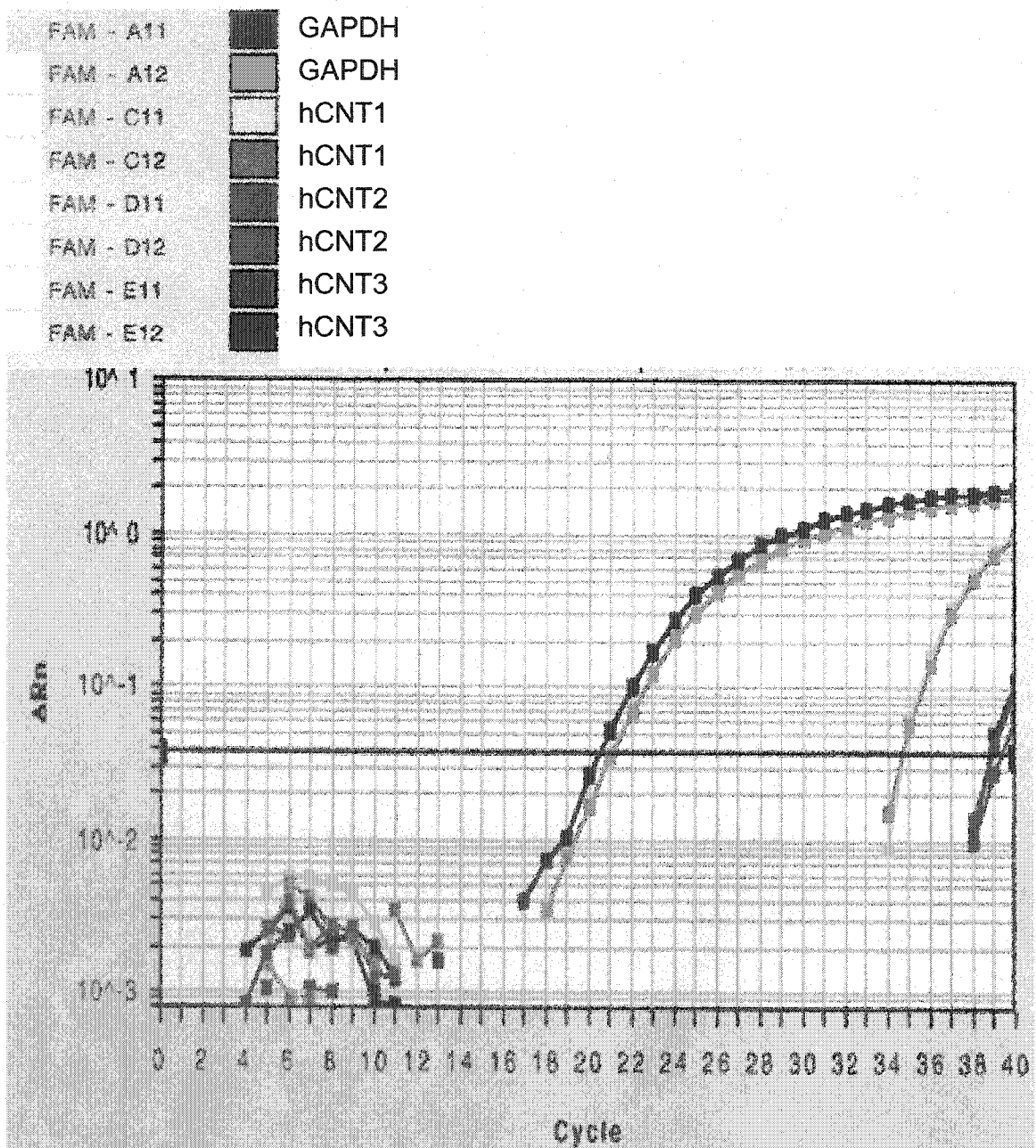


Figure III-6. Cycle time plot for real time Taqman RT-PCR analysis in HeLa cells

Taqman RT-PCR was performed according to procedures described in Materials and Methods (section II.7). The change in reporter fluorescence (ΔR_n) is plotted against the PCR cycle number. Depicted here is the visual representation of the fluorescence emitted by the formation of specific products for glyceraldehyde-3-phosphate dehydrogenase (GAPDH), hCNT1, hCNT2 and hCNT3. The threshold line indicated above was above background and within the linear phase of the exponential Taqman PCR reaction. Shown is one of two independent experiments that yielded similar results.

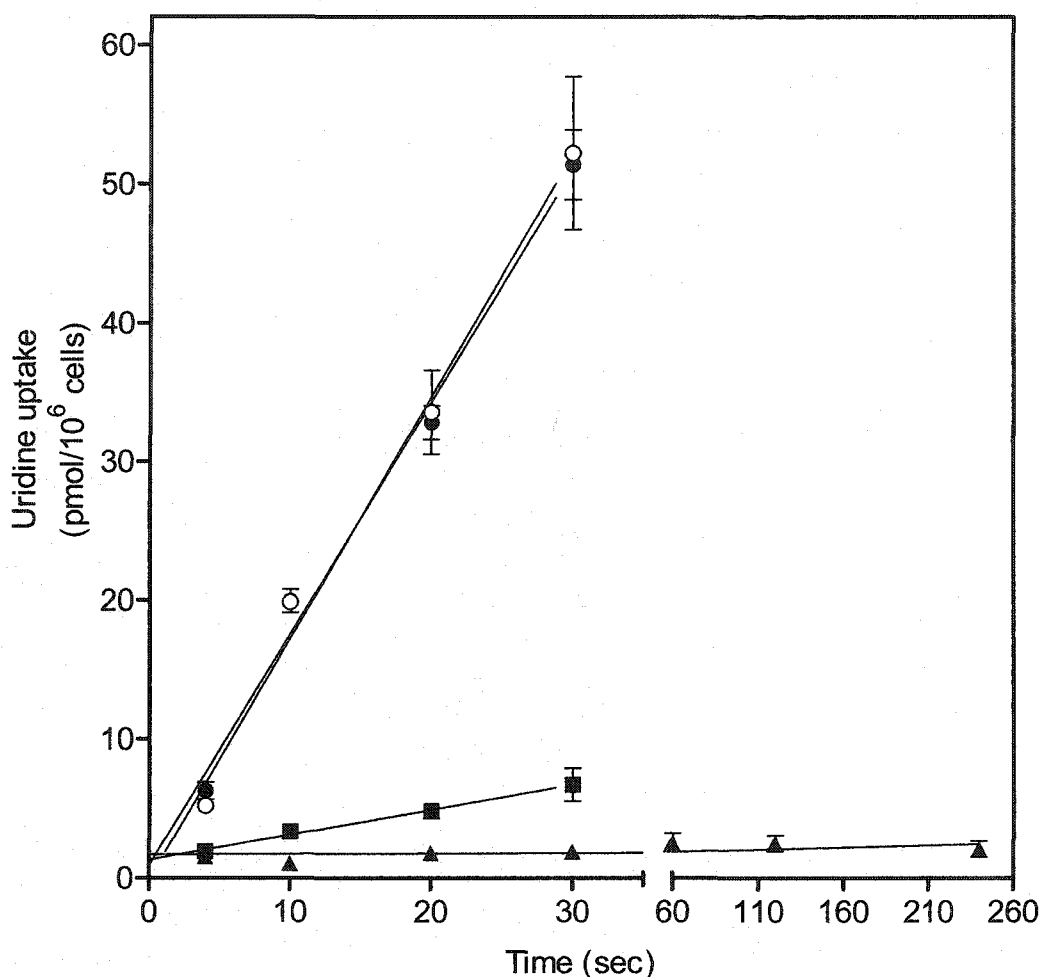


Figure III-7. Inhibitory effects of NBMPR or dilazep on uridine uptake by HeLa cells

Uptake of $10 \mu\text{M } ^3\text{H}$ -uridine was measured in Na^+ -free (open symbols) or Na^+ -containing (closed symbols) transport buffer in the absence of additives (\bullet, \circ) or in the presence of $0.1 \mu\text{M}$ NBMPR (\blacksquare) or $200 \mu\text{M}$ dilazep (\blacktriangle). Uridine uptake was measured over a period of 30 sec, with the exception of uptake measurements in the presence of dilazep, which were extended to 240 sec. Each value represents the mean \pm SD of three determinations and error bars are not shown where SD values were smaller than that represented by the symbols.

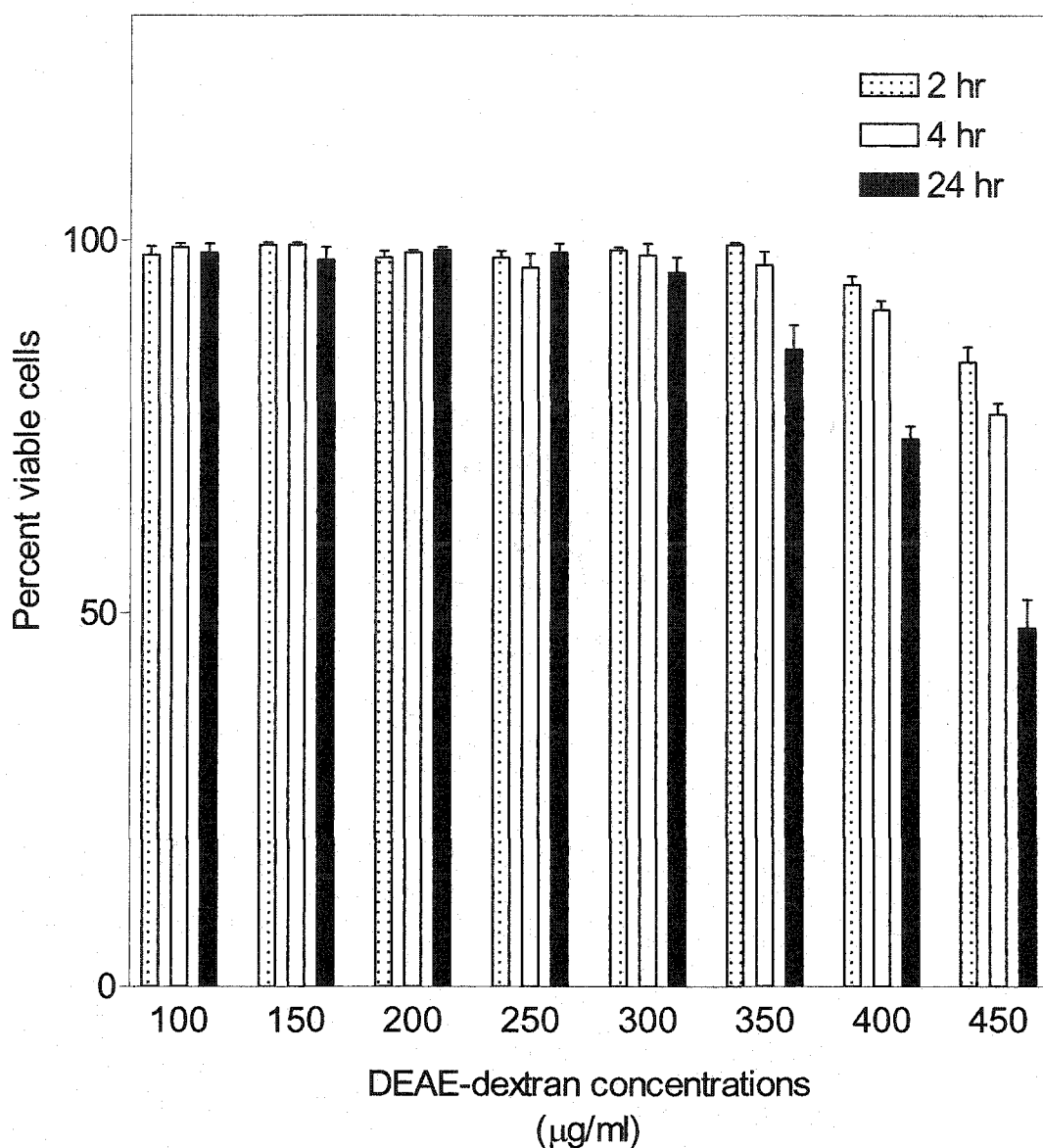


Figure III-8. Analysis of DEAE-dextran toxicity to HeLa cells

HeLa cells at approximately 50% confluency were exposed to graded concentrations of DEAE-dextran ranging from 100-450 µg/ml as indicated. Cell viability was assessed after exposures of 2, 4, and 24 hr by evaluating the ability of cells to exclude trypan blue under the hemocytometer viewed at 100x magnification with a light microscope as described in section 10.3. The fraction of viable cells was calculated by counting live (unstained) and dead (stained) cells and dividing the number of live cells by the total number of cells (live and dead). Each bar represents the mean \pm SD of triplicate determinations.

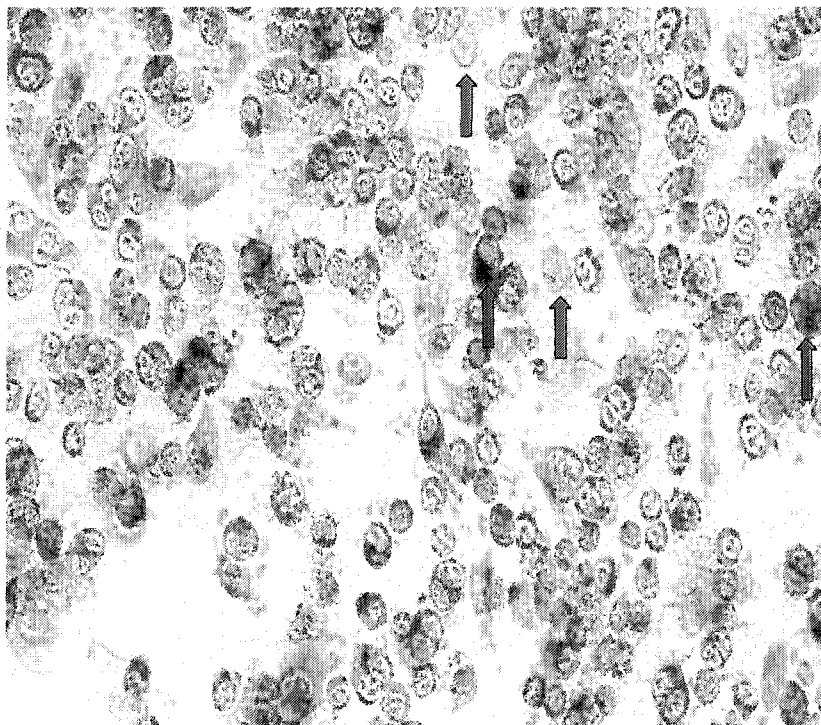


Figure III-9. A representative bright field image of *in situ* staining for β -galactosidase activity in HeLa cells

HeLa cells were transfected with pcDNA3/LacZ, fixed and stained as described in Materials and Methods (section II.13.1). Visualization was by bright field microscopy using an oil emersion lens at 40x magnification. Cellular staining of a green color, as shown by the red arrow, is indicative of positive staining for β -galactosidase activity. Non-transfected cells did not exhibit staining, as shown by the blue arrows, indicating the absence β -galactosidase activity.

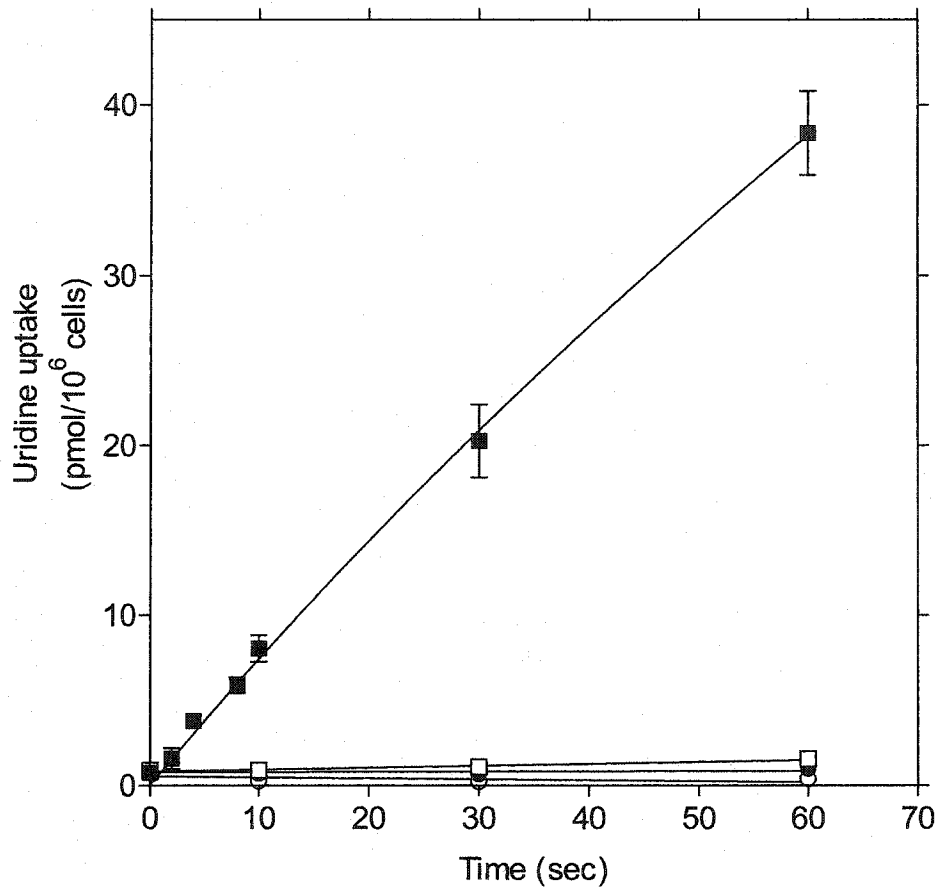


Figure III-10. Long time courses of uridine uptake by HeLa cells transiently transfected with hCNT1 cDNA

HeLa cells were transfected with either pcDNA3 or pcDNA3/hCNT1 as described in Materials and Methods (section II.11.1). ENT-mediated processes were inhibited by incubating cells for 15 min in transport buffer that contained 200 μ M dilazep prior to uptake measurements and also including 200 μ M dilazep in transport assays. Uptake of 10 μ M 3 H-uridine was performed in sodium-containing (closed symbols) or sodium-free (open symbols) transport buffer (as described in section II.16) with cells transfected with either pcDNA3 (●,○) or pcDNA3/hCNT1 (■,□). Each value represents the mean \pm SD of three determinations and error bars are not shown where SD values were smaller than the size of the data symbols. Shown is one of two independent experiments that yielded qualitatively similar results.

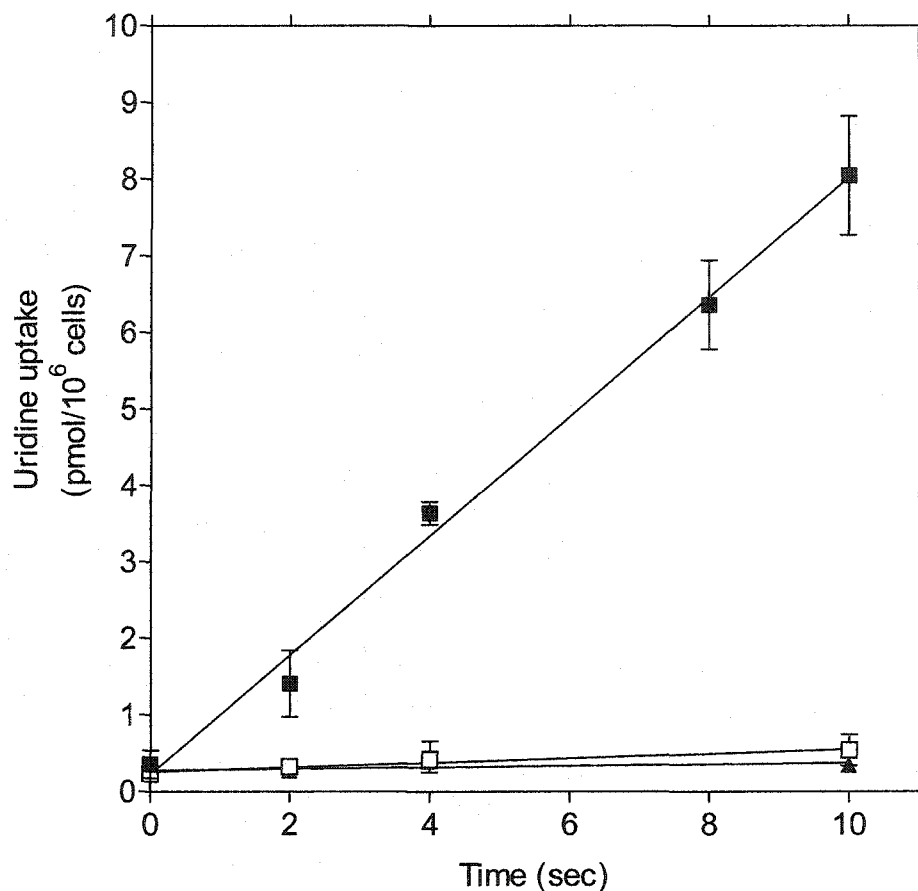


Figure III-11. Short-time courses of uridine uptake by HeLa cells transiently transfected with hCNT1 cDNA

HeLa cells were transfected with either pcDNA3 or pcDNA3/hCNT1 as described in Materials and Methods (section II.11.1). ENT-mediated processes were inhibited by incubating cells for 15 min in transport buffer that contained 200 μ M dilazep prior to uptake measurements and also including 200 μ M dilazep in transport assays. Uptake of 10 μ M 3 H-uridine over a 10-sec time period was performed in sodium-containing (closed symbols) or sodium-free (open symbols) transport buffer (as described in section II.16) with cells transfected with either pcDNA3 (\blacktriangle) or pcDNA3/hCNT1 (\blacksquare , \square). Each value represents the mean \pm SD of three determinations and error bars are not shown where SD values were smaller than the size of the data symbols. Shown is one of two independent experiments that yielded qualitatively similar results.

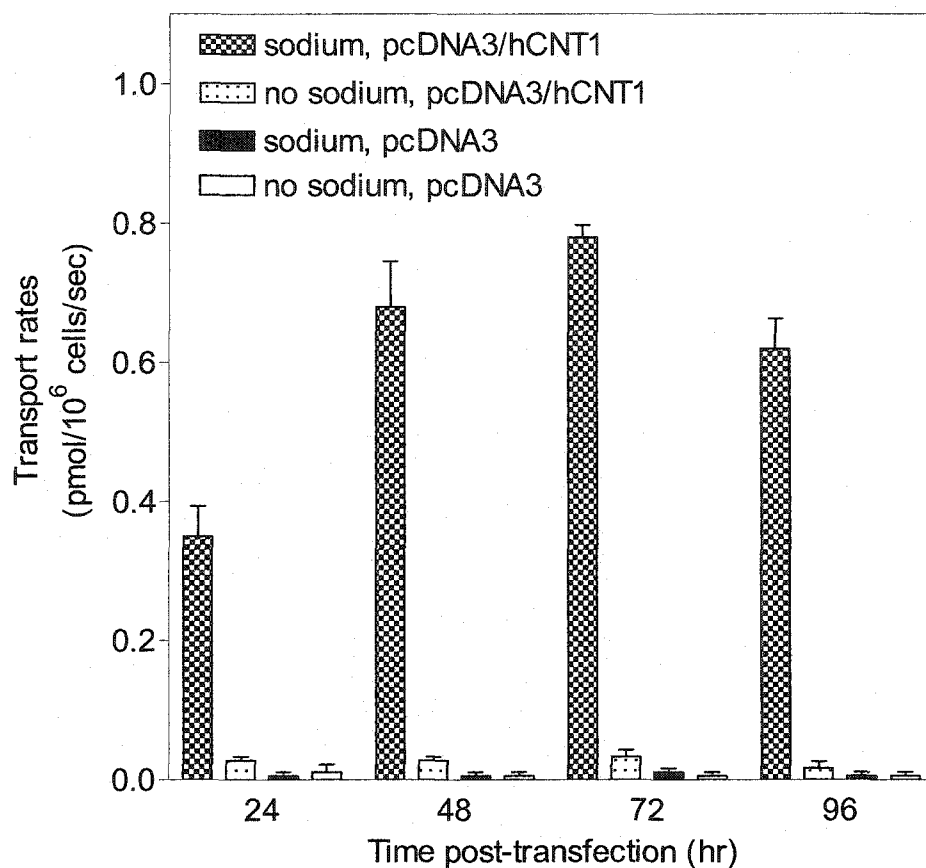


Figure III-12. Analysis of nucleoside transport activities in HeLa cells transiently transfected with hCNT1 cDNA at various times after transfection

HeLa cells were transfected with either pcDNA3 or pcDNA3/hCNT1 as described in Materials and Methods (section II.11.1). ENT-mediated processes were inhibited by incubating cells for 15 min in transport buffer that contained 200 μ M dilazep prior to uptake measurements and also including 200 μ M dilazep in transport assays. Transport assays with 10 μ M ³H-uridine were performed at various times (24, 48, 72 and 96) post-transfection in sodium-containing or sodium-free transport buffer as described in section II.16. Initial rates of uptake were obtained from 10-sec time courses similar to those shown in Figure III-11. Each value represents the mean \pm SD of three determinations.

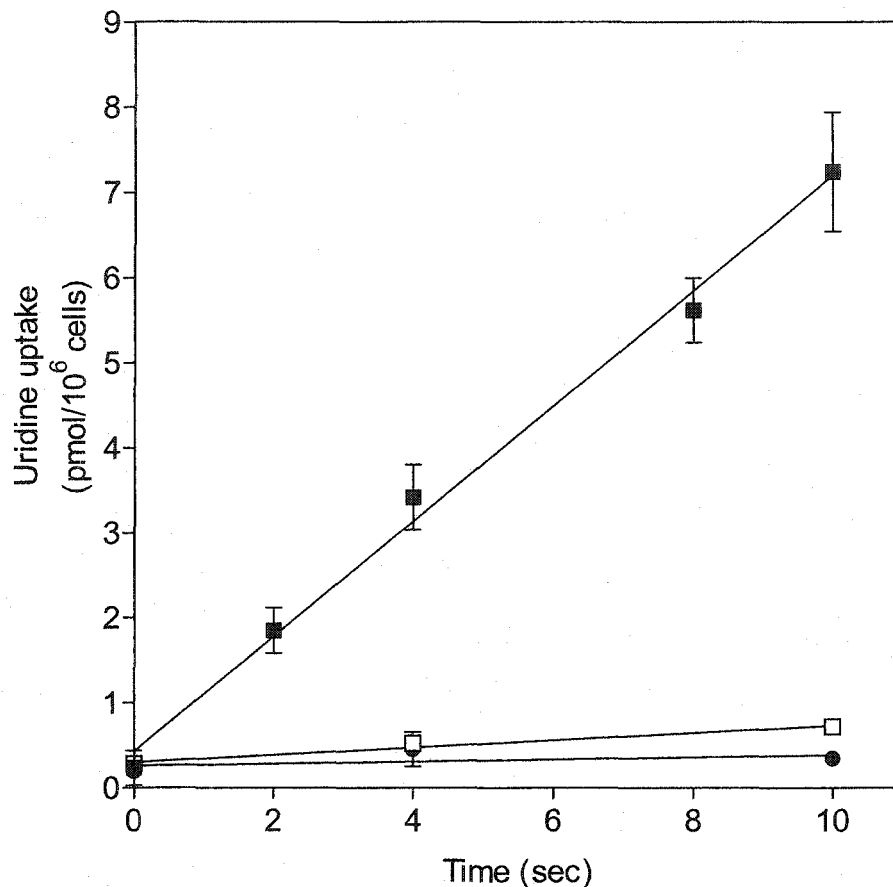


Figure III-13. Time course of uridine uptake by HeLa cells transiently transfected with hCNT2 cDNA

HeLa cells were transiently transfected with either pcDNA3 or pcDNA3/hCNT2 as described in Materials and Methods (section II.11.1). ENT-mediated processes were inhibited by incubating cells for 15 min in transport buffer that contained 200 μ M dilazep prior to uptake measurements and also including 200 μ M dilazep in transport assays. Transport measurements were performed 72-hr post-transfection with 10 μ M 3 H-uridine in the presence (closed symbols) or absence (open symbols) of sodium (as described in section II.16) with pcDNA3 (●) or pcDNA3/hCNT2 (■, □) transfected HeLa cells. Each value represents the mean \pm SD of triplicate determinations and error bars are not shown where SD values were smaller than the size of the data symbols.

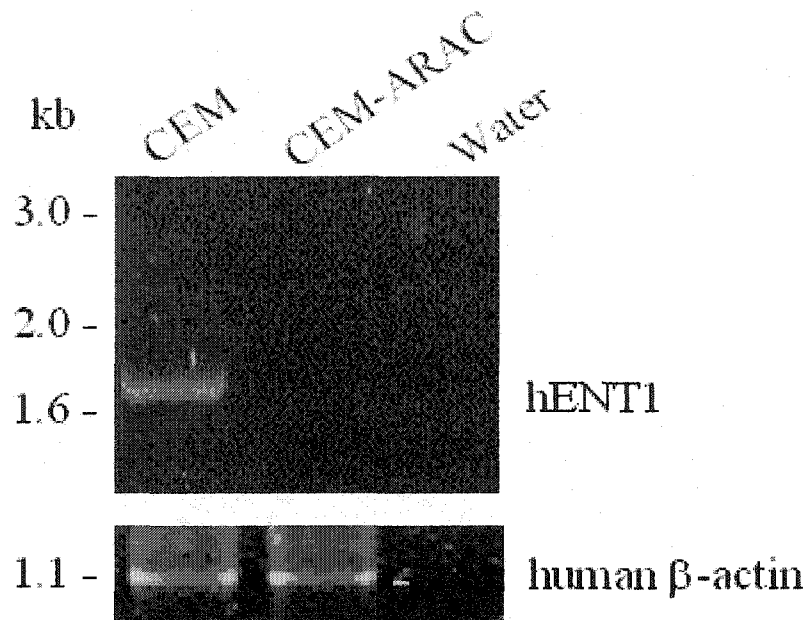


Figure III-14. RT-PCR analysis for the presence of hENT1 mRNA in CEM and CEM-ARAC cells

Poly(A)⁺ RNA was isolated from actively proliferating CEM and CEM-ARAC cell cultures and first-strand cDNA was synthesized by reverse transcription and then PCR-amplified with hENT1-specific or human β -actin specific primers as described in Materials and Methods (section II.6). PCR reactions in which DNA template was substituted with water served as negative controls. The products of PCR reactions were separated on a 1% agarose gel and the band that migrated with the expected hENT1 mobility was excised, gel-purified and sequenced. *Left*, positions of the DNA markers (in kb, kilobases)

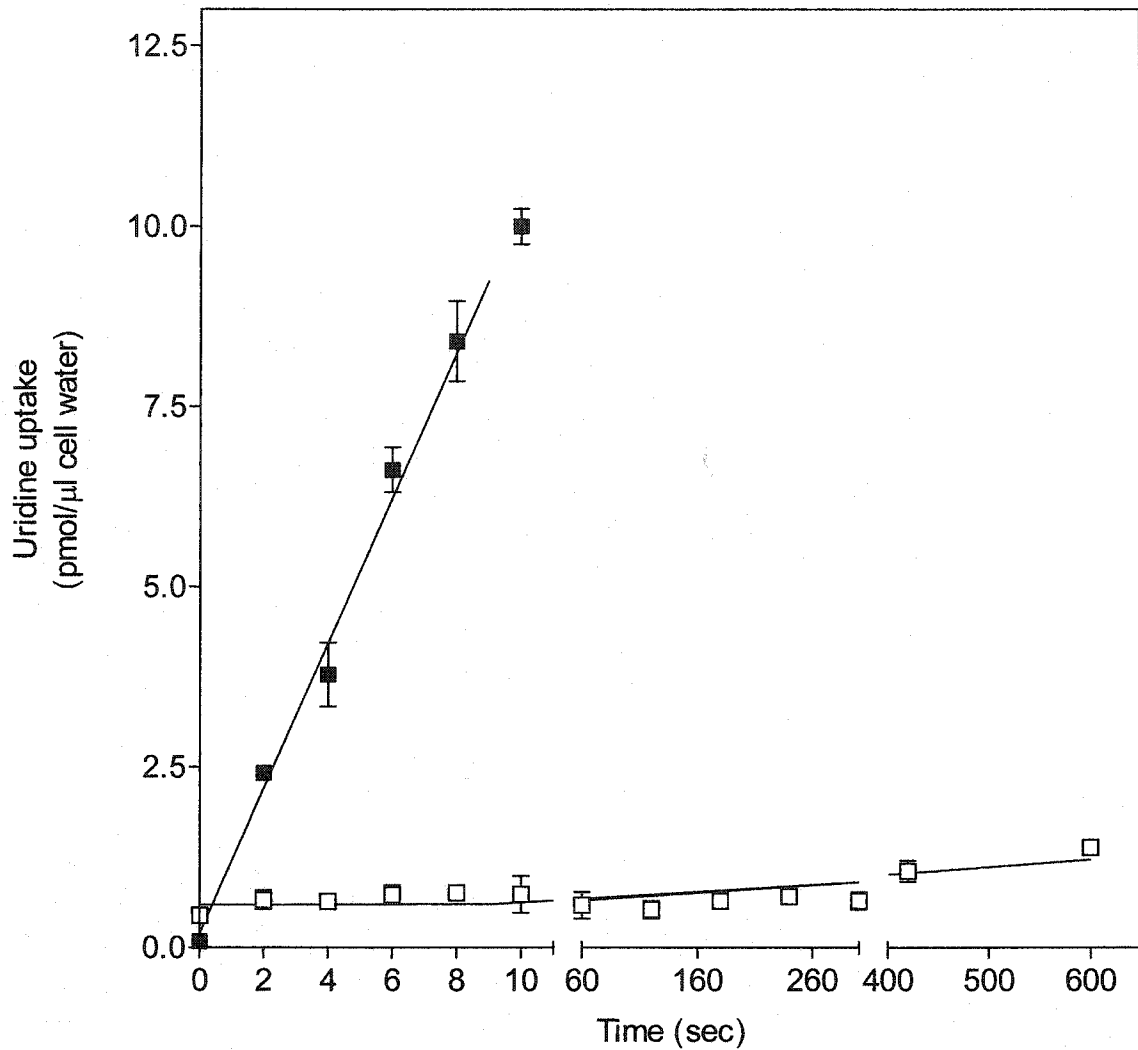


Figure III-15. Comparison of uridine uptake by CEM and CEM-ARAC cells over short and long time periods

Uptake of $10 \mu\text{M}$ ^3H -uridine by actively proliferating CEM (■) and CEM-ARAC (□) cells was measured over the time intervals shown in sodium-containing transport buffer as described in section II.15. Each value represents the mean \pm SD of three determinations and error bars are not shown where SD values were smaller than that represented by the symbols.

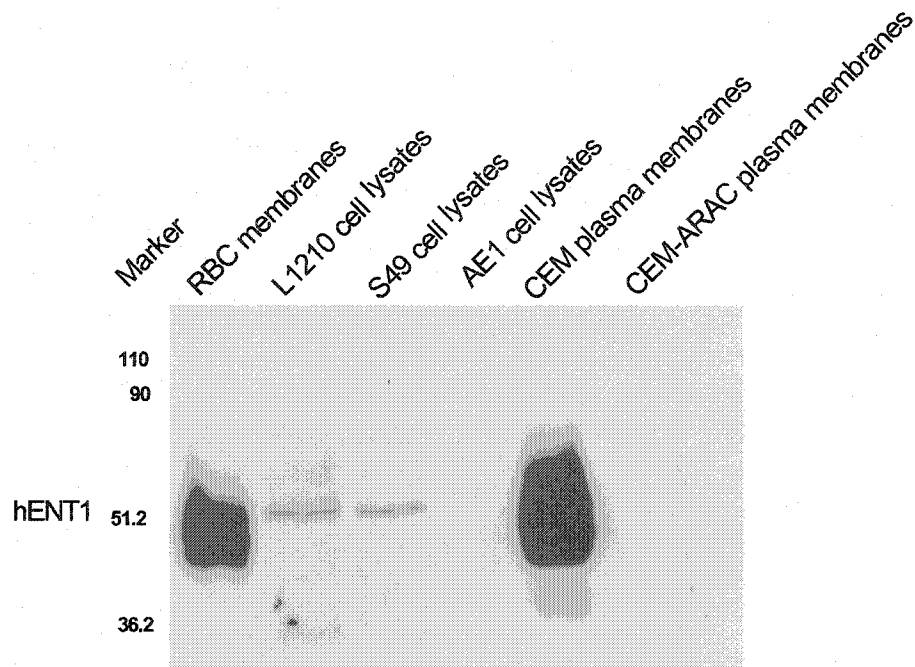


Figure III-16. Immunoblot analysis demonstrating hENT1 in CEM cells, but not in CEM-ARAC cells

Cell lysates of murine L1210 (L1210/B23.1), S49 and AE1 cells and enriched plasma membrane preparations of human CEM, CEM-ARAC and red blood cells (RBCs) were prepared as described in Materials and Methods (section II.17). Membrane preparations (15 μ g/lane) or cell lysates were electrophoresed through a 10% SDS-polyacrylamide gel and transferred to PVDF membrane (section II.8). The PVDF membrane was probed with 1:5000 dilution (v/v) of anti-hENT1 monoclonal antibodies followed by 1:7000 dilution (v/v) of anti-mouse HRP conjugated secondary antibodies. Detection was by ECL chemiluminescent and exposure to Fuji X-ray film. *Left*, positions of the protein markers (in kDa).

Consensus	---SA-GYFIT-C--I-L-I-CYL-LP-L-F-RYY---KL---P---ET	127
hENT1	LSESAFGYFITACAVIILTIICYLGLPRLEFYRYYQQLKL-EGPGEQ-ET	248
mENT1	AQTSALGYFITPCVIGILLSIVCYLSLPHLKFARYYLTERKLSQAPTQELT	236
Consensus	K--L----E----P-----S-----E-----S-----	134
hENT1	KLDLISKGEE---PRAGKEESGVSVSNSQPTNESH-----SIKAILK	287
mENT1	KAELLOADEKNGVPISPQOASPTLDDLPEKEPEPEEPQKPGKPSVFFVFR	286

Figure III-17. Amino acid sequence alignment of hENT1 and mENT1

The amino sequences of ENT1 proteins from human (h) and mouse (m) species were aligned using the BESTFIT program of the University of Wisconsin Genetics Computer Group (GCG) for the UNIX operating system. Shown is the amino acid sequence alignment of hENT1 and mENT1 in the region employed in raising anti-hENT1 antibodies (amino acid residues 254-271 of hENT1). Amino acid identities between hENT1 and mENT1 sequences are highlighted.

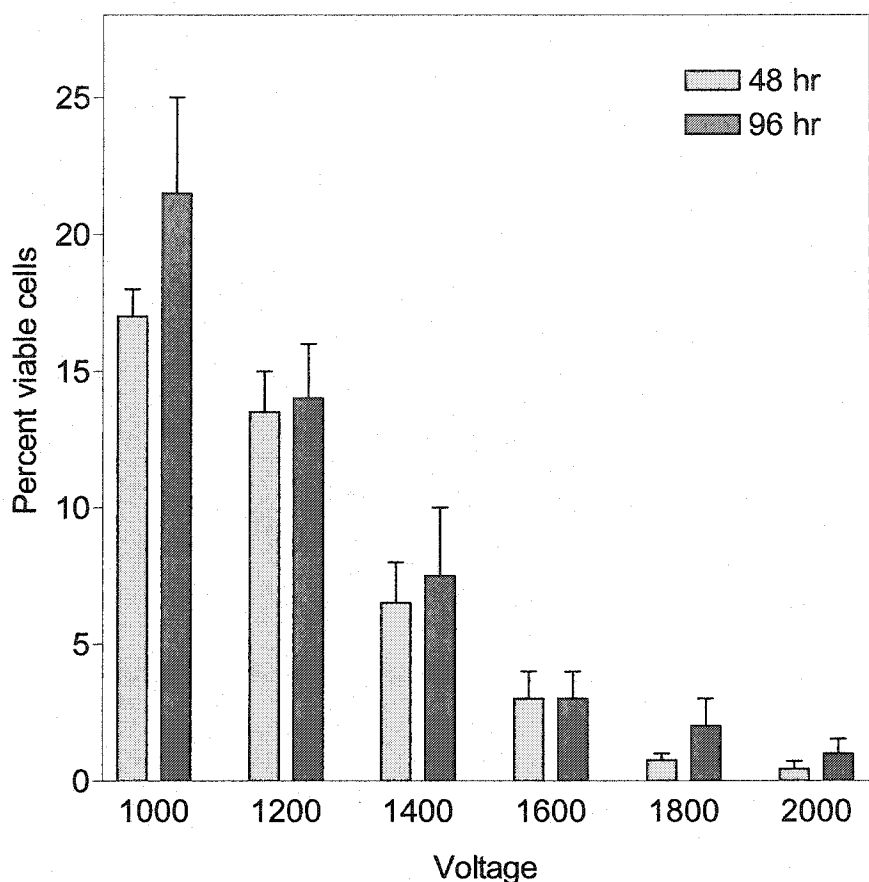


Figure III-18. Determination of viability of CEM-ARAC cells for electroporation using constant capacitance of 25 μ F and graded changes in voltage strength

Actively proliferating CEM-ARAC cells were harvested, resuspended in PBS (pH 7.4) at 3×10^8 cells/ml with or without 10 μ g of pcDNA3/LacZ and loaded into 4-mm gap cuvettes. Electroporations were performed using a Biorad Gene Pulser with graded changes to the voltage (ranging from 1000-2000 V) while maintaining constant capacitance at 25 μ F. Cell viabilities were assessed at 48 and 96 hr after transfection by evaluating the ability of cells to exclude trypan blue using a hemocytometer viewed at 100x magnification with a light microscope as described in section II.10.3. The fraction of viable cells was calculated by counting live (unstained) and dead (stained) cells and dividing the number of live cells by the total number of cells (live and dead). A representative experiment in which CEM-ARAC cells were electroporated with pcDNA3/LacZ is shown; experiments without pcDNA3/LacZ (not shown) yielded qualitatively similar results. Each bar represents the mean \pm SD of triplicate determinations.

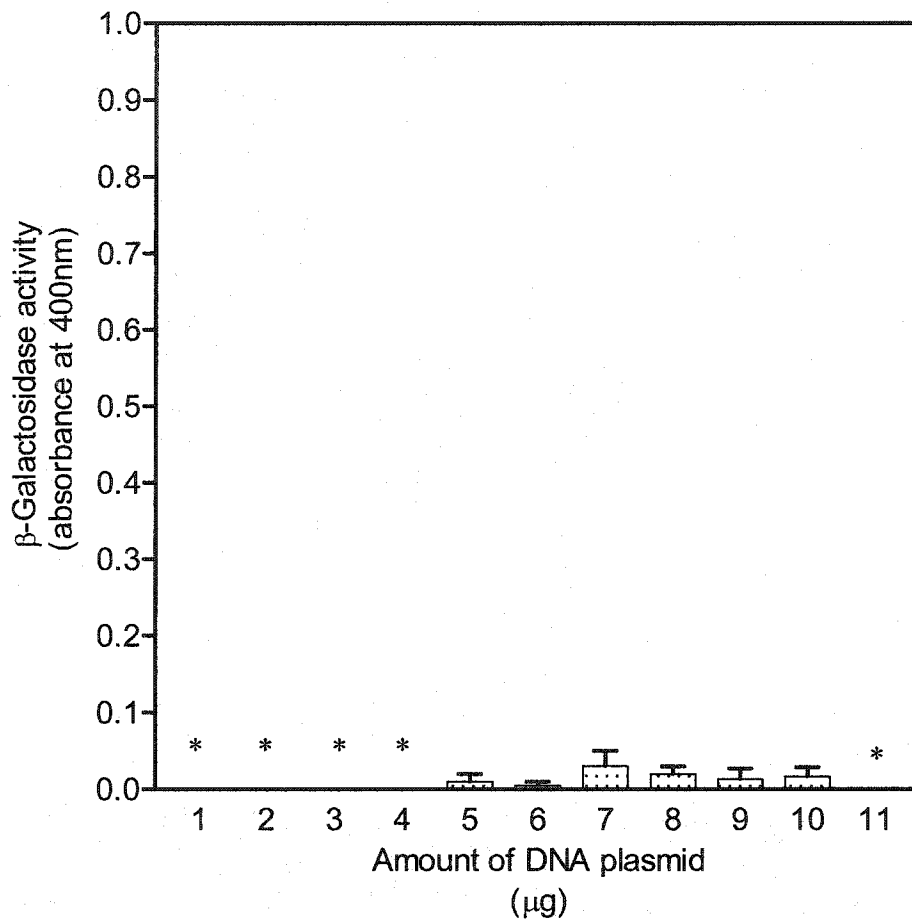


Figure III-19. The effects of DNA concentration on the transfection efficiency of CEM-ARAC cells electroporated at 25 μ F and 1000 V

CEM-ARAC cells were transfected with graded amounts (μ g) of pcDNA3/LacZ in PBS using the electroporation parameters of 1000 V and 25 μ F. The levels of β -galactosidase activity were examined 72 hr after transfection by measuring the hydrolysis of o-nitrophenyl- β -D-galactopyranoside (section II.13.2). Color development was monitored by measuring absorbance at 400 nm with a spectrophotometer. Levels of β -galactosidase activity were calculated by subtracting absorbance readings of CEM-ARAC cells (controls) that were electroporated in the absence of pcDNA3/LacZ. Each bar represents the mean \pm SD of triplicate determinations and the asterisk indicates values of β -galactosidase activity that were indistinguishable from control values.

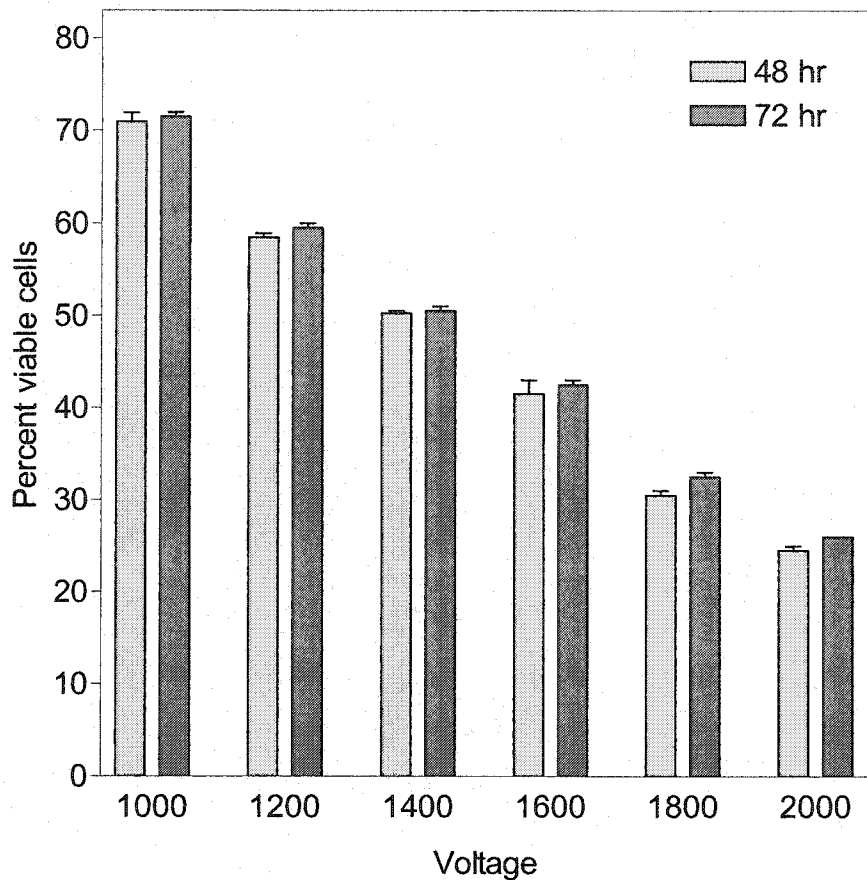


Figure III-20. Determination of viability of CEM-ARAC cells for electroporation using constant capacitance of 3 μ F and graded changes to voltage strength

Actively proliferating CEM-ARAC cells were harvested, resuspended in PBS (pH 7.4) at 3×10^8 cells/ml with or without 10 μ g of pcDNA3/LacZ and loaded into 4-mm gap cuvettes. Electroporations were performed using a Biorad Gene Pulser with graded changes to the voltage (ranging from 1000-2000 V) while maintaining constant capacitance at 3 μ F. Cell viabilities were assessed at 48 and 72 hr after transfection by evaluating the ability of cells to exclude trypan blue using a hemocytometer viewed at 100x magnification with a light microscope as described in section II.10.3. The fraction of viable cells was calculated by counting live (unstained) and dead (stained) cells and dividing the number of live cells by the total number of cells (live and dead). A representative experiment in which CEM-ARAC cells were electroporated with pcDNA3/LacZ is shown; experiments without pcDNA3/LacZ (not shown) yielded qualitatively similar results. Each bar represents the mean \pm SD of triplicate determinations and error bars are not shown where SD values were smaller than the size of the data symbols.

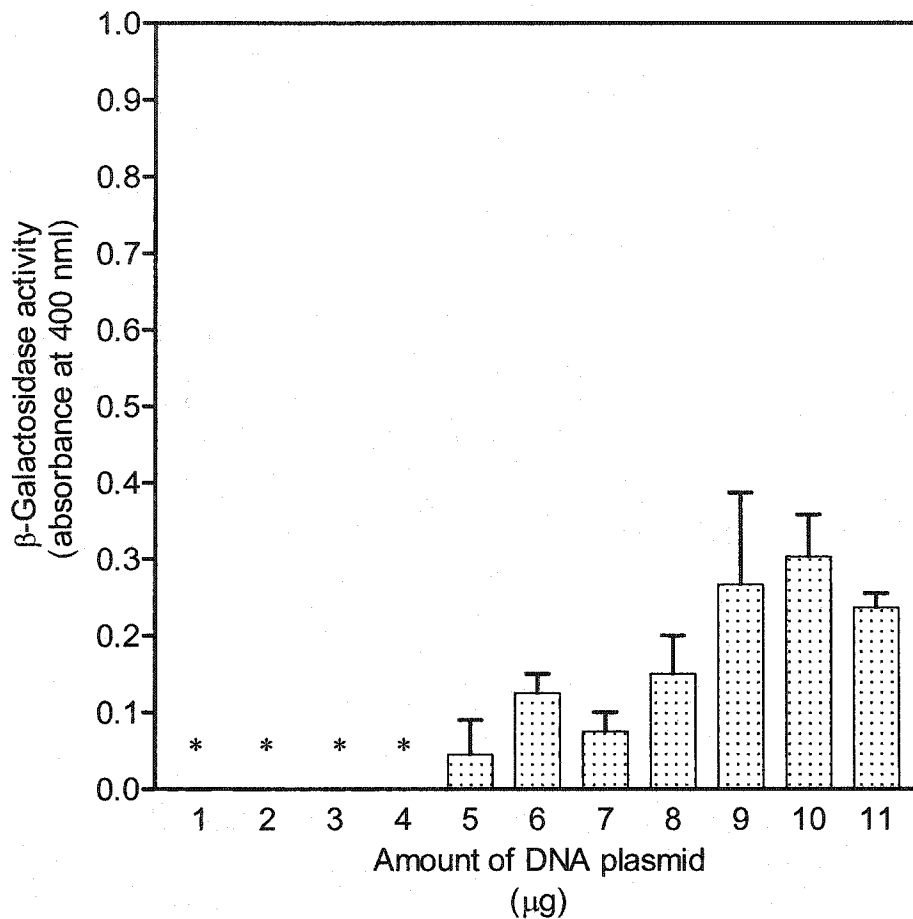


Figure III-21. The effect of DNA concentration on transfection efficiency of CEM-ARAC cells electroporated at 3 μF and 1400 V

CEM-ARAC cells were transfected with graded amounts (μg) of pcDNA3/LacZ in PBS using the electroporation parameters of 1400 V and 3 μF. The levels of β-galactosidase activity were examined 72 hr after transfection by measuring the hydrolysis of o-nitrophenyl-β-D-galactopyranoside (section II.13.2). Color development was monitored by measuring absorbance at 400 nm with a spectrophotometer. Levels of β-galactosidase activities were calculated by subtracting absorbance readings of CEM-ARAC cells (controls) that were electroporated in the absence of pcDNA3/LacZ. Each bar represents the mean ± SD of triplicate determinations and the asterisk indicates values of β-galactosidase activity that were indistinguishable from control values.

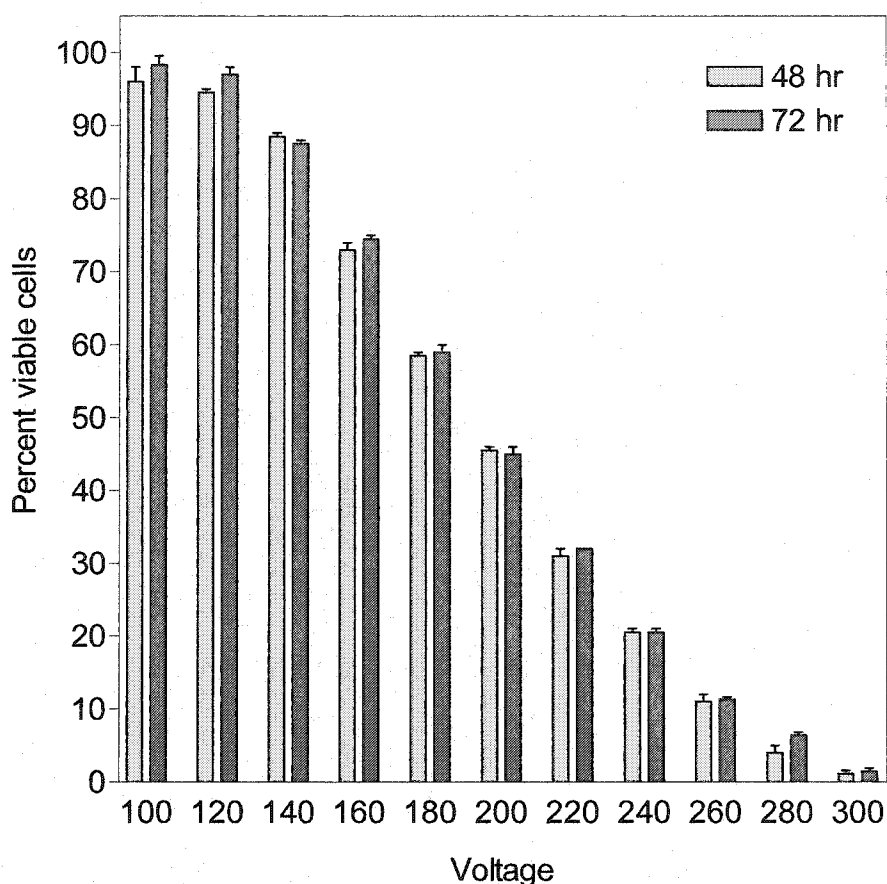


Figure III-22. Determination of viability of CEM-ARAC cells for electroporation using constant capacitance of 960 μ F and graded changes to voltage strength

Actively proliferating CEM-ARAC cells were harvested, resuspended in glutamine-free RPMI 1640 at 3×10^8 cells/ml with or without 10 μ g of pcDNA3/LacZ and loaded into 4-mm gap cuvettes. Electroporations were performed using a Biorad Gene Pulser equipped with a capacitance extender set at 960 μ F and graded changes to the voltage (ranging from 100-300 V) as shown. Cell viabilities were assessed at 48 and 72 hr after transfection by evaluating the ability of cells to exclude trypan blue using a hemocytometer viewed at 100x magnification with a light microscope as described in section II.10.3. The fraction of viable cells was calculated by counting live (unstained) and dead (stained) cells and dividing the number of live cells by the total number of cells (live and dead). A representative experiment in which CEM-ARAC cells were electroporated with pcDNA3/LacZ is shown; experiments without pcDNA3/LacZ (not shown) yielded qualitatively similar results. Each bar represents the mean \pm SD of triplicate determinations and error bars are not shown where SD values were smaller than the size of the data symbols.

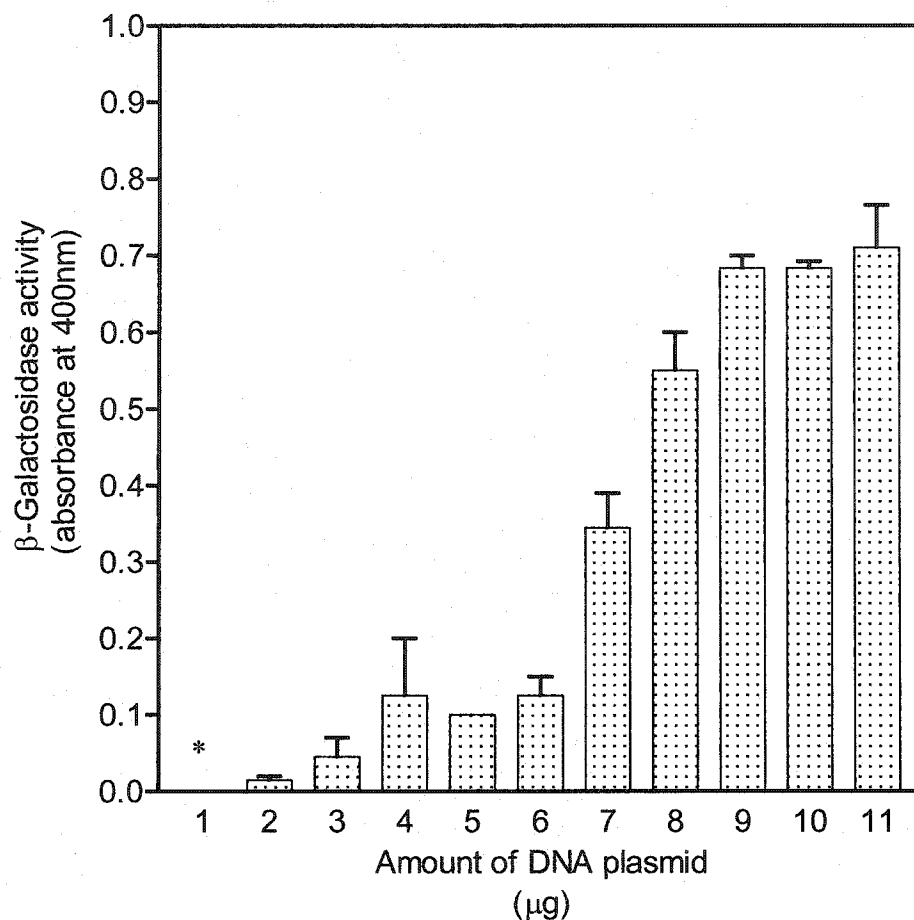


Figure III-23. The effect of DNA concentration on transfection efficiency of CEM-ARAC cells electroporated using optimized electroporation conditions of 960 μF and 190 V

CEM-ARAC cells were transfected with graded amounts (μg) of pcDNA3/LacZ in glutamine-free RPMI 1640 using the electroporation parameters of 190 V and 960 μF . The levels of β -galactosidase activity were examined 72 hr transfection by measuring the hydrolysis activity of o-nitrophenyl- β -D-galactopyranoside (section II.13.2). Color development was monitored by measuring absorbance at 400 nm with spectrophotometer. Levels of β -galactosidase were calculated by subtracting absorbance readings of CEM-ARAC cells (controls) that were electroporated in the absence of pcDNA3/LacZ. Each bar represents the mean \pm SD of triplicate determinations and the asterisk indicates values of β -galactosidase activity that were indistinguishable from the control values.

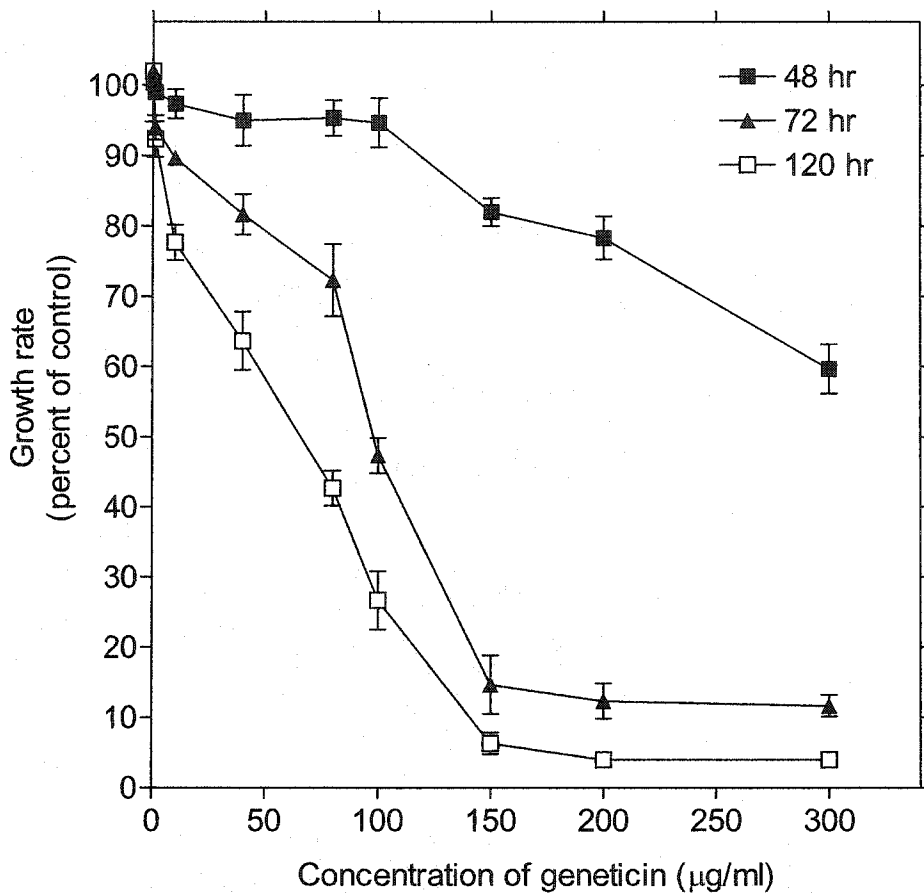


Figure III-24. The growth-inhibitory effects of geneticin on CEM-ARAC cells

CEM-ARAC cells in early exponential growth were incubated in 10 ml growth medium containing graded concentrations of geneticin (0, 1, 10, 40, 80, 100, 150, 200, 300 µg/ml). The number of cells in the presence and absence of geneticin was determined for the indicated incubation times (40, 72, 120 hr) using an electronic particle counter. Growth rates (population doublings/24 hr) in the presence of geneticin were calculated as the percentage of rates observed in the absence of geneticin and expressed as the mean \pm SD of triplicate determinations. Error bars are not shown where SD values were smaller than the size of data symbols. Untreated control cells exhibited a population doubling time of 21 ± 2 hr (mean \pm SD of triplicate determinations).

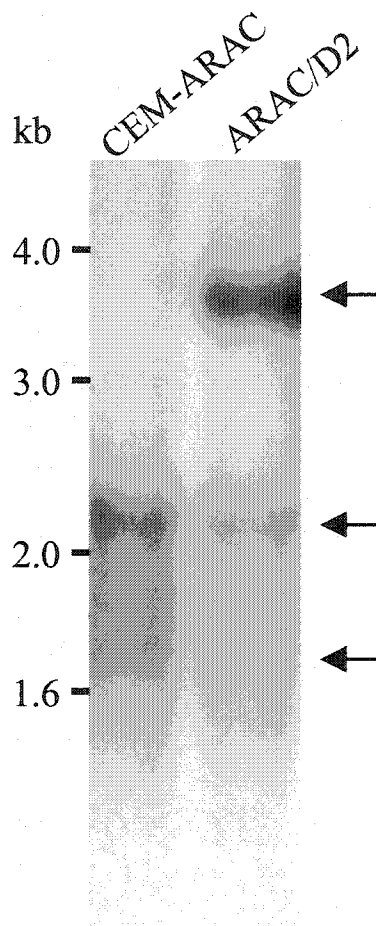


Figure III-25. Genomic integration of hCNT2 cDNA into ARAC/D2 cells

DNA from CEM-ARAC (15 μ g) and ARAC/D2 (10 μ g) cells was digested with EcoRI, resolved by electrophoresis on a 1% agarose gel, transferred to Hybond-N⁺ membranes and hybridized with a ³²P-labeled hCNT2 cDNA probe as described in Materials and Methods (section II.4). The positions of size markers (1-kb DNA ladder) are shown, *left*.

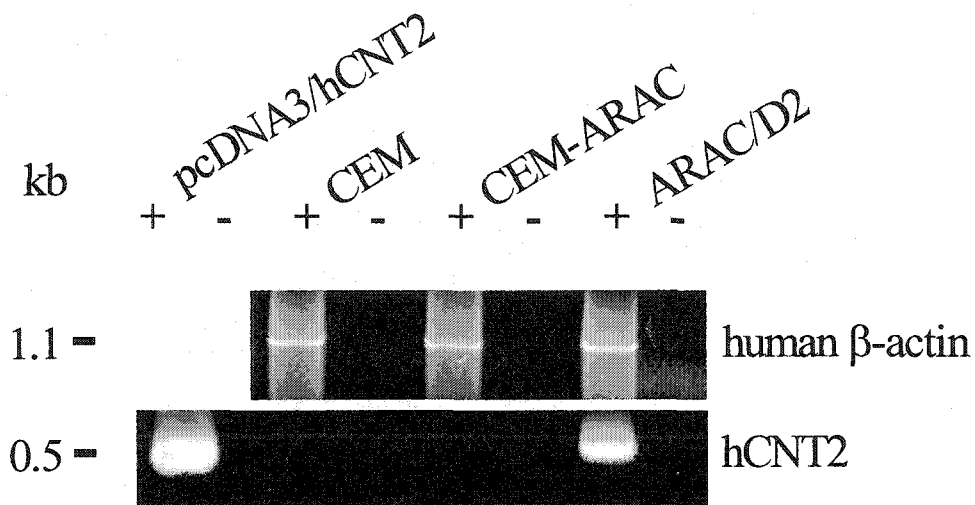


Figure III-26. Expression of hCNT2 mRNA in ARAC/D2 cells, but not in CEM or CEM-ARAC cells

Poly(A)⁺ RNA was isolated from CEM, CEM-ARAC and ARAC/D2 cells and reverse transcribed as described in section II.6. The resulting cDNAs and pcDNA3/hCNT2 (as a positive control) were used as templates for PCR with hCNT2-specific primers (NT2D and JM23) or human actin specific primers. PCR products were separated on a 1% agarose gel with size markers (1-kb DNA ladder). For each set of PCR conditions, reactions were conducted with (+) or without (-) DNA template.

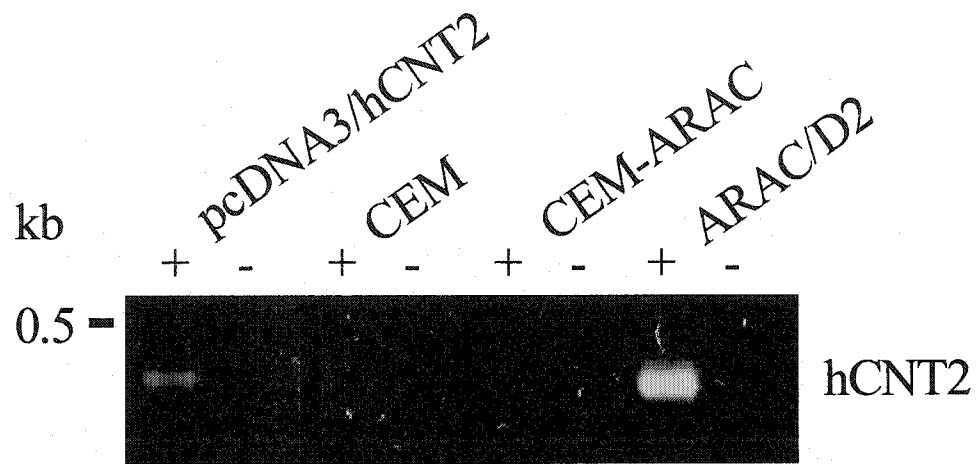


Figure III-27. Nested RT-PCR demonstrating hCNT2 mRNA in ARAC/D2 cells, but not in CEM or CEM-ARAC cells

RT-PCR of poly(A)⁺ RNA from CEM, CEM-ARAC and ARAC/D2 cells was performed as described in Figure III-26. The first-round PCR products were subjected to nested-PCR using internal hCNT2-specific primer sets (NT2KG25 and NT2KG26) as described in section II.6. The nested PCR products were separated on a 1% agarose gel with size markers (1-kb DNA ladder). For each set of PCR conditions, reactions were conducted with (+) or without (-) DNA template. The nested-PCR products were sequenced to verify their relationship to hCNT2 cDNA.

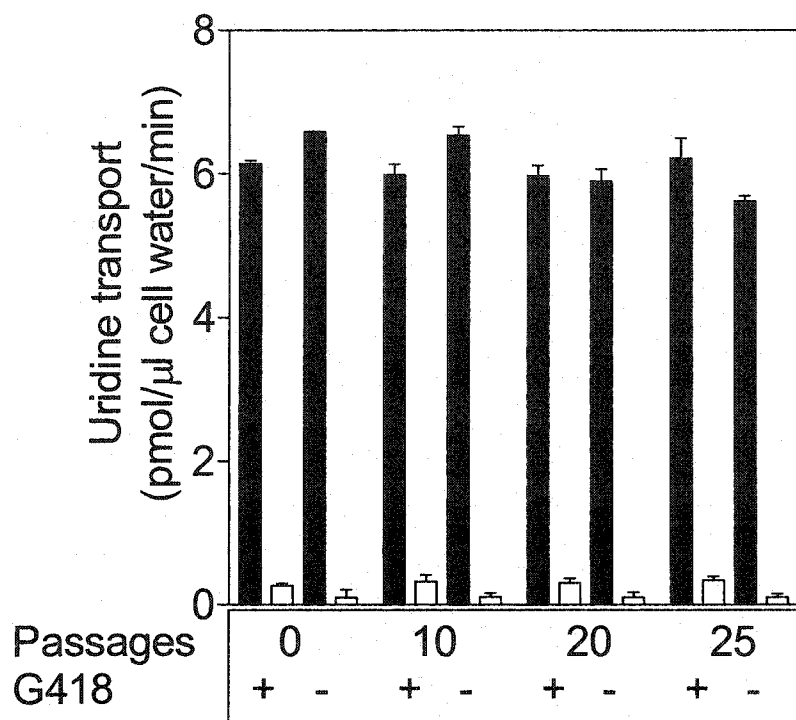


Figure III-28. Stability of hCNT2-mediated uridine transport activity in ARAC/D2 cells over 25 generations

ARAC/D2 cells were maintained in the presence (+) or absence (-) of G418 (geneticin) selection and after 10, 20 and 25 passages, ^3H -uridine uptake was measured in sodium-containing (solid bars) or sodium-free (open bars) transport buffer as described in section II.15. Values for uridine transport rates were obtained from the slopes of linear (180-sec) time courses. Each value represents the mean \pm S.D. of three determinations.

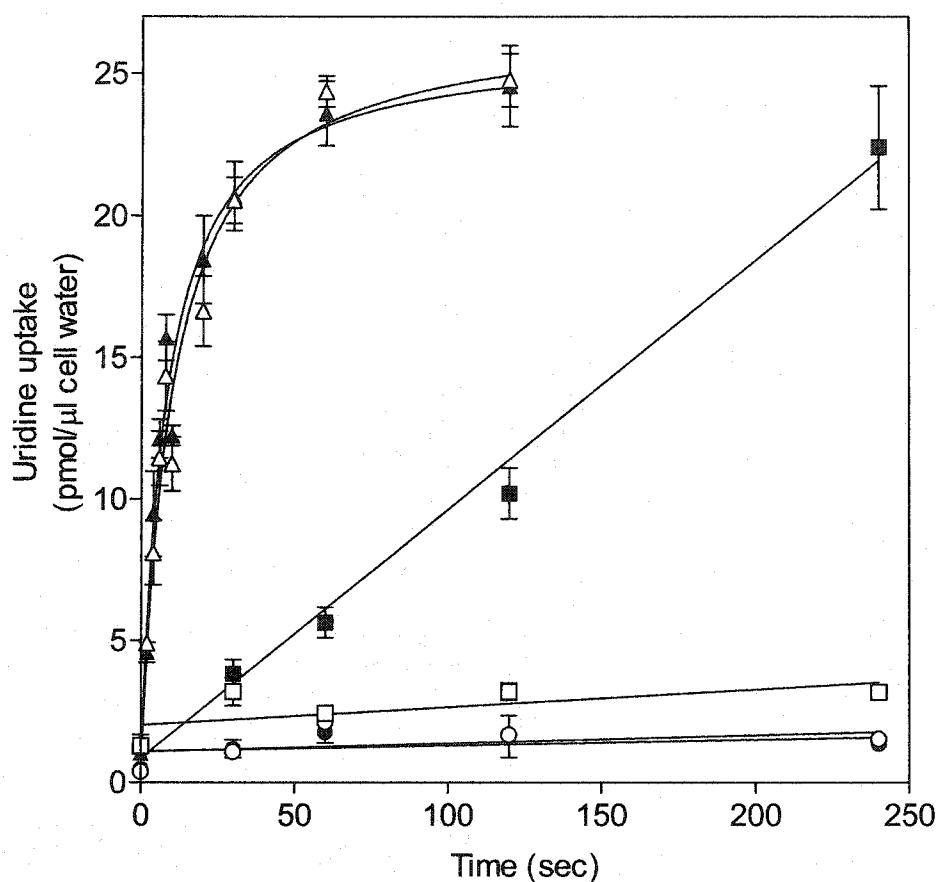


Figure III-29. Demonstration of sodium-dependent, hCNT2-mediated uptake by ARAC/D2 stable transfectants

Uptake of $10 \mu\text{M}$ ^3H -uridine was measured at the time intervals shown in the presence (closed symbols) or absence (open symbols) of sodium in ARAC/D2 (■, □), CEM-ARAC (●, ○) or CEM (▲, △) cells as described in section II.15. Each value represents the mean \pm SD of three determinations and error bars are not shown where SD values were smaller than that represented by the symbols.

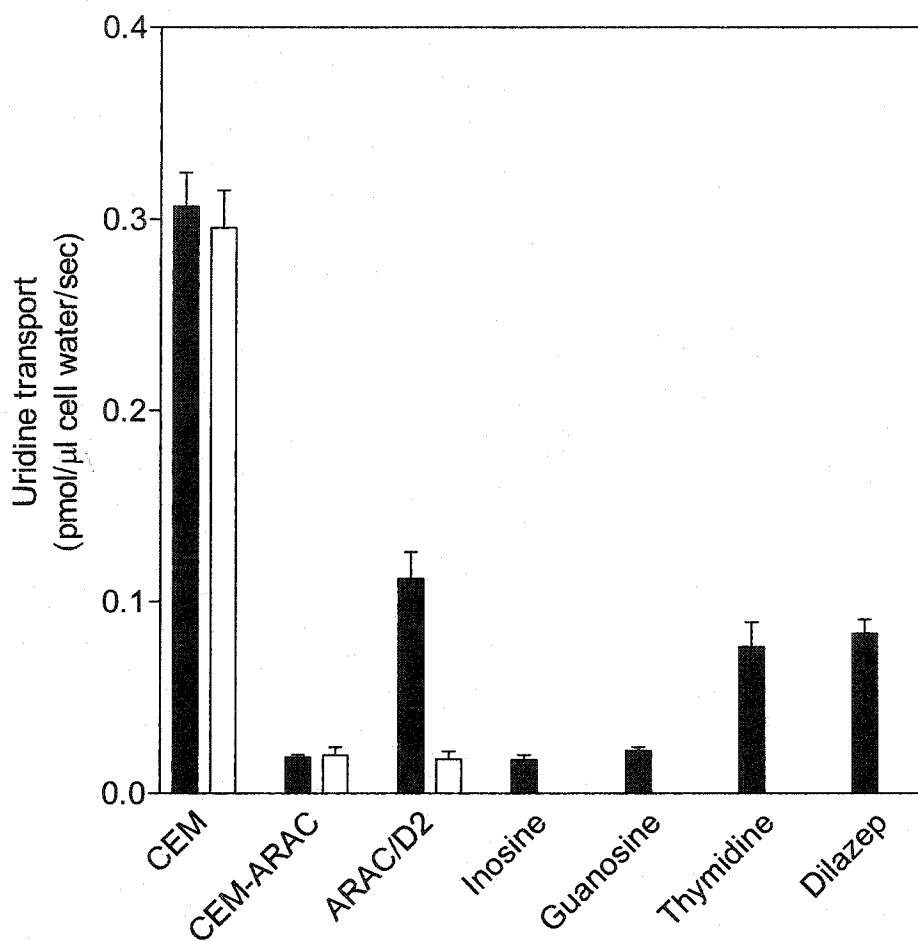


Figure III-30. Effects of natural nucleosides and dilazep on uridine influx into ARAC/D2 stable transfectants

Transport of 10 μM ^3H -uridine into CEM, CEM-ARAC and ARAC/D2 cells was measured in Na^+ -containing (filled bar) or sodium-free (open bar) transport buffer as described in section II.15. Inhibition of uridine transport into ARAC/D2 cells was performed in sodium-containing transport buffer with either 1 mM inosine, guanosine, thymidine or dilazep (filled bars). For transport assays, initial rates of uptake were obtained from 3-4 min linear time courses similar to those shown in Figure III-29. Each value represents the mean \pm SD of three determinations and error bars are not shown where SD values were smaller than those represented by the symbols.

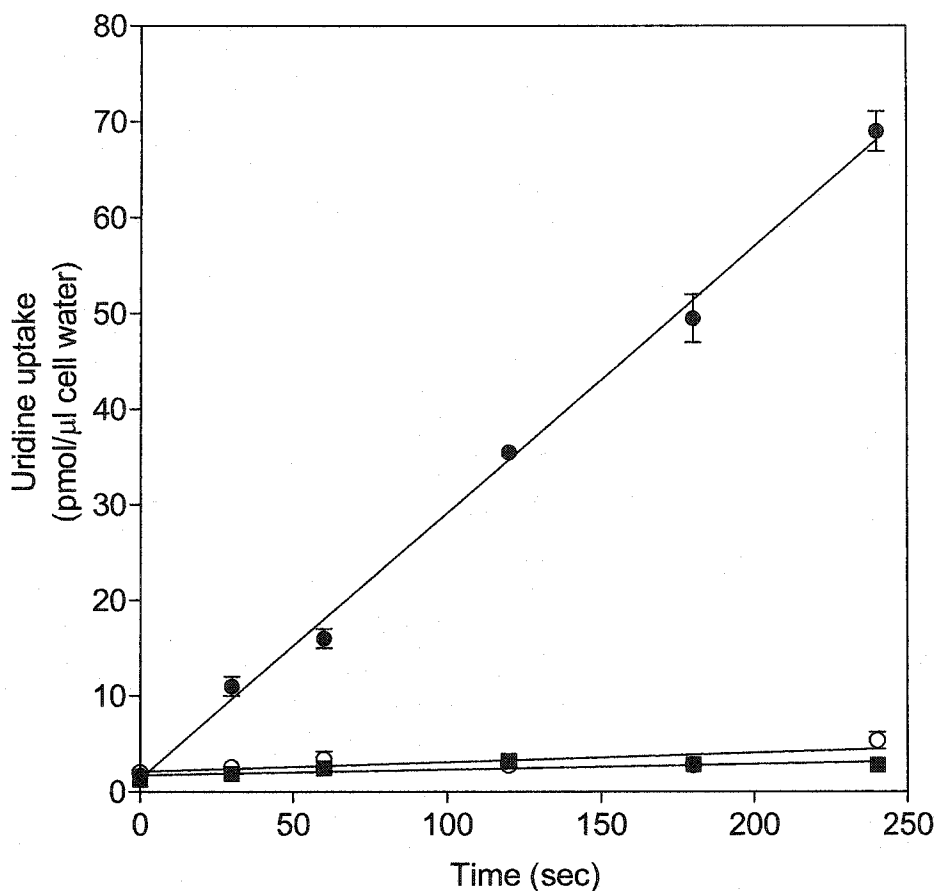


Figure III-31. Sodium-dependent, carrier-mediated uptake by TLCT1 stable transfectants

Uptake of $10 \mu\text{M}$ ^3H -uridine into TLCT1 cells was measured at the time intervals shown in sodium-containing (●) or sodium-free (○) transport buffer as described in section II.15. Non-mediated flux was identified by measuring uptake of $10 \mu\text{M}$ ^3H -uridine in sodium-containing transport buffer in the presence of excess 1 mM nonradiolabeled uridine (■). Each value represents the mean \pm SD of three determinations and error bars are not shown where SD values were smaller than that represented by the symbols.

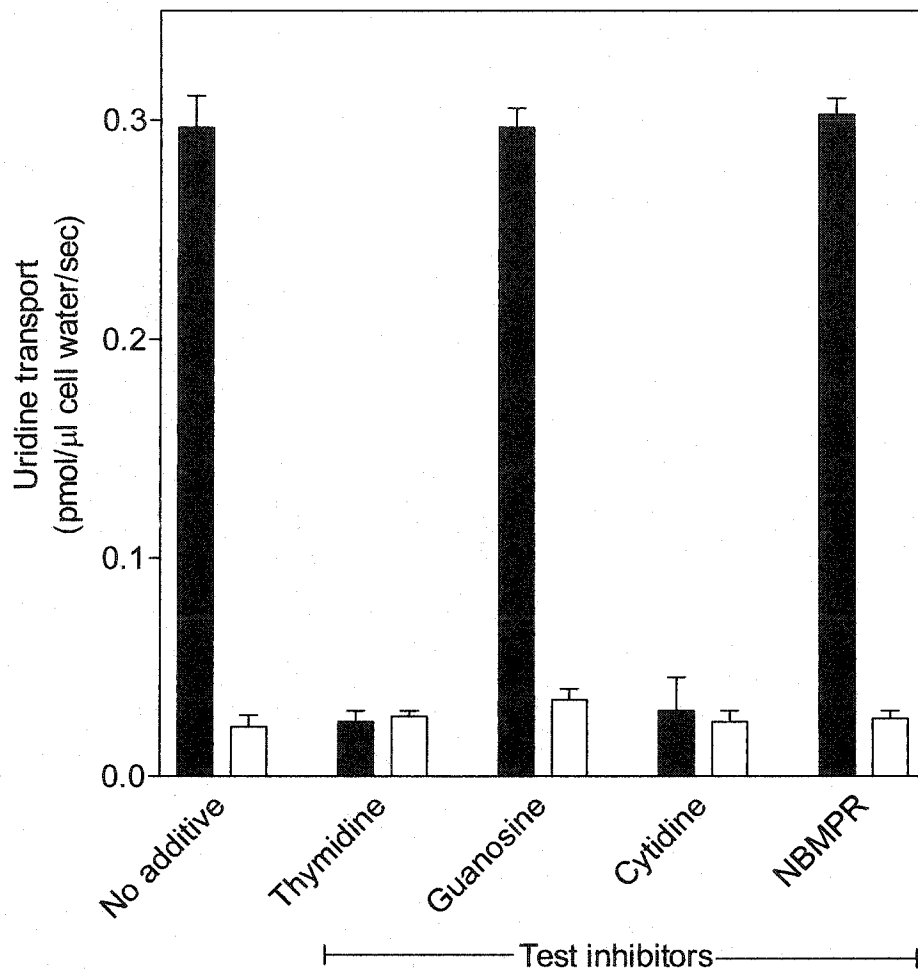


Figure III-32. Demonstration of *cit*-type activity by TLCT1 stable transfectants

Uptake of 10 μM ^3H -uridine into TLCT1 cells was measured in the presence (filled bars) or absence (unfilled bars) of sodium. Inhibition of uridine transport into TLCT1 cells was performed in sodium-containing transport buffer in the presence of 1 mM thymidine, guanosine, cytidine or 10 μM NBMPR. Initial rates of uptake were obtained from 60-sec linear time courses similar to those shown in Figure III-31. Each value represents the mean \pm SD of three determinations and error bars are not shown where SD values were smaller than those represented by the symbols.

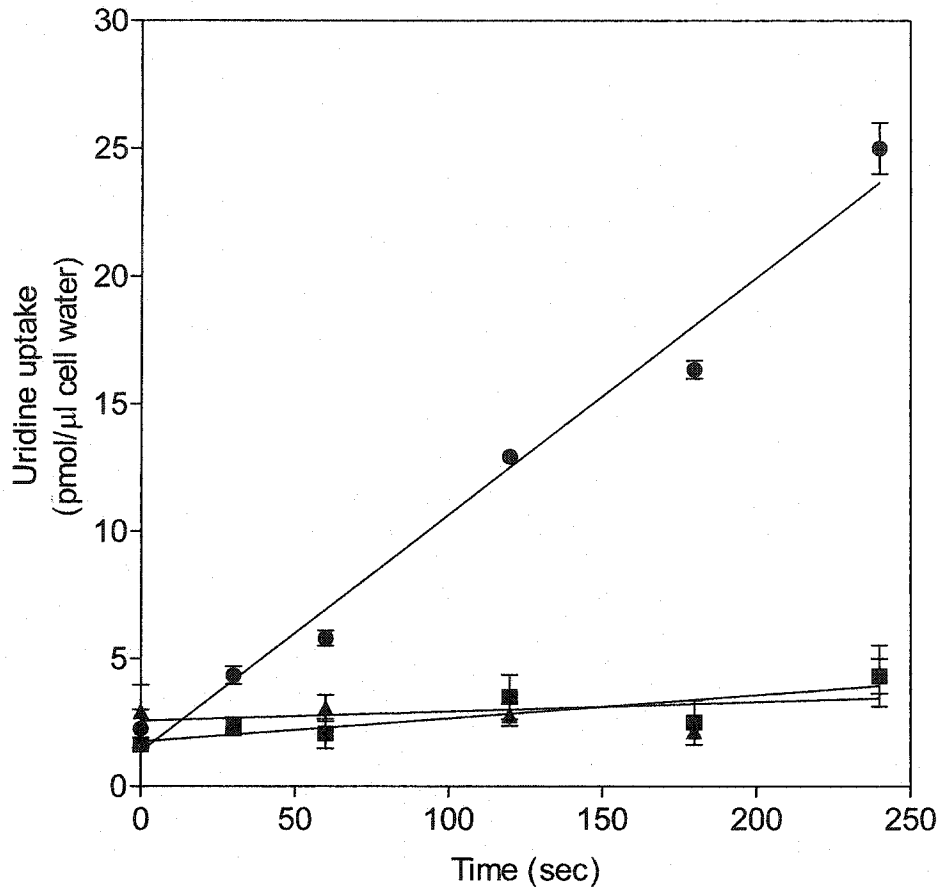


Figure III-33. Time course of uridine uptake by TLET2 stable transfectants

Uptake of $10 \mu\text{M } ^3\text{H}$ -uridine into TLET2 cells over the time intervals indicated was performed in sodium-containing transport buffer in the absence (●) or presence of either $200 \mu\text{M}$ dilazep (▲) or 3 mM uridine (■). Each value represents the mean \pm SD of three determinations and error bars are not shown where SD values were smaller than those represented by the symbols. Shown is one of two independent experiments that yielded qualitatively similar results.

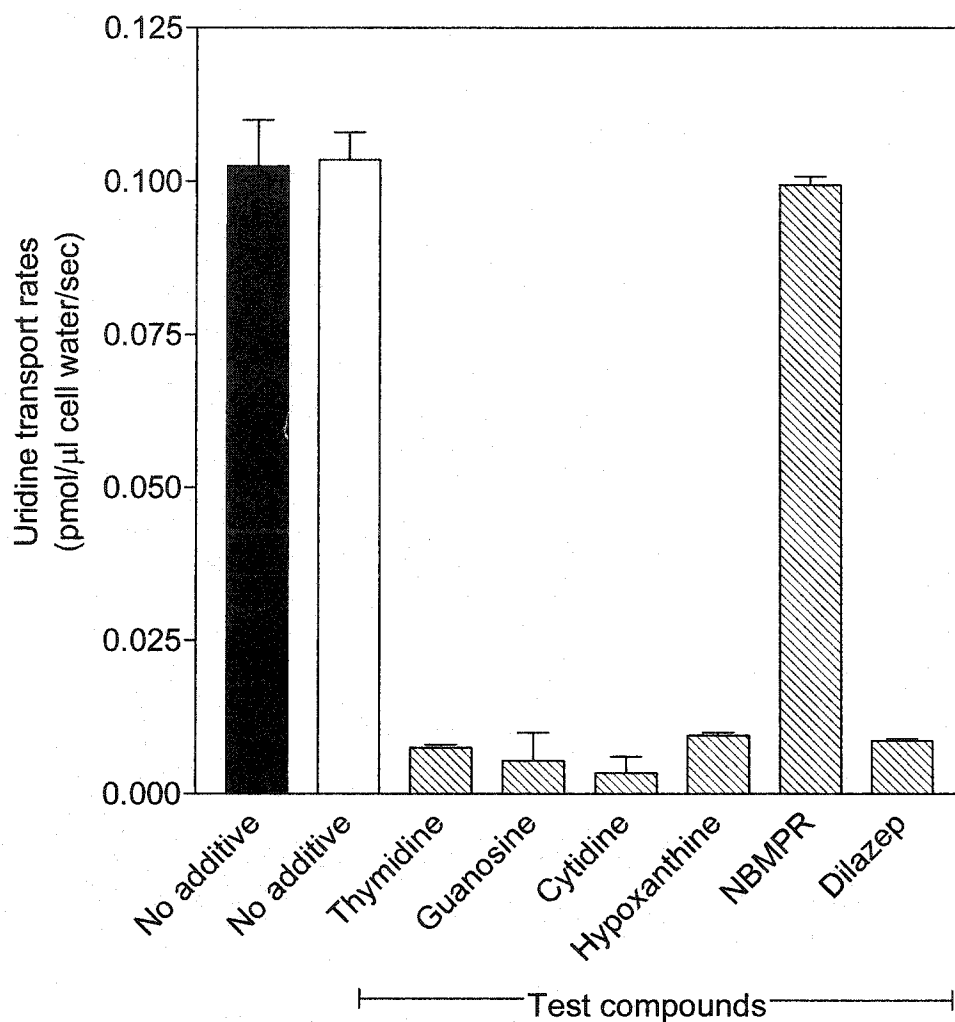


Figure III-34. Demonstration of *ei*-type activity by TLET2 stable transfectants

Uptake of 10 μM ^3H -uridine into TLET2 cells was measured in the presence (filled bars) or absence (unfilled bars) of sodium as described in section II.15. Uridine transport was performed in sodium-containing transport buffer in the presence of 3 mM thymidine, guanosine, cytidine, hypoxanthine or 0.1 μM NBMPR or 200 μM dilazep (hatched bars). Initial rates of uptake were obtained from 240-sec linear time courses similar to those shown in Figure III-33. Each value represents the mean \pm SD of three determinations and error bars are not shown where SD values were smaller than those represented by the symbols.

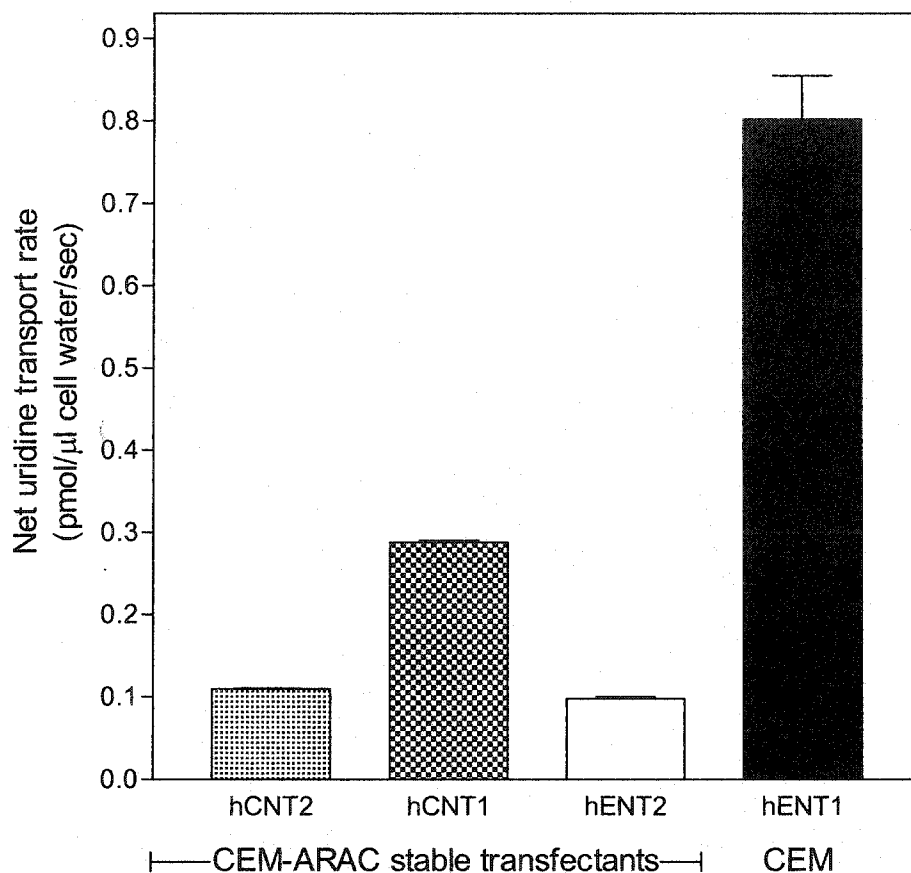


Figure III-35. Comparison of uridine transport activity in T-lymphoblastoid cell lines producing either hCNT2, hCNT1, hENT2 or hENT1

Uptake of $10 \mu\text{M}$ ^3H -uridine was measured in sodium-containing transport buffer. Values for uridine transport rates were obtained from the slopes of linear portions of 120-sec time courses for CEM-ARAC stable transfectants and 10-sec time courses for CEM cells. Each value represents the mean \pm SD of three determinations and error bars are not shown where SD values were smaller than those represented by the symbols.

Chapter IV

IV. Structure-Activity and Structure-Cytotoxicity Studies of hCNT1 and hCNT2 in TLCT1 and ARAC/D2 Stable Transfectants*

* Portions of this chapter have been published previously [74].

IV.1. Introduction

Uridine is a permeant of all mammalian nucleoside transporters identified to date [15, 53] and possesses similarly diverse properties to adenosine in that it appears to act as a signaling molecule as well as a therapeutic agent [55-57]. Analogs of uridine such as the fluoropyrimidine nucleoside drugs (5-fluorouridine, 5-fluoro-2'-deoxyuridine, 5-fluoro-5'-deoxyuridine) are important in the treatment of disseminated human cancers, especially of the gastrointestinal tract, breast and ovary [299, 300]. 5-Fluoro-5'-deoxyuridine is an active metabolite of the new orally administered drug capecitabine [301, 302], which is currently in clinical trials and demonstrates significant activity against solid tumors [303, 304]. Adenosine analogs such as cladribine and fludarabine are used for the treatment of different hematologic malignancies [94, 95, 97, 98]. Caffeine and nicotine exhibit multi-faceted actions through interactions with cell surface receptors in the central nervous system, and there is evidence of their neuroprotective effects against Parkinson's disease [305, 306]. Despite the importance of some uridine and adenosine analogs in anticancer therapy and caffeine and nicotine in nervous-tissue effects, the interactions of these substances with the CNTs and the possible role of the CNTs in cellular pharmacology of these drugs remains uncertain.

Studies with mammalian cells have established that the *cit* and *cif* processes mediated by the two major CNT family members, hCNT1 and hCNT2, exhibit preferences, respectively, for physiologic pyrimidine and purine nucleosides [53]. The CNTs have been identified mainly in specialized

mammalian cells (e.g., intestinal and renal epithelia) and in several neoplastic cell types [119, 121, 172, 196, 200, 231]. Functional characteristics of hCNT1 and hCNT2 are understood primarily from analyses of radioisotopic fluxes of physiologic nucleosides by recombinant transporters produced in oocytes of *Xenopus laevis* [131-133]. Such studies have established that hCNT1 and hCNT2 proteins exhibit permeant selectivities, respectively, for physiologic pyrimidine nucleosides and purine nucleosides. The apparent contrasting permeant preferences between hCNT1 and hCNT2 have lead to the speculation that they have complementary roles in tissues where both transporters are present, such as the brain and intestine [182, 196].

Although the *Xenopus laevis* expression system is a powerful tool for assessing transportability of nucleosides, it cannot be used to establish relationships between nucleoside drug transportability and cytotoxicity. Analysis of the molecular mechanisms of nucleoside transport in mammalian cells was for many years hampered by the presence in most cell types of more than one transporter type. In the present study, stable transfectants of hCNT1 and hCNT2 (named respectively, TLCT1 and ARAC/D2) produced in transport-deficient human leukemia cells were employed as model cell lines to study the transport properties of hCNT1 and hCNT2. The work in this chapter includes structure-activity and structure-cytotoxicity relationships of nucleoside and non-nucleoside drugs by hCNT2, followed by a comparison of the substrate selectivities and transport properties of hCNT2 and hCNT1. A variety of nucleoside analogs were examined, including nucleoside with substitution or elimination of the hydroxyl

group at the 2'- or 3'-positions of the sugar and addition of bulky, hydrophobic substituents or halogens at, respectively, the N6 and C5 positions of the base to determine if modifications of natural nucleosides affect their interactions with transporters and, in some cases, transportability.

Analysis of the molecular determinants for interaction with the purine-nucleoside selective hCNT2 identified several halogenated uridine analogs (e.g., 5-fluorouridine and 5-fluoro-2'-deoxyuridine) as high-affinity permeants and adenosine analogs (e.g., cladribine and fludarabine) as poorer permeants. A correlation was made between transport activities of uridine and adenosine analogs, and their antiproliferative activities against cancer cells containing or lacking particular transporters. In addition, the apparent contrasting permeant selectivities of hCNT2 and hCNT1 were examined by comparison of the capacity of these transporters to interact with a variety of therapeutically important uridine and adenosine analogs, as well as with caffeine and nicotine.

IV.2. Results

IV.2.1. Analysis of the nucleoside structural determinants for interaction with hCNT2 in ARAC/D2 cells

The ARAC/D2 stable transfectant that produced recombinant hCNT2 in isolation (described in Chapter III, section III.2.8.3) was employed in studies designed to analyze the permeant selectivity of hCNT2 by examining various nucleoside analogs with different structural modifications for their ability to interact with hCNT2. Uridine has been used extensively in inhibition experiments to assess permeant selectivity and/or inhibitory activity of nucleoside analogs. The extent to which various test nucleoside analogs inhibited uridine uptake into ARAC/D2 cells was examined by measuring uptake of 10 μM ^3H -uridine over 240-sec time periods in sodium-containing or sodium-free transport buffer in the absence or presence of a single high concentration (1000 μM) of test compound. A representative experiment is presented in Figure IV-1, in which the results revealed that uridine uptake by hCNT2 was inhibited completely in the presence of 2'-deoxyuridine, partially in the presence of 5-methyluridine and not at all in the presence of 3'-deoxyuridine. Negligible uridine uptake was observed in the absence of sodium over this time period.

IV.2.2. Structure-activity relationships of hCNT2: inhibition of uridine uptake by purine and pyrimidine nucleosides and by nucleobases

Rates of uptake of 10 μM ^3H -uridine were determined from uptake time courses similar to those shown in Figure IV-1 in which uptake was measured in

the absence or presence of 1 mM concentrations of (i) physiologic purine and pyrimidine nucleosides, nucleobases and ribose, (ii) purine and pyrimidine arabinonucleosides and arabinose, and (iii) analogs of adenosine and uridine. Studies involving adenosine and deaminase-sensitive adenosine analogs were conducted in the presence of 2 μ M 2'-deoxycoformycin to prevent deamination [268]. Deoxycoformycin did not inhibit hCNT2-mediated 3 H-uridine influx when tested at concentrations of 10 μ M since uridine transport rates in the presence and absence of deoxycoformycin were, respectively, 0.11 ± 0.019 pmol/ μ l cell water/sec and 0.11 ± 0.010 pmol/ μ l cell water/sec.

The results shown in Table IV-1 reveal that 3 H-uridine uptake by hCNT2 was inhibited completely by the physiologically occurring ribosyl and 2'-deoxyribosyl purine nucleosides, uridine, 2'-deoxyuridine, partially by thymidine and uracil, and not at all by ribose, cytidine, 2'-deoxycytidine or the other nucleobases that were tested. Although 2'-deoxyuridine and 2'-deoxyribosyl purine nucleosides inhibited uridine transport completely, 3'-deoxyuridine and 2',3'-dideoxyribosyl derivatives of uridine and adenosine had no effect, suggesting a requirement of the hydroxyl group at the 3' position of the ribosyl moiety for interaction with hCNT2.

The results of Table IV-1 also showed that hCNT2-mediated 3 H-uridine uptake was markedly inhibited by purine arabinonucleosides (9- β -D-arabinofuranosyladenine, 9- β -D-arabinofuranosylhypoxanthine), whereas it was not inhibited or only partially inhibited by pyrimidine arabinonucleosides (1- β -D-arabinofuranosyluracil, 1- β -D-arabinofuranosylcytosine, 2-fluoro-9- β -D-

arabinofuranosyladenine (fludarabine) and arabinose. 2'-Deoxyadenosine inhibited ^3H -uridine influx completely and exhibited greater inhibitory activity than either 2-chloroadenosine or 2-chloro-2'-deoxyadenosine (cladribine). Modifications of the purine ring to create 7-deazaadenosine (tubercidin) resulted in a compound that had no effect on hCNT2-mediated ^3H -uridine transport.

Substitutions with a series of halogens with decreasing electronegativities at position 5 of uridine (5-fluorouridine, 5-bromouridine, 5-iodouridine) resulted in complete inhibition of hCNT2-mediated ^3H -uridine transport. However, 5-methyluridine and thymidine were less potent inhibitors of ^3H -uridine transport (62% and 26% inhibition respectively). The different 5-halogenated 2'-deoxyribosyl uridine analogs showed different magnitudes of inhibition of ^3H -uridine transport, with 5-fluoro-2'-deoxyuridine being the most effective (82% inhibition), followed by 5-bromo-2'-deoxyuridine and 5-iodo-2'-deoxyuridine (44% and 31% inhibition, respectively). 5-Fluoro-5'-deoxyuridine, an intermediate metabolite of the oral fluoropyrimidine capecitabine [303], showed 20% inhibition of hCNT2-mediated ^3H -uridine transport.

The combined results of Table IV-1 demonstrated that hCNT2 exhibited (i) tolerance for substitution of the hydroxyl group for a hydrogen in the 2', but not the 3', position of the ribosyl moiety, (ii) preference for the 2'-hydroxyl substituent in the α - rather than β -configuration, (iii) low tolerance for modifications of position 2 on the purine base of adenosine analogs with halogen and (iv) higher tolerance for modifications of position 5 on the pyrimidine base of uridine analogs with halogen substituents than with a methyl group.

IV.2.3. Kinetics of uridine uptake and interactions of halogenated-uridine analogs with hCNT2

The kinetic parameters of hCNT2-mediated uridine transport into ARAC/D2 cells were estimated by determining the concentration dependence of ^3H -uridine influx at graded concentrations from 0 to 1000 μM (Figure IV-2). Uridine transport rates derived from linear regression analysis of uptake time courses were plotted as a function of uridine concentrations. The relationship between uridine influx (V) and concentration (S) was analyzed by non-linear regression using the classical equation $V=(S \times V_{\text{max}})/(K_m + S)$, where V_{max} and K_m represent, respectively, the maximal limiting influx and permeant concentration that produced the half maximal influx [307]. The graphical representation of this relationship is shown in Figure IV-2, in which uridine influx by hCNT2 conformed to Michaelis-Menten kinetics and yielded apparent K_m and V_{max} values, respectively, of $46 \pm 4 \mu\text{M}$ and $0.42 \pm 0.05 \text{ pmol}/\mu\text{l cell water}/\text{sec}$.

Since hCNT2 exhibited remarkably high tolerance for halogens at position 5 in several uridine analogs, inhibition experiments were performed with graded concentrations of the halogenated analogs to quantify the relative effects of these modifications in ribosyl and deoxyribosyl derivatives of uridine. Several important fluoropyrimidine nucleosides used at one time or another in cancer chemotherapy regimens were examined in this work for their ability to interact with hCNT2. As shown in the representative concentration-effect relationships of Figure IV-3 that compared 5-fluorouridine, 5-fluoro-2'-deoxyuridine and 5-fluoro-5'-deoxyuridine, hCNT2-mediated ^3H -uridine transport was inhibited by 5-

halogenated uridine analogs to varying degrees. The IC_{50} values (concentration that reduced uridine uptake by 50%) for 5-fluorouridine, 5-fluoro-2'-deoxyuridine and 5-fluoro-5'-deoxyuridine inhibition of 3H -uridine transport were 41, 99 and 498 μM , respectively.

The calculated inhibitor constants (K_i values) for uridine-containing analogs determined from the equation of Cheng and Prusoff [308] are shown in Table IV-2. The K_i values for 5-fluorouridine and 5-iodouridine (34 and 50 μM , respectively) were similar to the K_m value of 46 ± 4 μM observed for uridine transport by hCNT2. A much higher K_i value (197 μM) was obtained for 5-methyluridine, which was consistent with its poor ability to inhibit hCNT2-mediated 3H -uridine transport in the inhibition studies of Table IV-1. The halogen substituents at the 5 position in the pyrimidine ring of ribosyl analogs did not alter the apparent K_i values, whereas there was a progressive increase in K_i values that paralleled the increase in size and/or decrease in electronegativities of the halogen atoms in the 2'-deoxyribosyl analogs (5-fluoro-2'-deoxyuridine < 5-bromo-2'-deoxyuridine < 5-iodo-2'-deoxyuridine).

A comparison of 5-fluoro-2'-deoxyuridine and 5-fluoro-5'-deoxyuridine demonstrated the importance of the hydroxyl group at the 5' position for inhibitor-transporter interaction. Removal of the hydroxyl group at the 5' position of 5-fluorouridine increased the K_i value from 34 to 411 μM , whereas removal of the hydroxyl group at the 2' position increased the K_i value to 82 μM . These results indicated that the 5-halogenated uridine analogs, 2'-deoxyuridine and 5-fluoro-2'-deoxyuridine bound well to hCNT2. Although these results demonstrated

interaction between the inhibiting substances and hCNT2, the experimental protocol did not provide information on the transportability of the inhibiting substances.

IV.2.4. Transport characteristics of ARAC/D2 cells: hCNT2-mediated transport of physiological and modified nucleosides

The initial rates of uptake of adenosine and uridine analogs that exhibited inhibitory activities in the inhibition experiments were examined to determine if these compounds were transported by hCNT2 and, if so, to compare their transport rates with those of the universal permeant uridine. The results of Figure IV-4 showed that the sodium-dependent transport rates, which represented the hCNT2-mediated component, were generally higher for physiologic purine nucleosides than for pyrimidine nucleosides. Both adenosine and 2'-deoxyadenosine, which completely inhibited hCNT2-mediated ³H-uridine transport (Table IV-1), exhibited approximately 2-fold higher transport rates than uridine (adenosine > 2'-deoxyadenosine). Guanosine exhibited slightly higher rates of transport than 2'-deoxyguanosine. The adenosine analogs, fludarabine (9-β-D-arabinofuranosyl-2-fluoroadenine) and cladribine (2-chloro-2'-deoxyadenosine), exhibited relatively low transport rates compared to the natural nucleosides that were permeants of hCNT2.

Since hCNT2-mediated uridine transport was inhibited strongly by several modified uridine analogs in the experiments of Table IV-1, a series of pyrimidine nucleosides and nucleobases were examined for transportability in the experiments of Figure IV-4. The sodium-dependent component of the transport

rate for 5-fluorouridine (0.132 ± 0.003 pmol/ μ l cell water/sec) was rapid and higher than that observed for uridine (0.097 ± 0.009 pmol/ μ l cell water/sec). Although uracil and thymidine partially inhibited hCNT2-mediated 3 H-uridine transport (Table IV-1), direct measurement of 3 H-uracil and 3 H-thymidine influx into ARAC/D2 cells indicated that these inhibitors were not permeants of hCNT2. The uptake of 3 H-uracil observed in the presence and absence of extracellular sodium may have been due to uptake by a nucleobase transporter and/or passive diffusion.

IV.2.5. Transport of 5-fluorouridine by hCNT2

The kinetics of transport of 5-fluorouridine by hCNT2- and hENT1-containing cells were compared with those of the naturally occurring nucleoside uridine in the experiment of Table IV-3. Initial rates of uptake by hCNT2-containing ARAC/D2 cells were determined as a function of concentration and the relationship so obtained conformed to Michaelis-Menten kinetics, with apparent K_m and V_{max} values (mean \pm S.D.) of 43 ± 7 μ M and 0.38 ± 0.07 pmol/ μ l cell water/sec, respectively. The apparent K_m value (43 μ M) for 5-fluorouridine influx was similar to the K_i value (34 μ M) determined from the inhibition experiments of Table IV-2. The K_m and V_{max} values for 5-fluorouridine were almost identical to those obtained in the same experiment for uridine (46 ± 4 μ M and 0.42 ± 0.05 pmol/ μ l cell water/sec, respectively). The calculated V_{max}/K_m ratios for the two compounds were similar, indicating that hCNT2 transports 5-fluorouridine and uridine with equal efficiencies.

To compare the abilities of hCNT2 and hENT1 to interact with 5-fluorouridine and uridine, transport assays with ARAC/D2 and CEM cells were undertaken (Table IV-3). Analysis of the kinetic parameters of the hENT1-mediated transport mechanism in CEM cells revealed substantially higher apparent K_m values for 5-fluorouridine and uridine than those obtained in ARAC/D2 cells, with the 5-fluorouridine K_m value being slightly higher than that of uridine (217 versus 192 μM). The V_{max} values for uridine and 5-fluorouridine obtained in CEM cells were much higher than the values obtained for the same compounds in ARAC/D2 cells.

IV.2.6. Analysis of the chemosensitivity of cytotoxic nucleoside drugs in ARAC/D2, CEM and CEM-ARAC cells

The fluoropyrimidine nucleosides, 5-fluorouridine, 5-fluoro-2'-deoxyuridine and 5-fluoro-5'-deoxyuridine exhibited differences in their affinities for hCNT2 with 5-fluorouridine > 5-fluoro-2'-deoxyuridine > 5-fluoro-5'-deoxyuridine. 5-Fluoro-5'-deoxyuridine is an active metabolite of the prodrug capecitabine, and their chemical structures are shown in Figure IV-5. The relationship between drug transportability and cellular toxicity was addressed by examination of the antiproliferative activities of various nucleoside drugs that differed with respect to their transport efficiency by hCNT2. Cultures of hCNT2-producing ARAC/D2 cells were exposed continuously to graded concentrations of 5-fluorouridine, 5-fluoro-2'-deoxyuridine or 5-fluoro-5'-deoxyuridine. The antiproliferative activities of the drugs were estimated by linear regression analysis of growth rates, and the resulting growth rates were plotted as a function of drug concentrations as

shown in the representative experiment of Figure IV-6. The results showed concentration dependent inhibition of cell proliferation by all the fluoropyrimidine nucleosides tested. The antiproliferative activities of 5-fluorouridine, 5-fluoro-2'-deoxyuridine and 5-fluoro-5'-deoxyuridine, expressed as the concentration of drug that inhibited cell proliferation by 50% (IC_{50}), were, respectively, 0.05, 0.25 and 47 μ M.

IV.2.7. Enhanced sensitivity to purine and pyrimidine nucleoside drugs in hCNT2-producing ARAC/D2 cells

The nature of the association between efficiency of transport and cellular toxicity was addressed further by comparative examination of a group of cytotoxic nucleoside drugs for their ability to inhibit cell proliferation in cancer cell lines (ARAC/D2, CEM and CEM-ARAC) that possessed, respectively, hCNT2, hENT1 and no nucleoside transporters (Table IV-4). Antiproliferative activities of the various drugs, expressed as IC_{50} values, were determined from concentration-effect relationships similar to those shown in Figure IV-6. The anthracycline doxorubicin was included in the experimental analysis to demonstrate that the resistance of CEM-ARAC cells was not associated with multidrug resistance (MDR) proteins. All of the cell lines tested exhibited similar sensitivities to doxorubicin, indicating that cellular resistance to nucleoside drugs was not likely linked to plasma membrane efflux of drugs by MDR proteins.

The results of Table IV-4 showed that CEM cells were sensitive, whereas CEM-ARAC cells were highly resistant, to all of the nucleoside drugs tested. This result showed that hENT1-mediated permeation across the plasma

membrane greatly enhanced antiproliferative activity of both purine and pyrimidine nucleoside drugs. Although cladribine was relatively more cytotoxic to ARAC/D2 cells than fludarabine, both drugs were much more effective against CEM cells. Tubercidin (7-deazaadenosine), a known permeant of *es* (i.e., hENT1-mediated) processes [75], exhibited markedly different activities against hENT1-containing CEM and hCNT2-containing ARAC/D2 cells, with IC_{50} values, respectively, of 0.08 and 16.7 μM , a 200-fold difference. A qualitatively similar result was obtained with cytarabine, which is a known *es* permeant [82]; IC_{50} values, respectively, of 0.10 and $> 100 \mu\text{M}$ were obtained with CEM and ARAC/D2 cells. ARAC/D2 cells appeared to be relatively insensitive to tubercidin and cytarabine, suggesting that these drugs were likely not permeants of hCNT2.

The cytotoxic fluoropyrimidine nucleoside, 5-fluorouridine, which was shown in Table IV-3 to be a high-affinity permeant of hCNT2, was considerably more toxic to ARAC/D2 and CEM cells (IC_{50} values, respectively, 0.05 and 0.06 μM) than to CEM-ARAC cells ($IC_{50} > 50 \mu\text{M}$). Similarly, 5-fluoro-2'-deoxyuridine was cytotoxic, albeit moderate compared to 5-fluorouridine, against ARAC/D2 cells and much less so against CEM-ARAC cells. In contrast, 5-fluoro-5'-deoxyuridine was only slightly less effective against ARAC/D2 cells ($IC_{50} = 47 \mu\text{M}$) than against CEM-ARAC cells ($IC_{50} > 50 \mu\text{M}$). CEM-ARAC cells were highly resistant to the antiproliferative effects of most of the nucleoside drugs investigated.

IV.2.8. Comparative studies of hCNT1 and hCNT2 in TLCT1 and ARAC/D2 stable transfectants: transporter interactions with analogs of uridine and adenosine

The general permeant selectivities of hCNT1 and hCNT2 have been defined for key natural nucleosides in studies with recombinant transporters produced in *Xenopus* oocytes [131-133]. These studies have classified hCNT1 and hCNT2 as mediating, respectively, either the *cit* or *cif* processes in mammalian cells [53, 131-133]. The hCNT1 and hCNT2 proteins are generally referred to as pyrimidine-nucleoside selective and purine-nucleoside selective transporters [134, 140, 208].

The studies in this section further explored the differences between hCNT1 and hCNT2 in their abilities to interact with uridine and adenosine analogs. Inhibition and transport experiments were undertaken with TLCT1 and ARAC/D2 stable transfectants that produce, respectively, hCNT1 and hCNT2 in isolation. The isolation and characterization of both transfectants are described in Chapter III (section III.2.8).

IV.2.8.1. Kinetics of uridine transport by hCNT1 in TLCT1 cells

Uridine is a universal permeant of all mammalian nucleoside transporters [53] and therefore has been employed frequently in inhibition experiments to determine permeant selectivities and/or inhibitory activities of other nucleosides. The kinetic properties of hCNT1-mediated uridine transport into TLCT1 cells were determined by calculating initial rates of uridine transport, derived from uptake time courses as a function of graded uridine concentrations as presented

in Figure IV-7. Uridine influx into TLCT1 cells was saturable and the Michaelis-Menten kinetic parameters were (K_m and V_{max}), respectively, $34 \pm 2 \mu\text{M}$ and $1.01 \pm 0.17 \text{ pmol}/\mu\text{l cell water}/\text{sec}$

IV.2.8.2. *Comparison of the inhibitory activities of uridine analogs on uridine uptake by hCNT1 and hCNT2 in stable transfectants*

The prodrug capecitabine (see Figure IV-5) is metabolized by extracellular enzymes carboxylesterase and cytidine deaminase to 5-fluoro-5'-deoxyuridine [301, 309], which is believed to be the form that enters target tumor cells. The inhibitory activities of 5-fluoro-5'-deoxyuridine on ^3H -uridine transport by hCNT1 and hCNT2 were compared in the concentration-effect relationships of Figure IV-8. A reduction in uridine transport rates was observed for both transporters with increasing concentrations of 5-fluoro-5'-deoxyuridine, although there was a marked difference in their sensitivities to inhibition by 5-fluoro-5'-deoxyuridine. The IC_{50} values for 5-fluoro-5'-deoxyuridine inhibition of ^3H -uridine transport by hCNT1 and hCNT2, respectively, were 31 and 498 μM .

The inhibitory effects of uridine analogs were further addressed using additional structurally similar analogs that were tested for their relative abilities to inhibit ^3H -uridine influx into either TLCT1 (hCNT1-containing) or ARAC/D2 (hCNT2-containing) cells. The concentration-effect relationships of several other uridine analogs were determined in experiments similar to those of Figure IV-8 and K_i values were computed according to the equation of Cheng and Prusoff [308]. The results are presented in Table IV-5. K_i values in the range of 22 to 33 μM were obtained in hCNT1-containing TLCT1 cells for 5-fluorouridine, 2'-

deoxyuridine, 5-fluoro-2'-deoxyuridine and 5-fluoro-5'-deoxyuridine. Although similarly low K_i values were obtained in hCNT2-containing ARAC/D2 cells for 5-fluorouridine and 2'-deoxyuridine (34 and 39 μM respectively), the K_i values for 5-fluoro-2'-deoxyuridine and 5-fluoro-5'-deoxyuridine were, respectively, slightly higher (82 μM) and much higher (411 μM). Capecitabine itself did not inhibit ^3H -uridine uptake into either TLCT1 or ARAC/D2 cells when tested at 1 mM.

IV.2.8.3. Inhibition of ^3H -uridine transport into TLCT1 and ARAC/D2 cells by L-adenosine, but not by L-uridine

Earlier studies with murine cells have demonstrated that the equilibrative NBMPR-sensitive (i.e., hENT1-mediated) transport process exhibits stereoselectivity for the D-enantiomer of various nucleosides [310]. The majority of studies conducted in the nucleoside transporter field have been with D-enantiomers of various natural and synthetic nucleosides. The interaction of nucleosides of the L-configuration with CNT family members has not been determined. Nucleoside analogs of the L-configuration make up some of the nucleoside drugs currently employed in treatment of viral diseases [61]. The extent to which L-enantiomers of uridine and adenosine inhibited uptake of ^3H -labeled D-uridine by TLCT1 or ARAC/D2 cells producing, respectively, hCNT1 and hCNT2, was assessed in the experiments of Figure IV-9. Transport rates of D-uridine in the presence and absence of high concentrations of either L-uridine or L-adenosine were derived from linear regression analysis of uptake time courses. Uridine transport rates, which were higher for TLCT1 cells (0.291 ± 0.009 pmol/ μl cell water) than for ARAC/2 cells (0.098 ± 0.006 pmol/ μl cell

water), were reduced to negligible levels in the presence of nonradiolabeled D-uridine. In the presence of 1 mM L-uridine, there were no apparent changes in the uridine transport rates observed for either cell line. In the presence of L-adenosine, there were a small reductions in uridine transport rates to 0.212 ± 0.008 and 0.079 ± 0.009 pmol/ μ l cell water, respectively, in hCNT1-containing TLCT1 and hCNT2-containing ARAC/D2 cells. The inhibition by L-adenosine of hCNT1-mediated uridine influx was greater than that of hCNT2-mediated influx, although the inhibitions by L-adenosine were much less than those observed with D-uridine. These results indicated that L-adenosine was not a permeant, or was a poor permeant, of hCNT1 and hCNT2. Assessment of the transportability of L-adenosine was not pursued in this study.

IV.2.8.4. Comparison of the inhibitory activities of adenosine analogs on uridine uptake by hCNT1 and hCNT2 in stable transfectants

Adenosine was once thought to be a universal permeant of mammalian nucleoside transporters [13], a property similar to that of uridine. Adenosine now appears to exhibit a dual role, acting more as an inhibitor of CNT1-mediated process, while behaving as a high-affinity, high-activity permeant of CNT2-mediated process [15, 132, 133]. The role of adenosine in mammalian tissues is multi-faceted, particularly in excitable tissues such as the heart and brain, where it exhibits protective effects during pathological conditions [22-25, 35, 36]. The rapid creation and depletion of extracellular pools of adenosine involved in stimulation and inactivation of adenosine receptors, respectively, are attributed, in part, to fluxes mediated by nucleoside transporters. Adenosine analogs such

as N⁶-(p-aminobenzyl)adenosine and caffeine are known to bind to adenosine receptors [311-313] and were examined in the present study as potential inhibitors of hCNT1 and/or hCNT2.

Derivatives of adenine and adenosine, as well as nicotine, were examined for their ability to inhibit uridine transport into either TLCT1 or ARAC/D2 cells. Initial rates of uptake of 10 μ M ³H-uridine were measured in the presence of 1 mM test compounds and the results are presented in Table IV-6. Excess (1 mM) nonradiolabeled uridine reduced ³H-uridine transport to negligible levels in both TLCT1 and ARAC/D2 cells (0.005 ± 0.002 and 0.002 ± 0.003 pmol/ μ l cell water/sec, respectively). Transport of ³H-uridine into TLCT1 cells was inhibited completely by N⁶-(p-aminobenzyl)adenosine, nicotine, caffeine, adenosine and 2'-deoxyadenosine, almost completely by 5'-deoxyadenosine, 2-chloroadenosine, partially by 8-chloroadenosine, and not at all by erythro-9-(2-hydroxy-3-nonyl)adenine, 2'-3'-dideoxyadenosine and adenine. Transport of ³H-uridine transport into ARAC/D2 cells was inhibited completely by N⁶-(p-aminobenzyl)adenosine, caffeine, adenosine and 2'-deoxyadenosine, partially by nicotine, 5'-deoxyadenosine, erythro-9-(2-hydroxy-3-nonyl)adenine and 2-chloroadenosine and poorly, or not all, by 8-chloroadenosine, 2'-3'-dideoxyadenosine and adenine. Since ³H-uridine transport was not inhibited in either cell line by 2'-3'-dideoxyadenosine, erythro-9-(2-hydroxy-3-nonyl)adenine or adenine, these compounds evidently did not bind to either hCNT1 or hCNT2, and thus were not permeants. The differences in sensitivities of TLCT1 and

ARAC/D2 cells to inhibition of ^3H -uridine transport by nicotine and 5'-deoxyadenosine were pursued in subsequent studies.

IV.2.8.5. Concentration-effect relationships of adenosine analogs and nicotine for inhibition of ^3H -uridine transport into TLCT1 and ARAC/D2 cells

It has been shown that N^6 -(p-aminobenzyl)adenosine is a high-affinity ligand of A1 and A3-type adenosine receptors as well as a potent inhibitor of the es transporter [311, 312, 314]. The relative inhibitory activities of N^6 -(p-aminobenzyl)adenosine and 5'-deoxyadenosine on ^3H -uridine transport into TLCT1 and ARAC/D2 cells were determined in the experiment of Figure IV-10. The IC_{50} values, which were determined from analysis of the concentration-effect relationships of Figure IV-10, for N^6 -(p-aminobenzyl)adenosine and 5'-deoxyadenosine inhibition of ^3H -uridine transport into TLCT1 cells were 36 and 88 μM , respectively, and into ARAC/D2 cells were 43 and 287 μM , respectively. These results demonstrated that N^6 -(p-aminobenzyl)adenosine exhibited similarly moderate inhibitory activities on hCNT1- and hCNT2-mediated uridine influx, whereas 5'-deoxyadenosine, a less active inhibitor, exhibited more pronounced inhibition against TLCT1 cells (IC_{50} = 88 μM) than against ARAC/D2 cells (IC_{50} = 287 μM).

Both caffeine and nicotine exert important physiological effects on the central nervous system in association with adenosine [305, 306, 313, 315]. The molecular structure of caffeine is similar to that of adenine and it can act as a

ligand of adenosine receptors ([313] see Figure IV-11). To compare the relative abilities of caffeine and nicotine to inhibit ^3H -uridine transport into TLCT1 and ARAC/D2 cells, their IC_{50} values, derived from concentration-effect relationships for inhibition of ^3H -uridine transport, were determined. As shown in the experiments of Figure IV-12, caffeine and nicotine produced concentration-dependent reductions in uridine transport rates and yielded IC_{50} values of 59 and 82 μM , respectively, in TLCT1 cells, and IC_{50} values of 125 and 276 μM , respectively, in ARAC/D2 cells. These IC_{50} values for caffeine and nicotine inhibition of ^3H -uridine transport were 2- to 3- fold higher for ARAC/D2 cells than for TLCT1 cells, suggesting differences in the ability of these compounds to interact with hCNT1 or hCNT2.

IV.2.8.6. Comparison of the inhibitory constants of adenosine analogs and nicotine in TLCT1 and ARAC/D2 cells

Since several of the adenosine analogs and nicotine inhibited uridine transport, other adenosine analogs were also examined in similar inhibition experiments. The IC_{50} values from concentration-effect relationships were used to calculate K_i values and the results are presented in Table IV-7. For both TLCT1 and ARAC/D2 cells, K_i values for N^6 -(p-aminobenzyl)adenosine, adenosine and 2'-deoxyadenosine were in the range of 28 to 44 μM . The K_i values for TLCT1 cells were lower for caffeine, nicotine and 5'-deoxyadenosine (46, 63 and 68 μM , respectively) than for ARAC/D2 cells (103, 227 and 237 μM , respectively). The K_i value for 2-chloroadenosine was 37 μM in ARAC/D2 cells and 101 μM in TLCT1 cells. The other analogs of adenosine (8-

chloroadenosine, L-adenosine and 2'-3'-dideoxyadenosine) exhibited little, if any, inhibitory effects on uridine transport in either cell line.

IV.2.8.7. Assessment of transportability of natural and therapeutic nucleosides by hCNT1 and hCNT2 in TLCT1 and ARAC/D2 cells

The inhibition experiments presented above revealed differences in the inhibitory activities of uridine and adenosine analogs on ³H-uridine transport into the TLCT1 and ARAC/D2 stable transfectants, suggesting differences in interactions of these compounds with hCNT1 and hCNT2. The nature of this interaction was addressed further by analysis of uptake of ³H-labeled uridine analogs, adenosine analogs and nicotine. Initial rates were determined from time courses of uptake of ³H-labeled compounds and the results are summarized in Table IV-8. TLCT1 cells, which possessed hCNT1, exhibited approximately 3-fold higher sodium-dependent transport of 2'-deoxyuridine and uridine than ARAC/D2 cells, which possessed hCNT2. Thymidine was not transported by ARAC/D2 cells, but was transported by TLCT1 cells, albeit at relatively low levels (net rate, 0.067 pmol/μl cell water/sec) compared to uridine (net rate, 0.293 pmol/μl cell water/sec). Adenosine was the only purine nucleoside among the compounds examined that was transported by TLCT1 cells, although the net rate (0.040 pmol/μl cell water/sec) was only 16% of that observed with ARAC/D2 cells (net rate, 0.248 pmol/μl cell water/sec). ARAC/D2 cells exhibited approximately 2-fold higher transport rates of adenosine analogs than uridine analogs and the purine 2'-deoxynucleosides were transported with almost similar rates as the purine ribonucleosides. These results suggested that

hCNT2 exhibited a greater capacity to transport adenosine analogs than uridine analogs whereas hCNT1 exhibited a greater capacity to transport uridine analogs than adenosine analogs.

Since the hCNT1 and hCNT2 proteins differed in their capacity to transport physiologic uridine and adenosine analogs, further experiments were conducted in attempt to compare their relative abilities to transport drug analogs of uridine and adenosine and nicotine. As shown in Table IV-8, both TLCT1 and ARAC/D2 cells transported 5-fluorouridine, although the rate in TLCT1 cells was 2.4-fold greater than that in ARAC/D2 cells. TLCT1 cells exhibited no detectable cladribine or fludarabine transport, whereas ARAC/D2 cells transported both compounds, although at low rates. The sodium-dependent transport rate for cladribine (0.023 pmol/ μ l cell water/sec) in ARAC/D2 cells was 2.3-fold higher than that for fludarabine ((0.010 pmol/ μ l cell water/sec). Therefore, hCNT2 transported the two adenosine analogs and 5-fluorouridine, and the rate of 5-fluorouridine transport was 4.8- and 11-fold higher than the rates of cladribine and fludarabine, respectively. In contrast, although hCNT1 was capable of transporting adenosine and 2'-deoxyadenosine, it did not transport either cladribine (2-chloro-2'-deoxyadenosine) or fludarabine (2-fluoro-9- β -D-arabinofuranosyladenine).

Since inhibition experiments revealed that caffeine and nicotine differentially inhibited uridine influx by hCNT1 and hCNT2, the transportability of these substances was assessed by measuring their uptake directly in TLCT1 and ARAC/D2 cells (Table IV-8). There was little, if any, uptake of either

caffeine or nicotine in TLCT1 or ARAC/D2 cells, indicating that caffeine and nicotine were not transported by hCNT1 and hCNT2 at 10 μ M, although both transporters exhibited the capacity to bind caffeine and nicotine.

IV.3. Discussion

The present work utilized the stable transfectants TLCT1 and ARAC/D2 producing, respectively, hCNT1 and hCNT2 in the same genetic background to study and compare the two major members of the CNT family. This specific approach avoided some of the difficulties associated with the multiplicity of nucleoside transporters in cell preparations employed for analysis of nucleoside fluxes [121, 200, 201]. By studying hCNT1 and hCNT2 in the human null background of CEM-ARAC cells (described in Chapter III), differences and similarities between the transporters could be defined more reliably.

IV.3.1. Analysis of the molecular determinants for interaction with hCNT2 and correlation of drug transport with in vitro sensitivity

The ARAC/D2 stable transfectant was used to identify molecular determinants for nucleoside analog interaction with hCNT2. Uridine inhibition experiments with structurally modified nucleosides revealed that the 3'- and 5'-hydroxyl groups of the ribosyl moiety were important for interaction of uridine analogs with hCNT2, whereas removal of the hydroxyl at the 2'-position did not significantly affect interaction with hCNT2. Therefore, it appears that the 3'- and 5'-hydroxyl groups were important structural features for permeant recognition, whereas the 2'-hydroxyl group was less important, although there was a preference for the 2'-hydroxyl group in the α - rather than β -configuration. hCNT2 exhibited a tolerance for modifications of the 5, but not the 3, position of the base with halogen substituents.

The apparent tolerance for hCNT2 interaction with purine 2'-deoxyribonucleosides was demonstrated by the complete blockade of uridine transport into ARAC/D2 cells by 2'-deoxyguanosine, 2'-deoxyadenosine and 2'-deoxyinosine and the capacity for inwardly directed transport of ³H-labeled 2'-deoxyguanosine and 2'-deoxyadenosine. Guanosine and 2'-deoxyguanosine transport rates were almost identical, whereas adenosine transport rates were somewhat greater than those of 2'-deoxyadenosine.

Although hCNT2 exhibited the typical purine-nucleoside selectivity [131, 132], it also displayed an unexpected tolerance for substitution of 5-fluoropyrimidine for uracil since 5-fluorouridine was transported with i) a similar affinity and ii) somewhat higher activity than uridine, when their net transport rates (at 10 μM) were compared directly. The clinically useful adenosine analog drugs, cladribine and fludarabine, were relatively weak inhibitors of recombinant hCNT2 in comparison to uridine analog drugs. Their sodium-dependent mediated transport rates (at 10 μM) were relatively low in comparison to that of 5-fluorouridine. In contrast, studies of cladribine transport by the rat homolog of hCNT2 (also termed SPNT), produced by transient expression of its cDNA in cultured HeLa cells, demonstrated that cladribine was a relatively good permeant [198]. These results indicate species differences in the interaction of cladribine with rat and human CNT2 proteins. The difference in transportability of cladribine between the human and rat CNT2 proteins is perhaps not surprising, given that these proteins share less amino acid identity (69%) in the amino-terminal half where the substrate binding domain of hCNTs reside [177].

Analysis of the chemosensitivity of cells to uridine and adenosine analog drugs demonstrated that cladribine was relatively more cytotoxic to ARAC/D2 cells than fludarabine, which was consistent with their apparent low-affinity interaction with hCNT2 and their low transport rates. Their relatively high antiproliferative activities against CEM cells were likely related to the greater capacity for uptake of cladribine and fludarabine via hENT1. Cladribine uptake by the equilibrative NBMPR-sensitive (i.e., hENT1-mediated) process has been demonstrated in cultured human leukemic cells [316]. In freshly isolated leukemic lymphoblasts, *in vitro* sensitivity to cladribine correlated with *es* (i.e., hENT1) abundance in plasma membranes as determined by SAENTA-fluorescein binding [220]. The relative insensitivities of hCNT2-containing cells to tubercidin and cytarabine were consistent with the inability of these compounds to inhibit hCNT2-mediated uridine influx, and they were therefore concluded to not be permeants of hCNT2. Cytarabine and tubercidin were also poor permeants of the human and rat pyrimidine-nucleoside selective (CNT1) transporters [66, 159].

The cytotoxic fluoropyrimidine nucleoside 5-fluorouridine, which was a high-affinity hCNT2 permeant, was considerably more toxic to ARAC/D2 and CEM cells than to transport-deficient CEM-ARAC cells. For ARAC/D2 cells, the acquired sensitivity to 5-fluorouridine was associated with, and most likely due to, the acquisition of hCNT2 activity by introduction of hCNT2 cDNA, whereas for CEM cells, the intrinsic sensitivity to 5-fluorouridine was attributed to endogenous hENT1-mediated uptake. RT-PCR and northern blot analysis have detected only

hENT1 mRNA in CEM cells, and this was associated with the presence of hENT1 protein in CEM cell membranes (see Chapter III). Similarly, 5-fluoro-2'-deoxyuridine was cytotoxic, although less so than 5-fluorouridine, against ARAC/D2 cells whereas CEM-ARAC cells were resistant. These results suggested that 5-fluoro-2'-deoxyuridine likely utilized hCNT2 to cross the cell membrane, since transport-deficient cells were far less sensitive to this analog than hCNT2-containing cells.

5-Fluoro-5'-deoxyuridine was less active against ARAC/D2 than CEM cells, consistent with the conclusion that its entry was not, or poorly, mediated by hCNT2. 5-Fluoro-5'-deoxyuridine is a metabolite of the novel orally administered drug capecitabine [301, 302], and there is recent evidence of its transportability by hCNT1 produced heterologously in Chinese hamster ovary cells [86]. Capecitabine, however, was not a permeant of either hCNT1 or hCNT2 since it did not inhibit uridine influx into either TLCT1 or ARAC/D2 cells when tested at 1 mM.

Collectively, the results suggested that the degree of antiproliferative activity against ARAC/D2 cells by uridine and adenosine analog drugs was reflected in their affinities and patterns of transport activity by hCNT2. The presence of recombinant hCNT2 in ARAC/D2 cells resulted in the acquisition of sensitivity to 5-fluorouridine and 5-fluoro-2'-deoxyuridine, whereas transport-deficient CEM-ARAC cells were resistant. This result was the first demonstration of the importance of hCNT2 in overcoming drug resistance arising from a deficiency in nucleoside transport capability.

IV.3.2. Comparative studies of hCNT1 and hCNT2 in TLCT1 and ARAC/D2 stable transfectants: transporter interactions with analogs of uridine, adenosine and adenine and with nicotine

Studies with mammalian cells have established that the *cit* and *cif* processes mediated by the two major CNT family members, hCNT1 and hCNT2, exhibit preferences, respectively, for physiologic pyrimidine and purine nucleosides [53, 132, 133]. Specialized tissues such as brain, kidney and intestine appear to possess both transporters [119, 182, 196], and there is evidence that substrate availability modulates their expression in rat jejunum *in vivo* [317]. There have also been speculations that hCNT1 and hCNT2 complement each other in the salvage of nucleosides from dietary sources and body fluids [140, 208].

While the general substrate selectivities of hCNT1 and hCNT2 have been established for key natural nucleosides [13, 131-133], there may be differences between the two transporters in their abilities to bind and transport nucleoside analogs. Indeed, substantial alterations in permeant selectivities of hCNT1 and hCNT2 were produced after small changes by site-directed mutagenesis of amino acid residues in the identified substrate binding domain [177].

The inhibition and transport studies presented in this chapter compared hCNT1 and hCNT2 in their capacity to interact with various analogs of uridine and adenosine, including several anticancer drugs, using the stable transfectants, TLCT1 and ARAC/D2. The K_i values for uridine analogs (5-fluorouridine, 2'-deoxyuridine, 5-fluoro-2'-deoxyuridine and 5-fluoro-5'-

deoxyuridine) were similarly low for hCNT1 in the range of 22 to 33 μM , suggesting that hCNT1 exhibited high affinities for these compounds. The purine-nucleoside selective hCNT2 exhibited moderate to high-affinity interactions with 5-fluorouridine, 2'-deoxyuridine and 5-fluoro-2'-deoxyuridine, but low-affinity interactions with 5-fluoro-5'-deoxyuridine. It has been shown that 5-fluoro-5'-deoxyuridine, a metabolite of the orally administered fluoropyrimidine derivative capecitabine, is a permeant of recombinant hCNT1 produced in *Xenopus laevis* oocytes by analysis of sodium currents induced by exposure to drug using voltage-clamp technique [318]. The work in this chapter indicated that capecitabine itself is not likely to be transported by either hCNT1 or hCNT2 since it was unable to inhibit ^3H -uridine influx into either TLCT1 or ARAC/D2 cells when tested at 1 mM.

Analyses of the inhibitory activities of adenine and adenosine analogs on uridine uptake into TLCT1 and ARAC/D2 cells demonstrated that erythro-9-(2-hydroxy-3-nonyl)adenine, 2'-3'-dideoxyadenosine and adenine exhibited low or negligible inhibitory effects, and therefore were likely not permeants of either hCNT1 or hCNT2. The inability of 2'-3'-dideoxyadenosine to reduce hCNT1- or hCNT2-mediated ^3H -uridine transport rates was consistent with the inability of 2'-3'-dideoxyuridine to inhibit hCNT2-mediated uridine uptake, suggesting the importance of the 3'-hydroxyl moiety for interaction with CNT proteins. The 3'-hydroxyl group is evidently an important structural feature for permeant recognition for most nucleoside transporters since the *es* transporter in human red cells was also poorly inhibited by several 2',3'-dideoxynucleosides, including

2',3'-dideoxyguanosine and 2',3'-dideoxyadenosine [223]. Interestingly, rat CNT1, which shares 83% amino acid identity with hCNT1, exhibits the ability to mediate the uptake of the antiviral nucleoside 2',3'-dideoxycytidine when produced in *Xenopus* oocytes [109, 133].

Several highly effective nucleoside drugs against viral and cancer diseases are nucleoside analogs of the L-configuration [61, 68]. L-Enantiomers of antiviral drugs are important in that they have been shown to be more potent than their corresponding D-enantiomers, and they are essentially noncytotoxic to human peripheral blood mononuclear cells [319]. The extent to which L-enantiomers of uridine and adenosine inhibited ³H-labeled D-uridine uptake into TLCT1 or ARAC/D2 cells was examined, and the results demonstrated negligible inhibitory activities by L-nucleosides. D-Nucleosides inhibited ³H-uridine uptake completely, suggesting that the enantiomeric configuration of the ribofuranosyl moiety was an important determinant for interaction with hCNT1 and hCNT2. Examination of adenosine uptake into murine L1210 leukemia cells and erythrocytes revealed that the equilibrative nucleoside transport process was stereoselective, and there was a marked preference for the D-enantiomer of adenosine over the L-enantiomer [310].

Ligands of adenosine receptors, N⁶-(p-aminobenzyl)adenosine, 2-chloroadenosine and caffeine [311-314, 320-322], were examined for their ability to inhibit hCNT1- and hCNT2-mediated ³H-uridine transport. All of these compounds demonstrated complete blockade of uridine influx by hCNT1 and hCNT2. The K_i value for N⁶-(p-aminobenzyl)adenosine inhibition of uridine influx

was similarly low for hCNT1 (28 μM) and hCNT2 (35 μM), suggesting that both transporters possessed fairly high affinities for this compound. N^6 -(*p*-aminobenzyl)adenosine has been shown to inhibit adenosine transport by cultured glial cells from chick embryo brain [323]. The K_i value for 2-chloroadenosine was 37 μM in ARAC/D2 cells and 101 μM in TLCT1 cells, suggesting that this substance has higher affinity for hCNT2 than hCNT1.

The K_i value for caffeine inhibition of hCNT2-mediated uridine transport was more than 2-fold greater than the K_i value for its inhibition of hCNT1-mediated transport, suggesting that hCNT2 and hCNT1 differ in their affinities for caffeine. Although hCNT1 exhibited a moderate affinity for caffeine, direct measurement of uptake of radiolabeled caffeine (at 10 μM) did not reveal any mediated uptake in either of the stable transfectants, suggesting that caffeine is either a non-permeant or a poor permeant of hCNT1 or hCNT2. Similarly, flux analysis with radiolabeled nicotine (at 10 μM) demonstrated that it was also not transported, despite the apparent moderate affinity of this substance (K_i value, 63 μM) for hCNT1.

Caffeine and nicotine exhibit important effects in the CNS, and there is evidence of their protective function against the development and progression of neurodegenerative diseases [306, 324, 325]. The average caffeine in a 150-ml cup of instant coffee is approximately 90 mg (more in freshly brewed coffee) [326], which equates to a concentration of 3.09 mM. The half-life of caffeine ranges from 3-6 hours in humans, and the serum levels achieved after an average cup of coffee are about 0.95 mg per liter of blood [326], which equates

to 4.9 μM . Caffeine has been shown to enhance locomotor activity in animal models of Parkinson's disease through its antagonistic action on adenosine receptors [327]. Similarly, both retrospective and prospective epidemiological studies have consistently demonstrated an inverse association between cigarette smoking and neurodegenerative illnesses such as Parkinson's disease, leading to speculations that smoking in general and nicotine in particular might be neuroprotective [324, 325]. An average cigarette contains approximately 1.5-2 mg of nicotine depending on the brand, resulting in nicotine concentrations in blood of 0.23 to 0.32 μM [328]. The physiological significance of the normal concentrations of caffeine and nicotine on the CNTs is uncertain, although it is tempting to speculate that an increased consumption above normal levels may potentially affect the ability of the CNTs to transport other permeants.

A comparison of the transport of uridine analogs in TLCT1 and ARAC/D2 cells showed that the transport rates of 2'-deoxyuridine, uridine and 5-fluorouridine for hCNT1 were higher than the rates observed for hCNT2. This suggested that hCNT1 exhibited a greater capacity for mediating the uptake of uridine analogs than hCNT2. In contrast, the transport rates of purine nucleosides (guanosine, 2'-deoxyguanosine, adenosine and 2'-deoxyadenosine) by hCNT2 were approximately 4-fold higher than the rates of adenosine transport by hCNT1.

IV.3.3. Conclusion

For many cell types, the presence of heterogeneous nucleoside transporters and complex overlapping permeant selectivities poses difficulties in

the interpretation of flux measurements and determination of mechanisms of drug transport or inhibition. The results presented in this chapter are the first concerted attempt to define the transport properties of hCNT2 and hCNT1 using isogenic stably transfected cell lines, each containing a particular nucleoside transporter. These studies demonstrated that introduction of hCNT2 into transport-defective cells conferred the capacity for enhanced drug transport and sensitivity to pharmacologically important fluoropyrimidine nucleosides. Several important substances that mediate effects on the CNS were shown to exhibit moderate affinities for hCNT1 and hCNT2. Although hCNT1 is pyrimidine-nucleoside selective, it possessed a greater capacity for interaction with several adenosine analogs than hCNT2. hCNT2, which is considered to be purine-nucleoside selective, was capable of interacting and transporting several uridine analogs with high affinity.

The identification of important structural features of nucleoside analogs for interaction with two of the three major members of the CNT family yielded important information that could potentially provide useful information in the design of new nucleoside analogs as therapeutic agents in human diseases. Perhaps more importantly, knowledge of differences between hCNT1 and hCNT2 in their transport activities and abilities to transport nucleoside analogs may provide clues as to the origin of selectivity and efficacy of nucleoside drugs.

Table IV-1. Inhibition of uridine uptake by hCNT2 in ARAC/D2 cells by ribonucleosides, arabinonucleosides and nucleobases: identification of candidate permeants and inhibitors of hCNT2

Rates of transport of 10 μM ^3H -uridine were obtained from uptake time courses of 3-4 min in sodium-containing or sodium-free transport buffer in the absence or presence of 1 mM test compounds listed as described in Figure IV-1. Sodium-dependent transport rates were calculated from the difference in uptake measurements performed in sodium-containing and sodium-free transport buffers as described in section II.15. The rate of uridine transport in the absence of additives (controls) was 0.12 ± 0.013 pmol/ μl cell water/sec. Transport rates are expressed as percentages of values obtained in the absence of additives (control) and are means \pm SD of triplicate determinations.

Additive (test compound)	Net ^3H -uridine transport (percent of control)
Pyrimidine nucleosides, nucleobases and ribose	
None	100
Uridine	2 ± 0.8
5-Fluorouridine	1 ± 0.6
5-Bromouridine	7 ± 5
5-Iodouridine	9 ± 7
5-Methyluridine	38 ± 3
2'-Deoxyuridine	3 ± 1.4
3'-Deoxyuridine	99 ± 7
2',3'-Dideoxyuridine	101 ± 5
5-Fluoro-2'-deoxyuridine	18 ± 2
5-Bromo-2'-deoxyuridine	56 ± 3
5-Iodo-2'-deoxyuridine	69 ± 5
5-Fluoro-5'-deoxyuridine	80 ± 5
Thymidine	74 ± 3
Cytidine	94 ± 7
2'-Deoxycytidine	96 ± 6
Uracil	68 ± 3
5-Fluorouracil	82 ± 3
Thymine	85 ± 2
Cytosine	99 ± 5
Ribose	97 ± 4
Purine nucleosides and nucleobases	
Inosine	4 ± 2.8
2'-Deoxyinosine	5 ± 4
Guanosine	1 ± 0.8

2'-Deoxyguanosine	3 ± 2
Adenosine	2 ± 1.7
2'-Deoxyadenosine	2 ± 1.3
2',3'-Dideoxyadenosine	96 ± 3
2-Chloroadenosine	15 ± 3
2-Chloro-2'-deoxyadenosine	32 ± 4
7-Deazaadenosine	100 ± 2
Adenine	98 ± 3
Hypoxanthine	96 ± 5
Guanine	101 ± 2
Arabinonucleosides and arabinose	
1-β-D-Arabinofuranosyluracil	70 ± 4
1-β-D-Arabinofuranosylcytosine	102 ± 6
9-β-D-Arabinofuranosyladenine	31 ± 2
2-Fluoro-9-β-D-arabinofuranosyladenine	84 ± 3
9-β-D-Arabinofuranosylhypoxanthine	20 ± 2
Arabinose	99 ± 3

Table IV-2. Inhibitor constants (K_i values) for inhibition of uridine transport by hCNT2 in ARAC/D2 cells

The concentrations of test compounds that reduced uridine uptake rates by 50% (IC_{50} values) were determined from concentration-effect relationships similar to those shown in Figure IV-3. These values were then used to calculate K_i values according to the equation of Cheng and Prusoff [308] using the average K_m values for uridine transport of three independent experiments obtained as shown in Figure IV-2.

Nucleoside	IC_{50} (μM)	K_i (μM)
5-Fluorouridine	41	34
5-Iodouridine	61	50
5-Methyluridine	240	197
2'-Deoxyuridine	47	39
5-Fluoro-2'-deoxyuridine	99	82
5-Bromo-2'-deoxyuridine	267	219
5-Iodo-2'-deoxyuridine	299	246
5-Fluoro-5'-deoxyuridine	>500	>411

Table IV-3. Comparison of Michaelis-Menten constants for the transport of uridine and 5-fluorouridine by hCNT2 in ARAC/D2 and hENT1 in CEM cells

Transport assays with ARAC/D2 and CEM cells were performed with graded concentrations of ³H-nucleoside in sodium-containing and sodium-free transport buffer. Initial rates of uptake were determined from the slopes of linear portions of uptake time courses over 180-sec and 10-sec time periods for ARAC/D2 and CEM cells, respectively, that were similar to those shown in Figure IV-2. The rates of hCNT2- and hENT1- mediated transport are plotted as a function of the substrate concentrations tested (0-1000 μM). The transport rates mediated by hCNT2 were calculated from the difference in uptake measurements performed in sodium-containing and sodium-free transport buffers. The data were analyzed by nonlinear regression using Graphpad Prism software. The K_m and V_{max} values are the means ± SD of triplicate determinations.

Nucleoside	ARAC/D2			CEM		
	K _m ¹	V _{max} ²	V _{max} /K _m	K _m ¹	V _{max} ²	V _{max} /K _m
Uridine	46 ± 4	0.42 ± 0.05	0.009	192 ± 10	27 ± 11	0.14
5-Fluorouridine	43 ± 7	0.38 ± 0.07	0.009	217 ± 16	22 ± 9	0.10

¹ Expressed as μM

² Expressed as pmol/μl cell water/sec

Table IV-4. Effects of continuous exposures to cytotoxic nucleoside drugs and doxorubicin on proliferation rates of CEM, CEM-ARAC and ARAC/D2 cells

Cultures of actively proliferating ARAC/D2, CEM and CEM-ARAC cells at 1×10^5 cells/ml were exposed continuously to graded concentrations of various drugs for 48 hr as described in Figure IV-6. Cell concentrations in the presence and absence of drug were quantitated at 24, 36 and 48 hr by electronic particle counting. Growth rates in the presence of drug were calculated as the percentage of rates observed in the absence of drug and plotted as a function of the logarithmic concentration of drug. Antiproliferative activities were expressed as the concentration of drug (in μM) that inhibited cell proliferation by 50% (IC_{50}). Resistance factors (in brackets) for each drug were calculated by dividing IC_{50} values for CEM-ARAC and ARAC/D2 cells by IC_{50} values for CEM cells. The values reported are the means of duplicate experiments.

Drugs	IC_{50} for inhibition of cell proliferation		
	CEM (hENT1)	CEM-ARAC (NT-deficient)	ARAC/D2 (hCNT2)
cladribine	0.05 (1)	1.96 (39)	0.19 (3.8)
fludarabine	1.5 (1)	40 (26.7)	30 (20)
tubercidin	0.08 (1)	17.9 (224)	16.7 (209)
cytarabine	0.10 (1)	>100 (>1000)	>100 (>1000)
5-fluorouridine	0.06 (1)	>50 (>833)	0.05 (0.8)
5-fluoro-2'-deoxyuridine	0.11 (1)	22.7 (206)	0.25 (2.3)
5-fluoro-5'-deoxyuridine	0.98 (1)	>50 (>51)	47 (48)
doxorubicin	0.04 (1)	0.09 (2.3)	0.12 (3)

Table IV-5. K_i values for inhibition of uridine transport by hCNT1 in TLCT1 and hCNT2 in ARAC/D2 cells by analogs of uridine

The concentrations of test compounds that reduced uridine uptake rates by 50% (IC_{50} values) were determined from concentration-effect relationships as shown in Figure IV-8. These values were used to calculate K_i values according to the equation of Cheng and Prusoff [308] using the average K_m values for uridine transport in TLCT1 and ARAC/D2 cells from three independent experiments as shown in Figures IV-5 and IV-2.

Compounds	IC_{50} (μM)	K_i (μM)
<i>TLCT1</i>		
5-Fluorouridine	28	22
2'-Deoxyuridine	43	33
5-Fluoro-2'-deoxyuridine	34	26
5-Fluoro-5'-deoxyuridine	31	24
Capecitabine	>1000 ¹	ND ²
<i>ARAC/D2</i>		
5-Fluorouridine	41	34
2'-Deoxyuridine	47	39
5-Fluoro-2'-deoxyuridine	99	82
5-Fluoro-5'-deoxyuridine	500	411
Capecitabine	>1000 ¹	ND ²

¹No inhibition observed at 1000 μM

²Not determined since inhibition was not observed at highest concentration tested

Table IV-6. Inhibitory activities of adenine and adenosine analogs and nicotine on uridine transport by hCNT1 in TLCT1 and hCNT2 in ARAC/D2 cells

Transport of 10 μM ^3H -uridine into TLCT1 and ARAC/D2 cells was measured in sodium-containing transport buffer in the absence or presence of 1 mM test compound as described in section II.15. Initial rates of uptake were obtained from 180-sec uptake time courses. The results are the means \pm SD of triplicate determinations. The ratios of transport rates were determined by dividing rates in the presence of test compound by rates obtained in their absence.

Test compounds	TLCT1		ARAC/D2	
	Transport rates ¹	Ratio	Transport rates ¹	Ratio
<i>No additive</i>	0.290 \pm 0.004	1	0.105 \pm 0.002	1
Uridine	0.005 \pm 0.002	0.02	0.002 \pm 0.003	0.02
N ⁶ -(p-aminobenzyl)adenosine	0.004 \pm 0.003	0.01	0.003 \pm 0.001	0.03
Erythro-9-(2-hydroxy-3-nonyl)adenine	0.276 \pm 0.004	0.95	0.052 \pm 0.004	0.49
2'-3'-Dideoxyadenosine	0.281 \pm 0.003	0.97	0.092 \pm 0.003	0.88
Nicotine	0.002 \pm 0.006	0.01	0.025 \pm 0.002	0.24
Caffeine	0.003 \pm 0.005	0.01	0.003 \pm 0.001	0.03
Adenine	0.289 \pm 0.004	0.99	0.098 \pm 0.003	0.93
Adenosine	0.005 \pm 0.004	0.02	0.002 \pm 0.004	0.02
5'-Deoxyadenosine	0.037 \pm 0.002	0.13	0.023 \pm 0.003	0.22
2'-Deoxyadenosine	0.003 \pm 0.003	0.01	0.002 \pm 0.001	0.02
2-Chloroadenosine	0.032 \pm 0.004	0.11	0.016 \pm 0.004	0.15
8-Chloroadenosine	0.191 \pm 0.002	0.66	0.064 \pm 0.002	0.61

¹Uridine transport rates, mean \pm SD (pmol/ μl cell water/sec)

Table IV-7. K_i values for inhibition of uridine transport by hCNT1 in TLCT1 and hCNT2 in ARAC/D2 cells by analogs of adenine and adenosine

The concentrations of test compounds that reduced uridine uptake rates by 50% (IC_{50} values) were determined from concentration-effect relationships of Figures IV-10 and IV-12 or from similar experiments (not shown). The IC_{50} values were used to calculate K_i values according to the equation of Cheng and Prusoff [308] using the average K_m values for uridine transport in TLCT1 and ARAC/D2 cells from three independent experiments as shown in Figures IV-5 and IV-2.

Test compounds	TLCT1		ARAC/D2	
	IC_{50} (μ M)	K_i (μ M)	IC_{50} (μ M)	K_i (μ M)
N^6 -(p-Aminobenzyl)adenosine ¹	36	28	43	35
8-Chloroadenosine	>300	>232	>300	>246
5'-Deoxyadenosine ¹	88	68	288	237
L-Adenosine	>250	>193	>300	>246
Adenosine	49	39	30	25
2'-Deoxyadenosine	57	44	35	29
2-Chloroadenosine	131	101	45	37
Nicotine ²	81	63	276	227
Caffeine ²	59	46	125	103
2'-3'-Dideoxyadenosine	>500 ³	ND ⁴	>500 ³	ND ⁴

¹From Figure IV-10

²From Figure IV-12

³No inhibition observed at 500 μ M

⁴Not determined since inhibition was not observed at the highest concentration tested

Table IV-8. Comparison of the levels of nucleoside and drug transport by hCNT1 and hCNT2 in TLCT1 and ARAC/D2 cells

Uptake of 10 μM ^3H -compound into TLCT1 and ARAC/D2 cells was measured as described in Materials and Methods (section II.15) and initial rates of uptake were determined from linear regression analysis of 3-min time courses of uptake in sodium-containing or sodium-free transport buffer. Net transport rates (i.e., sodium-dependent transport) were determined by subtracting uptake rates in the absence of sodium from uptake rates in the presence of sodium and are expressed as the mean \pm SD of triplicate determinations.

Nucleosides	Transport rates					
	Sodium	TLCT1 No sodium	Net	Sodium	ARAC/D2 No sodium	Net
2'-Deoxyuridine	0.275 \pm 0.008	0.004 \pm 0.001	0.271	0.100 \pm 0.001	0.001 \pm 0.002	0.099
Uridine	0.297 \pm 0.009	0.003 \pm 0.002	0.293	0.108 \pm 0.002	0.003 \pm 0.002	0.105
Thymidine	0.072 \pm 0.002	0.005 \pm 0.002	0.067	0.005 \pm 0.003	0.004 \pm 0.001	0
Guanosine	0.006 \pm 0.005	0.008 \pm 0.002	0	0.237 \pm 0.008	0.010 \pm 0.003	0.227
2'-Deoxyguanosine	0.007 \pm 0.004	0.007 \pm 0.002	0	0.214 \pm 0.008	0.008 \pm 0.005	0.206
Adenosine	0.047 \pm 0.001	0.007 \pm 0.004	0.040	0.256 \pm 0.009	0.008 \pm 0.003	0.248
2'-Deoxyadenosine	0.028 \pm 0.003	0.007 \pm 0.005	0.021	0.197 \pm 0.006	0.011 \pm 0.003	0.186
Drugs						
5-Fluoruridine	0.271 \pm 0.012	0.004 \pm 0.002	0.267	0.119 \pm 0.013	0.008 \pm 0.003	0.111
Cladribine	0.011 \pm 0.006	0.010 \pm 0.008	0.001	0.0310 \pm 0.003	0.008 \pm 0.006	0.023
Fludarabine	0.014 \pm 0.012	0.015 \pm 0.009	0	0.0210 \pm 0.004	0.011 \pm 0.004	0.010
Caffeine	0.003 \pm 0.001	0.005 \pm 0.003	0	0.006 \pm 0.004	0.005 \pm 0.003	0.001
Nicotine	0.015 \pm 0.008	0.018 \pm 0.014	0	0.013 \pm 0.010	0.012 \pm 0.008	0.001

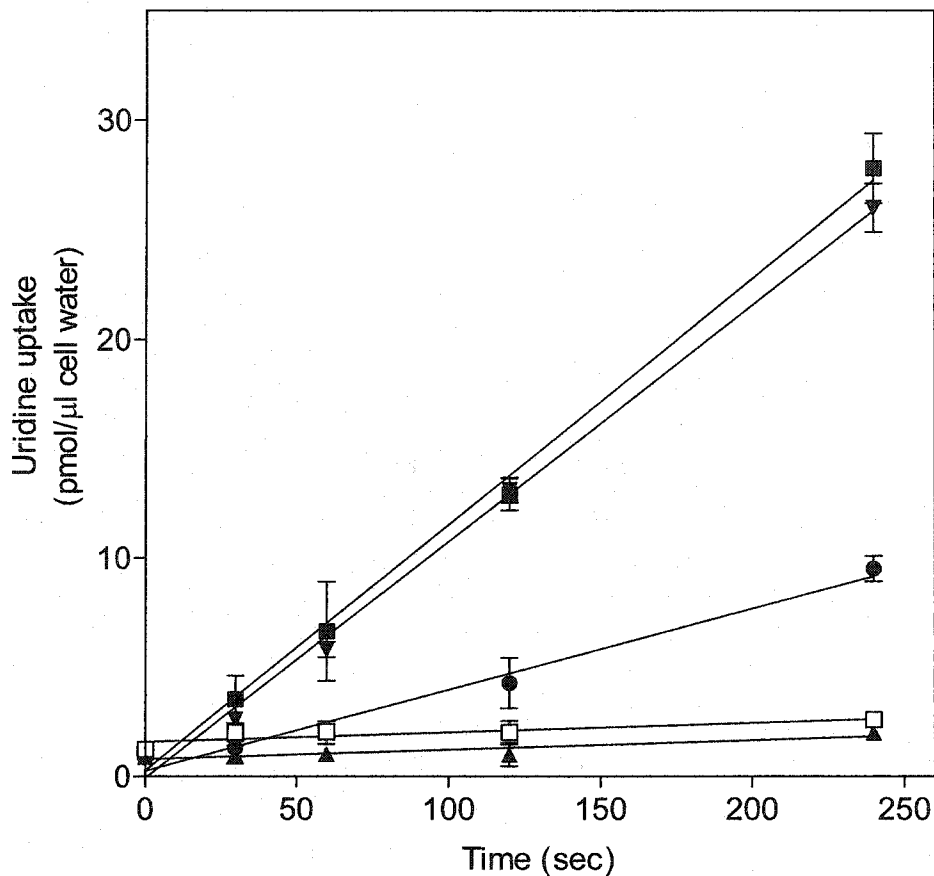


Figure IV-1. Effects of nucleoside analogs on uridine uptake by hCNT2 in ARAC/D2 cells

Uptake of $10 \mu\text{M}$ ^3H -uridine over 240-sec time periods into ARAC/D2 cells was determined as described in section II.15 in sodium-containing (closed symbols) or sodium-free (open symbols) transport buffer in the absence (■, □) or presence of $1000 \mu\text{M}$ test compound (2'-deoxyuridine (▲), 3'-deoxyuridine (▼) or 5-methyluridine (●)). Each value represents the mean \pm SD of three determinations and error bars are not shown where SD values were smaller than that represented by the symbols.

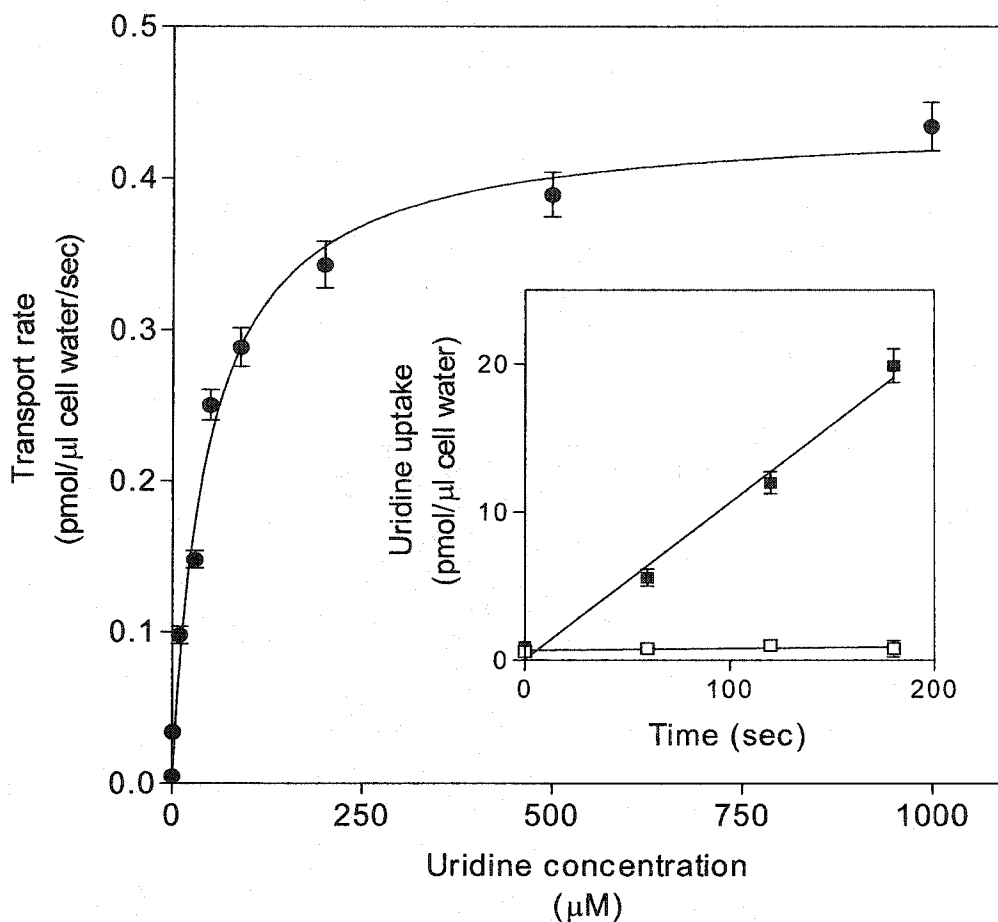


Figure IV-2. Kinetic analysis of uridine transport mediated by hCNT2 in ARAC/D2 cells

Transport assays with ARAC/D2 cells were performed with graded concentrations of ^3H -uridine in sodium-containing (■) and sodium-free (□) transport buffer as described in section II.15. *Inset*, a representative uptake time course with $10\ \mu\text{M}$ ^3H -uridine is shown. Initial rates of uptake were determined from the slopes of linear portions of uptake time courses over 180-sec time periods similar to those shown in the inset. The sodium-dependent ^3H -uridine transport rates, calculated from the difference in uptake measurements performed in sodium-containing and sodium-free transport buffers, are plotted as a function of the uridine concentrations tested (0-1000 μM). Results are the means \pm SD of triplicate determinations and error bars are not shown where SD values were smaller than the size of the data symbols. The data were analyzed by nonlinear regression using Graphpad Prism software. Shown is one of three independent experiments that yielded similar results. Kinetic constants were $K_m = 46 \pm 4\ \mu\text{M}$ and $V_{\text{max}} = 0.42 \pm 0.05\ \text{pmol}/\mu\text{l cell water}/\text{sec}$.

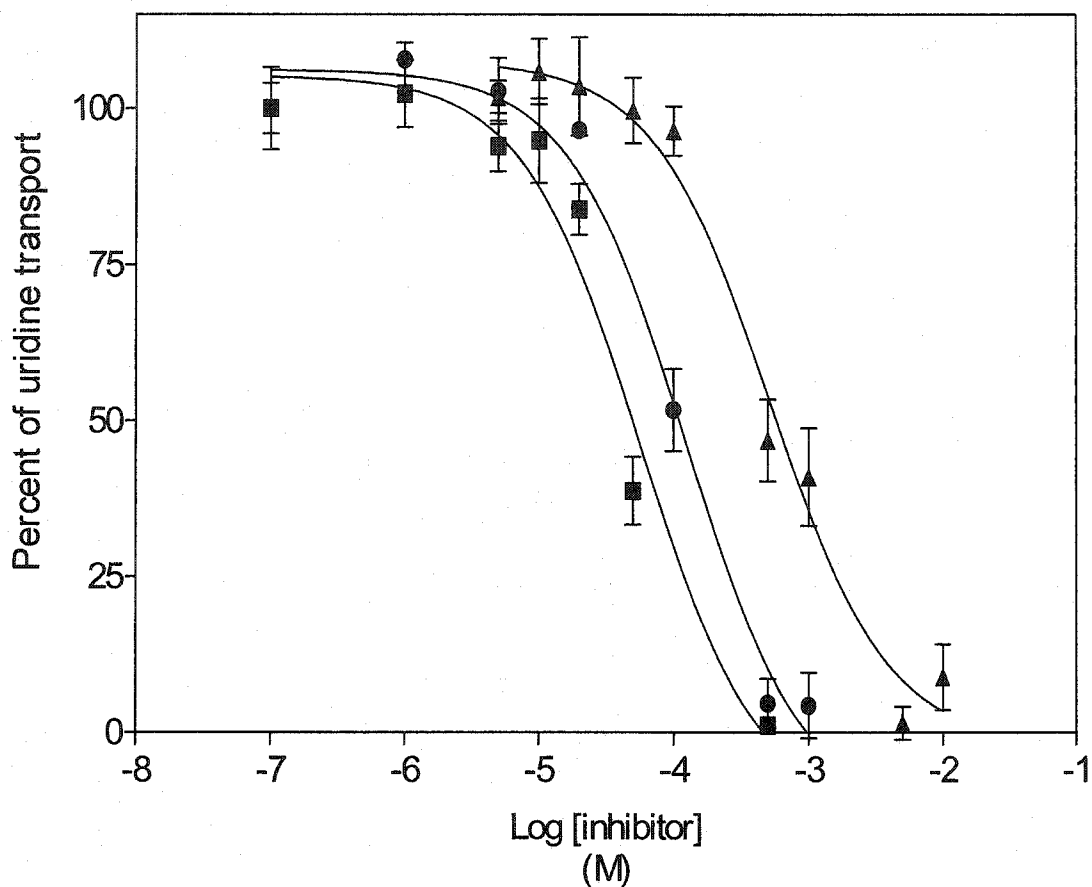


Figure IV-3. The concentration dependence of hCNT2-mediated uridine transport into ARAC/D2 cells by fluorinated uridine analogs

^3H -Uridine uptake was measured in sodium-containing transport buffer alone or with graded concentrations of either 5-fluorouridine (■, 0.1-500 μM), 5-fluoro-2'-deoxyuridine (●, 0.1-1000 μM) or 5-fluoro-5'-deoxyuridine (▲, 5 μM -10 mM) as described in Figure IV-1. Sodium-dependent transport rates were calculated by subtracting uptake measurements performed in sodium-free transport buffer from uptake measurements performed in sodium-containing transport buffer. The data are presented as the fraction of sodium-dependent uridine transport remaining in the presence of test compound as a function of the logarithm of the concentration of test compound, and are the means \pm SD data obtained from triplicate determinations. Results were analyzed by non-linear regression using GraphPad Prism[®] analysis software. The IC_{50} values (concentration of inhibitor that reduced uridine uptake by 50%) for 5-fluorouridine, 5-fluoro-2'-deoxyuridine and 5-fluoro-5'-deoxyuridine inhibition of uridine transport were 41, 99 and 500 μM respectively.

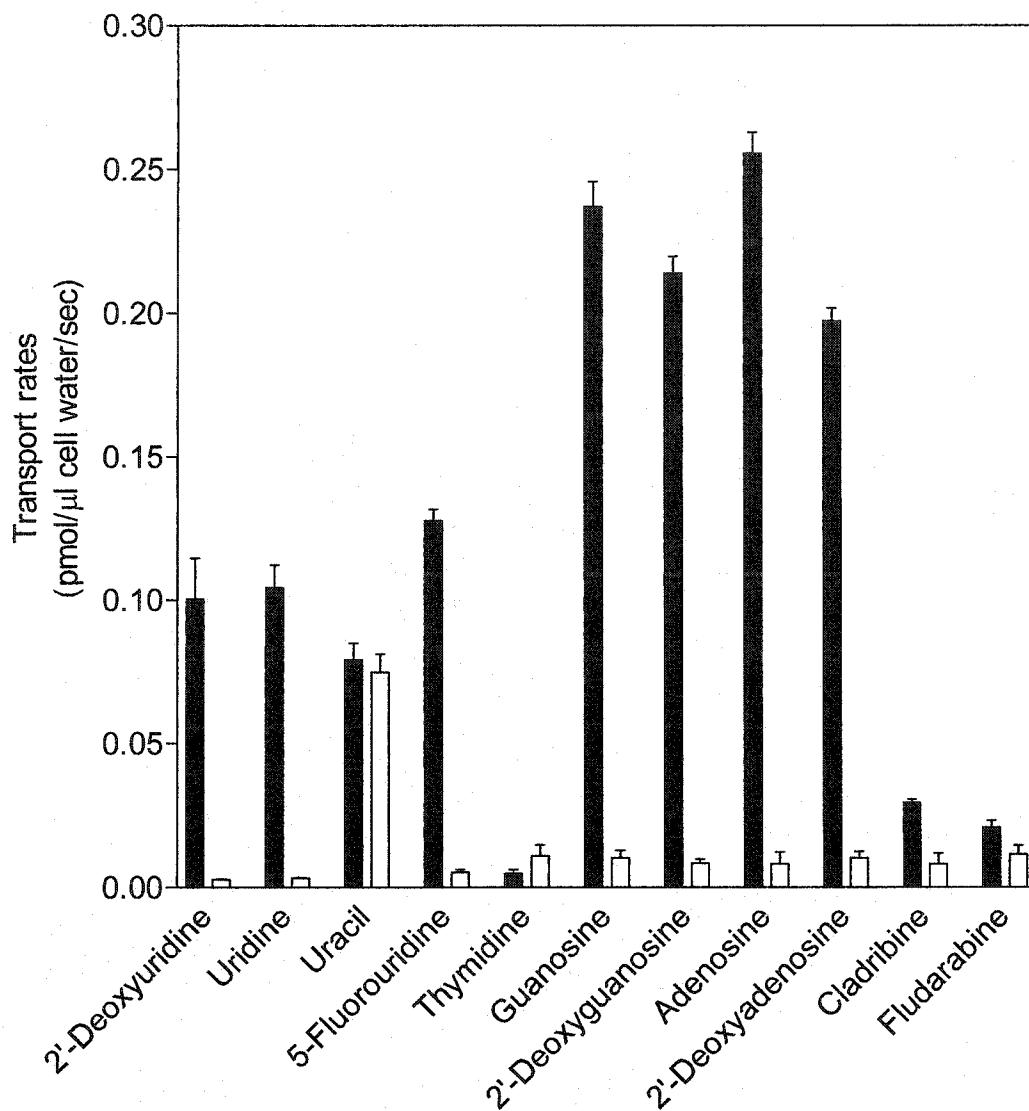
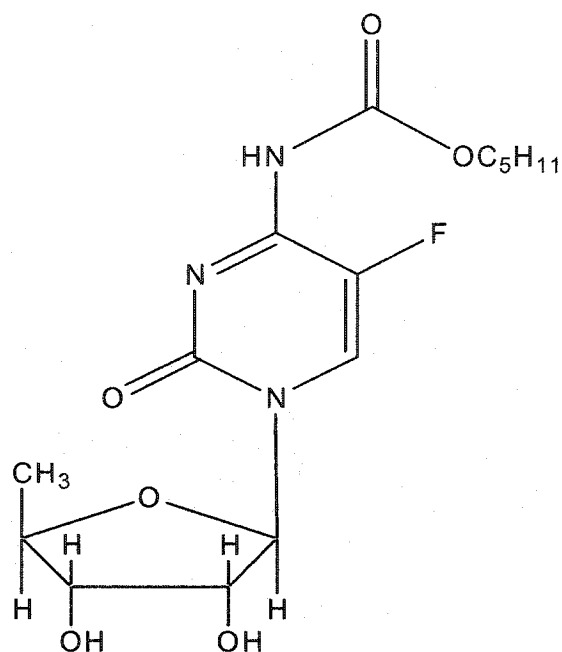
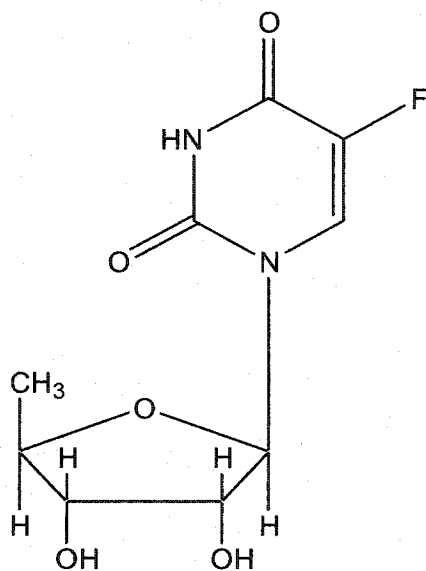


Figure IV-4. Transport of purine and pyrimidine nucleosides by hCNT2 in ARAC/D2 cells

Uptake of $10 \mu\text{M}$ ^3H -nucleoside into ARAC/D2 cells was performed as described in Materials and Methods (section II.15) and initial rates were determined from the linear portions of time courses of isotopic fluxes in sodium-containing (filled bar) or sodium-free (open bar) transport buffer. Each bar represents the mean \pm SD of three determinations and error bars are not shown where SD values were smaller than those represented by the symbols. Test compounds were: fludarabine (9- β -D-arabinofuranosyl-2-fluoroadenine), cladribine (2-chloro-2'-deoxyadenosine), 2'-deoxyadenosine, adenosine, 2'-deoxyguanosine, guanosine, thymidine, 5-fluorouridine, uracil, uridine and 2'-deoxyuridine.



Capecitabine



5-Fluoro-5'-deoxyuridine

Figure IV-5. Chemical structures of capecitabine and 5-fluoro-5'-deoxyuridine

Depicted are the chemical structures of the prodrug capecitabine and its active metabolite 5-fluoro-5'-deoxyuridine.

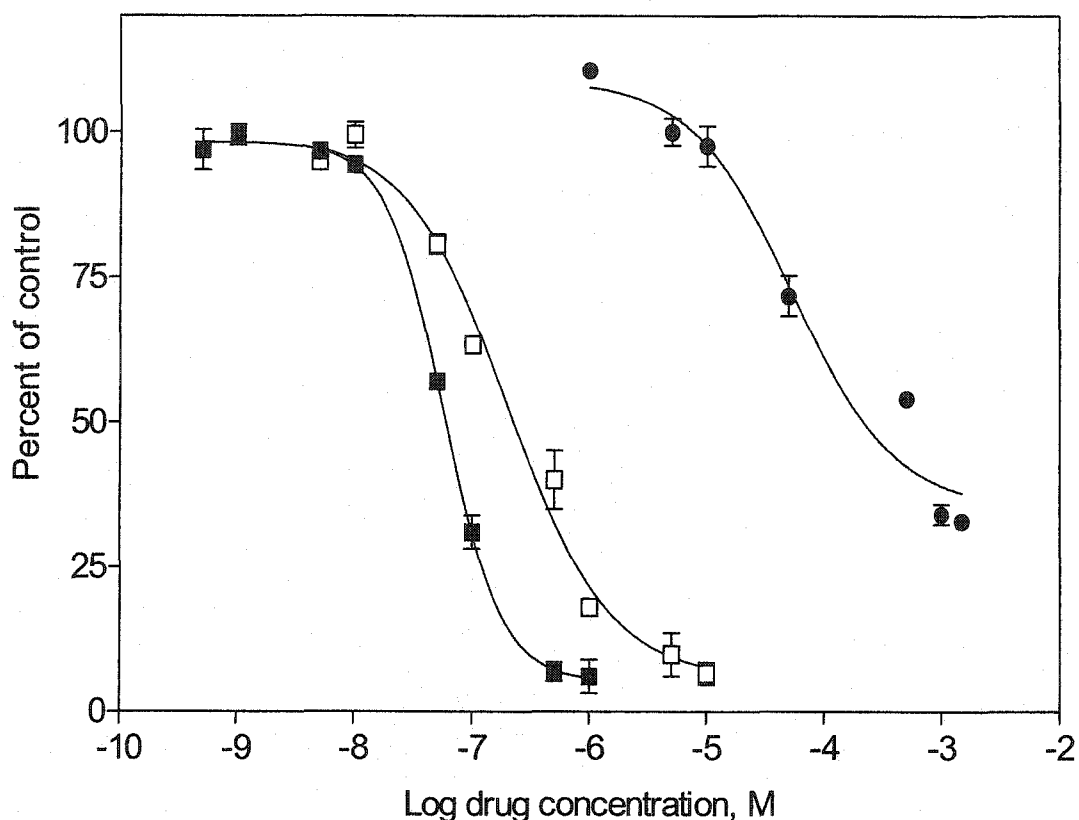


Figure IV-6. Antiproliferative activities of 5-fluorouridine, 5-fluoro-2'-deoxyuridine and 5-fluoro-5'-deoxyuridine on ARAC/D2 cells

Cultures of actively proliferating ARAC/D2 cells at 1×10^5 cells/ml were incubated (in triplicate) in growth medium containing graded concentrations of 5-fluorouridine (0-1 μ M, ■), 5-fluoro-2'-deoxyuridine (0-10 μ M, □) or 5-fluoro-5'-deoxyuridine (0-500 μ M, ●) for 48 hr. The number of cells in the presence and absence of drug was determined at 24, 36 and 48 hr by electronic particle counting as described in section II.10. Growth rates in the presence of drug were calculated as the percentage of rates observed in the absence of drug and plotted as a function of the logarithmic concentration of drug. Results were analyzed by non-linear regression using GraphPad Prism[®] analysis software. Values are means \pm SD of triplicate determinations and error bars are not shown where SD values were smaller than the size of data symbols.

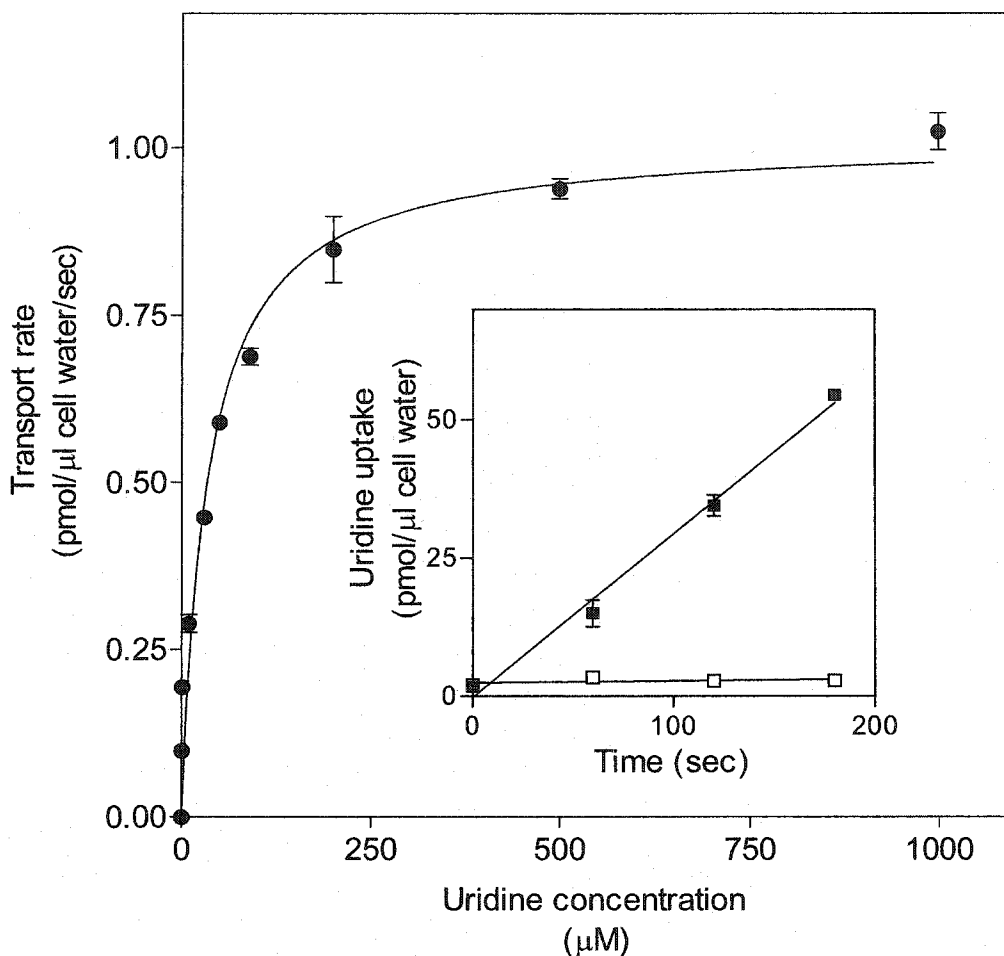


Figure IV-7. Kinetic analysis of uridine transport mediated by hCNT1 in TLCT1 cells

Transport assays with TLCT1 cells were performed with graded concentrations of ^3H -uridine in sodium-containing (■) and sodium-free (□) transport buffer as described in section II.15. *Inset*, a representative uptake time course with $10\ \mu\text{M}$ ^3H -uridine is shown. Initial rates of uptake were determined from the slopes of linear portions of uptake time courses over 180-sec time periods similar to those shown in the inset. The sodium-dependent ^3H -uridine transport rates, calculated from uptake measurements performed in sodium-containing and sodium-free transport buffers, are plotted as a function of the uridine concentrations tested (0-1000 μM). Results are the means \pm SD of triplicate determinations and error bars are not shown where SD values were smaller than the size of the data symbols. The data were analyzed by nonlinear regression using Graphpad Prism software. The calculated kinetic parameters K_m and V_{max} were $34 \pm 2\ \mu\text{M}$ and $1.01 \pm 0.17\ \text{pmol}/\mu\text{l cell water}/\text{sec}$ respectively. Shown is one of three independent experiments that yielded similar results.

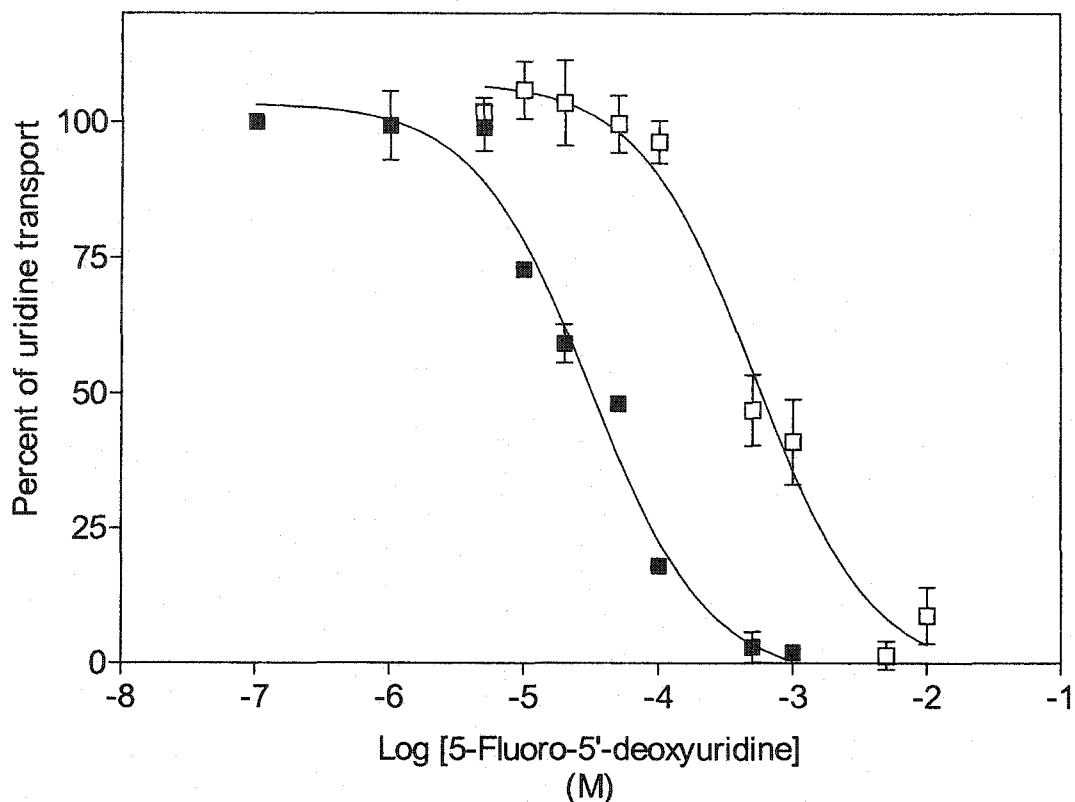


Figure IV-8. Concentration dependent inhibition of uridine transport by 5-fluoro-5'-deoxyuridine in hCNT1- and hCNT2-producing stable transfectants

³H-Uridine uptake was measured as described in section II.15 in sodium-containing transport buffer alone or with graded concentrations of 5-fluoro-5'-deoxyuridine (0-10 mM) in TLCT1 (hCNT1-containing) (■) and ARAC/D2 (hCNT2-containing) (□) cells. Sodium-dependent transport rates were calculated by subtracting uptake measurements performed in sodium-free transport buffer from uptake measurements performed in sodium-containing transport buffer. The data are presented as the percentage of sodium-dependent uridine transport remaining in the presence of 5-fluoro-5'-deoxyuridine as a function of the logarithm of the concentration of 5-fluoro-5'-deoxyuridine, and are the means \pm SD data obtained from triplicate determinations. Results were analyzed by non-linear regression using GraphPad Prism[®] analysis software. The IC₅₀ values (concentration of inhibitor that reduces uridine uptake by 50%) for 5-fluoro-5'-deoxyuridine inhibition of uridine transport in TLCT1 and ARAC/D2 cells, respectively, were 31 and 500 μ M.

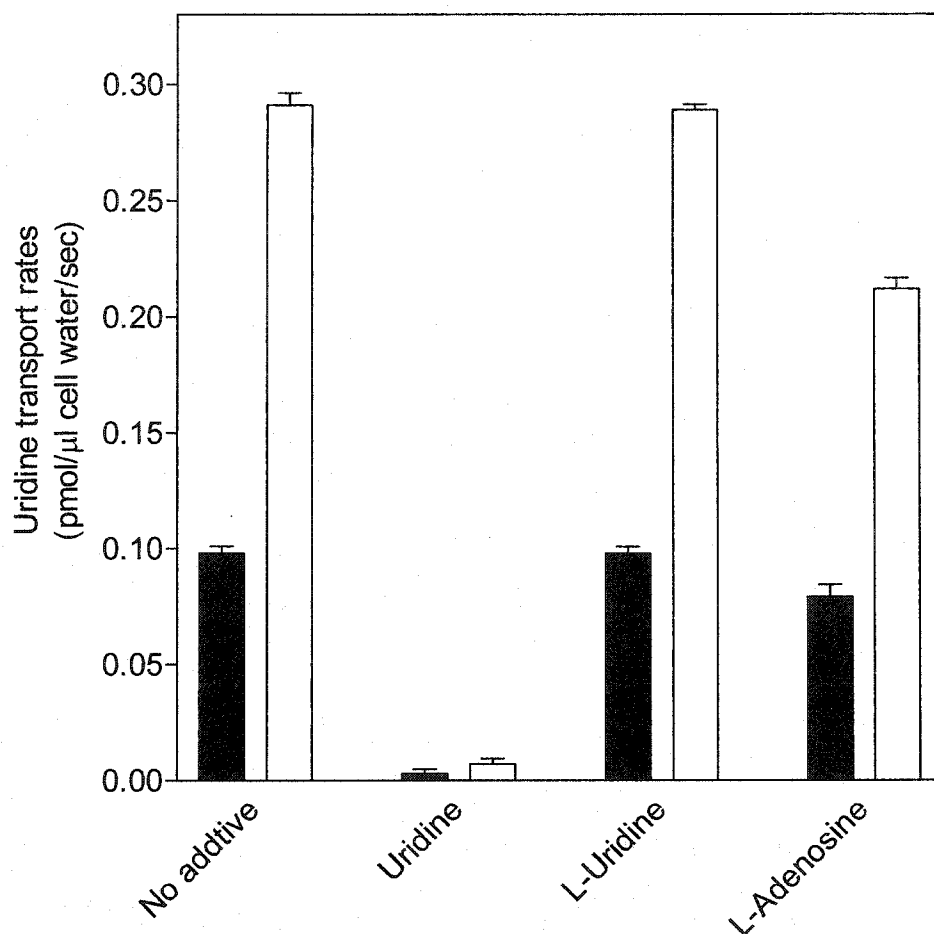


Figure IV-9. Effects of L-uridine and L-adenosine on uridine influx into hCNT1-containing TLCT1 and hCNT2-containing ARAC/D2 cells

Transport of 10 μM ^3H -uridine into TLCT1 (open bars) and ARAC/D2 (filled bars) cells was measured in sodium-containing transport buffer in the absence or presence of 1 mM uridine, L-uridine or L-adenosine as described in section II.15. Initial rates of uptake were obtained from 180-sec time courses similar to those shown in Figure IV-1. Each value represents the mean \pm SD of three determinations.

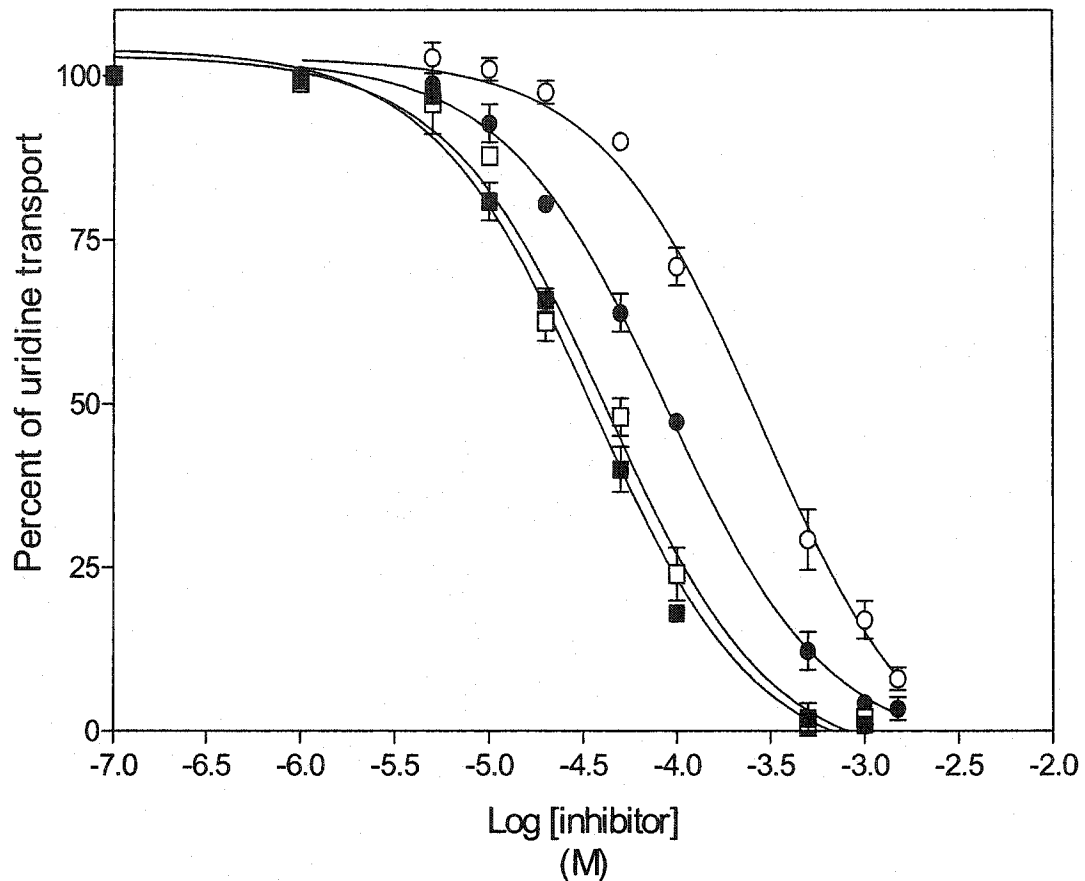
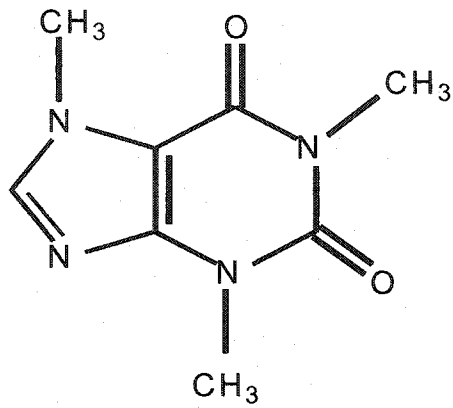
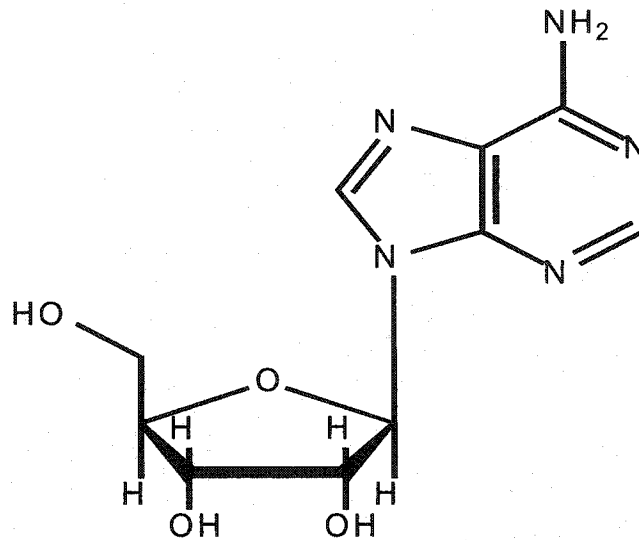


Figure IV-10. Inhibition of uridine transport by N⁶-(p-aminobenzyl)adenosine and 5'-deoxyadenosine in hCNT1-containing TLCT1 and hCNT2-containing ARAC/D2 cells

Initial rates of ³H-uridine uptake were measured as described in section II.15 in sodium-containing transport buffer alone or with graded concentrations of either N⁶-(p-aminobenzyl)adenosine (■, □; 0.1 μM–1 mM) or 5'-deoxyadenosine (●, ○; 0.1 μM–1.5 mM) in TLCT1 (■, ●) or ARAC/D2 (□, ○) cells. Sodium-dependent transport rates were calculated from the difference in uptake measurements performed in sodium-containing and sodium-free transport buffers. The data are presented as the percentage of sodium-dependent uridine transport remaining in the presence of test compound as a function of the logarithm of the concentration of test compound, and are the means ± SD of triplicate determinations. Results were analyzed by non-linear regression using GraphPad Prism[®] analysis software. The IC₅₀ values for N⁶-(p-aminobenzyl)adenosine and 5'-deoxyadenosine inhibition of uridine transport into TLCT1 cells were 36 and 88 μM, respectively. The IC₅₀ values for N⁶-(p-aminobenzyl)adenosine and 5'-deoxyadenosine inhibition of uridine transport into ARAC/D2 cells were 43 and 287 μM, respectively.



Caffeine



Adenosine

Figure IV-11. Structural similarities between caffeine and adenosine
Depicted is the chemical structure of adenosine and its analog caffeine.

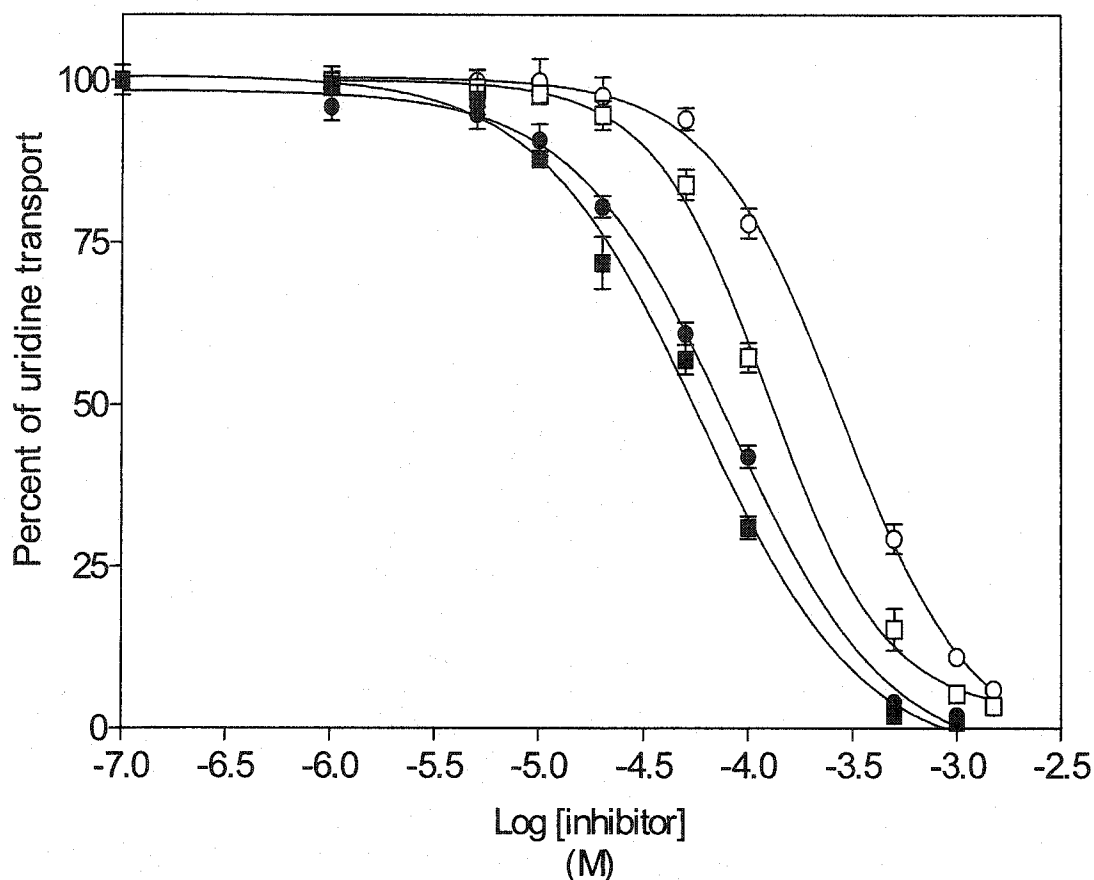


Figure IV-12. Inhibition of uridine transport by caffeine and nicotine in hCNT1-containing TLCT1 and hCNT2-containing ARAC/D2 cells

Initial rates ^3H -uridine uptake were measured as described in section II.15 in sodium-containing transport buffer alone or with graded concentrations of either caffeine (■, □; 0.1 μM –1 mM) or nicotine (●, ○; 0.1 μM –1.5 mM) in TLCT1 (■, ●) or ARAC/D2 (□, ○) cells. Sodium-dependent transport rates were calculated from the difference in uptake measurements performed in sodium-containing and sodium-free transport buffers. The data are presented as the percentage of sodium-dependent uridine transport remaining in the presence of test compound as a function of the logarithm of the concentration of test compound, and are the means \pm SD of triplicate determinations. Results were analyzed by non-linear regression using GraphPad Prism[®] analysis software. The IC_{50} values for caffeine and nicotine inhibition of uridine transport into TLCT1 cells were 59 and 82 μM , respectively. The IC_{50} values for caffeine and nicotine inhibition of uridine transport into ARAC/D2 cells were 125 and 276 μM , respectively.

Chapter V

V. Production and Characterization of Antibodies Against hCNT2 and hCNT3

V.1. Introduction

When this work was initiated, antibodies against human concentrative nucleoside transporters were not available. Polyclonal antibodies against rCNT1 and SPNT (rCNT2) from rats have been raised against oligopeptides corresponding to residues 45-67 and 30-53, respectively, of rCNT1 and rCNT2 [329]. These anti-rCNT1 and anti-rCNT2 polyclonal antibodies have been shown to recognize immunoreactive bands with apparent molecular masses of 74 kDa and 103 kDa, corresponding, respectively, to rCNT1 and rCNT2, in immunoblot analysis of preparations from rat liver parenchymal cells and kidney [329]. Polyclonal antibodies against rCNT1 have also been reported [141].

The detection of rCNT1 in the apical membranes of polarized epithelial cells of jejunum and renal tubules was demonstrated by immunofluorescence analysis using anti-rCNT1 polyclonal antibodies raised against amino acid residues 505-524 of rCNT1 [141]. The region used as the antigen for generating anti-rCNT1 polyclonal antibodies shared high (85%) amino acid sequence identities with sequences of hCNT1, and these antibodies also recognized hCNT1 in immunoblots of membranes of *Xenopus* oocytes producing hCNT1 proteins [141].

After the cloning of hCNT1 cDNA [133], initial efforts focused on generating antibodies that specifically recognized hCNT1. Synthetic peptides corresponding to residues 503-512 near the predicted carboxy-terminal tail of hCNT1 were used as antigen for raising polyclonal antibodies against hCNT1. These antibodies did not recognize recombinant hCNT1 in membrane

preparations of HeLa cells transiently transfected with hCNT1 cDNA (J. Marjan, T. Lang and C. Cass, Unpublished results). Polyclonal antibodies directed against an epitope corresponding to amino acid residues 390-399 of hCNT1 were also generated (J. Marjan, T. Lang and C. Cass, Unpublished results). Flow cytometry using these polyclonal antibodies together with secondary antibodies conjugated to fluorescein isothiocyanate showed that cells transiently transfected with hCNT1 cDNA exhibited a higher percentage of positive fluorescent staining of hCNT1-transfected cells compared to mock transfected cells (J. Marjan, M. Selner and C. Cass, Unpublished results). However, the anti-hCNT1 antibodies did not recognize recombinant hCNT1 in immunoblot analysis of membrane preparations of hCNT1-producing HeLa cells (K. Graham, T. Lang, P. Carpenter and C. Cass, Unpublished results). Other epitopes against various regions near the amino terminus and large loop domains between transmembrane segments have been selected for raising anti-hCNT1 antibodies, but have not yielded useful antibodies (K. Graham, T. Lang, P. Carpenter and C. Cass, Unpublished results).

This chapter describes the production of polyclonal and monoclonal antibodies specifically against hCNT2 and hCNT3. Algorithms for prediction of transmembrane segments, secondary structures and hydrophilic regions of CNT proteins were used to design potential immunogenic epitopes for raising peptide antibodies. The reactivities and specificities of the generated antibodies were characterized by ELISA (enzyme-linked immunosorbent assay), immunoblot and immunofluorescence analysis.

The results demonstrated that polyclonal and monoclonal antibodies against either hCNT2 and hCNT3 recognized the corresponding recombinant CNT proteins produced in either yeast or human cells in immunoblot and immunofluorescence analysis. The availability of these antibodies allowed for the first time detection and visualization of hCNT2 and hCNT3 proteins. In addition, these antibodies enabled the examination of native CNT proteins as described in subsequent chapters.

V.2. Results

V.2.1. *Generation of anti-hCNT2 antibodies*

The aim of the work in this section was to raise polyclonal and monoclonal antibodies against hCNT2 that would be useful in detection of denatured and non-denatured proteins by various immunological techniques such as immunoblotting and immunofluorescence. Anti-peptide antibodies have been successfully raised against rCNT1 [141]. Earlier studies suggested that synthetic peptides containing hydrophilic amino acids and proline residues exhibited high probability of being exposed on the surface of the native protein [330, 331].

V.2.1.1. *Choosing appropriate peptide sequences of hCNT2 for raising anti-peptide antibodies*

The amino acid sequences of hCNT2, deduced from the nucleotide sequences (GenBank accession number, AF036109), were analyzed for hydrophilic and charged regions of at least seven residues that would constitute potential immunogenic epitopes. The results of Figure V-1, which is the hydrophilicity plot of the hCNT2 protein sequence, showed several hydrophilic regions near the amino terminus and a few near the carboxyl terminus or the interior of the protein. Examination of the amino acid sequences near the amino terminus (residues 10-60) of hCNT2 revealed a stretch of 22 hydrophilic and charged amino acid sequences.

The hydrophobicity index of each amino acid in the chosen 22 amino acid residues (named TL3273) were determined and plotted as a function of the

residue number as shown in Figure V-2. A positive value would indicate that free energy is required for transfer to water (i.e., the polypeptide is hydrophobic) [331]. The results showed that all of the amino acids in the chosen peptide sequence were below 0 kcal/mol, indicating that they were hydrophilic.

The chosen 22 amino acid peptide sequence (KEVEPEGSKRTDAQGHSLGDGL) corresponded to residues 29-50 of hCNT2, which is located in the large intracellular stretch of amino acids near the amino terminus of the protein as shown in the putative topology model prediction of Figure V-3.

Multiple alignments of amino acid sequences of the chosen peptide sequence TL3273 with other sequences of CNT proteins from human, rabbit and rat were determined as shown in Figure V-4. The alignment results showed no amino acid identity between chosen TL3273 sequences and human CNT1 and CNT3 sequences. However, there was a 32% and 41% amino acid identity between the TL3273 and the corresponding rabbit and rat CNT2 sequences, respectively.

V.2.1.2. Characterization of anti-hCNT2 antibodies

The chosen TL3273 polypeptide was synthesized and conjugated to either keyhole limpet hemacyanin (KLH) or bovine serum albumin (BSA) by the Alberta Peptide Institute (API, University of Alberta, AB, Canada). Rabbits and mice were injected with TL3273-KLH peptide conjugate as described in Materials and Methods (sections II.18 and II.20)

V.2.1.3. Assessment of anti-hCNT2 peptide antibody production by ELISA

The immune response of rabbits and mice to the TL3273-KLH peptide conjugate was monitored by ELISA using TL3273-BSA coated plates as shown, respectively, in the experiments of Figures V-5 and V-6. The results revealed that pre-immune sera from either rabbits or mice exhibited negligible absorbance at 650 nm. In the experiment of Figure V-5, the immune sera of test bleeds from the two rabbits (named 783 and 812) showed a progressive increase in absorbance after successive test bleeds, reaching a maximum at test bleed 3. Test bleed 4 from both rabbits did not result in any substantial increase in absorbance reading. Similarly, the immune sera of test bleeds from mice showed a large increase in absorbance between test bleeds 1 and 2. No significant increase in absorbance was apparent after the second test bleed from mice 4.1, 4.3 and 2.3. Mice 4.2, 2.1 and 2.2 reached maximum absorbance readings after the third test bleed.

V.2.1.4. Demonstration of specificity of anti-hCNT2 peptide antibodies by immunoblot analysis

The rabbit antisera and hybridoma supernatants were immunoaffinity enriched as described in Materials and Methods (sections II.21 and II.22) and the resulting enriched polyclonal and monoclonal antibody preparations (hereafter referred to as polyclonal and monoclonal antibodies) were assessed for reactivity against denatured hCNT2 proteins by immunoblot analysis. Membrane preparations were prepared from yeast and cultured cells either containing or lacking hCNT2, and probed with anti-hCNT2 antibodies as shown

in the experiment of Figure V-7. The immunoblot of Panel A revealed immunoreactive species in membrane preparations of yeast and ARAC/D2 cells producing hCNT2 when probed with anti-hCNT2 polyclonal antibodies. However, no bands were evident in membrane preparations of yeast or CEM-ARAC cells lacking hCNT2.

The specificity of the anti-hCNT2 monoclonal antibodies was examined in Panel B of Figure V-7. A unique immunoreactive band was detected with the anti-hCNT2 monoclonal antibodies in membrane preparations of yeast containing hCNT2 whereas no bands were observed in yeast that lacked hCNT2.

The electrophoretic mobility of the hCNT2 immunoreactive species produced by pYES2/hCNT2myc transformed yeast was examined further in Panel C of Figure V-7. The results showed that the anti-myc antibodies detected an immunoreactive band in membrane preparations of pYES2/hCNT2myc transformed yeast that migrated with similar mobilities to hCNT2 immunoreactive bands observed in Panels A and B.

The specificities of the anti-hCNT2 antibodies were addressed further in cultured HeLa cells that produced recombinant hCNT2 by transient transfection of hCNT2 cDNA (Figure V-8). Following the transfection of pcDNA3/hCNT2 into HeLa cells, the production of hCNT2 protein was assessed by immunoblot analysis using the polyclonal antibodies against hCNT2 (Lane B), and the results were compared with those obtained with cells transfected with pcDNA3 (Lane A). The immunoblot results of Figure V-8 showed a unique band with an apparent molecular mass between 70 and 75 kDa in HeLa cells transfected with

pcDNA3/hCNT2, which was consistent with the calculated molecular mass of hCNT2 protein deduced from the amino acid sequence. No unique band of the predicted size for hCNT2 was detected in cells transfected with pcDNA3.

V.2.1.5. Demonstration of anti-hCNT2 antibody reactivity with hCNT2 in ARAC/D2 cells by immunofluorescence

To ascertain whether the anti-hCNT2 antibodies recognized non-denatured hCNT2 in cell staining protocols, indirect immunofluorescence analyses of hCNT2-containing ARAC/D2 cells and transport-deficient CEM-ARAC cells (both described in Chapter III) were undertaken. ARAC/D2 and CEM-ARAC cells, which were grown on poly-L-lysine coated coverslips, were stained with either anti-hCNT2 polyclonal or monoclonal antibodies, and images were collected by LSM-510 confocal microscopy as shown in Figure V-9. The anti-hCNT2 polyclonal antibodies labeled primarily cell membranes of ARAC/D2 cells (Panel A) whereas little or no fluorescent signal was detected in CEM-ARAC cells (Panel C) that lacked production of hCNT2. Similarly, the anti-hCNT2 monoclonal antibodies labeled mainly cell membranes of ARAC/D2 cells (Panel B) and did not produce any detectable fluorescent signal in CEM-ARAC cells (Panel D). These experiments demonstrated that the anti-hCNT2 monoclonal antibodies, like the anti-hCNT2 polyclonal antibodies, could be employed to detect hCNT2 by immunofluorescence.

As a control, immunofluorescence experiments were performed in which ARAC/D2 cells were stained with pre-immune sera from the same rabbit that was used to generate anti-hCNT2 polyclonal antibodies. The

immunofluorescence experiment of Figure V-10 showed no detectable fluorescent signal in ARAC-D2 cells that were stained with pre-immune sera, whereas the expected plasma membrane staining of ARAC/D2 cells resembling that of Figure V-9 was apparent when stained with anti-hCNT2 polyclonal antibodies. Collectively, the results demonstrated the specificity and utility of the anti-hCNT2 antibodies in immunofluorescence.

V.2.2. Generation of anti-hCNT3 antibodies

A similar methodology to that described in section VB.1 for production of anti-hCNT2 antibodies was employed to raise peptide antibodies against hCNT3. Identification of amino acid sequences of hCNT3 that had high probability of being immunogenic was undertaken as described below.

V.2.2.1. Choosing appropriate peptide sequence of hCNT3 for raising anti-peptide antibodies

The hydropathy plot of the hCNT3 protein sequences deduced from the nucleotide sequence of the open reading frame (GenBank accession number, AF305210) using algorithms by Kyte and Doolittle [331] revealed a large hydrophilic stretch of amino acid sequence near the amino terminus and several hydrophilic regions in the interior of the protein. Analysis of the hydrophobicity values of a stretch of 25 amino acids near the amino terminus (Figure V-11) showed that all of the amino acids in that region exhibited values below 0 kcal/mol. This potential immunogenic epitope (named TL3360) corresponds to residues 45-69, which is located in a large region close to the amino terminus

that is predicted to be intracellular, as shown in the putative hCNT3 topology model of Figure V-12. Amino acid sequence alignment of the polypeptide TL3360 sequence (REHTNTKQDEEQVTVEQDSPRNREH) with other sequences of CNT proteins is shown in Figure V-13. The results showed 4% amino acid identity between polypeptide TL3360 and corresponding regions of other hCNT proteins.

Hydropathy analysis of the 23-amino acid sequence named TL3361 as shown in Figure V-14 revealed that the majority of the amino acids had values below 0 kcal/mol. This second potential immunogenic epitope was located in the predicted extracellular loop domain between transmembrane segments 11 and 12 of the putative hCNT3 topology model of Figure V-12. Amino acid sequence alignment of polypeptide TL3361 sequences (HLRKEGGPKFVNGVQQYISIRSE) with other sequences of hCNT proteins are shown in Figure V-15. The results revealed a 30% amino acid identity between TL3361 and corresponding regions of other hCNT sequences.

V.2.2.2. Characterization of anti-hCNT3 antibodies

The chosen TL3360 and TL3361 sequences of hCNT3 were synthesized, conjugated and injected into rabbits and mice as described in section II.20. The immune response of rabbits and mice to the TL3360-KLH and TL3361-KLH peptide conjugates were monitored by ELISA as described earlier in section VB.1.2.1. Two mice demonstrated relatively poor immune response against the injected peptide-conjugates as shown by ELISA. Furthermore, their antisera did not recognize any bands corresponding to hCNT3 in immunoblots of membranes

from cells producing recombinant hCNT3. These mice were subsequently terminated. All other mice and rabbits were kept for either (i) hybridoma production to generate anti-hCNT3 monoclonal antibodies or (ii) generation of anti-hCNT3 polyclonal antibodies, respectively.

V.2.2.3. Demonstration of specificity of anti-hCNT3 antibodies by immunoblot analysis

The rabbit antisera and hybridoma supernatants were immunoaffinity purified as described in Materials and Methods (section II.22.) and the resulting purified polyclonal and monoclonal antibody preparations (hereafter referred to as polyclonal and monoclonal antibodies) against hCNT3 were used in subsequent immunological experiments. To assess the specificity of the anti-hCNT3 antibodies, yeast transformed with either pYGE15 (no insert) or with pYGE15/hCNT3myc were subjected to immunoblot analysis as shown in the experiment of Figure V-16. The immunoblot of Panel A, which was probed with anti-hCNT3 (TL3360) polyclonal antibodies directed against the predicted intracellular region near the amino terminus (described in section V.2.2.1), revealed a unique immunoreactive band in membranes of yeast transformed with pYGE15/hCNT3myc, but not in yeast transformed with pYGE15. The immunoblot of Panel B demonstrated recognition of a unique immunoreactive material of similar electrophoretic mobility to that observed in Panel A by the anti-hCNT3 (TL3361) polyclonal antibodies in membranes of yeast harboring pYGE15/hCNT3myc. No such bands were apparent in yeast harboring pYGE15. Collectively, these experiments demonstrated the ability of the polyclonal

antibodies, directed either against intracellular (TL3360) or extracellular (TL3361) epitopes, to recognize recombinant hCNT3 by immunoblot analysis.

To determine the usability and specificity of the anti-hCNT3 monoclonal antibodies, immunoblots of membranes of yeast harboring either pYGE15/hCNT3myc or pYGE15 were probed with the anti-hCNT3 monoclonal antibodies in Panel C of Figure V-16. The results showed a single immunoreactive band of similar electrophoretic mobility to those of Panels A and B in membranes of yeast harboring pYGE15/hCNT3myc. No immunoreactive bands were detected in membranes of yeast with pYGE15.

Yeast producing recombinant hCNT3, which was immunologically tagged with the myc epitope, were used to determine whether anti-myc monoclonal antibodies recognized similar immunoreactive species as the anti-hCNT3 antibodies. The immunoblot of Panel D of Figure V-16, which contained membranes of yeast harboring either pYGE15/hCNT3myc or pYGE15, were probed with the anti-myc monoclonal antibodies. The results showed a similar immunoreactive material to those observed in Panels A, B and C in membranes of yeast harboring pYGE15/hCNT3myc, whereas no bands were detected in membranes of yeast harboring pYGE15.

V.2.2.4. Production of hCNT3 and hCNT3 tagged with green fluorescent protein (GFP) in HeLa cells

The experiments that follow aimed at examining further the specificity of the anti-hCNT3 antibodies against hCNT3 when produced in lower quantities in cultured cells. Functional production of recombinant hCNT3 produced in

mammalian cells has not been previously described. HeLa cells, which have been used successfully in transient transfection of cDNAs corresponding to hCNT1 and hCNT2 (described in Chapter III, section III.2.3) were employed as host cells to introduce hCNT3 cDNA. The demonstration of hCNT3 as the protein responsible for the *cib* process by molecular cloning of its cDNA was recently reported by Ritzel *et al* [2, 134].

The hCNT3 open reading frame was PCR-amplified from the original cloning vector pBluescript II KS with addition of necessary restriction sites for subcloning into pcDNA3 and pGFP-C1. The introduction of pcDNA3/hCNT3 and pGFP/hCNT3 into HeLa cells was accomplished by employing similar transfection methodologies using DEAE-dextran described in section III.2.3. The functional production of either hCNT3 or hCNT3-GFP was examined by conducting isotopic flux analysis using 10 μ M uridine. The rates of uridine uptake were calculated from 10-sec time courses and are presented in the bar graph of Figure V-17. The results showed a large stimulation of uridine transport activity in the presence of sodium in both hCNT3 and hCNT3-GFP transfected HeLa cells, whereas in the absence of sodium, the amount of uptake observed was low. This result suggested that the GFP tag in hCNT3-GFP did not influence the uridine transport activity of hCNT3 when produced in HeLa cells. The uridine transport rates obtained for cells producing hCNT3 and hCNT3-GFP were, respectively, 1.16 ± 0.06 and 1.14 ± 0.11 pmol/ 10^6 cells/sec.

V.2.2.5. Detection of recombinant hCNT3 in HeLa cells transiently transfected with hCNT3 cDNA

To determine whether the anti-hCNT3 antibodies recognized recombinant hCNT3 produced in HeLa cells, lysates of cells transfected with either pcDNA3/hCNT3 or pcDNA3 were subjected to immunoblot analysis in the experiment of Figure V-18. The PVDF membrane was probed with anti-hCNT3 polyclonal antibodies (TL3360, described in section V.2.2.1) directed against an intracellular epitope of hCNT3. The results revealed a prominent single band that migrated at an apparent molecular mass between 75 and 80 kDa in lysates from pcDNA3/hCNT3 transfected cells, but not in lysates from pcDNA3 transfected cells. These results demonstrated the specificity of the TL3360-directed antibodies against hCNT3 produced in cultured cells.

V.2.2.6. Detection of hCNT3 in transiently transfected HeLa cells by immunofluorescence with anti-hCNT3 antibodies

The experiments that follow attempted to determine the utility of the anti-hCNT3 monoclonal antibodies that were directed against TL3360 (an intracellular epitope of hCNT3) in immunofluorescent detection of hCNT3 in cells. HeLa cells either transfected with pcDNA3/hCNT3 or pcDNA3 were subjected to immunofluorescence analysis by confocal microscopy. HeLa cells transiently transfected with pcDNA3/hCNT3 were (i) fixed, (ii) permeabilized and (iii) stained with DAPI to visualize the nucleus and anti-hCNT3 monoclonal antibodies to localize hCNT3. Immunofluorescence images of DAPI and hCNT3 labeling shown in Figure V-19 revealed that DAPI stained the nucleus of the

majority of HeLa cells (Panel A), whereas the anti-hCNT3 monoclonal antibodies stained only a few HeLa cells. The superimposed image (Panel C) showed staining of the plasma membrane as well as the endoplasmic reticulum by the anti-hCNT3 antibodies and no colocalization of the blue (DAPI) and green (antibodies) images was apparent.

To assess the specificity of the staining pattern observed in the experiment of Figure V-19, HeLa cells transiently transfected with pcDNA3 were stained with anti-hCNT3 monoclonal antibodies as shown in the experiment of Figure V-20. The results showed a low level of background staining that was apparent in all the HeLa cells (Panel A). The superimposed image (Panel C) of the immunofluorescence and differential interference contrast signal revealed that the background staining was localized to the nucleus of HeLa cells and the fluorescence was relatively weak, at best, in comparison to that observed in Figure V-19.

V.2.2.7. Detection of hCNT3-GFP staining in HeLa cells transiently transfected with pGFP-C1/hCNT3 by immunofluorescence analysis

Transport experiments described in section V.2.2.4 demonstrated that pGFP-C1/hCNT3, when introduced into HeLa cells, resulted in functional hCNT3-mediated transport activity, indicating the presence of hCNT3-GFP fusion proteins at the cell surface. The nucleoside transport activity observed in HeLa cells transfected with pGFP-C1/hCNT3 was similar to that of cells transfected with pcDNA3/hCNT3 (see Figure V-17).

The experiment of Figure V-21 was undertaken to determine the location of hCNT3-GFP fusion proteins in HeLa cells transiently transfected with pGFP-C1/hCNT3. Transfected HeLa cells were analyzed by double-label immunofluorescence using anti-hCNT3 monoclonal antibodies to label hCNT3 and DAPI to visualize nuclei. Detection of hCNT3-GFP was accomplished by excitation at 488 nm using the argon laser and collection of emission spectra with appropriate filter sets. The immunofluorescence image presented in Panel B shows the green fluorescent signal of hCNT3-GFP in HeLa cells. The immunofluorescence image shown in Panel C represented staining patterns in HeLa cells by the anti-hCNT3 monoclonal antibodies (TL3360). The superimposed images of Panels A, B and C are shown in Panel D. The immunofluorescence image of Panel D demonstrated colocalization of immunofluorescent signals from Panel B (GFP) and Panel C (anti-hCNT3 monoclonal antibodies).

V.3. Discussion

The overall focus of the work in this chapter was to raise peptide antibodies against the human CNT proteins, hCNT2 and hCNT3. Attempts were also made to generate anti-hCNT1 antibodies directed against amino acid sequences QDLSKYKQRR corresponding to residues 503-512 near the predicted carboxyl-terminal tail of hCNT1, but these were unsuccessful (J. Marjan, T. Lang and C. Cass, Unpublished observations). Because rCNT1 is glycosylated at the carboxyl-terminal tail [141], it was assumed that failure to obtain anti-hCNT1 antibodies that recognized hCNT1 was due to the presence of a carbohydrate moiety near the epitope that was used to raise these antibodies. Other epitopes against various regions near the amino terminus and large loop domains between transmembrane segments have been selected for raising anti-hCNT1 antibodies, but have not yielded useful antibodies (K. Graham, T. Lang, P. Carpenter and C. Cass, Unpublished observations).

In the present work, polyclonal and monoclonal antibodies directed against an intracellular epitope near the amino terminus of hCNT2 were produced and characterized. The specificities of the anti-hCNT2 polyclonal and monoclonal antibodies were demonstrated by immunoblot analyses of membrane preparations of yeast and cultured cells either lacking or containing hCNT2. The anti-hCNT2 polyclonal and monoclonal antibodies recognized the same immunoreactive species, which exhibited electrophoretic mobility that corresponded with the predicted size of hCNT2. These immunoreactive bands were absent in membrane preparations of yeast and cultured cells that lacked

hCNT2. The antibodies also recognized an immunoreactive band of apparent molecular mass between 70 and 75 kDa corresponding to recombinant hCNT2, which was produced in HeLa cells by transient transfection of hCNT2 cDNA. The utility of the anti-hCNT2 antibodies in immunoblotting was further extended to immunofluorescence.

Immunofluorescence confocal microscopy established that anti-hCNT2 polyclonal and monoclonal antibodies bound to similar immunoreactive species located at the plasma membrane that corresponded to hCNT2 in ARAC/D2 stable transfectants. No detectable fluorescent signal was apparent in CEM-ARAC cells that lacked hCNT2 when they were stained with anti-hCNT2 polyclonal or monoclonal antibodies. The pre-immune sera from the same rabbit used to raise anti-hCNT2 polyclonal antibodies did not produce any detectable fluorescent signal when used to stain ARAC/D2 cells. These results established the specificity of these antibodies in immunofluorescence experiments.

The anti-hCNT3 antibodies were raised against two different immunogenic epitopes, TL3360 and TL3361 of hCNT3 corresponding, respectively, to (i) a hydrophilic region near the amino terminus predicted to be intracellular and (ii) a large loop domain between the putative transmembrane segments 11 and 12, predicted to be extracellular.

Polyclonal and monoclonal antibodies against epitope TL3360 and polyclonal antibodies against epitope TL3361 were characterized by immunoblot analysis of membranes of yeast transformed with either pYGE15 or pYGE15/hCNT2myc. All of the antibodies recognized the same immunoreactive

materials of similar electrophoretic mobilities in membranes of yeast producing recombinant hCNT3, whereas no immunoreactive bands were detected in membranes of yeast with pYGE15. Demonstration of the detection of recombinant hCNT3 in yeast cells was further extended to human cells.

The anti-hCNT3 (TL3360) antibodies recognized a broad immunoreactive band with an apparent molecular mass between 75 and 80 kDa corresponding to hCNT3 in HeLa cells transiently transfected with pcDNA3/hCNT3. Isotopic flux analysis of transiently transfected HeLa cells demonstrated that the transport rates obtained for hCNT3 (1.16 ± 0.06 pmol/ 10^6 cells/sec) and hCNT3-GFP (1.14 ± 0.11 pmol/ 10^6 cells/sec) were similar, indicating that the GFP tag did not influence the transport activity of hCNT3. The transport rates of hCNT3 and hCNT3-GFP were approximately 1.5-fold greater than those observed for hCNT1 (0.76 ± 0.022 pmol/ 10^6 cells/sec) and hCNT2 (0.72 ± 0.032 pmol/ 10^6 cells/sec) transfected HeLa cells (described in Chapter III, sections III.2.3.3 and III.2.3.5). The relatively higher hCNT3-mediated transport activity suggested possible differences between hCNT3 and other CNT family members in its capacity for mediating uridine uptake. This conclusion was supported by data obtained using yeast to express nucleoside transporter cDNAs. The results of such studies using similar transport-assay conditions with 10 μ M uridine demonstrated a more robust uridine uptake by recombinant hCNT3 compared to that by hCNT1 and hCNT2 (J. Zhang, F. Visser, M. Vickers, T. Lang, J. Young, S. Baldwin, C. Cass, Unpublished results).

The monoclonal antibodies against epitope TL3360 of hCNT3 were characterized further to determine their utility in immunofluorescence. These antibodies stained primarily the plasma membrane and the endoplasmic reticulum in HeLa cells producing hCNT3-GFP, and the antibody-staining patterns demonstrated colocalization with the hCNT3-GFP fluorescent signal, establishing the specificity of the anti-hCNT3 antibodies in immunofluorescence.

This was the first time that anti-hCNT2 and anti-hCNT3 antibodies have been successfully produced. The generation of useful antibodies against two major members of the human CNT family has provided important methodologies and tools for generating antibodies against other nucleoside transport proteins. Perhaps more importantly, these antibodies will permit a greater variety of approaches to the study of CNT proteins.

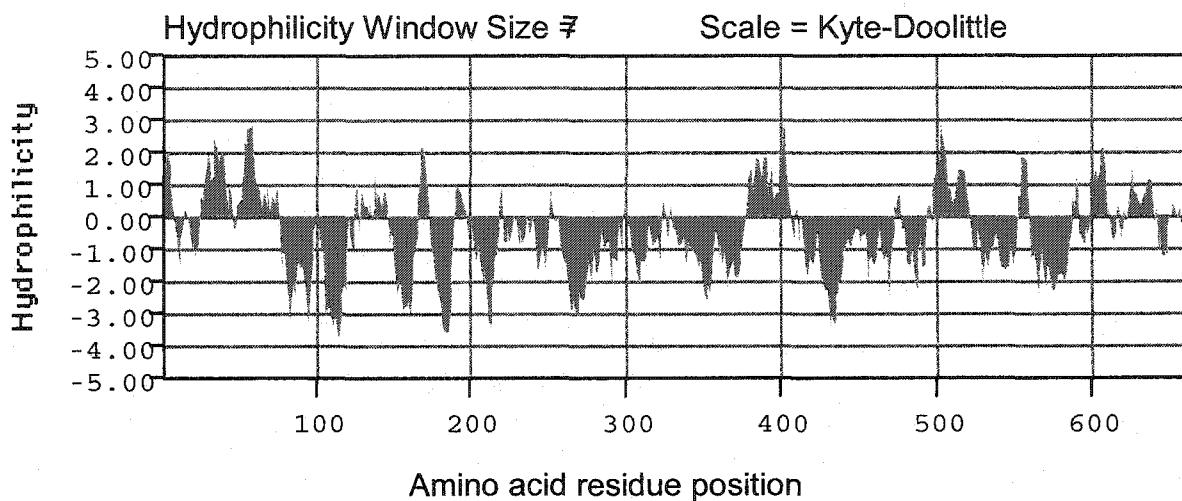


Figure V-1. Hydrophilicity plot of hCNT2 protein sequence identifying hydrophilic regions

The amino acid sequence of hCNT2 was deduced from the nucleotide sequences (accession number, AF036109) obtained from GenBank data bases by using GeneTool. The hCNT2 protein sequence was imported into PepTool and analyzed for hydrophilic regions using the algorithm of Kyte and Doolittle. [337]

Hydrophobicity for: hCNT2 peptide TL3273

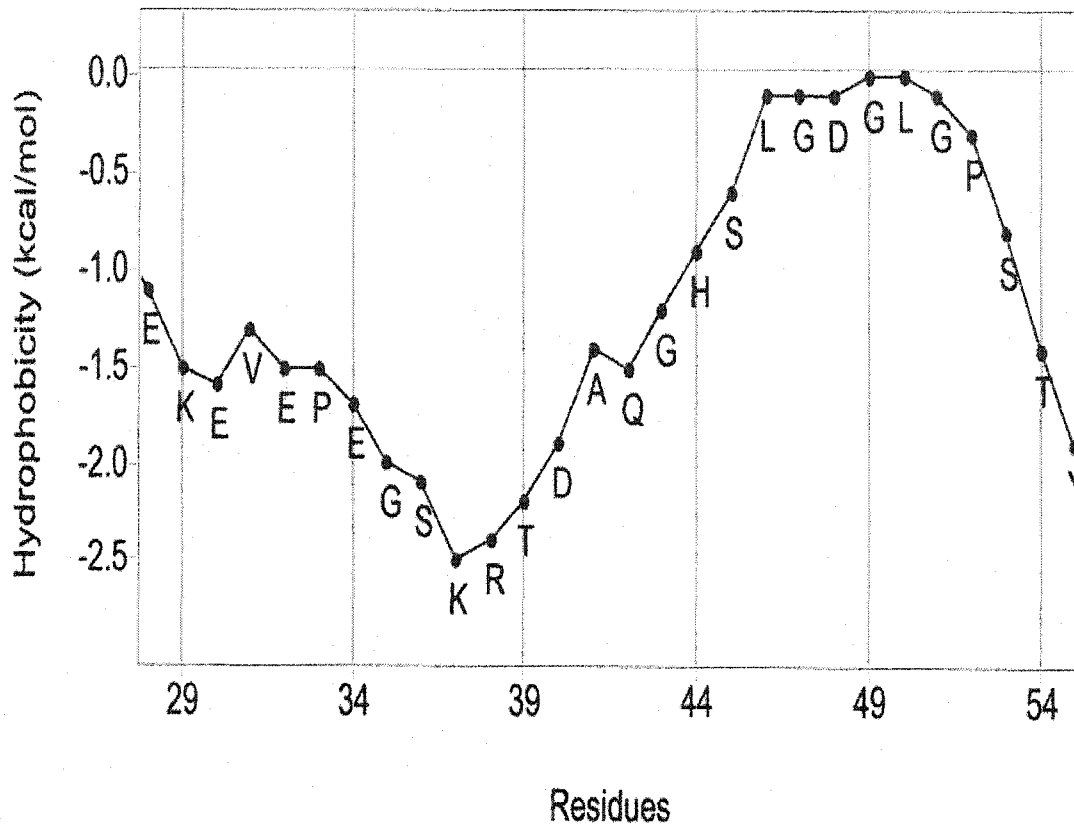


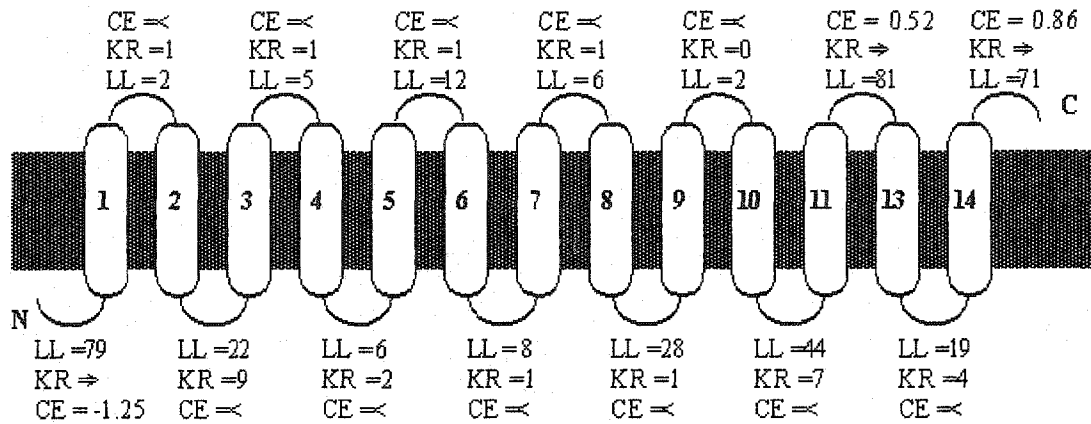
Figure V-2. Hydropathy plot of the chosen polypeptide TL3273 of hCNT2

The chosen 22-amino acid sequence (TL3273) of hCNT2 was imported into PepTool software and the hydrophobicity index (kcal/mol) was calculated from the amino acid composition of each segment according to the method of Kyte and Doolittle [337]. The hydrophobicity index is the free energy needed to transfer successive segments of a polypeptide from a nonpolar solvent to water. The results are presented as hydrophobicity as a function of residue number. A positive value indicates that free energy is required for transfer to water (that is, the segment is hydrophobic). Values above 0 kcal/mol are indicative of hydrophobes.

hCNT2

> : Too long to be significant
 < : Too short to be significant
 LI : Loop length
 KR : Number of Lys and Arg

KR Diff: Positive charge difference
 CE : Net charge energy
 CE Diff: Net charge difference
 CH Diff: Charge difference over N-term segments



KR Diff=20 **CYTOPLASM**
 CH Diff= 4 **CYTOPLASM**
 CE Diff= -2.62 **CYTOPLASM**
 Integral Membrane Protein

Structure no. 4

Figure V-3. Topological prediction of hCNT2

The hCNT2 protein sequence was imported into TopPredII protein structure analysis software and analyzed using TopPredII calculations for polytopic membrane proteins [338]. Shown is the putative topology model of hCNT2 in the membrane depicting the lengths of loop (LL) domains, 13 transmembrane segments, intracellular amino terminus and extracellular carboxy-terminus. The chosen peptide sequence TL3273 is located in the large intracellular region near the amino terminus of the protein.

Consensus	-----	
hCNT2	GLELMEKEVEPEGSKRTDA--QGHS LGDGLGPSTYQR-RSRWPFSKARSF	69
TL3273	-----KEVEPEGSKRTDA--QGHS LGDGL-----	22
rbCNT2	GLELTEEGINSEQTRRMEV--QGHS LDDVVRPATHQR-SYLQPLTKARTF	69
rCNT2	GLELMEVG-NLEQGKTL EEVTQGHSLKDGLGHSSLWR-RILQPFTKARSF	70
hCNT1	GADFLESLEEGQLPRSDLSPA EIRSSWSEAAPKPF SRWRNLQPALRARSF	74
hCNT3	KQDEEQVTVEQDS PRNRE----H-MEDDDE-EMQQKGLERR YDTVCGF	93

Figure V-4. Amino acid sequence alignment of polypeptides TL3273, CNT2, CNT1 and CNT3

The sequences of CNT proteins hCNT2, rCNT2, rbCNT2, hCNT1 and hCNT3 from human (h), rat (r) and rabbit (rb) species were aligned with TL3273 polypeptide using the BESTFIT program of the University of Wisconsin Genetics Computer Group (GCG) for the UNIX operating system. Amino acid sequence positions are shown on the right.

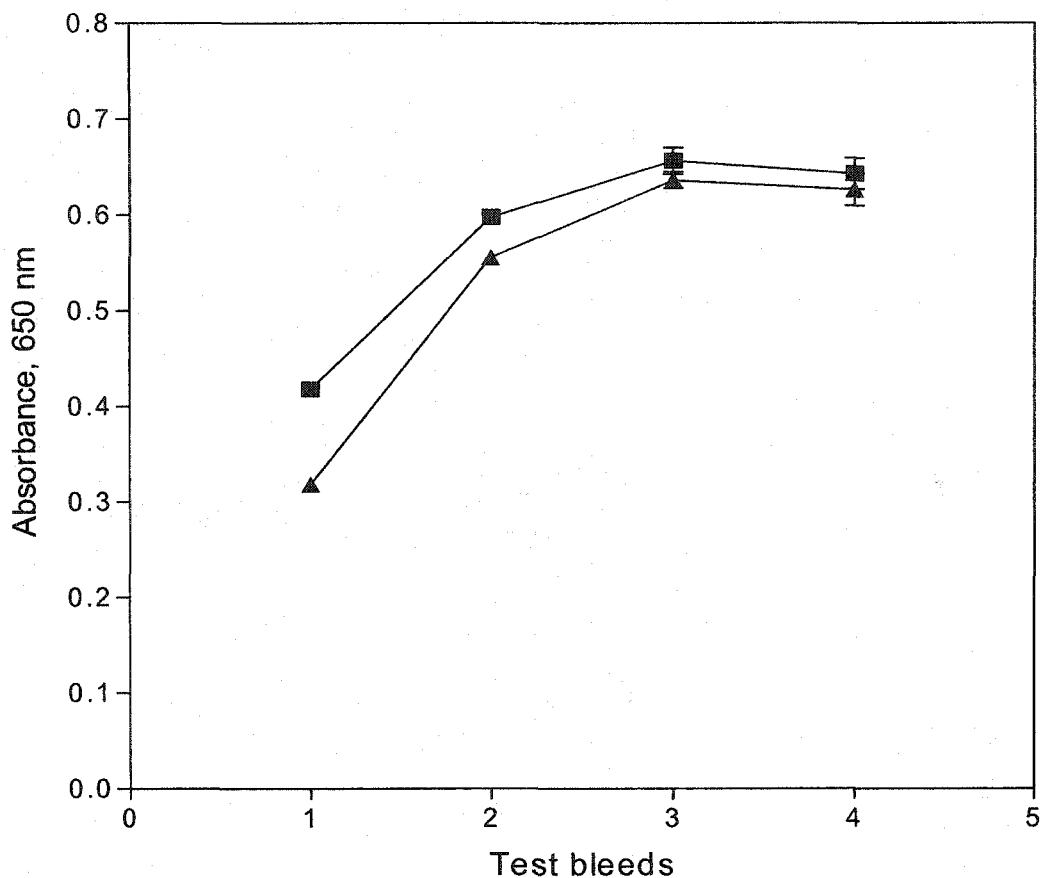


Figure V-5. Monitoring anti-hCNT2 peptide antibody production in rabbits by ELISA

Serum from test bleeds (1-4) of rabbits 783 (■) and 812 (▲) were diluted 1:10000 (v/v) with PBS and subjected to ELISA using 96-well plates coated with hCNT2 peptide TL3273 conjugated to BSA as described in section II.19. Absorbance at 650 nm was determined using a UVmax 96-well plate reader along with SOFTmax software. Each value represents the mean \pm SD of triplicate determinations and error bars are not shown where SD values were smaller than the size of the data symbols. The absorbance for preimmune sera was 0.009 ± 0.005 .

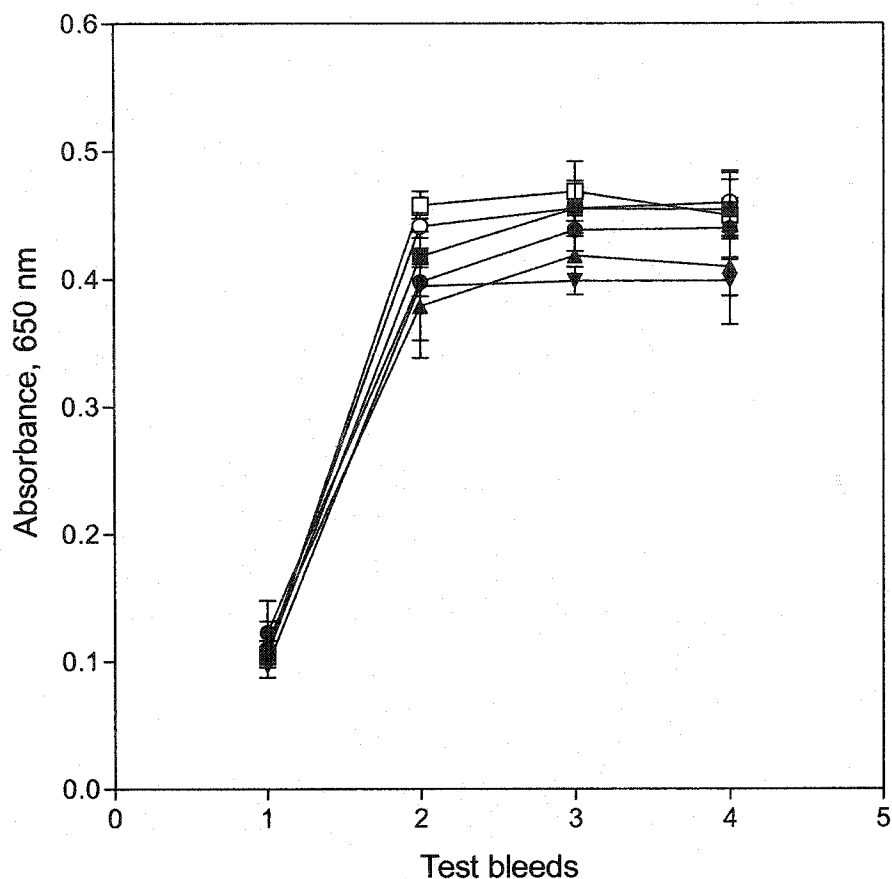


Figure V-6. Monitoring anti-hCNT2 peptide antibody production in mice by ELISA

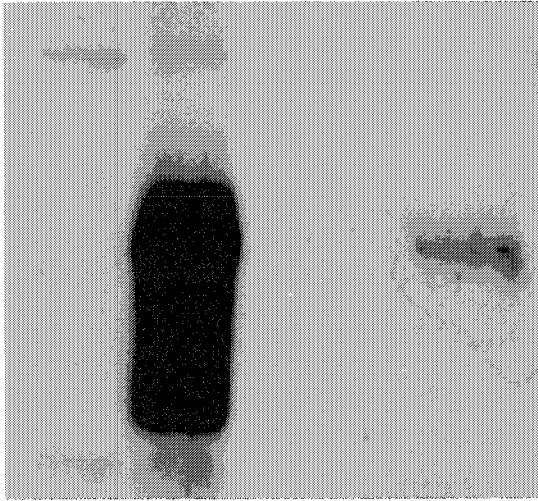
Serum from test bleeds (1-4) of mice 4.1 (■), 4.2 (▲), 4.3 (▼), 2.1 (●), 2.2 (○) and 2.3 (□) were diluted 1:10000 (v/v) with PBS and subjected to ELISA using 96-well plates coated with hCNT2 peptide TL3273 conjugated to BSA as described in section II.19. Absorbance at 650 nm was determined using a UVmax 96-well plate reader along with SOFTmax software. Each value represents the mean \pm SD of triplicate determinations and error bars are not shown where SD values were smaller than the size of the data symbols. The absorbance for preimmune sera were 0.005 ± 0.003 .

Figure V-7. Immunoreactivity of anti-hCNT2 antibodies against recombinant hCNT2 produced in yeast and ARAC/D2 stable transfectant

Yeast harboring pYES2 (lane 1) or pYES2/hCNT2myc (lane 2), CEM-ARAC (lane 3) and ARAC/D2 (lane 4) cells were subjected to immunoblot analysis as described in section II.8. Membrane preparations were prepared from yeast and cultured cells according to procedures described in section II.17. Equal quantities (5 μ g) of protein were loaded, electrophoresed through a 10% SDS-polyacrylamide gel and transferred to PVDF membrane. The PVDF membrane were probed with 1:7000 dilution (v/v) of anti-hCNT2 polyclonal antibodies (Panel A), 1:9000 dilution (v/v) of anti-hCNT2 monoclonal antibodies (Panel B), 1:4000 dilution (v/v) of anti-myc monoclonal antibodies (Panel C), followed by either 1:10000 dilution (v/v) of anti-goat HRP conjugated (Panel A) or 1:8000 dilution (v/v) of anti-mouse HRP conjugated (Panels B, C) secondary antibodies. Detection was by ECL chemiluminescent and exposure to Fuji X-ray film. Protein markers are not shown for clarity.

A

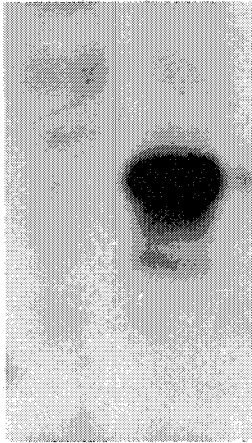
1 2 3 4



Anti-hCNT2 polyclonal
antibodies

B

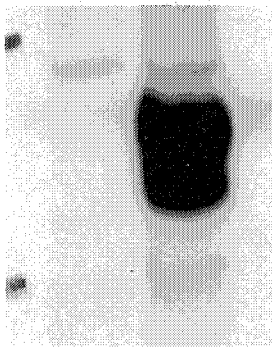
1 2



Anti-hCNT2 monoclonal
antibodies

C

1 2



Anti-myc monoclonal
antibodies

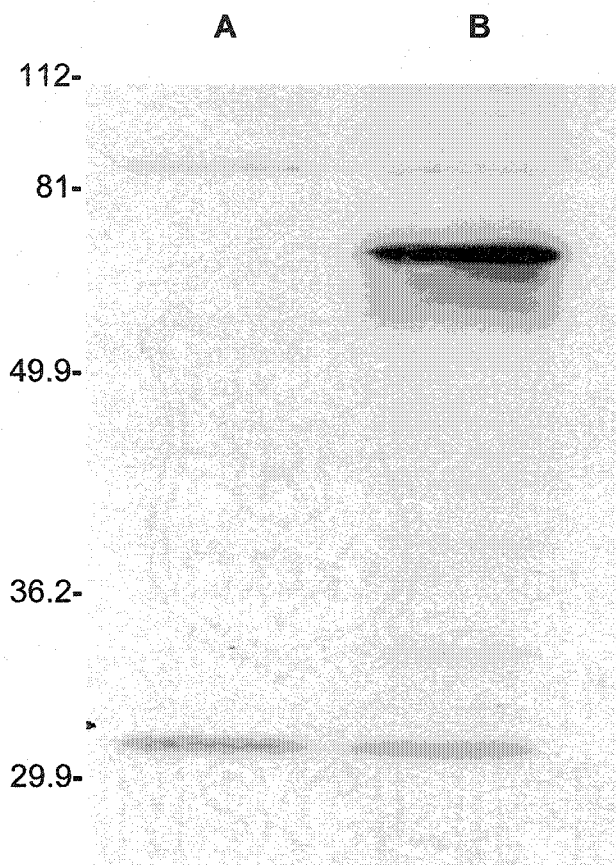


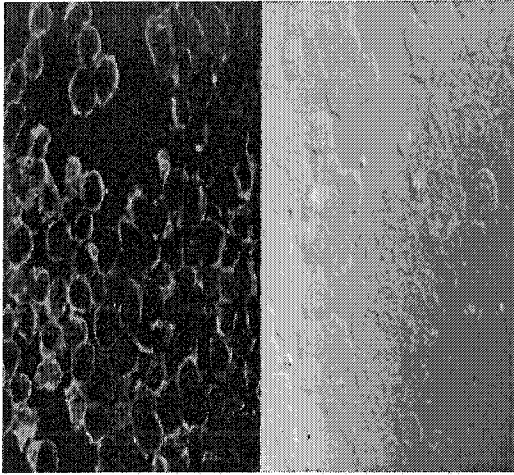
Figure V-8. Detection of recombinant hCNT2 in HeLa cells transiently transfected with hCNT2 cDNA by immunoblot analysis

HeLa cells were transiently transfected with either pcDNA3 (lane **A**) or pcDNA3/hCNT2 (lane **B**) by DEAE-dextran transfection as described in section II.11.1. Membrane preparations were prepared from HeLa cells according to procedures described in section II.17. Equal quantities (10 μ g) of protein were loaded, electrophoresed through a 10% SDS-polyacrylamide gel and transferred to PVDF membrane. The PVDF membrane was probed with 1:7000 dilution (v/v) of anti-hCNT2 polyclonal antibodies followed by 1:8000 dilution (v/v) of anti-goat HRP conjugated secondary antibodies. Detection was by ECL chemiluminescence and exposure to Fuji X-ray film. *Left*, positions of the protein markers (in kDa).

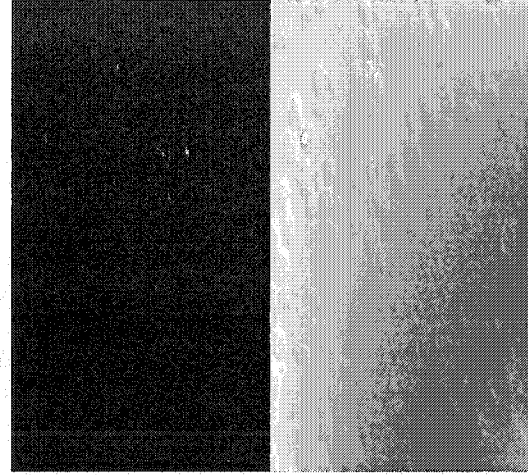
ARAC/D2 (hCNT2-containing)

CEM-ARAC (transporter-deficient)

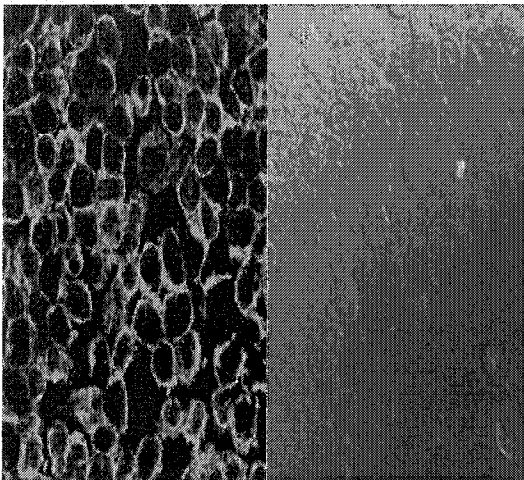
A



C



B



D

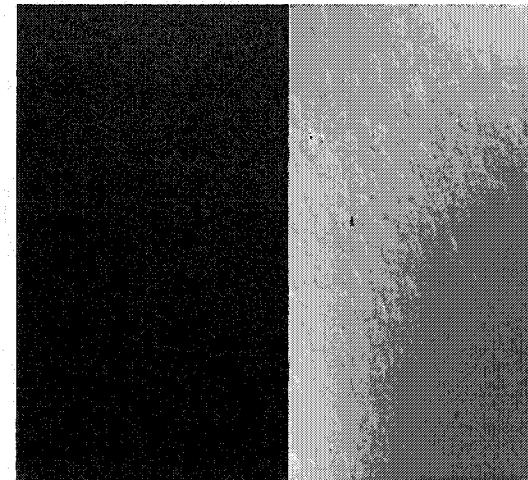


Figure V-9. Anti-hCNT2 antibodies stained plasma membranes of hCNT2 stably transfected ARAC/D2 cells but not of transporter-deficient CEM-ARAC cells

ARAC/D2 (A, B) and CEM-ARAC (C, D) cells were grown on poly-L-lysine coated coverslips overnight. Coverslips were fixed, permeabilized in methanol for 5 min, stained with anti-hCNT2 polyclonal (A, C) or anti-hCNT2 monoclonal (B, D) antibodies, followed with either Alexa Fluoro 488 conjugated goat anti-rabbit (A, C) or goat anti-mouse antibodies (B, D), and mounted on slides in 90% glycerol. Slides were visualized by LSM-510 confocal microscopy as described in section II.22. Shown are immunofluorescence (left side) and differential interference contrast (right side) images.

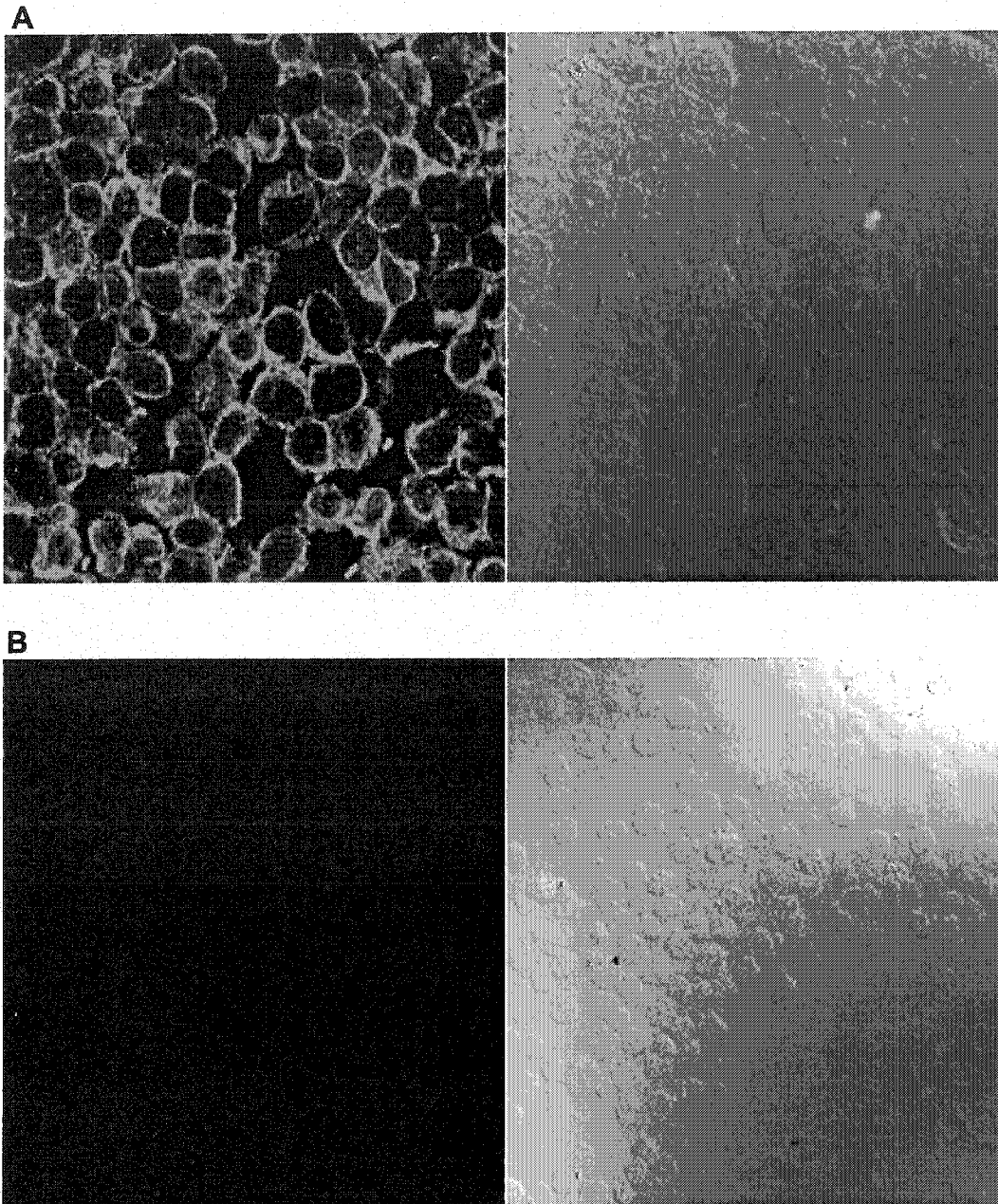


Figure V-10. Plasma membrane labeling of hCNT2 stably transfected ARAC/D2 cells in the presence, but not in the absence, of anti-hCNT2 antibodies

ARAC/D2 cells were grown on poly-L-lysine coated coverslips overnight. Coverslips were fixed, permeabilized in methanol for 5 min, incubated with anti-hCNT2 polyclonal antibodies (A) or with pre-immune sera (B), followed with Alexa Fluoro 488 conjugated goat anti-rabbit antibodies (A, B), and mounted on slides in 90% glycerol. Slides were visualized by LSM-510 confocal microscopy as described in section II.22. Shown are immunofluorescence (left side) and differential interference contrast (right side) images.

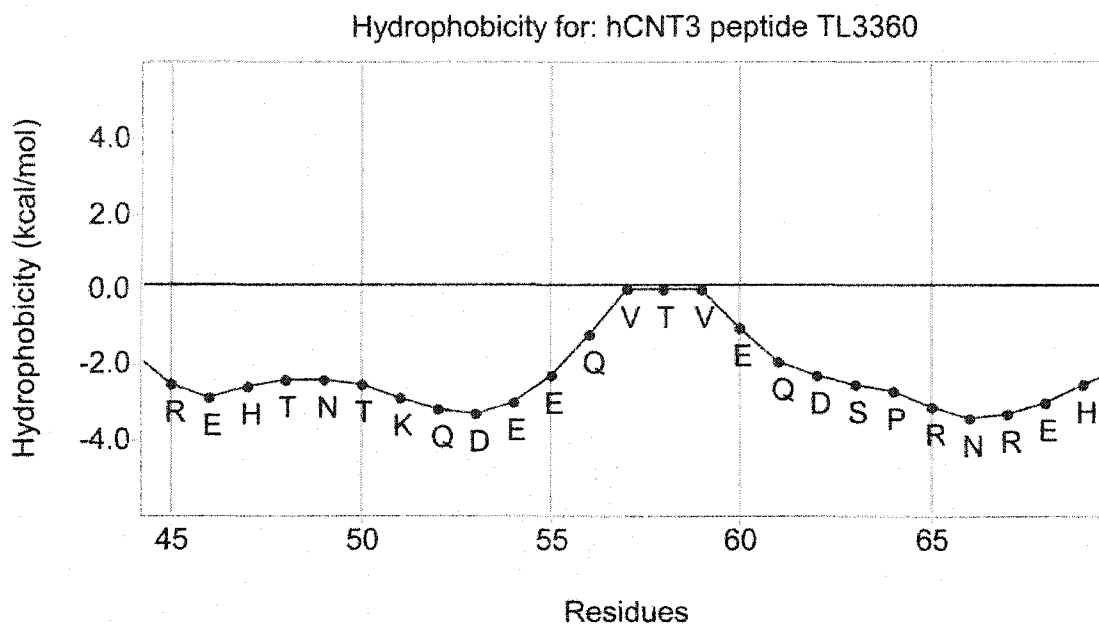
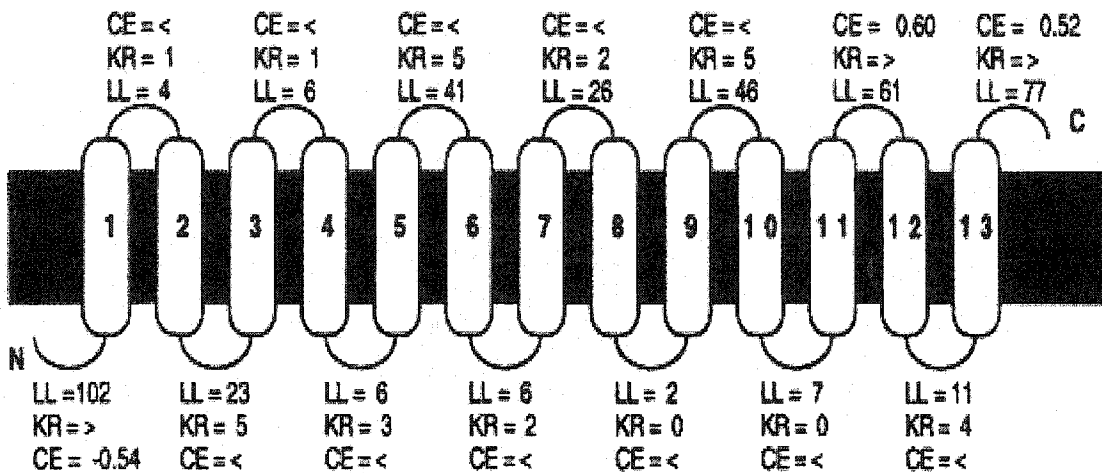


Figure V-11. Hydropathy plot of the chosen polypeptide TL3360 of hCNT3

The chosen 25-amino acid sequences TL3360 of hCNT3 was imported into PepTool software and the hydrophobicity index (in kcal/mol) was calculated from the amino acid composition of each segment according to the method of Kyte and Doolittle [337]. The hydrophobicity index is the free energy needed to transfer successive segments of a polypeptide from a nonpolar solvent to water. The results are presented as hydrophobicity as a function of residue number. A positive value indicates that free energy is required for transfer to water (that is, the segment is hydrophobic). Values above 0 kcal/mol are indicative of hydrophobes.

> : Too long to be significant
 < : Too short to be significant
 LI : Loop length
 KR : Number of Lys and Arg

KR Diff : Positive charge difference
 CE : Net charge energy
 CE Diff : Net charge difference
 CH Diff : Charge difference over N-term segments



KR Diff = 0 **Undecided**
 CH Diff = 2 **CYTOPLASM**
 CE Diff = -1.66 **CYTOPLASM**
 Integral Membrane Protein

Structure no. 1

Figure V-12. Topological prediction of hCNT3 orientation in the membrane

The hCNT3 protein sequence was imported into TopPredII protein structure analysis software and analyzed using TopPredII calculations for polytopic membrane proteins [338]. Shown is the putative topology model of hCNT2 in the membrane depicting the lengths of loop (LL) domains, 13 transmembrane segments, intracellular amino terminus and extracellular carboxy-terminus. The chosen peptide sequences TL3360 and TL3361 are respectively located in the large intracellular loop close to the amino terminus and extracellular loop between transmembrane segments 11 and 12.

Consensus	-----	
hCNT3	MELRSTAAPRAEGYSNVGFQNEENFLENENTSGNNSIRSRVQSREHTNT	50
TL3360	-----REHTNT	6
hCNT1	-----MENDPSRRRESISLTPVAKGLENMGADFLES	31
hCNT2	-----MEKASGRQSIALSTVETGTVNPGLELME-	28
Consensus	---E-----	1
hCNT3	KQDEEQVTVEQDSPRN-REHMEDDDEEMQKGLERRYDTVCGFCRKHKT	99
TL3360	KQDEEQVTVEQDSPRN-REH-----	25
hCNT1	LE-EGQLPRSDLSPAIEIRSSWSEAAPKPFSSRWRNLQPALRARSFCREHMQ	80
hCNT2	KEVEPEGSKRTDA--QGHS LGDGLGPSTYQR-RSRWPFSKARSFCKTHAS	75

Figure V-13. Amino acid sequence alignment of polypeptides TL3360, hCNT3, hCNT2 and hCNT1

The sequences of CNT proteins hCNT3, hCNT2 and hCNT1 were aligned with TL3360 polypeptide using the BESTFIT program of the University of Wisconsin Genetics Computer Group (GCG) for the UNIX operating system. Shown is the amino acid identity of the chosen polypeptide sequence TL3360 with other sequences of hCNT proteins. The identical amino acid is highlighted.

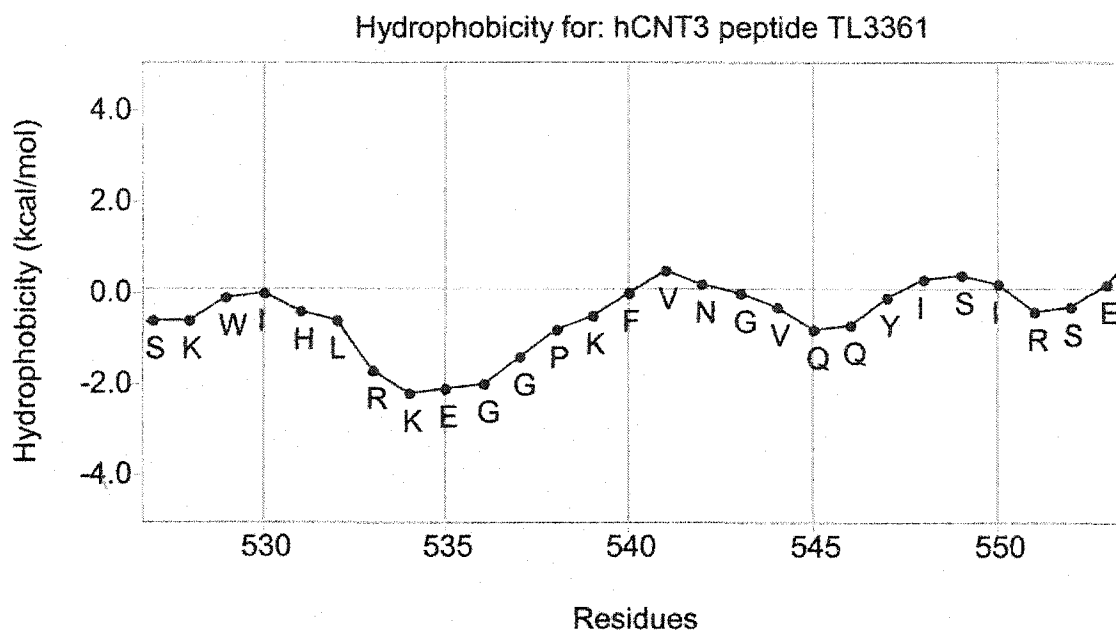


Figure V-14. Hydropathy plot of the chosen polypeptide TL3361 of hCNT3

The chosen TL3361 23-amino acid sequence of hCNT3 was imported into PepTool software and the hydrophobicity index (kcal/mol) was calculated from the amino acid composition of each segment according to the method of Kyte and Doolittle [337]. The hydrophobicity index is the free energy needed to transfer successive segments of a polypeptide from a nonpolar solvent to water. The results are presented as hydrophobicity as a function of residue number. A positive value indicates that free energy is required for transfer to water (that is, the segment is hydrophobic). Values above 0 kcal/mol are indicative of hydrophobes.

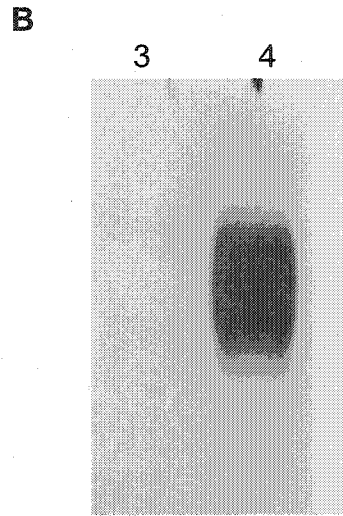
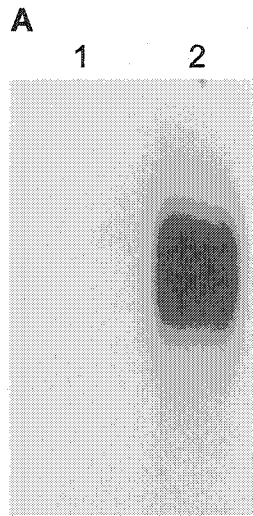
Consensus	-----R--G-----Q-IS-	5
hCNT3	WQDSFMVARLIGYKTFNFVAYEHLKWIHLRKEGGPKFVNGVQOYISI	550
TL3361	-----HLRKEGGPKFVNGVQOYISI	20
hCNT1	WEDCPVVAELLGIKLFLNEFVAYQDLSKYKQRRLAGAEWVGNRKOWISV	528
hCNT2	WTDCPMVAEMVGIKFFINEFVAYQQLSQYKNKRLSCMEEWIEGKOWISV	523
Consensus	R-E-----	7
hCNT3	RSEI IATYALCGFANIGSLGIVIGGLTSMAPSRKRDIASGAVRALIAGTV	600
TL3361	RSE-----	23
hCNT1	RAEVLTTFALCGFANFSSIGIMLGGLTSMVPQRKSDFSQIVLRALFTGAC	578
hCNT2	RAEIIITTFSLCGFANLSSIGITLGGLTSIVPHRKSDDLKVVVRLFTGAC	573

Figure V-15. Amino acid sequence alignment of polypeptides TL3361, hCNT3, hCNT2 and hCNT1

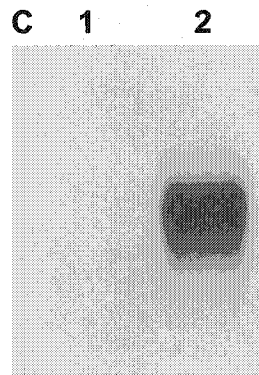
The sequences of TL3361, hCNT3, hCNT2 and hCNT1 were aligned using the BESTFIT program of the University of Wisconsin Genetics Computer Group (GCG) for the UNIX operating system. Shown is the amino acid identity of the chosen peptide sequence TL3361 with other sequences of hCNT proteins. Identical amino acids are highlighted.

Figure V-16. Immunoreactivity of anti-hCNT3 antibodies against recombinant hCNT3 produced in yeast

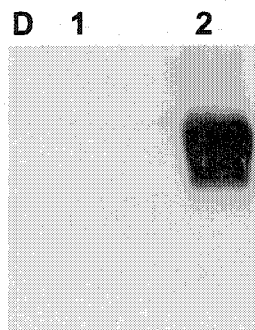
Yeast harboring pYGE15 (lanes 1, 3) or pYGE15/hCNT2myc (lanes 2, 4) were subjected to immunoblot analysis as described in section II.8. Membrane preparations were prepared from yeast according to procedures described in section II.17.1. Equal quantities (5 μ g) of protein were loaded, electrophoresed through a 10% SDS-polyacrylamide gel and transferred to PVDF membranes. The PVDF membranes were probed with either 1:10000 dilution (v/v) of anti-hCNT3 (TL3360) polyclonal antibodies (Panel A), anti-hCNT3 (TL3361) polyclonal antibodies (Panel B), 1:9000 dilution (v/v) of anti-hCNT3 monoclonal antibodies (Panel C), 1:4000 dilution (v/v) of anti-myc monoclonal antibodies (Panel D), followed by either 1:10000 dilution (v/v) of anti-goat HRP conjugated (Panels A, B) or 1:9000 dilution (v/v) of anti-mouse HRP conjugated (Panels C, D) secondary antibodies. Detection was by ECL chemiluminescence and exposure to Fuji X-ray film. Protein markers are not shown for clarity.



Anti-hCNT3 polyclonal antibodies



Anti-hCNT3 monoclonal antibodies



Anti-myc monoclonal antibodies

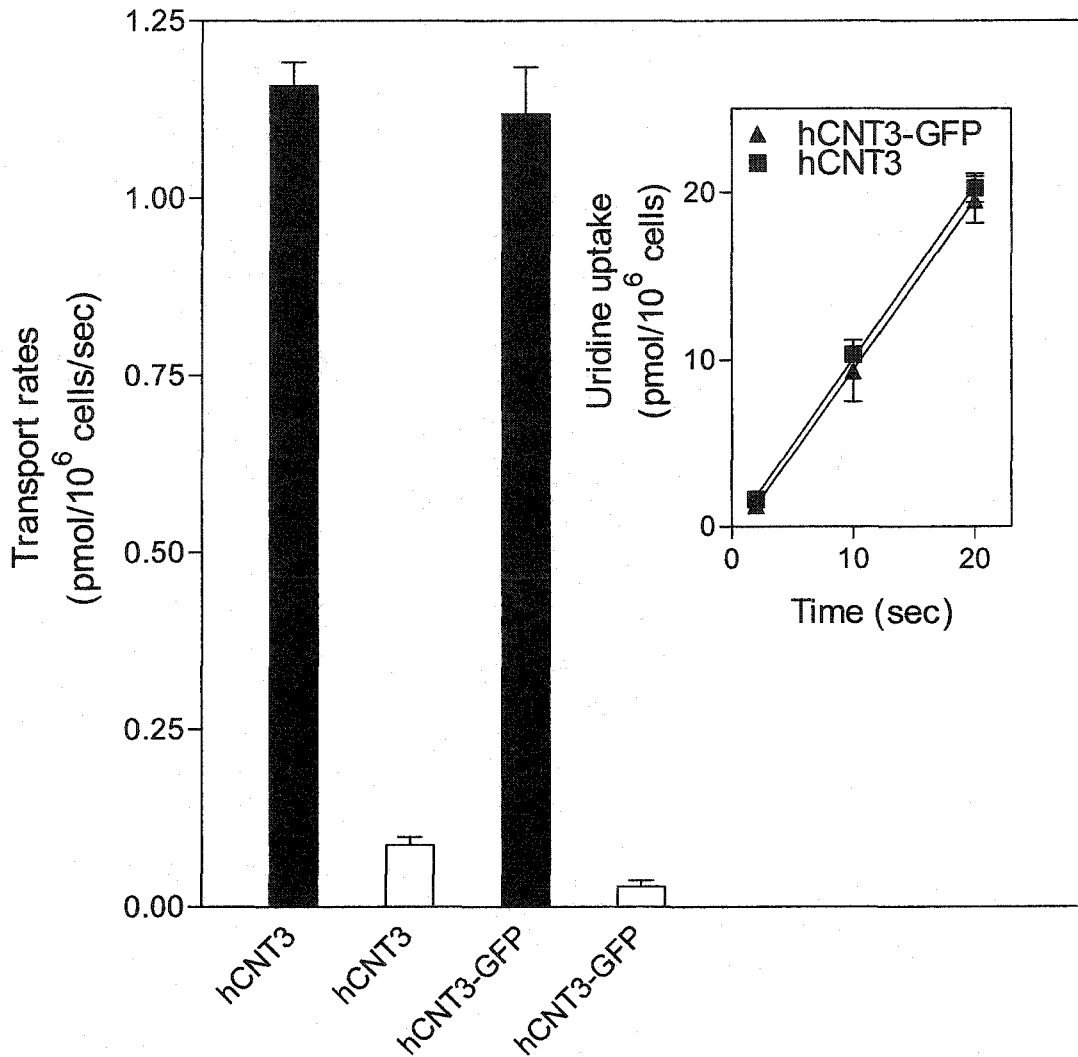


Figure V-17. Uridine transport activities in HeLa cells transiently transfected with untagged or GFP-tagged hCNT3 cDNA

HeLa cells were transiently transfected with pcDNA3/hCNT3 or pGFP/hCNT3 as described in section II.11. ENT-mediated processes were inhibited by incubating cells for 15 min in transport buffer that contained 200 μ M dilazep prior to uptake measurements and also including 200 μ M dilazep in transport assays. Uptake of 10 μ M uridine was performed in sodium-containing (solid bars) or sodium-free (open bars) transport buffer as described in section II.16. Inset, initial rates of uptake in sodium-containing transport buffer were obtained from 20-sec time courses. Each value represents the mean \pm SD of three determinations. Shown is one of two independent experiments that yielded qualitatively similar results.

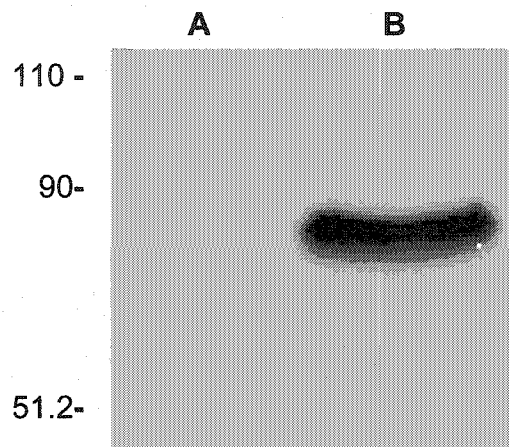


Figure V-18. Detection of recombinant hCNT3 in HeLa cells transiently transfected with hCNT3 cDNA by immunoblot analysis

HeLa cells were transiently transfected with either pcDNA3 (lane A) or pcDNA3/hCNT3 (lane B) by DEAE-dextran transfection as described in section II.11. Total cell lysates of HeLa cells prepared by lysis in sample buffer at 65°C for 10 min and were electrophoresed through a 10% SDS-polyacrylamide gel and transferred to a PVDF membrane. The PVDF membrane was probed with a 1:8000 dilution (v/v) of anti-hCNT3 polyclonal antibodies (TL3360) followed by a 1:7000 dilution (v/v) of anti-goat HRP conjugated secondary antibodies. Detection was by ECL chemiluminescence and exposure to Fuji X-ray film. *Left*, positions of the protein markers (in kDa).

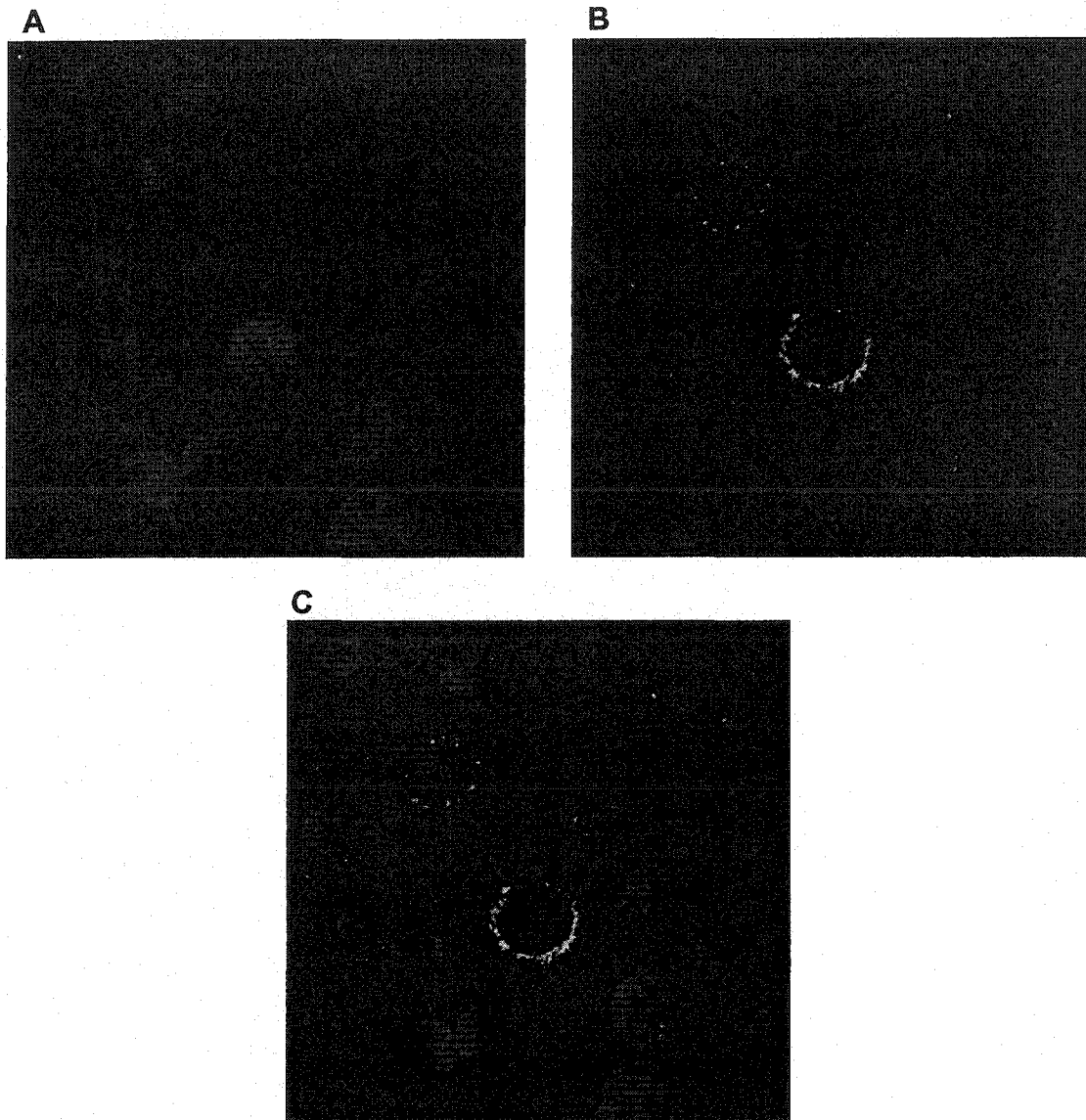


Figure V-19. Detection of hCNT3 in pcDNA3/hCNT3 transiently transfected HeLa cells by immunofluorescence analysis with anti-hCNT3 antibodies

HeLa cells that had been transiently transfected with pcDNA3/hCNT3 as described in section II.11.1 were grown on poly-L-lysine coated coverslips for 12 hr. Coverslips were fixed in paraformaldehyde, permeabilized in Triton X-100, stained with anti-hCNT3 monoclonal antibodies directed against epitope TL3360 of hCNT3, followed with Alexa Fluoro 488 conjugated goat anti-mouse antibodies, labeled with DAPI and mounted on slides in 90% glycerol. Slides were visualized by LSM-510 confocal microscopy as described in section II.22. Shown are immunofluorescence staining of DAPI (Panel A), hCNT3 (Panel B) and merged (Panel C) images.

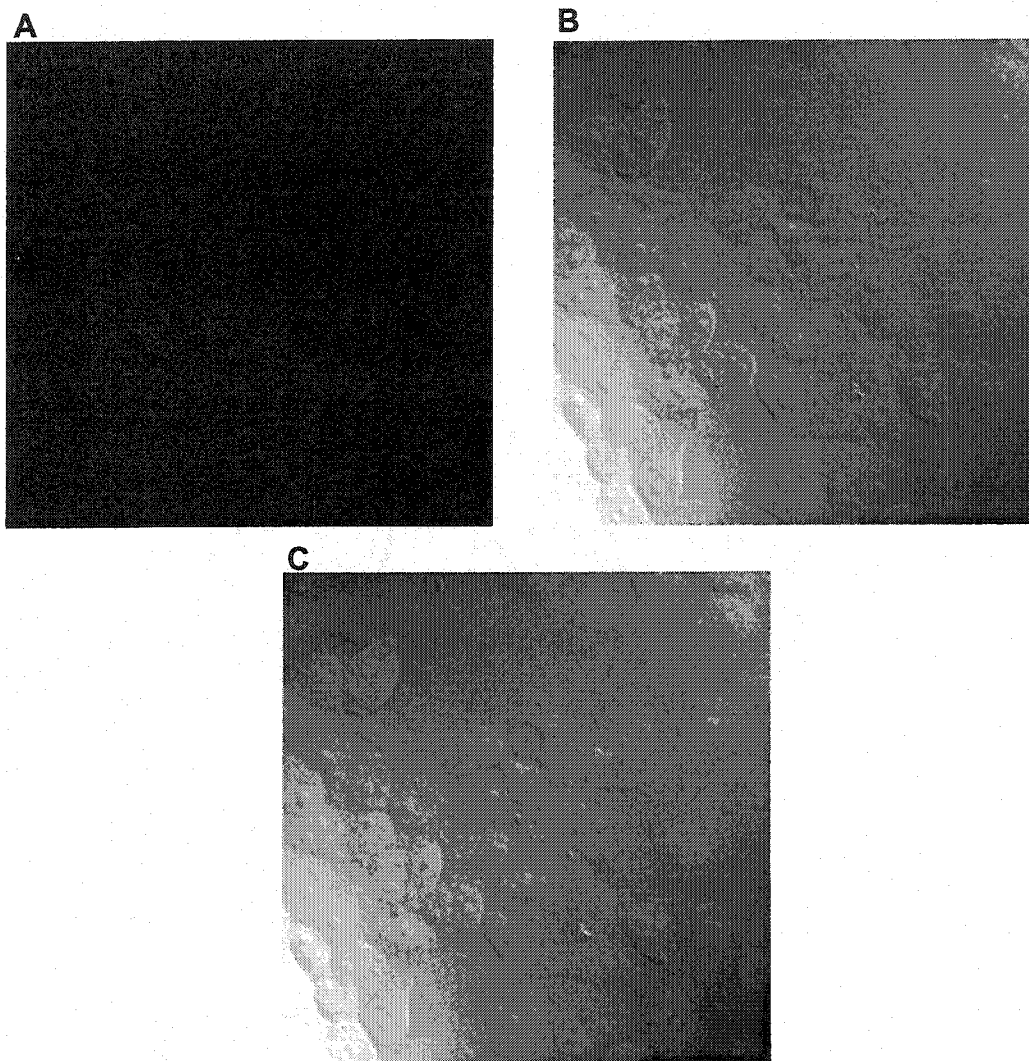


Figure V-20. Immunofluorescence analysis of pcDNA3 transiently transfected HeLa cells with anti-hCNT3 antibodies

HeLa cells that had been transiently transfected with pcDNA3 as described in section II.11.1. were grown on poly-L-lysine coated coverslips overnight. Coverslips were fixed in paraformaldehyde, permeabilized in Triton X-100, stained with anti-hCNT3 monoclonal antibodies directed against epitope TL3360 of hCNT3, followed with Alexa Fluoro 488 conjugated goat anti-mouse antibodies, and mounted on slides in 90% glycerol. Slides were visualized by LSM-510 confocal microscopy as described in section II.22. Shown are immunofluorescence (Panel A), differential interference contrast (Panel B) and merged (Panel C) images.

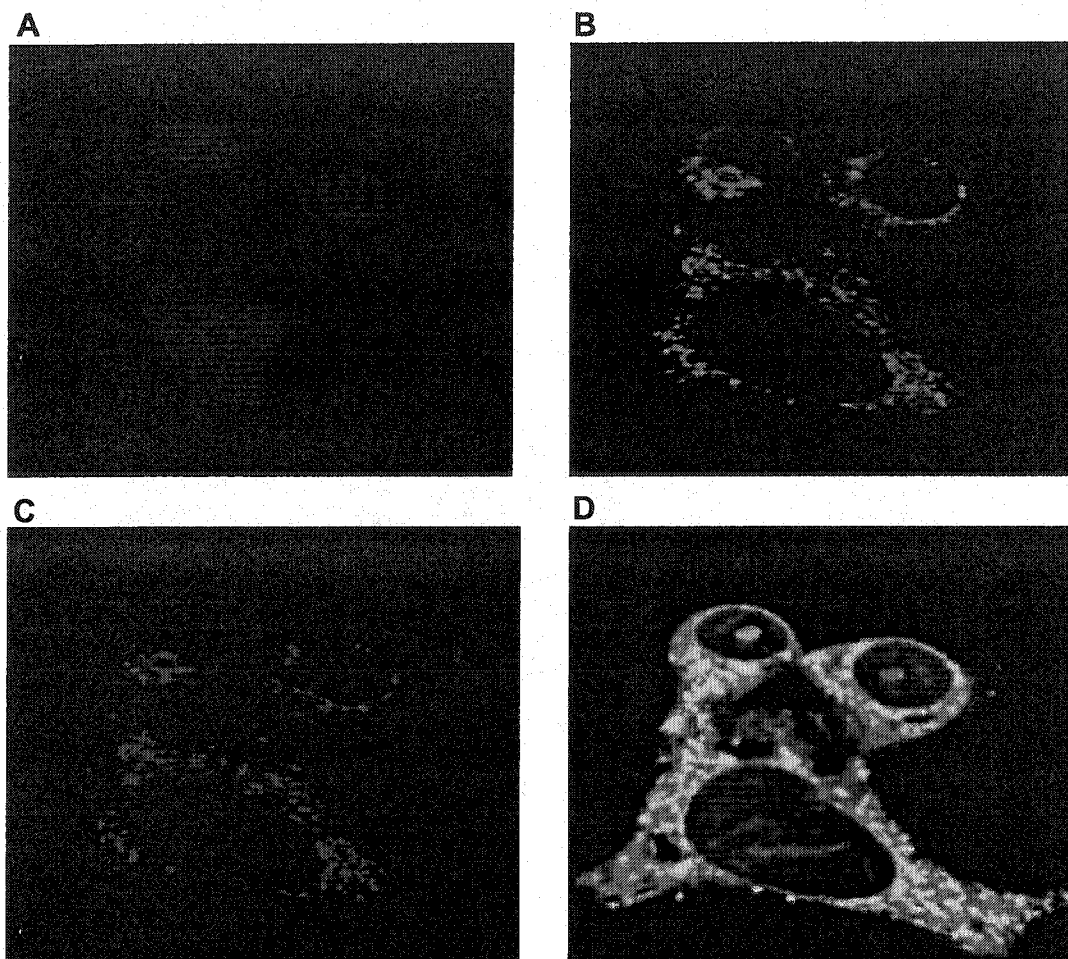


Figure V-21. Detection of hCNT3 in pGFP-C1/hCNT3 transiently transfected HeLa cells by immunofluorescence analysis

HeLa cells that had been transiently transfected with pcGFP-C1/hCNT3 as described in section II.11.1 were grown on poly-L-lysine coated coverslips overnight. Coverslips were fixed in paraformaldehyde, permeabilized in Triton X-100, stained with anti-hCNT3 monoclonal antibodies directed against an intracellular epitope TL3360 of hCNT3, followed with Alexa Fluoro 594 conjugated goat anti-mouse antibodies, labeled with DAPI and mounted on slides in 90% glycerol. Slides were visualized by LSM-510 confocal microscopy as described in section II.22. Shown are immunofluorescence staining of DAPI (Panel A), GFP (Panel B), hCNT3 (Panel C) and merged (Panel D) images.

Chapter VI

VI. Localization of Recombinant hCNT2 in Stably Transfected Cells and Alterations in Distribution of Native hCNT3 in Caco-2 Cells

VI.1. Introduction

The gastrointestinal mucosa maintains a rapid rate of cellular proliferation and metabolic activity [332], and therefore may have an increased need for exogenous nucleotides. Like bone marrow cells and leukocytes, small intestinal epithelial cells possess a limited capacity for *de novo* synthesis of nucleotides [333, 334]. The salvage pathway for acquiring nucleotides is energetically more favorable and likely to be of particular importance for rapidly dividing cells in the intestine. Nucleotides do not passively diffuse across the plasma membrane of cells and dietary nucleotides are metabolized to nucleosides and nucleobases by various enzymes before being absorbed in the intestine [335, 336].

Immunolocalization studies in rat intestine have shown that the pyrimidine-nucleoside selective rCNT1 is located in the brush-border membranes of epithelial cells [141]. The expression of various CNT mRNAs in intestine [2, 132, 133] and the capacity of CNT proteins to transport nucleosides with high-affinity (see Chapter IV, [2, 53, 132, 133]) suggest that these transporters may play an important role in nucleoside salvage in the intestine. Perhaps more importantly, they may also be potential targets for improving the absorption of nucleoside drugs across intestinal epithelia.

Enterocytes are the first cells to encounter preformed nucleosides and orally administered nucleoside drugs. As such, the presence of sodium-dependent nucleoside transporters at the plasma membrane of cells is important in the uptake process. Both hCNT2 and hCNT3 mRNAs have been detected in intestinal tissues [2, 132], although at varying levels in different regions of the

intestine. The naturally occurring *cif* process (i.e., hCNT2) has been observed in brush border membrane vesicles prepared from human intestine [196]. It is thought that hCNT1 and hCNT2 complement each other in the salvage of nucleosides from dietary sources and body fluids [140, 208], and recent evidence suggests that substrate availability modulates their expression in jejunum *in vivo* [317].

While there is a substantial amount of information pertaining to the mechanisms that underlie the regulation of other membrane transporters [7, 8], much less is known about the regulation of nucleoside transporters. Nucleoside uptake varies throughout the cell cycle [1], and as a result of cellular differentiation and other growth-related stimuli [2-6].

In hepatocytes, rCNT2 mRNA expression and nucleoside transport activity are highly regulated during cell-cycle progression and differentiation [9]. In murine bone marrow macrophages, the inhibition of cell proliferation by interferon-gamma results in selective down-regulation of ENT1 and a concurrent stimulation of CNT1 and CNT2 mRNA expression [205]. Differentiation of human promyelocytic leukemic HL-60 cells to monocyte/macrophage-like cells by exposure to phorbol esters [206, 207] is accompanied by an increase in sodium-dependent transport of both purine and pyrimidine nucleosides in conjunction with a decline in nucleoside uptake of the NBMPR-sensitive process [3, 199]. Quantitative Taqman RT-PCR analyses combined with nucleoside transport assays comparing parental and differentiated HL-60 cells have shown that cell differentiation results in a stimulation of hCNT3 mRNA levels that is

paralleled by augmentation of *cib*-type nucleoside transport activity ([2, 337]. In a few examples that have been studied, epithelial differentiation appears to ultimately lead to an increase in CNT-mediated nucleoside transport activity and a reduction in ENT-mediated transport, although there are likely cell- and tissue-specific differences.

The intestinal epithelium exhibits a high intrinsic requirement for nucleosides, and there is evidence that nucleosides stimulate the expression of brush border enzymes as well as promote epithelia cell proliferation and differentiation [336, 338]. It is speculated that intestinal cell proliferation and differentiation may be linked with regulatory changes in the subcellular distribution, abundance and transport activity of the concentrative nucleoside transporters.

Caco-2 cells, originally isolated from human colon adenocarcinoma, have been used as an *in vitro* model of human intestinal epithelia physiology as well as to predict intestinal absorption of drugs and chemicals in humans [339-342]. Caco-2 cells possess a capacity to differentiate spontaneously in culture over time and form polarized monolayers possessing intercellular tight junctions and microvilli commonly associated with enterocytes in human intestinal epithelia [247, 343, 344]. The levels of expression of a few endogenous transport proteins in Caco-2 cells have been shown to be upregulated as a function of increasing time in culture and differentiation status [345]. For example, the levels of mRNAs corresponding to several hexose transporters were increased

as Caco-2 cells progressed from exponential growth to stationary phase, in parallel with the differentiation status of the cells [345].

The results of chapter III (section III.2.1.3) demonstrated for the first time the presence of hCNT3 mRNA in Caco-2 cells. No expression of either hCNT1 or hCNT2 mRNAs was detected in Caco-2 cells. Although Ward *et al* also reported the lack of hCNT1 and hCNT2 transcripts in Caco-2 cells by RT-PCR analysis [269], identification of hCNT3 mRNA was not included in that study.

While both hCNT2 and hCNT3 likely play an important physiological role in nucleoside uptake across plasma membranes of epithelial cells in the intestine, their cellular locations have not been explored. To achieve the objective of the work in this chapter, ARAC/D2 T-lymphoblastoid leukemia cells stably transfected with hCNT2 cDNA were used to determine the cellular location of recombinant hCNT2. Both polyclonal and monoclonal antibodies against hCNT2 were employed in conjunction with various membrane markers to examine the location of recombinant hCNT2 by indirect immunofluorescence confocal microscopy.

The second objective examined the cellular location of native hCNT3 at various times during Caco-2 differentiation by immunofluorescence confocal microscopy using anti-hCNT3 antibodies and cellular markers for various organelles. The differentiation status of Caco-2 cells was assessed by monitoring transepithelial electrical resistance (TEER) [247, 343, 344]. The results revealed a different cellular location for native hCNT3 in non-differentiated (day 4) Caco-2 cells compared to the primarily plasma membrane

localization of recombinant hCNT2 in ARAC/D2 cells. The subcellular distribution of hCNT3 changed from a predominantly intracellular localization to the cell surface as Caco-2 cells progressed towards a more differentiated phenotype. The increased presence of hCNT3 in the plasma membrane in well-differentiated (day 18) Caco-2 cells was associated with an increase in hCNT3 abundance and transport activity detected at apical membranes of Caco-2 monolayers.

Examination of hCNT3 in different regions of the human gastrointestinal tract revealed higher hCNT3 protein levels in jejunum and duodenum, and lower levels in colon. These differences in hCNT3 abundance between the small and large intestine, suggest a role of hCNT3 in tissues primarily involved in nutrient and drug absorption.

The results of this work demonstrated for the first time the plasma membrane localization of recombinant hCNT2 in cells and explored the trafficking of native hCNT3 from intracellular sites to the cell surface during Caco-2 cellular differentiation into enterocyte-like cells.

VI.2. Results

VI.2.1. Localization of recombinant hCNT2 in stably transfected human T-lymphoblastoid cells

Immunoaffinity purified anti-hCNT2 polyclonal antibodies (hereafter referred to as anti-hCNT2 polyclonal antibodies) were characterized in immunoblot and immunofluorescence analysis in the results of Chapter V. These antibodies were employed in the work described in this chapter to determine the subcellular location of hCNT2 in the ARAC/D2 stable transfectants producing recombinant hCNT2 (see Chapter III). The host transporter-deficient cell line, CEM-ARAC, which was used in the generation of the stable transfectants, was employed as a control to assess specificity of the anti-hCNT2 polyclonal antibodies. ARAC/D2 and CEM-ARAC cells were grown on poly-L-lysine coated coverslips overnight and labeled with anti-hCNT2 polyclonal antibodies in the experiment of Figure VI-1. The results revealed primarily plasma membrane staining of ARAC/D2 cells (Panel A), whereas no significant immunofluorescence signal was detected in the host CEM-ARAC cells, which lacked hCNT2 (Panel C).

To more precisely define the location of hCNT2 in ARAC/D2 cells by using higher magnification, fewer cells were attached onto poly-L-lysine coated coverslips for analysis by indirect double-label immunofluorescence using Alexa Fluor 488 phalloidin to label F-actin and anti-hCNT2 polyclonal antibodies to label hCNT2 (Figure VI-2). The results showed hCNT2 localization at or near the

cell surface above the staining of actin filaments, which appeared to form a dense network beneath the cell surface typically observed with actin cytoskeleton.

Since CD3 (cluster differentiation) are accessory proteins located specifically at the cell surface of all T cells, monoclonal antibodies against CD3 were employed to detect CD3 on the surface of ARAC/D2 cells in double-labeling immunofluorescent experiment with anti-hCNT2 polyclonal antibodies. ARAC/D2 cells were derived from CEM cells, which originated from a patient with T-lymphocytic leukemia [75, 93, 214]. ARAC/D2 cells were attached to coverslips by a different method to that utilized in the experiment of Figure VI-2. They were cytocentrifuged onto coverslips in order to spread the cells slightly and allow better resolution of internal structures. Coverslips were double-labeled with anti-hCNT2 polyclonal antibodies and anti-CD3 FITC-conjugated monoclonal antibodies. The results of Figure VI-3 showed mainly cell surface staining by both anti-CD3 antibodies (Panel B) and anti-hCNT2 antibodies (Panel C), and the antibody-staining patterns demonstrated colocalization as shown in the superimposed image of Panel D.

The same antibody preparations against hCNT2 and CD3 were used to investigate the host transport-deficient CEM-ARAC cells in the experiment of Figure VI-4. The results showed no immunofluorescence when CEM-ARAC cells were stained with the anti-hCNT2 polyclonal antibodies, whereas the anti-CD3 FITC conjugated monoclonal antibodies labeled, as expected, immunoreactive materials at the cell surface. The results of this experiment

demonstrated the specificity of the anti-hCNT2 polyclonal antibodies against hCNT2 since reactivity was observed only in hCNT2-producing cells.

VI.2.2. Localization of hCNT3 during Caco-2 cellular differentiation

In the experiments described in Chapter III, northern blot and RT-PCR analyses identified transcripts corresponding to hENT1, hENT2 and hCNT3 in Caco-2 cells. No mRNAs corresponding to other CNT family members were detected in Caco-2 cells. Therefore, Caco-2 cells were employed in experiments described in this chapter as an *in vitro* model for studying native hCNT3 in relation to its intestinal epithelial function. Fluxes by the equilibrative nucleoside transporters were inhibited by incubation of cells with dilazep, which has been previously shown to potently inhibit hENT1- and hENT2-mediated processes [75, 108, 127]. While the expression profiles of nucleoside transporter mRNAs in Caco-2 cells may have been predictive of the transporter protein produced, they did not provide confirmation of transporter functionality.

VI.2.2.1. Functional characterization of nucleoside transporters present in Caco-2 cells

To determine the endogenous nucleoside transport activities present in Caco-2 cells, radioisotopic flux analyses were performed with ³H-uridine. Uridine was employed since it is a known permeant of the nucleoside transporters of human cells, and also exhibits important characteristics such as high solubility and stability in solution.

VI.2.2.1.1 Demonstration of hENT1-, hENT2- and hCNT3-mediated uptake into Caco-2 cells.

The uptake of 10 μM uridine into Caco-2 cells was measured in sodium-containing or sodium-free transport buffer using 200 μM dilazep, a concentration that was well in excess of that needed to completely block *es* and *ei* processes (i.e., hENT1- and hENT2-mediated transport, respectively) [246]. The results of Figure VI-5 revealed a low level of uridine uptake in the presence of dilazep that was linear over the time course examined, when uptake measurements were conducted in sodium-containing transport buffer. When uridine uptake was measured using similar transport conditions, with the exception of the removal of sodium from the transport buffer, the level of uptake was negligible (transport rate = 0.039 ± 0.002 pmol/mg protein) and similar to that observed for the control (uptake performed in sodium-containing transport buffer in the presence of excess uridine and dilazep, transport rate = 0.021 ± 0.009 pmol/mg protein). These results suggested the presence of a sodium-dependent transport process in Caco-2 cells, most likely mediated by hCNT3 since hCNT3 mRNA was the only CNT family member expressed (see Chapter III).

To determine whether Caco-2 cells exhibited functional hENT1- and hENT2-mediated transport activities, in addition to hCNT3-mediated activity, time courses similar to those described in Figure VI-5 were determined using shorter time intervals that were selected to remain in the linear portions of uptake time courses. Since there is a large difference (> 4 -log) in sensitivity to NBMPR among ENT processes [170, 171], NBMPR was used to distinguish between *es*

(hENT1) and *ei* (hENT2) functional activities. Transport studies were undertaken in the presence of a concentration (100 nM) of NBMPR known to completely inhibit the *es*-component of nucleoside uptake [75], thereby permitting measurement of uptake by the *ei* process. The uptake of 10 μ M uridine into Caco-2 cell monolayers was measured at different time intervals over a 120-sec time period as illustrated in Figure VI-6. The results revealed a component of NBMPR-insensitive uridine uptake that was greater than the uptake observed in the presence of dilazep or in the presence of dilazep plus excess nonradiolabeled uridine. The amount of uridine uptake in the presence of dilazep, which inhibited both the *es* and *ei* components of uridine uptake, was lower than the uptake observed in the presence of NBMPR, which inhibited the *es* component of uridine uptake. The combined results suggested that the *es* (hENT1-mediated) transport process accounted for most of the uridine uptake observed in Caco-2 cells, followed by the *ei* (hENT2-mediated) and then the *cib* (hCNT3-mediated) processes.

VI.2.2.2. *Growth properties and differentiation of Caco-2 cells*

Caco-2 cells differentiate spontaneously in culture over time. The change of Caco-2 cells from a non-differentiated to well-differentiated phenotype is associated with a progressive increase in TEER readings and a decrease in permeability of membrane impermeable substances [247, 343, 344]. To gain a better understanding of the differentiation process of Caco-2 cells over time in culture, the growth pattern and adoption of enterocyte-like characteristics were examined.

VI.2.2.2.1 Growth characteristics of Caco-2 cells

To examine the growth characteristics of the lab's Caco-2 cells, the experiment of Figure VI-7 was undertaken. Caco-2 cells were seeded onto collagen-coated flasks, and grown under the conditions that would be used throughout this study. The experiment of Figure VI-7 showed that the proliferation of Caco-2 cells began after a lag period of approximately three days and stationary phase was reached at approximately day 12. Visualization of Caco-2 cells by light microscopy during the phase of active growth (days 7-11) revealed that the cells grew as spheroid-like clusters of well outlined polygonal cells similar to those described in Madine-Darby canine kidney (MDCK) cultures, a model cell type for kidney epithelia. Cell densities reached a maximum at day 12, and remained relatively constant thereafter until the end of the time period of analysis on day 21. The morphological appearance of Caco-2 cells visualized by light microscopy did not appear to change during stationary phase (days 12-21). Trypan blue dye exclusion, which was performed on day 22, indicated that the majority of the cells ($\geq 98\%$) were viable since they were able to exclude the dye, indicating that the integrity of plasma membranes was intact.

VI.2.2.2.2 Transepithelial electrical resistance (TEER): assessment of differentiation status in Caco-2 cells

To assess whether Caco-2 cells adopted characteristics of small intestinal epithelial cells during differentiation in culture over time, the formation of intercellular tight junctions was evaluated by measuring the transepithelial electrical resistance (TEER) as shown in Figure VI-8. TEER values across

collagen-coated membrane inserts without cells ranged between 33-48 ohm-cm². Tests on non-collagen coated membrane inserts indicated that the electrical resistance due to the collagen layer was 7.0-8.8 ohm-cm². For the first four days following the seeding of Caco-2 cells, TEER values were 68 ± 3 ohm-cm², which was only slightly higher than background values observed in the absence of cells. After day 5, the TEER values increased gradually and reached a maximum of 283 ± 4 ohm-cm² on day 18, which was indicative of the presence of intercellular tight junctions and polarization of Caco-2 cells [247, 344]. The maximum TEER readings for day-18 Caco-2 cells were similar, and in some cases higher, than those reported elsewhere for Caco-2 cells [247], indicating that cultures had achieved a well-differentiated phenotype, as reported by others [247, 343, 346]. Constant TEER readings were achieved thereafter until the end of the time period of analysis on day 23, suggesting that the membrane barrier produced by the Caco-2 monolayers was intact during stationary phase.

VI.2.2.3. Localization of endogenous hCNT3 at different times during Caco-2 differentiation

The detection of native hCNT3 in Caco-2 cells was examined by indirect immunofluorescence confocal microscopy with multiple antibodies against hCNT3 and various commercial organellar markers. The specificity of the anti-hCNT3 antibodies was demonstrated using recombinant hCNT3 and hCNT3-GFP proteins produced in HeLa cells (described in Chapter V, section V2.2.4). Initially, the fluorophore-conjugated secondary antibodies were assessed for cross-reactivity in Caco-2 cells. Caco-2 cells were grown on collagen-coated

inserts for 18 days and were stained with Alexa Fluoro 594 conjugated goat anti-mouse secondary antibodies alone in the absence of anti-hCNT3 antibodies. The results of Figure VI-9 showed no immunofluorescent signal when Caco-2 cells were stained with the fluorophore-conjugated secondary antibodies alone.

The cellular location of endogenous hCNT3 was determined in day-4 Caco-2 cell cultures as shown in Figure VI-10. Caco-2 cells were grown on collagen-coated inserts for four days, and the TEER values obtained were 67 ± 2 ohm-cm², indicative of the non-differentiated status of the Caco-2 cells [247, 344]. Caco-2 cells were fixed, permeabilized and stained with anti-hCNT3 monoclonal antibodies (detected with fluorophore-conjugated secondary antibodies) directed against an intracellular epitope TL3360 (described in Chapter V) of hCNT3. The nucleus and endoplasmic reticulum were visualized, respectively, with the use of a DNA-intercalating agent DAPI (4',6-diamidino-2-phenylindole, Panel A) and a endoplasmic reticulum dye DIOC5 (3',3'-dipentylloxacarbocyanine iodide, Panel B). The results showed immunoreactive staining close to the nucleus of Caco-2 cells by the anti-hCNT3 antibodies (Panel C), and the staining pattern resembled that of endoplasmic reticulum localization (Panel B). The superimposed image of immunofluorescent signals exhibited by the different fluorochromes demonstrated colocalization of hCNT3 and endoplasmic reticulum immunofluorescent signals as shown by the yellow staining obtained in Panel D, suggesting that hCNT3 was predominately located at or near the endoplasmic reticulum. No overlap of immunofluorescent staining of hCNT3 and the cell nucleus was apparent.

The subcellular location of hCNT3 was further examined in more highly differentiated Caco-2 cells in the experiment of Figure VI-11. Caco-2 cells, which were grown on collagen-coated inserts for 11 days exhibited TEER values of $213 \pm 1 \text{ ohm}\cdot\text{cm}^2$. The cells were doubly stained with the anti-hCNT3 monoclonal and polyclonal antibodies that were directed against different epitopes of hCNT3. The nucleus and the endoplasmic reticulum were visualized by labeling Caco-2 cells with DAPI (Panel A) and DIOC5 (Panel B), respectively. The staining by the monoclonal and polyclonal antibodies (detected with fluorophore-conjugated secondary antibodies), which were raised against different epitopes of hCNT3, was mainly at or near cell surfaces and the staining patterns were strikingly similar (Panels C and D). The abundant intracellular staining that was apparent in day 4 Caco-2 cell cultures (Figure VI-10) was absent in day 11 Caco-2 cultures (Figure VI-11). The superimposed image of all immunofluorescent signals of Panels A, B, C and D revealed that the staining patterns of the nuclear, endoplasmic reticulum and hCNT3 probes were distinct from one another (Panel E). There was little, if any, colocalization of staining by the anti-hCNT3 antibody preparations with that by the endoplasmic reticulum marker (Panel E).

To further examine changes in distribution of hCNT3 from intracellular sites to mainly cell surface sites during the differentiation process, Caco-2 cell cultures were analyzed at day 15 in a similar manner as described in Figure VI-11. In the experiment of Figure VI-12, Caco-2 cells were stained with anti-hCNT3 (TL3360) monoclonal antibodies, followed by labeling with DAPI (nuclear

marker) and DIOC5 (endoplasmic reticulum marker). The results revealed immunoreactive labeling mainly at or near cell surfaces by the anti-hCNT3 antibodies (Panel C), and the staining patterns resembled that observed in Figure VI-11, which showed the predominance of hCNT3 proteins at or near cell surfaces. The superimposed image in Panel D (Figure VI-12) showed distinct staining patterns exhibited by the anti-hCNT3 antibodies, DAPI and DIOC5. There was little or no overlap of the different fluorescent signals.

Lastly, the cellular location of hCNT3 was examined in day-18 (well-differentiated) Caco-2 cultures by employing similar experimental procedures to those described for Figures VI-10 to VI-12. The TEER values for day-18 cultures were $283 \pm 3 \text{ ohm}\cdot\text{cm}^2$, which were consistent with TEER readings associated with fully differentiated epithelial cells [247, 344]. The results of the experiment of Figure VI-13 revealed staining by the anti-hCNT3 antibodies of mainly cell surfaces (Panel C). The antibody-staining patterns at the cell surface in some areas were punctate, and in a few areas appeared to localize to distinct regions of the cell surface. The superimposed images showed little or no colocalization of fluorescent staining of the anti-hCNT3 antibodies with organellar markers for the endoplasmic reticulum or the nucleus (Panel D).

VI.2.2.4. Abundance of hCNT3 in plasma membranes at different times during Caco-2 differentiation

To ascertain whether the changes observed in the distribution of native hCNT3 between intracellular sites and cell surfaces during differentiation of Caco-2 cultures was associated with an increase in protein abundance at the

plasma membrane, the experiment of Figure VI-14 was undertaken. Enriched plasma membranes prepared from Caco-2 cells at different times (days 4, 11 and 18) were subjected to immunoblot analysis with anti-hCNT3 antibodies. The experiments of Figure VI-14 showed the presence of immunoreactive bands with apparent molecular weights between 75 and 80 kDa corresponding to hCNT3 in the day-4, day-11 and day-18 enriched plasma membrane preparations from Caco-2 cells. Although similar immunoreactivities with anti-hCNT3 antibodies were observed in membrane preparations from the day-4 and day-11 Caco-2 cultures, a much greater signal intensity was evident in the immunoreactive band from day-18 cultures. This result indicated an increased abundance of hCNT3 in plasma membranes in well-differentiated Caco-2 cells.

VI.2.2.5. Stimulation of hCNT3-mediated uridine transport activities detected at the apical membrane of Caco-2 cells over time in culture

It has recently been shown by immunofluorescence imaging of fluorescently-tagged hCNT1 fusion proteins produced by stable transfection in MDCK canine kidney cells that recombinant hCNT1 primarily distributed to the apical membrane [204]. The experiment of Figure VI-15 was undertaken to determine if the increase in protein abundance in enriched plasma membranes of Caco-2 cells (Figure VI-14) was linked with a stimulation of functional nucleoside transport activities detectable at apical membranes. Prior to transport measurements, Caco-2 monolayers were subjected to TEER readings to assess differentiation status. The 4- and 11-day Caco-2 cultures exhibited TEER values of $77 \pm 3 \text{ ohm}\cdot\text{cm}^2$ and $213 \pm 4 \text{ ohm}\cdot\text{cm}^2$, respectively, whereas the day-18

cultures exhibited TEER values of $281 \pm 2 \text{ ohm}\cdot\text{cm}^2$. The uptake of $10 \mu\text{M } ^3\text{H}$ -uridine across the apical (upper) compartment of Caco-2 cultures grown on collagen-coated transwell inserts was measured in sodium-containing transport buffer at various times during the differentiation process (Figure VI-15). The results showed that the day-4 (non-differentiated) cultures exhibited similar uptake rates to those observed for the non-mediated component of uptake in day-18 cultures. A large stimulation of uridine uptake was evident in day-18 (well-differentiated) cultures and a lesser stimulation was observed in day-11 (moderately-differentiated) cultures.

VI.2.3. Relative abundance of hCNT3 protein in the gastrointestinal tract

The presence of hCNT3 protein and functional activity in colon-derived Caco-2 cancer cells led to the speculation that hCNT3 may also be present in human colon as well as other regions of intestine. Membranes were prepared from biopsied tissues from different regions of the small and large intestine, and from day 18 (well-differentiated) Caco-2 cells as described in Materials and Methods (sections II.17.2 and II.17.4). Equal quantities of protein were electrophoresed through a 10% SDS-polyacrylamide gel, transferred to a PVDF membrane and subjected to immunoblotting with anti-hCNT3 antibodies. The results presented in Figure VI-16 showed immunoreactive species that migrated with apparent molecular weights between 75 and 80 kDa in all samples analyzed. The hCNT3 protein abundance varied between the small and large intestine, with relatively higher hCNT3 levels detected in jejunum and duodenum

than in colon. A greater abundance of hCNT3 protein was also evident in well-differentiated day 18 Caco-2 cells than in colon.

VI.3. Discussion

Intestinal epithelial cells are important in absorption of dietary nucleosides, and nucleoside transport systems in intestinal-cell plasma membranes may be involved in the movement of nucleosides and nucleoside drugs from the intestinal lumen into the blood. In rat jejunum, rCNT1 was found specifically in the brush-border membranes of absorptive epithelial cells [141]. This location of rCNT1 was consistent with functional activity measurements that demonstrated both *cit*- and *cif*-type sodium-dependent processes in rat and human intestinal brush-border membranes [196, 347]. In contrast, nucleoside transport across basolateral membranes of epithelial cells of rabbit jejunum lacked sodium dependency, suggesting the absence of CNT-mediated processes and the presence of ENT-mediated processes in basolateral membranes [190]. Localization studies using GFP-tagged rat CNT1 and CNT2 proteins revealed that both proteins are present in apical membranes of renal epithelial Madin-Darby canine kidney (MDCK) cells [203]. The cellular locations of recombinant hCNT1 and hENT1 produced as fluorescently-labeled fusion proteins in MDCK cells were determined recently using immunofluorescence confocal microscopy, and the results showed that hCNT1 localized to apical membranes, and hENT1 localized to basolateral membranes [204].

It may be possible to exploit nucleoside transporters for enhancing absorption of orally administered drugs in the treatment of certain diseases.

However, the distribution of the various nucleoside transporters in the GI tract and their cellular locations need to be determined before their exploitation in nucleoside drug delivery can be realized. The study of nucleoside transporters in intestine has been difficult because of the fragility and limited viability of intestinal enterocytes. One model system that is considered to closely represent human intestinal epithelia is the human colon adenocarcinoma Caco-2 cell line [343, 348-350]. Caco-2 cells form monolayers of differentiated epithelia cells over time in culture and exhibit characteristics typical of intestinal enterocytes such as development of cellular polarization and intercellular tight junctions [247, 343, 344]. Numerous transport proteins studied in Caco-2 cells exhibit similar kinetic parameters as those observed for the naturally occurring transporters in membrane vesicles isolated from human intestine [340], suggesting that the transporters in both experimental systems are functionally similar.

Characterization of the nucleoside transporters present in Caco-2 cells revealed the presence of hCNT3 transcripts (see Chapter III, section III.2.1.3) as well as hCNT3 activity. No other CNT family members were detected in Caco-2 cells, although hCNT1- and hCNT2-mediated activities have been reported in human intestine [172, 196]. The absence of hCNT1 and hCNT2 in Caco-2 cells may have been due to the colonic origin of the Caco-2 cell line. Indeed, CNT1 mRNA was expressed in different regions of the rat small intestine including jejunum, ileum and duodenum at varying levels [63, 181], but not in rat colon [181]. Establishing that Caco-2 cells possessed endogenous hCNT3 at levels

appropriate for examining transport kinetics enabled further studies of this important CNT family member.

Localization experiments examined the subcellular locations of recombinant hCNT2 and native hCNT3 in, respectively, stably transfected leukemia cells and cultured Caco-2 cells. The ARAC/D2 T-lymphoblastic leukemia cells, which were derived from transport-deficient CEM-ARAC cells, were characterized in Chapter III and produced recombinant hCNT2 in isolation. Caco-2 cells were characterized in the present chapter and possessed endogenous hCNT3.

Recombinant hCNT2 was found primarily at or near cell surfaces of ARAC/D2 cells and the hCNT2-staining pattern colocalized with the T-cell specific cell surface marker. Staining the cells with phalloidin-conjugated Alexa Fluor 488, which binds F-actin, suggested that the location of recombinant hCNT2 was mostly in plasma membranes, above the actin cytoskeleton network.

The cellular location of native hCNT3 differed in non-differentiated and differentiated Caco-2 cells. Using two different antibodies, each against a different epitope of hCNT3, revealed that hCNT3 was localized mainly to intracellular sites in non-differentiated day-4 Caco-2 cells. The intracellular localization of anti-hCNT3 antibody staining corresponded with that of an endoplasmic reticulum marker, suggesting that hCNT3 was at, or close, to the endoplasmic reticulum. A reduction in intracellular staining with anti-hCNT3 antibodies was apparent in day-11 Caco-2 cultures, and predominantly cell

surface staining with anti-hCNT3 antibodies was maintained thereafter as Caco-2 cells became more differentiated.

It has been shown that hCNT3 mRNA expression and hCNT3-mediated nucleoside transport activity increases upon differentiation of human promyelocytic leukemia HL-60 cells into adherent monocyte/macrophage-like cells by treatment of phorbol esters [2, 3, 199]. A similar phenomenon was observed in the current study, in which the abundance of endogenous hCNT3 in plasma membrane-enriched preparations from well-differentiated day-18 Caco-2 cultures was substantially higher than that in preparations from day-4 cultures. The increase in hCNT3 abundance in plasma membranes in day-18 Caco-2 cultures was accompanied by a 4-fold increase in hCNT3-mediated nucleoside transport activity in apical membranes of Caco-2 cells. This result was consistent with results of an independent investigation that demonstrated a 5-fold increase in mRNA levels in differentiated Caco-2 cells over that in non-differentiated cells by quantitative Taqman RT-PCR [337]. No measurable hCNT3-mediated nucleoside transport activity was detected in apical membranes of non-differentiated day-4 Caco-2 cultures, whereas hCNT3-mediated activity was detected, albeit at a low level, in day-11 cultures. The presence of hCNT3-mediated activity in apical membranes of well-differentiated Caco-2 epithelial cells was consistent with previous work with hCNT1-cyan fluorescence fusion protein produced in canine MDCK kidney epithelial cells, which showed recombinant hCNT1 in apical membranes in differentiated MDCK cells [204].

While this was the first demonstration of regulated hCNT3 trafficking from intracellular sites, possibly the endoplasmic reticulum, to plasma membranes, with alterations in hCNT3 protein content and transport activities, membrane trafficking of other transporters has been well documented. The classical example is the recruitment of the facilitated glucose transporter, GLUT4, from intracellular compartments to cell surfaces in response to insulin, resulting in increased sugar transport capacity [351, 352]. There is also some evidence that N-glycosylation is important in the functional activity and trafficking of membrane transporters to cell surfaces [353], but it is not known if this applies to the CNTs. The pyrimidine-nucleoside selective CNT1 of rats has been shown to be glycosylated at the carboxyl terminus [141] and it is expected that other CNT family members are also glycoproteins since they possessed consensus sequences for N-linked glycosylation at their carboxyl-termini. Loss of N-linked glycosylation capability in hENT1 did not appear to affect its transport activity, although the binding characteristics of the transporter for NBMPR, dilazep and dipyridamole were substantially altered [270].

Protein kinase C has also been implicated in the regulation of nucleoside transport activities as shown by the phorbol 12-myristate 13-acetate (PMA)-dependent reduction in equilibrative NBMPR-sensitive transport activity in HL-60 cells induced to differentiate [3, 199]. Stimulation of protein kinase C activity has been shown to produce an increase in hENT1-mediated nucleoside transport activity in cultured cervical cancer HeLa and breast cancer MCF7 cell lines [354]. The CNT family members, hCNT2 and hCNT3, possess consensus sites for

phosphorylation by protein kinase C, but whether or not these proteins are regulated by phosphorylation has not been determined. Caco-2 cells would be well-suited for studies examining the regulation of hCNT3 by protein kinase C.

The colonic origin of Caco-2 cells leads to the speculation that hCNT3 may also be present in tissues of the human gastrointestinal tract. The level of hCNT3 abundance varied greatly between regions of the small and large intestine, which is consistent with variations of hCNT3 transcripts observed in different regions of the intestine [2]. Relatively higher hCNT3 protein levels were present in jejunum and duodenum in comparison to colon, suggesting that hCNT3 is more abundant in tissues that are involved in nutrient absorption. hCNT3 may, therefore, be important as a mediator of nutrient and drug absorption in the intestine. Caco-2 cells will be a useful *in vitro* model of human intestinal epithelia for further studies of the regulation of hCNT3 in nucleoside utilization in the intestine.

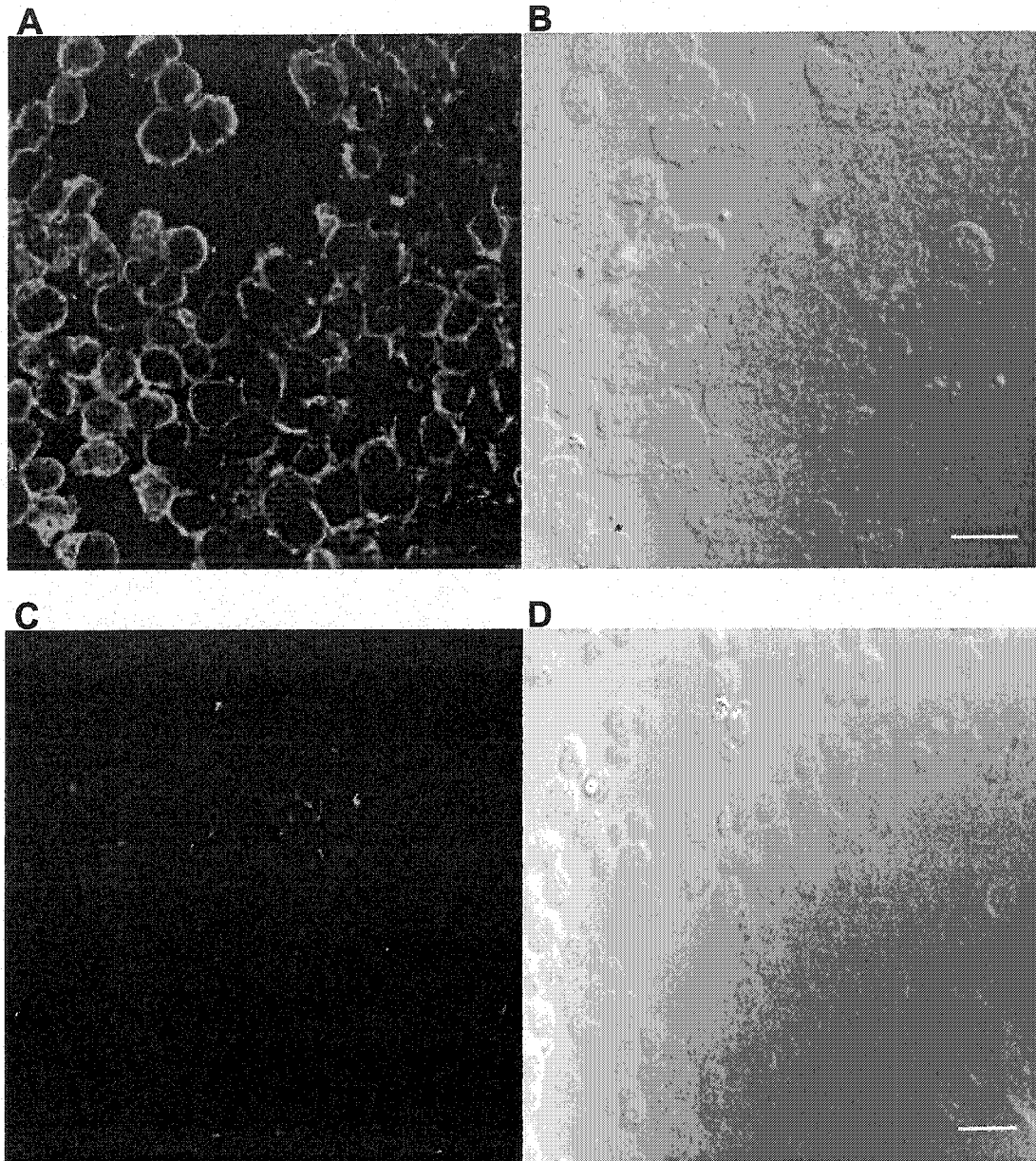


Figure VI-1. Anti-hCNT2 antibodies with reactivity of plasma membranes of hCNT2-producing ARAC/D2 cells but not of transporter-deficient CEM-ARAC cells

ARAC/D2 (Panels A, B) and CEM-ARAC (Panels C, D) cells were grown on poly-L-lysine-coated coverslips overnight as described in section II.22. Coverslips were fixed, permeabilized in methanol for 5 min, incubated with anti-hCNT2 polyclonal antibodies, followed with Alexa Fluoro 488 conjugated goat anti-rabbit antibodies, and mounted on slides in 90% glycerol. Slides were visualized by LSM-510 confocal microscopy as described in section II.22. Shown are immunofluorescence (Panels A, C) and differential interference contrast (Panels B, D) images. *Bar*, 15 μm .

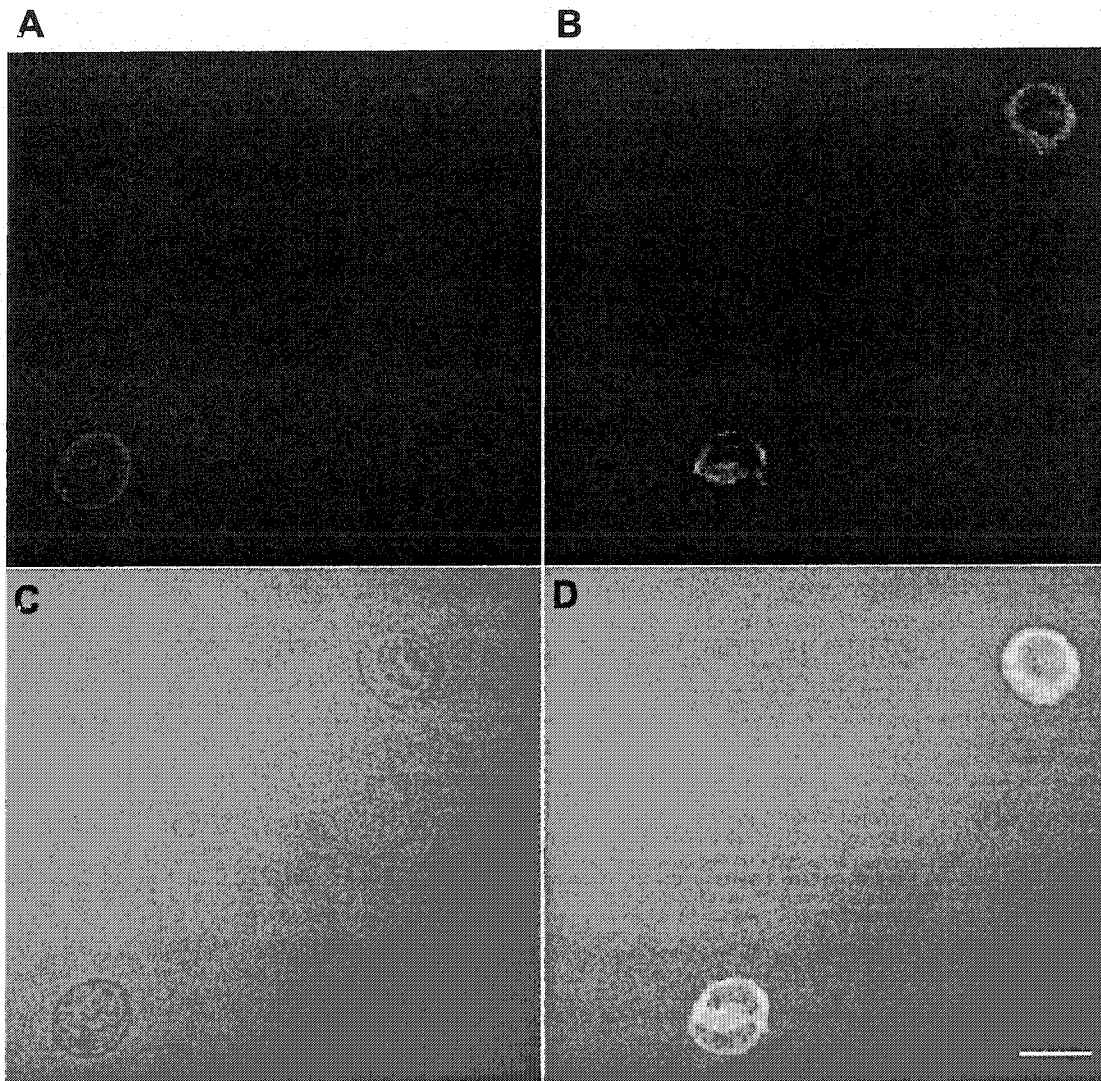


Figure VI-2. Localization of hCNT2 to the cell surface above the actin cytoskeleton in hCNT2-producing ARAC/D2 cells

ARAC/D2 cells were grown on poly-L-lysine-coated coverslips overnight as described in section II.22. Coverslips were fixed, permeabilized in methanol for 5 min, incubated with anti-hCNT2 polyclonal antibodies and Alexa Fluor 488 phalloidin, followed with Alexa Fluor 594 conjugated goat anti-rabbit antibodies, and mounted on slides in 90% glycerol. Slides were visualized by LSM-510 confocal microscopy as described in section II.22. Shown are fluorescence staining of hCNT2 (Panel A), F-actin (Panel B), differential interference contrast (Panel C) and merged (Panel D) images. *Bar*, 15 μm .

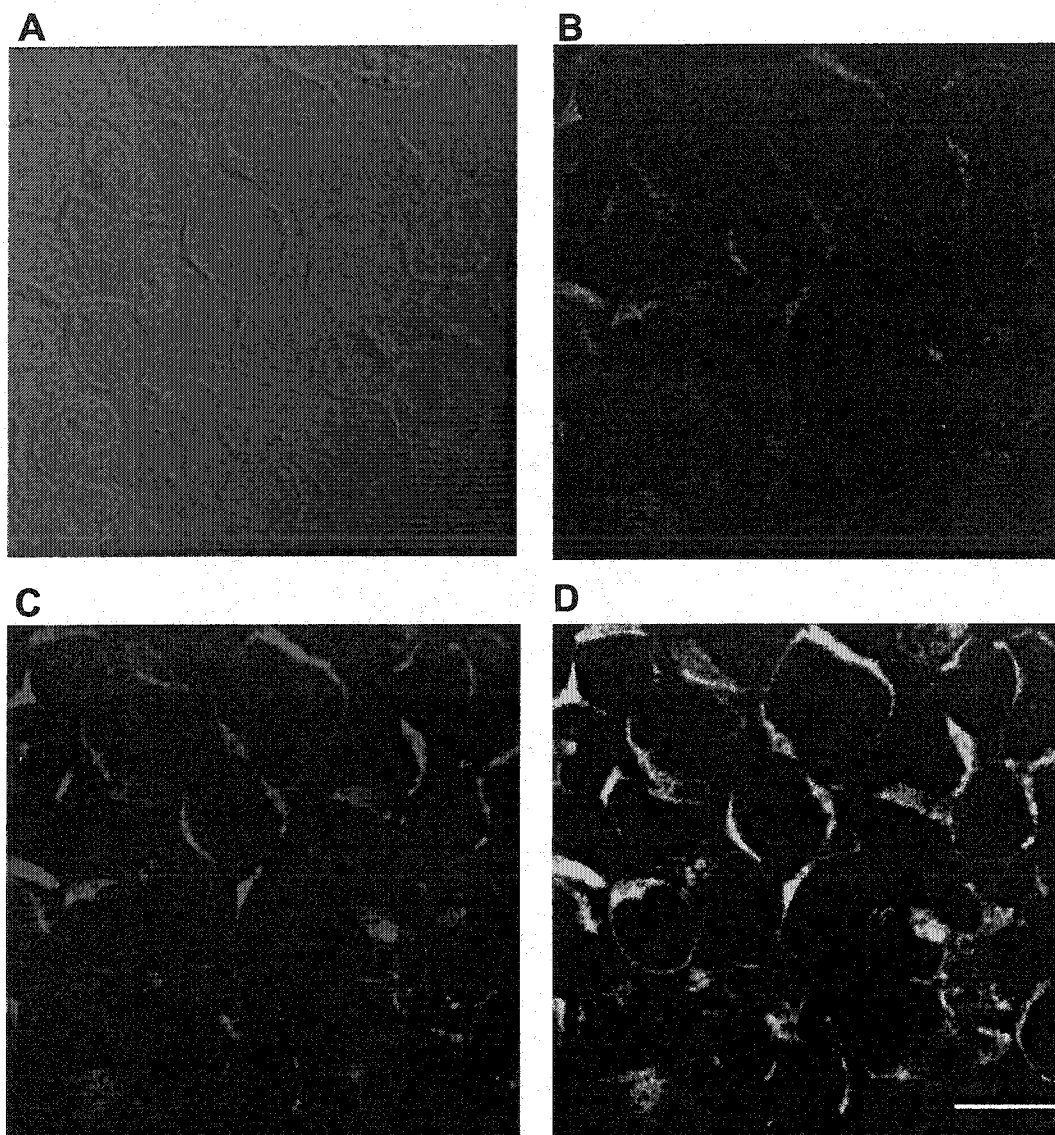


Figure VI-3. Colocalization of hCNT2 staining with the T-cell specific CD3 cell surface marker

ARAC/D2 cells were cytocentrifuged onto coverslips. Coverslips were fixed, permeabilized in methanol for 5 min, incubated with anti-hCNT2 polyclonal antibodies and with anti-CD3 conjugated FITC antibodies, followed with Alexa Fluoro 594 conjugated goat anti-rabbit antibodies, and mounted on slides in 90% glycerol. Slides were visualized by LSM-510 confocal microscopy as described in section II.22. Shown are differential interference contrast (Panel A) and immunofluorescence staining of CD3 (Panel B), hCNT2 (Panel C) and merged (Panel D) images. *Bar*, 15 μm .

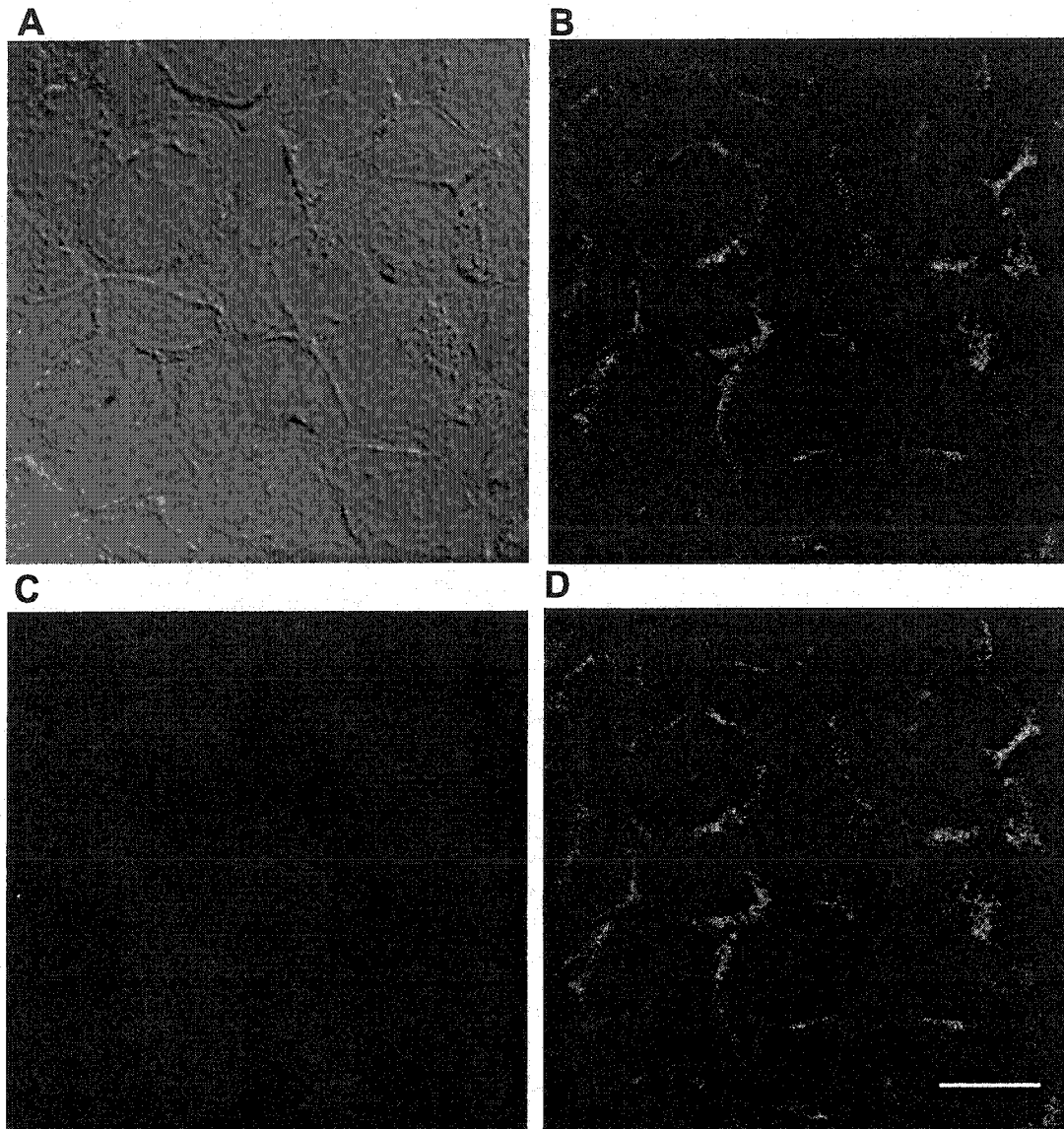


Figure VI-4. The absence of immunostaining of hCNT2 in transporter-deficient CEM-ARAC cells

CEM-ARAC cells were cytocentrifuged onto glass coverslips. Coverslips were fixed, permeabilized in methanol for 5 min, incubated with anti-hCNT2 polyclonal antibodies and with anti-CD3 FITC conjugated antibodies, followed with Alexa Fluoro 594 conjugated goat anti-rabbit antibodies, and mounted on slides in 90% glycerol. Slides were visualized by LSM-510 confocal microscopy as described in section II.22. Shown are differential interference contrast (Panel A) and immunofluorescence staining of CD3 (Panel B), hCNT2 (Panel C) and merged (Panel D) images. *Bar*, 15 μm .

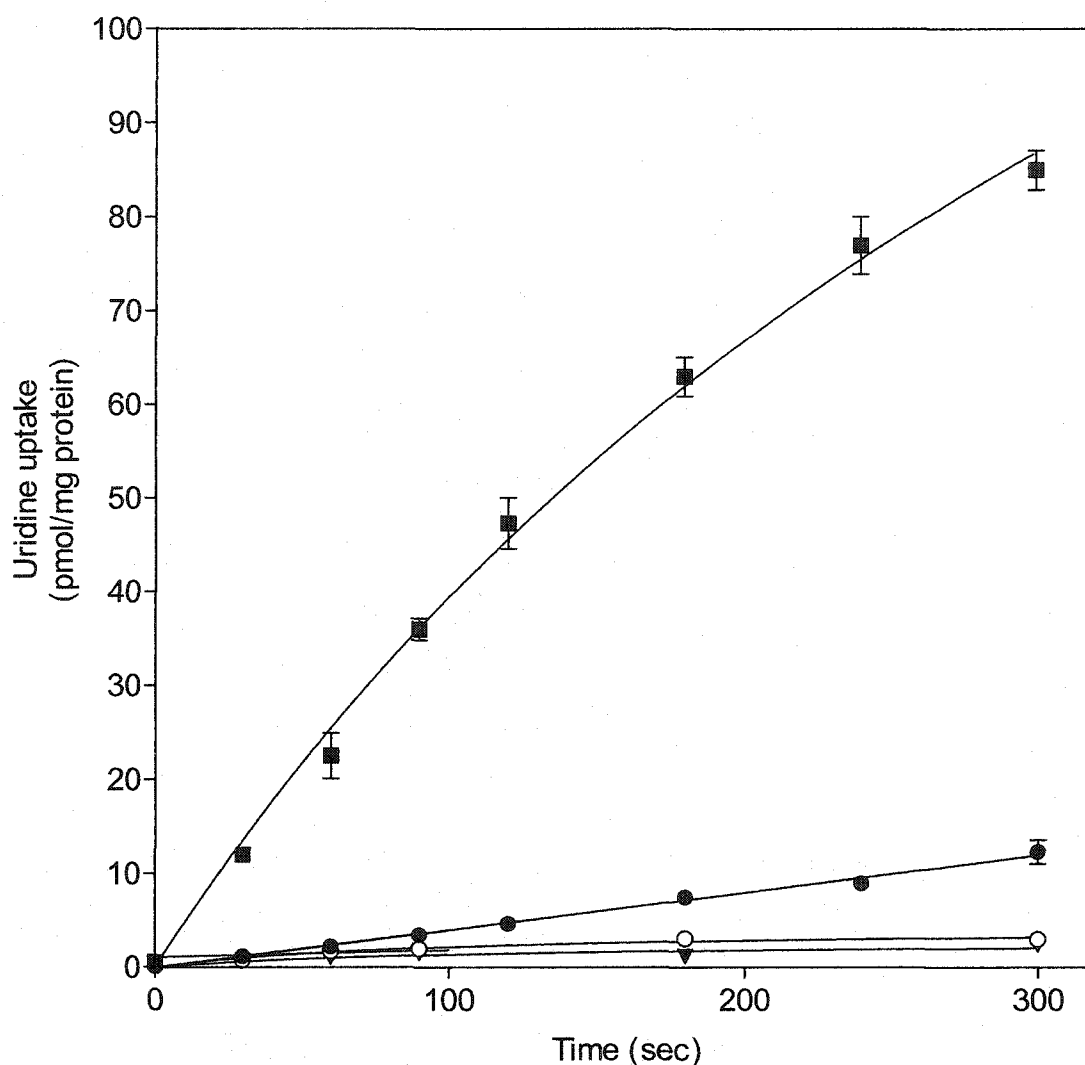


Figure VI-5. Time course of uridine uptake by Caco-2 cells in the presence and absence of sodium

Caco-2 cells were cultured on collagen-coated plates for 18 days as described in section II.10.2. Uptake of $10 \mu\text{M}$ ^3H -uridine into Caco-2 cells (as described in section II.16) was measured in sodium-free (open symbols) or sodium-containing (closed symbols) transport buffer in the absence of additives (■) or in the presence of $200 \mu\text{M}$ dilazep (●,○), or $200 \mu\text{M}$ dilazep plus excess 3 mM nonradioactive uridine (▼). Each value represents the mean \pm SD of triplicate determinations and error bars are not shown where SD values were smaller than that represented by the symbols. Shown is one of two independent experiments that yielded qualitatively similar results.

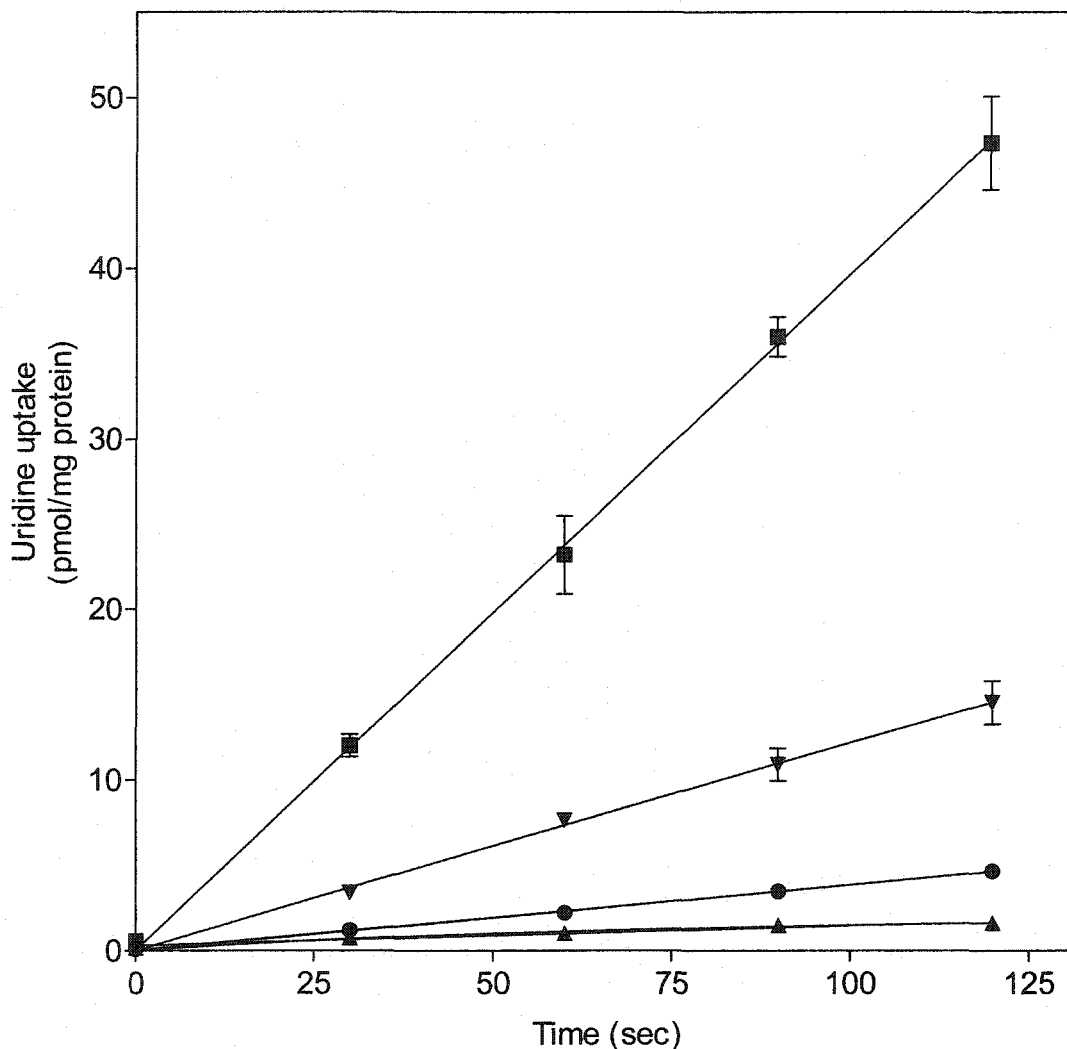


Figure VI-6. Inhibitory effects of dilazep and NBMPR on uridine uptake by Caco-2 cells

Caco-2 cells were cultured on collagen-coated plates for 18 days as described in section II.10.2. Uptake of $10 \mu\text{M}$ ^3H -uridine into Caco-2 cells (as described in section II.16) was performed in sodium-containing transport buffer in the absence of additives (■) or in the presence of $0.1 \mu\text{M}$ NBMPR (▼), $200 \mu\text{M}$ dilazep (●) or $200 \mu\text{M}$ dilazep plus 3mM uridine (▲). Each value represents the mean \pm SD of triplicate determinations and error bars are not shown where SD values were smaller than that represented by the symbols. Shown is one of two independent experiments that yielded qualitatively similar results.

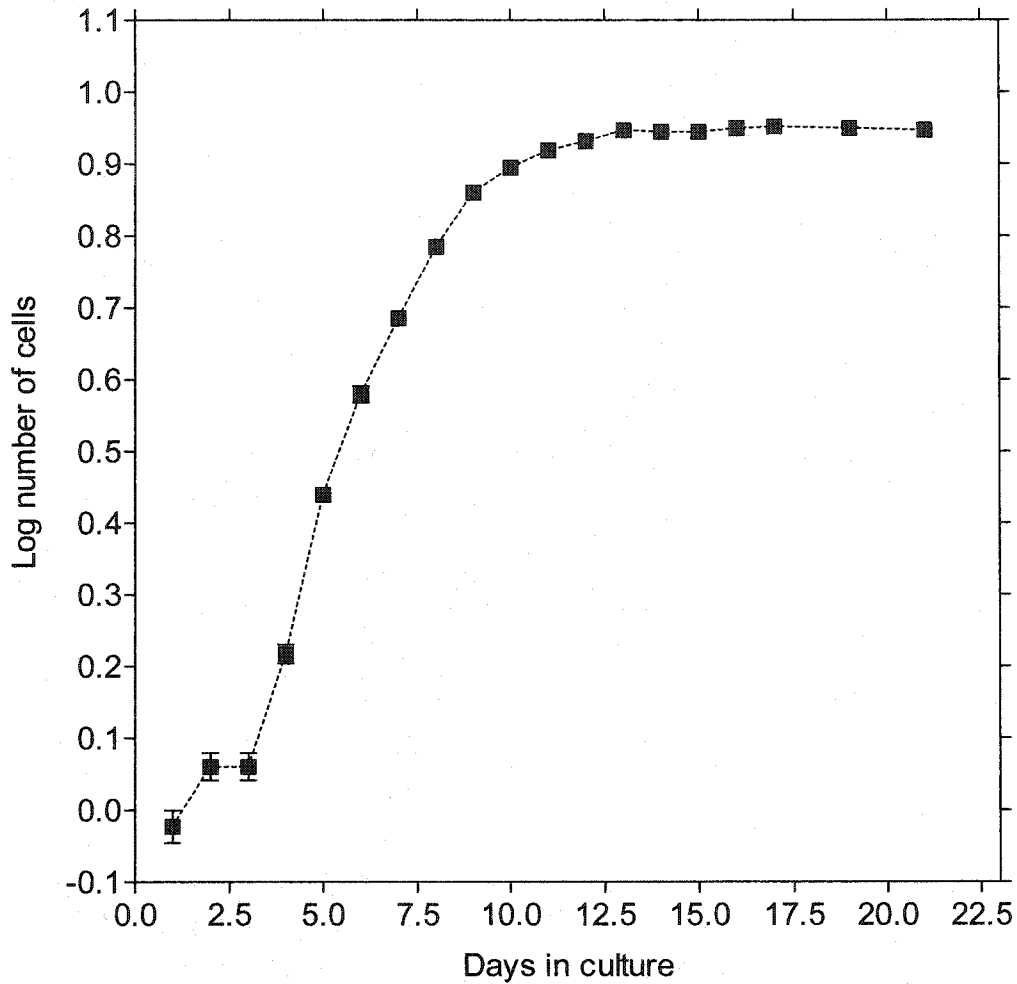


Figure VI-7. Growth curve of Caco-2 cells

Caco-2 cells were seeded onto collagen-coated flasks and grown for the period of time indicated as described in section II.10.2. Cells densities were determined by electronic particle counting and are expressed as the mean \pm SD of three determinations. Error bars are not shown where SD values were smaller than that represented by the symbols.

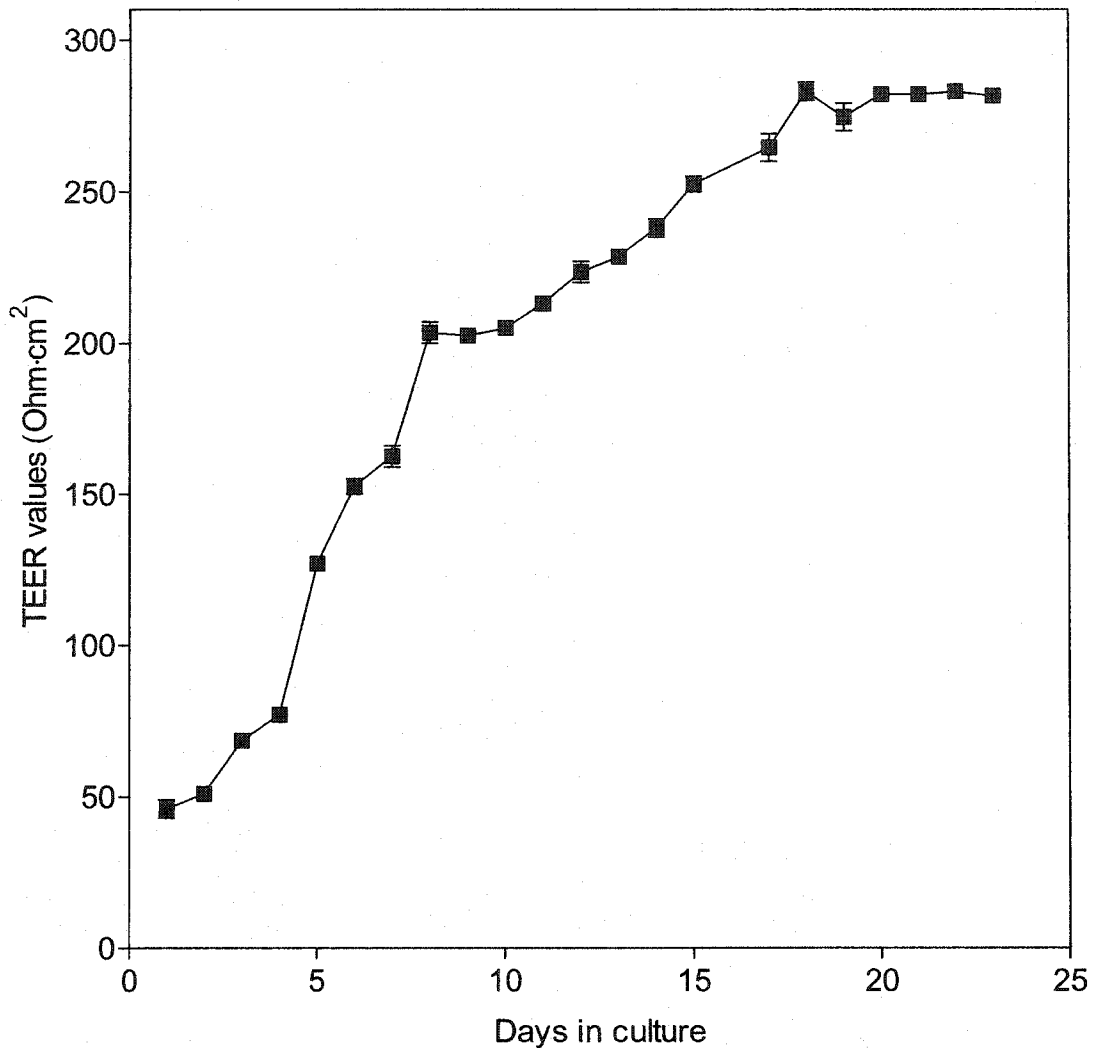


Figure VI-8. Transepithelial electrical resistance (TEER) values of Caco-2 cell monolayers cultured on collagen-coated polycarbonate inserts

Caco-2 cells were seeded onto collagen-coated inserts and grown for the period of time indicated, with media changes daily. TEER values of cell monolayers were measured daily as described in Materials and Methods (section II.14) using the Millicell-(ERS) Epithelial Resistance System. TEER values were calculated by multiplying the voltage changes by the surface area of the insert and then applying Ohm's law. The reported TEER values were corrected for background by subtraction of TEER values obtained in the absence of cells. Each value represents the mean \pm SD of 3 inserts and error bars are not shown where SD values were smaller than the size of the data symbols.

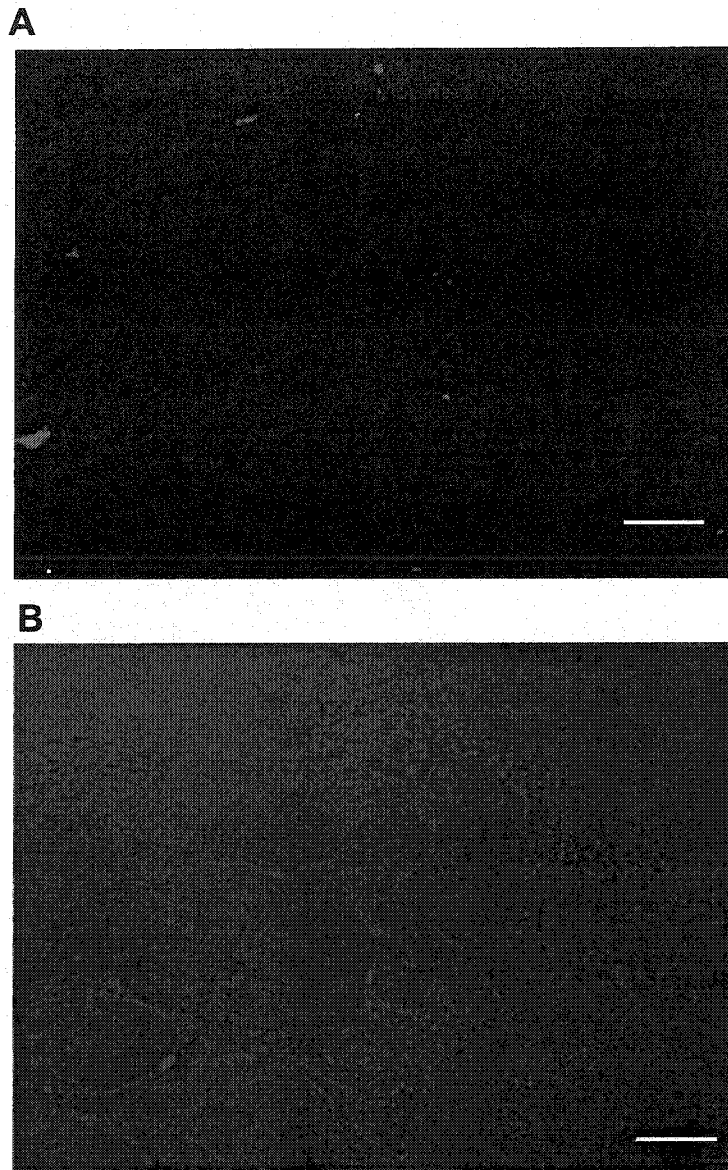


Figure VI-9. Absence of immunofluorescent signal in Caco-2 cells stained with secondary antibodies alone

Caco-2 cells were grown on collagen-coated inserts for 18 days as described in section II.10.2. Inserts were fixed in paraformaldehyde, permeabilized in Triton X-100, stained with Alexa Fluoro 594 conjugated goat anti-mouse secondary antibodies and mounted on slides in 90% glycerol. Slides were visualized by LSM-510 confocal microscopy as described in section II.22. Panel A shows immunofluorescence staining by the secondary antibodies alone (Panel A). Panel B shows the differential interference contrast image. *Bar*, 20 μm .

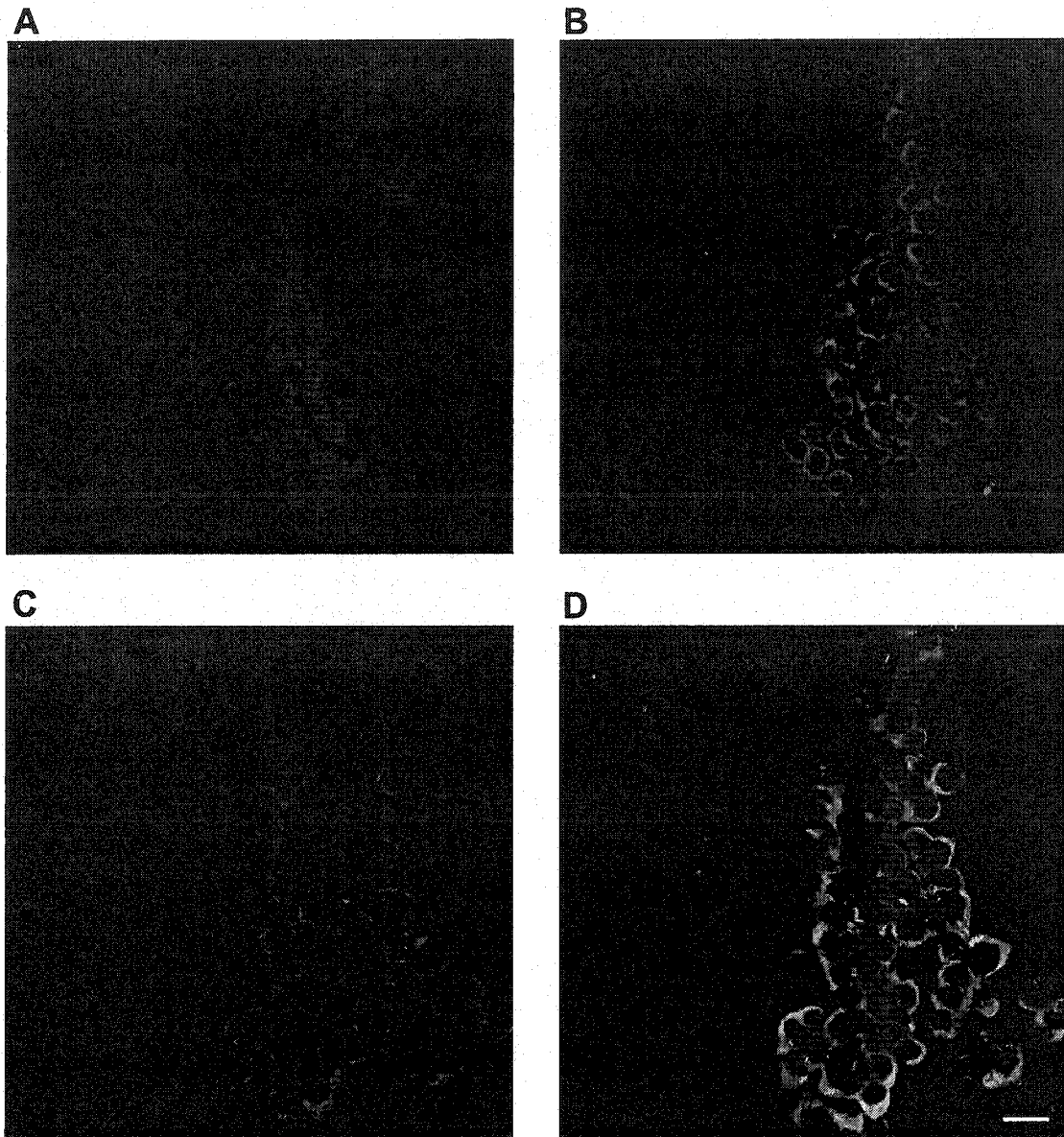
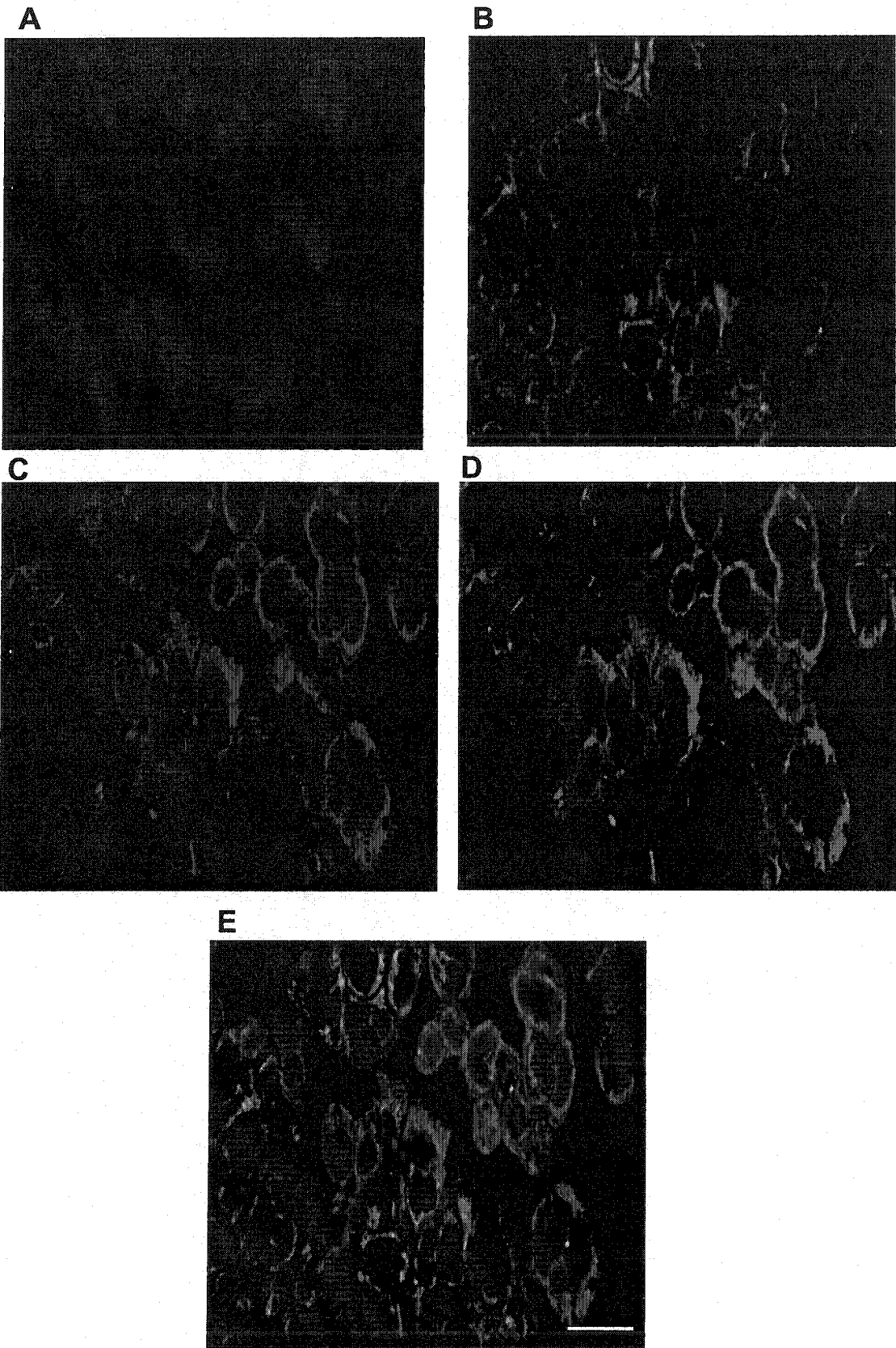


Figure VI-10. Localization of hCNT3 to the endoplasmic reticulum in day 4 Caco-2 cell cultures

Caco-2 cells were grown on collagen-coated inserts for 4 days as described in section II.10.2. Inserts were fixed in paraformaldehyde, permeabilized in Triton X-100, incubated with anti-hCNT3 monoclonal antibodies directed against epitope TL3360 of hCNT3, followed with Alexa Fluoro 594 conjugated goat anti-mouse antibodies, incubated with DAPI and DIOC5 and mounted on slides in 90% glycerol. Slides were visualized by LSM-510 confocal microscopy as described in section II.22. Shown are fluorescence staining by DAPI (Panel A), DIOC5 (Panel B) and anti-hCNT3 monoclonal antibodies (Panel C). The merged image is shown in Panel D. *Bar, 20 μ m.*



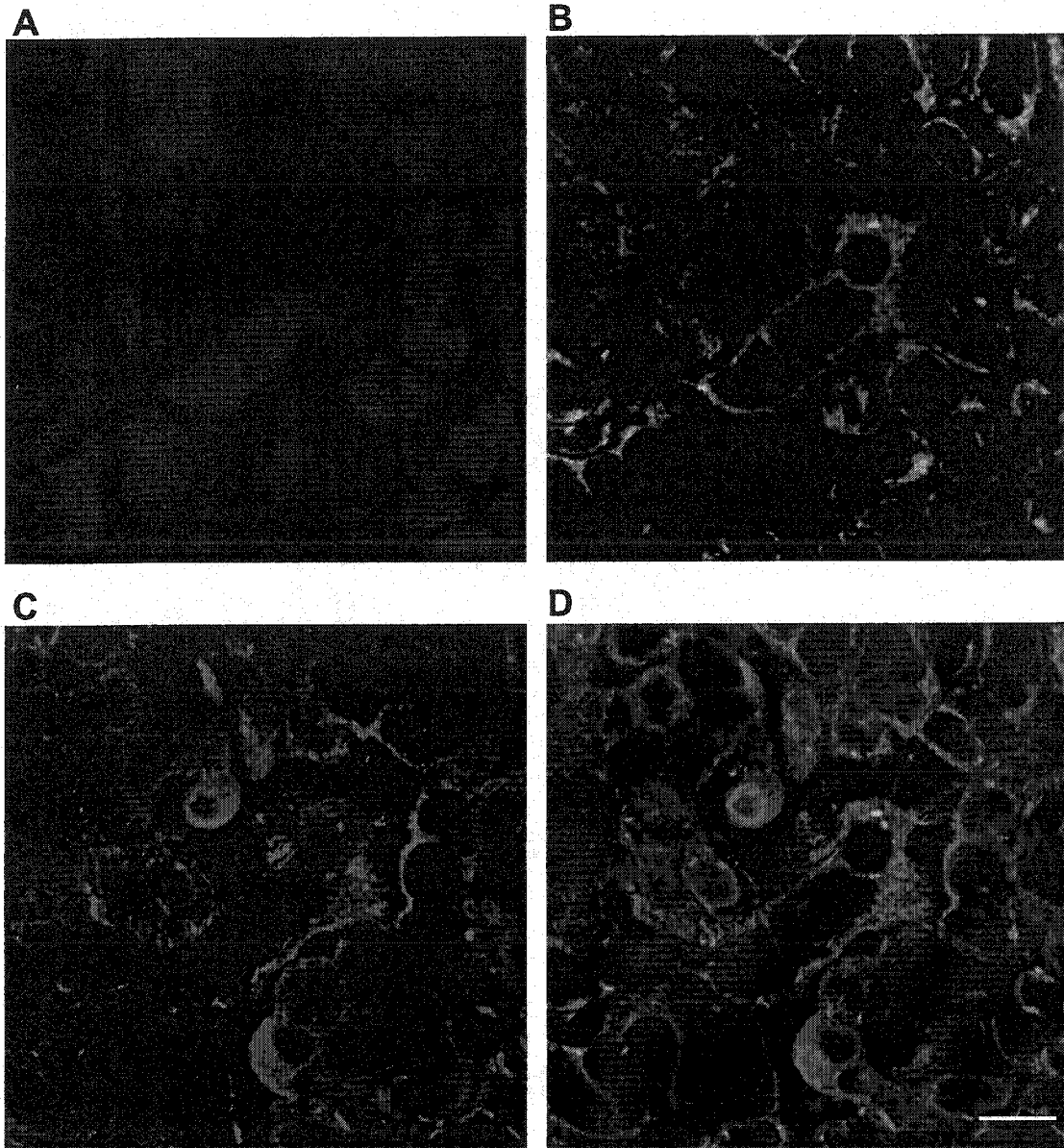


Figure VI-12. Cell surface localization of hCNT3 in day 15 Caco-2 cell cultures

Caco-2 cells were grown on collagen-coated inserts for 15 days as described in section II.10.2. Inserts were fixed in paraformaldehyde, permeabilized in Triton X-100, incubated with anti-hCNT3 monoclonal antibodies directed against epitope TL3360 of hCNT3, followed with Alexa Fluor 594 conjugated goat anti-mouse antibodies, and subsequently incubated with DAPI and DIOC5 and mounted on slides in 90% glycerol. Slides were visualized by LSM-510 confocal microscopy as described in section II.22. Shown are fluorescence staining by DAPI (Panel A), DIOC5 (Panel B) and anti-hCNT3 monoclonal antibodies (Panel C). The merged image of all the fluorescence is shown in Panel D. *Bar*, 20 μ m.

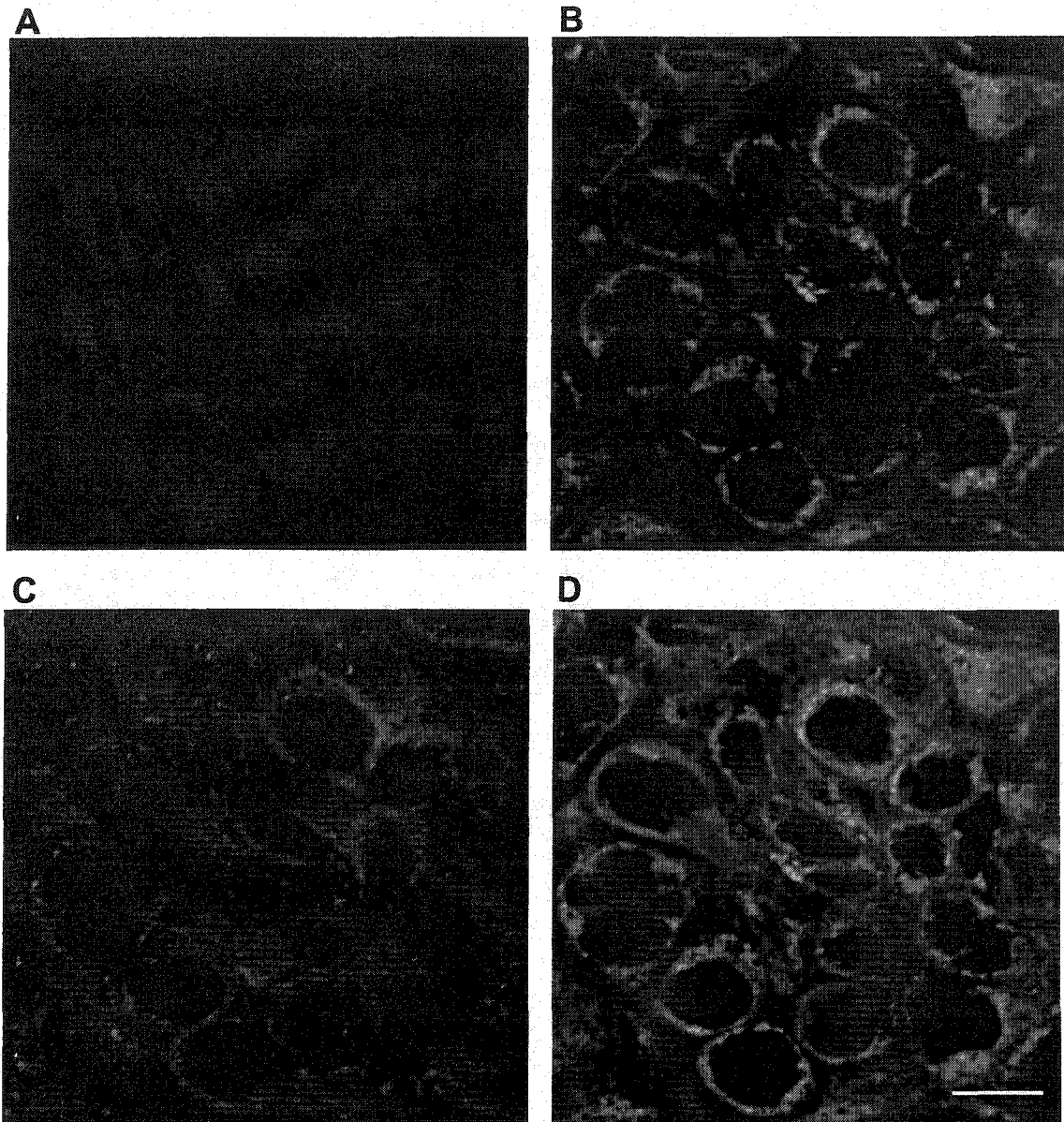


Figure VI-13. Predominant cell surface localization of hCNT3 in day 18 Caco-2 cell cultures

Caco-2 cells were grown on collagen-coated inserts for 18 days as described in section II.10.2. Inserts were fixed in paraformaldehyde, permeabilized in Triton X-100, incubated with anti-hCNT3 monoclonal antibodies directed against epitope TL3360 of hCNT3, followed with Alexa Fluor 594 conjugated goat anti-mouse antibodies, and subsequently incubated with DAPI and DIOC5 and mounted on slides in 90% glycerol. Slides were visualized by LSM-510 confocal microscopy as described in section II.22. Shown are fluorescence staining by DAPI (Panel A), DIOC5 (Panel B), and anti-hCNT3 monoclonal antibodies (Panel C). The merged image of all the fluorescence is shown in Panel D. *Bar*, 20 μm .

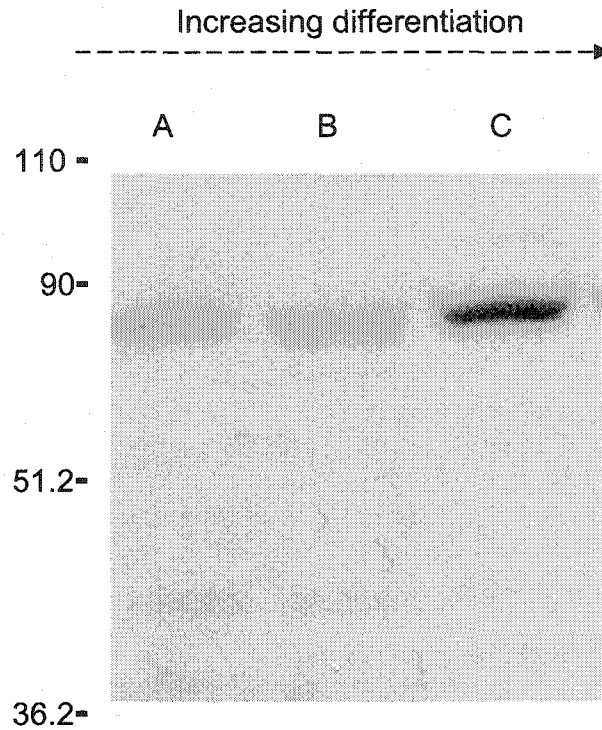


Figure VI-14. Immunoblot analysis of hCNT3 production in membrane preparations from Caco-2 cells after 4, 11, and 18 days in culture

Caco-2 cells were cultured on collagen-coated plates for 4 (Lane A), 11 (Lane B) and 18 (Lane C) days as described in section II.10.2. Enriched plasma membrane preparations were prepared from Caco-2 cells as described in section II.17.2. Equal quantities (15 μ g) of protein were loaded, electrophoresed through a 10% SDS-polyacrylamide gel and transferred to PVDF membrane. The PVDF membrane was probed with 1:8000 dilution (v/v) of anti-hCNT3 monoclonal antibodies followed by 1:7000 dilution (v/v) of goat anti-mouse HRP conjugated secondary antibodies. Detection was by ECL chemiluminescent and exposure to Fuji X-ray film. Left, positions of the protein markers (in kDa).

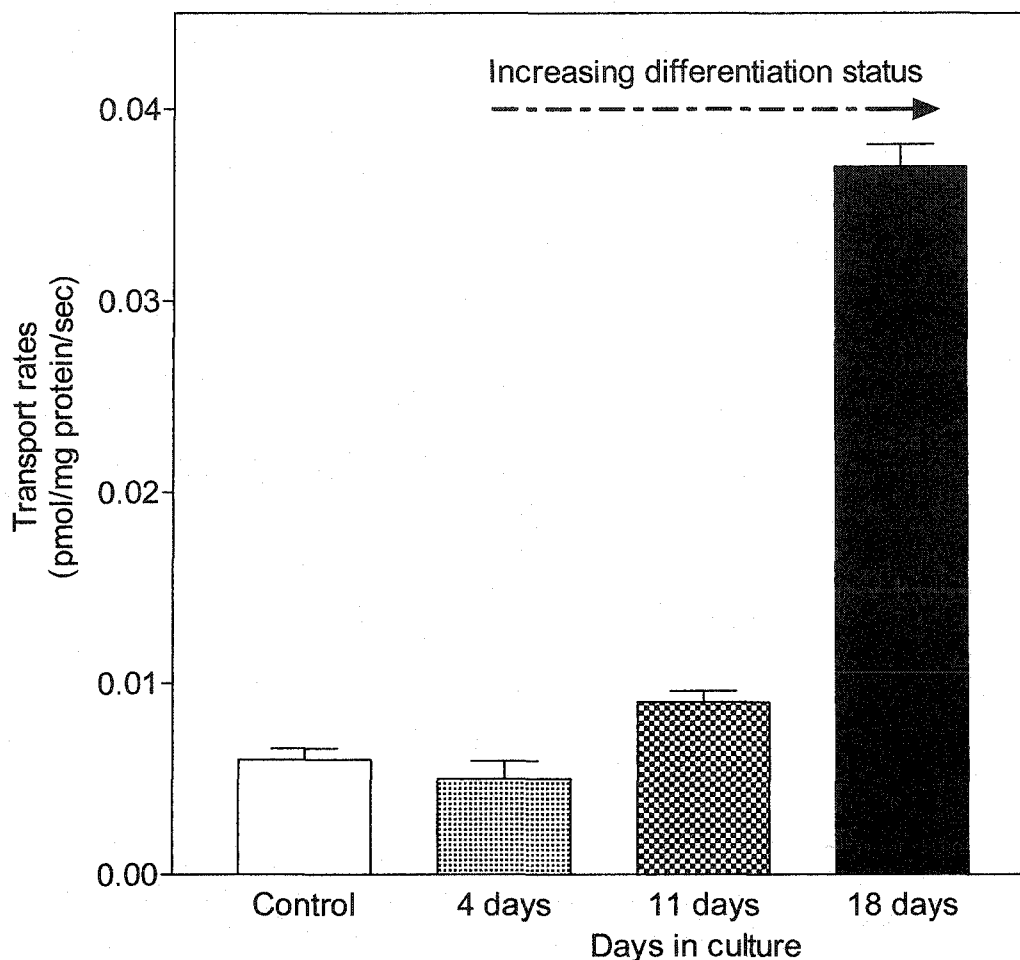


Figure VI-15. Sodium-dependent uridine transport activities in Caco-2 cultures after 4, 11, and 18 days

Caco-2 cells were cultured on collagen-coated inserts for the time periods indicated as described in section II.10.2. TEER readings were assessed prior to transport assays as an indicator of differentiation status as described in section II.14. ENT-mediated processes were inhibited by incubating Caco-2 cells for 15 min in 200 μ M dilazep prior to uptake measurements and including 200 μ M dilazep in transport buffers. Uptake of 10 μ M 3 H-uridine across the apical (upper) compartment of Caco-2 cultures was measured in sodium-containing transport buffer as described in section II.16. Initial rates of uptake were obtained from linear portions of 5-min time courses as shown in Figure VI-5. The non-mediated uptake (control) rates were determined for day 18 cultures under identical transport conditions except for the presence of 3 mM excess nonradiolabeled uridine. Each value represents the mean \pm SD of three inserts.

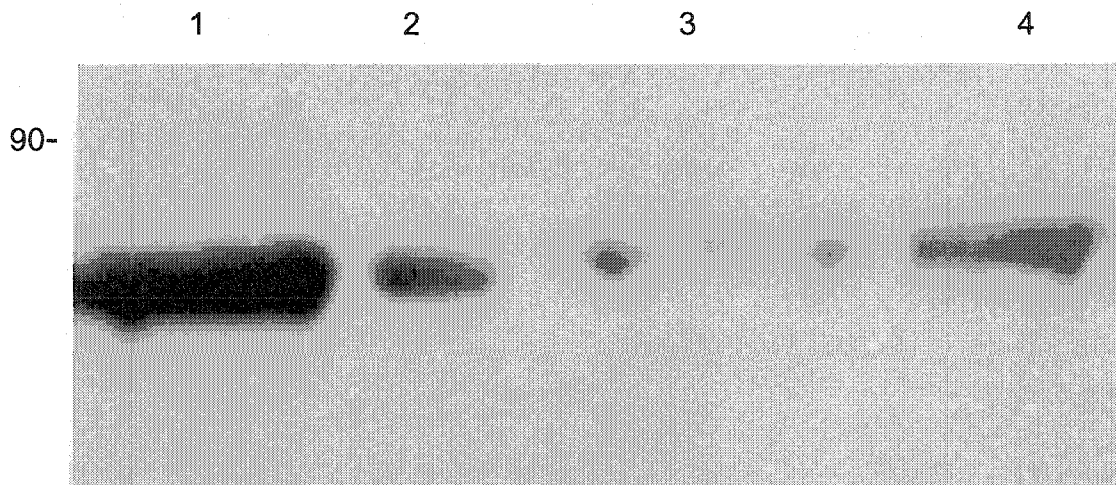


Figure VI-16. Immunoblot analysis of well-differentiated Caco-2 cells and biopsies of human tissues from different regions of gastrointestinal tract

Caco-2 cells were grown on collagen-coated plates for 18 days as described in section II.10.2. Membrane preparations were prepared from biopsies of human jejunum (Lane 1), duodenum (Lane 2), colon (Lane 3) and day-18 Caco-2 cells (Lane 4) as described in section II.17.4. Equal quantities (15 μ g) of protein were loaded, electrophoresed through a 10% SDS-polyacrylamide gel and transferred to PVDF membrane. The PVDF membrane was probed with 1:5000 dilution (v/v) of anti-hCNT3 monoclonal antibodies followed by 1:7000 dilution (v/v) of goat anti-mouse HRP conjugated secondary antibodies. Detection was by ECL chemiluminescent and exposure to Fuji X-ray film. Left, position of the protein markers (in kDa).

Chapter VII

VII. Distribution and Localization of CNT Proteins in Human Brain and Vascular Endothelial Cells: Relationship Between Their Location and Site of Adenosine Action

VII.1. Introduction

Adenosine exhibits multi-faceted effects in mammalian tissues, particularly in excitable tissues such as the heart and brain, where it has been proposed to be a mediator in local vasoregulation, cardiac mechanical and electrical function, synaptic transmission in the central nervous system (CNS) and modulator of platelet function and cell adhesion [16-18]. These actions by adenosine are, for the most part, mediated by its interactions with adenosine receptors located at the plasma membranes of target cells [19, 20]. Adenosine has been shown to reduce the activity of excitable tissues (e.g., by slowing the heart rate) or increase the delivery of metabolic substrates (e.g., by inducing vasodilation) [16, 21], and therefore helps to couple the rate of energy expenditure to the energy supply.

In the CNS, adenosine appears to exhibit neuroprotective properties through its regulatory actions on cell surface adenosine receptors [355]. Of the four adenosine receptors identified, the adenosine A₁ receptor is the most prominent in human brain [166]. The regulation of extracellular adenosine levels in the human brain is complex, involving numerous enzymes for the production and metabolism of adenosine, in addition to nucleoside transporters [17, 356]. The presence of adenosine in the CNS and the regional distribution of adenosine receptors, such as the A₁ subtype, imply that adenosine is likely an intercellular mediator with specific roles in the brain [357]. The source of extracellular adenosine has been the subject of intense research and there is evidence that it

is derived from several cell types, including brain neuronal and glial cells as well as endothelial cells [10].

Endothelium blood vessels represent both a physical and a metabolic barrier to adenosine. In the brain, endothelial cells form the blood-brain barrier and are largely responsible for restricting movement of substances into brain interstitium. Although no cell culture model can truly be representative of the blood-brain barrier *in situ*, human umbilical vein endothelial cells (HUVEC) have been used as an *in vitro* model of the blood-brain barrier [358-360]. An NBMPR-sensitive process mediating the transport of adenosine across the blood-brain barrier has been described in conjunction with adenosine A₁ receptors in human cerebral microvessels [361, 362]. Recently, CNT2 cDNA was cloned from isolated rat brain capillaries, demonstrating for the first time the existence of a CNT family member in brain endothelial cells [363]. The presence of CNTs, if any, in HUVEC has not been demonstrated.

Both equilibrative and sodium-dependent (concentrative) nucleoside transport processes, characterized by radioisotopic flux analysis with ³H-adenosine, have been demonstrated in whole brain from humans and lower mammals [164, 165, 183, 364]. Sodium-dependent nucleoside transport has been suggested to be present in rat brain. The distribution of es-type transporters in human and rat brain has been examined by ligand-binding studies utilizing radiolabeled NBMPR [166, 167, 365, 366]. The density of NBMPR-binding sites has been found to be the highest in the thalamus and midbrain, with lower levels found in the hippocampus and cerebellum [367, 368].

The recent availability of antibodies against hENT1 and hENT2 proteins has provided the essential immunological reagents to investigate the distribution of the two ENT proteins in human brain via immunoblot analysis [144].

Molecular techniques employing RT-PCR have identified CNT1 and CNT2 mRNAs in all regions of rat brain, including choroid plexus, brain stem, cerebral cortex, cerebellum, striatum, superior colliculus and hippocampus [182]. Although the detection of transcripts corresponding to rCNT1 and rCNT2 may not be quantitative, the relative signals detected varied considerably between different brain regions examined [182]. In contrast to the more localized expression in mainly specialized cell types exhibited by hCNT1 and hCNT2 mRNAs [132, 133, 168], the distribution pattern of hCNT3 mRNA is much more widespread than anticipated, and is present in most tissues examined, including various regions of human brain [2]. Since CNT activity appears to be regulated [2, 208], it is uncertain whether mRNA levels reflect the presence of physiologically significant amounts of CNT proteins. The presence of CNT proteins in human brain has not yet been demonstrated.

Early studies identifying transcripts for multiple CNT family members throughout various regions of the brain [168, 182] suggested that the widespread distribution of these transporters in the CNS reflects their role in mediating the uptake of adenosine. Gaining a better understanding of the physiological function of the CNTs in relation to adenosine-mediated neuromodulation will require knowledge, not only of their tissue distributions and abundance levels, but also of their subcellular locations.

Although both of the sodium-dependent nucleoside transporters, hCNT2 and hCNT3, exhibit the capacity for high-affinity transport of adenosine, their abundance levels and locations in the human brain have not been explored. In the present study, antibodies specific for hCNT2 and hCNT3 were employed to assess the distribution of the two major sodium-dependent transporters of adenosine (see Chapter IV) in human brain. Membrane fractions from different brain regions, including cerebral cortex, brainstem, cerebellum and basal ganglia, were subjected to immunoblot analysis using the Typhoon 9400 Variable Mode Imager and image analysis software to quantitate the relative abundance of CNT proteins. Their abundance levels were compared with the levels of adenosine A₁ receptors in different regions of the brain to ascertain whether the distribution of CNTs correlated with the distribution of adenosine A₁ receptors, therefore providing a possible functional association between CNTs and adenosine-mediated neuromodulation.

Since the site of adenosine action is at the cell surface [22, 311], the presence of CNT proteins in plasma membranes may have an important impact on extracellular adenosine pools. Vascular endothelial cells and their functions in vasoregulation are subjected to adenosine-mediated effects through adenosine receptors [10, 34, 321, 369, 370]. In the present investigation, primary cultures of human umbilical vein endothelial cells (HUVEC) were employed to determine the subcellular location of hCNT2 and hCNT3 by immunofluorescence confocal microscopy. The results provided evidence of sodium-dependent transporters in primary cultures of human endothelial cells.

VII.2. RESULTS

VII.2.1. *Distribution of hCNT2, hCNT3 and adenosine A1 receptors within the major divisions of the human brain*

Human brain was dissected by Dr. C. Hao (Laboratory Medicine and Pathology, University Hospital and University of Alberta, see Chapter II, section II.17.3) into its major divisions consisting of cerebral cortex (divided into frontal, parietal, temporal and occipital lobes), hippocampus, thalamus, brainstem (divided into the medulla, midbrain and pons), cerebellum and basal ganglia (divided into caudate nucleus, putamen and globus pallidus). The enriched membrane fractions of different brain regions in the present work were prepared from the same original human brain tissue used by Jennings *et al.* [144] in their study of the distribution of hENT1 and hENT2 in the CNS.

Equal quantities of enriched membrane preparations prepared as described in Materials and Methods (Chapter II, section II.17.3) from different regions of human brain were subjected to immunoblotting with antibodies directed against either hCNT2 or hCNT3. Detection of bands was by ECL chemiluminescence and exposure to Fuji X-ray film as shown in the experiment of Figure VII-1. The results showed detection by the anti-hCNT2 polyclonal antibodies of immunoreactive bands with an apparent molecular mass between 70 and 75 kDa in all regions of the brain investigated (Panel A). The signal intensities of immunoreactive bands varied substantially among brain regions, with high intensities in the cerebral cortex and thalamus and very low in the medulla.

The anti-hCNT3 monoclonal antibodies recognized immunoreactive materials with an apparent molecular mass between 75 and 80 kDa in all regions of the brain analyzed (Panel B, Figure VII-1). In contrast to the variations observed in hCNT2 abundance in the different regions of the brain, hCNT3 was present at higher and more uniform levels in most regions of the brain investigated.

Since adenosine A₁ receptors are known to be present in high abundance in the brain [11], the experiment of Figure VII-2 was undertaken to detect adenosine A₁ receptors in the human brain tissues used in the current work. As expected, immunoreactive species of apparent molecular weights between 35 and 40 kDa were detected in all the brain areas by commercial antibodies against adenosine A₁ receptors [144]. The adenosine A₁ receptors were present in varying abundance in different regions of the brain, with much higher levels in the cerebral cortex, hippocampus, thalamus and basal ganglia, and lower levels in the brainstem regions and the cerebellum.

VII.2.2. Correlation of hCNT2 and hCNT3 protein abundance with adenosine A₁ receptor

To compare the relative levels in hCNT2 and hCNT3 protein abundance with adenosine A₁ receptor abundance in the different brain areas, signal intensities of immunoreactive bands corresponding to different regions of the brain were quantified using a Typhoon 9400 Variable Mode Imager. The calculated volume, which was expressed in arbitrary units of the Typhoon signal, of each immunoreactive band corresponding to hCNT2 protein abundance in the

different brain regions is shown in Figure VII-3. The results indicated the presence of hCNT2 in all regions of the brain and the protein abundance levels corresponded well with those observed using film detection in Panel A of Figure VII-1. The cerebral cortex, particularly the occipital lobe, contained the highest levels of hCNT2 protein, whereas the frontal, parietal and temporal regions of the cortex contained lower levels. Moderate levels of hCNT2 were apparent in the hippocampus, thalamus, caudate nucleus and putamen. Lower levels were evident in the medulla, midbrain, pons, cerebellum, and globus pallidus when compared to other brain areas.

The pattern of hCNT3 protein distribution (Figure VII-4) in the different brain areas differed from that of hCNT2 (Figure VII-3). Much higher levels of hCNT3 were apparent in most brain areas compared to hCNT2, as shown by the relatively larger calculated volumes determined for the majority of hCNT3 immunoreactive bands. The levels of hCNT3 protein abundance were generally invariably high throughout the brain, with the exception of the hippocampus, medulla and globus pallidus, where hCNT3 protein levels were relatively lower.

The quantitation of adenosine A₁ receptor abundance in the major divisions of the human brain is shown in Figure VII-5. The results revealed that all brain areas examined possessed adenosine A₁ receptors, although the relative levels of the adenosine receptors in the different regions of the brain were variable.

A comparison of the relative abundance of hCNT2 and adenosine A₁ receptors in human brain was undertaken by plotting the normalized volume of

the immunoreactive band corresponding to hCNT2 in the different brain regions as a function of those corresponding to adenosine A₁ receptors (Figure VII-6). The results demonstrated a positive correlation with a r^2 value of 0.8306 and P value of <0.0001 between the relative levels of hCNT2 and adenosine A₁ receptors in the different brain areas. A similar correlation analysis with hCNT3 and adenosine A₁ receptor abundance, as shown in Figure VII-7, could not demonstrate a correlation between the relative levels of hCNT3 and adenosine A₁ receptor in the different brain regions (r^2 value of 0.2400 and P value of 0.0893).

VII.2.3. Demonstration of hCNT2 and hCNT3 in human endothelial cells by immunoblot analysis

Previous studies of the distribution of human equilibrative nucleoside transporters in the central nervous system showed that all the brain regions investigated lacked endothelial cells as revealed by the absence of immunoreactive bands in immunoblots probed with anti-CD34 antibodies [144]. Since the present study employed the same original brain tissue as Jennings *et al.* [144] to prepare enriched membrane fractions of the different brain areas, experiments were undertaken to determine the presence and location of CNTs in endothelial cells. Due to the difficulty in obtaining human endothelial cells from brain capillaries, human umbilical vein endothelial cells (HUVEC) were employed. HUVEC have been shown to be responsive to adenosine-mediated protective effects through adenosine receptors [10, 34, 321]. Since the site of adenosine action is at cell surfaces [22, 311], it follows that the presence of CNT

proteins at plasma membranes may possibly have an effect on extracellular adenosine levels near adenosine receptors.

Primary cultures of human umbilical vein endothelial cells were grown on 1% gelatin-coated tissue culture flasks as described in Materials and Methods (section II.10.2). Cell lysates of HUVEC were subjected to immunoblotting with either anti-hCNT2 or anti-hCNT3 antibodies. The experiment of Figure VII-8 showed detection by the anti-hCNT2 antibodies of an immunoreactive band with an apparent molecular weight between 70 and 75 kDa in HUVEC, whereas no immunoreactivity was present, as expected, in CEM-ARAC cells (Panel A). Similarly, the anti-hCNT3 antibodies recognized an immunoreactive band between 75 and 80 kDa in HUVEC, corresponding to the predicted size of hCNT3. No bands were detected in CEM-ARAC or ARAC/D2 cells with antibodies against hCNT3 suggesting the absence of cross-reactivity of these antibodies against hCNT2.

VII.2.4. Localization of hCNT2 and hCNT3 to plasma membranes of HUVEC by immunofluorescence confocal microscopy

To determine the cellular location of hCNT2 and hCNT3, HUVEC were grown on gelatin-coated inserts overnight, and labeled with preimmune rabbit sera or double labeled with anti-hCNT2 polyclonal and monoclonal antibodies as shown in Figure VII-9. The results demonstrated the lack of immunofluorescence signal when HUVEC were stained with the preimmune rabbit sera. However, anti-hCNT2 polyclonal antibodies obtained from the same rabbit labeled immunoreactive materials in plasma membranes of HUVEC (Panel

B). Similar staining patterns of HUVEC were evident with the anti-hCNT2 monoclonal antibodies (Panel C). The superimposed image of Panels B and C demonstrated colocalization of immunofluorescent signals by the anti-hCNT2 polyclonal and monoclonal antibodies. As an added assurance of the colocalization of the anti-hCNT2 antibodies, a comparison of the signal intensities produced by the two antibodies in a selected region of the superimposed image (Panel D) was profiled as shown in Figure VII-10. The results showed that the signal intensities of the anti-hCNT2 polyclonal antibodies corresponded well with those of the anti-hCNT2 monoclonal antibodies, indicating that the two antibodies likely bound to the same immunoreactive materials, which were located predominately at cell surfaces.

The cellular location of hCNT3 in HUVEC was examined by double-label immunofluorescence with polyclonal antibodies against a putative extracellular epitope and monoclonal antibodies against an intracellular epitope of hCNT3 as shown in Figure VII-11. The specificity of labeling with the anti-hCNT3 antibodies was demonstrated by the absence of HUVEC staining when rabbit preimmune sera were used to stain the cells (Panel A). However, when HUVEC were stained simultaneously with anti-hCNT3 polyclonal and monoclonal antibodies raised against different immunogenic epitopes of hCNT3, similar staining patterns were observed for both antibody preparations (Panels B and C). The superimposed image of the staining by the two antibodies showed a predominant yellow-color staining localized to plasma membranes of HUVEC, demonstrating that the immunofluorescent signals from the two antibodies

colocalized (Panel D). The immunofluorescence staining was analyzed further by measuring the signal intensities exhibited by the two antibodies in a selected distance across several cells in the superimposed image of Panel D. The profile of the signal intensities of the immunofluorescent staining of HUVEC shown in Figure VII-12 demonstrated colocalization of immunofluorescent signals by the two antibodies.

VII.3. Discussion

Adenosine is implicated in a variety of physiological and pathophysiological responses related to the central nervous system and cardiovascular system through its association with cell surface adenosine receptors [16, 17, 371, 372]. Since adenosine receptors may be activated by different range of endogenous adenosine concentrations [38], the levels of adenosine available to bind and activate these receptors help control the different physiological responses to adenosine. Accordingly, identification of the various nucleoside transport processes that mediate adenosine uptake and release, and therefore influence the adenosine pools in the extracellular space may be instrumental in understanding the degree of adenosine receptor stimulation and the central actions of adenosine.

While numerous studies have implicated equilibrative nucleoside transport processes in the modulation of local adenosine concentrations near adenosine receptors [21, 373], the contribution of sodium-dependent nucleoside transport systems is uncertain. Both hCNT2 and hCNT3 are sodium-dependent active transporters and share a similar ability of being able to transport adenosine with high affinities [2, 132]. However, the distribution and location of these two proteins in brain tissues and vascular endothelial cells, which are capable of influencing extracellular adenosine concentrations as well as being subjected to adenosine-mediated regulation [10, 34, 321], have not been explored. The generation of highly specific antibodies against both hCNT2 and hCNT3 provided the prerequisite immunological reagents to examine their distribution within

different brain areas as well as their presence and location in human umbilical vein endothelial cells (HUVEC).

Immunoblot analysis of the major divisions of the human brain and quantitation of protein abundance by the Typhoon 9400 Variable Mode Imager showed that the hCNT2 protein was present in all brain areas investigated, with the highest hCNT2 protein abundance in the cerebral cortex, particularly the occipital lobe, followed by relatively lower hCNT2 abundance in the frontal, parietal and temporal regions of the cortex. The hippocampus, thalamus, caudate nucleus and putamen possessed moderate levels of hCNT2 protein, whereas the medulla, midbrain, pons, cerebellum, and globus pallidus contained much lower levels when compared to other brain areas. Earlier work using RT-PCR analysis of various regions of rat brain has provided evidence of rCNT2 mRNAs in the hypothalamus, cerebellum and cerebral cortex [182], a result that is consistent with the present demonstration of hCNT2 protein in these areas of human brain. Unfortunately a comparison of the hCNT2 protein levels with mRNA levels in these brain regions cannot be made since the RT-PCR analysis employed [182] was not quantitative.

The pattern of hCNT3 distribution in the different brain areas was very distinct from that of hCNT2. While hCNT2 protein levels varied substantially between the different brain areas, hCNT3 levels were much more uniform and invariably high throughout most brain areas, with the exception of the hippocampus, medulla and globus pallidus, where hCNT3 protein levels were slightly lower compared to other brain areas. The use of multiple tissue RNA

arrays probed with a cDNA fragment corresponding to hCNT3 also revealed fairly uniform levels of hCNT3 transcripts in human brain, including cerebral cortex, cerebellum, hippocampus, thalamus, caudate nucleus, putamen, medulla and pons, although the levels of hCNT3 transcripts appeared to be comparatively lower in brain tissues than other tissues examined such as the intestine [2].

The prevalence of hCNT2 and hCNT3 proteins throughout the human brain suggests the existence of multiple routes for translocation of purine as well as pyrimidine nucleosides across plasma membranes. It is perhaps not surprising, given the diverse actions of adenosine in the human brain, that the concentrative transporters are present, in addition to the equilibrative transporters, hENT1 and hENT2 [144], to maintain adenosine concentrations under physiological and pathological situations. Such precedence has already been described for other compounds such as amino acids and glucose, which are transported across brain cell membranes by active sodium-dependent transport systems as well as sodium-independent equilibrative systems [374, 375].

There is evidence of sodium-dependent adenosine and uridine transport activities in mixed populations of dissociated brain cells from adult rats [183], however these studies did not identify the type of concentrative process observed. Identification of *cib*-type transporters by functional transport assays in choroid plexus tissue slices obtained from rabbit brain has been described [128, 236]. A novel sodium-dependent transport process with broad substrate

selectivity and the ability to transport hypoxanthine, a metabolized product of adenosine, has also been reported in rabbit choroid plexus [376]. Because much of what is inferred about sodium-dependent adenosine transport in brain stems from research conducted on other tissues, the extent to which these data can be extrapolated to human central nervous system is uncertain.

A comparison of the distribution of hCNT2 and hCNT3 with that of adenosine A₁ receptor protein abundance in the major divisions of human brain was made. While adenosine A₁ receptors were present throughout the CNS, relatively higher receptor levels were evident in the cerebral cortex, hippocampus, thalamus, and basal ganglia compared to the brainstem region and the cerebellum, a result that is consistent with the pattern of A₁ receptor distribution typically observed in brain [11, 144, 166]. The relative abundance of A₁ receptors demonstrated a strong positive correlation (r^2 value of 0.8306 and P value of <0.0001) with the relative abundance of hCNT2 protein observed in the brain areas examined, suggesting an anatomical and/or neurochemical relationship between hCNT2 and adenosine receptor-mediated events. A relationship between the distribution of adenosine A₁ receptors and hCNT3 in human brain could not be demonstrated.

Although there was a lack of relationship between the levels of A₁ receptors and hCNT3, hCNT3 may be involved at sites of adenosine action with other P1 purinoceptors such as the A_{2a}, A_{2b} or A₃ subtypes or the P2 purinoceptors. Also, the prevalence of hCNT3 protein throughout the brain may reflect a role in cellular salvage of nucleosides from the extracellular environment

of the brain. This role is perhaps substantiated by the unique ability of hCNT3, among CNTs, to possess the capacity to transport both purine and pyrimidine nucleosides with high affinity, both of which are undoubtedly important in brain function. Uridine possesses similar properties to adenosine in that it appears to act as a signaling molecule as well as a therapeutic agent [55-57]. Its basal concentration in plasma and brain interstitial fluid ranges from 3 to 8 μM , and it is actively salvaged by cells of the brain, resulting in an intracellular uridine concentration that is typically higher than the extracellular concentration [51].

The finding that the two CNTs are found in varying abundance in particular areas of brain suggests that they may also be localized to discrete populations of cells that are capable of producing changes in extracellular adenosine levels. Several cell types, such as neuronal cells, glial cells and endothelial cells have been identified as sources of extracellular adenosine [40, 377-379]. However, the membrane preparations of human brain employed in this study did not contain endothelial cells since they were derived from the same original brain tissues that were shown to lack endothelium as revealed by immunoblot analysis with anti-CD34 antibodies [144].

Due to the difficulty in obtaining human brain endothelial cells, vascular endothelial cells were examined for the presence of either hCNT2 or hCNT3. While vascular endothelial cells are likely different from brain endothelial cells, they have been shown to be a source of extracellular adenosine, and are responsive to adenosine-mediated protective effects through adenosine receptors [10, 34, 321, 370]. The action of adenosine on its receptors occurs at

the cell surface [22, 311], and therefore the existence of CNT proteins at the plasma membrane could potentially influence extracellular adenosine levels near adenosine receptors.

Lysates from primary cultures of HUVEC that were subjected to immunoblotting exhibited immunoreactive materials with apparent molecular masses corresponding to the predicted sizes expected for hCNT2 and hCNT3 proteins. A cDNA encoding an adenosine transporter identical in sequence to rCNT2 has recently been isolated from rat brain capillaries [363]. Although brain capillaries consist primarily of endothelial cells, other cell types, such as astrocytes, are also present, and rCNT2 could, therefore, be present in either or both of these cell types. Sodium-dependent transport processes have been described in primary cultures of rat cerebellar and spinal cord astrocytes [380].

The cellular location of hCNT2 and hCNT3 in HUVEC was determined by double-labeling immunofluorescence with monoclonal and polyclonal antibodies against different epitopes of CNT proteins and visualized by confocal microscopy. The results showed hCNT2 and hCNT3 in plasma membranes of HUVEC. The plasma membrane location of hCNT2 and hCNT3 suggests that these proteins, which likely play an important role in mediating physiological functions of adenosine, may also be involved in salvage of purine and pyrimidine nucleosides from the extracellular milieu. If the CNT proteins are presumed to also be present in brain endothelial cells, depending on their location with respect to luminal or abluminal membranes, they could play a role in either uptake or release of nucleosides from the vascular system into brain interstitium.

In situ hybridization of isolated rat brain capillaries has demonstrated rCNT2 mRNA localization to the capillary endothelial cells [363]. While sodium-dependent transport activity across the luminal endothelial membrane in brain has been demonstrated *in vivo* [381], nucleoside transporters of the concentrative type have not been previously described in endothelial cells. Whether or not the presence of CNT proteins in vascular endothelial cells shown in this study reflect those in brain endothelial cells is not clear.

In conclusion, the current work provided evidence that hCNT2 and hCNT3 proteins are present in human brain tissues and in vascular endothelial cells. The positive correlation between the regional distribution of hCNT2 with adenosine A₁ receptors in brain suggested a functional link between mediators of adenosine flux and sites of adenosine action. This raises the possibility that hCNT2 proteins in brain may act to control adenosine concentrations near adenosine receptors, and therefore influence adenosine binding and signaling functions under physiological and pathological conditions.

The demonstration of the presence of both hCNT2 and hCNT3 proteins and their immunolocalization in primary cultures of HUVEC for the first time make these cells a useful model for further study of the functional and regulatory aspects of these sodium-dependent transporters with respect to adenosine-mediated events.

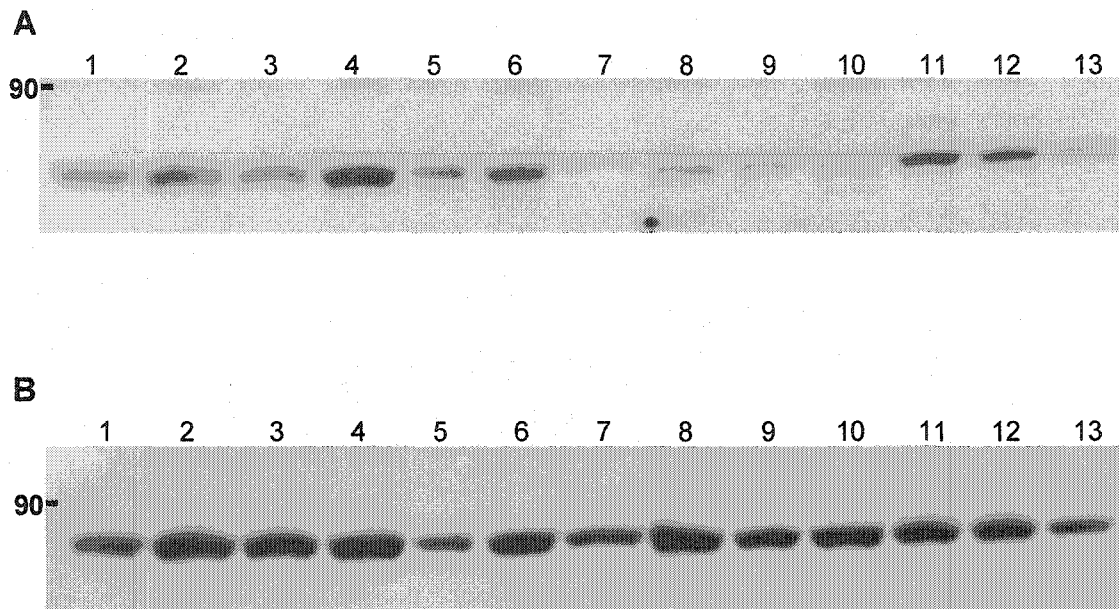


Figure VII-1. Differential distribution and abundance of hCNT2 and hCNT3 within the major divisions of the human brain

Human brain was obtained at autopsy <4 hr postmortem and dissected into the major divisions of the human brain, which are: cerebral cortex (divided into frontal (Lane 1), parietal (Lane 2), temporal (Lane 3) and occipital (Lane 4) lobes), hippocampus (Lane 5), thalamus (Lane 6), brainstem (divided into the medulla (Lane 7), midbrain (Lane 8) and pons (Lane 9)), cerebellum (Lane 10) and basal ganglia (divided into caudate nucleus (Lane 11), putamen (Lane 12) and globus pallidus (Lane 13)). Membranes of human brain prepared as described in section II.17.3 were equally loaded (30 μ g of protein), resolved by SDS-PAGE and transferred to PVDF membranes. PVDF membranes were probed with 1:8000 dilution of anti-hCNT2 polyclonal antibodies (Panel A) or 1:7000 dilution of anti-hCNT3 monoclonal antibodies (Panel B), followed by either 1:7000 dilution of goat anti-rabbit HRP conjugated secondary antibodies (Panel A) or 1:5000 dilution of goat anti-mouse HRP conjugated secondary antibodies (Panel B). Detection was by ECL chemiluminescence and exposure to Fuji X-ray film. *Left*, positions of the protein markers (in kDa).

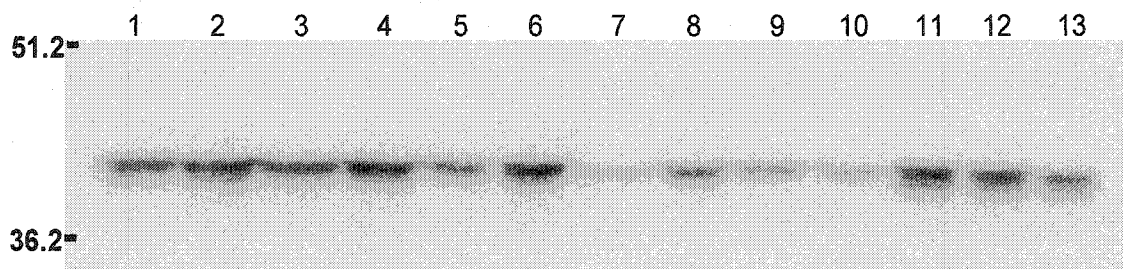


Figure VII-2. Immunodetection of adenosine A1 receptors within the major divisions of the human brain

Human brain was obtained at autopsy <4 hr postmortem and dissected into the major divisions of the human brain, which are: cerebral cortex (divided into frontal (Lane 1), parietal (Lane 2), temporal (Lane 3) and occipital (Lane 4) lobes), hippocampus (Lane 5), thalamus (Lane 6), brainstem (divided into the medulla (Lane 7), midbrain (Lane 8) and pons (Lane 9)), cerebellum (Lane 10) and basal ganglia (divided into caudate nucleus (Lane 11), putamen (Lane 12) and globus pallidus (Lane 13)). Membranes of human brain prepared as described in section II.17.3 were equally loaded (30 μ g of protein), resolved by SDS-PAGE and transferred to PVDF membranes. PVDF membranes were probed with 1:2000 dilution of anti-adenosine A1 receptor polyclonal antibodies, followed by 1:9000 dilution of goat anti-rabbit HRP conjugated secondary antibodies. Detection was by ECL chemiluminescence and exposure to Fuji X-ray film. *Left*, positions of the protein markers (in kDa).

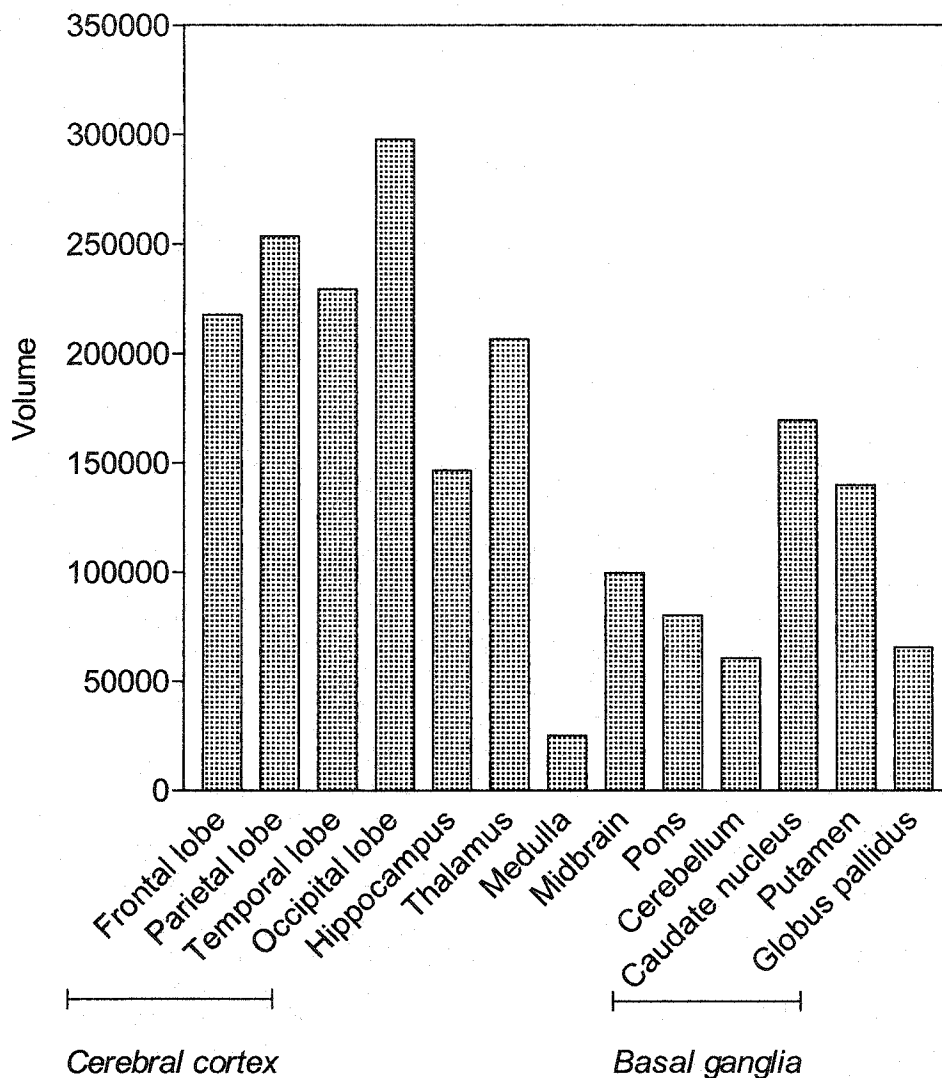


Figure VII-3. Quantitation of the relative abundance of hCNT2 in the major divisions of the human brain

Quantitative immunoblotting of brain membrane preparations with anti-hCNT2 polyclonal antibodies was performed as described in Figure VII-1 and section II.8. The PVDF membrane was incubated in ECL Plus Western Blotting Detection Reagents (0.1 ml/cm² membrane) for 5 min and scanned by Typhoon 9400 Variable Mode Imager. Electronic images were imported into ImageQuant version 5.2 software for data analysis. Signal intensities of immunoreactive bands corresponding to different regions of the brain were quantitatively determined using volume analysis with object-average background correction applied. The calculated volume, which is the integrated intensity, excluding background, of all pixels in each immunoreactive band corresponding to hCNT2 in the different regions of the brain, was imported into Prism and plotted. Shown are the mean values of three independent experiments.

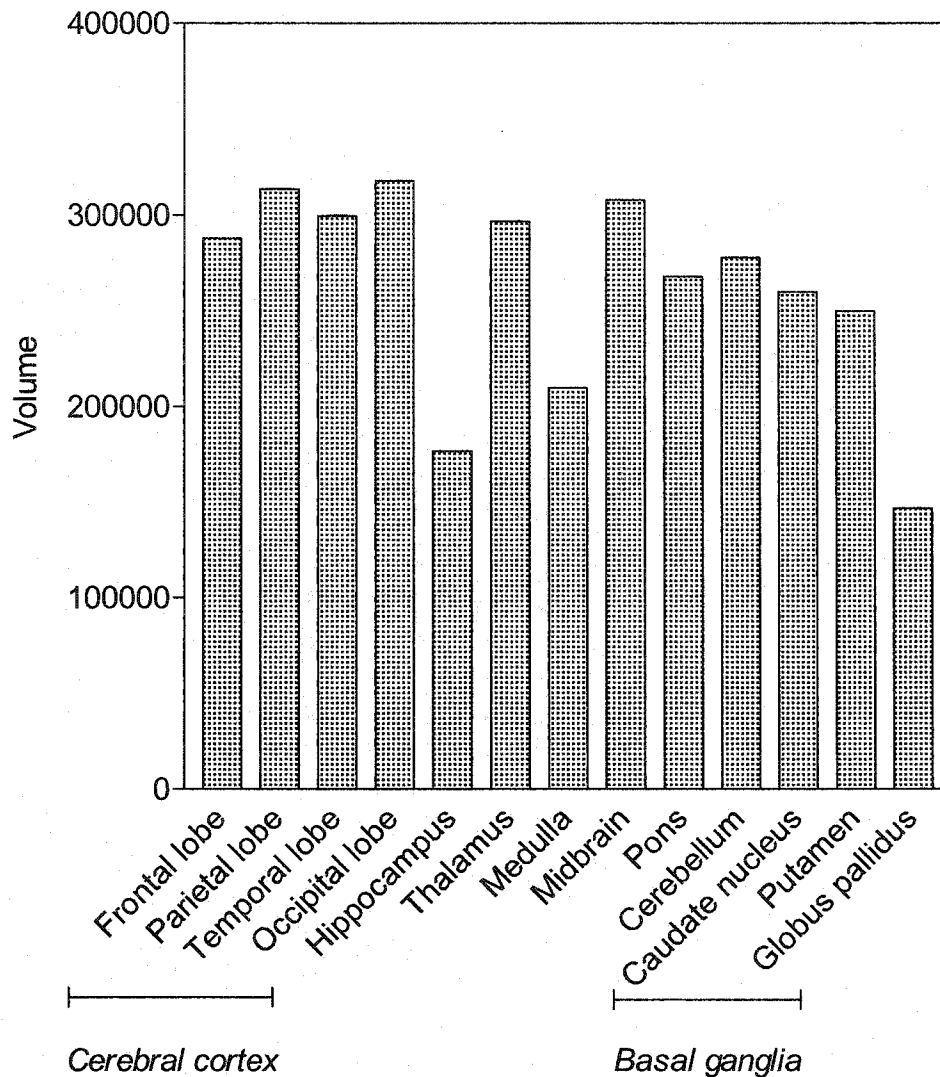


Figure VII-4. Quantitation of the relative abundance of hCNT3 in the major divisions of the human brain

Quantitative immunoblotting of brain membrane preparations with anti-hCNT3 monoclonal antibodies was performed as described in Figure VII-3. The PVDF membrane was incubated in ECL Plus Western Blotting Detection Reagents (0.1 ml/cm² membrane) for 5 min and scanned by Typhoon 9400 Variable Mode Imager. Electronic images were imported into ImageQuant version 5.2 software for data analysis. Signal intensities of immunoreactive bands corresponding to different regions of the brain were quantitatively determined using volume analysis with object-average background correction applied. The calculated volume, which is the integrated intensity, excluding background, of all pixels in each immunoreactive band corresponding to hCNT3 in the different regions of the brain, was imported into Prism and plotted. Shown are the mean values of three independent experiments.

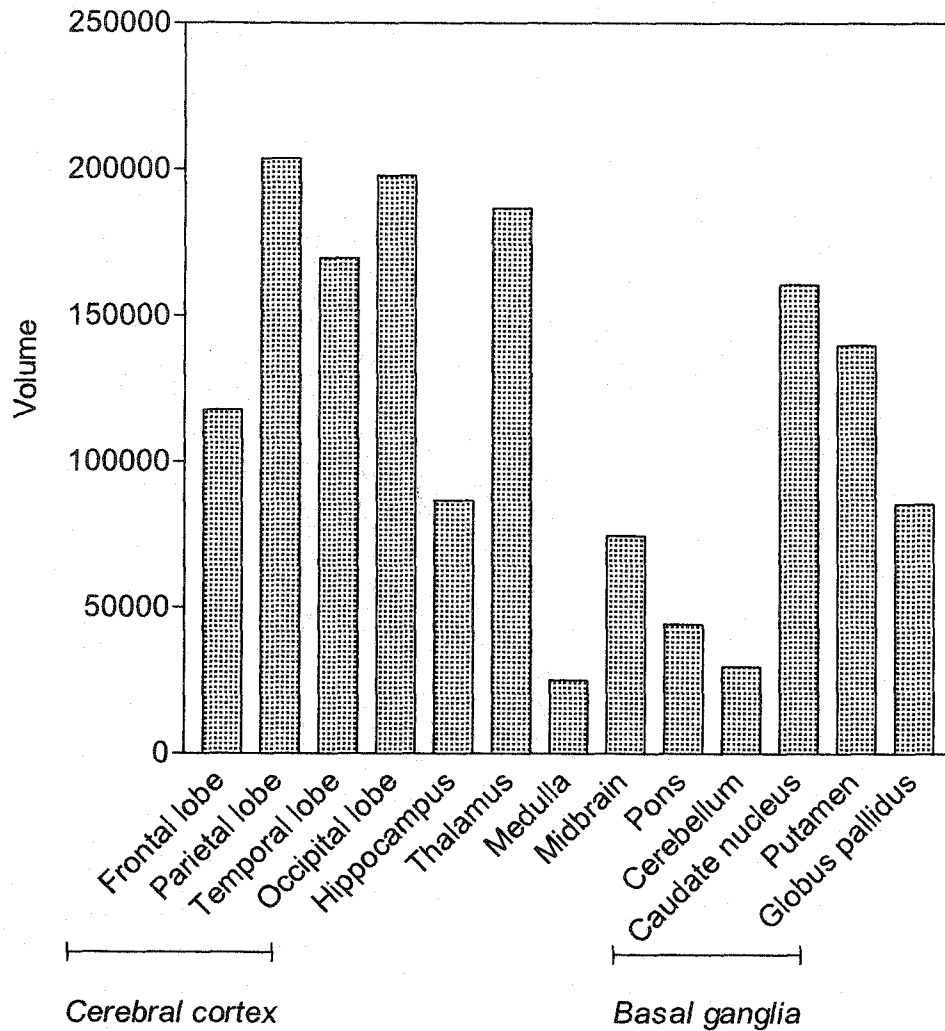


Figure VII-5. Quantitation of the relative abundance of adenosine A1 receptors in the major divisions of the human brain

Quantitative immunoblotting of brain membrane preparations with anti-adenosine A1 receptors polyclonal antibodies was performed as described in Figure VII-3. The PVDF membrane was incubated in ECL Plus Western Blotting Detection Reagents (0.1 ml/cm² membrane) for 5 min and scanned by Typhoon 9400 Variable Mode Imager. Electronic images were imported into ImageQuant version 5.2 software for data analysis. Signal intensities of immunoreactive bands corresponding to different regions of the brain were quantitatively determined using volume analysis with object-average background correction applied. The calculated volume, which is the integrated intensity, excluding background, of all pixels in each immunoreactive band corresponding to adenosine A1 receptors in the different regions of the brain, was imported into Prism and plotted. Shown are mean values of three independent experiments.

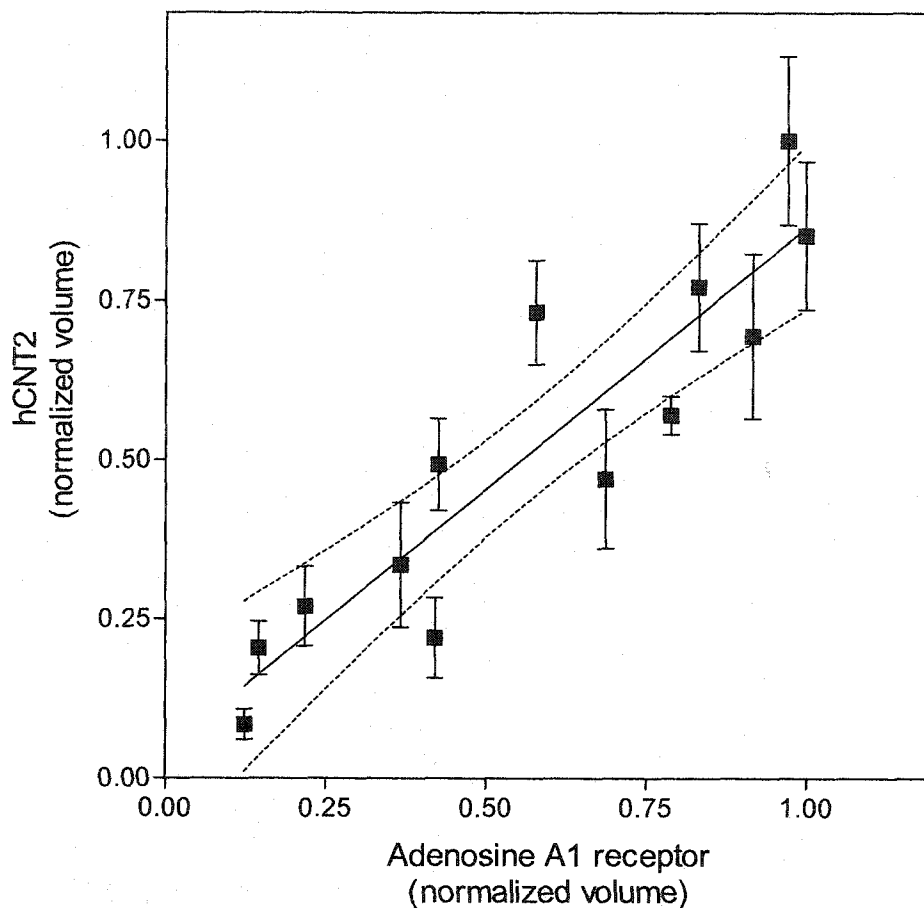


Figure VII-6. Comparison of the abundance of hCNT2 and adenosine A1 receptors in human brain

Signal intensities of immunoreactive bands obtained from Typhoon 9400 Variable Mode Imager corresponding to different regions of the brain were quantitatively determined by ImageQuant version 5.2 software using volume analysis with object-average background correction applied as described in section II.8. The immunoreactive band that exhibited the highest volume (signal intensity) was expressed as 1.0 and the other bands were expressed as a fraction of that value. Data numbers were exported to Prism and the normalized volume of each immunoreactive band corresponding to hCNT2 in the different brain regions was plotted as a function of the normalized volume of adenosine A1 receptors. Correlation analysis was performed showing positive correlation (r^2 value of 0.8306, P value of <0.0001 and slope of 0.82 ± 0.11) between the signal intensities of hCNT2 and adenosine A1 receptors in the different brain areas. The 95% confidence intervals of the linear regression line is depicted as the dashed lines. Each value represents the mean \pm SD of triplicate determinations and error bars are not shown where SD values were smaller than the size of the data symbols.

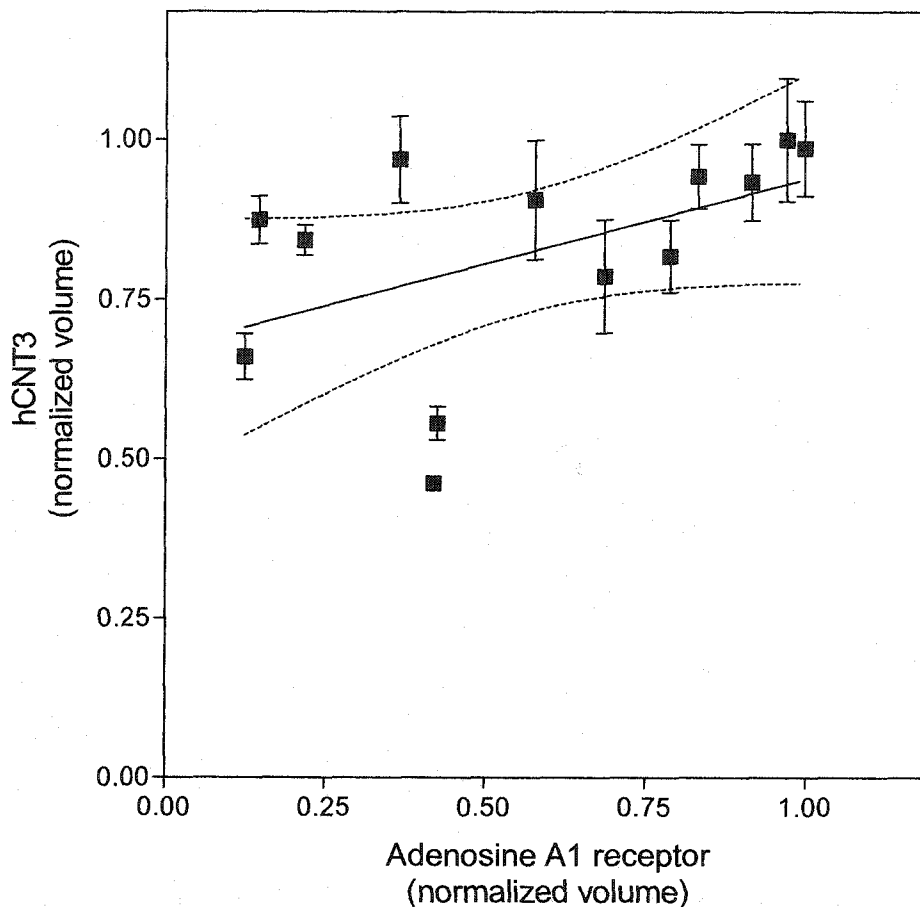


Figure VII-7. Comparison of the abundance of hCNT3 and adenosine A1 receptors in human brain

Signal intensities of immunoreactive bands obtained from Typhoon 9400 Variable Mode Imager corresponding to different regions of the brain were quantitatively determined by ImageQuant version 5.2 software using volume analysis with object-average background correction applied as described in Figure VII-6. The immunoreactive band that exhibited the highest volume (signal intensity) was expressed as 1.0 and the other bands were expressed as a fraction of that value. Data numbers were exported to Prism and the normalized volume of each immunoreactive band corresponding to hCNT3 in the different brain regions is plotted as a function of the normalized volume of adenosine A1 receptors. Correlation analysis was performed showing no correlation (r^2 value of 0.2400, P value of 0.0893 and slope of 0.26 ± 0.14) between the signal intensities of hCNT3 and adenosine A1 receptors in the different brain areas. The 95% confidence intervals of the linear regression line is depicted as the dashed lines. Each value represents the mean \pm SD of triplicate determinations and error bars are not shown where SD values were smaller than the size of the data symbols.

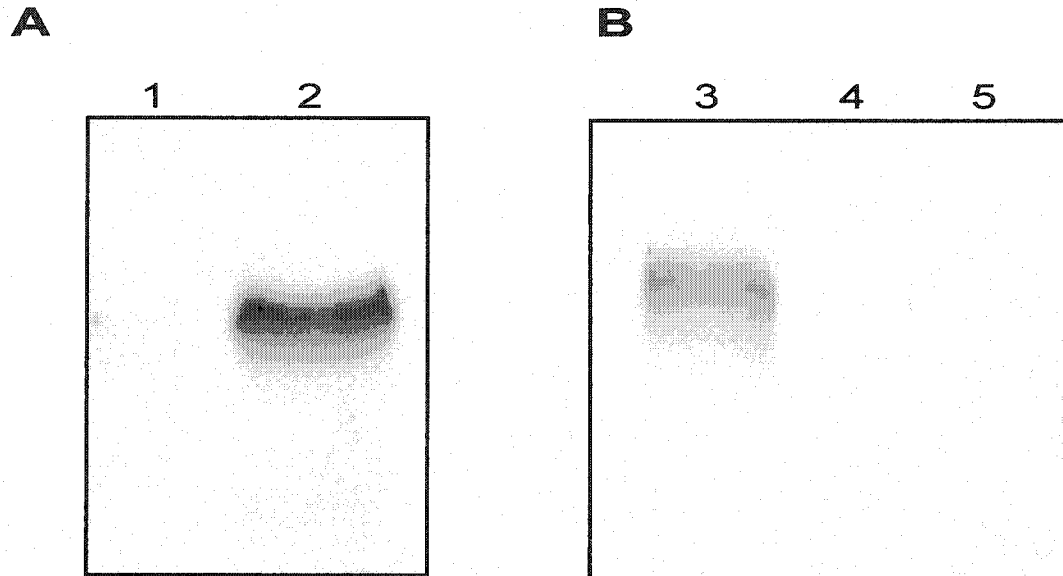


Figure VII-8. Demonstration of hCNT2 and hCNT3 in human umbilical vein endothelial cells (HUVEC)

Cell lysates from CEM-ARAC (Lanes 1 and 4), HUVEC (Lanes 2 and 3) and ARAC/D2 (Lane 5) were electrophoresed through a 10% SDS-polyacrylamide gel and transferred to PVDF membrane as described in sections II.8, II.10.2 and II.17.2. The PVDF membrane was probed with either 1:7000 dilution (v/v) of anti-hCNT2 polyclonal antibodies (Panel A) or 1:5000 dilution (v/v) anti-hCNT3 monoclonal antibodies, followed by 1:8000 dilution (v/v) of goat anti-rabbit (Panel A) or goat anti-mouse (Panel B) HRP conjugated secondary antibodies. Detection was by ECL chemiluminescence and exposure to Fuji X-ray film. *Left*, positions of the protein markers (in kDa).

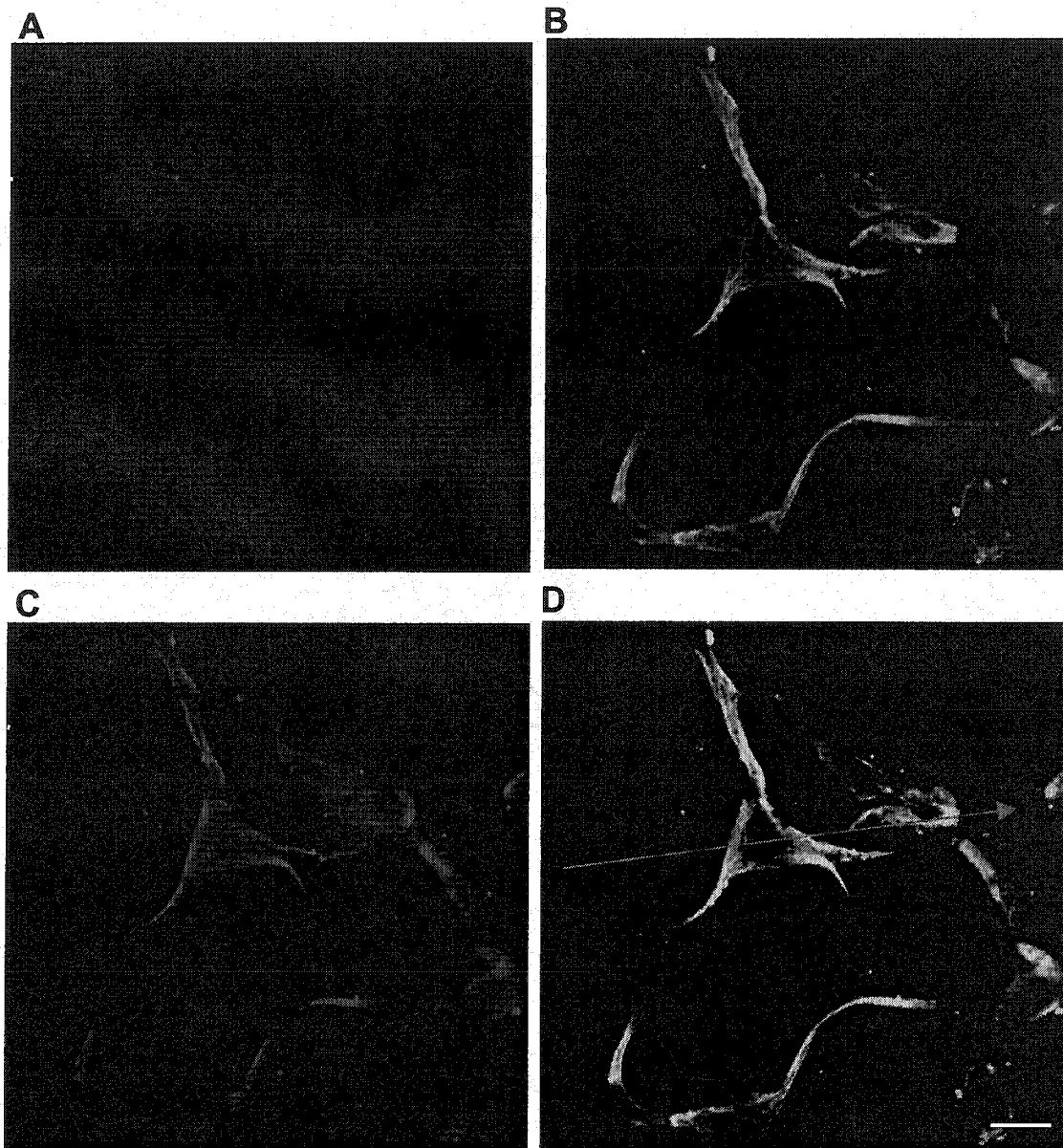


Figure VII-9. Localization of hCNT2 to cell surfaces of human umbilical vein endothelial cells (HUVEC)

HUVEC (generations 2-4) were grown on gelatin-coated inserts overnight as described in section II.10.2. Inserts were fixed in paraformaldehyde, permeabilized in Triton X-100, incubated with either preimmune rabbit sera (Panel A) or anti-hCNT2 polyclonal and monoclonal antibodies (Panels B, C, D), followed with Alexa Fluor 488 conjugated goat anti-rabbit antibodies and Alexa Fluor 594 conjugated goat anti-mouse antibodies, and mounted on slides in 90% glycerol. Slides were visualized by LSM-510 confocal microscopy as described in section II.22. Shown are immunofluorescence staining with preimmune rabbit sera (Panel A), anti-hCNT2 polyclonal antibodies (Panel B), and anti-hCNT2 monoclonal antibodies (Panel C). Panel D is the superimposed image of Panels B and C. *Bar*, 15 μm . *Arrowed line* depicts region of interest for colocalization profiling in Figure VII-10.

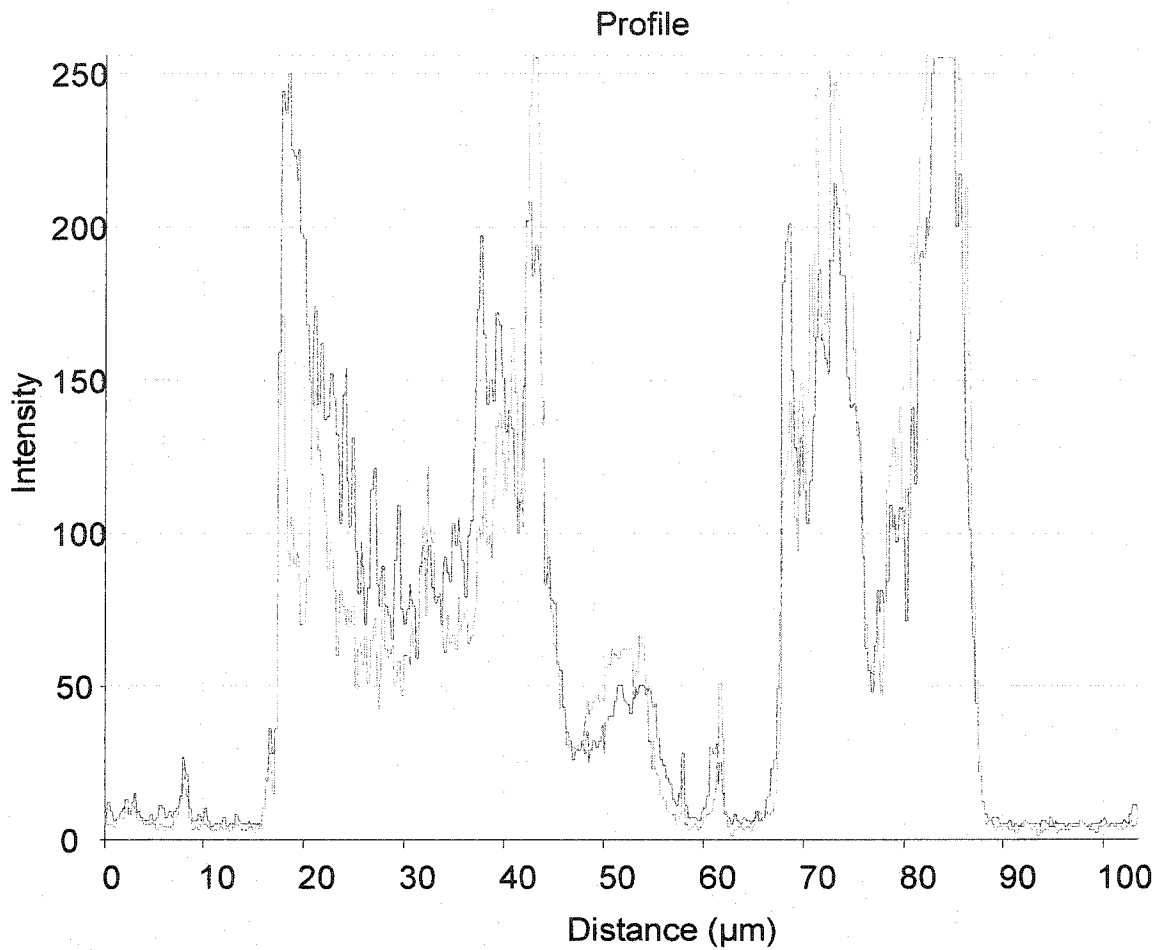


Figure VII-10. Profile of colocalized immunofluorescent signals from anti-hCNT2 polyclonal and monoclonal antibody staining of HUVEC

Colocalization analysis was performed on the superimposed image of Panel D in Figure VII-9 using LSM-510 software. Signal intensities of immunofluorescent staining patterns by anti-hCNT2 polyclonal and monoclonal antibodies were profiled in a selected region of interest as denoted by the arrowed line in Figure VII-9. Signal intensities shown in red and green are, respectively, from anti-hCNT2 monoclonal and polyclonal antibodies.

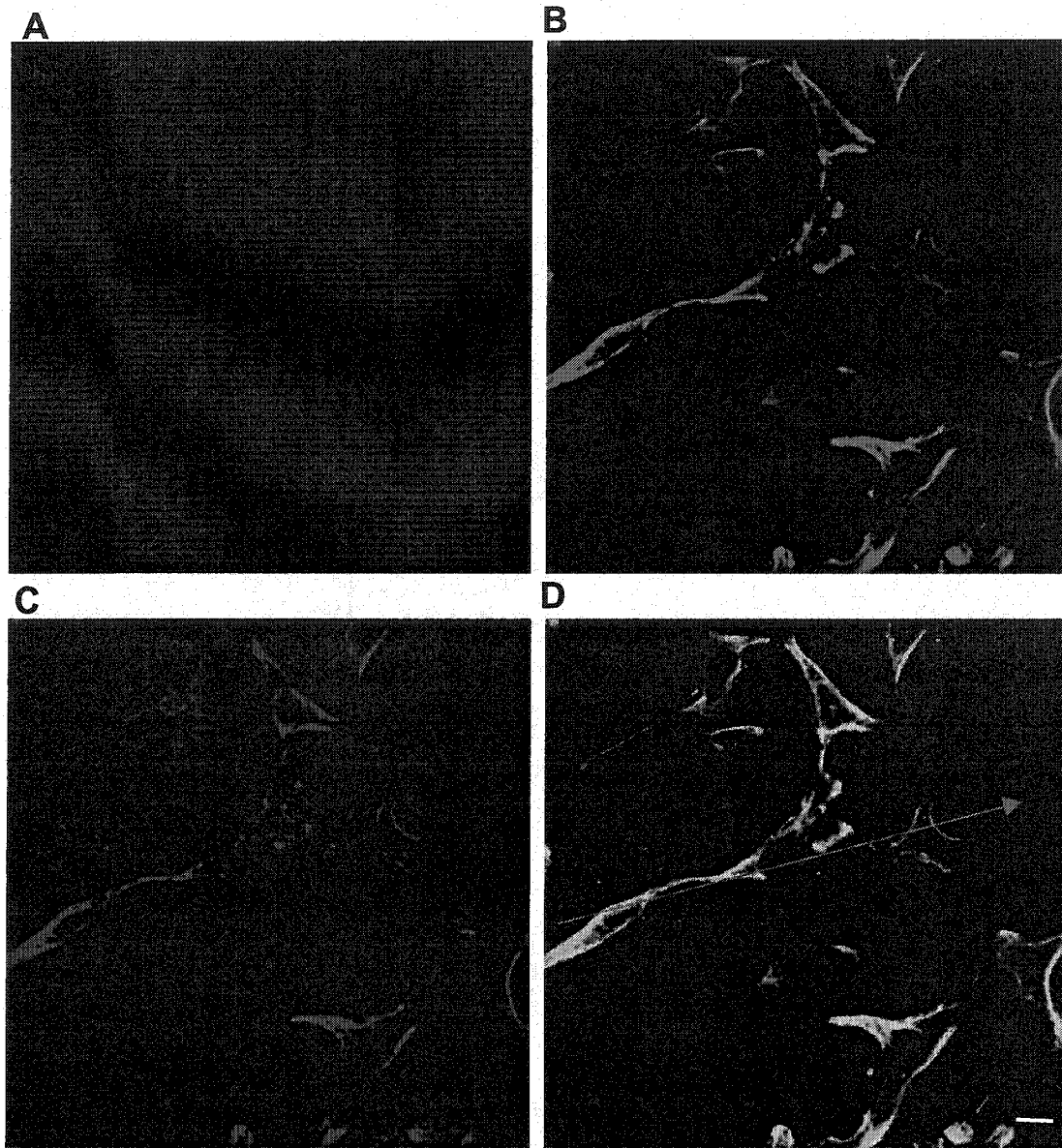


Figure VII-11. Localization of hCNT3 to cell surfaces of human umbilical vein endothelial cells (HUVEC)

HUVEC (generations 2-4) were grown on gelatin-coated inserts overnight as described in VII-9. Inserts were fixed in paraformaldehyde, permeabilized in Triton X-100, incubated with either preimmune rabbit sera (Panel A) or anti-hCNT3 polyclonal antibodies directed against epitope TL3361 and monoclonal antibodies directed against epitope TL3360 (Panels B, C, D) of hCNT3, followed with Alexa Fluor 488 conjugated goat anti-rabbit antibodies and Alexa Fluor 594 conjugated goat anti-mouse antibodies, and mounted on slides in 90% glycerol. Slides were visualized by LSM-510 confocal microscopy as described in section II.22. Shown are immunofluorescence staining by preimmune rabbit sera (Panel A), anti-hCNT3 polyclonal antibodies (Panel B), and anti-hCNT3 monoclonal antibodies (Panel C). Panel D is the superimposed image of Panels B and C. *Bar*, 20 μm . *Arrowed line* depicts region of interest for colocalization profiling in Figure VII-12.

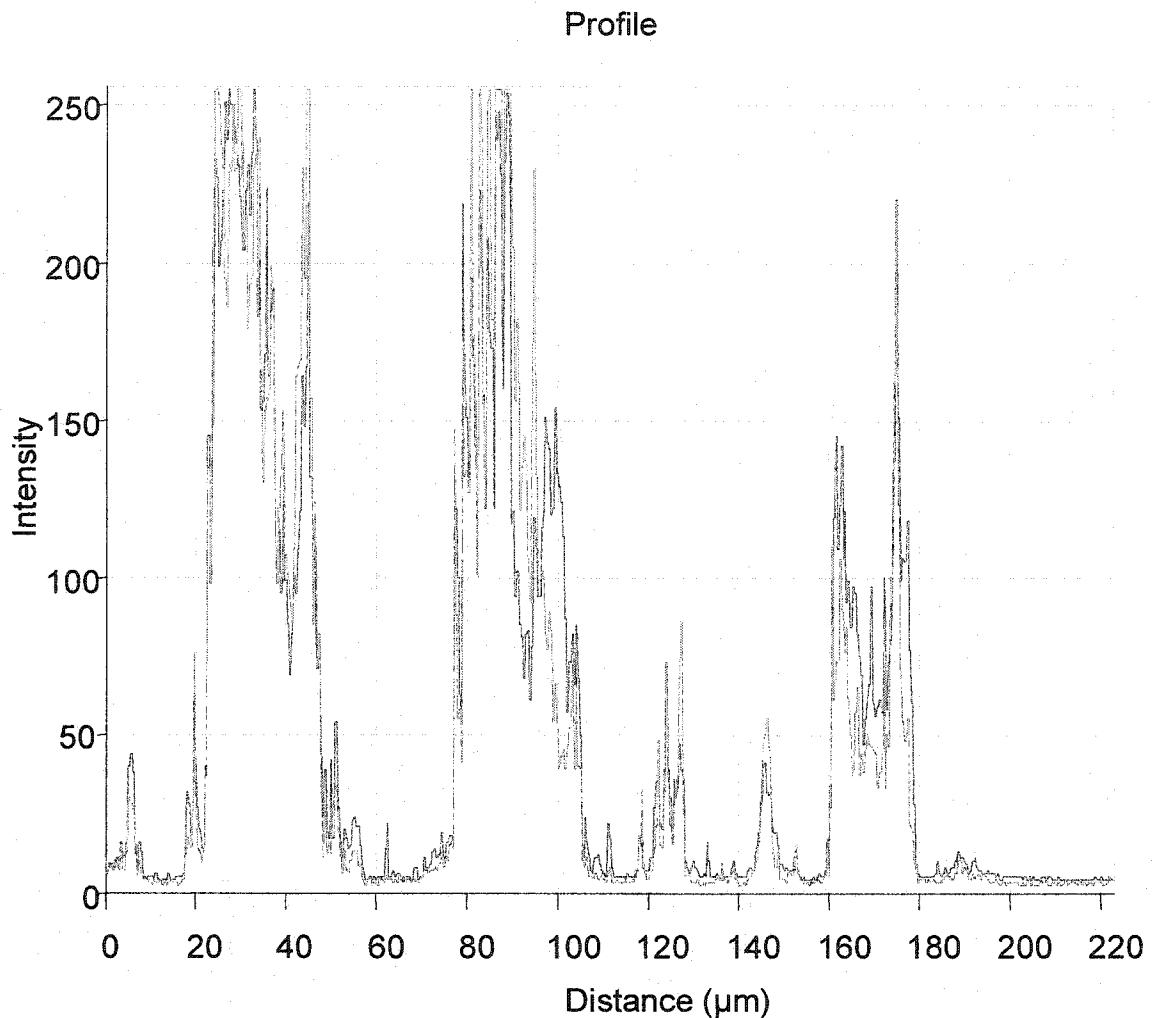


Figure VII-12. Profile of colocalized immunofluorescent signals from anti-hCNT3 polyclonal and monoclonal antibody staining of HUVEC

Colocalization analysis was performed on the superimposed image of Panel D in Figure VII-11 using LSM-510 software. Signal intensities of immunofluorescent staining patterns by anti-hCNT3 polyclonal antibodies against epitope TL3361 and monoclonal antibodies against epitope TL3360 were profiled in a selected region of interest as denoted by the arrowed line in Figure VII-11. Signal intensities shown in red and green are, respectively, from anti-hCNT3 monoclonal and polyclonal antibodies

Chapter VIII

VIII. General Conclusions and Discussion

The significant achievements of the present work were the development of *in vitro* model systems based on human cell lines and the generation of polyclonal and monoclonal antibodies that specifically recognized either hCNT2 or hCNT3. The production of stable transfectants in transport-deficient human leukemia cells provided new model cell lines to study and compare the properties of hCNTs with respect to their interactions with nucleoside analogs. The generation and characterization of antibodies against hCNT2 and hCNT3 provided the prerequisite immunological tools to conduct research aimed at determining their subcellular locations, tissue distributions, and their roles in nucleoside utilization and pharmacology. The studies described in this thesis provided insights into the importance of hCNT family members in nucleoside drug uptake and adenosine-mediated signaling in the brain, and also provided evidence that suggested regulation of hCNT3 during intestinal epithelia differentiation.

VIII.1. Characterization of endogenous nucleoside transporters present in cultured human cell lines

Multiple nucleoside transporters with overlapping substrate selectivities are naturally present in mammalian cells [153, 200, 201]. An important aspect of generating transfectants was to first acquire knowledge of the endogenous nucleoside transport proteins present in potential recipient cells. Analysis of the expression profiles of nucleoside transporter mRNAs and characterization of the associated nucleoside transport activities in various human cell lines derived from different tissues identified two human lines, HeLa and CEM-ARAC, as

potential recipients for production, respectively, of transient and stable transfectants.

While the molecular and functional characterization of the cultured cell lines provided useful information for generation of transfectants, they also contributed to a body of knowledge with respect to the types of nucleoside transporters present in particular cell types. This information may be potentially useful in the selection of appropriate nucleoside drugs in chemotherapy regimens. For instance, hENT mRNAs were expressed in all the leukemic cell lines examined whereas hCNT mRNAs were not detected in any of these cell lines. Thus, it may be postulated that hENT1 plays a more prominent role in chemotherapy against leukemia utilizing cladribine since hENT1 also exhibited a greater capacity for the transport of cladribine than either hCNT2 or hCNT1. Indeed, CEM cells, which possessed only hENT1, were demonstrated to be much more sensitive to cladribine than ARAC/D2 cells that produced recombinant hCNT2. In freshly isolated leukemic lymphoblasts, *in vitro* sensitivity to cladribine correlated with es (i.e., hENT1) abundance in plasma membranes as determined by SAENTA-fluorescein binding [220]. In contrast, a low abundance or deficiency of nucleoside transporters that mediated the uptake of gemcitabine and cytarabine has been shown to contribute to decreased sensitivity to the drugs *in vitro* and *in vivo* [69, 220].

VIII.2. Generation of transfectants for assessing nucleoside analog interactions with hCNTs

Knowledge of the expression profiles and functional activities of nucleoside transporters present in the different cell lines analyzed aided in the choice of two cell lines (HeLa and CEM-ARAC) to be used as recipients for gene transfer of exogenous nucleoside transporter cDNAs. HeLa cells, which lacked functional expression of hCNTs, were transiently transfected with coding sequences corresponding to hCNT1, hCNT2, hCNT3 or hCNT3-GFP. This work provided transient transfectants of HeLa cells for study of recombinant hCNTs and characterization of antibodies against hCNT proteins by immunoblot and immunofluorescence analyses.

CEM-ARAC cells were shown to exhibit a complete deficiency in nucleoside transport capability due to the lack of hENT1 mRNA expression, and hENT1 protein production at the cell surface, and this was associated with *in vitro* resistance to nucleoside drugs that were permeants of hENT1. In contrast, wildtype CEM cells expressed hENT1 mRNA and were capable of nucleoside transport mediated by endogenous hENT1. Gene transfer techniques were used to introduce cDNAs encoding hCNT1, hCNT2 and hENT2 into transport-deficient CEM-ARAC cells, thereby generating a series of stable cell lines to undertake structure-activity and structure-cytotoxicity relationship studies. Future work, which has already been initiated, will be aimed at generating hCNT3 and hENT1 stable transfectants to provide a complete panel of stable cell lines to be used as

model systems for (i) drug screening, (ii) identification of potent CNT inhibitors and (iii) comparison of the different human nucleoside transporters.

To determine if modifications of natural nucleosides affected their interactions with hCNT proteins and, in some cases, transportability, a variety of nucleoside analogs were examined, including nucleosides with substitution or elimination of the hydroxyl group at the 2'- and 3'-position of the pentose ring sugar and addition of bulky, hydrophobic substituents or halogens at, respectively, the N6 and C5 positions of the base. These studies identified key structural features that enable predictions of whether or not a particular nucleoside drug is likely to be accepted as a permeant. For example, hCNT1 and hCNT2 appeared to be highly stereoselective with preferences for the naturally occurring D- over the L-enantiomers. This stereoselectivity is not only pertinent to the hCNTs, but also extends to the hENTs [310]. Therefore, it may be expected that nucleoside drugs with the L-configuration, such as some of the antiviral nucleoside drugs [61, 319] are not likely transported by nucleoside transporters. Another example of the influence of stereoselectivity on transportability is the novel deoxycytidine analogue, troxicitabine, also an L-nucleoside, which has potent antitumor activity in animal models, and is currently in clinical trials. Troxicitabine is not transported by either hENTs or hCNTs [68].

Loss or substitution of the 3'- and 5'-hydroxyl groups of the ribosyl moiety decreased, or eliminated altogether, nucleoside analog binding to both hCNT1 and hCNT2. This result was similar to results of early studies with the *es*-type transporter, in which the presence of the 3'-hydroxyl group was shown to be an

important determinant of transportability [65, 223]. The removal of the hydroxyl at the 2'-position did not significantly affect interaction of nucleoside analogs with hCNTs. Therefore, it appears that the 3'- and 5'-hydroxyl groups were important structural features for permeant recognition, and the 2'-hydroxyl group was less important. There was also a preference for the 2'-hydroxyl group in the α - rather than β -configuration (i.e., ribose versus arabinose). Future experiments should be focused on assessing the substrate selectivities, inhibitory activities and kinetics of transport for uridine and adenosine analogs by hCNT3. These results could then be compared against those of hCNT1 and hCNT2 to gain a better understanding of the origin of selectivity and efficacy of nucleoside drugs.

Nicotine and ligands of adenosine receptors such as caffeine, N⁶-p-aminobenzyladenosine and 2-chloroadenosine, which exhibit effects in the CNS, differed in their abilities to interact with either hCNT1 or hCNT2. Given that CNT1 and CNT2 mRNAs are expressed in rat brain [182], and hCNT2 was distributed with varied abundance in human brain, it is tempting to speculate that these substances may have differential effects on hCNT1- and hCNT2-mediated adenosine influx in the CNS. Future work should be directed at determining the inhibitory activities of these substances on adenosine influx by native CNT1 and CNT2 proteins in preparations of brain cells. There is evidence of tissue-specific differences in the kinetics of adenosine transport between CNT2 cloned from rat blood-brain barrier and intestine [363, 382]. To further address the nature of these differences, characterization of the inhibitory effects of adenosine analogs, caffeine and nicotine on CNT-mediated adenosine influx should be performed on

specific cell types in brain such glial cells and endothelial cells. It has been well documented that adenosine acts as an inhibitor of CNT1, while behaving as a high-affinity, high-capacity permeant of CNT2 [15]. Perhaps further characterization of other adenosine analogs would potentially identify potent inhibitors of hCNT1, which this study aimed at achieving, but without success.

VIII.3. Correlation of nucleoside drug transport capabilities with *in vitro* drug sensitivities

The purine-nucleoside selective hCNT2 exhibited a tolerance for uridine analogs with modifications of the 5, but not the 3, position of the base with halogen substituents, which included several fluoropyrimidine nucleoside drugs. These were transported by hCNT2 with greater activity than some of the adenosine analog drugs, such as cladribine and fludarabine, and this correlated with a greater *in vitro* chemosensitivity of ARAC/D2 cells, which contained hCNT2. The degree of sensitivity of cells to uridine- and adenosine-analog drugs was reflected in their affinities and patterns of transport activity by hCNT2.

The difference in kinetics of transport between hCNT2 (higher affinity, lower activity) and hENT1 (lower affinity, higher activity) for several anticancer nucleoside drugs suggests that it may be possible to rationally design chemotherapeutic schedules that take advantage of these differences. If an expression profile of a given tumor was assessed to exhibit mainly hCNT2, one might target the cancer cells with low-dose, long-duration exposures to fluoropyrimidine nucleosides, which would be actively concentrated in cancer cells through the action of hCNT2, while minimizing toxicity to surrounding cells.

Since hENT1 appears to be present in most tissues, another strategy to increase the therapeutic index of fluoropyrimidine nucleosides might be to use ENT inhibitors (e.g., dipyridamole or NBMPR phosphate) to block drug efflux by hENT1, while the inward transport of drug by hCNT2 is maintained. A similar strategy exhibited enhanced anti-proliferative activity of araA (9-beta-D-arabinofuranosyladenine) against L1210/C2 murine leukemia cells [227] due to intracellular accumulation of araA in cells mediated by the *cif* (i.e., CNT2-mediated) process and inhibition of outward araA transport by the *es* and *ei* (i.e., ENT1- and ENT2-mediated) processes using dipyridamole [201]. In HL-60 human leukemia cells, which possess hENTs as well as hCNT3 [2], an increased sensitivity to araC was achieved by utilizing dipyridamole to block araC efflux, while maintaining drug uptake through the action of hCNT3 [383].

The availability of specific antibodies against members of the CNT family will enable future determinations of the tissue and tumor distribution of these proteins and their relationship to malignant progression. Knowledge of the type of hCNT proteins present in a tumor may allow rational nucleoside drug selection or prediction of response to nucleoside chemotherapy. For example, hCNT1 and hCNT2 differed in their abilities to transport 5-fluoro-5'-deoxyuridine, which is the metabolite of orally administered capecitabine utilized in the treatment of a variety of solid tumors, including breast and GI cancers [301, 302]. Therefore, if a given malignancy possessed little or no hCNT1, even though it contained hCNT2, it might not be beneficial to use capecitabine since the transported metabolite is a poor permeant of hCNT2, but a good permeant of hCNT1 [86].

On the other hand, breast-derived MCF7 cancer cells were shown to possess hCNT1 transcripts (this study), and breast tissues were shown to possess hENT1 protein [294], suggesting that it may be beneficial to treat this type of malignancy with capecitabine since transport of its metabolite (5-fluoro-5'-deoxyuridine) is mediated by both type of transporters [294].

VIII.4. Production of antibodies against CNT proteins

Studies in the field of nucleoside transport have primarily focused on plasma membrane transport, whereas the cellular and tissue locations of the transport proteins, for the most part, have not been addressed. This work generated antibodies specifically against hCNT2 and hCNT3, which enabled the detection and visualization of these transporters by immunoblot and immunofluorescence analyses.

Further efforts should be aimed at generating antibodies against hCNT1, which would provide a complete panel of antibodies to study members of the hCNT family. Antibodies raised against extracellular epitopes of nucleoside transporters would also be advantageous since they allow for analysis of intact cells without permeabilization. The production of antibodies against intracellular and extracellular epitopes of hCNT1 (T. Lang, K. Graham, P. Carpenter, C. Cass) and hENT2 (T. Lang, P. Carpenter, C. Cass) have commenced. Characterization of anti-hENT2 polyclonal and monoclonal antibodies have demonstrated the specificity of these antibodies against recombinant hENT2. Further characterization of anti-hCNT1 antibodies is required. The availability of these antibodies will enable different types of biochemical and cell biological

approaches to further study the regulation of native transporters in cells or tissues.

VIII.5. Subcellular location of recombinant hCNT2 and regulation of hCNT3 distribution and abundance during intestinal cell differentiation

Recombinant hCNT2 was primarily found in the plasma membranes of the cell line stably transfected with hCNT2 cDNA. In contrast, native hCNT3 was localized to intracellular compartments of non-differentiated Caco-2 intestinal epithelial cells. As Caco-2 cells progressed towards a more differentiated phenotype, the subcellular location of hCNT3 was altered from primarily intracellular to cell surface. The increased hCNT3 localization to cell surfaces in well-differentiated Caco-2 cells was associated with increased hCNT3 abundance and transport activity detected at apical membranes of Caco-2 monolayers. Examination of hCNT3 in different regions of human gastrointestinal tract revealed higher hCNT3 levels in jejunum and duodenum, and lower levels in colon, suggesting a physiological basis for the difference in hCNT3 abundance between the small and large intestine, and the prevalence of hCNT3 in tissues involved in nutrient and drug absorption. These observations raise the possibility that hCNT3 abundance and distribution may be regulated as intestinal epithelial cells undergo morphological and functional changes as they migrate from the crypts up the villi. It has been well documented that the levels of brush-border enzymes and the capacity for absorption are higher in intestinal epithelial cells at the villus tips than in the crypts [332, 340, 384]. Further

experiments, which have been initiated, are aimed at determining the subcellular location of hCNT3 in frozen jejunum sections by immunofluorescence confocal microscopy (C. Wong, T. Lang, C. Cass). Development of techniques for immunohistochemistry employing paraffin-embedded, formalin-fixed jejunum sections and antibodies against hCNT2 and hCNT3 is currently underway (C. Wong, L. Dabbagh, T. Lang, J. Mackey, C. Cass).

The CNT family members, hCNT2 and hCNT3, possess consensus sites for phosphorylation by protein kinase C, but whether or not these proteins are regulated by phosphorylation has not been determined. Further studies should examine whether protein kinase C regulates hCNT3-mediated nucleoside transport activity in Caco-2 cells. To determine the effects of protein kinase C on hCNT3-mediated activity, 10 μ M uridine transport into Caco-2 cells could be measured following up-regulation or down-regulation of protein kinase C activity by exposure of Caco-2 cells to 100 nM of PMA for, respectively, 10 min or 24 hr.

The pyrimidine-nucleoside selective CNT1 of rats has been shown to be glycosylated [141] and it may be expected that other CNT family members are also glycoproteins since they possessed consensus sites for N-linked glycosylation. N-Glycosylation is important in the functional activity and trafficking of other membrane transporters to cell surfaces [353], but whether or not this applies to the hCNTs is not known. Loss of N-linked glycosylation capability in hENT1 does not appear to affect its transport activity, although the binding characteristics of the transporter for NBMPR, dilazep and dipyridamole were substantially altered [270].

Experiments have been initiated to determine the glycosylation status of hCNT2 and hCNT3 produced in HeLa cells by transient transfection of their cDNAs. The use of endoglycosidase F to remove N-linked carbohydrates from proteins and immunoblot analysis of the treated and untreated membrane preparations revealed that recombinant hCNT2 and hCNT3 were glycoproteins (T. Lang and C. Cass, Unpublished results). Future experiments should also assess location of the glycosylation sites utilized, which could be accomplished by systematically removing the potential glycosylation sites on the protein by site-directed mutagenesis and analyzing the different mutant proteins using procedures similar to those described by Hamilton *et al* [141]. The importance of N-linked glycosylation could be assessed by introducing the different glycosylation mutants generated by site-directed mutagenesis into HeLa cells and testing for nucleoside transport activity.

VIII.6. Relationships between the distribution and location of CNTs and sites of adenosine action

To gain a better understanding of the role of concentrative nucleoside transporters in the regulation of adenosine-mediated physiological and pathological events, this study investigated the distribution and location of hCNT2 and hCNT3 in human brain and vascular endothelial cells. The relative levels of hCNT2 in different regions of human brain revealed a strong positive correlation with relative levels of adenosine A1 receptors, suggestive of an anatomical and/or neurochemical relationship between hCNT2 and sites of adenosine action. It was not possible to establish whether or not there was a

relationship between the distribution of hCNT3 and adenosine A₁ receptors in human brain from the studies presented in this thesis. While hCNT3 may also modulate extracellular adenosine pools near adenosine A₁ receptors, hCNT2 and hCNT3 may act at sites of adenosine action with other P1 purinoceptors such as the A_{2a}, A_{2b} or A₃ subtypes or the P2 purinoceptors. Future experiments should compare the distribution of hCNT2 and hCNT3 with those of other P1 purinoceptor subtypes or P2 purinoceptors. These experiments may provide clues as to the reason for the prevalence of hCNT3 throughout most regions of human brain investigated. The unique ability of hCNT3, among hCNTs, to accept both purine and pyrimidine nucleosides as permeants, both of which are undoubtedly important in brain functions, suggests that hCNT3 may play a role in salvage of these nucleosides from brain interstitium.

Future research should be aimed at assessing the location of hCNT2 and hCNT3 in tissue sections of human brain by immunohistochemical analysis with antibodies against hCNT2 and hCNT3. If antibodies against hCNT1 become available, they should also be included in the analysis to define the tissue location of hCNT1 and compare it with the distribution of adenosine A₁ receptors. Paraffin-embedded formalin-fixed normal brain tissue sections have been obtained from Dr. C. Hao (Laboratory Medicine and Pathology, University Hospital and University of Alberta) with the intention of conducting immunohistochemistry on brain tissues to further define the anatomical distribution and cellular location of the CNTs. These studies may identify specific cell types in brain (e.g. neurons, astrocytes and glial cells) that possess

particular members of the CNT family. Antigen retrieval techniques involving high-temperature treatment of brain tissues with aqueous salt solutions [385, 386] have been employed in an effort to achieve uniform and reproducible staining of formalin-fixed brain sections. These experiments so far have not yielded meaningful results. An alternative approach will be to use frozen sections of brain tissue for immunofluorescence confocal microscopic analysis with antibodies against the various CNT proteins. This approach has yielded much success in immunohistochemical determination of hENT1 in cryosectioned tissue of breast cancer [294].

Chapter IX

IX. Bibliography

1. Cass, C.E., E. Dahlig, E.Y. Lau, T.P. Lynch, and A.R. Paterson, *Fluctuations in nucleoside uptake and binding of the inhibitor of nucleoside transport, nitrobenzylthioinosine, during the replication cycle of HeLa cells*. *Cancer Res*, 1979. **39**(4): p. 1245-52.
2. Ritzel, M.W., A.M. Ng, S.Y. Yao, K. Graham, S.K. Loewen, K.M. Smith, R.G. Ritzel, D.A. Mowles, P. Carpenter, X.Z. Chen, E. Karpinski, R.J. Hyde, S.A. Baldwin, C.E. Cass, and J.D. Young, *Molecular identification and characterization of novel human and mouse concentrative Na⁺-nucleoside cotransporter proteins (hCNT3 and mCNT3) broadly selective for purine and pyrimidine nucleosides (system cib)*. *J Biol Chem*, 2001. **276**(4): p. 2914-27.
3. Lee, C.W., J.A. Sokoloski, A.C. Sartorelli, and R.E. Handschumacher, *Induction of the differentiation of HL-60 cells by phorbol 12-myristate 13-acetate activates a Na⁽⁺⁾-dependent uridine-transport system. Involvement of protein kinase C*. *Biochem J*, 1991. **274**(Pt 1): p. 85-90.
4. Sokoloski, J.A., C.W. Lee, R.E. Handschumacher, A. Nigam, and A.C. Sartorelli, *Effects of uridine on the growth and differentiation of HL-60 leukemia cells*. *Leukemia Research*, 1991. **15**(11): p. 1051-8.
5. Soler, C., A. Felipe, J.F. Mata, F.J. Casado, A. Celada, and M. Pastor-Anglada, *Regulation of nucleoside transport by lipopolysaccharide, phorbol esters, and tumor necrosis factor-alpha in human B-lymphocytes*. *J Biol Chem*, 1998. **273**(41): p. 26939-45.
6. Meckling-Gill, K.A., L. Guilbert, and C.E. Cass, *CSF-1 stimulates nucleoside transport in S1 macrophages*. *J Cell Physiol*, 1993. **155**(3): p. 530-8.
7. McGowan, K.M., S.D. Long, and P.H. Pekala, *Glucose transporter gene expression: regulation of transcription and mRNA stability*. *Pharmac Ther*, 1995. **66**: p. 465-505.
8. Chin, K.-V., I. Pastan, and M.M. Gottesman, *Function and regulation of the human multidrug resistance gene*. *Adv Cancer Res*, 1993. **60**: p. 157-180.

9. del Santo, B., R. Valdes, J. Mata, A. Felipe, F.J. Casado, and M. Pastor-Anglada, *Differential expression and regulation of nucleoside transport systems in rat liver parenchymal and hepatoma cells*. *Hepatology*, 1998. **28**(6): p. 1504-11.
10. Latini, S. and F. Pedata, *Adenosine in the central nervous system: release mechanisms and extracellular concentrations*. *J Neurochem*, 2001. **79**(3): p. 463-84.
11. Ralevic, V. and G. Burnstock, *Receptors for purines and pyrimidines*. *Pharmacological Reviews*, 1998. **50**: p. 413-492.
12. Griffith, D.A. and S.M. Jarvis, *Nucleoside and nucleobase transport systems of mammalian cells*. *Biochimica et Biophysica Acta Reviews on Biomembranes*, 1996. **1286**(3): p. 153-181.
13. Cass, C.E., *Nucleoside Transport*, in *Drug Transport in Antimicrobial and Anticancer Chemotherapy*, N.H. Georgopapadaku, Editor. 1995, Marcel Dekker: New York, NY. p. 403-451.
14. Murray, A.W., *The biological significance of purine salvage*. *Ann Rev Biochem*, 1971. **40**: p. 811-826.
15. Cass, C.E., J.D. Young, and S.A. Baldwin, *Recent advances in the molecular biology of nucleoside transporters of mammalian cells*. *Biochem Cell Biol*, 1998. **76**(5): p. 761-70.
16. Pelleg, A., *Adenosine in the heart: Its emerging roles*. *Hospital Practice*, 1993. **28**(3).
17. Thorn, J.A. and S.M. Jarvis, *Adenosine transporters*. *General Pharmacology*, 1996. **27**: p. 613-620.
18. Hiddemann, W., R. Rottmann, B. Wormann, A. Thiel, M. Essink, C. Ottensmeier, M. Freund, T. Buchner, and J. van de Loo, *Treatment of advanced chronic lymphocytic leukemia by fludarabine - Results of a clinical phase-II study*. *Ann Hematol*, 1991. **63**: p. 1-4.
19. Collis, M.G. and S.M.O. Hourani, *Adenosine receptor subtypes*. *TIPS Reviews*, 1993. **14**: p. 360-366.

20. Klotz, K.N., *Adenosine receptors and their ligands*. Naunyn-Schmiedeberg's Arch Pharmacol, 2000. **362**: p. 382-391.
21. Geiger, D.D. and D.M. Fyda, *Adenosine Transport in Nervous System Tissues*, T.E. Stone, Editor. 1991. p. 1-23.
22. Delicado, E.G., A. Rodrigues, R.P. Sen, A.M. Sebastiao, J.A. Ribeiro, and M.T. Miras-Portugal, *Effect of 5'-(N-ethylcarboxamido)adenosine on adenosine transport in cultured chromaffin cells*. J Neurochem, 1990. **54**(6): p. 1941-6.
23. Abd-Elfattah, A.S., M.E. Jessen, J. Lekven, and A.S. Wechsler, *Differential cardioprotection with selective inhibitors of adenosine metabolism and transport: role of purine release in ischemic and reperfusion injury*. Mol Cell Biochem, 1998. **180**(1-2): p. 179-91.
24. Abd-Elfattah, A.S., S. Mardini, J.H. Guo, M.I. Shehab, N. El-Singaby, S.P. Gao, and E.M. El-Guessab, *Nucleoside transport protein: Properties and regulation*, in *Purines and Myocardial Protection*, A.S. Abd-Elfattah and A.S. Wechsler, Editors. 1996, Kluwer Academic Publishers. p. 151-163.
25. Robertson, J.I.S., *Adenosine, cardioprotection and its clinical application*. Expert Opinion on Investigational Drugs, 1995. **4**(2): p. 157-158.
26. Brown, J.R., K. Cornell, and P.W. Cook, *Adenosine- and adenine-nucleotide-mediated inhibition of normal and transformed keratinocyte proliferation is dependent upon dipyridamole-sensitive adenosine transport*. J Invest Dermatol, 2000. **115**(5): p. 849-59.
27. Cook, P.W., N.M. Ashton, and M.R. Pittelkow, *Adenosine and adenine nucleotides inhibit the autonomous and epidermal growth factor-mediated proliferation of cultured human keratinocytes*. J Invest Dermatol, 1995. **104**(6): p. 976-81.
28. Barry, C.P. and S.E. Lind, *Adenosine-mediated killing of cultured epithelial cancer cells*. Cancer Res, 2000. **60**(7): p. 1887-94.
29. Sellers, L.A., J. Simon, T.S. Lundahl, D.J. Cousens, P.P. Humphrey, and E.A. Barnard, *Adenosine Nucleotides Acting at the Human P2Y1*

- Receptor Stimulate Mitogen-activated Protein Kinases and Induce Apoptosis.* J Biol Chem, 2001. **276**(19): p. 16379-16390.
30. Peyot, M.L., A.P. Gadeau, F. Dandre, I. Belloc, F. Dupuch, and C. Desgranges, *Extracellular Adenosine Induces Apoptosis of Human Arterial Smooth Muscle Cells via A(2b)-Purinoceptor.* Circ Res, 2000. **86**(1): p. 76-85.
 31. Schrier, S.M., E.W. van Tilburg, H. van der Meulen, A.P. Ijzerman, G.J. Mulder, and J.F. Nagelkerke, *Extracellular adenosine-induced apoptosis in mouse neuroblastoma cells studies on involvement of adenosine receptors and adenosine uptake.* Biochem Pharmacol, 2001. **61**(4): p. 417-425.
 32. Ceruti, S., C. Franceschi, D. Barbieri, W. Malorni, A. Camurri, A.M. Giammarioli, A. Ambrosini, G. Racagn, F. Cattabeni, and M.P. Abbracchio, *Apoptosis induced by 2-chloro-adenosine and 2-chloro-2'-deoxy-adenosine in a human astrocytoma cell line: differential mechanisms and possible clinical relevance.* J Neurosci Res, 2000. **60**: p. 388-400.
 33. Dawicki, D.D., D. Chatterjee, J. Wyche, and S. Rounds, *Extracellular ATP and adenosine cause apoptosis of pulmonary artery endothelial cells.* Am J Physiol, 1997. **273**: p. L485-L494.
 34. Rounds, S., W.L. Yee, D.D. Dawicki, E. Harrington, N. Parks, and M.V. Cutaia, *Mechanism of extracellular ATP- and adenosine-induced apoptosis of cultured artery endothelial cells.* Am J Physiol, 1998. **275**: p. L379-L388.
 35. Dunwiddie, T.V. and S.A. Masino, *The role and regulation of adenosine in the central nervous system.* Annu Rev Neurosci, 2001. **24**: p. 31-55.
 36. Pearson, T., F. Nuritova, D. Caldwell, N. Dale, and B.G. Frenguelli, *A depletable pool of adenosine in area ca1 of the rat hippocampus.* J Neurosci, 2001. **21**(7): p. 2298-307.

37. Imura, T. and S. Shimohama, *Opposing effects of adenosine on the survival of glial cells exposed to chemical ischemia*. J Neurosci Res, 2000. **62**(4): p. 539-46.
38. Fredholm, B.B., M.P. Abbracchio, G. Burnstock, J.W. Daly, T.K. Harden, K.A. Jacobson, P. Leff, and M. Williams, *Nomenclature and classification of purinoceptors*. Pharmacol Rev, 1994. **46**: p. 143-156.
39. Geiger, J.D., M.E. Johnston, and V. Yago, *Pharmacological characterization of rapidly accumulated adenosine by dissociated brain cells from adult rat*. J Neurochem, 1988. **51**(1): p. 283-91.
40. Thampy, K.G. and E.M. Barnes, Jr., *Adenosine transport by primary cultures of neurons from chick embryo brain*. J Neurochem., 1983. **40**: p. 874 -879.
41. Thampy, K.G. and E.M. Barnes, Jr., *Adenosine transport by cultured glial cells from chick embryo brain*. Arch. Biochem. Biophys., 1986. **220**: p. 340-346.
42. Miras-Portugal, M.T., E.G. Delicado, T. Casillas, and R.P. Sen, *Control of nucleoside transport in neural cells. Effect of protein kinase C activation*. Adv Exp Med Biol, 1991. **309A**: p. 435-8.
43. Marijnen, Y.M., D. de Korte, D. Roos, and A.H. van Gennip, *Purine and pyrimidine metabolism of normal and leukemic lymphocytes*. Adv Exp Med Biol . 1989. **253A**: p. 433-438.
44. Meisel, H., S. Gunther, D. Martin, and E. Schlimme, *Apoptosis induced by modified ribonucleosides in human cell culture systems*. FEBS Lett, 1998. **433**: p. 265-268.
45. Piga, A., K. Ganeshaguru, E.S. Green, B. Sheridan, and A.V. Hoffbrand, *Selective toxicity of purine nucleosides to human leukaemic cells*. Adv Exp Med Biol . 1989. **253**: p. 291-298.
46. De Fouw, N.J., D.D. Ma, R. Michalevicz, D.A. Gray, and A.V. Hoffbrand, *Differential cytotoxicity of deoxyguanosine and 8-aminoguanosine for human leukemic cell lines and normal bone marrow progenitor cells*. Hematol Oncol, 1984. **2**: p. 189-197.

47. Kim SG, Kim CW, Ahn ET, Lee KY, Hong EK, Y. BI, and H. YB., *Enhanced anti-tumour effects of acriflavine in combination with guanosine in mice*. J Pharm Pharmacol, 1997. **49**: p. 216–222.
48. Osti, F., F.G. Corradini, S. Hanau, M. Matteuzzi, and R. Gambari, *Human leukemia K562 cells: induction to erythroid differentiation by guanine, guanosine and guanine nucleotides*. Haematologica, 1997. **82**: p. 395–401.
49. Van der Kraan, P.M., P.M. van Zandvoort, R.A. De Abreu, and J.A. Bakkeren, *Effects of 8-aminoguanosine on the toxicity of guanosine and deoxyguanosine for malignant and normal lymphoid cells*. J Leukoc Biol, 1988. **44**: p. 46–50.
50. Kelly, K.J., Z. Plotkin, and P.C. Dagher, *Guanosine supplementation reduces apoptosis and protects renal function in the setting of ischemic injury*. J Clin Invest, 2001. **108**(9): p. 1291-8.
51. Traut, T.W., *Physiological concentrations of purines and pyrimidines*. Mol Cell Biochem, 1994. **140**(1): p. 1-22.
52. Connolly, G.P. and J.A. Duley, *Uridine and its nucleotides: biological actions, therapeutic potentials*. Trends Pharmacol Sci, 1999. **20**(5): p. 218-25.
53. Cass, C.E., J.D. Young, S.A. Baldwin, M.A. Cabrita, K.A. Graham, M. Griffiths, L.L. Jennings, J.R. Mackey, A.M. Ng, M.W. Ritzel, M.F. Vickers, and S.Y. Yao, *Nucleoside transporters of mammalian cells*. Pharm Biotechnol, 1999. **12**: p. 313-52.
54. Rudolph, F.B., *The biochemistry and physiology of nucleotides*. J Nutr, 1994. **124**: p. 124S-130S.
55. Anderson, C.M. and F.E. Parkinson, *Potential signalling roles for UTP and UDP: sources, regulation and release of uracil nucleotides*. Trends Pharmacol Sci, 1997. **18**(10): p. 387-92.
56. Connolly, G.P. and J.A. Duley, *Uridine and its nucleotides: biological actions, therapeutic potentials*. Trends Pharmacol Sci, 1999. **20**(5): p. 218-25.

57. Silei, V., V. Politi, and G.M. Lauro, *Uridine induces differentiation in human neuroblastoma cells via protein kinase C epsilon*. J Neurosci Res, 2000. **61**(2): p. 206-11.
58. Communi, D. and J.M. Boeynaems, *Receptors responsive to extracellular pyrimidine nucleotides*. Trends Pharmacol Sci, 1997. **18**(3): p. 83-6.
59. O'Dwyer, P.J., S.A. King, D.F. Hoth, and B. Leyland-Jones, *Role of thymidine in biochemical modulation: a review*. Cancer Res, 1987. **47**(15): p. 3911-9.
60. Perigaud, C., G. Gosselin, and J.-L. Imbach, *Nucleoside analogues as chemotherapeutic agents: a review*. Nucleosides and Nucleotides, 1992. **11**: p. 903-945.
61. Pastor-Anglada, M., A. Felipe, and F.J. Casado, *Transport and mode of action of nucleoside derivatives used in chemical and antiviral therapies*. Trends Pharmacol Sci, 1998. **19**(10): p. 424-30.
62. Mackey, J.R., S.A. Baldwin, J.D. Young, and C. E. Cass, *Nucleoside transport and its significance for anticancer drug resistance*. Drug resistance update, 1998: p. 310-324.
63. Huang, Q.Q., S.Y. Yao, M.W. Ritzel, A.R. Paterson, C.E. Cass, and J.D. Young, *Cloning and functional expression of a complementary DNA encoding a mammalian nucleoside transport protein*. J Biol Chem, 1994. **269**(27): p. 17757-60.
64. Hu, M., *Comparison of uptake characteristics of thymidine and zidovudine in a human intestinal epithelial model system*. Journal of Pharmaceutical Sciences, 1993. **82**(8): p. 829-833.
65. Zimmerman, T.P., W.B. Mahony, and K.L. Prus, *3'-Azido-3'-deoxythymidine. An unusual nucleoside analogue that permeates the membrane of human erythrocytes and lymphocytes by nonfacilitated diffusion*. J Biol Chem, 1987. **262**(12): p. 5748-54.
66. Graham, K.A., J. Leithoff, I.R. Coe, D. Mowles, J.R. Mackey, J.D. Young, and C.E. Cass, *Differential transport of cytosine-containing nucleosides by*

- recombinant human concentrative nucleoside transporter protein hCNT1. Nucleosides Nucleotides Nucleic Acids, 2000. 19(1-2): p. 415-34.*
67. August, E.M., E.M. Birks, and W.H. Prusoff, *3'-Deoxythymidin-2'-ene permeation of human lymphocyte H9 cells by nonfacilitated diffusion. Mol Pharmacol, 1991. 39(2): p. 246-9.*
 68. Gourdeau, H., M.L. Clarke, F. Ouellet, D. Mowles, M. Selner, A. Richard, N. Lee, J.R. Mackey, J.D. Young, J. Jolivet, R.G. Lafreniere, and C.E. Cass, *Mechanisms of uptake and resistance to troxacitabine, a novel deoxycytidine nucleoside analogue, in human leukemic and solid tumor cell lines. Cancer Res, 2001. 61(19): p. 7217-24.*
 69. Mackey, J.R., R.S. Mani, M. Selner, D. Mowles, J.D. Young, J.A. Belt, C.R. Crawford, and C.E. Cass, *Functional nucleoside transporters are required for gemcitabine influx and manifestation of toxicity in cancer cell lines. Cancer Res, 1998. 58(19): p. 4349-57.*
 70. Wright, A.M., A.R. Paterson, B. Sowa, J.J. Akabutu, P.E. Grundy, and W.P. Gati, *Cytotoxicity of 2-chlorodeoxyadenosine and arabinosylcytosine in leukaemic lymphoblasts from paediatric patients: significance of cellular nucleoside transporter content. Br J Haematol, 2002. 116(3): p. 528-37.*
 71. Ullman, B., *Dideoxycytidine metabolism in wild type and mutant CEM cells deficient in nucleoside transport or deoxycytidine kinase. Adv Exp Med Biol, 1989. 253B: p. 415-20.*
 72. Cohen, A., B. Ullman, and D.W. Martin, *Characterization of a mutant mouse lymphoma cell with deficient transport of purine and pyrimidine nucleosides. J Biol Chem, 1979. 254(1): p. 112-6.*
 73. Sobrero, A.F., R.E. Handschumacher, and J.R. Bertino, *Highly selective drug combinations for human colon cancer cells resistant in vitro to 5-fluoro-2'-deoxyuridine. Cancer Res, 1985. 45(7): p. 3161-3.*
 74. Lang, T.T., M. Selner, J.D. Young, and C.E. Cass, *Acquisition of human concentrative nucleoside transporter 2 (hCNT2) activity by gene transfer confers sensitivity to fluoropyrimidine nucleosides in drug-resistant leukemia cells. Mol Pharmacol, 2001. 60(5): p. 1143-52.*

75. Cass, C.E., K.M. King, J.T. Montano, and A. Janowska-Wieczorek, *A comparison of the abilities of nitrobenzylthioinosine, dilazep, and dipyridamole to protect human hematopoietic cells from 7-deazaadenosine (tubercidin)*. *Cancer Res*, 1992. **52**(21): p. 5879-86.
76. Kaplinsky, C., H. Yeger, Z. Estrov, J. Barankiewicz, G. Pawlin, M.H. Freedman, and A. Cohen, *Selective protection of tubercidin toxicity by nitrobenzyl thioinosine in normal tissues but not in human neuroblastoma cells*. *Cancer Chemotherapy & Pharmacology*, 1986. **17**(3): p. 264-8.
77. Fu, N.W., *Protection of cells by nucleoside transport inhibitor combined with nebularine and the therapeutic effect on transplantable mouse tumors*. *Chung-Hua Chung Liu Tsa Chih Chinese Journal of Oncology*, 1985. **7**(2): p. 94-8.
78. Adjei, A.A., L. Dagnino, M.M. Wong, and A.R. Paterson, *Protection against fludarabine neurotoxicity in leukemic mice by the nucleoside transport inhibitor nitrobenzylthioinosine*. *Cancer Chemotherapy & Pharmacology*, 1992. **31**(1): p. 71-5.
79. Baer, H.P., V. Serignese, A. Moorji, and H. Van Belle, *In vivo effectiveness of several nucleoside transport inhibitors in mice and hamsters*. *Naunyn-Schmiedebergs Archives of Pharmacology*, 1991. **343**(4): p. 365-9.
80. White, J.C., J.P. Rathmell, and R.L. Capizzi, *Membrane transport influences the rate of accumulation of cytosine arabinoside in human leukemia cells*. *J Clin Invest*, 1987. **79**(2): p. 380-7.
81. Zittoun, R., M. Jean-Pierre, S. Delanian, A.-M. Suberville, and D. Thevenin, *Prognostic value of in vitro uptake and retention of cytosine arabinoside in acute myelogenous leukemia*. *Seminars in Oncology*, 1987. **14**: p. 269 - 275.
82. Wiley, J.S., S.P. Jones, W.H. Sawyer, and A.R. Paterson, *Cytosine arabinoside influx and nucleoside transport sites in acute leukemia*. *J Clin Invest*, 1982. **69**(2): p. 479-89.

83. Zuhlsdorf, M., J. Vormoor, and J. Boos, *Cytosine arabinoside resistance in childhood leukemia*. International Journal Of Pediatric Hematologyoncology, 1997. 4(6): p. 565-581.
84. Galmarini, C.M., X. Thomas, F. Calvo, P. Rousselot, M. Rabilloud, A. Jaffari, E. Cros, and C. Dumontet, *In vivo mechanisms of resistance to cytarabine in acute myeloid leukaemia*. British Journal of Haematology, 2002. 117: p. 860-868.
85. Plunkett, W. and V. Gandhi, *Nucleoside analogs: cellular pharmacology, mechanisms of action, and strategies for combination therapy*, in *Nucleoside Analogs in Cancer Therapy*, B.D. Cheson, M.J. Keating, and W. Plunkett, Editors. 1997, Marcel Dekker: New York, NY. p. 1-35.
86. Mata, J.F., J.M. Garcia-Manteiga, M.P. Lostao, S. Fernandez-Veledo, E. Guillen-Gomez, I.M. Larrayoz, J. Lloberas, F.J. Casado, and M. Pastor-Anglada, *Role of the human concentrative nucleoside transporter (hCNT1) in the cytotoxic action of 5'-deoxy-5-fluorouridine*. Mol Pharmacol, 2001. 59(6): p. 1542-48.
87. Beranek, J., *A study on structure-activity relationships of nucleoside analogues*. Drugs Exp Clin Res, 1986. 12(4): p. 355-67.
88. Weckbecker, G., *Biochem Pharmacol and analysis of fluoropyrimidines alone and in combination with modulators*. Pharmacol Ther, 1991. 50(3): p. 367-424.
89. Boring, C.C., T.S. Squires, T. Tong, and S. Montgomery, *Cancer statistics, 1994*. CA Cancer J Clin, 1994. 44(1): p. 7-26.
90. Song, D., M.G. Wientjes, Y. Gan, and J.L. Au, *Bladder tissue pharmacokinetics and antitumor effect of intravesical 5- fluorouridine*. Clin Cancer Res, 1997. 3(6): p. 901-9.
91. Heinemann, V. and U. Jehn, *Rationales for a pharmacologically optimized treatment of acute nonlymphocytic leukemia with cytosine arabinoside*. Leukemia, 1990. 4: p. 790-796.

92. Galmarini, C.M., J.R. Mackey, and C. Dumontet, *Nucleoside analogues: mechanisms of drug resistance and reversal strategies*. *Leukemia*, 2001. **15**(6): p. 875-90.
93. Gati, W.P., A.R. Paterson, L.M. Larratt, A.R. Turner, and A.R. Belch, *Sensitivity of acute leukemia cells to cytarabine is a correlate of cellular es nucleoside transporter site content measured by flow cytometry with SAENTA-fluorescein*. *Blood*, 1997. **90**(1): p. 346-53.
94. Bryson, H.M. and E.M. Sorkin, *Cladribine. A review of its pharmacodynamic and pharmacokinetic properties and therapeutic potential in haematological malignancies*. *Drugs*, 1993. **46**(5): p. 872-94.
95. Ahmad, I., A.M. Al-Katib, F.W. Beck, and R.M. Mohammad, *Sequential treatment of a resistant chronic lymphocytic leukemia patient with bryostatin 1 followed by 2-chlorodeoxyadenosine: case report*. *Clin Cancer Res*, 2000. **6**(4): p. 1328-32.
96. Guchelaar, H.-J., D.J. Richel, and M.R. Schaafsma, *Clinical and toxicological aspects of the antineoplastic drug cladribine: a review*. *Ann Hematol*, 1994. **69**: p. 223-230.
97. Feldman, E.J. and M.J. Keating, *Fludarabine in the treatment of lymphoproliferative malignancies*. *Cancer Invest*, 1993. **11**(3): p. 314-8.
98. Gandhi, V. and W. Plunkett, *Cellular and clinical pharmacology of fludarabine*. *Clin Pharmacokinet*, 2002. **41**(2): p. 93-103.
99. Robertson, L.E., S. Chubb, R.E. Meyn, M. Story, and W. Plunkett, *Induction of apoptotic cell death in chronic lymphocytic leukemia by 2-chloro-2'-deoxyadenosine and 9-B-D-arabinosyl-2-fluoroadenine*. *Blood*, 1993. **81**: p. 143-150.
100. Cohen, A., J.W.W. Lee, and E.W. Gelfand, *Selective toxicity of deoxyguanosine and arabinosyl guanine for T-leukemic cells*. *Blood*, 1983. **61**: p. 660-66.
101. Verhoef, V. and A. Fridland, *Metabolic basis of arabinonucleoside selectivity for human leukemic T- and B-lymphoblasts*. *Cancer Res.*, 1985. **45**: p. 3646-50.

102. Curbo, S., C. Zhu, M. Johansson, J. Balzarini, and A. Karlsson, *Dual mechanisms of 9-beta-D-arabinofuranosylguanine resistance in CEM T-lymphoblast leukemia cells*. *Biochem Biophys Res Commun*, 2001. **285**(1): p. 40-5.
103. Kisor, D.F., W. Plunkett, J. Kurtzberg, B. Mitchell, J.P. Hodge, T. Ernst, M.J. Keating, and V. Gandhi, *Pharmacokinetics of nelarabine and 9-beta-D-arabinofuranosyl guanine in pediatric and adult patients during a phase I study of nelarabine for the treatment of refractory hematologic malignancies*. *J Clin Oncol*, 2000. **18**(5): p. 995-1003.
104. Fletcher, C.V., *Treatment of herpesvirus infections in HIV-infected individuals*. *Ann Pharmacother*, 1992. **26**(7-8): p. 955-62.
105. Morse, G.D., M.J. Shelton, and A.M. O'Donnell, *Comparative pharmacokinetics of antiviral nucleoside analogues*. *Clin Pharmacokinet*, 1993. **24**(2): p. 101-23.
106. De Clercq, E., *New selective antiviral agents active against the AIDS virus*. *TIPS Reviews*, 1987. **8**: p. 339 - 345.
107. Li, X. and W.K. Chan, *Transport, metabolism and elimination mechanisms of anti-HIV agents*. *Adv Drug Deliv Rev*, 1999. **39**(1-3): p. 81-103.
108. Fang, X., F.E. Parkinson, D.A. Mowles, J.D. Young, and C.E. Cass, *Functional characterization of a recombinant sodium-dependent nucleoside transporter with selectivity for pyrimidine nucleosides (cNT1rat) by transient expression in cultured mammalian cells*. *Biochem J*, 1996. **317**(Pt 2): p. 457-65.
109. Yao, S.Y., C.E. Cass, and J.D. Young, *Transport of the antiviral nucleoside analogs 3'-azido-3'-deoxythymidine and 2',3'-dideoxycytidine by a recombinant nucleoside transporter (rCNT) expressed in *Xenopus laevis* oocytes*. *Mol Pharmacol*, 1996. **50**(2): p. 388-93.
110. Wada, S., M. Tsuda, T. Sekine, S.H. Cha, M. Kimura, Y. Kanai, and H. Endou, *Rat Multispecific Organic Anion Transporter 1 (rOAT1) Transports Zidovudine, Acyclovir, and Other Antiviral Nucleoside Analogs*. *J Pharmacol Exp Ther*, 2000. **294**(3): p. 844-849.

111. Rando, R.F. and N. Nguyen-Ba, *Development of novel nucleoside analogues for use against drug resistant strains of HIV-1*. Drug Discov Today, 2000. 5(10): p. 465-476.
112. Hatzis, P., A.S. Al-Madhoon, M. Jullig, T.G. Petrakis, S. Eriksson, and I. Talianidis, *The intracellular localization of deoxycytidine kinase*. J Biol Chem, 1998. 273(46): p. 30239-43.
113. Arner, E.S.J. and S. Eriksson, *Mammalian deoxyribonucleoside kinases*. Pharmac Ther, 1995. 67: p. 155-186.
114. Jullig, M. and S. Eriksson, *Mitochondrial and submitochondrial localization of human deoxyguanosine kinase*. Eur J Biochem, 2000. 267(17): p. 5466-72.
115. Belt, J.A., *Heterogeneity of nucleoside transport in mammalian cells. Two types of transport activity in L1210 and other cultured neoplastic cells*. Mol Pharmacol, 1983. 24(3): p. 479-84.
116. Jarvis, S.M. and J.D. Young, *Nucleoside transport in human and sheep erythrocytes. Evidence that nitrobenzylthioinosine binds specifically to functional nucleoside-transport sites*. Biochem J, 1980. 190(2): p. 377-83.
117. Figueredo, V.M., I. Diamond, H.Z. Zhou, and S.A. Camacho, *Chronic dipyridamole therapy produces sustained protection against cardiac ischemia-reperfusion injury*. Am J Physiol, 1999. 277(5 Pt 2): p. H2091-H2097.
118. Buolamwini, J.K., *Nucleoside transport inhibitors: Structure-activity relationships and potential therapeutic applications*. Current Medicinal Chemistry, 1997. 4(1): p. 35-66.
119. Gutierrez, M.M., C.M. Brett, R.J. Ott, A.C. Hui, and K.M. Giacomini, *Nucleoside transport in brush border membrane vesicles from human kidney*. Biochim Biophys Acta, 1992. 1105(1): p. 1-9.
120. Paterson, A.R., W.P. Gati, D. Vijayalakshmi, C.E. Cass, M.J. Mant, J.D. Young, and A.R. Belch, *Inhibitor-sensitive, Na(+)-linked transport of nucleoside analogs in leukemia cells from patients (Meeting abstract)*. Proc Annu Meet Am Assoc Cancer Res, 1993. 34: p. A84.

121. Flanagan, S.A. and K.A. Mecklinggill, *Characterization of a novel Na⁺ dependent, guanosine specific, nitrobenzylthioinosine-sensitive transporter in acute promyelocytic leukemia cells*. J Biol Chem, 1997. **272** (29): p. 18026-32.
122. Dagnino, L., L.L. Bennett, Jr., and A.R. Paterson, *Sodium-dependent nucleoside transport in mouse leukemia L1210 cells*. J Biol Chem, 1991. **266**(10): p. 6308-11.
123. Williams, T.C. and S.M. Jarvis, *Multiple sodium-dependent nucleoside transport systems in bovine renal brush-border membrane vesicles*. Biochem J, 1991. **274**(Pt 1): p. 27-33.
124. Dagnino, L., L.L. Bennett, Jr., and A.R. Paterson, *Substrate specificity, kinetics, and stoichiometry of sodium-dependent adenosine transport in L1210/AM mouse leukemia cells*. J Biol Chem, 1991. **266**(10): p. 6312-7.
125. Gutierrez, M.M. and K.M. Giacomini, *Substrate selectivity, potential sensitivity and stoichiometry of Na⁽⁺⁾-nucleoside transport in brush border membrane vesicles from human kidney*. Biochimica et Biophysica Acta, 1993. **1149**(2): p. 202-8.
126. Moseley, R.H., S. Jarose, and P. Permod, *Adenosine transport in rat liver plasma membrane vesicles*. Am J Physiol, 1991. **261**(5 Pt 1): p. G716-22.
127. Plagemann, P.G. and J.M. Aran, *Characterization of Na⁽⁺⁾-dependent, active nucleoside transport in rat and mouse peritoneal macrophages, a mouse macrophage cell line and normal rat kidney cells*. Biochim Biophys Acta, 1990. **1028**(3): p. 289-98.
128. Wu, X., G. Yuan, C.M. Brett, A.C. Hui, and K.M. Giacomini, *Sodium-dependent nucleoside transport in choroid plexus from rabbit. Evidence for a single transporter for purine and pyrimidine nucleosides*. J Biol Chem, 1992. **267**(13): p. 8813-18.
129. Hong, M., L. Schlichter, and R. Bendayan, *A Na⁽⁺⁾-dependent nucleoside transporter in microglia*. J Pharmacol Exp Ther, 2000. **292**(1): p. 366-74.

130. Che, M., D.F. Ortiz, and I.M. Arias, *Primary structure and functional expression of a cDNA encoding the bile canalicular, purine-specific Na⁺-nucleoside cotransporter*. J Biol Chem, 1995. **270**(23): p. 13596-13599.
131. Wang, J., S.-F. Su, M.J. Dresser, M.E. Schnaner, C.B. Washington, and K.M. Giacomini, *Na⁺-dependent purine nucleoside transporter from human kidney: cloning and functional characterization*. Am J Physiol, 1997. **273**(42): p. F1058-F1065.
132. Ritzel, M.W., S.Y. Yao, A.M. Ng, J.R. Mackey, C.E. Cass, and J.D. Young, *Molecular cloning, functional expression and chromosomal localization of a cDNA encoding a human Na⁺/nucleoside cotransporter (hCNT2) selective for purine nucleosides and uridine*. Mol Membr Biol, 1998. **15**(4): p. 203-11.
133. Ritzel, M.W.L., S.Y.M. Yao, M.Y. Huang, J.F. Elliott, C.E. Cass, and J.D. Young, *Molecular cloning and functional expression of cDNAs encoding a human Na⁺-nucleoside cotransporter (hCNT1)*. Am J Physiol, 1997. **272**: p. C707-C714.
134. Ritzel, M.W., A.M. Ng, S.Y. Yao, K. Graham, S.K. Loewen, K.M. Smith, R.J. Hyde, E. Karpinski, C.E. Cass, S.A. Baldwin, and J.D. Young, *Recent molecular advances in studies of the concentrative Na⁺-dependent nucleoside transporter (CNT) family: identification and characterization of novel human and mouse proteins (hCNT3 and mCNT3) broadly selective for purine and pyrimidine nucleosides (system cib)*. Mol Membr Biol, 2001. **18**(1): p. 65-72.
135. Griffiths, M., N. Beaumont, S.Y. Yao, M. Sundaram, C.E. Boumah, A. Davies, F.Y. Kwong, I. Coe, C.E. Cass, J.D. Young, and S.A. Baldwin, *Cloning of a human nucleoside transporter implicated in the cellular uptake of adenosine and chemotherapeutic drugs*. Nature Medicine, 1997. **3**(1): p. 89-93.
136. Griffiths, M., S.Y. Yao, F. Abidi, S.E. Phillips, C.E. Cass, J.D. Young, and S.A. Baldwin, *Molecular cloning and characterization of a*

- nitrobenzylthioinosine- insensitive (ei) equilibrative nucleoside transporter from human placenta. Biochem J, 1997. 328(Pt 3): p. 739-43.*
137. Crawford, C.R., D.H. Patel, C. Naeve, and J.A. Belt, *Cloning of the human equilibrative, nitrobenzylmercaptapurine riboside (NBMPR)-insensitive nucleoside transporter ei by functional expression in a transport-deficient cell line. J Biol Chem, 1998. 273(9): p. 5288-93.*
 138. Crawford, C., D. Patel, and J. Belt, *Isolation of a human cDNA that confers equilibrative, nitrobenzylmercaptapurine riboside-insensitive nucleoside transport activity (ei) to a transport deficient human leukemia cell line. Proc Annu Meet Am Assoc Cancer Res, 1997. 38: p. A406.*
 139. Yao, S.Y., M. Sundaram, E.G. Chomey, C.E. Cass, S.A. Baldwin, and J.D. Young, *Identification of Cys140 in helix 4 as an exofacial cysteine residue within the substrate-translocation channel of rat equilibrative nitrobenzylthioinosine (NBMPR)-insensitive nucleoside transporter rENT2. Biochem J, 2001. 353(Pt 2): p. 387-393.*
 140. Baldwin, S.A., J.R. Mackey, C.E. Cass, and J.D. Young, *Nucleoside transporters: molecular biology and implications for therapeutic development. Mol Med Today, 1999. 5(5): p. 216-24.*
 141. Hamilton, S.R., S.Y. Yao, J.C. Ingram, D.A. Hadden, M.W. Ritzel, M.P. Gallagher, P.J. Henderson, C.E. Cass, J.D. Young, and S.A. Baldwin, *Subcellular distribution and membrane topology of the mammalian concentrative Na⁺-nucleoside cotransporter rCNT1. J Biol Chem, 2001. 276(30): p. 27981-27988.*
 142. Sundaram, M., S.Y. Yao, J.C. Ingram, Z.A. Berry, F. Abidi, C.E. Cass, S.A. Baldwin, and J.D. Young, *Topology of a human equilibrative, nitrobenzylthioinosine (NBMPR)- sensitive nucleoside transporter (hENT1) implicated in the cellular uptake of adenosine and anti-cancer drugs. J Biol Chem, 2001. 2: p. 2.*
 143. Kwong, F.Y., J.S. Wu, M.M. Shi, H.E. Fincham, A. Davies, P.J. Henderson, S.A. Baldwin, and J.D. Young, *Enzymic cleavage as a probe*

- of the molecular structures of mammalian equilibrative nucleoside transporters. *J Biol Chem*, 1993. **268**(29): p. 22127-34.
144. Jennings, L.L., C. Hao, M.A. Cabrita, M.F. Vickers, S.A. Baldwin, D.Y. J, and C.E. Cass, *Distinct regional distribution of human equilibrative nucleoside transporter proteins 1 and 2 (hENT1 and hENT2) in the central nervous system*. *Neuropharmacology*, 2001. **40**(5): p. 722-31.
145. Wu, J.S., F.Y. Kwong, S.M. Jarvis, and J.D. Young, *Identification of the erythrocyte nucleoside transporter as a band 4.5 polypeptide. Photoaffinity labeling studies using nitrobenzylthioinosine*. *J Biol Chem*, 1983. **258**(22): p. 13745-51.
146. Kwong, F.Y., H.E. Fincham, A. Davies, N. Beaumont, P.J. Henderson, J.D. Young, and S.A. Baldwin, *Mammalian nitrobenzylthioinosine-sensitive nucleoside transport proteins. Immunological evidence that transporters differing in size and inhibitor specificity share sequence homology*. *J Biol Chem*, 1992. **267**(30): p. 21954-60.
147. Plagemann, P.G. and C. Woffendin, *Species differences in sensitivity of nucleoside transport in erythrocytes and cultured cells to inhibition by nitrobenzylthioinosine, dipyridamole, dilazep and lidoflazine*. *Biochimica et Biophysica Acta*, 1988. **969**(1): p. 1-8.
148. Jarvis, S.M., J.R. Hammond, A.R. Paterson, and A.S. Clanachan, *Species differences in nucleoside transport. A study of uridine transport and nitrobenzylthioinosine binding by mammalian erythrocytes*. *Biochem J*, 1982. **208**(1): p. 83-8.
149. Kiss, A., K. Farah, J. Kim, R.J. Garriock, T.A. Drysdale, and J.R. Hammond, *Molecular cloning and functional characterization of inhibitor-sensitive (mENT1) and inhibitor-resistant (mENT2) equilibrative nucleoside transporters from mouse brain*. *Biochem J*, 2000. **352**(Pt 2): p. 363-372.
150. Hammond, J.R., *Interaction of a series of draflazine analogues with equilibrative nucleoside transporters: species differences and transporter*

- subtype selectivity*. Naunyn Schmiedebergs Arch Pharmacol, 2000. **361**(4): p. 373-82.
151. Shi, M.M. and J.D. Young, [³H]Dipyridamole binding to nucleoside transporters from guinea-pig and rat lung. Biochem J, 1986. **240**(3): p. 879-83.
152. Gati, W.P. and A.R.P. Paterson, *Nucleoside transport*, in *The Red Cell Membrane: Structure, Function, and Clinical Implications*, J.C. Parker, Editor. 1989, Marcel Dekker: New York. p. 635-61.
153. Boleti, H., I.R. Coe, S.A. Baldwin, J.D. Young, and C.E. Cass, *Molecular identification of the equilibrative NBMPR-sensitive (es) nucleoside transporter and demonstration of an equilibrative NBMPR-insensitive (ei) transport activity in human erythroleukemia (K562) cells*. Neuropharmacology, 1997. **36**(9): p. 1167-79.
154. Mani, R.S., J.R. Hammond, J.M.J. Marjan, K.A. Graham, J.D. Young, S.A. Baldwin, and C.E. Cass, *Demonstration of equilibrative nucleoside transporters (hENT1, hENT2) in intracellular membranes of cultured human choriocarcinoma (BeWo) cells by functional reconstitution in proteoliposomes*. J Biol Chem, 1998. **273**(46): p. 30818-25.
155. Coe, I.R., M. Griffiths, J.D. Young, S.A. Baldwin, and C.E. Cass, *Assignment of the human equilibrative nucleoside transporter (hENT1) to 6p21.1-p21.2*. Genomics, 1997. **45**(2): p. 459-60.
156. Plagemann, P.G., R.M. Wohlhueter, and C. Woffendin, *Nucleoside and nucleobase transport in animal cells*. Biochimica et Biophysica Acta, 1988. **947**(3): p. 405-43.
157. Jarvis, S.M., *Inhibition by nucleosides of glucose-transport activity in human erythrocytes*. Biochem J, 1988. **249**(2): p. 383-89.
158. Kwong, F.Y., A. Davies, C.M. Tse, J.D. Young, P.J. Henderson, and S.A. Baldwin, *Purification of the human erythrocyte nucleoside transporter by immunoaffinity chromatography*. Biochem J, 1988. **255**(1): p. 243-49.
159. Crawford, C.R., C.E. Cass, J.D. Young, and J.A. Belt, *Stable expression of a recombinant sodium-dependent, pyrimidine-selective nucleoside*

- transporter (CNT1) in a transport-deficient mouse leukemia cell line. Biochem Cell Biol, 1998. 76(5): p. 843-51.*
160. Osses, N., J.D. Pearson, D.L. Yudilevich, and S.M. Jarvis, *Hypoxanthine enters human vascular endothelial cells (ECV 304) via the nitrobenzylthioinosine-insensitive equilibrative nucleoside transporter. Biochem J, 1996. 317(Pt 3): p. 843-48.*
161. Yao, S.Y., M. Sundaram, E.G. Chomey, C.E. Cass, S.A. Baldwin, and J.D. Young, *Transport of antiviral 3'-deoxynucleoside drugs by recombinant human and rat equilibrative, nitrobenzylthioinosine (NBMPR)-insensitive (ENT2) nucleoside transporter proteins produced in Xenopus oocytes. Mol Membr Biol, 2001. 18(2): p. 161-67.*
162. Anderson, C.M., S.A. Baldwin, J.D. Young, C.E. Cass, and F.E. Parkinson, *Distribution of mRNA encoding a nitrobenzylthioinosine-insensitive nucleoside transporter (ENT2) in rat brain. Brain Res Mol Brain Res, 1999. 70(2): p. 293-97.*
163. Anderson, C.M., W. Xiong, J.D. Geiger, J.D. Young, C.E. Cass, S.A. Baldwin, and F.E. Parkinson, *Distribution of equilibrative, nitrobenzylthioinosine-sensitive nucleoside transporters (ENT1) in brain. J Neurochem, 1999. 73(2): p. 867-73.*
164. Gu, J.G., G. Kala, and J.D. Geiger, *[3H]adenosine transport in synaptoneurosomes of postmortem human brain. J Neurochem, 1993. 60(6): p. 2232-37.*
165. Johnston, M.E. and J.D. Geiger, *Adenosine transport systems on dissociated brain cells from mouse, guinea-pig, and rat. Neurochem-Res, 1990. 15(9): p. 911-15.*
166. Glass, M., R.L.M. Faull, and M. Dragunow, *Localisation of the adenosine uptake site in the human brain: a comparison with the distribution of adenosine A1 receptors. Brain Research, 1996. 710 (1-2): p. 79-91.*
167. Marangos, P.J., J. Patel, R. Clark-Rosenberg, and A.M. Martino, *[3H]Nitrobenzylthioinosine binding as a probe for the study of adenosine uptake sites in brain. J Neurochem, 1982. 39(1): p. 184-91.*

168. Pennycooke, M., N. Chaudary, I. Shuralyova, Y. Zhang, and I.R. Coe, *Differential expression of human nucleoside transporters in normal and tumor tissue*. *Biochem Biophys Res Commun*, 2001. **280**(3): p. 951-59.
169. Yao, S.Y., A.M. Ng, W.R. Muzyka, M. Griffiths, C.E. Cass, S.A. Baldwin, and J.D. Young, *Molecular cloning and functional characterization of nitrobenzylthioinosine (NBMPR)-sensitive (es) and NBMPR-insensitive (ei) equilibrative nucleoside transporter proteins (rENT1 and rENT2) from rat tissues*. *J Biol Chem*, 1997. **272**(45): p. 28423-30.
170. Dahlig-Harley, E., Y. Eilam, A.R. Paterson, and C.E. Cass, *Binding of nitrobenzylthioinosine to high-affinity sites on the nucleoside-transport mechanism of HeLa cells*. *Biochem J*, 1981. **200**(2): p. 295-305.
171. Boumah, C.E., D.L. Hogue, and C.E. Cass, *Expression of high levels of nitrobenzylthioinosine-sensitive nucleoside transport in cultured human choriocarcinoma (BeWo) cells*. *Biochem J*, 1992. **288**(Pt 3): p. 987-96.
172. Chandrasena, G., R. Giltay, S.D. Patil, A. Bakken, and J.D. Unadkat, *Functional expression of human intestinal Na⁺-dependent and Na⁺-independent nucleoside transporters in Xenopus laevis oocytes*. *Biochem Pharmacol*, 1997. **53**(12): p. 1909-18.
173. Leung, G.P., J.L. Ward, P.Y. Wong, and C.M. Tse, *Characterization of nucleoside transport systems in cultured rat epididymal epithelium*. *Am J Physiol Cell Physiol*, 2001. **280**(5): p. C1076-82.
174. Craig, J.E., Y. Zhang, and M.P. Gallagher, *Cloning of the nupC gene of Escherichia coli encoding a nucleoside transport system, and identification of an adjacent insertion element, IS 186*. *Molecular Microbiology*, 1994. **11**(6): p. 1159-68.
175. Zhang, Y., J.E. Craig, and M.P. Gallagher, *Location of the nupC gene on the physical map of Escherichia coli K-12*. *J Bacteriol*, 1992. **174**(17): p. 5758-59.
176. Vickers, M.F., J.D. Young, S.A. Baldwin, M.J. Ellison, and C.E. Cass, *Functional production of mammalian concentrative nucleoside*

- transporters in Saccharomyces cerevisiae*. Mol Membr Biol, 2001. **18**(1): p. 73-9.
177. Loewen, S.K., A.M. Ng, S.Y. Yao, C.E. Cass, S.A. Baldwin, and J.D. Young, *Identification of amino acid residues responsible for the pyrimidine and purine nucleoside specificities of human concentrative Na(+) nucleoside cotransporters hCNT1 and hCNT2*. J Biol Chem, 1999. **274**(35): p. 24475-84.
178. Wang, J. and K.M. Giacomini, *Serine 318 is essential for the pyrimidine selectivity of the N2 Na⁺-nucleoside transporter*. J Biol Chem, 1999. **274**(4): p. 2298-302.
179. Mackey, J.R., S.Y. Yao, K.M. Smith, E. Karpinski, S.A. Baldwin, C.E. Cass, and J.D. Young, *Gemcitabine transport in xenopus oocytes expressing recombinant plasma membrane mammalian nucleoside transporters*. J Natl Cancer Inst, 1999. **91**(21): p. 1876-81.
180. Huang, Q.Q., C.M. Harvey, A.R. Paterson, C.E. Cass, and J.D. Young, *Functional expression of Na(+)-dependent nucleoside transport systems of rat intestine in isolated oocytes of Xenopus laevis. Demonstration that rat jejunum expresses the purine-selective system N1 (cif) and a second, novel system N3 having broad specificity for purine and pyrimidine nucleosides*. J Biol Chem, 1993. **268**(27): p. 20613-19.
181. Wang, J., M.E. Schaner, S. Thomassen, S.F. Su, M. Piquette-Miller, and K.M. Giacomini, *Functional and molecular characteristics of Na(+)-dependent nucleoside transporters*. Pharm Res, 1997. **14**(11): p. 1524-32.
182. Anderson, C.M., W. Xiong, J.D. Young, C.E. Cass, and F.E. Parkinson, *Demonstration of the existence of mRNAs encoding N1/cif and N2/cit sodium/nucleoside cotransporters in rat brain*. Brain Research. Molecular Brain Research, 1996. **42**(2): p. 358-61.
183. Johnston, M.E. and J.D. Geiger, *Sodium-dependent uptake of nucleosides by dissociated brain cells from the rat*. J Neurochem, 1989. **52**(1): p. 75-81.

184. Plagemann, P.G., *Na(+)-dependent, active nucleoside transport in S49 mouse lymphoma cells and loss in AE-1 mutant deficient in facilitated nucleoside transport.* J Cell Biochem, 1991. **46**(1): p. 54-59.
185. Plagemann, P.G., *Na(+)-dependent, concentrative nucleoside transport in rat macrophages. Specificity for natural nucleosides and nucleoside analogs, including dideoxynucleosides, and comparison of nucleoside transport in rat, mouse and human macrophages.* Biochem Pharmacol, 1991. **42**(2): p. 247-52.
186. Baer, H.P. and A. Moorji, *Sodium-dependent and inhibitor-insensitive uptake of adenosine by mouse peritoneal exudate cells.* Biochim Biophys Acta, 1990. **1026**(2): p. 241-47.
187. Plagemann, P.G., J.M. Aran, and C. Woffendin, *Na(+)-dependent, active and Na(+)-independent, facilitated transport of formycin B in mouse spleen lymphocytes.* Biochim Biophys Acta, 1990. **1022**(1): p. 93-102.
188. Baer, H.P., A. Moorji, P.O. Ogbunude, and V. Serignese, *Sodium-dependent nucleoside transport in mouse lymphocytes, human monocytes, and hamster macrophages and peritoneal exudate cells.* Canadian Journal of Physiology & Pharmacology, 1992. **70**(1): p. 29-35.
189. Marina, N.M. and J.A. Belt, *Effect of nucleoside transport inhibitors on thymidine salvage and the toxicity of nucleoside analogs in mouse bone marrow granulocyte-macrophage progenitor cells.* Cancer Communications, 1991. **3**(12): p. 367-72.
190. Roden, M., A.R. Paterson, and K. Turnheim, *Sodium-dependent nucleoside transport in rabbit intestinal epithelium.* Gastroenterology, 1991. **100**(6): p. 1553-62.
191. Bronk, J.R. and J.G. Hastewell, *The specificity of pyrimidine nucleoside transport and metabolism by rat jejunum in vitro.* J Physiol, 1989. **408**: p. 405-11.
192. Bronk, J.R. and J.G. Hastewell, *The transport and metabolism of the uridine mononucleotides by rat jejunum in vitro.* J Physiol, 1989. **408**: p. 129-35.

193. Holstege, A., H.M. Gengenbacher, L. Jehle, and J. Hoppmann, *Facilitated diffusion and sodium-dependent transport of purine and pyrimidine nucleosides in rat liver*. *Hepatology*, 1991. **14**(2): p. 373-80.
194. Ungemach, F.R. and D. Hegner, *Uptake of thymidine into isolated rat hepatocytes. Evidence for two transport systems*. *Hoppe-Seylers Zeitschrift fur Physiologische Chemie*, 1978. **359**(7): p. 845-56.
195. Brett, C.M., C.B. Washington, R.J. Ott, M.M. Gutierrez, and K.M. Giacomini, *Interaction of nucleoside analogues with the sodium-nucleoside transport system in brush border membrane vesicles from human kidney*. *Pharmaceutical Research*, 1993. **10**(3): p. 423-6.
196. Patil, S.D. and J.D. Unadkat, *Sodium dependent nucleoside transport in the human intestinal brush border membrane*. *Am J Physiol Gastrointest Liver Physiol*, 1997. **35** (6): p. G1314-G1320.
197. Ngo, L.Y., S.D. Patil, and J.D. Unadkat, *Ontogenic and longitudinal activity of Na(+)-nucleoside transporters in the human intestine*. *Am J Physiol Gastrointest Liver Physiol*, 2001. **280**(3): p. G475-G481.
198. Schaner, M.E., J. Wang, S. Zevin, K.M. Gerstin, and K.M. Giacomini, *Transient expression of a purine-selective nucleoside transporter (SPNTint) in a human cell line (HeLa)*. *Pharm Res*, 1997. **14**(10): p. 1316-21.
199. Lee, C.W., J.A. Sokoloski, A.C. Sartorelli, and R.E. Handschumacher, *Differentiation of HL-60 cells by dimethylsulfoxide activates a Na(+)-dependent nucleoside transport system*. *In Vivo*, 1994. **8**(5): p. 795-801.
200. Roovers, K.I. and K.A. Meckling-Gill, *Characterization of equilibrative and concentrative Na+-dependent (cif) nucleoside transport in acute promyelocytic leukemia NB4 cells*. *J Cell Physiol*, 1996. **166**(3): p. 593-600.
201. Crawford, C.R., C.Y. Ng, L.D. Noel, and J.A. Belt, *Nucleoside transport in L1210 murine leukemia cells. Evidence for three transporters*. *J Biol Chem*, 1990. **265**(17): p. 9732-6.

202. Le Hir, M., *Evidence for separate carriers for purine nucleosides and for pyrimidine nucleosides in the renal brush border membrane*. Renal Physiol. Biochem., 1990. **13**(3): p. 154-61.
203. Mangravite, L.M., J.H. Lipschutz, K.E. Mostov, and K.M. Giacomini, *Localization of GFP-tagged concentrative nucleoside transporters in a renal polarized epithelial cell line*. Am J Physiol Renal Physiol, 2001. **280**(5): p. F879-85.
204. Lai, Y., A.H. Bakken, and J.D. Unadkat, *Simultaneous expression of hCNT1-CFP and hENT1-YFP in Madin-Darby canine kidney cells. Localization and vectorial transport studies*. J Biol Chem, 2002. **277**(40): p. 37711-17.
205. Soler, C., J. Garcia-Manteiga, R. Valdes, J. Xaus, M. Comalada, F.J. Casado, M. Pastor-Anglada, A. Celada, and A. Felipe, *Macrophages require different nucleoside transport systems for proliferation and activation*. Faseb J, 2001. **15**(11): p. 1979-88.
206. Rovera, G., D. Santoli, and C. Damsky, *Human promyelocytic leukemia cells in culture differentiate into macrophage-like cells when treated with a phorbol diester*. Proc Natl Acad Sci USA, 1979. **76**(6): p. 2779-83.
207. Sachs, L., *Control of normal cell differentiation and the phenotypic reversion of malignancy in myeloid leukaemia*. Nature, 1978. **274**: p. 535-39.
208. Pastor-Anglada, M., F.J. Casado, R. Valdes, J. Mata, J. Garcia-Manteiga, and M. Molina, *Complex regulation of nucleoside transporter expression in epithelial and immune system cells*. Mol Membr Biol, 2001. **18**(1): p. 81-85.
209. Bogosian, G. and J. Kane, *Recombinant DNA Technology and Applications*, ed. A. Prokop, R. Bajpai, and H. C. 1991, McGraw Hill, New York. 285-15.
210. Norholm, M.H. and G. Dandanell, *Specificity and topology of the Escherichia coli xanthosine permease, a representative of the NHS*

- subfamily of the major facilitator superfamily*. J Bacteriol, 2001. **183**(16): p. 4900-04.
211. Schmidt, R., M.F. Manolson, and M.-R. Chevallier, *Photoaffinity labeling and characterization of the cloned purine-cytosine transport system in Saccharomyces cerevisiae*. Proc Natl Acad. Sci, 1984. **81**: p. 6276-80.
212. Gillissen, B., L. Burkle, B. Andre, C. Kuhn, D. Rentsch, B. Brandl, and W.B. Frommer, *A new family of high-affinity transporters for adenine, cytosine, and purine derivatives in Arabidopsis*. Plant Cell, 2000. **12**(2): p. 291-300.
213. Vickers, M.F., S.Y. Yao, S.A. Baldwin, J.D. Young, and C.E. Cass, *Nucleoside transporter proteins of Saccharomyces cerevisiae. Demonstration of a transporter (FUI1) with high uridine selectivity in plasma membranes and a transporter (FUN26) with broad nucleoside selectivity in intracellular membranes*. J Biol Chem, 2000. **275**(34): p. 25931-38.
214. Ullman, B., T. Coons, S. Rockwell, and K. McCartan, *Genetic analysis of 2',3'-dideoxycytidine incorporation into cultured human T lymphoblasts*. J Biol Chem, 1988. **263**(25): p. 12391-96.
215. Crawford, C.R., C.Y. Ng, B. Ullman, and J.A. Belt, *Identification and reconstitution of the nucleoside transporter of CEM human leukemia cells*. Biochimica et Biophysica Acta, 1990. **1024**(2): p. 289-97.
216. Ullman, B., *Mutational analysis of nucleoside and nucleobase transport, in resistance to antineoplastic drugs*, D. Kessel, Editor. 1989, CRC Press: New York, NY. p. 293-15.
217. Bowen, D., R.B. Diasio, and I.D. Goldman, *Distinguishing between membrane transport and intracellular metabolism of fluorodeoxyuridine in Ehrlich ascites tumor cells by application of kinetic and high performance liquid chromatographic techniques*. J Biol Chem, 1979. **254**(12): p. 5333-39.

218. Gati, W.P., E.E. Knaus, and L.I. Wiebe, *Interaction of 2'-halogeno-2'-deoxyuridines with the human erythrocyte nucleoside transport mechanism*. Mol Pharmacol, 1983. **23**(1): p. 146-52.
219. Mackey, J.R., L.L. Jennings, M.L. Clarke, C.L. Santos, L. Dabbagh, M. Vsianska, S.L. Koski, R.W. Coupland, S.A. Baldwin, J.D. Young, and C.E. Cass, *Immunohistochemical variation of human equilibrative nucleoside transporter 1 protein in primary breast cancers*. Clin Cancer Res, 2002. **8**(1): p. 110-16.
220. Gati, W.P., A.R. Paterson, A.R. Belch, V. Chlumecky, L.M. Larratt, M.J. Mant, and A.R. Turner, *Es nucleoside transporter content of acute leukemia cells: role in cell sensitivity to cytarabine (araC)*. Leuk Lymphoma, 1998. **32**(1-2): p. 45-54.
221. Wiley, J.S., J. Taupin, G.P. Jamieson, M. Snook, W.H. Sawyer, and L.R. Finch, *Cytosine arabinoside transport and metabolism in acute leukemias and T cell lymphoblastic lymphoma*. J Clin Invest, 1985. **75**(2): p. 632-42.
222. Plagemann, P.G. and C. Woffendin, *Dideoxycytidine permeation and salvage by mouse leukemia cells and human erythrocytes*. Biochem-Pharmacol, 1989. **38**(20): p. 3469-75.
223. Domin, B.A., W.B. Mahony, and T.P. Zimmerman, *Membrane permeation mechanisms of 2',3'-dideoxynucleosides*. Biochem Pharmacol, 1993. **46**(4): p. 725-729.
224. Chan, T.C., L. Shaffer, R. Redmond, and K.L. Pennington, *Permeation and metabolism of anti-HIV and endogenous nucleosides in human immune effector cells*. Biochem Pharmacol, 1993. **46**(2): p. 273-78.
225. King, K.M. and C.E. Cass, *Membrane transport of 2-chloro-2'-deoxyadenosine and 2-chloro-2'-arabino-fluoro-2'-deoxyadenosine is required for cytotoxicity*. Proc Annu Meet Am Assoc Cancer Res, 1994. **35**: p. A3436.
226. Cass, C.E. and A.R. Paterson, *Inhibition by nitrobenzylthioinosine of uptake of adenosine, 2'-deoxyadenosine and 9-beta-D-*

- arabinofuranosyladenine* by human and mouse erythrocytes. *Biochem Pharmacol*, 1975. **24**(21): p. 1989-93.
227. Dagnino, L. and A.R. Paterson, *Sodium-dependent and equilibrative nucleoside transport systems in L1210 mouse leukemia cells: effect of inhibitors of equilibrative systems on the content and retention of nucleosides*. *Cancer Res*, 1990. **50**(20): p. 6549-53.
228. Mahony, W.B., B.A. Domin, R.T. McConnell, and T.P. Zimmerman, *Acyclovir transport into human erythrocytes*. *J Biol Chem*, 1988. **263**(19): p. 9285-91.
229. Mahony, W.B., B.A. Domin, and T.P. Zimmerman, *Ganciclovir permeation of the human erythrocyte membrane*. *Biochem Pharmacol*, 1991. **41**(2): p. 263-71.
230. Gutierrez, M.M. and K.M. Giacomini, *Expression of a human renal sodium nucleoside cotransporter in Xenopus laevis oocytes*. *Biochem Pharmacol*, 1994. **48**(12): p. 2251-53.
231. Belt, J.A., N.M. Marina, D.A. Phelps, and C.R. Crawford, *Nucleoside transport in normal and neoplastic cells*. *Adv Enzyme Regul*, 1993. **33**: p. 235-52.
232. Ruiz-Montasell, B., F. Javier Casado, A. Felipe, and M. Pastor-Anglada, *Uridine transport in basolateral plasma membrane vesicles from rat liver*. *Journal of Membrane Biology*, 1992. **128**(3): p. 227-33.
233. Darnowski, J.W. and R.E. Handschumacher, *Tissue uridine pools: evidence in vivo of a concentrative mechanism for uridine uptake*. *Cancer Res*, 1986. **46**(7): p. 3490-94.
234. Darnowski, J.W., C. Holdridge, and R.E. Handschumacher, *Concentrative uridine transport by murine splenocytes: kinetics, substrate specificity, and sodium dependency*. *Cancer Res*, 1987. **47**(10): p. 2614-19.
235. Vijayalakshmi, D. and J.A. Belt, *Sodium-dependent nucleoside transport in mouse intestinal epithelial cells. Two transport systems with differing substrate specificities*. *J Biol Chem*, 1988. **263**(36): p. 19419-23.

236. Wu, X., M.M. Gutierrez, and K.M. Giacomini, *Further characterization of the sodium-dependent nucleoside transporter (N3) in choroid plexus from rabbit*. *Biochimica et Biophysica Acta Biomembranes*, 1994. **1191**(1): p. 190-96.
237. Belt, J.A. and L.D. Noel, *Nucleoside transport in Walker 256 rat carcinosarcoma and S49 mouse lymphoma cells. Differences in sensitivity to nitrobenzylthioinosine and thiol reagents*. *Biochem J*, 1985. **232**(3): p. 681-88.
238. Ausubel, M.R., B. R.E., D.D. Kingston, J.G. Moore, J.A. Deisman, and K.S. Smith, *Current protocols in molecular biology*. 1989, New York: John Wiley and Sons.
239. Laemmli, U.K., *Cleavage of structural proteins during the assembly of bacteriophage T4*. *Nature*, 1970. **227**: p. 680-685.
240. Burnette, W.N., "Western blotting": *Electrophoretic transfer of proteins from sodium dodecyl sulfate-polyacrylamide gels to unmodified nitrocellulose and radiographic detection with antibody and radioiodinated protein A*. *Anal. Biochem.*, 1981. **112**: p. 195-03.
241. Towbin, H., T. Staehelin, and J. Gordon, *Electrophoretic transfer of proteins from polyacrylamide gels to nitrocellulose sheets: Procedure and some applications*. *Proc Natl Acad Sci USA*, 1979. **76**: p. 4350-54.
242. Smith, P.K., R.I. Krohn, G.T. Hermanson, A.K. Mallia, F.H. Gartner, M.D. Provenzano, E.K. Fujimoto, N.M. Goeke, B.J. Olsen, and D.C. Klenk, *Measurement of protein using bicinchoninic acid*. *Anal Biochem*, 1985. **150**: p. 76-85.
243. Cohen, A., B. Ullman, and D.W. Martin, Jr., *Characterization of a mutant mouse lymphoma cell with deficient transport of purine and pyrimidine nucleosides*. *J Biol Chem*, 1979. **254**(1): p. 112-16.
244. Vijayalakshmi, D., L. Dagnino, J.A. Belt, W.P. Gati, C.E. Cass, and A.R. Paterson, *L1210/B23.1 cells express equilibrative, inhibitor-sensitive nucleoside transport activity and lack two parental nucleoside transport activities*. *J Biol Chem*, 1992. **267**(24): p. 16951-56.

245. Cass, C.E., N. Kolassa, Y. Uehara, E. Dahlig-Harley, E.R. Harley, and A.R. Paterson, *Absence of binding sites for the transport inhibitor nitrobenzylthioinosine on nucleoside transport-deficient mouse lymphoma cells*. *Biochimica et Biophysica Acta*, 1981. **649**(3): p. 769-77.
246. Gati, W.P. and A.R. Paterson, *Interaction of [3H]dilazep at nucleoside transporter-associated binding sites on S49 mouse lymphoma cells*. *Mol Pharmacol*, 1989. **36**(1): p. 134-41.
247. Hidalgo, I.J., T.J. Raub, and R.T. Borchardt, *Characterization of the human colon carcinoma cell line (Caco-2) as a model system for intestinal epithelial permeability*. *Gastroenterology*, 1989. **96**(3): p. 736-49.
248. Bonifacino, J.S., D. M., J.B. Harford, and K.M. Yamada, eds. *Current protocols in cell biology*. Vol. Volume 1. 2000, John Wiley and Sons, Inc.: New York, NY.
249. Ausubel, F.M., B. R., R.E. Kingston, D.D. Moore, J.G. Seidman, J.A. Smith, and K. Struhl, *Current protocols in molecular biology*. 1994, New York, NY: John Wiley and Sons, Inc.
250. Golub, E.I., H. Kim, and D.J. Volsky, *Transfection of DNA into adherent cells by DEAE-dextran/DMSO method increases drastically if the cells are removed from surface and treated in suspension*. *Nucleic Acids Res*, 1989. **17**(12): p. 4902.
251. Danna, K.J. and L.M. Sompayrac, *Efficient infection of monkey cells with SV40 DNA. II. Use of low- molecular-weight DEAE-dextran for large-scale experiments*. *J Virol Methods*, 1982. **5**(5-6): p. 335-41.
252. Lin, W.C. and L.A. Culp, *Selectable plasmid vectors with alternative and ultrasensitive histochemical marker genes*. *Biotechniques*, 1991. **11**(3): p. 344-51.
253. Andreason, G.L. and G.A. Evans, *Optimization of electroporation for transfection of mammalian cell lines*. *Anal Biochem*, 1989. **180**(2): p. 269-75.

254. Chu, G., H. Hayakawa, and P. Berg, *Electroporation for the efficient transfection of mammalian cells with DNA*. Nucl Acids Res, 1987. **15**(1311-1326).
255. Eustis-Turf, E., K. Wang, and L. Schook, *Transfer of MAC genes into hematopoietic stem cells by electroporation: A model of monitoring gene expression*. Animal Biotechnol, 1990. **1**: p. 47-60.
256. Potter, H., *Electroporation in biology*. Anal Biochem, 1988. **174**: p. 361-373.
257. Reid, L. and O. Smithies, *Gene targeting and electroporation*, in *Guide to electroporation and electrofusion*, D. Chang, et al., Editors. 1992, Academic Press: San Diego.
258. Potter, H., *Protocols for using electroporation to stably or transiently transfect mammalian cells*, in *Guide to electroporation and electrofusion*, D. Chang, et al., Editors. 1992, Academic Press: San Diego.
259. Sato, K., R. Slesinski, and J. Littlefield, *Chemical mutagenesis at the phosphoribosyltransferase locus in cultured human lymphoblasts*. Proc Natl Acad Sci USA, 1972. **69**(5): p. 1244-48.
260. Nolan, G.P., S. Fiering, J.F. Nicolas, and L.A. Herzenberg, *Fluorescence-activated cell analysis and sorting of viable mammalian cells based on beta-D-galactosidase activity after transduction of Escherichia coli lacZ*. Proc Natl Acad Sci USA, 1988. **85**(8): p. 2603-07.
261. MacGregor, G.R., A.E. Mogg, J.F. Burke, and C.T. Caskey, *Histochemical staining of clonal mammalian cell lines expressing E. coli beta galactosidase indicates heterogeneous expression of the bacterial gene*. Somat Cell Mol Genet, 1987. **13**(3): p. 253-65.
262. Inc, G.T.S., *ImaGene green lacZ gene expression kit (I-2904) for quantitating lacZ β -D-galactosidase activity in cells*. Gene Therapy Systems Inc., 1997. **4**: p. 1-4.
263. Fiering, S.N., M. Roederer, G.P. Nolan, D.R. Micklem, D.R. Parks, and L.A. Herzenberg, *Improved FACS-Gal: flow cytometric analysis and*

- sorting of viable eukaryotic cells expressing reporter gene constructs. Cytometry, 1991. 12(4): p. 291-301.*
264. Paterson, A.R., E.R. Harley, and C.E. Cass, *Inward fluxes of adenosine in erythrocytes and cultured cells measured by a quenched-flow method. Biochem J, 1984. 224(3): p. 1001-08.*
265. Harley, E.R., A.R. Paterson, and C.E. Cass, *Initial rate kinetics of the transport of adenosine and 4-amino-7-(beta-D-ribofuranosyl)pyrrolo[2,3-d]pyrimidine (tubercidin) in cultured cells. Cancer Res, 1982. 42(4): p. 1289-95.*
266. Cass, C.E. and T.H. Au-Yeung, *Enhancement of 9-beta-D-arabinofuranosyladenine cytotoxicity to mouse leukemia L1210 in vitro by 2'-deoxycoformycin. Cancer Res, 1976. 36(4): p. 1486-91.*
267. Paterson, A.R.P. and C.E. Cass, *Measurement and inhibition of membrane transport of adenosine, in Methods in Pharmacology, D.M. Paton, Editor. 1985, Plenum Publishing. p. 165-79.*
268. Barros, L.F., J.C. Bustamante, D.L. Yudilevich, and S.M. Jarvis, *Adenosine transport and nitrobenzylthioinosine binding in human placental membrane vesicles from brush-border and basal sides of the trophoblast. Journal of Membrane Biology, 1991. 119(2): p. 151-61.*
269. Ward, J.L. and C.M. Tse, *Nucleoside transport in human colonic epithelial cell lines: evidence for two Na⁺-independent transport systems in T84 and Caco-2 cells¹. Biochim Biophys Acta, 1999. 1419(1): p. 15-22.*
270. Vickers, M.F., R.S. Mani, M. Sundaram, D.L. Hogue, J.D. Young, S.A. Baldwin, and C.E. Cass, *Functional production and reconstitution of the human equilibrative nucleoside transporter (hENT1) in Saccharomyces cerevisiae. Interaction of inhibitors of nucleoside transport with recombinant hent1 and a glycosylation-defective derivative (hent1/n48q). Biochem J, 1999. 339(Pt 1): p. 21-32.*
271. Mani, R.S., J.R. Hammond, J.M. Marjan, K.A. Graham, J.D. Young, S.A. Baldwin, and C.E. Cass, *Demonstration of equilibrative nucleoside transporters (hENT1 and hENT2) in nuclear envelopes of cultured human*

- choriocarcinoma (BeWo) cells by functional reconstitution in proteoliposomes.* J Biol Chem, 1998. **273**(46): p. 30818-25.
272. Craik, J.D., A.H. Good, R. Gottschalk, S.M. Jarvis, A.R. Paterson, and C.E. Cass, *Identification of glucose and nucleoside transport proteins in neonatal pig erythrocytes using monoclonal antibodies against band 4.5 polypeptides of adult human and pig erythrocytes.* Biochemistry & Cell Biology, 1988. **66**(8): p. 839-52.
273. Good, A.H., J.D. Craik, S.M. Jarvis, F.Y. Kwong, J.D. Young, A.R. Paterson, and C.E. Cass, *Characterization of monoclonal antibodies that recognize band 4.5 polypeptides associated with nucleoside transport in pig erythrocytes.* Biochem J, 1987. **244**(3): p. 749-55.
274. Harlow, E. and D. Lane, *Using antibodies: a laboratory manual.* 1999, Cold Spring Harbor, NY: Cold Spring Harbor Laboratory Press.
275. Harlow, E. and D. Lane, *in Antibodies: a Laboratory manual.* 1988, New York: Cold Spring Harbor Laboratory.
276. Barnstable, C.J. and e. al., *Production of monoclonal antibodies to group A erythrocytes, HLA and other human cell surface antigens-new tools for genetic analysis.* Cell, 1978. **14**(1): p. 9-20.
277. Farr, A.G. and P.K. Nakane, *Immunocytochemistry with enzyme labeled antibodies: A brief review.* J Immunol Methods, 1981. **47**: p. 129-144.
278. Shulman, M., C.D. Wilde, and G. Kohler, *A better cell line for making hybridomas secreting specific antibodies.* Nature, 1978. **276**: p. 269-70.
279. Lang, T.T., J.D. Young, and C.E. Cass, *Stable expression of a human concentrative nucleoside transporter implicated in transport of anticancer and antiviral nucleosides.* Faseb J., 1999. **13** (7): p. A1391:349.
280. Young, J.D., S.M. Jarvis, M.J. Robins, and A.R. Paterson, *Photoaffinity labeling of the human erythrocyte nucleoside transporter by N6-(p-Azidobenzyl)adenosine and nitrobenzylthioinosine. Evidence that the transporter is a band 4.5 polypeptide.* J Biol Chem, 1983. **258**(4): p. 2202-08.

281. Yin, J.L., N.A. Shackel, A. Zekry, P.H. McGuinness, C. Richards, K.V. Putten, G.W. McCaughan, J.M. Eris, and G.A. Bishop, *Real-time reverse transcriptase-polymerase chain reaction (RT-PCR) for measurement of cytokine and growth factor mRNA expression with fluorogenic probes or SYBR Green I*. *Immunol Cell Biol*, 2001. **79**(3): p. 213-21.
282. Miyajima, K., S. Tamiya, Y. Oda, T. Adachi, T. Konomoto, H. Toyoshiba, K. Masuda, and M. Tsuneyoshi, *Relative quantitation of p53 and MDM2 gene expression in leiomyosarcoma; real-time semi-quantitative reverse transcription- polymerase chain reaction*. *Cancer Lett*, 2001. **164**(2): p. 177-88.
283. Sussman, D.J. and G. Milman, *Short-term, high-efficiency expression of transfected DNA*. *Mol. Cell. Biol.*, 1984: p. 1641-43.
284. Koren, R., C.E. Cass, and A.R. Paterson, *The kinetics of dissociation of the inhibitor of nucleoside transport, nitrobenzylthioinosine, from the high-affinity binding sites of cultured hamster cells*. *Biochem J*, 1983. **216**(2): p. 299-08.
285. Sirotnak, F.M. and J.R. Barrueco, *Membrane transport and the antineoplastic action of nucleoside analogues*. *Cancer & Metastasis Reviews*, 1987. **6**(4): p. 459-80.
286. Cass, C.E., L.A. Gaudette, and A.R. Paterson, *Mediated transport of nucleosides in human erythrocytes. Specific binding of the inhibitor nitrobenzylthioinosine to nucleoside transport sites in the erythrocyte membrane*. *Biochimica et Biophysica Acta*, 1974. **345**(1): p. 1-10.
287. Chang, D.C. and T.S. Reese, *Changes in membrane structure induced by electroporation as revealed by rapid-freezing electron microscopy*. *Biophys J*, 1990. **58**(1): p. 1-12.
288. Santerre, R., J. Walls, and B. Grinnell, *Use of vectors to confer resistance to antibiotic G418 and hygromycin in stably transfected cell lines*, in *Methods in Molecular Biology*, E. Murray, Editor. 1991, Humana Press: Clifton.

289. Ward, J.L., A. Sherali, Z.P. Mo, and C.M. Tse, *Kinetic and pharmacological properties of cloned human equilibrative nucleoside transporters, ENT1 and ENT2, stably expressed in nucleoside transporter-deficient PK15 cells. Ent2 exhibits a low affinity for guanosine and cytidine but a high affinity for inosine.* J Biol Chem, 2000. **275**(12): p. 8375-81.
290. Yao, S.Y., A.M. Ng, M.F. Vickers, M. Sundaram, C.E. Cass, S.A. Baldwin, and J.D. Young, *Functional and molecular characterization of nucleobase transport by recombinant human and rat ENT1 and ENT2 equilibrative nucleoside transport proteins: Chimeric constructs reveal a role for the ENT2 helix 5-6 region in nucleobase translocation.* J Biol Chem, 2002. **277**: p. 2.
291. Hammond, J.R. and A.S. Clanachan, *Species differences in the binding of [³H]nitrobenzylthioinosine to the nucleoside transport system in mammalian central nervous system membranes: evidence for interconvertible conformations of the binding site/transporter complex.* J Neurochem, 1985. **45**(2): p. 527-35.
292. Schaner, M.E., J. Wang, L. Zhang, S.F. Su, K.M. Gerstin, and K.M. Giacomini, *Functional characterization of a human purine-selective, Na⁺-dependent nucleoside transporter (hSPNT1) in a mammalian expression system.* J Pharmacol Exp Ther, 1999. **289**(3): p. 1487-91.
293. Boyer, C.R., P.L. Karjian, G.M. Wahl, M. Pegram, and S.T. Neuteboom, *Nucleoside transport inhibitors, dipyridamole and p-nitrobenzylthioinosine, selectively potentiate the antitumor activity of NB1011.* Anticancer Drugs, 2002. **13**(1): p. 29-36.
294. Mackey, J.R., L.L. Jennings, M.L. Clarke, C.L. Santos, L. Dabbagh, M. Vsianska, S.L. Koski, R.W. Coupland, S.A. Baldwin, J.D. Young, and C.E. Cass, *Immunohistochemical variation of human equilibrative nucleoside transporter 1 protein in primary breast cancers.* Clin Cancer Res, 2002. **8**(1): p. 110-16.

295. Fregeau, C.J. and R.C. Bleackley, *Factors influencing transient expression in cytotoxic T cells following DEAE dextran-mediated gene transfer*. *Somat Cell Mol Genet*, 1991. **17**(3): p. 239-57.
296. Southern, P.J. and P. Berg, *Transformation of mammalian cells to antibiotic resistance with a bacterial gene under control of the SV40 early region promoter*. *J Mol Appl Genet*, 1982. **1**(4): p. 327-41.
297. Chen, X.J. and H. Fukuhara, *A gene fusion system using the aminoglycoside 3'-phosphotransferase gene of the kanamycin-resistance transposon Tn903: use in the yeast Kluyveromyces lactis and Saccharomyces cerevisiae*. *Gene*, 1988. **69**(2): p. 181-92.
298. Spandidos, D.A., *Transfer of human globin genes to human erythroleukemia cells*. *Mol Biol Med*, 1984. **2**(3): p. 167-75.
299. Nishimura, G., I. Terada, T. Kobayashi, I. Ninomiya, H. Kitagawa, S. Fushida, T. Fujimura, M. Kayahara, K. Shimizu, T. Ohta, and K. Miwa, *Thymidine phosphorylase and dihydropyrimidine dehydrogenase levels in primary colorectal cancer show a relationship to clinical effects of 5'-deoxy-5-fluorouridine as adjuvant chemotherapy*. *Oncol Rep*, 2002. **9**(3): p. 479-82.
300. Sadahiro, S., Y. Otani, K. Oya, H. Ike, H. Shimada, S. Yamaguchi, Y. Hiki, H. Fujita, and T. Mitomi, *Thymidine phosphorylase expression and effect of doxifluridine: a phase II study*. *Oncol Rep*, 2001. **8**(4): p. 753-58.
301. Budman, D.R., *Capecitabine*. *Invest New Drugs*, 2000. **18**(4): p. 355-63.
302. Shimma, N., I. Umeda, M. Arasaki, C. Murasaki, K. Masubuchi, Y. Kohchi, M. Miwa, M. Ura, N. Sawada, H. Tahara, I. Kuruma, I. Horii, and H. Ishitsuka, *The design and synthesis of a new tumor-selective fluoropyrimidine carbamate, capecitabine*. *Bioorg Med Chem*, 2000. **8**(7): p. 1697-06.
303. Di Costanzo, F., A. Sdrobolini, and S. Gasperoni, *Capecitabine, a new oral fluoropyrimidine for the treatment of colorectal cancer*. *Crit Rev Oncol Hematol*, 2000. **35**(2): p. 101-08.

304. Evans, T.R., G. Pentheroudakis, J. Paul, A. McInnes, R. Blackie, N. Raby, R. Morrison, G.M. Fullarton, M. Soukop, and A.C. McDonald, *A phase I and pharmacokinetic study of capecitabine in combination with epirubicin and cisplatin in patients with inoperable oesophago-gastric adenocarcinoma*. *Ann Oncol*, 2002. **13**(9): p. 1469-78.
305. von Borstel, R.W., A.A. Renshaw, and R.J. Wurtman, *Adenosine strongly potentiates pressor responses to nicotine in rats*. *Proc Natl Acad Sci USA*, 1984. **81**(17): p. 5599-603.
306. Ross, G.W. and H. Petrovitch, *Current evidence for neuroprotective effects of nicotine and caffeine against Parkinson's disease*. *Drugs Aging*, 2001. **18**(11): p. 797-06.
307. Stein, W.D., *Transport and diffusion across cell membranes*. 1986, Orlando, CA: Academic Press Inc.
308. Cheng, Y.-C. and W.H. Prusoff, *Relationship between the inhibition constant (Kt) and the concentration of inhibitor which causes 50 percent inhibition (I50) of an enzymatic reaction*. *Biochem. Pharmacol.*, 1973. **22**: p. 3099-08.
309. Desmoulin, F., V. Gilard, M. Malet-Martino, and R. Martino, *Metabolism of capecitabine, an oral fluorouracil prodrug: (19)F NMR studies in animal models and human urine*. *Drug Metab Dispos*, 2002. **30**(11): p. 1221-29.
310. Gati, W.P., L. Dagnino, and A.R. Paterson, *Enantiomeric selectivity of adenosine transport systems in mouse erythrocytes and L1210 cells*. *Biochem J*, 1989. **263**(3): p. 957-60.
311. Linden, J., A. Patel, and S. Sadek, *[¹²⁵I]Aminobenzyladenosine, a new radioligand with improved specific binding to adenosine receptors in heart*. *Circ Res*, 1985. **56**(2): p. 279-84.
312. Munshi, R., I.H. Pang, P.C. Sternweis, and J. Linden, *A1 adenosine receptors of bovine brain couple to guanine nucleotide-binding proteins Gi1, Gi2, and Go*. *J Biol Chem*, 1991. **266**(33): p. 22285-89.

313. Evoniuk, G., K.A. Jacobson, M.T. Shamim, J.W. Daly, and R.J. Wurtman, *A1- and A2-selective adenosine antagonists: in vivo characterization of cardiovascular effects*. *J Pharmacol Exp Ther*, 1987. **242**(3): p. 882-87.
314. Durand, I.H. and R.D. Green, *Cloning of a chick A3 adenosine receptor: characterization of ligand binding and receptor-effector coupling of chick A1 and A3 adenosine receptors*. *Naunyn Schmiedebergs Arch Pharmacol*, 2001. **363**(1): p. 81-86.
315. von Borstel, R.W., G.E. Evoniuk, and R.J. Wurtman, *Adenosine potentiates sympathomimetic effects of nicotinic agonists in vivo*. *J Pharmacol Exp Ther*, 1986. **236**(2): p. 344-49.
316. Wright, A.M., W.P. Gati, and A.R. Paterson, *Enhancement of retention and cytotoxicity of 2-chlorodeoxyadenosine in cultured human leukemic lymphoblasts by nitrobenzylthioinosine, an inhibitor of equilibrative nucleoside transport*. *Leukemia*, 2000. **14**(1): p. 52-60.
317. Valdes, R., M.A. Ortega, F.J. Casado, A. Felipe, A. Gil, A. Sanchez-Pozo, and M. Pastor-Anglada, *Nutritional regulation of nucleoside transporter expression in rat small intestine*. *Gastroenterology*, 2000. **119**(6): p. 1623-30.
318. Mata, J.F., J.M. Garcia-Manteiga, M.P. Lostao, S. Fernandez-Veledo, E. Guillen-Gomez, I.M. Larrayoz, J. Lloberas, F.J. Casado, and M. Pastor-Anglada, *Role of the human concentrative nucleoside transporter (hcnt1) in the cytotoxic action of 5*. *Mol Pharmacol*, 2001. **59**(6): p. 1542.
319. Stuyver, L.J., S. Lostia, M. Adams, J.S. Mathew, B.S. Pai, J. Grier, P.M. Tharnish, Y. Choi, Y. Chong, H. Choo, C.K. Chu, M.J. Otto, and R.F. Schinazi, *Antiviral activities and cellular toxicities of modified 2',3'-dideoxy-2',3'-didehydrocytidine analogues*. *Antimicrob Agents Chemother*, 2002. **46**(12): p. 3854-60.
320. Borowicz, K.K., J. Luszczki, and S.J. Czuczwar, *2-Chloroadenosine, a preferential agonist of adenosine A1 receptors, enhances the anticonvulsant activity of carbamazepine and clonazepam in mice*. *Eur Neuropsychopharmacol*, 2002. **12**(2): p. 173-79.

321. Dubey, R.K., D.G. Gillespie, and E.K. Jackson, *A(2B) adenosine receptors stimulate growth of porcine and rat arterial endothelial cells*. Hypertension, 2002. **39**(2 Pt 2): p. 530-35.
322. Flood, A. and J.P. Headrick, *Functional characterization of coronary vascular adenosine receptors in the mouse*. Br J Pharmacol, 2001. **133**(7): p. 1063-72.
323. Thampy, K.G. and E.M. Barnes, Jr., *Adenosine transport by cultured glial cells from chick embryo brain*. Arch Biochem Biophys, 1983. **220**(2): p. 340-46.
324. Picciotto, M.R. and M. Zoli, *Nicotinic receptors in aging and dementia*. J Neurobiol, 2002. **53**(4): p. 641-55.
325. Jonnala, R.R., A.V. Terry, Jr., and J.J. Buccafusco, *Nicotine increases the expression of high affinity nerve growth factor receptors in both in vitro and in vivo*. Life Sci, 2002. **70**(13): p. 1543-54.
326. Nehlig, A. and G. Debry, *Potential teratogenic and neurodevelopmental consequences of coffee and caffeine exposure: a review on human and animal data*. Neurotoxicol Teratol, 1994. **16**(6): p. 531-43.
327. Chen, J.F., K. Xu, J.P. Petzer, R. Staal, Y.H. Xu, M. Beilstein, P.K. Sonsalla, K. Castagnoli, N. Castagnoli, Jr., and M.A. Schwarzschild, *Neuroprotection by caffeine and A(2A) adenosine receptor inactivation in a model of Parkinson's disease*. J Neurosci, 2001. **21**(10): p. RC143.
328. Lawson, G.M., R.D. Hurt, L.C. Dale, K.P. Offord, I.T. Croghan, D.R. Schroeder, and N.S. Jiang, *Application of serum nicotine and plasma cotinine concentrations to assessment of nicotine replacement in light, moderate, and heavy smokers undergoing transdermal therapy*. J Clin Pharmacol, 1998. **38**(6): p. 502-09.
329. Felipe, A., R. Valdes, B. Santo, J. Lloberas, J. Casado, and M. Pastor-Anglada, *Na⁺-dependent nucleoside transport in liver: two different isoforms from the same gene family are expressed in liver cells*. Biochem J, 1998. **330**(Pt 2): p. 997-01.

330. Hopp, T.P. and K.R. Woods, *Prediction of protein antigenic determinants from amino acid sequences*. Proc Natl Acad Sci USA, 1981. **78**: p. 3824-28.
331. Kyte, J. and R.F. Doolittle, *A simple method for displaying the hydropathic character of a protein*. J Mol Biol, 1982. **157**: p. 105-32.
332. Creamer, B., *The turnover of the epithelium of the small intestine*. Br Med Bull, 1967. **23**(3): p. 226-30.
333. Mackinnon, A.M. and D.J. Deller, *Purine nucleotide biosynthesis in gastrointestinal mucosa*. Biochim Biophys Acta, 1973. **319**(1-4).
334. Sonada, T. and M. Tatibana, *Metabolic fate of pyrimidines and purines in dietary nucleic acids ingested by mice*. Biochim Biophys Acta, 1978. **521**: p. 55-56.
335. Schlimme, E., D. Martin, and H. Meisel, *Nucleosides and nucleotides: natural bioactive substances in milk and colostrum*. Br J Nutr, 2000. **84 Suppl 1**: p. S59-68.
336. Sanderson, I.R. and Y. He, *Nucleotide uptake and metabolism by intestinal epithelial cells*. J Nutr, 1994. **124**(1 Suppl): p. 131S-137S.
337. Graham, K., P. Carpenter, T.T. Lang, J. Listgarten, D. Mowles, H. Razavy, S.A. Baldwin, J.D. Young, J.R. Mackey, and C.E. Cass, *Nucleoside transporter expression in differentiating cellular systems*. Alberta Cancer Board Research Conference, 2002: p. Meeting Abstract.
338. He, Y., S.W. Chu, and W.A. Walker, *Nucleotide supplements alter proliferation and differentiation of cultured human (Caco-2) and rat (IEC-6) intestinal epithelial cells*. J Nutr, 1993. **123**: p. 1017-27.
339. Anderson, K.E., L.A. Eliot, B.R. Stevenson, and J.A. Rogers, *Formulation and evaluation of a folic acid receptor-targeted oral vancomycin liposomal dosage form*. Pharm Res, 2001. **18**(3): p. 316-22.
340. Hidalgo, I.J. and J.Y. Li, *Carrier-mediated transport and efflux mechanisms in Caco-2 cells*. Advanced Drug Delivery Reviews, 1996. **22**: p. 53-66.

341. Barrett, M.A., M.J. Lawrence, A.J. Hutt, and A.B. Lansley, *Stereoselective absorption and hydrolysis of cefuroxime axetil diastereomers using the Caco-2 cell monolayer model*. Eur J Drug Metab Pharmacokinet, 1997. **22**(4): p. 409-13.
342. Le Visage, C., P. Couvreur, E. Mysiakine, P. Breton, N. Bru, and E. Fattal, *In vitro and in vivo evaluation of poly(methylidene malonate 2.1.2) microparticles behavior for oral administration*. J Drug Target, 2001. **9**(2): p. 141-53.
343. Pinto, M., S. Robine-Leon, M. Appay, M. Kedingner, N. Triadou, E. Dussaulx, B. Lacroix, K. Haffen, and A. Zweidbaum, *Enterocyte-like differentiation and polarization of human colon carcinoma cell line Caco-2 in culture*. Biol Cell, 1983. **47**: p. 323-30.
344. Rousset, M., *The human colon carcinoma cell lines HT-29 and Caco-2: two in vitro models for the study of intestine differentiation*. Biochemistry, 1986. **68**: p. 1035-40.
345. Mahraoui, L., A. Rodolosse, A. Barbat, E. Dussaulx, A. Zweibaum, M. Rousset, and E. Brot-Laroche, *Presence and differential expression of SGLT1, GLUT1, GLUT2, GLUT3 and GLUT5 hexose-transporter mRNAs in Caco-2 cell clones in relation to cell growth and glucose consumption*. Biochem J, 1994. **298 Pt 3**: p. 629-33.
346. Peters, W.H. and H.M. Roelofs, *Time-dependent activity and expression of glutathione S-transferases in the human colon adenocarcinoma cell line Caco-2*. Biochem J, 1989. **264**(2): p. 613-16.
347. Iseki, K., M. Sugawara, T. Fujiwara, I. Naasani, M. Kobayashi, and K. Miyazaki, *Transport mechanisms of nucleosides and the derivative, 6-mercaptopurine riboside across rat intestinal brush-border membranes*. Biochimica et Biophysica Acta, 1996. **1278**(1): p. 105-10.
348. Hidalgo, I.J. and R.T. Borchardt, *Transport of a large neutral amino acid (phenylalanine) in a human intestinal epithelial cell line: Caco-2*. Biochim Biophys Acta, 1990. **1035**: p. 25-30.

349. Dix, C.J., I.F. Hassan, H.Y. Obray, R. Shah, and G. Wilson, *The transport of vitamine B12 through polarized monolayers of Caco-2 cells*. Gastroenterology, 1990. **98**: p. 1272-79.
350. Dantzig, A.H. and L. Bergin, *Uptake of the cephalosporin, cephalixin, by a dipeptide transport carrier in the human intestinal cell line Caco-2*. Biochim Biophys Acta, 1990. **1027**: p. 211-17.
351. Cushman, S.W. and L.J. Wardzala, *Potential mechanism of insulin action on glucose transport in the isolated rat adipose cell*. J Biol Chem, 1980. **255**: p. 4758-62.
352. Suzuki, K. and T. Kono, *Evidence that insulin causes translocation of glucose transport activity to the plasma membrane from an intracellular storage site*. Proc Natl Acad Sci USA, 1980. **77**: p. 2542-45.
353. Bradbury, N.A. and R.J. Bridges, *Role of membrane trafficking in plasma membrane solute transport*. Am J Physiol, 1994. **267**: p. C1-C24.
354. Coe, I., Y. Zhang, T. McKenzie, and Z. Naydenova, *PKC regulation of the human equilibrative nucleoside transporter, hENT1*. FEBS Lett, 2002. **517**: p. 201-05.
355. Von Lubitz, D.K., *Adenosine and cerebral ischemia: therapeutic future or death of a brave concept?* Eur J Pharmacol, 1999. **365**: p. 9-25.
356. Geiger, J.D., F.E. Parkinson, and E.A. Kowaluk, *Regulators of endogenous adenosine levels as therapeutic targets*, in *Purinergic approaches in experimental therapeutics*, K.A. Jacobson and M.F. Jarvis, Editors. 1997, Wiley-Liss: New York, NY. p. 55-84.
357. Impagnatiello, F., E. Bastia, E. Ongini, and A. Monopoli, *Adenosine receptors in neurological disorders*. Emerging Therapeutic Targets, 2000. **4**: p. 635-64.
358. Defazio, G., D. Ribatti, B. Nico, F. Ricchiuti, R. De Salvia, L. Roncali, and P. Livrea, *Endocytosis of horseradish peroxidase by brain microvascular and umbilical vein endothelial cells in culture: an ultrastructural and morphometric study*. Brain Res Bull, 1997. **43(5)**: p. 467-72.

359. Hurst, R.D. and I.B. Fritz, *Properties of an immortalised vascular endothelial/glioma cell co-culture model of the blood-brain barrier*. J Cell Physiol, 1996. **167(1)**: p. 81-88.
360. Ramschoye, P.V. and I.B. Fritz, *Preliminary characterization of glial-secreted factors responsible for the induction of high electrical resistances across endothelial monolayers in a blood-brain barrier model*. J Lab Clin Med, 1998. **132(4)**: p. 341-50.
361. Kalaria, R.N. and S.I. Harik, *Nucleoside transporter of cerebral microvessels and choroid plexus*. J Neurochem, 1986. **47(6)**: p. 1849-56.
362. Kalaria, R.N. and S.I. Harik, *Adenosine receptors and the nucleoside transporter in human brain vasculature*. J Cereb Blood Flow Metab, 1988. **8(1)**: p. 32-39.
363. Li, J.Y., R.J. Boado, and W.M. Pardridge, *Cloned blood-brain barrier adenosine transporter is identical to the rat concentrative Na⁺ nucleoside cotransporter CNT2*. J Cereb Blood Flow Metab, 2001. **21(8)**: p. 929-36.
364. Lawrence, A.J., M. Castillo-Melendez, and B. Jarrott, *[³H]Adenosine transport in rat dorsal brain stem using a crude synaptosomal preparation*. Neurochem Int, 1994. **25**: p. 221-26.
365. Marangos, P.J., R.R. Clark-Rosenberg, and J. Patel, *(³H)Nitrobenzylthioinosine is a photoaffinity probe for adenosine uptake sites in brain*. Eur. J. Pharmacol., 1982. **85**: p. 359-60.
366. Snell, B.J., J.L. Short, J. Drago, C. Ledent, and A.J. Lawrence, *Characterisation of central adenosine A(1) receptors and adenosine transporters in mice lacking the adenosine A(2a) receptor*. Brain Res, 2000. **877(2)**: p. 160-69.
367. Castillo-Melendez, M., B. Jarrott, and A.J. Lawrence, *Markers of adenosine removal in normotensive and hypertensive rat nervous tissue*. Hypertension, 1996. **28**: p. 1026-33.
368. Geiger, J.D. and J.I. Nagy, *Heterogenous distribution of adenosine transport sites labelled by NBTI in rat brain: An autoradiographic and membrane binding study*. Brain Res Bull, 1984. **13**: p. 657-66.

369. Kenny, D., M.G. Coughlan, J.P. Kampine, R.R. Montgomery, Z.J. Bosnjak, and D.C. Wartier, *Cultured endothelial cells restore vasodilator responses to coronary arteries with impaired endothelial function and alter the response to a nitric oxide donor*. *Pharmacology*, 1994. **49**(4): p. 249-56.
370. Kitakaze, M., M. Fong, M. Yoshitake, T. Minamino, K. Node, Y. Okuyama, N. Terada, T. Kambayashi, and M. Hori, *Vesnarinone inhibits adenosine uptake in endothelial cells, smooth muscle cells and myocytes, and mediates cytoprotection*. *J Mol Cell Cardiol*, 1997. **29**(12): p. 3413-17.
371. Moreau, J.L. and G. Huber, *Central adenosine A(2A) receptors: an overview*. *Brain Research Reviews*, 1999. **31**: p. 65-82.
372. Rakic, L.M. and G. Burnstock, *Receptors for purines and pyrimidines*. *Pharmacological Reviews*, 1998. **50**: p. 413-492.
373. Barankiewicz, J., *Transport of adenosine vai cell membrane and its modulation*. 1995: Poland.
374. Duelli, R. and W. Kuschinsky, *Brain glucose transporters: relationship to local energy demand*. *News Physiol Sci*, 2001. **16**: p. 71-76.
375. Smith, Q.R., *Drug delivery to brain and the role of carrier-mediated transport*. *Adv Exp Med Biol*, 1993. **331**: p. 83-93.
376. Washington, C.B. and K.M. Giacomini, *Mechanisms of nucleobase transport in rabbit choroid plexus. Evidence for a Na⁺-dependent nucleobase transporter with broad substrate selectivity*. *J Biol Chem*, 1995. **270**(39): p. 22816-19.
377. Sinclair, C.J., C.G. LaRiviere, J.D. Young, C.E. Cass, S.A. Baldwin, and F.E. Parkinson, *Purine uptake and release in rat C6 glioma cells: nucleoside transport and purine metabolism under ATP-depleting conditions*. *J Neurochem*, 2000. **75**(4): p. 1528-38.
378. Meghji, P., J.B. Tuttle, and R. Rubio, *Adenosine formation and release by embryonic chick neurons and glia in cell culture*. *J Neurochem*, 1989. **53**(6): p. 1852-60.
379. Buchwald, A., B.R. Ito, and W. Schaper, *Influence of mioflazine on canine coronary blood flow and on adenine nucleotide and nucleoside content*

- under normal and ischemic conditions. Journal of Cardiovascular Pharmacology, 1987. 10(2): p. 213-21.*
380. Hosli, E. and L. Hosli, *Autoradiographic studies on the uptake of adenosine and on binding of adenosine analogues in neurons and astrocytes of cultured rat cerebellum and spinal cord. Neuroscience, 1988. 24: p. 621-628.*
381. Ennis, S.R., X.D. Ren, and A.L. Beltz, *Mechanisms of sodium transport at the blood-brain barrier studies with in situ perfusion of rat brain. J Neurochem, 1996. 66: p. 756-63.*
382. Li, J.Y., R.J. Boado, and W.M. Pardridge, *Differential kinetics of transport of 2',3'-dideoxyinosine and adenosine via concentrative Na⁺ nucleoside transporter CNT2 cloned from rat blood-brain barrier. J Pharmacol Exp Ther, 2001. 299(2): p. 735-40.*
383. Chan, T.C., *Augmentation of 1-beta-D-arabinofuranosylcytosine cytotoxicity in human tumor cells by inhibiting drug efflux. Cancer Res, 1989. 49(10): p. 2656-60.*
384. Quaroni, A., *Crypt cell development in newborn rat small intestine. J Cell Biol, 1985. 100(5): p. 1601-10.*
385. Pileri, S.A., G. Roncador, C. Ceccarelli, M. Piccioli, A. Briskomatis, E. Sabbatini, S. Ascani, D. Santini, P.P. Piccaluga, O. Leone, S. Damiani, C. Ercolessi, F. Sandri, F. Pieri, L. Leoncini, and B. Falini, *Antigen retrieval techniques in immunohistochemistry: comparison of different methods. J. Pathol., 1997. 183: p. 116-23.*
386. Shi, S.-R., R.J. Cote, and C.R. Taylor, *Antigen retrieval immunohistochemistry: past, present, and future. J. Histochem. Cytochem., 1997. 45: p. 327-343.*